

## DOCTOR OF PHILOSOPHY

### Investigation into the effects of age and diet induced obesity on cardiac contractility and its effect on drug responses

Ribeiro, Ralfe Alibhai

*Award date:*  
2021

*Awarding institution:*  
Coventry University

[Link to publication](#)

#### **General rights**

Copyright and moral rights for the publications made accessible in the public portal are retained by the authors and/or other copyright owners and it is a condition of accessing publications that users recognise and abide by the legal requirements associated with these rights.

- Users may download and print one copy of this thesis for personal non-commercial research or study
- This thesis cannot be reproduced or quoted extensively from without first obtaining permission from the copyright holder(s)
- You may not further distribute the material or use it for any profit-making activity or commercial gain
- You may freely distribute the URL identifying the publication in the public portal

#### **Take down policy**

If you believe that this document breaches copyright please contact us providing details, and we will remove access to the work immediately and investigate your claim.



**Investigation into the effects of age  
and diet induced obesity on cardiac  
contractility and its effect on drug  
responses**

**By**

**Ralfe Alibhai Ribeiro BSc (Hons), MSc**

**PhD**

**Coventry University**

**June 2020**

# **Investigation into the effects of age and diet induced obesity on cardiac contractility and its effect on drug responses**

**By**

**Ralfe Alibhai Ribeiro BSc (Hons), MSc**

***A thesis submitted in partial fulfilment of the University's requirements for the Degree of Doctor of Philosophy***

**Coventry University**

**June 2020**

Content removed on data protection grounds



## **Certificate of Ethical Approval**

Applicant:

Ralfe Alibhai Ribeiro

Project Title:

Effects of a high fat diet on cardiac contractile function in naive and stressed condition

This is to certify that the above named applicant has completed the Coventry University Ethical Approval process and their project has been confirmed and approved as Medium Risk

Date of approval:

24 November 2015

Project Reference Number:

P37057



## **Certificate of Ethical Approval**

Applicant:

Ralfe Alibhai Ribeiro

Project Title:

Effects of a high fat diet on cardiac contractile function in naive and stressed condition

This is to certify that the above named applicant has completed the Coventry University Ethical Approval process and their project has been confirmed and approved as Medium Risk

Date of approval:

23 November 2016

Project Reference Number:

P45504



## **Certificate of Ethical Approval**

Applicant:

Ralfe Alibhai Ribeiro

Project Title:

The effects of a high-fat diet induced obesity and ageing on the contractile function of the heart

This is to certify that the above named applicant has completed the Coventry University Ethical Approval process and their project has been confirmed and approved as Medium Risk

Date of approval:

04 July 2019

Project Reference Number:

P90389

Content removed on data protection grounds

# Table of Contents

---

Acknowledgements.....	15
Abstract .....	16
List of Figures .....	19
List of Tables.....	26
List of Abbreviations.....	27
Chapter One: Introduction .....	30
1.1    General overview .....	30
1.2    Parameters of cardiac contractility .....	31
1.2.1    Cardiac excitation-contraction coupling and action potential.....	35
1.3    Contractility measurements and muscle mechanics .....	37
1.3.1    The heart machinery: pressure-volume relationship.....	38
1.3.2    The Langendorff Heart model as a measure for contractility.....	40
1.3.3    The Work-loop technique and isometric contractions .....	41
1.4    The old heart .....	43
1.4.1    Frailty in cardiovascular disease.....	49
1.4.2    Impact of age on cardiac contractility.....	50
1.5    Obesity and the heart .....	53
1.5.1    Pathophysiology of obesity .....	54
1.5.2    Cardiac remodelling in obesity.....	57
1.6    Cardiovascular mitochondrial regulation.....	63
1.6.1    Peroxisome proliferator-activated receptor alpha (PPAR $\alpha$ ).....	66
1.6.2    Pyruvate Dehydrogenase (PDH).....	69
1.6.3    Uncoupling Protein 3 (UCP3).....	71
1.7    Inotropic drugs and their modes of action .....	75
1.7.1    Isoprenaline.....	75
1.7.2    Dobutamine.....	78
1.7.3    Atenolol .....	81
1.7.4    Itraconazole.....	84
Chapter Two: Aims and hypotheses.....	89
Chapter Three: Materials and Methods.....	91
3.1    Model Characterisation.....	91
3.1.1    Aged models.....	91
3.1.2    High-fat diet-induced obesity models (HFD).....	93

3.2	Langendorff Isolated Heart Model .....	97
3.2.1	Drugs and chemicals utilised .....	97
3.2.2	Haemodynamics Data Collection .....	98
3.2.3	Dose response protocol .....	100
3.3	Work-Loop and Muscle mechanic studies .....	101
3.3.1	Muscle preparation .....	101
3.3.2	Contraction studies .....	102
3.3.3	Muscle length optimisation.....	104
3.4	Western Blotting .....	104
3.4.1	Antibodies and reagents used for Western Blotting.....	105
3.4.2	Tissue Collection for Western Blot Analysis.....	105
3.4.3	Protein Quantification using Bicinchoninic Acid Assay (BCA) .....	106
3.4.4	Gel Electrophoresis, protein transfer and antibody probing .....	106
3.4.5	Visualisation, Densitometry and Quantification .....	107
3.5	Compliance with the 3Rs.....	108
3.6	Statistical Analysis .....	108
3.7	Optimised and attempted techniques .....	110
3.7.1	Langendorff short administration dose response protocol .....	110
3.7.2	Langendorff ECG measurements .....	111
3.7.3	Enzyme-linked immunosorbent assay (ELISA) .....	111
3.7.4	Reverse transcription PCR (RT-PCR).....	114
Chapter Four: The effects of age on the contractile function of the heart.....		117
4.1	Introduction .....	118
4.2	Materials and Methods .....	121
4.2.1	Animal Models .....	121
4.2.2	Langendorff Isolated Heart Model (full review in section 3.2) .....	122
4.2.3	Work-loop Assay (full review in section 3.3).....	123
4.2.4	Western Blotting (full review in section 3.4).....	124
4.2.5	Statistical Analysis (full review in section 3.6) .....	127
4.3	Results .....	127
4.3.1	Langendorff Isolated Heart Model.....	127
4.3.2	Work-Loop Assay.....	133
4.3.3	Western Blot .....	136
4.4	Discussion and Conclusion .....	138
4.5	Summary, limitations and final comments .....	144

Chapter Five: The effects of high fat -diet-induced obesity on the contractile function of the heart .....	146
5.1 Introduction .....	147
5.2 Materials and Methods .....	151
5.2.1 Animal Models .....	151
5.2.2 Langendorff Isolated Heart Model (full review in section 3.2) .....	153
5.2.3 Work-loop Assay (full review in section 3.3) .....	154
5.2.4 Western Blotting (full review in section 3.4) .....	156
5.2.5 Statistical Analysis (full review in section 3.6) .....	158
5.3 Results .....	159
5.3.1 Langendorff Isolated Heart Model .....	159
5.3.2 Work-Loop Assay .....	166
5.3.3 Western Blot .....	169
5.4 Discussion and Conclusion .....	171
5.5 Summary, limitations and final comments .....	176
Chapter Six: Inotropic drug effects on the contractile function of the heart in an age-dependant study .....	178
6.1 Introduction .....	179
6.2 Materials and Methods .....	184
6.2.1 Animal Models .....	184
6.2.2 Langendorff Isolated Heart Model (full review in section 3.2) .....	185
6.2.3 Work-loop assay (full review in section 3.3) .....	186
6.2.4 Western Blotting (full review in section 3.4) .....	188
6.2.5 Statistical Analysis (full review in section 3.6) .....	190
6.3 Results .....	191
6.3.1 Langendorff Isolated Heart Model .....	191
6.3.2 Work-loop Assay .....	205
6.3.3 Western Blots .....	211
6.3.3.1 Pyruvate Dehydrogenase .....	211
6.3.3.2 UCP3 .....	214
6.4 Discussion and Conclusion .....	217
6.5 Summary, limitations and final comments .....	228
Chapter Seven: Inotropic drug effects on the contractile function of the heart in High-fat diet-induced obesity, in differently aged animals .....	230
7.1 Introduction .....	231
7.2 Materials and Methods .....	237

7.2.1	Animal Models .....	237
7.2.2	Langendorff Isolated Heart Model (full review in section 3.2) .....	239
7.2.3	Western Blotting (full review in section 3.4).....	240
7.2.4	Statistical Analysis (full review in section 3.6) .....	242
7.3	Results .....	243
7.3.1	Langendorff Isolated Heart Model.....	243
7.3.2	Western Blots .....	270
7.3.2.1	Pyruvate Dehydrogenase .....	270
7.3.2.2	UCP3 .....	274
7.4	Discussion and Conclusion .....	277
7.5	Summary, limitations and final comments .....	285
Chapter Eight: General conclusions .....		287
8.1	Summary of key findings .....	287
8.2	Study limitations.....	290
Chapter Nine: Future work.....		292
References.....		295
Appendix .....		336

# Acknowledgements

*“When the Almighty tests you, He’s testing how well you’re able to restore faith in your heart. Be patient. Do not lose faith. Ease will come.” – Mufti Ismail bin Musa Menk.*

I would like to start by thanking my supervisory team (Dr. Jason Tallis, Dr. Mayel Gharanei, Dr. Mike Dodd and Professor Helen Maddock) for providing me with the necessary tools to develop my critical thinking and for helping me develop as an independent researcher.

Secondly, I would like to thank Mark and Bethan for their technical and moral support. You helped and guided me through the data collection period of my project and I would not have any data to defend if you had not been there for me. I would also like to take a moment to thank all of my colleagues that participated in this journey with me.

To my friends (G, Gui, Flu, J and Weiu), thank you for putting up with me at my best and my worst and for the (always entertaining) distractions. You are the best group of friends anyone could hope for and this completion would not be possible without you.

I could not write an acknowledgement section without thanking my parents and my siblings, who saw me grow and were there for me for every high and low point for these past years (and forever). They taught me the value of perseverance and patience and I would not have gotten to where I am, both academically and in life, without your invaluable support. This degree is mine as much as it is yours, if not more.

Last but certainly not least, I would like to give a big thank you to my best friend and the most supportive wife one could ask for. You picked me up when I needed, and you gave me the confidence boost to get me through this. Thank you for never wavering in your faith in me and for seeing something that no one else saw.

# Abstract

Cardiac contractility is often defined as the ability of the cardiac muscle to generate power and results from a number of mechanisms. Contractile work is also the trigger that causes an increase or decrease in ATP generation, via one of two main processes: fatty acid (FA) oxidation or carbon substrate metabolism. These two mechanisms are crucial in contraction and any changes can lead to cardiac dysfunction. To this effect, both age and obesity have been previously shown to play a significant role in cardiac dysfunction, primarily via changes to contractility and ATP generation and in pathways involving the citric acid cycle and uncoupling proteins. The primary aim of this thesis was to investigate cardiac contractility in rodent models of aging and high fat diet-induced obesity (HFD) in the presence and absence of inotropic drugs.

The first part of this project was a physiological investigation into the effects of ageing (3, 6 and 18-month murine models) and high fat diet-induced obesity (6 and 18-month lean and obese murine models) on cardiac function. The second part of the project was a pharmacological investigation into the effects of inotrope-induced changes on cardiac contractility in ageing and high-fat diet-induced obesity (using the same models). To achieve this, three techniques were used: the Langendorff isolated heart model, the papillary muscle work-loop assay used to assess power output and western blotting protein analysis of Pyruvate dehydrogenase E1- $\alpha$  subunit (PDH) and Uncoupling protein 3 (UCP3).

Cardiac function of the whole heart diminished with age, showing significant differences for the Rare pressure product (RPP) on the 18-month models when compared to the 3 and 6-month models ( $p < 0.05$ ), but the cardiac muscles also suffer time and age-dependant decreases in performance, when comparing the 6-month models to the 3-month models.

This translated to reductions in power output ( $p < 0.05$ ) and total net-work done. In addition to this, and in agreement with previous literature, the results from the western blots on PDH have shown decreased phosphorylation in an age-dependant fashion and indicate that there is, in fact, a decrease in FA oxidation ( $p < 0.0001$  when comparing between the 6 and 18-month models with the 3-month model). The UCP3 results corroborate these findings and suggest that there is a decrease in the rate of FA oxidation, in an age-dependant fashion ( $p < 0.0001$  when comparing between the 6 and 18-month models with the 3-month model).

HFD functional changes were also recorded, as the 6-month lean heart showed significant decreases in the absolute values for the haemodynamic parameters when compared to the 6-month HFD model ( $p < 0.0001$ ); the 18-month model showed a significant increase compared to the 6-month lean model, but not when compared to the 6-month HFD model, which aligns with previous literature which associated these changes with hypertrophic changes to the heart. On the muscle assay, significant decreases in power output, fatigue and total net-work done were recorded when comparing between lean and HFD muscles ( $p < 0.01$ ). Finally, the pPDH and UCP3 were shown to be effective biomarkers of obesity, as the formers levels decreased in the presence of the high-fat diet ( $p < 0.0001$ ), while the latter increased significantly. The measured increase in UCP3, specifically, is indicative of increased FA availability and its consequent usage.

On the ageing pharmacological chapter, a phenomenon known as  $\beta$ -receptor desensitization was present, as the LVDP, HR and RPP for the 18-month dobutamine-treated hearts were shown to have age-dependant impairments, when compared to the 3 and 6-month models ( $p < 0.0001$ ). As for the western blot assay, it was found that PDH was reduced in an age-dependant fashion for all three drug-treated hearts, with seemingly no changes in expression between them ( $p < 0.0001$  when comparing between the 6 and 18-month models with the 3-month model).

This seems to indicate that FA oxidation and ATP production are being affected, but not detected in the isolated heart models (other than on the Dobutamine-treated hearts). As for UCP3, interestingly no change was recorded for atenolol or itraconazole across different ages, but a significant decrease was recorded for the 6 and 18-month dobutamine treated hearts when compared to the 3-month heart ( $p < 0.0001$ ). It is therefore possible that there is a correlation between the observed  $\beta$ -receptor desensitization and the UCP3 levels, even though the exact link between the two is unclear.

On the isolated heart model, between the lean and HFD atenolol-treated hearts, but both the Dobutamine and Itraconazole data showed severe impairment and exacerbation (respectively) in their inotropic effects on LVDP, HR and RPP, when treating the HFD models and comparing them to the lean models ( $p < 0.01$  for each parameter for Dobutamine and  $p < 0.0001$  for each parameter for Itraconazole). PDH was significantly changed for the HFD hearts treated with Dobutamine ( $p < 0.0001$ ) and Itraconazole ( $p < 0.0001$ ), with little to no change in our atenolol treated hearts. UCP3 on the other hand showed no significance between the dobutamine and atenolol treated HFD and lean hearts but showed a significant decrease for the itraconazole HFD treated hearts when compared to the lean hearts ( $p < 0.001$ ).

In conclusion, these results showed that both age and HFD cause functional changes in the heart in both absence and presence of drug treatments and their combined synergistic effect can cause further detrimental changes on different haemodynamic parameters. In addition, PDH activity, specifically, seems to be heavily linked to the inotropic effect of both Dobutamine and Itraconazole in the presence of obesity, but further work will still be necessary in order to confirm this observation.

# List of Figures

- Figure 1.2.1** Cardiac signalling pathways.
- Figure 1.2.2** Calcium influx in cardiomyocytes.
- Figure 1.2.3** Cardiac output calculations.
- Figure 1.2.1.1** Action potential of cardiac muscles in humans (left) and rodents (right).
- Figure 1.2.1.2** Calcium influx in the cardiomyocyte.
- Figure 1.3.1.1** Wiggers Diagram.
- Figure 1.3.2.1** Isolated heart apparatus.
- Figure 1.3.3.1** Cardiac papillary muscle.
- Figure 1.3.4.1** Mechanisms leading to the contraction and relaxation of the heart.
- Figure 1.4.1** The old heart.
- Figure 1.4.2** Risk factors of cardiovascular disease.
- Figure 1.4.3** Cardiac dysfunctions associated with age.
- Figure 1.4.4** Risk factors and structural changes in the heart.
- Figure 1.4.5** Changes in cardiac pressure as a result of age.
- Figure 1.4.1.1** Impact factors of frailty in age.
- Figure 1.5.1** BMI Formula.
- Figure 1.5.1.1** Different types of adipose tissue.
- Figure 1.5.1.2** Pathophysiology of obesity cardiomyopathy.
- Figure 1.5.2.1** Mechanisms leading to cardiac lipotoxicity.
- Figure 1.5.2.2** Effect of insulin on adipose storage.
- Figure 1.5.2.3** Effects of HFD on cardiac gene expression.
- Figure 1.5.2.4** Mechanisms involved in cardiac dysfunction as a result of obesity.

- Figure 1.6.1** ROS effect within the cells.
- Figure 1.6.1.1** Intracellular PPAR pathways.
- Figure 1.6.2.1** PDC regulatory processes.
- Figure 1.6.2.2** ATP production diagram.
- Figure 1.6.3.1** Intracellular role of UCPs.
- Figure 1.6.3.2** UCP list.
- Figure 1.7.1.1** Isoprenaline mode of action.
- Figure 1.7.2.1** Dobutamine mode of action and signalling pathways.
- Figure 1.7.2.2**  $\beta$ -AR effects on different heart models.
- Figure 1.7.3.1** Atenolol mode of action.
- Figure 1.7.4.1** Angiogenesis and CVD.
- Figure 1.7.4.2** Intracellular effects of CYPs.
- Figure 3.1.1.1** Kaplan Meier survival curve for the aging rats over time.
- Figure 3.1.1.2** Graph showcasing heart weight variations across all aged models.
- Figure 3.1.2.1** Comparison of animal body mass in both the 6 and the 18-month aged models, measured bi-weekly, for a total of 16 weeks.
- Figure 3.1.2.2** Graph showcasing heart weight variation across all obese and lean models.
- Figure 3.2.2.1** Langendorff isolated heart.
- Figure 3.2.2.2** A print screen is shown above representing the software used to analyse the different haemodynamic parameters (LVDP, heart rate, + dP/dtmax and - dP/dTmax).
- Figure 3.2.2.3** Langendorff trace further explained.
- Figure 3.2.3.1** Langendorff protocol.
- Figure 3.3.2.1** Work-loop protocol.
- Figure 3.4.5.1** Representative western blot gel run.
- Figure 4.2.2.1** Langendorff protocol.

- Figure 4.2.3.1** Work-loop protocol.
- Figure 4.3.1.1** Maximum ventricular pressure rise difference amongst rats of age 3-months, 6-months and 18-months (n = 4).
- Figure 4.3.1.2** Maximum ventricular pressure drop difference amongst rats of age 3-months, 6-months and 18-months (n = 4).
- Figure 4.3.1.3** Rate Pressure Product difference amongst rats of age 3-months, 6-months and 18-months (n = 4) – Normalised (top) vs raw data (bottom).
- Figure 4.3.1.4** LVDP and HR difference amongst rats of age 3-months, 6-months and 18-months (n = 4)
- Figure 4.3.2.1** Power Output in 3-month (n = 7) and 6-month (n = 6) age models.
- Figure 4.3.2.2** Age comparison at 45 minutes.
- Figure 4.3.2.3** Age comparison at 100 minutes.
- Figure 4.3.2.4** Age comparison at 120 minutes.
- Figure 4.3.3.1** Phosphorylated PDH expression in differently aged models (n = 4 for all).
- Figure 4.3.3.2** UCP3 expression in differently aged models (n = 4 for all).
- Figure 5.2.1.1** Comparison of animal body mass in both the 6 and the 18-month aged models, measured bi-weekly, for a total of 16 weeks.
- Figure 5.2.2.1** Langendorff protocol.
- Figure 5.2.3.1** Work-loop protocol.
- Figure 5.3.1.1** +dP/dT<sub>max</sub> for the 6-month models as seen in graph A and for the 18-month models as seen in graph B (n = 4 for both models).
- Figure 5.3.1.2** -dP/dT<sub>max</sub> for the lean and HFD 6-month models (n = 4 for both models).
- Figure 5.3.1.3** -dP/dT<sub>max</sub> for the lean and HFD 6-month models (n = 4 for both models).
- Figure 5.3.1.4** RPP for the 6 (A) and 18-month (B) lean and HFD models (n = 4 for both models).
- Figure 5.3.1.5** CF for the 6 (A) and 18-month (B) lean and HFD models (n = 4 for both models).

- Figure 5.3.1.6** MPR for the 6- and 18-month HFD models (n = 4 for both models).
- Figure 5.3.1.7** MPD for the 6- and 18-month HFD models (n = 4 for both models).
- Figure 5.3.1.8** RPP for the 6- and 18-month HFD models (n = 4 for both models).
- Figure 5.3.2.1** Power output for the lean and HFD 6-month models (n = 6 and 5, respectively).
- Figure 5.3.2.2** Comparison between a lean and an HFD model at the 45-minute mark.
- Figure 5.3.2.3** Comparison between a lean and an HFD model at the 100-minute mark.
- Figure 5.3.2.4** Comparison between a lean and an HFD model at the 120-minute mark.
- Figure 5.3.3.1** Phosphorylated PDH expression in 6- and 18-month-old HFD and lean animal models (n = 4 for all).
- Figure 5.3.3.2** UCP3 expression in 6- and 18-month-old HFD and lean animal models (n = 4 for all).
- Figure 6.2.2.1** Langendorff protocol.
- Figure 6.2.3.1** Work-loop protocol.
- Figure 6.3.1.1** LVDP for Atenolol across the different aged models (n = 4 for all).
- Figure 6.3.1.2** HR for Atenolol across the different aged models (n = 4 for all).
- Figure 6.3.1.3** RPP for Atenolol across the different aged models (n = 4 for all).
- Figure 6.3.1.4** +dP/dTmax (A) and – dP/dTmax (B) for Atenolol across the different aged models (n = 4 for all).
- Figure 6.3.1.5** LVDP for Itraconazole across the different aged models (n = 4 for all).
- Figure 6.3.1.6** HR for Itraconazole across the different aged models (n = 4 for all).
- Figure 6.3.1.7** RPP for Itraconazole across the different aged models (n = 4 for all).
- Figure 6.3.1.8** +dP/dTmax (A) and – dP/dTmax (B) for Itraconazole across the different aged models (n = 4 for all).
- Figure 6.3.1.9** LVDP for Dobutamine across the different aged models (n = 4 for all).
- Figure 6.3.1.10** HR for Dobutamine across the different aged models (n = 4 for all).
- Figure 6.3.1.11** RPP for Dobutamine across the different aged models (n = 4 for all).

- Figure 6.3.1.12** +dP/dTmax for Dobutamine across the different aged models (n = 4 for all).
- Figure 6.3.1.13** -dP/dTmax for Dobutamine across the different aged models (n = 4 for all).
- Figure 6.3.2.1** Power output for each drug group.
- Figure 6.3.2.2** Comparison between control and Dobutamine treated muscles.
- Figure 6.3.2.3** Comparison between control and Isoprenaline treated muscles.
- Figure 6.3.2.4** Comparison between control and Atenolol treated muscles.
- Figure 6.3.2.5** Comparison between control and Itraconazole treated muscles.
- Figure 6.3.3.1.1** Phosphorylated PDH expression in different dobutamine-treated aged models (n = 4 for all).
- Figure 6.3.3.1.2** Phosphorylated PDH expression in different atenolol-treated aged models (n = 4 for all).
- Figure 6.3.3.1.3** Phosphorylated PDH expression in different itraconazole-treated aged models (n = 4 for all)
- Figure 6.3.3.2.1** UCP3 expression in different dobutamine-treated aged models (n = 4 for all).
- Figure 6.3.3.2.2** UCP3 expression in different atenolol-treated aged models (n = 4 for all).
- Figure 6.3.3.2.3** UCP3 expression in different itraconazole-treated aged models (n = 4 for all).
- Figure 7.2.1.1** Comparison of animal weight in both the 6 and the 18-month aged models, measured bi-weekly, for a total of 16 weeks.
- Figure 7.2.2.1** Langendorff protocol.
- Figure 7.3.1.1** + and -dP/dTmax for the 6-month atenolol-treated lean and HFD models (n = 4 for both).
- Figure 7.3.1.2** RPP for the 6-month atenolol-treated lean and HFD models (n = 4 for both).
- Figure 7.3.1.3** + and -dP/dTmax for the 18-month atenolol-treated lean and HFD models (n = 4 for both).
- Figure 7.3.1.4** RPP for the 18-month atenolol-treated lean and HFD models (n = 4 for both).

- Figure 7.3.1.5** LVDP for the 6-month itraconazole-treated lean and HFD models (n = 4 for both).
- Figure 7.3.1.6** HR for the 6-month itraconazole-treated lean and HFD models (n = 4 for both).
- Figure 7.3.1.7** +dP/dTmax for the 6-month itraconazole-treated lean and HFD models (n = 4 for both).
- Figure 7.3.1.8** -dP/dTmax for the 6-month itraconazole-treated lean and HFD models (n = 4 for both).
- Figure 7.3.1.9** RPP for the 6-month itraconazole-treated lean and HFD models (n = 4 for both).
- Figure 7.3.1.10** LVDP for the 18-month itraconazole-treated lean and HFD models (n = 4 for both).
- Figure 7.3.1.11** HR for the 18-month itraconazole-treated lean and HFD models (n = 4 for both).
- Figure 7.3.1.12** + and - dP/dTmax for the 18-month itraconazole-treated lean and HFD models (n = 4 for both).
- Figure 7.3.1.13** RPP for the 18-month itraconazole-treated lean and HFD models (n = 4 for both).
- Figure 7.3.1.14** LVDP for the 6-month dobutamine-treated lean and HFD models (n = 4 for both).
- Figure 7.3.1.15** HR for the 6-month dobutamine-treated lean and HFD models (n = 4 for both).
- Figure 7.3.1.16** + and -dP/dTmax for the 6-month dobutamine-treated lean and HFD models (n = 4 for both).
- Figure 7.3.1.17** RPP for the 6-month dobutamine-treated lean and HFD models (n = 4 for both).
- Figure 7.3.1.18** LVDP for the 18-month dobutamine-treated lean and HFD models (n = 4 for both).
- Figure 7.3.1.19** HR for the 18-month dobutamine-treated lean and HFD models (n = 4 for both).
- Figure 7.3.1.20** + and - dP/dTmax for the 18-month dobutamine-treated lean and HFD models (n = 4 for both).
- Figure 7.3.1.21** RPP for the 18-month dobutamine-treated lean and HFD models (n = 4 for both).

- Figure 7.3.1.22** MPR for the 6- and 18-month HFD hearts treated with Atenolol (n = 4 for both).
- Figure 7.3.1.23** MPD for the 6- and 18-month HFD hearts treated with Atenolol (n = 4 for both).
- Figure 7.3.1.24** RPP for the 6- and 18-month HFD hearts treated with Atenolol (n = 4 for both).
- Figure 7.3.1.25** MPR for the 6- and 18-month HFD hearts treated with Itraconazole (n = 4 for both).
- Figure 7.3.1.26** MPD for the 6- and 18-month HFD hearts treated with Itraconazole (n = 4 for both).
- Figure 7.3.1.27** RPP for the 6- and 18-month HFD hearts treated with Itraconazole (n = 4 for both).
- Figure 7.3.1.28** MPR for the 6- and 18-month HFD hearts treated with Dobutamine (n = 4 for both).
- Figure 7.3.1.29** MPD for the 6- and 18-month HFD hearts treated with Dobutamine (n = 4 for both).
- Figure 7.3.1.30** RPP for the 6- and 18-month HFD hearts treated with Dobutamine (n = 4 for both).
- Figure 7.3.2.1.1** Phosphorylated PDH expression in 6- and 18-month-old HFD and lean Dobutamine treated animal models (n = 4 for all).
- Figure 7.3.2.1.2** Phosphorylated PDH expression in 6- and 18-month-old HFD and lean Atenolol treated animal models (n = 4 for all).
- Figure 7.3.2.1.3** Phosphorylated PDH expression in 6- and 18-month-old HFD and lean Itraconazole treated animal models (n = 4 for all).
- Figure 7.3.2.2.1** UCP3 expression in 6- and 18-month-old HFD and lean Dobutamine treated animal models (n = 4 for all).
- Figure 7.3.2.2.2** UCP3 expression in 6- and 18-month-old HFD and lean Atenolol treated animal models (n = 4 for all).
- Figure 7.3.2.2.3** UCP3 expression in 6- and 18-month-old HFD and lean Itraconazole treated animal models (n = 4 for all).

# List of Tables

<b>Table 3.1.2.1</b>	Table with the comparison of parameters between lean models and HFD models, in 6-month and 18-month aged animals.
<b>Table 3.1.2.2</b>	Table with the layout of each chapter presented.
<b>Table 4.3.1.1</b>	Performance assessment of the three age models in the first 20-minutes of the experimental protocol.
<b>Table 5.2.1.1</b>	Table with the comparison of parameters between lean models and HFD models, in 6-month and 18-month aged animals.
<b>Table 5.3.1.1</b>	Performance assessment of the four HFD models in the first 20-minutes of the experimental protocol.
<b>Table 6.3.1.1</b>	Table with the minimum and maximum drug response on the isolated heart, and respective EC50 value.
<b>Table 7.2.1.1</b>	Table with the comparison of parameters between lean models and HFD models, in 6-month and 18-month aged animals.
<b>Table 7.3.1.1</b>	Table with the minimum and maximum drug response on the 6-month lean and HFD isolated hearts, and respective EC50 value.
<b>Table 7.3.1.2</b>	Table with the minimum and maximum drug response on the 18-month lean and HFD isolated hearts, and respective EC50 value.

# List of Abbreviations

<b>AC-5 or AC</b>	Type 5 adenylyl cyclase
<b>ACC</b>	Acetyl-CoA carboxylase
<b>AD or MUSC</b>	Muscarinic receptor
<b>AKAP</b>	A-kinase-anchoring protein
<b>AMPK</b>	5' Amp-activated protein kinase
<b>ANOVA</b>	Analysis of variance
<b>ANP</b>	Atrial natriuretic peptide
<b>ATP</b>	Adenosine triphosphate
<b>AV</b>	Atrioventricular node
<b><math>\alpha/\beta</math> MHC</b>	Alpha/beta myosin heavy chain
<b><math>\beta</math>1/2 AR</b>	Beta-adrenergic receptor 1 and 2
<b>BAT</b>	Brown adipose tissue
<b>BCA</b>	Bicinchoninic acid assay
<b>BMAT</b>	Bone marrow adipose tissue
<b>BMI</b>	Body mass index
<b>BPM</b>	beats per minute
<b>BSA</b>	Bovine serum albumin
<b>Ca<sup>2+</sup></b>	Calcium
<b>CAC</b>	Citric acid cycle
<b>CamkII</b>	Ca <sup>2+</sup> /calmodulin-dependent protein kinase
<b>cAMP</b>	Cyclic adenosine monophosphate
<b>Cas</b>	Catecholamines
<b>CAT</b>	Carnitine acyl translocase
<b>CATf</b>	Carnitine acyl translocase transferase
<b>CD36</b>	Platelet glycoprotein 4
<b>CF</b>	Coronary flow
<b>CPT1</b>	Carnitine palmitoyl transferase 1
<b>CPT2</b>	Carnitine palmitoyl transferase 2
<b>CS</b>	Citrate Synthase
<b>CT</b>	Carboxyltransferase
<b>cTnT</b>	Cardiac troponin T
<b>CVD</b>	Cardiovascular disease
<b>CYP</b>	Cytochromes P450 enzyme superfamily
<b>DAG</b>	Diglyceride
<b>DCA</b>	Dichloroacetate
<b>DHPR</b>	Dihydropyridine receptor
<b>+dP/dTmax</b>	Maximum ventricular pressure increase/rise
<b>-dP/dTmax</b>	Maximum ventricular pressure decrease/drop
<b>EC</b>	Cardiac excitation coupling
<b>ECG</b>	Electrocardiogram
<b>EET</b>	Epoxyeicosatrienoic acid
<b>ELISA</b>	Enzyme-linked immunosorbent assay
<b>eNOS</b>	Endothelial nitric oxide synthetase

<b>ER</b>	Endoplasmic Reticulum
<b>ERK</b>	Extracellular signal-regulated kinase
<b>ETC</b>	Electron transport chain
<b>FA</b>	Fatty acid
<b>FACS</b>	Long chain fatty acyl-CoA synthetase
<b>FATP</b>	Long chain fatty acid transport protein
<b>FFA</b>	Free-fatty acid
<b>FAO</b>	Fatty acid oxidation
<b>FI</b>	Frailty index
<b>GAPDH</b>	Glyceraldehyde 3-phosphate dehydrogenase
<b>GLUT4</b>	Glucose transporter type 4
<b>GRK2</b>	G-protein coupled receptor kinase 2
<b>Gq <math>\alpha/\beta/\gamma</math></b>	G alpha/beta/gamma protein complex
<b>H<sup>+</sup></b>	Hydrogen
<b>HDAC</b>	Histone deacetylase
<b>HETE</b>	Hydroxyeicosatetraenoic acid
<b>HFD</b>	High-fat diet OR high-fat diet models
<b>HR</b>	Heart rate
<b>HRP</b>	Horseradish peroxidase
<b>ICa</b>	L-type calcium current
<b>IMM</b>	Inner mitochondrial membrane
<b>ISO</b>	Isoprenaline
<b>K<sup>+</sup></b>	Potassium
<b>KACH</b>	Potassium Channel
<b>KGDC</b>	Ketoglutarate dehydrogenase complex
<b>KHB</b>	Krebs-Henseleit buffer
<b>L95%</b>	Percentage of the original maximum muscle length
<b>LSD</b>	Least significant difference
<b>LVDP</b>	Left ventricular developed pressure
<b>LPL</b>	Lipoprotein lipase
<b>LysoPC</b>	Lysophosphatidylcholine
<b>MAPK</b>	Mitogen-activated protein kinase
<b>MCD</b>	Malonyl-CoA decarboxylase
<b>mRNA</b>	Messenger RNA
<b>MPD</b>	Maximum ventricular pressure decrease/drop
<b>MPR</b>	Maximum ventricular pressure increase/rise
<b>MPVD</b>	Maximum ventricular pressure decrease/drop
<b>MPVR</b>	Maximum ventricular pressure increase/rise
<b>mtDNA</b>	Mitochondrial DNA
<b>MVO2</b>	Myocardial volume oxygen
<b>Na<sup>+</sup></b>	Sodium
<b>NA-HX</b>	Sodium-Hydrogen exchanger
<b>NADH</b>	Nicotinamide adenine dinucleotide + hydrogen
<b>NCX/Na-CaX</b>	Sodium-calcium exchanger
<b>NO</b>	Nitric oxide
<b>Ob/ob</b>	Obese mutant mouse model

<b>OMM</b>	Outer mitochondrial membrane
<b>PC</b>	Pyruvate carboxylase
<b>PCG</b>	Phonocardiogram
<b>PCr</b>	Pyruvate carrier
<b>PDC or PDHc</b>	Pyruvate dehydrogenase complex
<b>PDEIII</b>	Phosphodiesterase 3
<b>PDH</b>	Pyruvate dehydrogenase
<b>PDK</b>	Pyruvate dehydrogenase kinase
<b>PDP</b>	Pyruvate dehydrogenase phosphatase
<b>PDP2</b>	Pyruvate dehydrogenase phosphatase catalytic subunit 2
<b>PGH2</b>	Prostaglandin H2
<b>PI3K</b>	Phosphoinositide 3-kinase
<b>PK</b>	Pharmacokinetics
<b>PKA/C</b>	Protein kinase A/C
<b>PLD</b>	Phospholipase D
<b>PLN/PLB</b>	Phospholamban
<b>PMCA</b>	Plasma membrane Ca <sup>2+</sup> ATPase
<b>PP1</b>	Protein phosphatase 1
<b>PPAR <math>\alpha/\gamma/\delta</math></b>	Peroxisome proliferator-activated receptor alpha/gamma/delta
<b>pPDH</b>	Phosphorylated pyruvate dehydrogenase E1-alpha subunit (S293)
<b>PVDF</b>	Polyvinylidene fluoride
<b>RAAS</b>	Renin angiotensin aldosterone system
<b>Rgl</b>	Protein Phosphatase 1 Subunit GL
<b>ROS</b>	Reactive oxygen species
<b>RPP</b>	Rate pressure product
<b>RT-PCR</b>	Reverse transcription polymerase chain reaction
<b>RyR2</b>	Ryanodine receptor
<b>SA</b>	Sinoatrial node
<b>SEM</b>	Standard error of the mean
<b>SERCA</b>	Sarco/endoplasmic reticulum Ca <sup>2+</sup> ATPase
<b>SIRT1</b>	Sirtuin 1
<b>SR</b>	Sarcoplasmic reticulum
<b>SV</b>	Stroke Volume
<b>TAG or TG</b>	Triglyceride
<b>TBST</b>	Tris-buffered saline with tween 20
<b>TCA</b>	Tricarboxylic acid cycle
<b>TMP</b>	Transmembrane potential
<b>TNF<math>\alpha</math></b>	Tumour-necrosis factor alpha
<b>TSA</b>	Trichostatin A
<b>TxA2</b>	Thromboxane A2
<b>UCP 1/2/3</b>	Uncoupling protein 1/2/3
<b>uORF</b>	Upstream open reading frame
<b>UPR</b>	Unfolded protein response
<b>VEGF</b>	Vascular endothelial growth factor
<b>VLDL</b>	Very low-density lipoprotein
<b>WAT</b>	White adipose tissue

# Chapter One: Introduction

## 1.1 General overview

The investigation into muscle contractility is of vital importance to understand how the heart adapts to both external and internal changes. The experimental work collected and presented in this thesis entails a novel investigation into the effects of various drug treatments on diet-induced obesity models and aging models with an aim of investigating how the contractile function of the heart changes and find the intracellular pathways associated with said changes. It was hypothesized that some of the commonly used inotropic drugs in the market have a reduced effect in obese patients. To explain these mechanisms, the introductory chapter gives a general overview on obesity and ageing and their effects on heart contractility, the drug treatments used and their potential molecular pathway changes, with an added importance to the mitochondrial pathways and proteins that were investigated. In addition, there are comparisons of different *in vitro* muscle biomechanics techniques with special emphasis on the use of the Langendorff isolated heart model and the work-loop technique for a more complete assessment of inotropic effects on both the whole organ and on the contractile function of the papillary muscle. Finally, a comparison into different mitochondrial metabolism regulators will also be done between diet induced, lean, aged and non-aged models, to further investigate potential changes in energy regulation. To the best of our knowledge, this is the first project to focus on these pathways in conjunction with the inotropic drugs used (Atenolol, Dobutamine, Isoprenaline and Itraconazole).

## 1.2 Parameters of cardiac contractility

Myocardial contractility represents the heart muscle's ability to contract due to increasingly high degrees of binding between myosin and actin filaments and it is regulated by calcium ions within the cells (Kobayashi and Solaro 2005; Kranias and Hajjar 2012; MacLennan and Kranias 2003; Rodriguez and Kranias 2005). The increase or decrease of the hearts' contractile strength is done through a variety of mechanisms, usually involving high or low calcium level mediation in the cytosol of cardiac myocytes during action potentials (Kass and Tsien 1976; Noble et al. 1991). The following list depicts the most important mechanisms to take into consideration when talking about muscle contractility:

- a) **Sympathetic activation and phospholamban phosphorylation** - Activation of the sympathetic nervous system through an increase of circulating catecholamines and sympathetic nerve stimulation leads to an increase in cyclic AMP (cAMP) level due to the action of adenylate cyclase; this process is possible due to the activation of the  $\beta$ -adrenergic receptors in the cell membrane; this then leads to the activation of several secondary messengers within the protein channels (Triposkiadis et al. 2009), among them the phosphorylation process of phospholamban (Meyer et al. 2010; Zhang et al. 2019). When not phosphorylated, phospholamban (PLN) inhibits the action of the Sarco/endoplasmic reticulum  $\text{Ca}^{2+}$  ATPase (SERCA), which affects the contraction and relaxation of the muscles (Lipskaia et al. 2010).

When phosphorylated, PLN increases the calcium levels within the muscles and enhances the rate of relaxation. It also triggers an inotropic effect as a result (MacLennan and Kranias 2003; Marks 2013; Rodriguez and Kranias 2005). Figure 1.2.1 depicts the general pathways involved in contractility.

**Figure 1.2.1 - Cardiac signalling pathways.** This image showcases the mechanisms and interactions between different signalling pathways involved in cardiac contractility, mainly via elevations in the levels of two very important cardiac intracellular messengers: cAMP and  $\text{Ca}^{2+}$  (MacLennan and Kranias 2003). The highlighted areas represent the points of interest for this project: the  $\beta$ -adrenergic receptors and the mitochondria ATP production. NCX – Sodium-calcium exchanger, DHPR – Dihydropyridine receptor, PMCA - Plasma membrane  $\text{Ca}^{2+}$  ATPase, PLN – Phospholamban, AKAP – A-kinase anchoring protein, PP1 – Protein phosphatase 1, Rgl – Protein phosphatase 1 subunit GL.

**b) L-type Calcium channels and binding of calcium by Troponin-C - L-type**

calcium channels are regulated by the adrenergic nervous system and very important in the cardiac excitation-contraction coupling of the heart, or EC (explained in detail in section 1.2.1). This coupling causes an increase in the intracellular sodium ions of the cells (see figure 1.2.2), which causes the opening of the L-type channels; this in turn leads to the movement of  $\text{Ca}^{2+}$  in and out of the sarcoplasmic reticulum (SR) via the ryanodine receptors (RyR2), which triggers a steep increase in the intracellular  $\text{Ca}^{2+}$  concentration up to the required level (between 100nM and 1 $\mu$ M) for optimal Troponin-C binding (Bodi et al. 2005; Yamakage and Namiki 2002). In cardiac muscle, Troponin C binds to cardiac troponin T (cTnT) and anchors itself to Troponin I and T, which then regulates diastolic and systolic heart function.

Some materials have been removed from this thesis due to Third Party Copyright. Pages where material has been removed are clearly marked in the electronic version. The unabridged version of the thesis can be viewed at the Lanchester Library, Coventry University

**Figure 1.2.2 – Calcium influx in cardiomyocytes.** The image represents the  $\text{Ca}^{2+}$  regulation within the cardiac myocyte; this is of particular importance, as it is one of the main processes behind the initiation of cardiac contraction and changes to this process can lead to significant contractile dysfunction (Wang, K. et al. 2018). Na-CaX – Sodium-calcium exchanger, Na-HX – Sodium-Hydrogen exchanger, Ica – L-type calcium current, PLB – Phospholamban.

These processes can be exacerbated or impaired by heart disease and drug effects.

(Davis and Tikunova 2008; van Eerd and Takahashi 1975). It is also important to mention that oxidative stress can play a major role in the impairment of calcium handling due to its effect on reducing  $\text{Ca}^{2+}$  activity via changes in the SERCA protein expression (Balderas-Villalobos et al. 2013; Steinberg 2013).

- c) **Cardiac output** – The cardiac output of the heart is defined as the blood pumped per minute; in other words, it is defined as the work being done by ventricles of the heart (Hamilton 1953; Vincent 2008). It has four very important determinants: heart rate, contractility, preload and afterload (see figure 1.2.3). Both the preload and afterload of the heart are calculated based on the Law of LaPlace (Basford 2002). The preload of the heart is defined as the initial cardiomyocyte stretch prior to contraction and represents the factors that are involved in the ventricular stress and the end of diastole (Norton 2001). On the other hand, the afterload represents the factors involved in the myocardial stress during systolic ejection (Norton 2001).

Effects that cause a change in ventricular output and require an increased pressure during systole will therefore always influence afterload (Norton 2001). An increase in afterload is directly correlated with a decreased cardiac output (Naito et al. 1996; Ratshin, Rackley and Russell Jr 1974).

Some materials have been removed from this thesis due to Third Party Copyright. Pages where material has been removed are clearly marked in the electronic version. The unabridged version of the thesis can be viewed at the Lanchester Library, Coventry University

**Figure 1.2.3 - Cardiac output calculations.** Diagram representing the major influencing factors of heart rate (HR) and stroke volume (SV) on cardiac output (Betts et al. 2014).

As seen above, a variety of mechanisms must be considered when talking about and studying contractility. In the next few sections, we will go through an in-depth explanation of what happens during the contraction of the heart muscles.

### 1.2.1 Cardiac excitation-contraction coupling and action potential

Cardiomyocytes comprise approximately 80% of the total ventricular mass and are usually measured at 60-140 $\mu$ M (Wiener et al. 2012; Woodcock and Matkovich 2005). It is within these cells that the process of contraction is initiated, and it is divided into four phases: Phase 4, Phase 0, Phase 1, Phase 2 and Phase 3 (see figure 1.2.1.1).

Phase 4 is the resting potential, in which the Na<sup>+</sup> and Ca<sup>2+</sup> channels are closed and the transmembrane potential (TMP) is at -90 mV (Antzelevitch 2005; Nerbonne and Kass 2005).

Phase 0 is the depolarization phase in which the Na<sup>+</sup> channels open and sodium leaks into the cells. The L-type Ca<sup>2+</sup> channels also open during this phase, once the TMP is greater than -40 mV (Antzelevitch 2005; Nerbonne and Kass 2005); the normal threshold potential for phase 0 in cardiomyocytes is -70 mV, although 0 mV is reached for a short period of time known as overshoot (Eisner et al. 2017; Santana, Cheng and Lederer 2010; Vornanen 1996). Phase 1, also known as the early repolarization phase, is the phase at which the TMP hits positive numbers and the K<sup>+</sup> channels start to slowly open (Vornanen 1996); Phase 2 is called the plateau phase, when the mV value is just below 0, and it is the phase in which the K<sup>+</sup> channels leak against the concentration gradient to the outside of the cell and the L-type calcium channels open fully to allow Ca<sup>2+</sup> ions to move into the cell and bind to the RyR to increase intracellular Ca levels, which increases overall muscle contraction (Santana, Cheng and Lederer 2010; Vornanen 1996). Finally, phase 3 is the repolarization phase, where the Ca<sup>2+</sup> channels are inhibited and the circulating K<sup>+</sup> brings the TMP down to -90 mV; the ionic gradient is also restored by the passage of Na<sup>+</sup> and Ca<sup>2+</sup> ions from an intracellular to an extracellular environment via a variety of pumps such as the NCX, the Ca<sup>2+</sup> ATPase and the Na<sup>+</sup>-K<sup>+</sup> ATPase (Eisner et al. 2017; Feridooni, Dibb and Howlett 2015; Santana, Cheng and Lederer 2010).

Figure 1.2.1.1 displays a diagram with the different ventricular action potential phases and a comparison between a human and a rodent cycle (Capasso et al. 1986; Luo and Rudy 1991; Nerbonne and Kass 2005; Watanabe et al. 1983). Contrary to the human heart, the rodent heart does not have a plateau in phase 2 due to rapidly increasing  $K^+$  outward currents (Nerbonne and Kass 2005). A very low plateau can be observed during repolarization, after the extrusion of  $Ca^{2+}$  from the cellular cytosol and the current generated by the  $Na^+/Ca^{2+}$ .

Some materials have been removed from this thesis due to Third Party Copyright. Pages where material has been removed are clearly marked in the electronic version. The unabridged version of the thesis can be viewed at the Lanchester Library, Coventry University

**Figure 1.2.1.1 – Action potential of cardiac muscles in humans (left) and rodents (right).** The cardiac action potential is generated as a result of changes in voltage due to ion movements within the cells and it starts within a group of cells with automatic action potential generation capabilities known as the sinoatrial node; the action potential then passes along the cells and initiates the contraction process, as explained above. As we can see by the figure, rodent models lack a plateau during phase 2 because of a faster repolarization as a consequence of a higher base heart rate when compared to humans (Nerbonne and Kass 2005).

The combination of the mechanisms outlined in sections 1.2 and 1.2.1 trigger what is known as the inotropic state of the heart; this state is described as the necessary conditions to modify muscle contractile strength, more specifically the myocardium (Hasenfuss, Gerd and Teerlink 2011). The heart possesses three main endogenous inotropic mechanisms: a length-dependant cross-bridge activation, a heart rate dependant activation of contractile force and a catecholamine-mediated inotropy (Bers 2008). The most important of the three is the length-dependant activation, which occurs without an increase in intracellular calcium and is a result of the Frank-Starling mechanism (Holubarsch et al. 1996).

The Frank Sterling mechanism is based on the principle that the stroke volume of the left ventricular increases as a response to the end diastolic volume (Jacob, Dierberger and Kissling 1992); as the ventricles get filled the cardiac muscle fibres are stretched, with a consequential contraction force increase. This mechanism allows for cardiac output to be maintained without external regulation and it is vital in maintaining ventricular output and is based on the principle that the stroke volume of the left ventricle increases due to an increase in the total left ventricular volume as a result of myocyte stretching (Ochsner et al. 2017). The heart rate dependant activation is calcium dependant, as an increase in heart rate implicates an increase in calcium levels and overall availability within the cardiomyocytes, which leads to an increase in contractility. The catecholamine-mediated inotropy is based on the usage of the  $\beta$ -adrenoceptor-adenylyl cyclase system to phosphorylate L-type calcium channels, via protein kinase A, in order to increase calcium influx and RyRs; phospholamban is also activated in order to accelerate calcium accumulation within the sarcoplasmic reticulum (Farrell and Howlett 2008; Grossman and Messerli 1998; Vallet, Dupuis and Chopin 1991).

### **1.3 Contractility measurements and muscle mechanics**

There are a few different methods to measure the contractility of the heart, according to the parameters of section 1.2. This section will review the ones used for this project.

### **1.3.1 The heart machinery: pressure-volume relationship**

To understand the techniques used in this project, it is important to first understand the cardiac pressure-volume relationship cycle. It represents a means to characterize left ventricular performance (Green et al. 2011). This cardiac cycle is a sequence of events that repeats with each heartbeat and it includes both the relaxation and the contraction phases of a single heartbeat (Krug et al. 2013). The points of maximal volume and minimal pressure are directly linked to the mitral valve opening and closure, explained further down (Green et al. 2011).

Pictured in figure 1.3.1.1 is a Wiggers diagram, with the different components of cardiac physiology (Krug et al. 2013; Lee and Smith 2012). The first and fourth stages represent the ventricular diastole, which begins with the relaxation and closing of the ventricular chambers (Mitchell and Wang 2014); this phase is often called isovolumetric relaxation phase. After that, the mitral and tricuspid valve open and blood rapidly rushes in from the atria and fills the chambers; this is known as the isovolumic contraction, where the volume remains but the pressure rises (Mitchell and Wang 2014). Final ejection occurs when the pressure in the ventricles is higher than the pressure in the aorta (Krug et al. 2013).

Diastolic and systolic function are two very important phases in the cardiac cycle and heavily linked to the contractility of the heart. The diastolic phase is composed of the isovolumic relaxation and ventricular filling (as mentioned above) and it is done via intracellular calcium uptake; relaxation of the left ventricle can be impaired by energy metabolism changes and this can have a severe influence on cardiac flow dynamics; as a result of this, cardiac output is severely reduced due to a reduction in the necessary energy to maintain it (García et al. 2006).

Diastolic pressure refers to the filling of the heart with blood in-between contractions. Systolic function refers to the cardiac cycle responsible for the contraction of the heart muscles after the diastolic phase finishes and is a commonly used left ventricular ejection fraction quantifier; in addition to this, systolic function is directly linked to an increase in intracellular calcium, which in turn uses ATP to generate mechanical force in the form of muscle contractions (Bers 2008; García et al. 2006).

Some materials have been removed from this thesis due to Third Party Copyright. Pages where material has been removed are clearly marked in the electronic version. The unabridged version of the thesis can be viewed at the Lanchester Library, Coventry University

**Figure 1.3.1.1 – Wiggers Diagram.** Different events of the cardiac cycle in the left ventricle (Krug et al. 2013). This cycle is crucial for cardiac physiology and clearly illustrates what occurs within a single contraction and relaxation loop, including the changes in aortic pressure, left ventricular pressure, left atrial pressure and left ventricular volume. These parameters are then analysed in relation to both an electrocardiogram (ECG) and a phonocardiogram (PCG).

### **1.3.2 The Langendorff Heart model as a measure for contractility**

The origin of isolated perfused heart preparations can be traced from the work of Carl Ludwig in the late 19<sup>th</sup> century (Bell, Mocanu and Yellon 2011; Zimmer 1999), to the frog heart isolations by Elias Cyon in 1866 (Zimmer 1998) and finally to the mammalian heart perfusion developed by Oskar Langendorff in 1895 (Sutherland and Hearse 2000).

It starts with the perfusion of the heart, with perfusion buffer (see figure 1.3.2.1), by means of cannulating the aorta, in a retrograde fashion, forcing the closing of the aortic valve as a result of a change in pressure. The buffer then passes through a vascular bed before being drawn to the coronary sinus in the right atria. This allows the preparation to be maintained without any fluid filling the ventricular chambers (Skrzypiec-Spring et al. 2007).

The advantages of this technique lie in the fact that it is quite simple and cheap to reproduce and allows for whole organ studies in an isolated system, which is beneficial for physiological and pharmacological research without the triggering of other responses and compensatory mechanisms. This is useful in contractile studies, as it allows us to measure the left ventricular pressure and, from that, calculate the total myocardial workload of the heart, by multiplying this pressure by the heart rate; simply put, it gives us the measurements to analyse the amount of stress that the myocardium is subjected to per heart rate cycle. This is incredibly useful, as it allows for the recording of parameters that indicate how different stressors (obesity, age and pharmacological compounds for this project) cause changes in the heart. The main limitation of the technique is that it is much less clinically relevant since it does not take the compensatory mechanisms of a whole organism into account (Bell, Mocanu and Yellon 2011). A detailed methodology used for this project will be presented in section 2.2.

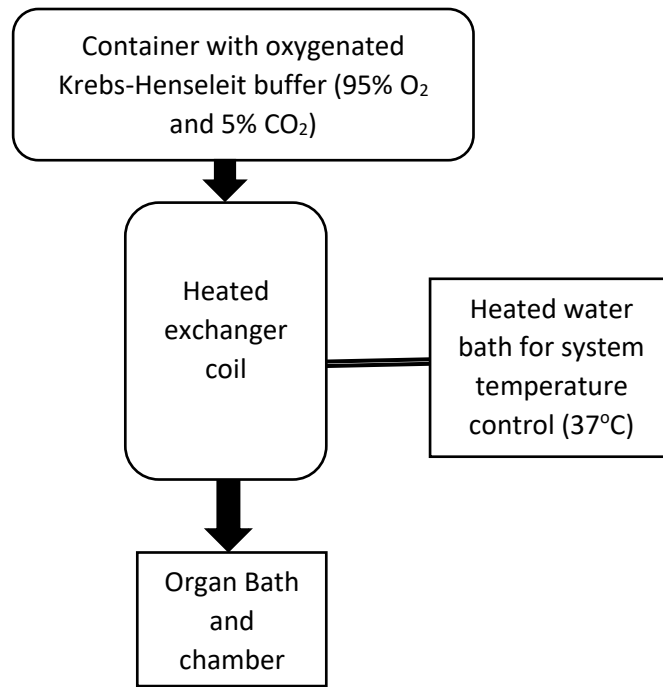


**Figure 1.3.2.1 – Isolated heart apparatus.** Simplified schematic of the constant pressure Langendorff heart perfusion system used for this project.

### 1.3.3 The Work-loop technique and isometric contractions

The papillary muscle of the left ventricle is a proven method to investigate ventricular contractile changes in the heart (Haycraft and Paterson 1896; Marzilli et al. 1980). Based on previous studies, it is therefore known that the work-loop is a reliable tool to study changes in muscle performance (Layland, Young and Altringham 1995; Layland, J. and Kentish 2000). To add to this, previous studies have also shown how not only is it possible to carry out age studies on it (Kiriiazis and Gibbs 2000), but compound effects on the muscle capacity to generate instantaneous power as well (Gharanei et al. 2014). The advantage of the work-loop technique is that it allows the study of a cyclical muscle length change, during both contraction and relaxation, in order to measure the total net-work and power output being generated by the muscle.

Applying this to the models used for this project (aged and High-fat diet-induced obesity) allows us to see how power generated is affected by physiological factors. As previously stated, the mitral valve plays quite an important role in cardiac contraction and the papillary muscle is a vital component of the mitral valve complex, due to its role in the lengthening and shortening of the valve (Marzilli, Sabbah and Stein 1980; Marzilli et al. 1980; Voci et al. 1995). This muscle is located on the left ventricle is one of the last portions of the heart to be perfused with coronary arterial blood and, because of this, is one of the most sensitive anatomic markers available in the heart. Dysfunction can occur in these muscles, usually because of acute myocardial infarction (Voci et al. 1995). As seen in figure 1.3.3.1, the positioning of the papillary muscle is between the mitral valve and the walls of the ventricular chamber (Gharanei et al. 2014b; Marzilli et al. 1980).

It is important to notice that although the muscles are generally the same thickness as the wall of the sputum, differences in size can be observed between them, with larger muscles being preferred for use with the work-loop assay. The work-loop assay uses the papillary muscle as an in-vitro method to assess force changes during contraction (Roberts, W. and Cohen 1972). The method previously used has been reviewed and tested with great success (Gharanei et al. 2014b). However, slight modifications were made to the method used for the study presented here (please refer to section 2.3 for a detailed review of these changes).

Some materials have been removed from this thesis due to Third Party Copyright. Pages where material has been removed are clearly marked in the electronic version. The unabridged version of the thesis can be viewed at the Lanchester Library, Coventry University

**Figure 1.3.3.1 – Cardiac papillary muscle.**  
Subvalvular apparatus of the mitral valve and how the papillary muscle plays a role in its opening and closing (Cooley 2010).

The next four sub-sections will now be comprised of reviews on the effects of aging and obesity on the heart and cardiovascular disease, on mitochondrial regulation in the heart and on the previous literature that mentions the inotropic drugs used for this project.

#### **1.4 The old heart**

As the average lifespan of humans increases, there is a growing need to understand how to maintain a high quality of life for the elder population (Ben-Haim et al. 2017; Crimmins 2015). The current population demographic worldwide is changing, with projected numbers of the elderly population being doubled compared to the number of children between 2010 and 2040 (Heidenreich et al. 2011). As ageing is inevitable, so are the risks and costs associated with it (Fleg, Aronow and Frishman 2011). It is known that there are genetic pathways involved in the regulation of age in organisms, but further research is still required when it comes to the exact mechanisms behind this (Bitto et al. 2015; Guarente and Kenyon 2000; North and Sinclair 2012). Aging is a very important factor when it comes to muscle effects and it can range from decreased muscle fibre size to loss of type 2 fibres within the muscle, among others (figure 1.4.1), but all causes lead to muscle strength loss (Wilson, D. et al. 2017). The mechanisms behind the effects of ageing in the cardiac muscle will be further explored in sub-sections 1.4.1 and 1.4.2.

Some materials have been removed from this thesis due to Third Party Copyright. Pages where material has been removed are clearly marked in the electronic version. The unabridged version of the thesis can be viewed at the Lanchester Library, Coventry University

**Figure 1.4.1 – The old heart.** Age related structural changes within the muscles of the body (Wilson, D. et al. 2017).

Amongst the main complications of age, cardiovascular diseases are the more relevant and the more heavily studied ones, partially due to their cost in most developed countries (Camici et al. 2015; Kovacic et al. 2011; Kuller et al. 2016; Newman et al. 2008). Statistics collected by the British Heart Foundation show that over half of the population within the UK is at risk or dying of a variety of cardiovascular diseases (CVDs), ranging from myocardial infarcts to atrial fibrillation, as seen in figure 1.4.2 (Biernacka and Frangogiannis 2011; Hacker et al. 2006; Heller and Whitehorn 1972; Nair and Nair 2001). It is very costly to treat CVDs and over £11 billion are invested every year in healthcare due to cardiac complications (BHF 2020). Due to the high mortality numbers related to CVDs, there is a consensus for the need of an investigation to find the mechanisms behind it, especially within the aging population.

Age associated changes	Organ	Cardiovascular disease
Increased intimal thickness	Vasculature	Systolic hypertension
Arterial stiffening		Coronary artery stenosis
Increased pulse pressure		Peripheral artery stenosis
Increased pulse wave velocity		Carotid artery stenosis
Early central wave reflections		
Decreased endothelium-mediated vasodilatation		
Increased left atrial size	Atria	Atrial fibrillation
Atrial premature complexes		
Decreased maximal heart rate	Sinus node	Sinus node dysfunction, sick sinus syndrome
Decreased heart rate variability		
Increased conduction time	Atrioventricular node	Second, third-degree block
Sclerosis, calcification	Valves	Stenosis, regurgitation
Increased left ventricular wall tension	Ventricles	Left ventricular hypertrophy
Prolonged myocardial contraction		
Prolonged early diastolic filling rate		Heart failure (with or without systolic dysfunction)
Decreased maximal cardiac output		
Right bundle branch block		
Ventricular premature complexes		Ventricular tachycardia, fibrillation

**Figure 1.4.2 – Risk factors of cardiovascular disease.** Major age-associated dysfunctions associated with cardiovascular disease in the aging population (Chen, M. A. 2015).

Aging is associated with a variety of physiological processes linked to high risk factors of CVD, as previously shown and mentioned. Aged cardiac tissue alterations can be due to a variety of factors such as arterial thickening and stiffness, impaired endothelial function, limited systolic capacity, hypertrophy, damaged tissue, fibrosis, among other factors (Chen, M. A. 2015; North and Sinclair 2012; Paneni et al. 2017). Most of these risk-factors are not present in younger hearts, although exceptions exist (see figure 1.4.3).

Some materials have been removed from this thesis due to Third Party Copyright. Pages where material has been removed are clearly marked in the electronic version. The unabridged version of the thesis can be viewed at the Lanchester Library, Coventry University

**Figure 1.4.3 –Cardiac dysfunctions associated with age.** Top: Comparison between a young and an aged human heart (North and Sinclair 2012) and bottom: the pathophysiology of an aging cardiovascular system (Paneni et al. 2017). SA – Sinoatrial, AV – atrioventricular,  $MVO_2$  – Myocardial volume oxygen.

Some of the mentioned risk factors are responsible for massive structural changes in the heart, especially heart rate and left ventricular contractility, although other risk factors can play a role in this (see figure 1.4.4).

Some materials have been removed from this thesis due to Third Party Copyright. Pages where material has been removed are clearly marked in the electronic version. The unabridged version of the thesis can be viewed at the Lanchester Library, Coventry University

**Figure 1.4.4 – Risk factors and structural changes in the heart.** Overview of the main cardiovascular pathophysiology developments that occur in the heart (Kim, Park and O'Rourke 2015).

In early ages the diastolic rate declines but is quickly compensated by an increase in arterial contraction. However, in aged models, there is a decrease in sympathetic heart modulation, as well as a decrease in response to  $\beta$ -adrenergic receptor activation (Dhingra and Vasan 2012; Lakatta and Levy 2003). This is of particular importance for this project because some of the inotropes used have a direct agonistic (Dobutamine) or antagonistic (Atenolol) effect on the  $\beta$ 1-receptors of the heart and it is therefore likely that the recorded changes in heart function will be as a direct, or at least partial, result of this. Please refer to the beginning of section 1.4 for a detailed review on this effect.

As mentioned before, vascular thickening and stiffness are some of the structural effects of ageing on the heart (Guarente and Kenyon 2000; Leblanc et al. 1998; Nair and Nair 2001). These changes can lead to various effects upon the heart, such as systolic and diastolic changes, as well as arterial fibrillation (see figure 1.4.5). Alongside the previously mentioned changes, this thickening of the vascular walls can also lead to a decline in endothelial cell function, as well as a loss of proliferation and movement, partially due to a reduction in eNOS (endothelial nitric oxide synthetase) activity (Izzo Jr and Shykoff 2001).

Some materials have been removed from this thesis due to Third Party Copyright. Pages where material has been removed are clearly marked in the electronic version. The unabridged version of the thesis can be viewed at the Lanchester Library, Coventry University

**Figure 1.4.5 – Changes in cardiac pressure as a result of age.** Main structural changes in the heart and vessels measured from both old and young patients (Izzo Jr and Shykoff 2001).

At a cellular level, cardiomyocytes also suffer changes, mainly in their numbers. Age causes a decrease in heart cells due to apoptosis and necrosis linked to reactive oxygen species (ROS) production.; in addition to this, there is also cardiomyocyte senescence, which is observed at a higher rate within the elder population and has been previously suggested as a potential biomarker to assess cardiac tissue viability in aged models (North and Sinclair 2012).

### 1.4.1 Frailty in cardiovascular disease

Frailty is a biological process defined as a geriatric syndrome prevalent amongst the elder population and it is defined as a state of life decline, vulnerability to stressors and general physical weakness (Chen, M. A. 2015; Feridooni, H. A. et al. 2014; Fried et al. 2001). It has become a high-priority focus in cardiovascular research due to the increasingly complex nature of older patients and their stressors, as highlighted in figure 1.4.1.1 (Afilalo et al. 2009; Bergman et al. 2007; Shamliyan et al. 2013).

Some materials have been removed from this thesis due to Third Party Copyright. Pages where material has been removed are clearly marked in the electronic version. The unabridged version of the thesis can be viewed at the Lanchester Library, Coventry University

**Figure 1.4.1.1 - Impact factors of frailty in age.** Pathophysiology of frailty and its links to cardiovascular dysfunction (Chen, M. A. 2015).

The link between frailty and CVDs is complex but can both be traced to low grade chronic inflammation; amongst the causes of these inflammations are things such as obesity, insulin resistance and redox imbalance (Csiszar et al. 2008; Rockwood et al. 2017). Inflammation in CVDs is known to cause lipoprotein oxidation and atherosclerotic plaque activation and it is known that most patients considered “frail” have similar traits to the ones present in CVD.

Therefore, it is a natural assumption that there are common biological pathways at play that either link the two or facilitate the damage one causes to the other (Chen, M. A. 2015). Past research has identified a variety of approaches to quantify frailty known as the frailty index (FI) and is based upon behavioural and physiological assessments of patients (Feridooni, H. A. et al. 2014; Kleipool et al. 2018; Rockwood et al. 2017). Evaluations of the different biological systems within the body as well as external factors are always taken into consideration when developing an FI score; this can, however, result in some problems due to its variable parameters and aspects, which can be detrimental when looking for consistency (Feridooni, H. A. et al. 2014; Rockwood et al. 2017). Nonetheless, it has been shown to provide useful insights into pre-clinical models and there is still research ongoing in an attempt to translate these results into human trials (Feridooni, H. A. et al. 2014; Rockwood et al. 2017). This study took the FI into consideration when talking about body mass, fat pad mass and length of the animal models used, as well as a controlled diet and environment (Kane et al. 2016).

#### **1.4.2 Impact of age on cardiac contractility**

Age is a dominant factor for cardiovascular disease, with senescence playing a major role in the vascular dysfunction of aged models (Heidenreich et al. 2011; North and Sinclair 2012); it is also known that adult hearts have a progressive size increase (hypertrophy) (Barton et al. 2016; Hacker et al. 2006). Cardiac performance is, as previously mentioned in section 1.2, carried out via an interaction of various factors (Abel, Litwin and Sweeney 2008).

Age associated myocardial changes have been documented and preload has been shown to have a direct effect in decreasing the velocity and extent of muscle shortening, in an age dependant manner, mainly due to its influence on enzymatic properties of the heart (myosin B being a prime example of this); this change has not been recorded in younger rat models (Feridooni et al. 2017; Heller and Whitehorn 1972; Leblanc et al. 1998). While talking about molecular pathways, Akt and autophagy (important biological process by which there is degradation of unwanted or dysfunctional cellular components) have been linked to contractile dysfunction via unsuppressed autophagy of aged cardiomyocytes; these effects were manifested by severe hypertrophy, prolonged re-lengthening and limited intracellular  $Ca^{2+}$  release (Camici et al. 2015; Hua et al. 2011). Although still under research, preliminary data suggests a direct involvement of Akt in the deteriorating effects of aging on contractility.

Another important component of contractility,  $\beta$ -adrenoreceptors, has also been shown to have limited functionality in aged models, with a clear indication that aged hearts have reduces responsiveness to adrenergic stimulation and this has been linked to the adenosine receptor signal transduction mechanism, since limited myocardial adenosine can be partially responsible for a reduction in  $\beta$ -adrenergic responses in older models (Dobson, Fenton and Romano 1990; Nair and Nair 2001). Finally, it is important to reinforce the effect of  $Ca^{2+}$  in heart contractility (a further explanation of action potential and calcium channels in the heart can be seen in section 1.2.1) and how it changes with age. Ventricular papillary muscles have been used to show a change in shortening velocity when immersing the muscle in a water bath containing  $Ca^{2+}$  via alterations in biomechanical parameters and a reduction in the velocity-load relation, alongside a dysfunction in contractile protein activity (Nair and Nair 2001).

Discrepancies were observed but there was a clear significant difference when comparing the between the 5, 10, 15 and 20-month year old rat models (Capasso et al. 1986; Nair and Nair 2001). A more recent study looked at the exact impact of age and frailty on the ventricular structure of older mice models and used a Langendorff heart study as well as cardiac myocyte isolations and western blotting, making it very relevant for the work being presented for this project (Feridooni et al. 2017). Feridooni et al recorded an age-dependant decline in the left ventricular developed pressure (LVDP), with a clear slowdown in heart contractions, as measured via the maximum ventricular pressure rise and drop (+dP/dTmax and -dP/dTmax, respectively); in the study, this was attributed mainly to L-type Ca<sup>2+</sup> channel changes, but the exact mechanism was not explored; due to the important role of the mitochondria in Ca<sup>2+</sup> channel regulation, it is possible that there is an involvement of energy regulatory agents and that they might be the cause of the dysfunction (Nagatsu 2006).

The myocytes in aged models have been shown to have not only a decrease in peak Ca<sup>2+</sup> currents, which causes changes in contractions, but also changes to the L-type Ca<sup>2+</sup> channels, which were shown to be directly influenced by the age of the animals (Albarwani et al. 2016). This study also validated the previously documented presence of cardiac hypertrophy in aged models (Feridooni, Dibb and Howlett 2015; Keller and Howlett 2016). Calcium channel voltage-dependent L type alpha 1C subunit, a known subunit of the L-type Calcium channels was also measured and was found to have its expression lowered when comparing between the aged and the young mice models, which supports the previously observed claim that there is a direct involvement of the L-type channels and the reduction of cardiac contractility (Feridooni, Dibb and Howlett 2015). The next section will be a review on the cardiac remodelling observed in obesity and how it affects heart contractility.

## 1.5 Obesity and the heart

Obesity is a disorder in which there is an imbalance in the homeostasis of a living organism; it is also a growing pandemic, with the numbers posing a high worldwide public health threat, as over 39% of adults aged 18 and over are obese (WHO 2020), and a costly global investment, with obesity-related illness costing over \$2 trillion annually, or 2.8% of the global GDP (Gregg and Shaw 2017; Tremmel et al. 2017). In the UK, one in every four adults is diagnosed with obesity, while half of the world population is estimated to be either overweight or obese (Baker 2018; Waumsley et al. 2011). The cost to maintain effective treatments against obesity are enormous due to the associated health risks such as cardiovascular diseases, type 2 diabetes, obstructive sleep apnoea and certain types of cancer, among others (Haslam 2007; Waumsley et al. 2011). The term “obesity” stems from the Latin ob-esum, which means “on account of having been eaten” and it is defined as excess of body fat accumulated on the body, leading to negative effects on health (Haslam 2007). The most common method to determine obesity levels is the body mass index (BMI), which is obtained by dividing weight by the square of a person’s height (see figure 1.5.1). The waist-hip ratio can also be used as a viable method to confirm obesity, when supported by the BMI. (Ho-Pham et al. 2015; Lean 2000).

$$\text{BMI} = \frac{\text{Weight (kilograms)}}{\text{Height (meters)}^2}$$

**Figure 1.5.1 – BMI formula.** General formula commonly used worldwide to calculate the BMI of patients.

As mentioned before, obesity is one of the leading preventable causes of death, alongside hypertension, smoking and sexually transmitted diseases (Barness, Opitz and Gilbert-Barness 2007). Causes for obesity include excessive food energy intake and a sedentary lifestyle, although genetics and other medical reasons have been reported to play a role in a pre-disposition to overweight and obesity (Baker 2018; Selthofer-Relatić, Bošnjak and Kibel 2016).

### **1.5.1 Pathophysiology of obesity**

Adipocytes are cells that exist primarily in the adipose tissue and play a major role in the storage of energy as fat (Birbrair et al. 2013). There are three functionally different types of adipose tissue described in mammals: bone marrow adipose tissue (BMAT), white adipose tissue (WAT) and brown adipose tissue (BAT); brown and white adipose tissue are fundamentally different when it comes to their anatomical location, morphology, function and regulation (Coelho, Oliveira and Fernandes 2013) White fat cells, also known as monovacuolar cells, are the primary site for storage of energy as lipids within organisms, while brown fat cells, also known as plurivacuolar cells, are so named due to its characteristic colour, originated from its vascularization and large mitochondrial numbers (Elsen, Raschke and Eckel 2014; Moisan et al. 2015). Although both tissues store energy in the form of triglycerides, the release of this energy is done in different ways (figure 1.5.1.1); white adipose cells store and release this energy to comply with the organisms needs while brown adipose cells convert it to heat and plays a major role in thermogenesis regulation (Hildebrand, Stümer and Pfeifer 2018; Rosell et al. 2014). An important note here that the developmental process of adipose tissue has been previously shown to be species-dependant (Redinger 2007).

Some materials have been removed from this thesis due to Third Party Copyright. Pages where material has been removed are clearly marked in the electronic version. The unabridged version of the thesis can be viewed at the Lanchester Library, Coventry University

**Figure 1.5.1.1 – Different types of adipose tissue.** Main characteristics of white (WAT) and brown (BAT) adipose tissues and their response to HFD (Hildebrand, Stümer and Pfeifer 2018).

The impact of obesity on the body (see figure 1.5.1.2) has been heavily investigated and has been found to be at the centre of the development of a wide array of cardiovascular complications, ranging from cardiac failure to coronary artery disease, as well as hypertension (Avelar et al. 2007; Carbone et al. 2020; Park et al. 2011). It is noteworthy to mention that obesity is characterized by an uncontrolled expansion of fat mass via adipocyte hypertrophy and hyperplasia, with an accompanying increase in metabolism regulators (e.g., glycerol, hormones and pro-inflammatory cytokines) which lead to the mentioned negative cardiac effects (Kahn, S. E., Hull and Utzschneider 2006).

Some materials have been removed from this thesis due to Third Party Copyright. Pages where material has been removed are clearly marked in the electronic version. The unabridged version of the thesis can be viewed at the Lanchester Library, Coventry University

**Figure 1.5.1.2 - Pathophysiology of obesity cardiomyopathy.** This diagram showcases the haemodynamic alterations that come from adipose deposits in the body (Alpert et al. 2018).

## 1.5.2 Cardiac remodelling in obesity

Adipocytes have an additional function within the organism: they protect nonadipocytes, which have a limited triacylglycerol storage capacity, from excessive lipid accumulation and their entry into nonoxidative metabolic pathways (Coelho, Oliveira and Fernandes 2013).

Lipotoxicity refers to a condition in which the stored fatty acids (FA) spill over into nonadipocytes and cause cellular dysfunction and apoptosis, as seen in figure 1.5.2.1

(Drosatos 2016; Marín-Royo et al. 2019; Unger and Zhou 2001; Wende and Abel 2010).

Some materials have been removed from this thesis due to Third Party Copyright. Pages where material has been removed are clearly marked in the electronic version. The unabridged version of the thesis can be viewed at the Lanchester Library, Coventry University

**Figure 1.5.2.1 - Mechanisms leading to cardiac lipotoxicity.** This figure shows that an increased dietary fat intake leads to increased free fatty acid circulation, which leads to an increased fatty acid uptake, decreased oxidation and increased lipid intermediates in the heart. These sudden changes lead to contractile dysfunction and apoptosis, amongst other negative effects (Wende and Abel, 2010). FFA – Free fatty acids, TG – Triglycerides.

The full range of the effects of lipotoxicity is not yet fully understood, but it is known that saturated fatty acid exposure exacerbates apoptosis (Drosatos and Schulze 2013). Studies have shown that increases in stimuli associated with obesity and lipid delivery cause a protein influx within the endoplasmic reticulum (ER); the regulation of this process is usually carried out by chaperone proteins, a process known as the unfolded protein response, or UPR (Eizirik, Cardozo and Cnop 2008).

Disturbances in the UPR causes ER stress, which increases  $\beta$ -cell dysfunction and triggers apoptosis; the described chain of reactions is the suggested mechanism that links obesity and the development of diabetes (Cnop, Foufelle and Velloso 2012). The exact mechanism by which obesity leads to ER stress is not fully understood, but it is known that ER stress induces  $\text{Ca}^{2+}$  release and signalling to the mitochondria, which activates two proapoptotic proteins, BAK and BAX (Cnop, Foufelle and Velloso 2012; Scorrano et al. 2003). A wide array of studies has been carried out to decipher the molecular mechanism of lipid-induced apoptosis in  $\beta$ -cell; while some papers describe the interaction as directly linked to ceramide synthesis and insulin resistance (Turpin et al. 2006), other papers mention the involvement of reactive oxygen species (Finck et al. 2003). More work is therefore still needed to understand the depth of how obesity triggers lipotoxic events in the heart. A paper by Drosatos and Schulze discussed the molecular pathways and signalling effects of lipids in cardiac lipotoxicity and dysfunction (Drosatos and Schulze 2013). The first discussed pathway was the apoptosis pathway, a pathway that has been previously shown to be involved in AMPK activation within cardiomyocytes of high fat diet induced obesity models (HFD), as one of the main causes of apoptosis (Drosatos and Schulze 2013). Palmitic acid also plays a major role in apoptosis and has been shown to alter mitochondrial physiology and triggering cell death (Sparagna et al. 2000). To explain the second pathway, it is important to give a brief introduction to insulin and insulin resistance. Insulin is an important regulator of adipocytes due to its effect in the differentiation of pre-adipocytes into adipocytes. It is also important in the stimulation of glucose transport, triglyceride synthesis and lipolysis inhibition in mature adipocytes, as seen in figure 1.5.2.2 (Kahn, B. B. and Flier 2000). Added to this, insulin also exerts an effect on intracellular  $\text{Ca}^{2+}$  handling and can have a cardioprotective effect. All these functions are possible due to downstream regulation of the Insulin/IRS1/PI3K/Akt pathway.

Some materials have been removed from this thesis due to Third Party Copyright. Pages where material has been removed are clearly marked in the electronic version. The unabridged version of the thesis can be viewed at the Lanchester Library, Coventry University

**Figure 1.5.2.2 - Effect of insulin on adipose storage.** Insulin stimulates differentiation and inhibits lipolysis. It also breaks down triglyceride (Kahn and Flier, 2000). GLUT4 – Glucose transporter type 4, PI3K – Phosphoinositide 3-kinase, VLDL – Very low-density lipoprotein, LPL – Lipoprotein lipase.

Insulin signalling defects develop early in obesity (Park et al. 2005). They can be caused by a variety of factors, but lipid accumulation in the heart is the most common one. This leads to an extensive utilization of fatty acids for cardiac energy, as well as defective contractile response to insulin and decreased cardiovascular efficiency due to a waste of oxygen for noncontractile purposes (Mazumder et al. 2004; Young, Guthrie, Razeghi, Leighton, Abbasi, Patil, Youker and Taegtmeyer 2002). ROS also play a major role in the development of insulin resistance, as suggested by a paper that reported an observable decrease in insulin resistance following ROS attenuation in obese rat models (Kim et al. 2000). Protein kinase C (PKC) activation is the third reviewed pathway associated with cardiac dysfunction and obesity (Drosatos et al. 2011). PKCs are implicated in the regulation of contractility gene expression and growth; overexpression of PKC $\beta$  has been linked to cardiomyopathy associated with myocardial necrosis, impaired Ca<sup>2+</sup> handling and thickened ventricular walls (Wakasaki et al. 1997). A follow-up study showed that high-fat diet rat models had increased PKC $\beta$  and developed cardiac hypertrophy (Jalili, Manning and Kim 2003).

PKC isoforms have been linked to a variety of heart conditions. PKC $\alpha$  and PKC $\epsilon$  have both been shown to affect the contractility of the heart due to their negative inotropic effect in cardiomyocytes (Belin et al. 2007; Narayan et al. 1998). Finally, the PKC pathway has also been associated with compromised  $\beta$ -adrenergic receptor responsiveness in lipotoxic animal models (Drosatos et al. 2011).

When talking about the concept of cardiac remodelling, it is commonly defined as any changes in size, shape or structure within the heart, normally associated with the left ventricle (Abel, Litwin and Sweeney 2008; Aurigemma, de Simone and Fitzgibbons 2013). In this regard, hypertension with left ventricular hypertrophy is one, if not the major, factor in cardiovascular related mortality, especially in the aged and aging population, as the co-existence of both conditions has been shown to be associated with an increase in metabolic and mitochondrial heart dysfunction (the latter will be further clarified in section 1.5) and it is hypothesized that HFD can accelerate cardiac remodelling and ventricular dysfunction (Katholi and Couri 2011; Shiou et al. 2018; Wang, X. et al. 2015). Recent studies have shown the effects of a high-fat diet on the ventricular remodelling in aged rats (Drosatos 2016; Shiou et al. 2018; Taylor 2014). In the aforementioned studies, researchers used HFD models and concluded that the high fat diet was causing significant hypertrophy in their 44-week-old animals, as well as an overexpression of PPAR $\alpha$  (explained in-depth in section 1.5.1, with a brief mention in figure 1.5.2.3), which has been previously linked to contractile dysfunctions (Luptak, Balschi et al. 2005; Shiou et al. 2018; Young, M. et al. 2001). The study concluded that the dietary fat was inducing cardiac changes, including lipotoxicity. It is therefore likely that HFD models can and should be linked to lipotoxicity, and that this should be taken into consideration when researching different obesity models.

Some materials have been removed from this thesis due to Third Party Copyright. Pages where material has been removed are clearly marked in the electronic version. The unabridged version of the thesis can be viewed at the Lanchester Library, Coventry University

**Figure 1.5.2.3 – Effects of HFD on cardiac gene expression.** Notable changes include  $\alpha$ -MHC, TNF-  $\alpha$  and left atrial dimensions (Shiou et al. 2018).  $\alpha$ -MHC - Alpha Myosin heavy chain, PPAR $\alpha$  – Peroxisome proliferator receptor alpha, TNF $\alpha$  – Tumour necrosis factor alpha, ANP – Atrial natriuretic peptide.

All the previously mentioned pathways and mechanisms are important when talking about the heart and how obesity can influence its structure and function (see figure 1.5.2.4). They are also relevant from a pharmacologic angle due to the impact that they have not only while under the influence of a disease like obesity, but also while under the influence of commonly used drugs to treat heart conditions. It is necessary to understand, in-depth, the mechanism behind these pathways in order to understand the exact interactions that occur when obese patients are subjected to treatment with inotropic drugs that exacerbate their condition or cause cardiac complications.

Some materials have been removed from this thesis due to Third Party Copyright. Pages where material has been removed are clearly marked in the electronic version. The unabridged version of the thesis can be viewed at the Lanchester Library, Coventry University

**Figure 1.5.2.4 – Mechanisms involved in cardiac dysfunction as a result of obesity.** Factors involved in structural and functional cardiac changes in obesity include both metabolic and haemodynamic changes such as lipotoxicity and hypertension (Abel, E., Litwin and Sweeney 2008).

For this project, the focus was mainly on the potential changes in the mitochondrial processes within the heart; more specifically on targets potentially involved in the contractile function of the heart. The following section will go into detail regarding the specific targets that were chosen for this thesis.

## 1.6 Cardiovascular mitochondrial regulation

In cardiomyocytes, mitochondria occupy between 30 to 50% of the total cell volume (Wang, K. et al. 2018). Mitochondria are known as the core of the cellular energy metabolism and the main source of adenosine triphosphate (ATP), which is used to fuel a variety of different cell functions (Taegtmeyer et al. 2005; Wang, K. et al. 2018). These functions include force generation (like the ones generated during a muscle contraction), the folding and degradation of proteins, and the generation and maintenance of different membrane potentials (Kühlbrandt 2015). As mentioned before, the contractility of the heart is very important and mechanical dysfunctions of the myocardium lead to various complications (Ross Jr and Sobel 1972). It is therefore important to keep the contractility of the heart well regulated, especially when it comes to the contractile proteins such as myosin, troponin and tropomyosin (for more details, please refer to the introduction in section 1.2).

Contraction occurs when a thin muscle filament (fibrillary actin) and a thick muscle filament (myosin filament) slide along each other, translating hydrolysed ATP into mechanical force. During contraction, Troponin acts as a  $\text{Ca}^{2+}$  sensor. Alteration of local  $\text{Ca}^{2+}$  concentration changes the conformation of troponin, which in turn leads to the displacement/association of tropomyosin from/with actin filaments. It is the attachment and detachment of myosin to actin filaments that drives myocyte contraction (for a full review on heart contractility and the contraction phases, please refer to section 1.2). As mentioned before, contraction occurs at the expense of an immense energy demand that the cardiomyocytes cannot store within them. To keep up with this high demand, a cardiac metabolic coupling is in place to ensure that a constant and efficient energy production takes place, via continuous synthesis of ATP (Kolwicz Jr, Purohit and Tian 2013).

It is therefore crucial to maintain a balance in the cardiac cellular bioenergetics, via modulation of specific metabolic substrates known to influence heart contraction, such as fatty acids, glucose and pyruvate, among others (Huss and Kelly 2005; Ingwall 2008; Neubauer 2007). The peroxisome-proliferator activated receptor (PPAR) family members play a major role in the regulation and activation of these substrates, due to their role in the expression of the genes required for fatty acid uptake and oxidative phosphorylation, with both being heavily responsible for a greater percentage of ATP production within cardiomyocytes, at around 95% (Arany et al. 2005; Finck et al. 2003; Prosdocimo et al. 2015).

In the heart, the mitochondria play a vital role in cardiac energy production, with 70% of its production coming from fatty acid oxidation and the remaining 30% from carbon substrate metabolism via the pyruvate complex and lactate (Korvald, Elvenes and Myrnes 2000; Kühlbrandt 2015). Wang et al did a full profile of how cardiac metabolism works under the effect of a regular diet vs a high fat diet (Wang, X. et al. 2015). These researchers found the expected increase in PPAR under HFD conditions, but also found that there was only a severe observable mitochondrial dysfunction at the 14-month-old mark. In addition to this, Wang et al also recorded that the increase in fatty acid oxidation (FAO) was accompanied by an increase in ROS production, which in turn activated uncoupling proteins as a mechanism to potentially reduce oxidative damage, which has been established in previous literature (Boudina et al. 2007; Dong et al. 2006; Echtay et al. 2002; Kienesberger et al. 2012; Russell et al. 2004; Son et al. 2010). To this effect, age also plays a major negative role in mitochondrial activity. In younger cells, mitochondrial fusion allows for an equal distribution of mitochondria among cells during mitosis and also allows for the selective degradation of damaged ones; however, studies have shown that this process is impaired with age due to a loss of protective mechanisms (Seo et al. 2006; Seo et al. 2008).

Some studies have proposed theories as to why this happens, with the currently most accepted one being that mitochondria experience a loss of plasticity with age and that this can be, to an extent, instigated by an age-related ROS production increase and subsequent oxidative stress in the cells, as seen in figure 1.6.1 (Qiang et al. 2007; Reznick et al. 2007); this and other studies have also shown that there is a reduced capacity for biogenesis due to a decline in peroxisome proliferator-activated receptor gamma coactivator a-alpha (PGC-1 $\alpha$ ), although this has been mostly researched in skeletal muscle (Crane et al. 2010; Sandri et al. 2006). The activation of pro-apoptotic pathways has also been proposed as a link to this mitochondrial dynamic dysfunction but has mainly been studied on skeletal muscles (Elmore et al. 2001; Wohlgemuth et al. 2010). It is therefore likely that these recorded dysfunctions in mitochondrial regulation might be one of the intrinsic causes which contributes to oxidative stress and cell death during the aging process.

Some materials have been removed from this thesis due to Third Party Copyright. Pages where material has been removed are clearly marked in the electronic version. The unabridged version of the thesis can be viewed at the Lanchester Library, Coventry University

**Figure 1.6.1 – ROS effect within the cells.** Proposed mechanism of mitochondrial dysfunction in aging (Seo et al. 2010). ETC – Electron transport chain, mtDNA – Mitochondrial DNA.

Because of the mitochondrial role in energy production, any changes or disruption can cause a variety of disorders, among them cardiac contractility dysfunction (Neubauer 2007; Taegtmeyer et al. 2005). This decrease in contractility has been previously investigated and linked to the inactivation and expression change of specific elements involved in the citric acid cycle (CAC or TCA), oxidative phosphorylation, and energy (ATP) transportation, such as pyruvate, uncoupling proteins (1-5) and the PPAR family (Boudina et al. 2012; Crewe, Kinter and Szweda 2013; Finck 2007; Moreau et al. 2004; Pohl et al. 2019). There are certain conditions that cause changes in the mitochondrial function of the heart, but the mechanism behind this is not fully understood, nor is it understood how pharmacological compounds can affect these molecular pathways (see figure 1.6.1). The next few sections will review the main mitochondrial targets investigated in this study, with an emphasis on energy regulatory mechanism and agents and how they change in the presence of obesity and age.

### **1.6.1 Peroxisome proliferator-activated receptor alpha (PPAR $\alpha$ )**

PPARs are members of a hormone receptor superfamily, comprised of three major isoforms: PPAR $\alpha$ , PPAR $\gamma$  and PPAR $\delta$ . Any of these isoforms has a regulatory job in several lipid metabolism aspects of one or more systems, as seen in figure 1.6.1.1 (la Cour Poulsen, Siersbæk and Mandrup 2012; Pol, Lieu and Drosatos 2015). It has been previously noted that cardiac PPAR $\alpha$  levels are markedly reduced in the presence of certain conditions, like myocardial infarctions, heart failure and reactive oxygen species, among others (Karbowska, Kochan and Smolenski 2003; Masamura et al. 2003). As for its activity, PPAR $\alpha$  has been shown to be modulated by phosphorylation of specific serine residues, primarily via kinases such as protein kinase A (PKA), protein kinase C (PKC) and AMP-activated protein kinase (AMPK) (Burns and Heuvel 2007).

Some materials have been removed from this thesis due to Third Party Copyright. Pages where material has been removed are clearly marked in the electronic version. The unabridged version of the thesis can be viewed at the Lanchester Library, Coventry University

**Figure 1.6.1.1 – Intracellular PPAR pathways.** Metabolic regulation by PPARs in different tissues, with the proteins of interest and their respective pathways highlighted (Kersten 2014). PDK4 – Pyruvate dehydrogenase kinase 4. The remaining pathways represented in the image were not investigated for this project.

Studies have also shown how PPARs regulate gene expression in cardiomyocytes and how changes in these genes can cause either a reduction in fatty-acid oxidation with an accompanying glucose oxidation increase, which can cause cardiac dysfunctions (Haemmerle et al. 2011; Leone, Weinheimer and Kelly 1999) or an increase in oxidation rate and associated ventricular hypertrophy and systolic dysfunction (Finck et al. 2002). It is therefore possible to conclude that PPARs play a major role in regulating key genes in cardiac function, such as cardiac fatty acid oxidation and glucose inhibition.

As mentioned before, PPARs have been investigated in the path due to their importance in the heart. With PPAR $\alpha$  specifically, it has been established while using both PPAR $\alpha$ -knockout mice and transgenic mice models of cardiac specific PPAR $\alpha$  (tg-PPAR $\alpha$ ), that there is an observable decrease in fatty acid metabolism and an increase in oxidative stress (Guellich et al. 2013; Young, Guthrie, Razeghi, Leighton, Abbasi, Patil, Youker and Taegtmeier 2002), as well as an associated cardiac hypertrophy and lipotoxicity (Oka et al. 2015; Young, M. et al. 2001) and, while there is some controversy regarding the exact interaction between PPARs and to the contractility of the heart, it is clearly established that PPARs can positively or negatively impact the cardiac function due to their effect on ATP production (Campbell et al. 2002; Loichot et al. 2006; Luptak, Balschi et al. 2005). It is also important to note that these effects have been shown to be exacerbated during aging, especially in adult and senescent animal models (Iemitsu et al. 2002; Sung, B. et al. 2004). Based on these papers, it is established that PPARs play a major role in cardiac metabolism and are therefore crucial to explore how different types of stressors can affect their expression or the expression of agents directly involved with PPAR in the heart, not only in physiological models like age or obesity, but also in how these models react to the administration of inotropic medication, since these compounds can cause major changes in the heart.

## 1.6.2 Pyruvate Dehydrogenase (PDH)

Many factors are involved in mammalian myocardial metabolism ranging from hormone levels to the inotropic state of the heart, all of which have a central role to play (Sun et al. 2015). The pyruvate dehydrogenase complex (PDC) is a multienzyme complex located in the mitochondria that plays a key role in the regulation of the energy homeostasis in the heart due to its direct effect on the citric acid cycle, as it is responsible for catalysing and converting pyruvate into Acetyl-CoA, which is then used to deliver the acetyl group for further oxidation to produce ATP, as depicted in figure 1.6.2.1.

Some materials have been removed from this thesis due to Third Party Copyright. Pages where material has been removed are clearly marked in the electronic version. The unabridged version of the thesis can be viewed at the Lanchester Library, Coventry University

**Figure 1.6.2.1 – Pyruvate regulatory processes.** Mechanisms involved in PDC regulation and its relationship with different mitochondrial processes (Sun et al. 2015). Not depicted are the various enzymes that make up the PDC, such as the PDH E1 alpha subunit enzyme. PDHc – Pyruvate dehydrogenase complex, PDP – Pyruvate dehydrogenase phosphatase, DCA – Dichloroacetate.

The PDC has two forms: its active, when it is dephosphorylated and its inactive form, when it is phosphorylated (Linn, Pettit and Reed 1969). Dephosphorylation occurs either via PDP (pyruvate dehydrogenase phosphatase), which is stimulated by calcium ions (Huang et al. 1998) or via PDP2 (pyruvate dehydrogenase phosphatase catalytic subunit 2), which indirectly regulates the activation of the PDH kinase family, consisting of PDK 1-4 (Sugden and Holness 2003). Under physiological conditions, the heart utilizes fatty acid oxidation as the primary source of energy (60-90%), with glucose and lactate oxidation making up the remaining 10-40% (Sharma et al. 2005).

Furthermore, it has been demonstrated that a high-fat diet can induce increases in mRNA PDK expression, as well as a reduction in the active fraction of PDH (Crewe, Kinter and Szweda 2013; Holness et al. 2000; Rinnankoski-Tuikka et al. 2012; Wilson, C. et al. 2007). Mitochondrial decay occurs with age and to maintain a normal function, the heart is required to sustain a constant supply of different high-energy phosphates, which depends on the conversion of FA to energy (Katz 1988; Nakai et al. 1997). Interestingly, recent studies have shown that aged hearts catalyse pyruvate decarboxylation with greater efficiency when compared to younger hearts (Lloyd, Brocks and Chatham 2003; Moreau et al. 2004). This seems to be a compensatory mechanism to maintain NADH levels and indicates that there is a definite shift from FA oxidation to a more glucose-heavy energy production mechanism

(see figure 1.6.2.2).

Some materials have been removed from this thesis due to Third Party Copyright. Pages where material has been removed are clearly marked in the electronic version. The unabridged version of the thesis can be viewed at the Lanchester Library, Coventry University

**Figure 1.6.2.2 – ATP production diagram.** NADPH has been shown to be linked to age-related changes to cardiac bioenergetics, via changes to the citric acid cycle (Moreau et al. 2004). PC – Pyruvate carboxylase, PDC – Pyruvate dehydrogenase complex, PCr – Pyruvate carrier, ACC – Acetyl-CoA carboxylase, CAT – Carnitine acyl translocase, CATf – Carnitine acyl transferase, CS – Citrate synthase, CPT1 – Carnitine palmitoyl transferase 1, CPT2 – Carnitine palmitoyl transferase 2, IMM – Inner mitochondrial membrane, KGDC – Ketoglutarate dehydrogenase complex, OMM – Outer mitochondrial membrane.

### 1.6.3 Uncoupling Protein 3 (UCP3)

Uncoupling proteins (UCPs) are mitochondrial proteins involved in the regulation of proton channels and/or transporters (Nedergaard, Ricquier and Kozak 2005). Their function is to dissipate the proton gradient over the inner mitochondrial membrane to generate heat; in other words, they separate the oxidative phosphorylation from ATP synthesis with the energy being dissipated as heat (figure 1.6.3.1) – also known as mitochondrial proton leak (Nedergaard and Cannon 2003; Nedergaard, Ricquier and Kozak 2005). Both UCP2 and UCP3 have been identified as incredibly important agents in different aging and diabetes studies, with a recent focus on obesity as well (Boudina et al. 2012; Brand and Esteves 2005; Goshovska et al. 2010; Pohl et al. 2019).

Some materials have been removed from this thesis due to Third Party Copyright. Pages where material has been removed are clearly marked in the electronic version. The unabridged version of the thesis can be viewed at the Lanchester Library, Coventry University

---

**Figure 1.6.3.1 – Intracellular role of UCPs.** Uncoupling proteins and their importance as both proton and fatty acid anion transporters to the outside of the mitochondrial matrix. Once moved to the outside of the mitochondrial matrix, the fatty acid anion associates with a proton and returns to the mitochondrial matrix to release it, causing a proton leak and driving ATP generation (Lopaschuk et al. 2010). VLDL – Very low-density lipoprotein, LPL – Lipoprotein lipase, FACS – Long-chain fatty acyl-CoA synthetase, MCD – Malonyl-CoA decarboxylase, TAG – Triglycerides, ACC – Acetyl-CoA carboxylase, UCP – Uncoupling protein, CT – Carboxyltransferase, FATP – Long-chain fatty acid transport protein, CD36 – Platelet glycoprotein 4.

As aforementioned, aging has been associated with whole body reductions in metabolic rate and energy expenditure (Choksi and Papaconstantinou 2008; Goshovska et al. 2010; Poehlman et al. 1990). This same study found that UCP3 mRNA expression increased with aging, albeit to a lesser degree when compared to UCP2, in ischaemic hearts. They found that this increase in mRNA expression actually had a protective effect on the heart, by inhibiting the production of free radicals and reducing the oxidative stress in the heart; this was also accompanied by a smaller decrease in contractile function of the aged hearts, but whether this was an effect of UCP3 or not is still under discussion and has not been clearly established (Brand and Esteves 2005; Goshovska et al. 2010; Kühlbrandt 2015).

UCP3 also has a very important role in fatty acid oxidation and has been shown to be directly linked to fatty acid metabolism mechanisms (see figure 1.6.3.2). In fact, studies have shown that there is a direct mediation in both obese and diabetic heart models by UCPs, independent of expression levels (Boudina et al. 2007; Hilse et al. 2018; Holloway et al. 2009). An important note here is that both UCP2 and UCP3 have been labelled as having an important role in regulating mitochondrial properties in the presence of FAs, due to their similarities (not to be confused with both having the same role) in expression and function (Barazzoni and Nair 2001; Bellanti et al. 2013; Boudina et al. 2012; Holloway et al. 2009); therefore, many of the published literature makes mention of them together when discussion their function in different tissues.

Some materials have been removed from this thesis due to Third Party Copyright. Pages where material has been removed are clearly marked in the electronic version. The unabridged version of the thesis can be viewed at the Lanchester Library, Coventry University

**Figure 1.6.3.2 – UCP list.** Different uncoupling proteins and their associated function (Pohl et al. 2019).

To support these studies, a recently published study was conducted on the exact mechanisms behind how UCP3 regulates cardiac efficiency and whether it is different when comparing between normal animal models and high-fat diet induced obesity models with a knockout UCP3 gene (Boudina et al. 2012). The group found that UCP3 expression was increased in the presence of FA, as well as in the hearts of *ob/ob* mice, and that deletion of the UCP3 gene caused a reduction in FA oxidation, which correlates with previous research that showed how fatty acid oxidation is regulated in the heart (Wilson, C. et al. 2007; Wright et al. 2009). It is therefore clear that UCP3 has a direct effect on the heart, but the exact mechanisms behind it are not yet clear.

While the above studies are very important in the understanding of UCP3 expression, there are some concerns amongst the scientific community regarding the mRNA expression of UCP3 vs its protein expression. Previous studies have found some discrepancies between the two techniques (Pecqueur et al. 2001; Rupprecht et al. 2012; Rupprecht et al. 2019), which stem from the fact that both UCP2 and UCP3 have an upstream open reading frame, or uORF (Hurtaud et al. 2006). UORFs are mRNA elements that can, in certain conditions, cause a reduction in protein expression by up to 80% (Calvo, Pagliarini and Mootha 2009). Due to this, the investigation of these protein levels is still in its infancy and there is a lot of work still left to understand their exact functions. In this study, the aim was to use the protein form of UCP3, but the previously mentioned concerns will be taken into consideration when carrying out the project and when analysing the data.

## **1.7 Inotropic drugs and their modes of action**

The drugs used in this project will be discussed in detail in the following sections (Isoprenaline, Dobutamine, Atenolol and Itraconazole). These drugs were chosen based on their known clinical usage and inotropic effects. The plasma half-life of each drug will also be mentioned, as an explanation for the slower effects observed throughout the investigation; this plasma half-life is a parameter used to determine the time it takes for a substance to lose half of its pharmacological activity (Roberts, F. and Freshwater-Turner 2007).

### **1.7.1 Isoprenaline**

Catecholamines are amines that are derived from tyrosine and function as neurotransmissions in the central nervous system and as hormones in the endocrine system (Nagatsu 2006). Isoprenaline, sometimes known as Isoproterenol, is a commonly used  $\beta_1$ - and  $\beta_2$ -adrenoreceptor agonist ( $\beta_1$ AR and  $\beta_2$ AR, respectively) in the treatment of bradycardia (slow heart rate) and heart block. Its mode of action is predominantly involved with the activation of beta-1 and beta-2 adrenergic receptors, which are G-protein coupled receptors predominantly expressed in cardiac tissue and involved in observable increases in contractility and cardiac automaticity or action potential generation (Hoffman 2001; Hoffmann et al. 2004). These receptors are tissue mediators and regulate the cardiac rate and force of contraction of the heart. The adrenoreceptors are stimulated by the intracellular adenylyl cyclase, known as the enzyme responsible for the conversion of ATP into cyclic AMP, which leads to an increased systolic blood pressure and consequent increased heart activity (Averin et al. 2010). Please refer to section 1.3 for an in-depth review on myocardial contractility.

Isoprenaline induced tachycardia is a common side effect of the drug usage; it has also been shown to cause severe damage in septic patients by myocardial weight induced changes that can lead to hypertrophy (Brooks and Conrad 2009). It is a commonly used drug in infarct-like lesions, mainly in areas prone to ischaemia. A paper published in 2013 investigated the effects of tyrosine kinase inhibitors using Isoprenaline as a positive inotropic control for cardiac damage (Henderson et al. 2013) and the result detailed that the levels of cardiac toxicity obtained were not the expected one from the preclinical trials and it was hypothesized that the results acquired were due to the usage of higher, non-standardized concentrations of the drugs. The authors conclude the paper mentioning the need for more tests with the drugs used (isoprenaline and sunitinib amongst others) and mention the use of some of the techniques utilized for this project and described in sections 2.3 and 2.4. Another study also conducted in 2013 investigated the link between isoprenaline and the metabolic disturbances in myocardial infarction in rat cardiac tissue (Liu et al. 2013). The study showed that the cardiac pump was unable to meet the energy requirements while under isoprenaline induced myocardial infarction and this was found to be linked to changes in the fatty acid  $\beta$ -oxidation pathway and glycolysis (see figure 1.7.1.1), as these pathways have been shown in the past to be adaptive in order to satisfy the energy requirements of the organism (Lu, Y. et al. 2011). There are conflicting studies regarding beta-adrenoreceptors ( $\beta$ AR) and their link to dysfunction in obesity, with some showing no cardiac dysfunction-related changes to the  $\beta$ AR system (Ferron et al. 2015; Vileigas et al. 2016) and others reporting a reduction in cardiac contractile function due, in part, to a  $\beta$ AR decreased responsiveness to stimulation in obesity (Carillion et al. 2015; Carroll et al. 1997; Jiang, C. et al. 2015).

Studies have also found that there is a catecholamine related preference for the  $\alpha$ -receptors in senescent rat hearts (Ferrara et al. 2014; Jiang, M., Moffat and Narayanan 1993). This was tested using phenylephrine and the results obtained showed a shift in mediation from both receptors to the  $\alpha$ -receptor, in 7-month-old rats. There is also a phenomenon that is very well documented and is known as a “ $\beta$ -adrenoreceptor desensitization” and it is commonly observed during physical stress (Abrass, Davis and Scarpace 1982; Ferrara et al. 2014; Hashimoto, Nakashima and Sugino 1983).

Some materials have been removed from this thesis due to Third Party Copyright. Pages where material has been removed are clearly marked in the electronic version. The unabridged version of the thesis can be viewed at the Lanchester Library, Coventry University

**Figure 1.7.1.1 – Isoprenaline mode of action.** Effects of Isoprenaline on the metabolic system of myocardial infarction in rats (Liu et al. 2013). ISO – Isoprenaline.

## 1.7.2 Dobutamine

Dobutamine is an example of a synthetic amine, as it was a result of structural modifications to Isoprenaline in an attempt to reduce its chronotropic and vascular side effects (Driscoll et al. 1979; Tuttle 1958). Its mode of action is predominantly involved in the binding to beta-1 adrenergic receptors (see figure 1.7.2.1), which are G-protein coupled receptors predominantly expressed in cardiac tissue and involved in observable increases in contractility and cardiac automaticity or action potential generation (Hoffman 2001; Ruffolo 1987) - please refer to section 1.3 for an in-depth review on myocardial contractility. Due to these properties, Dobutamine is one of the most commonly used positive inotropic agents in the treatment of congestive heart failure and cardiogenic shock worldwide (Gheorghide, Filippatos and Felker 2012). Its exact effect works by augmenting the stroke volume and heart rate, reducing the afterload and generally increasing cardiac output (Ruffolo 1987).

Some materials have been removed from this thesis due to Third Party Copyright. Pages where material has been removed are clearly marked in the electronic version. The unabridged version of the thesis can be viewed at the Lanchester Library, Coventry University

**Figure 1.7.2.1 - Dobutamine mode of action and signalling pathways.** Dobutamine binds to the  $\beta$ -receptors and triggers the production of adenylyl cyclase, which leads to an increase in  $\text{Ca}^{2+}$  production and an overall increase in contractility (Teerlink 2009). KACH – Potassium channel, PDEIII – Phosphodiesterase 3, AD/MUSC – Muscarinic receptor, Gq  $\alpha/\beta/\gamma$  – G alpha/beta/gamma protein complex.

At high doses, it causes arterial and venous constriction due to the activation of the  $\alpha 1$  receptor and it has been frequently associated with cases of severe tachycardia, mild arrhythmias and hypertension symptoms (Vallet, Dupuis and Chopin 1991; Wang, Zhu and Shan 2015). Apart from heart failure, it is also commonly used to treat cardiogenic shock. Dobutamine has been documented to have a high mortality rate when used at elevated concentrations, independent of intermittent or continuous treatments (Amin and Maleki 2012; Krell et al. 1986). Dobutamine has also been linked to eosinophilic myocarditis, which is a rare and fatal disease that causes necrosis and endomyocardial fibrosis (Al Ali et al. 2006; Sohn et al. 2015), peripheral eosinophilia and in-hospital deaths caused by heart failure exacerbation. In high doses, it has been shown to cause an increased onset of negative effect on patients with myocardial ischaemia. However, due to its very short half-life, it can be advantageous over other inotropes (Wang, XC, Zhu and Shan 2015). Due to the dosage-related complications associated with the drug, conducting a dose response study is very important and vital to the understanding of the drug mechanism in order to avoid the aforementioned negative effects and improve patient care (Follath et al. 2002; Sindone et al. 1997). Similar to isoprenaline, dobutamine has been linked to ineffective energy production in HFD model via changes to the fatty acid  $\beta$ -oxidation pathway and glycolysis (Haggerty et al. 2015; Liu, X. et al. 2016). As mentioned before (see section 1.4.2.1), there is conflicting data regarding beta-adrenoreceptors ( $\beta$ AR) and their link to dysfunction in obesity, with studies reporting inconsistencies between them (Carillion et al. 2015; Carroll et al. 1997; Ferron et al. 2015; Jiang, C. et al. 2015; Vileigas et al. 2016). It therefore possible that a link exists between Dobutamine and obesity-connected dysfunction, but this is still up for debate and no conclusion is, as of right now, fully accepted.

As mentioned in section 1.7.1, catecholamine related preference for the  $\alpha$ -receptors in senescent rat hearts has been heavily reported in the past (Ferrara et al. 2014; Jiang, M., Moffat and Narayanan 1993), alongside a phenomenon known as “ $\beta$ -adrenoreceptor desensitization”, both previously documented (Abrass, Davis and Scarpace 1982; Ferrara et al. 2014; Hashimoto, Nakashima and Sugino 1983). Most of these studies are fairly old due to the extensive work that has been done with the aid of the aforementioned compounds. In addition to this, a more recent study found that the positive inotropic effect of  $\beta$ -receptor agonist is altered and reduced due to dysfunctions in the  $\beta_1$  and  $\beta_3$ -adrenoreceptors and in ATP production within the cells, as seen in figure 1.7.2.2 (Carillion et al. 2015). This hypothesis is fairly new and there is, therefore, a lot of work still necessary in order to prove or disprove it.

Some materials have been removed from this thesis due to Third Party Copyright. Pages where material has been removed are clearly marked in the electronic version. The unabridged version of the thesis can be viewed at the Lanchester Library, Coventry University

Some materials have been removed from this thesis due to Third Party Copyright. Pages where material has been removed are clearly marked in the electronic version. The unabridged version of the thesis can be viewed at the Lanchester Library, Coventry University

**Figure 1.7.2.2 –  $\beta$ -AR effects on different heart models.** Three models are shown: (A) physiological conditions in a normal heart, (B) during a heart failure event and (C) while under the effects of aging (Lucia, Eguchi and Koch 2018). Both aging and heart failure have similar effects on the heart, manifested in the form of increased catecholamine circulation and downregulation of  $\beta$ -Ars, leading to an overall reduction in contractility. Cas – Catecholamines, AC – Adenylyl cyclase, GRK2 – G Protein-coupled receptor kinase 2.

### 1.7.3 Atenolol

Beta blockers are a heterogeneous class of drugs mainly used in the treatment of hypertension and cardiac arrhythmias (Bristow et al. 1986; Koshman et al. 2018). Their use as cardioprotective agents against repeated myocardial infarctions has also been suggested in previous studies (Freemantle et al. 1999). This class of drugs act as competitive antagonists by blocking receptor sites of the sympathetic nervous system either selectively, for each individual receptor ( $\beta_1$ ,  $\beta_2$  and  $\beta_3$ ) or globally, for all three (DiNicolantonio et al. 2015; Triposkiadis et al. 2009).

Each receptor is located in different areas of the body and control different pathways and mechanisms:  $\beta_1$  receptors are located in the heart and kidneys,  $\beta_2$  receptors encompass a wider group that includes the lungs, skeletal and vascular smooth muscles, liver and a few other organs and  $\beta_3$  receptors are mainly located in a wide variety of fat cells (Cohen et al. 1999; Engelhardt et al. 1999; Mysliveček et al. 2003). The inhibition of the  $\beta$ -adrenergic receptors causes a decrease in the work output of the heart, and essentially decreases the heart rate of the heart and, although they have a similar structure to catecholamines, their effect is the exact opposite (Bristow et al. 1986). They also combat the fatty acid catecholamine-induced release on the adipose tissue, which leads to a decrease in the myocardial oxidative stress (Gorré and Vandekerckhove 2010). To this effect, Atenolol is a cardio-selective  $\beta_1$  receptor antagonist with both negative inotropic and chronotropic properties and one of the most commonly used beta-blockers worldwide in the treatment of hypertension (Carlberg, Samuelsson and Lindholm 2004). However, recent studies have shown that equally effective drugs are being recommended as alternatives to atenolol, such as calcium channel blockers and drugs designed to inhibit the renin-angiotensin system (Chen, N. et al. 2010; Xue et al. 2015).

Atenolol is also used as an effective treatment for angina, acute myocardial infarction, ventricular tachycardia, supraventricular tachycardia and long QT syndrome (Morita, Wu and Zipes 2008). Atenolol has also been shown in recent studies, to increase the risk of mortality in the elder population, especially in patients suffering from high pulse arterial pressure. (Testa et al. 2014). In another study using 18-month mice models, it was found that Atenolol not only reduced the membrane fatty acid unsaturation of the heart, but also decreased the various markers of oxidative stress within the animals (Gómez et al. 2014; Sanchez-Roman et al. 2010; Sanchez-Roman et al. 2014). The Gómez study also recorded changes in the heart rate, systolic pressure and diastolic pressure in the hearts treated with atenolol, when compared to the control groups; added to this, the atenolol treated groups also showed a lower metabolic rate when compared to the young models, albeit non-significant; in addition, phosphorylated ERK activity was significantly increased in the heart muscles of atenolol treated hearts (Gómez et al. 2014). This is of particular importance because ERK activity has been directly linked, in both cancer and regular physiological processes, to the activation of pyruvate dehydrogenase kinases, which suppress pyruvate consumption and induce lactate production; in other words, ERK causes an impairment in the TCA cycle and the overall mitochondrial energy production via disruptions in pyruvate production (Chung et al. 2010; Hom et al. 2011).

Previous studies have looked at the effect of Atenolol and its mechanism on diet-induced obesity (see figure 1.7.3.1) and found that there is a blunting in the bradycardic response of atenolol and variability in heart rate measures, alongside a reduced sympathetic sensitivity (Williams et al. 2003; Xu et al. 2015). An older study used isolated papillary and atrial muscles taken from diabetic rats and showed that, while there a beta-adrenoreceptor blocking effect, this was seen for both the control and the diabetic models and no significance was recorded (Nagamine et al. 1989).

Whilst the exact remodelling between diabetes and high-fat diet induced obesity differs, enough parameters are similar and can still provide us with some useful information on how drugs cause metabolic changes.

Some materials have been removed from this thesis due to Third Party Copyright. Pages where material has been removed are clearly marked in the electronic version. The unabridged version of the thesis can be viewed at the Lanchester Library, Coventry University

**Figure 1.7.3.1 – Atenolol mode of action.** Proposed atenolol mode of action and its potential effect on circulating free fatty acids (Wikoff et al. 2013). PLD – Phospholipase D, TAG – Triglyceride, DAG – Diglyceride, LysoPC – Lysophosphatidylcholine.

Atenolol has also shown to cause changes in different metabolic effects, in overweight hypertensive patients, such as hyperinsulinaemia and hyperglycaemia (Konrady et al. 2006). This study was conducted with a limited number of patients, but what the researchers suggest is that atenolol might cause an exacerbation of the negative aspects of obesity on the metabolic system, although the exact mechanism behind this is not yet understood. Another study was conducted on obese patients treated with atenolol (Wofford et al. 2001); in this study, patients were given atenolol for a month, before tests were performed on their systolic, diastolic and mean arterial pressures. It was noted that, on the obese patients treated with atenolol, there was a significant decrease in all of the mentioned parameters. This result suggests that blood pressure in obesity is susceptible to changes under the effect of beta-blockers.

#### 1.7.4 Itraconazole

Itraconazole (commonly known as Sporanox) is one of the most commonly used synthetic triazole antifungal agent and it acts by inhibiting the effects of key members of the CYP 450 enzyme superfamily. It has been outlined by the WHO as one of its essential medications (WHO 2019) . but recent studies have found a worrying trend regarding its effects on cardiovascular function. Amongst the severe adverse effects of the drug, the most commonly observed is heart failure and a severe drop in left ventricular pressure (Fung, Chau and Yew 2008). Before elaborating on the drug effects in the context of cardiac function, it is first important to provide some background on the function of triazole antifungals, due to the limited information available for Itraconazole, specifically.

Triazole antifungals are drugs used in the treatment of fungal diseases in patients undergoing stem cell transplants and intensive chemotherapy treatments (Ceesay et al. 2016; Maertens et al. 2011) that work by inhibiting both the angiogenesis cascade and the cytochrome P450 enzyme superfamily (Borgers and Ven 1989; Ghannoum and Rice 1999; Meletiadiis et al. 2012). Angiogenesis is a vital and complex process that is particularly important in cardiovascular disease; it is the process by which new blood vessels are formed, via a variety of synergetic vascular endothelial growth factor (VEGF) effects (Durand, Ait-Aissa and Gutterman 2017; Liao, Y. et al. 2014; Zachary and Morgan 2011). Angiogenesis has been linked to increases in the development of atherosclerotic plaques in newly formed vessels, but the information and tests currently available are not very conclusive; however, inhibition of angiogenesis has been considered as a potential path to target atherosclerosis and other ischaemic heart conditions (Gogiraju, Bochenek and Schäfer 2019; Henry et al. 2003; Khurana et al. 2005). Figure 1.7.4.1 shows the link between angiogenesis and CVDs.

Some materials have been removed from this thesis due to Third Party Copyright. Pages where material has been removed are clearly marked in the electronic version. The unabridged version of the thesis can be viewed at the Lanchester Library, Coventry University

**Figure 1.7.4.1 – Angiogenesis and CVD.** Effect of angiogenesis and its links to cardiovascular diseases (Moraga, Lao and Zeng 2017). HDAC – Histone deacetylase, TSA – Trichostatin A, SIRT1 – Sirtuin 1.

The cytochrome P450 enzyme superfamily (CYPs) is a group of enzymes with a very important role in the metabolism of lipophilic compounds within the organism, as well as endogenous compounds such as vitamins and arachidonic fatty acids (Bieche et al. 2007). CYPs are localized in the endoplasmic reticulum and, whilst mainly expressed in the liver, can also be measured in heart tissue (Pavek and Dvorak 2008; Stegeman et al. 1982; Wu et al. 1997). Each CYP subfamily has specific functions in heart physiology and have been previously linked to both cardioprotective (Katragadda et al. 2009; Lu, T. et al. 2001) and cardiotoxic effects (Chehal and Granville 2006; Fleming et al. 2001) in the heart, such as ROS dysfunctions and mitochondrial changes (see figure 1.7.4.2).

**Figure 1.7.4.2 – Intracellular effects of CYPs.** Overview of the positive and negative effects of CYPs on the heart and how they can cause beneficial or harmful changes (Chaudhary, Batchu and Seubert 2009). EET – Epoxyeicosatrienoic acid, HETE – Hydroxyeicosatetraenoic acid.

Other studies have been done on HFD and diabetic models and have shown that, in hearts overexpressing CYPs, the cardiac contractility of the heart is maintained and the cardiac glucose uptake is improved, alongside an increase in pyruvate dehydrogenase complex expression, which has been linked to important mitochondrial metabolic regulations in diabetes and obesity (Dewey et al. 2013; Ma et al. 2013; Roche et al. 2015).

Age also plays an effect in CYP expression and a recent study has shown that younger mice overexpress CYPs and that this effect is lost with age, due partially to oxidative stress (Chaudhary et al. 2013). Another study showed that the decline in cardiac function that is observed with age is linked to a reduction in CYPs, when compared to younger models (Jamieson et al. 2017). These studies, while limited, suggest that age has a significant effect in heart function and that, to an extent, this is linked to changes to CYP expression.

Whilst this was not explored for this project, it is a hypothesis proposed to explain the potential changes that we expect to record on the hearts treated with Itraconazole, due to its effect on the CYP2C enzyme protein complex (see hypotheses and aims in chapter 2, as well as the future studies in chapter 9).

Regarding the effects of the drug on cardiovascular function, studies have shown that patients were more likely to develop congestive heart failure when under treatments with Itraconazole, even when different protocols were used to measure the negative inotropic effect of the drug (Guth et al. 2015; Okuyan and Altin 2013; Tucker et al. 1990). Other studies have shown that, on animal models, Itraconazole heavily decreases the contractility of the heart and has a direct negative inotropic effect on cardiomyocytes, with no involvement of the mitochondria or calcium channels (Cleary et al. 2013; Qu et al. 2013). The exact mechanism behind the effect of antifungal drugs and the negative inotropy documented up to this point is not yet understood, even though some mechanisms have been proposed (Ahmad, Singer and Leissa 2001). Itraconazole has also been shown to be cytotoxic to cells, with studies showing that this negative effect is directly linked to both ATP level reduction in hepatocytes and to cytochrome P450 inhibition (Somchit et al. 2009). In the mentioned study, the researchers used ATP assay kits to determine ATP levels and found that, in cells incubated with Itraconazole, the ATP levels dropped significantly. The drug has shown to induce congestive heart failure in aged patients, between the ages of 58 and 60 years (Cleary and Stover 2015; Jia et al. 2010; Okuyan and Altin 2013).

As mentioned above, there is very limited research on azole antifungals and their effect on the cardiac function of obese patients and most of this data comes from patient data. Studies have been conducted but used a similar azole known as Fluconazole and it was found that the drug was less effective in obese and morbidly obese patients, when compared to nonobese patients (Alobaid et al. 2016; Lopez and Phillips 2014; Sinnollareddy et al. 2015), but the exact reason for this and any associated pathways affected were not investigated. While the target of these studies was not to look at the cardiovascular function of the heart, it is likely that there are similar effects in place that cause severe changes in the hearts of obese models, as cytochrome P450 seems to be directly linked to obese cardiac dysfunction.

# Chapter Two: Aims and hypotheses

The primary aims for this thesis were focused on investigating the following:

- (1) To investigate the effects of age, high-fat diet induced obesity (HFD) and the synergistic effect of both on cardiac contractility using the Langendorff Isolated heart and the work-loop muscle assay (Chapters 4 and 5).
- (2) To investigate the effects of Dobutamine, Isoprenaline, Atenolol and Itraconazole on the contractile function of ageing and HFD cardiac models (Chapters 6 and 7).
- (3) To understand the inotropic effects of Dobutamine, Atenolol and Itraconazole on the aforementioned models, with regards to shifts in cardiac energy metabolism pathways looking at pyruvate dehydrogenase E1- $\alpha$  subunit (PDH) and uncoupling protein 3 (UCP3) (Chapters 6 and 7).

Based on reviews of past literature, the hypotheses for this thesis were the following:

- (1) Increasing age will cause a decrease in haemodynamic and metabolic function of the heart, especially on the left ventricular pressure and heart rate and in the phosphorylation levels of PDH and UCP3. Muscle power output will be decreased on the work-loop muscle assay, due to the effect of ageing on muscle fatigue.
- (2) HFD will cause a decrease in haemodynamic and metabolic cardiac function, and this effect will be exacerbated on the 18-month aged models. The combined effect of age and obesity, when compared to their lean counterparts, will also cause significant impairment in muscular power output and a decrease in the phosphorylation levels of PDH, due to its vital function in glucose metabolism, and an increase in UCP3, due to its function as an obesity marker.

- (3) Due to  $\beta$ -receptor desensitization in ageing, Dobutamine and Atenolol measurements will show significant impaired effects on the haemodynamic function of the heart. Itraconazole will cause a significant decrease in the haemodynamic function of the heart, in an age-dependant fashion, due to changes in CYP expression.
- (4) PDH and UCP3 Phosphorylation levels will be reduced in the presence of Dobutamine but will not change significantly in the presence of Atenolol and Itraconazole.
- (5) HFD will cause a blunted effect of Dobutamine and will exacerbate the negative inotropic effects of Atenolol and Itraconazole, across all age groups.
- (6) PDH phosphorylation levels will be significantly decreased in the combined presence of HFD and age for Dobutamine, Atenolol and Itraconazole. Due to the presence of HFD, UCP3 levels will not show significant differences between the three drugs.

# **Chapter Three: Materials and Methods**

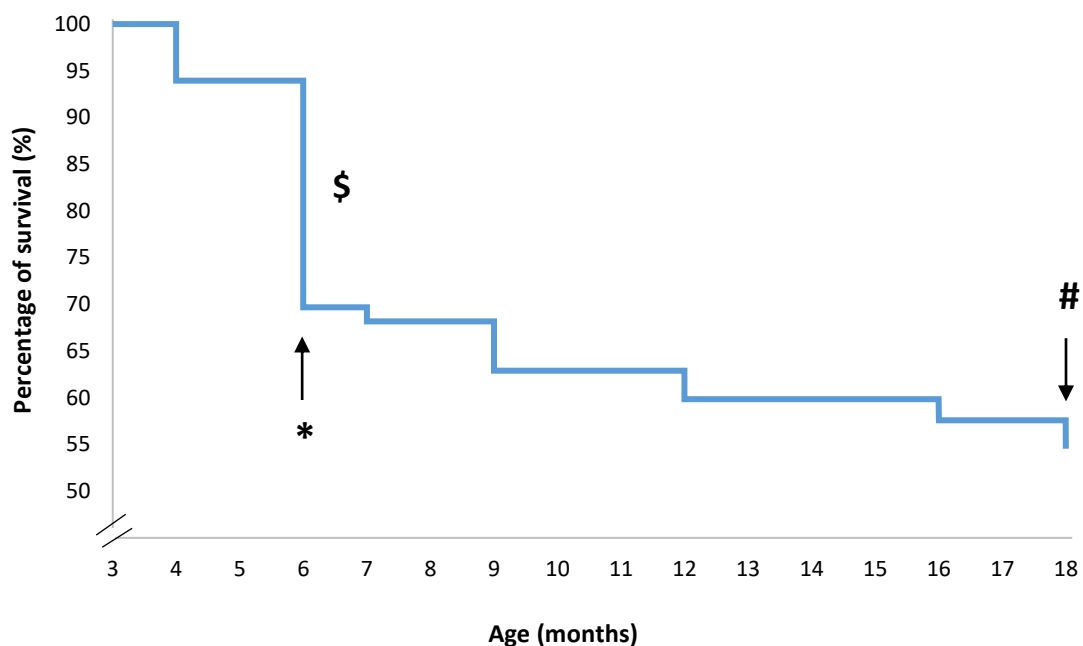
## **3.1 Model Characterisation**

Following ethics approval from the host institute, one hundred and thirty-two 3-month Sprague-Dawley male rats with an average body mass of  $350\text{g} \pm 3.2$  (standard error of the mean, or SEM) were purchased from Charles River UK Limited (Margate, UK) and received human care in accordance with the guidelines on the British Home Office Animals (Scientific Procedures) Act 1986 (Hollands 1986). Animals were aged in cages of 3 to 5 individuals, in 12h light and dark cycles, at around 50% relative humidity.

### **3.1.1 Aged models**

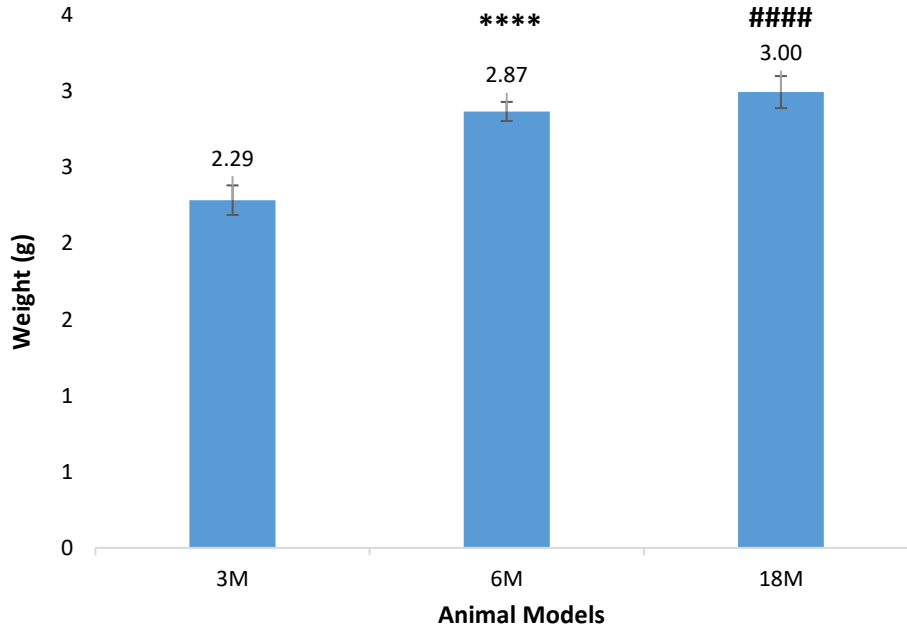
For this project, 3, 6 and 18-month models were used due to these ages being representative of a young, middle-aged and adult rat. For the purposes of this study, 3-month rats have been equated, in age, to a human child between 10-18 years, 6-month rats have been equated to a young adult between 20-30 years and 18-month rats have been equated to an older adult between 54-69 years (Andreollo et al. 2012; Capitanio et al. 2016; Jackson et al. 2017; Sengupta 2013). Previous results have varied from research group to research group and since there is no exact formula to calculate the age comparison between rats and humans, it was decided that the entirety of the previous published literature would be utilised to define the age groups for this thesis.

Figure 3.1.1.1 represents a plotted Kaplan-Meier curve showcasing the animal deaths throughout the project, although the numbers do not account for heart issues and losses post animal sacrifice. 30% of the animals were used for the 6-month project (40 animals) and the remaining 70% were aged up to 18-months (92 animals). Out of this, 22% (20 animals) died between month 6 and month 18; The exact causes of death were not determined, but it is possible that the effects of ageing and obesity might have played a role in this.



**Figure 3.1.1.1 – Kaplan-Meier survival curve for aging rats over time.** The graph illustrates the number of animals that survived by the end of the studies; the causes of death are not known but it is believed that the high-fat diet in combination with age caused an exacerbation of pathways which ultimately resulted in death. \* - 6-month data collection start, # - 18-month data collection start, \$ - Drop in animal numbers due to usage of animals for the 6-month data collection.

In addition, measurements for the heart weight of each animal were taken post-experimental procedures to confirm morphometric changes to the organ; figure 3.1.1.2 highlights the differences in weight across the three models, showcasing the hypertrophy commonly associated with older hearts. Body measurements were also taken, to confirm physical changes across all ages, as seen in table 3.1.2.1.



**Figure 3.1.1.2 – Graph showcasing heart weight variations across all aged models.** Significant changes were observed between the younger 3-month models and the aged 6 and 18-month models (\*\*\*\*and #### =  $p < 0.0001$ ; \* = 6-month model; # = 18-month model).

### 3.1.2 High-fat diet-induced obesity models (HFD)

For this project, “obesity” was defined as a significant increase in body mass, fat pad mass and body circumference as a result of a high-fat diet, when compared to a control lean group; the term used to refer to these physiological changes on the models will be “HFD”, to provide consistency to the discussion. Statistics published by the Health Survey for England have shown a worrying increase in the numbers of overweight and obese populations within the UK (HSE 2019). For the current study, 6 and 18-month lean and HFD models were used, similar to what was mentioned in section 3.1.1, with their human age equivalents being 20-30 years and 53-69 years, respectively. Obesity or overweight numbers for these populations are between the 15-34% for the former and 33-43% for the latter, making them among the most afflicted by this pandemic and the present research is therefore of paramount importance to look at how cardiac function changes within these specific populations.

The diets used for this project (both the standard diet and the high-fat diet) were similar to the ones seen in a study recently published by Messa et al (Messa et al. 2020), and their caloric compositions were as follows:

- **STANDARD CHOW**: protein 17.5%, fat 7.4%, carbohydrate, 75.1%; gross energy 3.52 kcal.g<sup>-1</sup>; metabolizable energy 2.57 kcal.g<sup>-1</sup> (CRM(P) SDS/Dietex International Ltd, Whitham, UK).
- **HIGH-FAT DIET**: protein 18.0%, fat 63.7%, carbohydrate, 18.4%; gross energy 5.2 kcal.g<sup>-1</sup>; metabolizable energy 3.8 kcal.g<sup>-1</sup> (Advance protocol PicoLab, Fort Worth, USA).

All the animal groups were given *ad libitum* access to their respective diet and water and feeding began 16 weeks prior to starting the experiments. For the 6 and 18-month lean and high-fat diet groups, the animals were divided into two groups each containing a randomized sample size of 60 and 80 Sprague-Dawley male rats, respectively, and a minimum of 4 n numbers were used per technique.

For the 6-month group, 30 were given standard chow *ad libitum* (average body mass of 539g ± 15.5 (SEM)) and the other 30 were given the high fat diet *ad libitum* (average body mass of 638g ± 7.2 (SEM)). For the 18-month group, 40 were given standard chow *ad libitum* (average body mass of 794g ± 8.4 (SEM)) and the other 40 were given the high fat diet *ad libitum* (average body mass of 929g ± 10.5 (SEM)).

Body mass for the 6 and 18-month animals was measured bi-weekly (see figure 2.1.1 and table 2.1.1) and both the mesenteric and epididymal pads (left and right) were weighed (see table 2.1.1) after the sacrifice of the animals to provide a two-step verification in their body mass difference, as seen in previous studies (Woods et al. 2003).

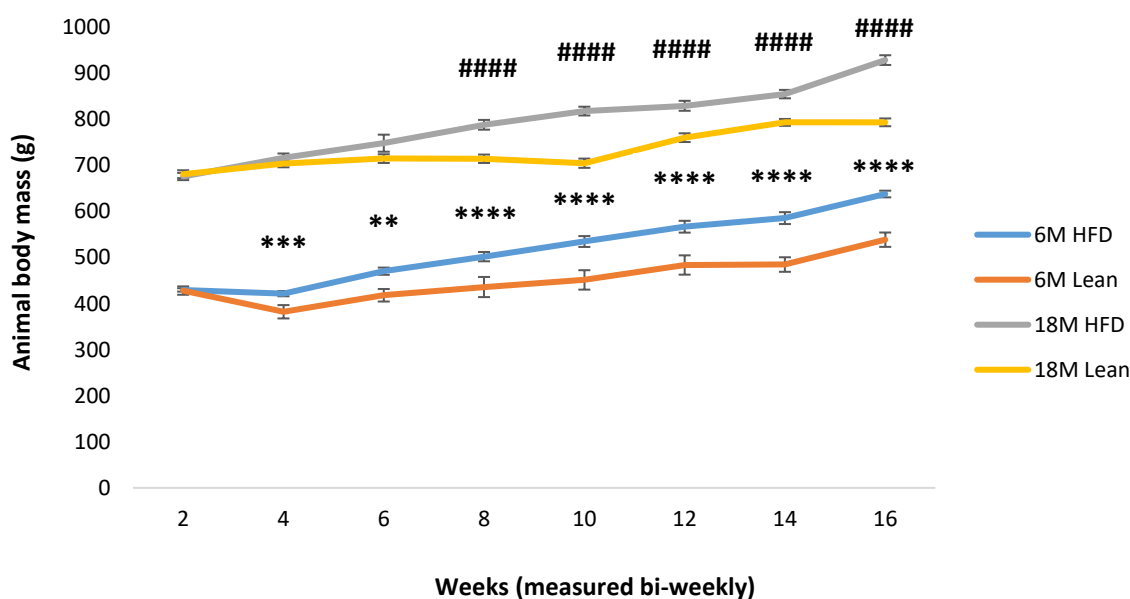


**Figure 3.1.2.1 – Comparison of animal body mass in both the 6 and the 18-month aged models, measured bi-weekly for a total of 16 weeks.** Significance was shown after the first month of feeding between the lean and the HFD models within each aged model (\*\*\*\*and ##### =  $p < 0.0001$ ; \* = 6-month model; # = 18-month model).

**Table 3.1.2.1 - Table with the comparison of parameters between lean models and HFD models, in 6-month and 18-month aged animals.** The mean values are a representation of the parameters at the start of the experimental protocols (\*\* =  $p < 0.01$ , \*\*\* =  $p < 0.001$  and \*\*\*\* =  $p < 0.0001$ , compared to the 6-month lean group and ### =  $p < 0.001$  and ##### =  $p < 0.0001$ , compared to the 18-month lean group).

Age group	6M Lean Mean $\pm$ SEM	6M HFD Mean $\pm$ SEM	18M Lean Mean $\pm$ SEM	18M HFD Mean $\pm$ SEM
<b>Body mass (g)</b>	539 $\pm$ 15.5	638 $\pm$ 7.2 ****	794 $\pm$ 8.4	929 $\pm$ 10.5 #####
<b>Body length (cm)</b>	43 $\pm$ 0.5	44 $\pm$ 0.4	49.5 $\pm$ 0.4	48.5 $\pm$ 0.4
<b>Left epididymal fat pad mass (g)</b>	7.01 $\pm$ 0.6	8.65 $\pm$ 0.5 ***	6.93 $\pm$ 0.4	12.05 $\pm$ 0.6 #####
<b>Right epididymal fat pad mass (g)</b>	6.64 $\pm$ 0.6	8.72 $\pm$ 0.5 **	6.97 $\pm$ 0.3	12.50 $\pm$ 0.6 #####
<b>Mesenteric fat pad mass (g)</b>	6.50 $\pm$ 0.6	10.63 $\pm$ 0.8 ****	8.70 $\pm$ 0.3	11.42 $\pm$ 0.4 ###
<b>Body circumference (cm)</b>	21.75 $\pm$ 0.2	25.75 $\pm$ 0.2 ****	26.25 $\pm$ 0.2	33.75 $\pm$ 0.3 #####

In addition to the parameters measured and similar to the aged models, the heart weight of each animal was also taken post-experimental procedures to confirm morphometric changes to the organ. Figure 3.1.2.2 highlights the heart weights across the used obese models.

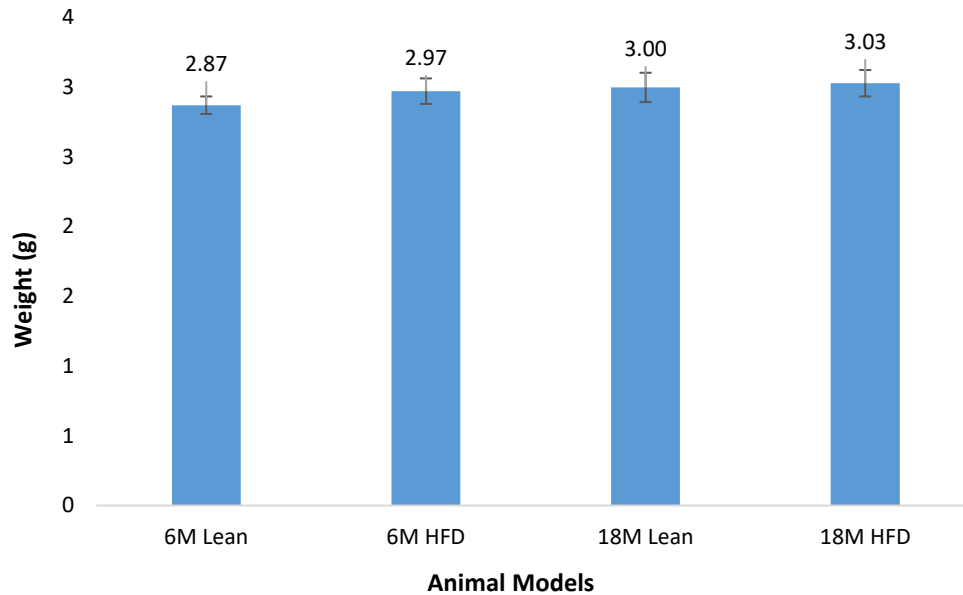


**Figure 3.1.2.2 – Graph showcasing heart weight variations across all obese and lean models.** Significant changes were observed between the younger 3-month models and the aged 6 and 18-month models.

Both genetic and diet-induced murine models exist as established models of obesity, such as AKR mice (Kless et al. 2017), C57BL/6J mice (Fleury Curado et al. 2018), ob/ob rats (Minhas et al. 2005), Zucker rat models of obesity (Bussey et al. 2018), Wistar rat models of obesity (Marques et al. 2016) and Sprague-Dawley rat models of obesity (Marques et al. 2016). All of these models have been used in the past to try and understand all the pathways involved in the obesity pathogenesis, due to their similarity to humans, particularly in the control of energy homeostasis (Barrett, Mercer and Morgan 2016). Murine models (and especially Sprague-Dawley rats) have also proven to be effective in detecting markers of obesity and cardiovascular diseases without being affected by other factors, making them excellent models for pre-clinical obesity-related projects (Marques et al. 2016; Rojas et al. 2018).

The animal models described above were divided according to each chapter and to each associated project, as seen in table 3.1.2.2:

**Table 3.1.2.2 - Table with the layout of each chapter presented.** A minimum of n=4 was produced per chapter, for each of the mentioned animal groups.

<b>Chapter 4 – Physiology age study</b>	3, 6 and 18-month animals
<b>Chapter 5 – Physiology HFD Study</b>	6 and 18-month animals (HFD vs Lean)
<b>Chapter 6 – Inotropic age study</b>	3, 6 and 18-month animals
<b>Chapter 7 – Inotropic HFD study</b>	6 and 18-month animals (HFD vs Lean)

## 3.2 Langendorff Isolated Heart Model

It starts with the perfusion of the heart with perfusion buffer, via cannulation of the aorta, in a retrograde fashion, forcing the closing of the aortic valve as a result of a change in pressure. The buffer then passes through a vascular bed before being drawn to the coronary sinus in the right atria. This allows the preparation to be maintained without any fluid filling the ventricular chambers (Skrzypiec-Spring et al. 2007). For a full background review on the technique, please refer to section 1.3.2.

### 3.2.1 Drugs and chemicals utilised

The drugs Itraconazole, Isoprenaline, Dobutamine and Atenolol were used throughout this project, all purchased from Abcam (UK), and diluted in Milli-Q<sup>®</sup> water to achieve the relevant concentrations used for the project (1nM, 3nM, 10nM, 100nM, 1µM, 10µM and 30µM). Please refer to section 1.7 for a full review on each of these compounds.

Krebs-Henseleit buffer (KHB) was also used and prepared daily, containing NaCl (118.5 mM), NaHCO<sub>3</sub> (25.0 mM), KCl (4.8 mM), MgSO<sub>4</sub> (1.2 mM), CaCl<sub>2</sub> (1.7 mM), KH<sub>2</sub>PO<sub>4</sub> (1.2 mM) and glucose (12 mM), with a pH of 7.4. The buffer was always gassed using 95% O<sub>2</sub> and 5% CO<sub>2</sub> and maintained at 37°C.

### 3.2.2 Haemodynamics Data Collection

Rats were sacrificed by means of cervical dislocation, in accordance with the British Home Office Animals (Scientific Procedures) Act 1986, Schedule 1 (Hollands 1986).

The diaphragm was cut to expose the thoracic cavity and the thorax was subsequently opened to expose the heart. The excised hearts were immediately placed in ice cold KHB before being mounted securely onto the Langendorff apparatus (figure 3.2.2.1). The preparation was subsequently retrogradely perfused for 20 minutes with KH buffer (maintained at a constant temperature of 37°C ± 0.5 at a pH of 7.4) and gassed with 95% O<sub>2</sub> and 5% CO<sub>2</sub>.

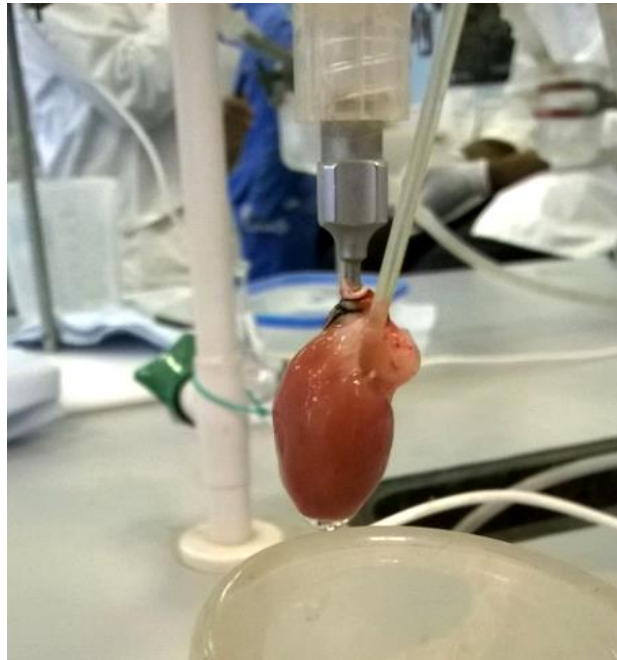


**Figure 3.2.2.1 – Langendorff isolated heart.** An image showing a heart mounted on the Langendorff apparatus, with a latex balloon inflated in the left ventricle, through the excised left atrium.

A latex balloon was inserted into the left ventricle through the excised left atrium and inflated at a constant pressure of 5-10 mmHg. Left Ventricular Developed Pressure (LVDP), heart rate (beats per minute – BPM), Maximum ventricular pressure increase (+dP/dTmax) and Maximum ventricular pressure decrease (-dP/dTmax) were recorded using a physiological pressure transducer connected to the latex balloon and to a PowerLab (ADInstruments, UK) linked to a PC with LabChart® software v7 (figures 3.2.2.2 and 3.2.2.3). The coronary flow, or CF, (ml.min<sup>-1</sup>) was also recorded by collecting the coronary perfusate at regular time intervals (once every 5-minutes).

The rate pressure product of the heart, or RPP (mmHg/min) was calculated by multiplying the LVDP by the HR (LVDP\*HR), at the end of the experimental protocol, as seen in previous papers (Dodd et al. 2018; Zuurbier and Van Beek 1997). The duration of the experimental protocol was 160 minutes for all hearts throughout the project. At the end of the protocol, the left ventricle was excised from each heart and divided into two; tissues were then rapidly frozen in liquid nitrogen before being stored at -80°C for future use.

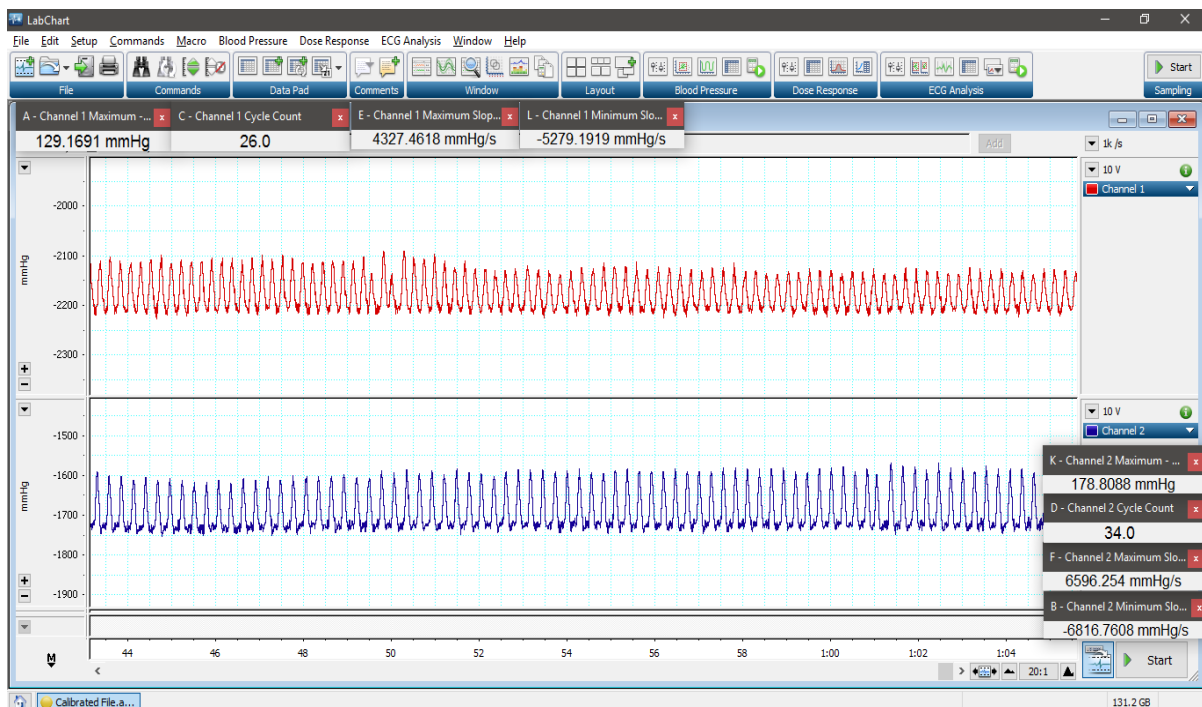


**Figure 3.2.2.2** - A print screen is shown above representing the software used to analyse the different haemodynamic parameters (LVDP, heart rate, + dP/dtmax and – dP/dTmax). The parameters were recorded at timed intervals as mentioned, by stopping the trace and highlighting 6 seconds of data.

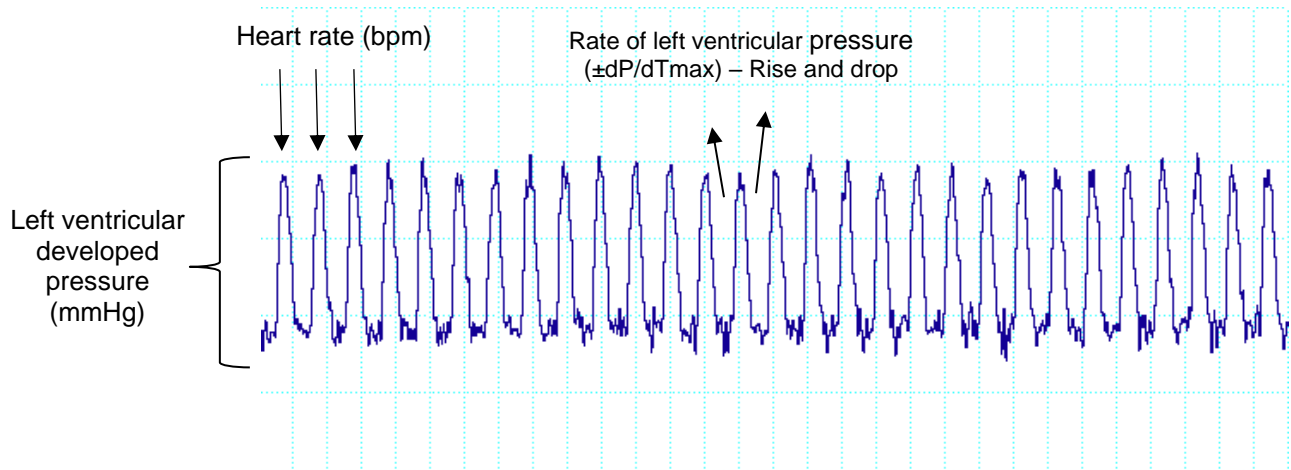


**Figure 3.2.2.3 - Langendorff trace further explained.** Each parameter measured by the software is shown on the trace above.

### 3.2.3 Dose response protocol

To record the haemodynamic parameters, the following protocol was developed and carried out, in order to accurately plot a dose response for the hearts:

- 20-minute administration dose response: The hearts were perfused for 20 minutes with KH buffer, to serve as the stabilisation period for each model. The experimental protocol for each of the inotropes used was then split into a 20-minute cumulative administration, for a total of 140 minutes of increasingly high drug concentrations for all hearts (ranging from 1nM to 30µM, for a total of seven different concentrations); a 20-minute cumulative protocol was chosen based on preliminary data that indicated that it was the adequate time to achieve a steady contractile response with each of the selected inotropic drugs (see figure 3.2.3.1).

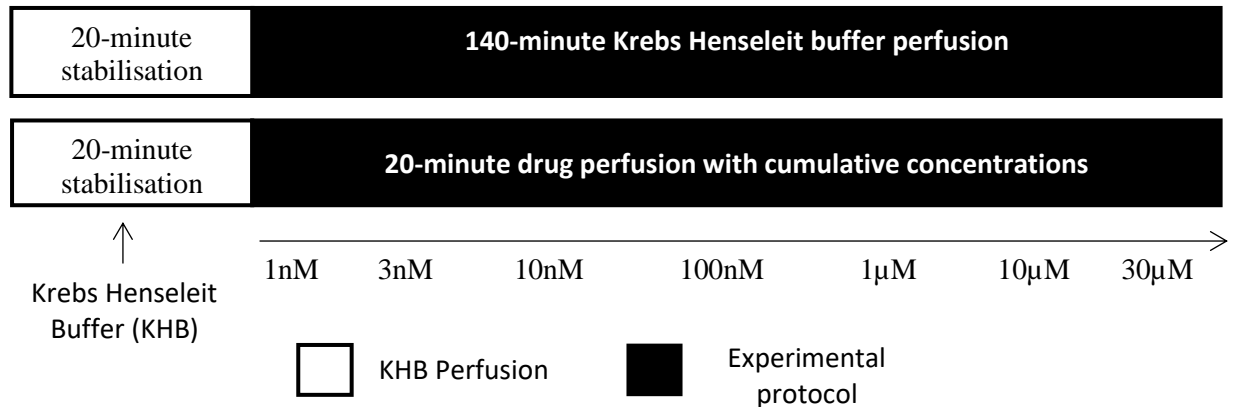


**Figure 3.2.3.1 - Langendorff protocol.** These were the protocols used for the isolated heart models, under base physiological conditions (top) and with our drug treatments (bottom). The hearts were perfused with KHB for a total of 160 minutes. For the inotrope protocol, we administered an increasingly higher dosage every 20-minutes, for a total of 140-minutes of drug perfusion.

### 3.3 Work-Loop and Muscle mechanic studies

The assessment of power output of the papillary muscle of the left ventricle is a proven method to investigate ventricular contractile changes in the heart (Haycraft and Paterson 1896; Marzilli et al. 1980). Based on previous studies, it is therefore known that it is possible to study changes in muscle performance with the use with the work-loop (Layland, Young and Altringham 1995; Layland, J., Young and Altringham 1995; Layland, J. and Kentish 2000). To add to this, previous studies have also shown how it is possible to not only carry out age studies on it (Kiriazis and Gibbs 2000), but compound effects on the muscle capacity to generate instantaneous power as well (Gharanei et al. 2014). Applying this to the models used (aged and HFD) allowed for the assessment of how power generated is affected by physiological factors. For a full background review, please refer to section 1.3.3.

#### 3.3.1 Muscle preparation

Rats were sacrificed by means of cervical dislocation, in accordance with the British Home Office Animals (Scientific Procedures) Act 1986, Schedule 1. The diaphragm was cut to expose the thoracic cavity and the thorax was subsequently opened to expose the heart.

The excised hearts were immediately placed in ice cold modified Ringers buffer (NaCl, 144mM; sodium pyruvate, 10mM; KCl, 6mM; MgCl<sub>2</sub>, 1mM; CaCl<sub>2</sub>, 2mM; NaH<sub>2</sub>PO<sub>4</sub>, 1mM; MgSO<sub>4</sub>, 1mM; Hepes, 10mM; with a pH of 7.4 at room temperature and oxygenated with 100% O<sub>2</sub>) and held in place on a silicone petri dish. This preparation was then placed under a microscope, to dissect the muscle as quickly as possible.

To start, a small incision was made from the apex and around the heart tissue, to expose the papillary muscles. The selection of the papillary muscles was based on structure of the chordae tendinaea (see figure 1.2.3.2 in section 1.2) and its attachment to the walls of the ventricular chamber. Muscles containing branches or smaller muscles attached to them were excluded due to the potential to disturb forces production and recording. The chosen muscles were carefully trimmed and dissected and were then clamped at both the tendon and the ventricular chamber wall by small aluminium foil T-shaped clips. The muscle was left untouched to avoid potential damage. The dissected muscle was then placed on a horizontal chamber in an organ bath with circulating modified Ringers buffer and maintained at 37°C.

### **3.3.2 Contraction studies**

For the actual work-loop protocol, the muscles were set to 95% of their original maximum length (L95%) and allowed a 30-minute stabilisation period. This number was based on a previous paper that optimised the length at which the muscle produces maximum power during length changes (Layland, J., Young and Altringham 1995). Once the L95% was calculated, the work-loop protocol (see figure 2.3.3.1) was carried out at a frequency of 6Hz and a strain amplitude of  $\pm 6\%$  which, again, has been shown to produce the maximum power output in the cardiac muscle (Layland, Young and Altringham 1995).

This protocol was repeated every 5 minutes for a total of 120 minutes (for a total of 24 loops produced per protocol). For the drug treatments, the muscles were allowed a 30-minute stabilisation period before being subjected to 90 minutes of circulating drugs (20µM Atenolol, 10µM Itraconazole, 5µM Dobutamine and 100nM Isoproterenol). Concentrations used for this study were derived from previous publications (Fletcher et al. 2020) and then optimised for this specific study.

At the end of the 120 minutes, the muscle was weighed to the nearest 0.00001g using an electronic balance. Instantaneous power output was calculated for every data point by multiplying instantaneous force generated by instantaneous velocity. This was done for each loop (1863 total data points per loop) and then averaged to generate a net-work value for each instance of a completed loop (Gharanei et al. 2014).

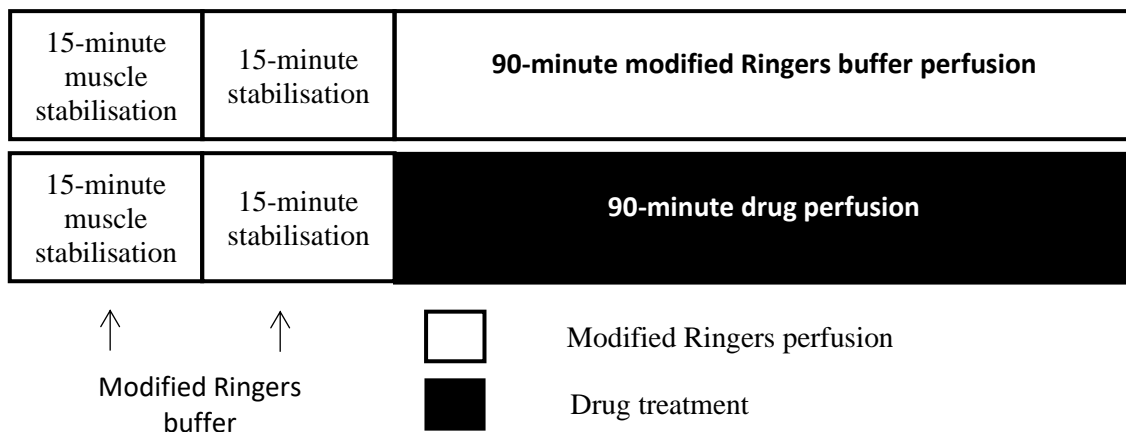


**Figure 3.3.2.1 – Work-loop protocol.** These were the protocols used for the work-loop technique, under base physiological conditions (top) and with drug treatments (bottom). The isolated papillary muscles were perfused with modified Ringers buffer for a total of 120 minutes. For the inotrope protocol, we administered the selected drug treatment for a total of 90-minutes.

### **3.3.3 Muscle length optimisation**

The muscles were also connected to a 50nM force transducer and a high-speed length controller that were later used to stimulate the muscles at a 60-mA amplitude. (Layland, Young and Altringham 1995). The resulting developed force was calculated by subtracting the maximum produced force from the minimum produced force. The optimal muscle length was obtained by gradually increasing the muscle length using a micromanipulator (all products were purchased from Aurora Scientific, Canada) until the maximum developed force was reached (L<sub>max</sub>). Once reached the muscle length was measured with an eyepiece.

### **3.4 Western Blotting**

The concept of protein transfers was first developed in 1979 (Towbin, Staehelin and Gordon 1979), where researchers used autoradiography to visualise and quantify protein contents; however, the term “western blot” did not gain traction until its inception in 1981, as a play on the Southern blot technique (Burnette 1981). Western blotting as we know it today, also known as protein immunoblotting, is a technique based on the principle of electrophoresis, whereby proteins are separated according to molecular weight, and then probed using specific antibodies raised to bind to the protein of interest (Bass et al. 2017; Mahmood and Yang 2012). Membranes probed with antibodies can be visualised using a conjugated secondary antibody, such as HRP-linked, the resultant protein bands can then be quantified using densitometry software. This method provides quantitative means of assessing the molecular mechanisms in various pathological conditions, through the identification of key protein mediators (Mahmood and Yang 2012).

### **3.4.1 Antibodies and reagents used for Western Blotting**

The following antibodies were used: anti-UCP3 antibody and phosphorylated and total Pyruvate Dehydrogenase E1-alpha subunit (S293) purchased from Abcam (UK). Biotinylated protein ladder detection pack, secondary antibodies for anti-biotin and HRP-linked anti-rabbit IgG and glyceraldehyde 3-phosphate dehydrogenase (GAPDH) were all purchased from Cell Signalling, UK. Any KDa and 4-12% Mini-PROTEAN® TGX™ pre-cast gels, Mini-PROTEAN tetra cell, Trans-blot® Turbo™, PVDF membranes and Precision Plus Protein™ Kaleidoscope™ Prestained ladder were all purchased from Bio-Rad Ltd (UK).

### **3.4.2 Tissue Collection for Western Blot Analysis**

Cardiac tissue was collected from each treatment group, as mentioned in section 2.2.3. Approximately half of the left ventricle (50 mg) was homogenized with lysis buffer (100 mM NaCl, 10 mM Tris base - pH 8.0, 1 mM EDTA - pH 8.0, 2 mM sodium pyrophosphate, 2 mM NaF, 2 mM  $\beta$ -glycerophosphate, SigmaFAST™ protease inhibitor cocktail tablets – 1 tablet/100ml and PhosStop™ - 1 tablet/10ml) on a IKA Ultra-Turrax® T 25 basic disperser, set to a speed of 21,500 RPM. This tissue was then centrifuged for 10 minutes at 11,000 RPM at 4°C to obtain the desired supernatant, which was then transferred into clean 1.5ml microcentrifuge tubes. Samples were diluted using Laemmli buffer (250 mM Tris-HCl – pH 6.8, 10% glycerol, 0.006% bromophenol blue, 4% SDS,  $\beta$ -mercaptoethanol – pH 6.8) and incubated at 100°C for 5 minutes before being stored at –20°C. Prior to using the samples, they were defrosted on ice and diluted further using Laemmli buffer to obtain a protein concentration of 50 $\mu$ g, following a concentration response.

### **3.4.3 Protein Quantification using Bicinchoninic Acid Assay (BCA)**

To calculate the protein content of homogenised sample we used a colorimetric Pierce™ BCA Protein assay kit (Thermo Fisher Scientific, UK). Concentrated albumin standards were serially diluted using lysis buffer to obtain a concentration range of 0 - 2000µg/ml. BCA working reagent was prepared following a 50:1 ratio of reagent A and reagent B, respectively. Standards and samples were pipetted at a volume of 10µl, in triplicate, onto a 96-well plate. Following this we added 200µl of working reagent to each well. Plates were then covered to protect from light and incubated for 30 minutes at 37°C, before being left to cool to room temperature. The plate reader was set to 562 nm and the measured absorbance values were then used to calculate the total protein content per unknown sample.

### **3.4.4 Gel Electrophoresis, protein transfer and antibody probing**

The previously collected samples were further diluted using laemmli buffer to obtain a concentration of 50µg/µl. These samples were then centrifuged at 1200 RPM for 2 minutes, at 4°C, before being loaded onto Precast TGX™ (Tris/glycine) gradient gels (Bio-Rad, UK). The gels were then placed inside of a Mini-PROTEAN™ vertical electrophoresis assembly unit before filling the chamber and outer tank with running buffer (14.42g/L Glycine, 1.0g/L SDS, 3.03g/L Tris base). The samples were then loaded into the wells, with at least one well loaded with a molecular protein marker acquired from Cell Signalling UK. Gels were run at 110V for 60 minutes using a Power-PAC 3000 (Bio-Rad, UK). Following electrophoretic separation, the gels were removed from their compartments and placed onto Trans-Blot® Turbo™ transfer packs, consisting of filter paper, buffer and a polyvinylidene fluoride (PVDF) membrane. The assembled cassettes were loaded into the Trans-Blot system (Bio-Rad, UK) and ran for the mixed molecular weight transfer protocol for a total of 7 minutes.

Following transfer, the membranes were cut into two using a scalpel blade. Blots were then incubated at room temperature in blocking buffer (5% w/v milk powder in Tris-buffered saline with Tween 20 (TBST) for 60 minutes on an orbital shaker (Cassambai et al. 2019). Following blocking, membranes were washed three times with TBST, for a total of 15 minutes, before being incubated with primary antibody (5% w/v bovine serum albumin (BSA) in TBST, at a concentration of 1/1000, on a roller shaker at 4°C overnight. The following day, membranes were once again washed three times with TBST to remove any unbound antibody. Blots were then incubated with secondary antibody (anti-rabbit HRP IgG – 1/1000, Cell Signalling, UK) in blocking solution (5% w/v milk powder in TBST) and incubated for 1 hour at room temperature, on an orbital shaker. The membranes were then washed one last time with TBST before being visualised.

### **3.4.5 Visualisation, Densitometry and Quantification**

To visualise the membranes, they were first placed onto an acetate sheet and coated with approximately 1 mL of SuperSignal West Femto kit (Thermo-Scientific), in a 1:1 dilution, to amplify the signals from the membranes. Images were then captured and visualised using a ChemiDoc with the ImageLab™ Touch software (Bio-Rad, UK). Membranes were exposed for 3 to 5 seconds (see representative blot in figure 3.4.5.1) in order to detect the bands corresponding to the proteins of interest. Images were subsequently analysed using the java-based software ImageJ (National Institutes of Health, USA). After visualising the membranes, they were stripped using Restore™ Western Blot Stripping Buffer (Thermo Fisher Scientific, UK) and re-probed for the total form of their respective primary antibody, to be used for normalisation during analysis. GAPDH (Cell Signalling, UK) was used as a loading control for all of the samples used in this project; to this effect, blots were only used if GAPDH stayed the same across the full extension of the blot.

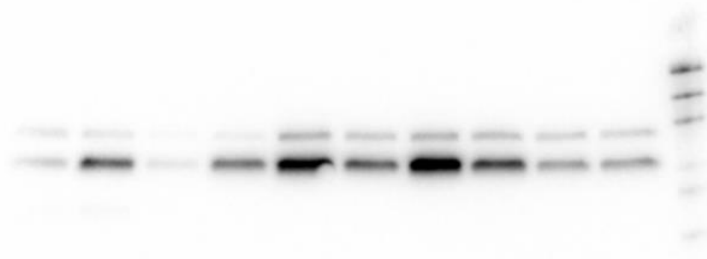


**Figure 3.4.5.1 - Representative western blot gel run.** The first eleven wells contain various samples, while the twelfth well contains a protein ladder.

### **3.5 Compliance with the 3Rs**

Animal research is a controversial topic, with ethical and moral concerns raised often; in an attempt to reassure the population, the principle of the Three Rs was developed: Replace, Reduce and Refine (NC3Rs 2019). For this project, these principles were considered and the models and protocols were adjusted to reflect that; by optimising a cumulative dose control response, a reduction of over 50% in animal usage was achieved, whilst still maintaining the expected levels of scientific integrity and reproducibility.

### **3.6 Statistical Analysis**

Animal body mass and fat pad weight was plotted as average mass/weight  $\pm$  standard error of the mean (SEM) and statistically analysed using One-Way analysis of variance (ANOVA) with Tukey's post hoc test, on IBM SPSS<sup>®</sup> Statistics 25 (IBM Corporation USA). A p value of  $p < 0.05$  was considered statistically significant.

The haemodynamics data was plotted as a percentage of the average stabilisation (first 20 minutes of the run - mean  $\pm$  standard error of the mean (SEM)). Coronary flow was first corrected to reflect the heart weight and then calculated as a percentage of average stabilisation.

For chapters 4 and 5, the Langendorff data was plotted using Microsoft® Excel and statistically analysed using a Two-Way analysis of variance (ANOVA) in order to firstly understand whether there was any interaction between the independent variables (age or HFD and time) and whether they affected the dependant variables (haemodynamic parameters). This was useful for this project, as it showed the degree of tissue viability across the different models. A Tukey's post hoc test was then ran for each time point as a function of each age and HFD group, as it was vital to use a reliable test with a reduced risk of false discovery rate alongside the Two-Way ANOVA, in order to better interpret the data collected. This analysis was done using IBM SPSS® Statistics 25 (IBM Corporation USA). A p value of  $p < 0.05$  was considered statistically significant. For chapters 6 and 7, the Langendorff data was plotted on Origin Pro 2015 (Origin Lab Corporation, USA), as the main focus was on producing the best fit concentration response curve for each of the inotropes used (Dobutamine, Itraconazole, Atenolol and Isoprenaline).

The work-loop data was plotted as a percentage of the average stabilisation (first 30 minutes of the run - mean  $\pm$  SEM). The instantaneous power output was calculated for each loop (1863 total data points per loop) and averaged to generate a net-work value for each instance of a completed loop. Peak forces and power output data were assessed for statistical difference using Two-way ANOVA with Tukey's post hoc test for each time point as a function of each age group and each HFD group, when applicable, on IBM SPSS® Statistics 25. A p value of  $p < 0.05$  was considered statistically significant. The same process was used to analyse the data from the different drug treatments used.

Western blot images were, once captured, analysed using One-Way ANOVA with Fisher's Least Significant Difference (LSD) post-hoc test for each blot (as we were interested in finding the minimum difference between protein expressions), on IBM SPSS® Statistics 25 (IBM Corporation USA). A p value of  $p < 0.05$  was considered statistically significant.

In order to establish high confidence levels, the groups sizes for this thesis were determined based on pilot data (data not shown) and as described in previous studies (Cassambai et al. 2019; Fletcher et al. 2020; Gharanei et al. 2013). The groups were designed to be equal and any loss in sample sizes were from experimental deviations and natural causes of death (please refer back to figure 3.1.1.1 for the Kaplan-Meier survival curve).

### **3.7 Optimised and attempted techniques**

This section will list any techniques attempted but not carried forward due to time and animal limitations. Future studies using these techniques will be discussed in-depth in section 8.2.

#### **3.7.1 Langendorff short administration dose response protocol**

Prior to choosing the mentioned dose response protocol (refer to section 3.2.4), optimisation was necessary to guarantee that an appropriate drug response on the hearts was obtained.

To do that, a short administration dose response was developed alongside the 20-minute dose response used:

Short administration dose response - The hearts were perfused for 20 minutes with KH buffer, to serve as the stabilisation period for each model, using the same reagents and parameters as the ones highlighted in sections 3.2.2 and 3.2.3. The experimental protocol for each of the selected inotropes used was then split into a short administration protocol, using an infusion of 100uL of increasing concentrations (ranging from 1nM to 30µM, for a total of seven different concentrations) directly into the heart, with a very short exposure time of 2 to 5 seconds. Wash-out periods were carried out in-between each dose to allow the heart to return to baseline values.

The data obtained from this technique was then plotted as a concentration response curve, with the baseline values of the heart prior to administration used to plot a % change of the drug response on the measured parameters. Due to time constraints and animal number concerns (as stated in section 3.5), this particular protocol was put aside and the 20-minute administration protocol was given priority. More information on the use of this protocol will be given in section 8.2.

### **3.7.2 Langendorff ECG measurements**

Hearts were perfused for 20 minutes with KH buffer, to serve as the stabilisation period for each model, using the same reagents and parameters as the ones highlighted in sections 3.2.2 and 3.2.3. Following stabilisation, a pair of monophasic action potential micro-hook electrode recorders connected to a Bio Amp (ADInstruments, UK) were placed in both the right atrium and the apex of the heart, in order to record the action potential changes of the heart, in an attempt to investigate the effects of our drugs on the cardiac conduction system. Unfortunately, due to budget and animal number concerns (as stated in section 3.5), this particular protocol had to be put aside but has been added to the future work section (section 8.2), as it is something worth exploring in future studies.

### **3.7.3 Enzyme-linked immunosorbent assay (ELISA)**

#### **Background**

ELISAs came as a necessity due to a lack of options to conduct immunoassays, as the only alternative before them was the use of radioimmunoassay, which carried a severe health risk due to their use of radioactivity (Engvall, Jonsson and Perlmann 1971; Van Weemen and Schuurs 1971).

To this effect, ELISAs use chromogenic substrates that cause observable changes in colouring when in the presence of proteins of interest. This is achieved via the use of specific antibodies designed to bind to said protein of interest. There are many types of ELISA, such as direct ELISA, sandwich ELISA, competitive ELISA and reverse ELISA. The attempted technique for this project was a sandwich ELISA, as we were looking to quantify the activity of PDH and its related phosphatases.

### **Sample preparation and protein assessment**

Following tissue collection and homogenisation (section 3.4.2), the protein content for each sample was determined using the BCA assay (section 3.4.1). A concentration response for Pyruvate Dehydrogenase was determined using the Pyruvate Dehydrogenase (PDH) Profiling ELISA kit (Abcam, UK). A standard curve was prepared as instructed by the assay manufacturer and used to determine the PDH concentrations (pmol b/ml) in protein concentrations of 0.5 mg/ml, 1 mg/ml, 1.5 mg/ml and 2 mg/ml, all groups were run in replicates. A protein concentration of 1.5 mg/ml was then used for subsequent assays.

### **Pyruvate Dehydrogenase ELISA Assay**

Several concentrations of each inotrope (1nM, 3nM, 10nM, 100nM, 1µM, 10µM and 30µM) were assessed in this assay, to determine the effect of each inotrope on the aged and obese models. All samples were prepared as described above and diluted to a final protein concentration of 1.5 mg/ml using Calibrator diluent RD5-55 to a volume of 100 µl. The standard curve sample was also serially diluted with Calibrator diluent according to the manufacturer's instructions.

Microplate strips were washed with wash buffer three times, ensuring that there was no liquid remaining in each well following each wash; following the final wash, the microplate was inverted and blotted on clean paper towels to ensure that the wash buffer had drained from the wells. Primary antibody at 50 µl was then added to each well, except for the non-specific binding (NSB) well, the plate was then sealed and left to incubate at room temperature for 1 hour on an orbital shaker ( $500 \pm 50$  RPM).

Following the incubation period, wells were aspirated and then washed with wash buffer for a total of four times, without allowing the wells to dry before the addition of 50 µl of the PDH conjugate to each well. Standards, unknown samples and control samples were then added at 100 µl per well, both the NSB and zero standard well had 100 µl of the calibrator diluent. The microplate was then sealed once again and incubated at room temperature for 2 hours on an orbital shaker. The wells were once again aspirated and washed four times with wash buffer, before the addition of 100 µl of substrate solution to each well, and a final incubation of 30 minutes at room temperature on an orbital shaker, protected from light. A 100 µl Stop solution was then added to each well to suspend the reaction occurring, observed by a colour change of blue to yellow (figure 2.6.2.1.), the plate was gently agitated to ensure mixing before quantifying.

### **Quantification using a plate reader**

Following cessation of the reaction, the plates were assessed quantitatively using a Bio-Tek plate reader, set to read values at both 450 nm and 540 nm, to account for any corrections, absorbance values from the 540 nm wavelength were compared to the 570 nm wavelength and showed no difference, therefore the 540 nm wavelength was subtracted from the 450 nm absorbance values. The NSB absorbance value was subtracted from all the other values.

A standard curve was then plotted and a line of best fit was determined to enable the calculation of the unknown samples. Samples were duplicated and assayed as an n of 4, where absorbance values did not lie within the range of the individual sample groups, these were discounted in the final determination of the average therefore representing an n of 3/4.

### **3.7.4 Reverse transcription PCR (RT-PCR)**

#### **Background**

Reverse transcription PCR, or RT-PCR, allows the use of RNA as a template. An additional step allows the detection and amplification of RNA. The RNA is reverse transcribed into complementary DNA (cDNA), using reverse transcriptase. The quality and purity of the RNA template is essential for the success of RT-PCR. The first step of RT-PCR is the synthesis of a DNA/RNA hybrid. Reverse transcriptase also has an RNase H function, which degrades the RNA portion of the hybrid. The single stranded DNA molecule is then completed by the DNA-dependent DNA polymerase activity of the reverse transcriptase into cDNA. The efficiency of the first-strand reaction can affect the amplification process. From here on, the standard PCR procedure is used to amplify the cDNA. The possibility to revert RNA into cDNA by RT-PCR has many advantages. RNA is single-stranded and very unstable, which makes it difficult to work with. Most commonly, it serves as a first step in qPCR, which quantifies RNA transcripts in a biological sample.

#### **Reagents utilised**

Reagents for sample preparation, including RNase Zap<sup>®</sup> and RNA Later<sup>®</sup> were purchased from Ambion<sup>®</sup>, ThermoFisher, UK. SYBR Green, dNTPs, PrimePCR pathway plates, GAPDH, PPAR- $\alpha$ , UCP3 and PDH primers were all purchased from Bio-Rad Ltd. (UK).

### **Tissue collection**

Myocardial tissue from the treatment groups (section 3.1) were collected. RNaseZap<sup>®</sup> was used to decontaminate all surfaces before tissue excision. The left ventricle was excised from each heart and divided into two; all tissues were rapidly frozen in liquid nitrogen before storage at -80°C. Tissue was then homogenised in TRIsure reagent (Bioline, UK) for RNA extraction, followed by 5-minute incubation at room temperature for phase separation. Chloroform was added to homogenised tissue (0.2ml/ml of TRIsure) and vigorously shaken for 15 seconds, incubated for 3 minutes at room temperature, then centrifuged (12000 x g, 15 minutes) at 4°C to separate into the different phases; organic phase, interphase and aqueous layer containing RNA. The aqueous layer was used to precipitate RNA, by addition of ice-cold isopropyl alcohol (0.5ml/ml of TRIsure) and incubated at room temperature for 10 minutes. Samples were centrifuged (12000 x g, 10 minutes) at 4°C. The pellet obtained was washed with 75% ethanol (1ml/ml of TRIsure) mixed, and centrifuged (7500 x g, 5 minutes) at 4°C. Pellets were airdried and dissolved in diethyl pyrocarbonate (DEPC)-treated water (10 µl) before analysis of RNA content. The RNA content of each sample was calculated using a Nanodrop One spectrophotometer. 260/280 ratios of 2.0 were assumed to be pure RNA; samples which had low ratios indicative of impurity were discarded and re-done.

### **cDNA synthesis and optimisation**

cDNA was synthesised using 1 µl of the Oligo dT (20) primer kit, 1 µl of premixed dNTP solution (10 mM), 1000 ng or a maximum volume of 8 µl of RNA, with a volume made to 10 µl using DEPC water, following the protocol from Invitrogen. The reaction mix was prepared in RNase and DNase free tubes and denatured at 65°C for 5 mins in a thermal cycler and immediately placed on ice before brief centrifuging (quick spin setting).

Once on ice, mastermix consisting of SuperScript Reverse transcriptase (1  $\mu$ l per reaction), 0.1 M DTT (1  $\mu$ l per reaction) and 5x First strand buffer (4  $\mu$ l per reaction) were used. Samples were vortexed, centrifuged (quick spin setting), and incubated at 50°C for 50 minutes, followed by 85°C for 5 minutes to terminate the reaction, before placing the samples on ice. The cDNA was quantified using a NanoDrop One. Following this, a concentration response was determined for glyceraldehyde 3-phosphate dehydrogenase (GAPDH). cDNA at 1, 3, 10, 30, 50, 80 and 100 ng as well as no template controls (NTC) were prepared in DNase- and RNase-free tubes before being plated into a PCR microplate in triplicate. GAPDH primer (2  $\mu$ l) and SYBR Green (10  $\mu$ l) were added to the cDNA and the volume made up to 20  $\mu$ l using DEPC treated water. Samples were vortexed and centrifuged (quick spin setting) before plating, plates were sealed then briefly centrifuged (quick spin setting) and set up in the PCR machine with: activation at 95°C (2 minute cycle), denaturation at 95°C (5 seconds, 40 cycles), annealing/extension at 60°C (30 seconds, 40 cycles), followed by a melt curve at 65-95°C (5 second cycle). Ct values were analysed and a concentration response curve (not shown) determined 80 ng as optimal. DNA was prepared with SYBR green and DEPC treated water and added to wells pre-prepared with each of the desired primers, with a total volume of 20  $\mu$ l per well. PrimePCR™ pathway plates were used for gene expression analysis. Run files for the plates were obtained from Bio-Rad, which provided the run instructions for the CFX Connect PCR machine (Bio-Rad, UK).

## **Chapter Four: The effects of age on the contractile function of the heart**

Some of the data in this chapter was presented as following:

- **Coventry University PGR Symposium 2016 – Poster presentation**
- **“Working Across Boundaries” HLS Conference 2016 – Poster presentation**
- **Midlands Cardiovascular Research Network Conference 2018 - Abstract**

Manuscripts in preparation which will include part of the data presented in this chapter:

- The impact of a high-fat diet on rat heart contractility, in different aged models  
– *RA Ribeiro, Maddock, H, Tallis, J, Dodd, M, Gharanei, AM – The Journal of Experimental Biology.*

## 4.1 Introduction

Aging is associated with a variety of physiological processes linked to high risk factors of CVD and aged cardiac tissue alterations can occur through a variety of factors such as vascular thickening and stiffness, impaired endothelial function, limited systolic capacity, hypertrophy and fibrosis, among other factors (Cheng et al. 2009; North and Sinclair 2012; Paneni et al. 2017). These changes can lead to negative effects upon the heart, such as systolic and diastolic changes, which cause severe decreases in inotropic and chronotropic cardiac function and eventual heart failure (Hamlin et al. 2004; Norton 2001). A study by Feridooni et al (Feridooni et al. 2017) looked at the exact impact of age and frailty on the ventricular structure of older mice models and used a Langendorff heart study as well as cardiac myocyte isolations and western blotting; Feridooni et al observed that the LVDP was shown to have a sharp decline directly linked to age, with a clear slowdown in heart contractions, as indicated by the  $+dP/dT_{max}$  and  $-dP/dT_{max}$ , as a result of calcium changes; however, the exact mechanisms were not explored. It is possible that these changes also occurred, partially, as a result of energy metabolism changes. This study is particularly relevant as it measured the same parameters as the ones presented in this project.

Several studies have demonstrated that severe changes can occur in the papillary muscle of the heart that are age-dependant. These include changes in shortening velocity in addition to contractile protein activity when comparing different ages of rats from 5, 10, 15 and 20-month year old rat models (Capasso et al. 1986; Nair and Nair 2001). Other studies have observed a potential decrease in muscle shortening and maximal force produced using 6-, 15-, 27- and 32-month-old rats (Kiriakis and Gibbs 2000); in their study, the researchers found that there were significant reductions, in isotonic experiments, on the total work output of the muscles on the 27 and 32-month models.

This reduction was explained to be due to a decrease in muscle shortening and maximal force produced. It is, therefore, obvious that there are severe changes in the heart papillary muscle that are age-dependant. In addition to this, mitral valve insufficiency is another factor that has been proposed to cause alterations in diastolic function in the dysfunctions seen with age, in both human and animal models (Avierinos et al. 2013; Klein et al. 1990; Marzilli, Sabbah and Stein 1980); this is of particular importance due to the role diastolic pressure plays in cardiac flow dynamics and, consequently, on cardiac output (García et al. 2006).

As mentioned in section 1.6, mitochondrial decay is a consequence of age; a fact that makes the conversion of fatty acids (FA) to energy all the more important in aged models (Katz 1988; Nakai et al. 1997). Research has shown that aged hearts catalyses certain mitochondrial reactions, mainly pyruvate decarboxylation, with great efficiency when compared to their younger counterparts (Lloyd, Brocks and Chatham 2003; Moreau et al. 2004). In addition to this, Moreau et al found that the phosphorylation of pyruvate dehydrogenase (PDH) and the pyruvate dehydrogenase complex (PDC) is significantly reduced in old hearts, when compared to young ones (Moreau et al. 2004); this seems to point to a compensatory mechanism to maintain NADH levels, as a result of a switch from FA oxidation to a more glucose-heavy energy production mechanism in the aged heart. Furthermore, aging has been associated with whole body reductions in metabolic rate and energy expenditure (Choksi and Papaconstantinou 2008; Goshovska et al. 2010; Poehlman et al. 1990). These studies also found that uncoupling protein 3 (UCP3) messenger RNA expression not only increased with aging, but also conferred a protective effect to the heart; however, this seemed to be accompanied by decreases in heart contractility (Brand and Esteves 2005; Goshovska et al. 2010; Kühlbrandt 2015).

Younger cells mitochondrial fusion allows for an equal distribution of mitochondria among cells during mitosis and also allows for the selective degradation of damaged ones; however, studies have shown that this process is impaired with age due to a loss of protective mechanisms (Seo et al. 2006; Seo et al. 2008). Some studies have proposed theories as to why this happens, with the currently most accepted one being that mitochondria experience a loss of plasticity with age and that this can be, to an extent, instigated by an age-related ROS production increase and subsequent oxidative stress in the cells (Qiang et al. 2007; Reznick et al. 2007). However, limited research has been undertaken which links ageing, function and intracellular mechanisms which makes these projects all the more important.

The aim of the present study was to examine how the effects of ageing (3, 6 and 18-months) can affect whole heart cardiac functions, isolated muscle contractions and intracellular proteins associated with mitochondrial energetic metabolism. The main hypotheses for this chapter were that **(a)** increasing age will cause a decrease in haemodynamic and metabolic function of the heart, especially on the left ventricular pressure and heart rate and in the phosphorylation levels of PDH and UCP3 and **(b)** a similar effect will also be recorded on the work-loop muscle assay, due to the effect of ageing on muscle fatigue.

The main objectives for this study were: **(a)** to elucidate how age-dependant tissue viability changes can affect the energy metabolism of the heart and how this can impact cardiac contractility and **(b)** to investigate whether there are changes to key mitochondrial energy metabolic agents such as pyruvate dehydrogenase E1- $\alpha$  subunit (PDH) and uncoupling protein 3 (UCP3) as a consequence of ageing.

## 4.2 Materials and Methods

### 4.2.1 Animal Models

Following ethics approval from the host institute, 3-month animals were purchased from Charles River UK Limited (Margate, UK) and received human care in accordance with the guidelines of the British Home Office Animals (Scientific Procedures) Act 1986 (Hollands 1986). For this project, 3, 6 and 18-month models were used due to these ages being representative of a young middle-aged and adult rat; the 3-month animals were used as controls for the studies to compare with the 6 and 18-month groups. The body mass measurements for the animals were as follows: 3-month group (n=11) with an average body mass of  $350\text{g} \pm 3.2$  (SEM), 6-month group (n=10) with an average body mass of  $539\text{g} \pm 15.5$  (SEM) and 18-month group (n=4) with an average body mass of  $794\text{g} \pm 8.4$ (SEM). All animals were sacrificed by means of cervical dislocation, in accordance with the British Home Office Animals (Scientific Procedures) Act 1986, Schedule 1 (Hollands 1986). For more information on the animal models used, please refer to section 2.1.

As mentioned before in section 3.1, for the purposes of this study 3-month rats have been equated, in age, to a human child between 10-18 years, 6-month rats have been equated to a young adult between 20-30 years and 18-month rats have been equated to an older adult between 54-69 years (Andreollo et al. 2012; Capitanio et al. 2016; Jackson et al. 2017; Sengupta 2013). For this study, it was decided that the entirety of the previous published literature would be utilised to define the age groups for this thesis.

#### 4.2.2 Langendorff Isolated Heart Model (full review in section 3.2)

The technique starts with the perfusion of the heart with Krebs-Henseleit buffer (maintained at a constant temperature of  $37^{\circ}\text{C} \pm 0.5$  at a pH of 7.4) and gassed with 95%  $\text{O}_2$  and 5%  $\text{CO}_2$ , by means of cannulating the aorta, in a retrograde fashion, forcing the closing of the aortic valve as a result of a change in pressure. The buffer then passes through a vascular bed before being drawn to the coronary sinus in the right atria. This allows the preparation to be maintained without any fluid filling the ventricular chambers (Skrzypiec-Spring et al. 2007). The Langendorff preparations were run as described in section 3.2.2 and as seen in figure 4.2.2.1, under normal physiological conditions. Measurements for the coronary flow (CF), left ventricular developed pressure (LVDP), heart rate (HR) and the Maximum ventricular pressure increase (+dP/dtmax or MPR) and decrease (-dP/dTmax or MPD) were recorded using a physiological pressure transducer connected to the latex balloon and to a PowerLab (ADInstruments, UK) linked to a PC with LabChart<sup>®</sup> software v7 and the rate pressure product (RPP) was calculated using the function mentioned in section 3.2.2. At the end of the protocol, the left ventricle was excised from each heart and divided into two; tissues were then rapidly frozen in liquid nitrogen before being stored at  $-80^{\circ}\text{C}$  for future use. For a full background review, please refer to section 3.2.

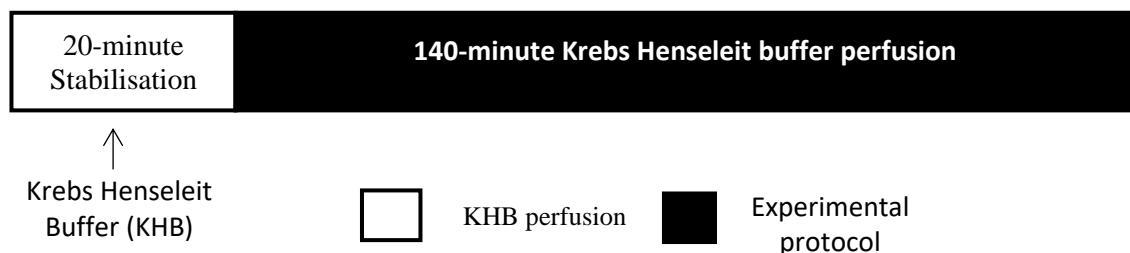


**Figure 4.2.2.1 - Langendorff Protocol.** This was the protocol used for this chapter. The hearts were perfused with KHB for a total run time of 160 minutes.

### 4.2.3 Work-loop Assay (full review in section 3.3)

Following the sacrifice of the animal, the diaphragm was cut to expose the thoracic cavity and the thorax was subsequently opened to expose the heart. The excised hearts were immediately placed in ice cold modified Ringers buffer (NaCl, 144mM; sodium pyruvate, 10mM; KCl, 6mM; MgCl<sub>2</sub>, 1mM; CaCl<sub>2</sub>, 2mM; NaH<sub>2</sub>PO<sub>4</sub>, 1mM; MgSO<sub>4</sub>, 1mM; Hepes, 10mM; with a pH of 7.4 at room temperature and oxygenated with 100% O<sub>2</sub>) and held in place on a silicone petri dish.

This preparation was then placed under a microscope, to dissect the muscle as quickly as possible. Muscles containing branches or smaller muscles attached to them were excluded due to the potential to disturb forces production and recording. The chosen muscles were carefully trimmed and dissected and were then clamped at both the tendon and the ventricular chamber wall by small aluminium foil T-shaped clips. The muscle was left untouched to avoid potential damage. The dissected muscle was then placed on a horizontal chamber in an organ bath with circulating modified Ringers buffer and maintained at 37°C. The muscles were also connected to a 50nM force transducer and a high-speed length controller that were later used to stimulate the muscles at a 60-mA amplitude. (Layland, Young and Altringham 1995). The resulting developed force was calculated by subtracting the maximum produced force from the minimum produced force. The optimal muscle length was obtained by gradually increasing the muscle length using a micromanipulator (all products were purchased from Aurora Scientific, Canada) until the maximum developed force was reached (L<sub>max</sub>). Once reached the muscle length was measured with an eyepiece. For the actual work-loop protocol, the muscles were calibrated to 95% of their original maximum length (L<sub>95%</sub>) and allowed a 30-minute stabilisation period.

Once the L95% was calculated, the work-loop protocol (see figure 4.2.3.1) was carried out at a frequency of 6Hz and a strain amplitude of  $\pm 6\%$  which, again, has been shown to produce the maximum power output in the cardiac muscle (Layland, Young and Altringham 1995). This protocol was repeated every 5 minutes for a total of 120 minutes (for a total of 24 loops produced per protocol). At the end of the 120 minutes, the muscle was weighed to the nearest 0.00001g using an electronic balance. Instantaneous power output was calculated for every data point by multiplying instantaneous force generated by instantaneous velocity. This was done for each loop (1863 total data points per loop) and then averaged to generate a net-work value for each instance of a completed loop (Gharanei et al. 2014). Final data was plotted as total power output and force, and ages were compared as described in section 3.2.1.

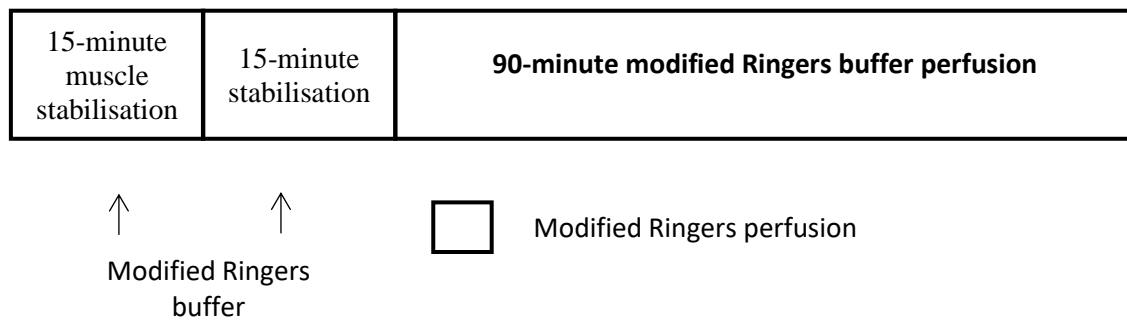


**Figure 4.2.3.1 – Work-loop protocol.** This was the protocol used for this chapter. The hearts were perfused with modified Ringers buffer for a total run time of 120-minutes.

#### 4.2.4 Western Blotting (full review in section 3.4)

Cardiac tissue was collected from each treatment group, as mentioned in table 3.1.2.2. Approximately half of the left ventricle (50 mg) was then homogenized with lysis buffer (100 mM NaCl, 10 mM Tris base - pH 8.0, 1 mM EDTA - pH 8.0, 2 mM sodium pyrophosphate, 2 mM NaF, 2 mM  $\beta$ -glycerophosphate, SigmaFAST™ protease inhibitor cocktail tablets – 1 tablet/100ml and PhosStop™ - 1 tablet/10ml) on a IKA Ultra-Turrax® T 25 basic disperser, set to a speed of 21,500 RPM.

This tissue was then centrifuged for 10 minutes at 11,000 RPM at 4°C to obtain the desired supernatant, which was then transferred into clean 1.5ml microcentrifuge tubes. Samples were diluted using Laemmli buffer (250 mM Tris-HCl – pH 6.8, 10% glycerol, 0.006% bromophenol blue, 4% SDS, β-mercaptoethanol – pH 6.8) and incubated at 100°C for 5 minutes before being stored at –20°C. Prior to using the samples, they were defrosted on ice and diluted further using Laemmli buffer to obtain a protein concentration of 50µg. To calculate the protein content of homogenised samples, a colorimetric Pierce™ BCA Protein assay kit (Thermo Fisher Scientific, UK) was used. Concentrated albumin standards were serially diluted using lysis buffer to obtain a concentration range of 0 - 2000µg/ml.

BCA working reagent was prepared following a 50:1 ratio of reagent A and reagent B, respectively. Standards and samples were pipetted at a volume of 10µl, in triplicate, onto a 96-well plate. Following this, 200µl of working reagent was added to each well. Plates were then covered to protect from light and incubated for 30 minutes at 37°C, before being left to cool to room temperature. The plate reader was set to 562 nm and the measured absorbance values were then used to calculate the total protein content per unknown sample.

The previously collected samples were further diluted using laemmli buffer to obtain a concentration of 50µg/µl. These samples were then centrifuged at 1200 RPM for 2 minutes, at 4°C, before being loaded onto Precast TGX™ (Tris/glycine) gradient gels (Bio-Rad, UK). The gels were then placed inside of a Mini-PROTEAN™ vertical electrophoresis assembly unit before filling the chamber and outer tank with running buffer (14.42g/L Glycine, 1.0g/L SDS, 3.03g/L Tris base). The samples were then loaded into the wells, with at least one well loaded with a molecular protein marker acquired from Cell Signalling UK. Gels were run at 110V for 60 minutes using a Power-PAC 3000 (Bio-Rad, UK).

Following electrophoretic separation, the gels were removed from their compartments and placed onto Trans-Blot<sup>®</sup> Turbo<sup>™</sup> transfer packs, consisting of filter paper, buffer and a polyvinylidene fluoride (PVDF) membrane. The assembled cassettes were loaded into the Trans-Blot system (Bio-Rad, UK) and ran for the mixed molecular weight transfer protocol for a total of 7 minutes. Following transfer, the membranes were cut into two using a scalpel blade. Blots were then incubated at room temperature in blocking buffer (5% w/v milk powder in Tris-buffered saline with Tween 20 (TBST) for 60 minutes on an orbital shaker (Cassambai et al. 2019). Blots were then incubated overnight in 5% w/v bovine serum albumin (BSA) in TBST - 1/1000, at 4°C, with anti-UCP3 antibody and phosphorylated Pyruvate Dehydrogenase E1-alpha subunit purchased from Abcam (UK).

The following day, blots were then incubated with secondary antibody (anti-rabbit HRP IgG – 1/1000, Cell Signalling, UK) in blocking solution (5% w/v milk powder in TBST) and incubated for 1 hour at room temperature on an orbital shaker.

To visualise the membranes, they were first placed onto an acetate sheet and coated with approximately 1 mL of SuperSignal West Femto kit (Thermo-Scientific), in a 1:1 dilution, to amplify the signals from the membranes. Images were then captured and visualised using a ChemiDoc with the ImageLab<sup>™</sup> Touch software (Bio-Rad, UK). Membranes were exposed for 3 to 5 seconds (see representative blot in figure 2.4.6.1) in order to detect the bands corresponding to the proteins of interest. Images were subsequently analysed using the java-based software ImageJ (National Institutes of Health, USA). After visualising the membranes, they were stripped using Restore<sup>™</sup> Western Blot Stripping Buffer (Thermo Fisher Scientific, UK) and re-probed for the total form of Pyruvate Dehydrogenase E1-alpha subunit and GAPDH, to be used as controls for the data.

#### **4.2.5 Statistical Analysis (full review in section 3.6)**

The haemodynamics and work-loop data were plotted as a percentage of the average stabilisation (mean  $\pm$  standard error of the mean (SEM)). Two-Way analysis of variance (ANOVA) was used with Tukey's LSD (least significant difference) for each time point as a function of each age group, for both the Langendorff and the work-loop data. Fisher's LSD was used for the western blot data, as the main interest was in finding the minimum difference between protein expression. A p-value of  $p < 0.05$  was considered statistically significant.

### **4.3 Results**

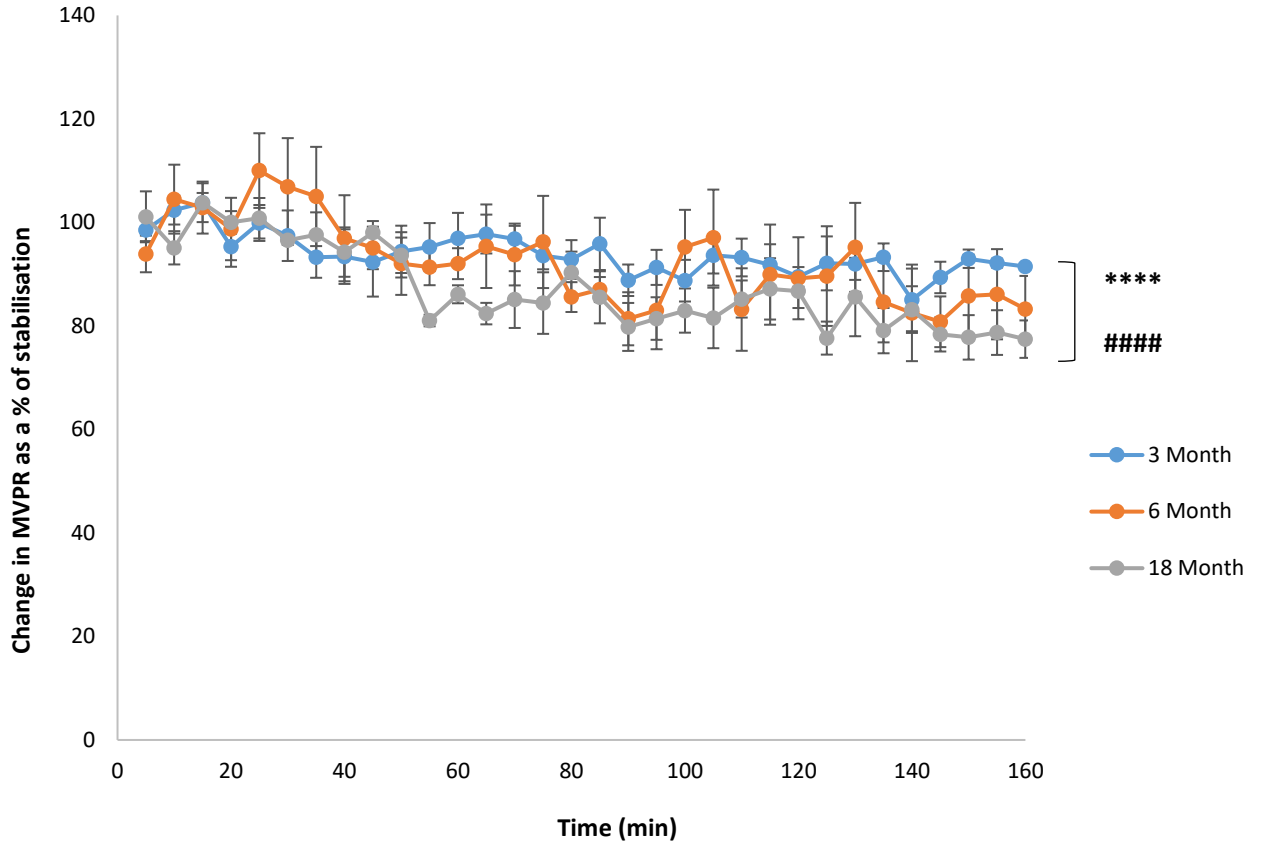
#### **4.3.1 Langendorff Isolated Heart Model**

As explained in section 3.6, a two-way ANOVA was done to confirm the interaction between age and time on the three haemodynamic parameters: maximum pressure rise, maximum pressure drop and rate pressure product. No statistically significant interaction was recorded (p values of 0.69, 0.82 and 0.99, respectively). However, the post hoc tests showed significances in the independent variables of time and age (p values of 0.000 for both MPR and RPP). Following this, analyses was done on performance based on the absolute values for the 6 and 18-month groups when compared to the 3-month group, during the first 20-minutes of the protocol (table 4.3.1.1). This showed significant changes in performance, as the 18-month group generally presented itself with higher average values for the 20-minute stabilisation time, in the calculated rate pressure product –  $p < 0.05$ , when compared to the younger models. Finally, the results were plotted and analysed after normalising them to stabilisation values, as seen in the graphs below.

**Table 4.3.1.1 – Performance assessment of the three age models in the first 20-minutes of the experimental protocol.** The table shows the absolute values of each of the haemodynamic parameters for each age group. The 18-month group shows higher initial numbers for all parameters, but only showed significance on the RPP measurements, when compared to both the 3 and 6-month models (n = 4 for all). No significance was recorded between the 3 and 6-month models (18-month model: \*\*\* = p < 0.001 in relation to the 3-month control; ## < 0.01 and ##### < 0.0001 in relation to the 6-month control).

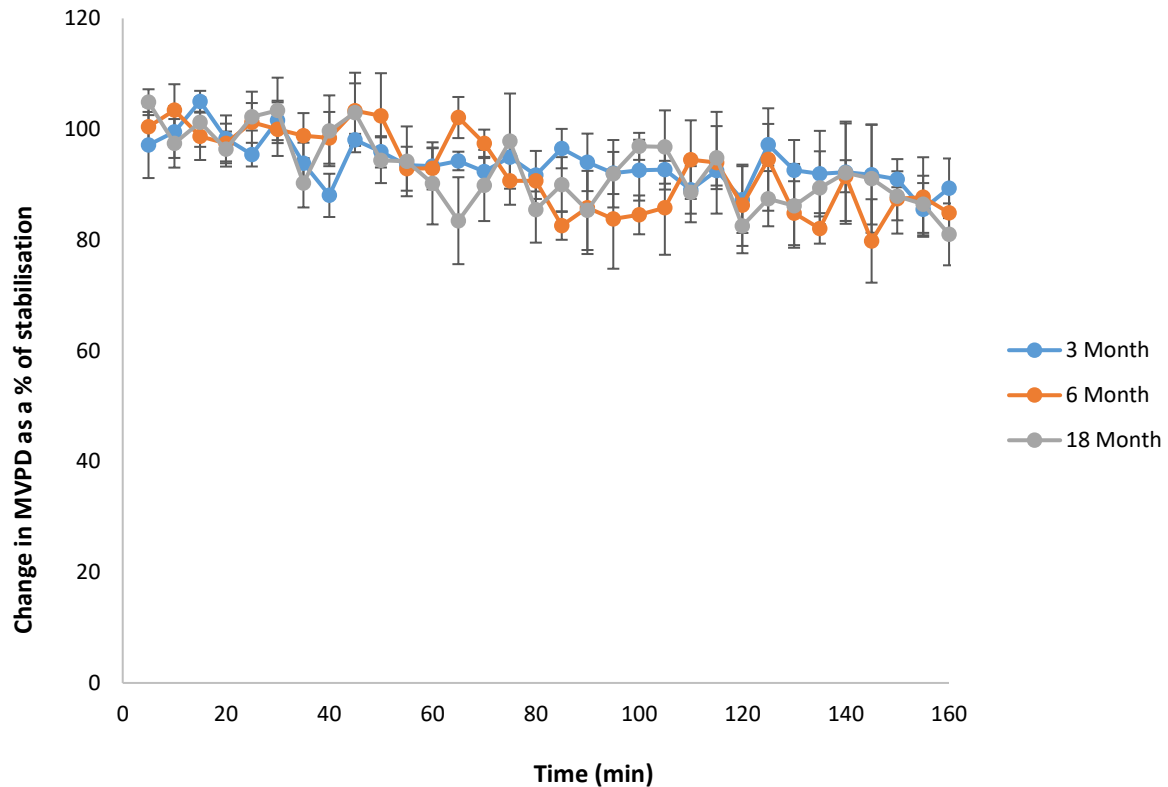
Age group	3-month	6-month	18-month	18-month significance
<b>MPR</b>				
Mean ± SEM	5316.5 ± 260.7	4757.5 ± 55.2	6022.7 ± 636.4	#####
<b>MPD</b>				
Mean ± SEM	-4757.7 ± 457.3	-4686.5 ± 310.1	-5169.5 ± 425.6	##
<b>RPP</b>				
Mean ± SEM	36874.1 ± 2621.4	37188.5 ± 3960.9	51477.9 ± 5847.6	*** #####

Figure 4.3.1.1 represents the rate at which the pressure on the left ventricle of the heart develops, plotted as both a % of the stabilisation time. When looking at the % of stabilisation, the Two-Way ANOVA and the post hoc tests showed a significant effect of ageing on the 18-month tissue viability and performance on the Langendorff isolated heart (-6.4% ± 1.1 (SEM), p<0.0001 when compared to the 3-month controls data and -4.8% ± 1.1 (SEM), p<0.0001 when compared to the 6-month hearts. However, no time-dependant significant effect was recorded between the three age models.



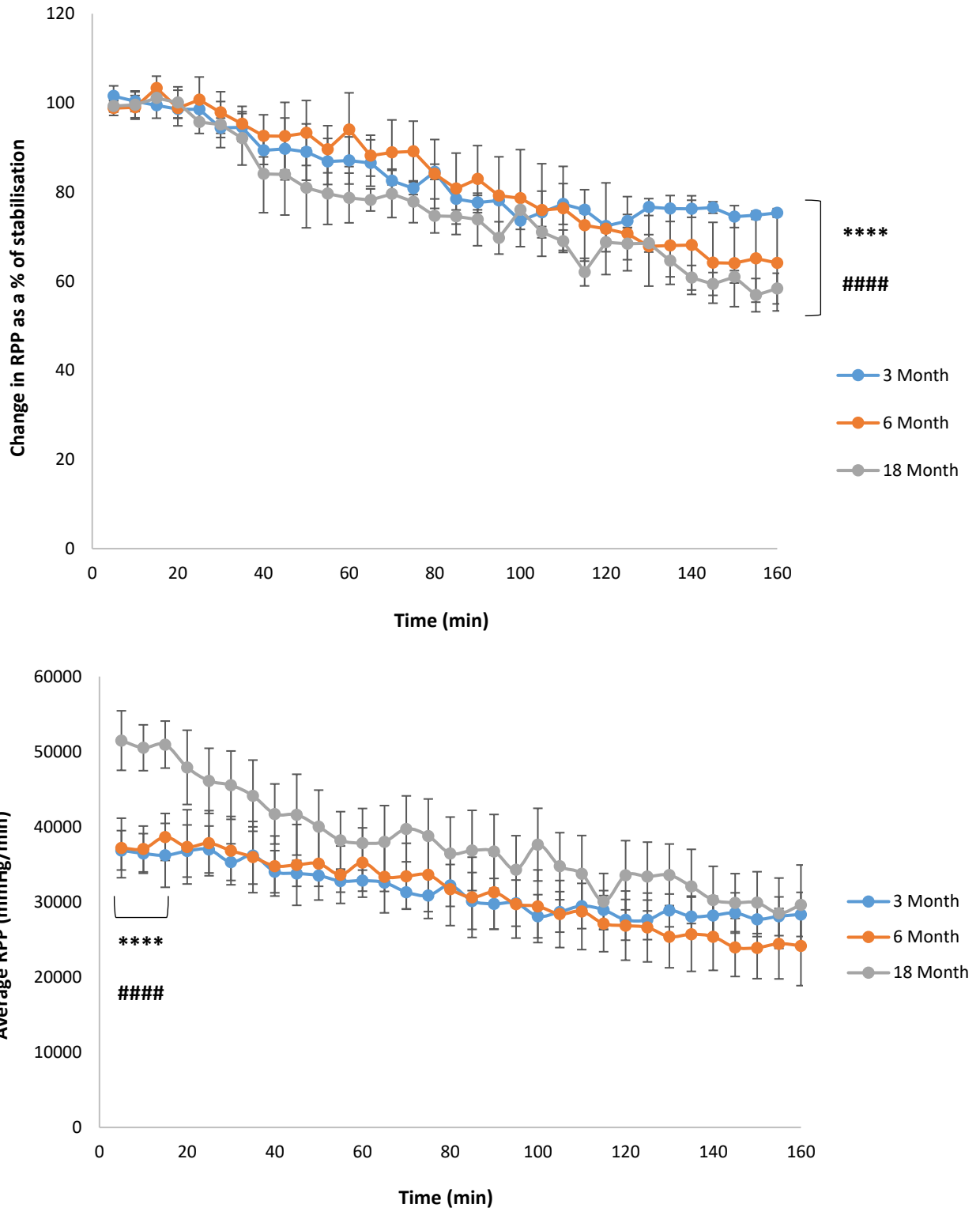
**Figure 4.3.1.1 – Maximum ventricular pressure rise difference amongst rats of age 3-months, 6-months and 18-months (n = 4).** Hearts were allowed a 20-minute stabilisation period and were then subsequently perfused with KH buffer for another 140 minutes. Measurements for maximum ventricular pressure rise are displayed above (18-month model: \*\*\*\* =  $p < 0.0001$  in relation to the 3-month model and #### =  $p < 0.0001$ , in relation to the 6-month model).

Figure 4.3.1.2 represents the rate at which the pressure on the left ventricle of the heart decays plotted as a % of the stabilisation time. When looking at the % of stabilisation, the post-hoc test showed no significant effects of age nor time on tissue viability, when compared between the different aged models.



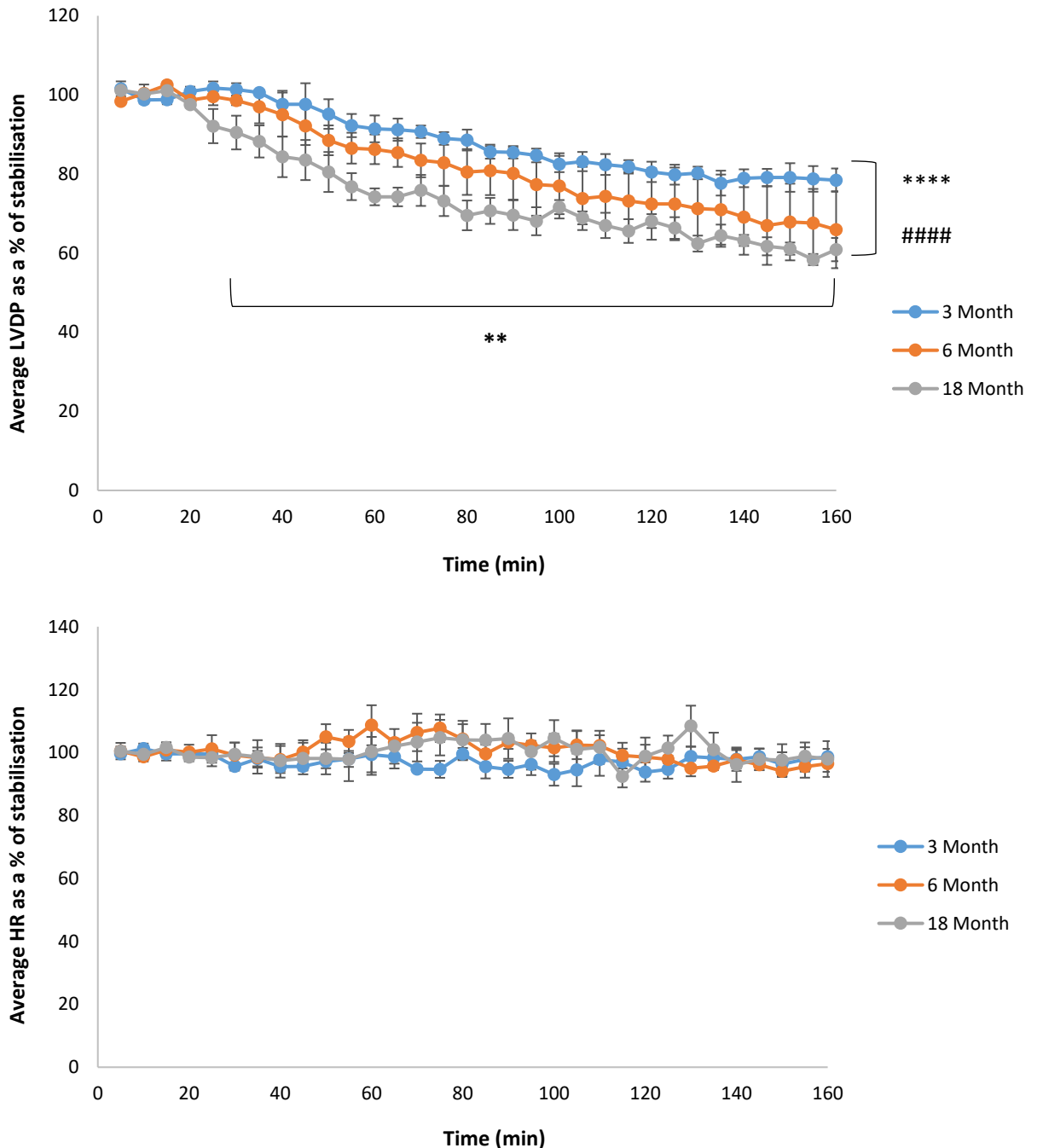
**Figure 4.3.1.2 – Maximum ventricular pressure drop difference amongst rats of age 3-months, 6-months and 18-months (n = 4).** Hearts were allowed a 20-minute stabilisation period and were then subsequently perfused with KH buffer for another 140 minutes.

Figure 4.3.1.3 represents a calculation for the total myocardial workload of the heart, obtained by multiplying the LVDP by the HR, plotted as a % of the stabilisation time. In other words, it represents the stress put on the myocardium per heart rate cycle, plotted as a % of the stabilisation time. When looking at the % of stabilisation, the post-hoc test showed a significant effect of age on the 18-month tissue viability and performance ( $-6.6\% \pm 1.2$  (SEM),  $p < 0.0001$  when compared to the 3-month controls data and  $-6.0\% \pm 1.2$  (SEM),  $p < 0.0001$  when compared to the 6-month hearts). As for the post hoc test for time, it showed no significant effect recorded between the three age models but it did record a similar trend between the three models. As seen by the raw data graph, the 18-month models show a significant difference in the first 15 minutes ( $+14603 \pm 2639.7$  (SEM),  $p < 0.0001$ ), when compared to the 3 and 6-month models; however, a sharper decrease in function was also recorded, which seems to be directly linked to an ageing effect upon the heart.



**Figure 4.3.1.3 – Rate Pressure Product difference amongst rats of age 3-months, 6-months and 18-months (n = 4) – Normalised (top) vs raw data (bottom). To calculate the RPP, the LVDP was multiplied by the HR and a measurement of myocardial workload over-time was obtained for each model. Measurements for the rate pressure product are displayed above (18-month model: \*\*\*\* =  $p < 0.0001$  in relation to the 3-month model and #### =  $p < 0.0001$ , in relation to the 6-month model).**

To calculate the RPP (figure 4.3.1.3), both the LVDP and the HR (figure 4.3.1.4) were taken into consideration, as previously explained. As seen by the graphs, no significance was found for the HR. The LVDP for the 18-month model, however, showed a significant decrease ( $-40\% \pm 2.04$  (SEM),  $p < 0.01$ ) when compared to the 3-month model.



**Figure 4.3.1.4 – LVDP and HR difference amongst rats of age 3-months, 6-months and 18-months (n = 4) – LVDP (top) and HR (bottom).** Hearts were allowed a 20-minute stabilisation period and were then subsequently perfused with KH buffer for another 140 minutes. Measurements for LVDP and HR are displayed above (18-month model: \* =  $p < 0.05$  and \*\*\*\* =  $p < 0.0001$  in relation to the 3-month model and 6-month model: #### =  $p < 0.05$  in relation to the 3-month model).

### 4.3.2 Work-Loop Assay

For this assay, only 3 and 6-month animals were compared. The two-way anova showed a non-significant interaction between AGE\*TIME ( $p$  value = 0.46) but the independent variables were significant, as seen in figure 4.3.2.1, indicated by both a significant interaction between the two ages (Y axis =  $p < 0.05$ ) and on aged tissue viability and performance over-time (X axis =  $p < 0.05$ ). The figure shows the average plots for the power output of the muscles throughout the experimental protocol. A decrease of up to 40% was considered normal and within the pre-defined parameters for the assay, according to previous literature (Layland, Young and Altringham 1995). When comparing between the two models, an initial significant decrease in power output (PO) was recorded for the 6-month model at the 35-minute mark ( $-14\% \pm 1.6$  (SEM),  $p < 0.05$ ). A further significant decrease was observed, at the 60-minute mark of  $-15\% \pm 3.7$  (SEM),  $p < 0.05$ . The peak significant decrease recorded between the two models occurred at the 105-minute mark, at  $-18\% \pm 4.5$  (SEM),  $p < 0.05$ . A significant over-time effect was also recorded, starting at the 35-minute mark and lasting until the end of the protocol ( $-14\% \pm 2.2$  (SEM),  $p < 0.05$ ).

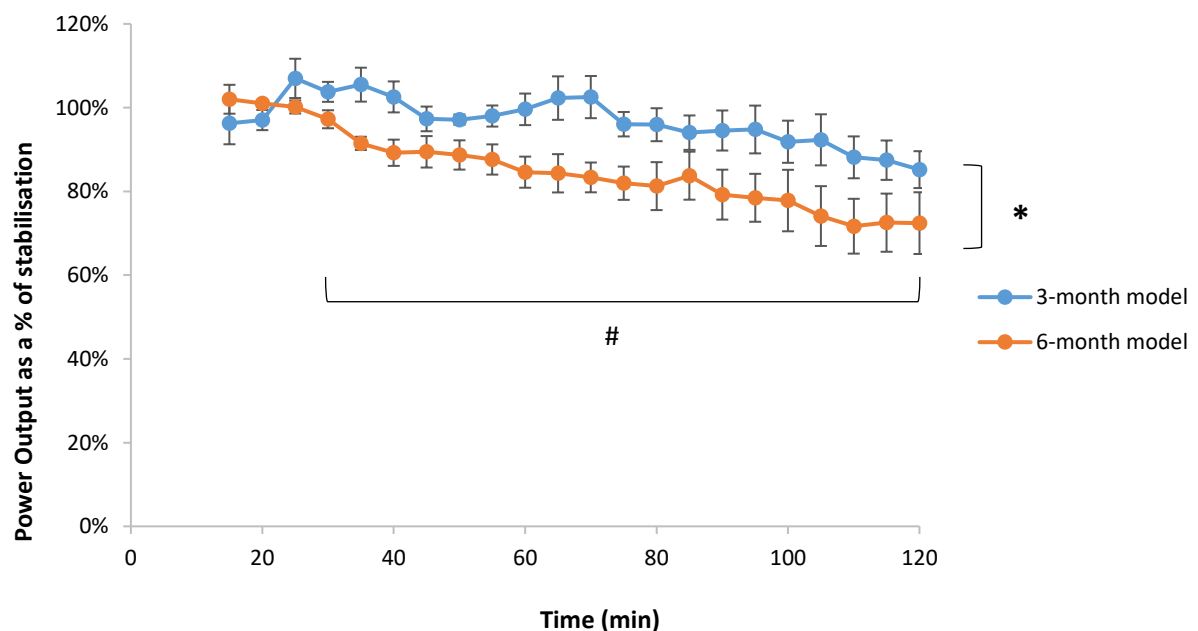


**Figure 4.3.2.1 – Power Output in 3-month ( $n = 7$ ) and 6-month ( $n = 6$ ) age models.** This graph represents the power output produced by the muscle under similar conditions but in two age models. The 3-month model was used as a control (\* and # =  $p < 0.05$ , for direct age comparison and tissue viability over-time comparison, respectively).

The next three graphs (figures 4.3.2.2 to 4.3.2.4) represent the difference in loop shape when comparing between the two age groups, at the 45, 100 and 120-minute marks. They are presented as a plot of force against % length change (or strain). The loops shown are all averages of the work produced by the muscles at certain time points and do not represent the full extent of the experimental protocol, although a pattern was clearly recorded. No change was documented in peak force measurements, based on visual inspection alone (A), indicated by the lack of change in the ascending limb of the loop. An increase was recorded for the passive re-lengthening of the muscles (C) and a consistent decrease in muscle work during shortening (B) and muscle activation rate (D) was also documented, when comparing the 6-month to the 3-month muscle. Finally, a decrease in the total net work done during the loop was recorded throughout the protocol, as indicated by the decreasing total area inside the loop.

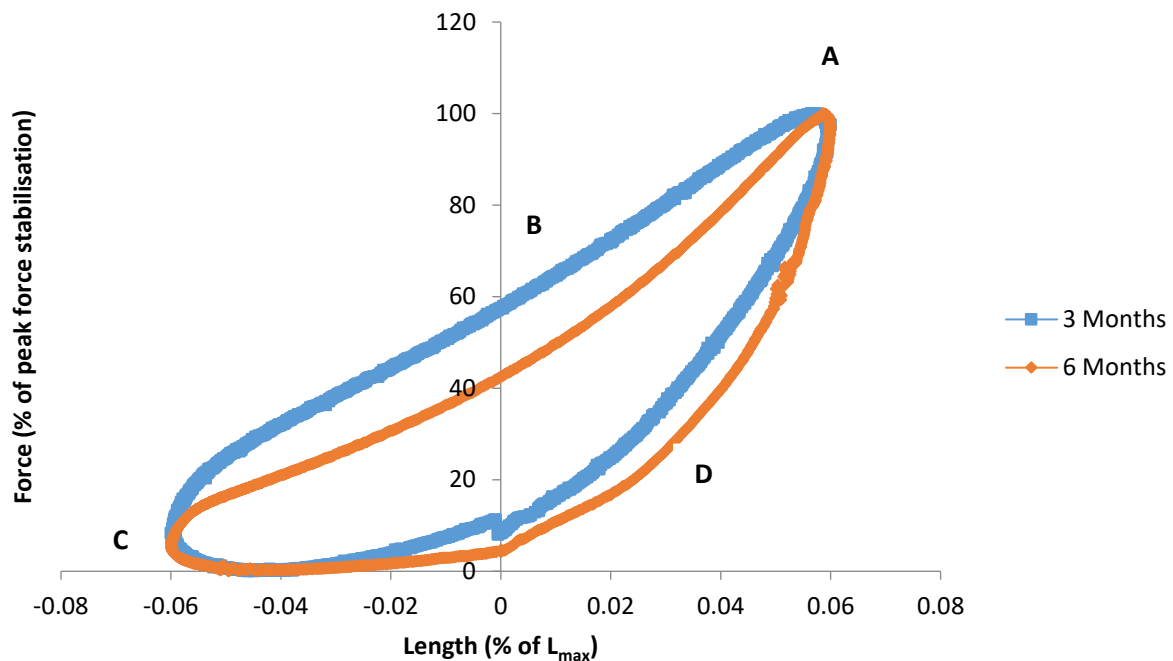


**Figure 4.3.2.2 – Age comparison at 45 minutes.** This graph represents the changes in muscle power at the 45-minute mark of the experimental protocol, when comparing between the two aged models (representative graph only). A = Peak force; B = Muscle shortening. C = Passive re-lengthening; and D = Activation rate.

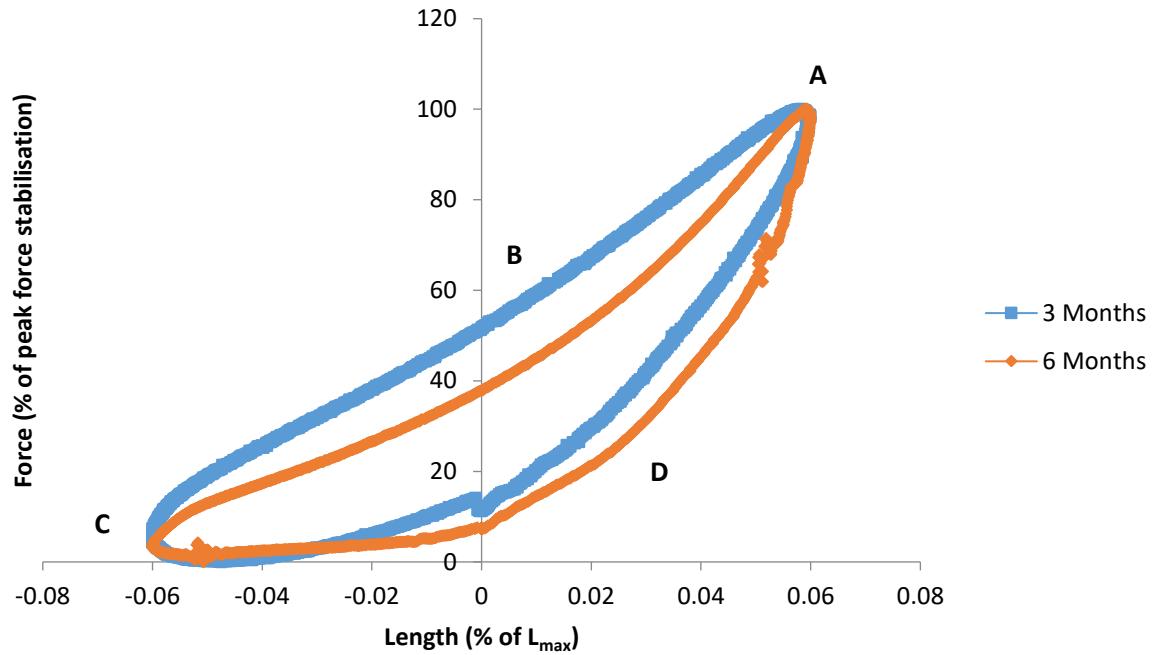


**Figure 4.3.2.3 - Age comparison at 100 minutes.** This graph represents the changes in muscle power at the 100-minute mark of the experimental protocol, when comparing between the two aged models (representative graph only). A = Peak force; B = Muscle shortening. C = Passive re-lengthening; and D = Activation rate.

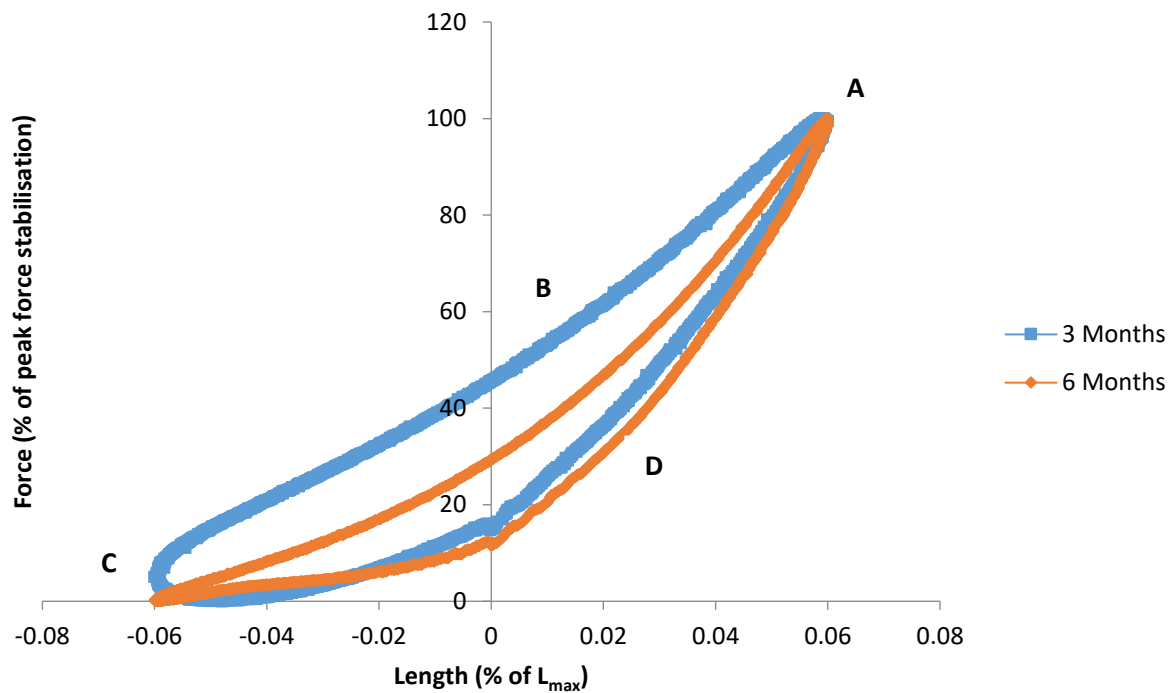
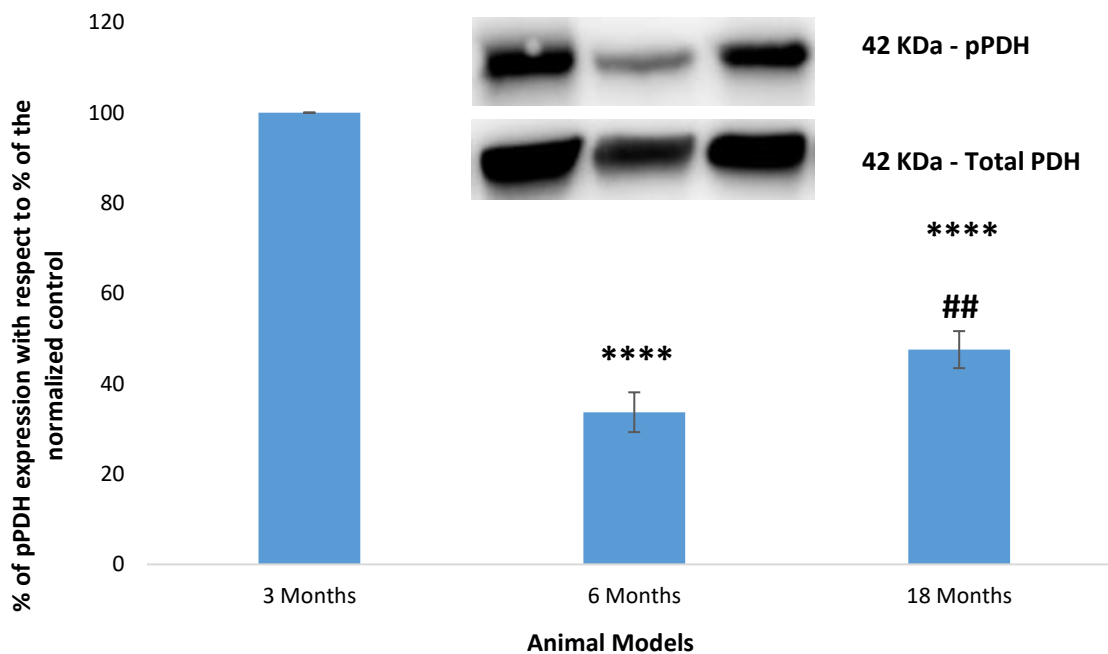


**Figure 4.3.2.4 - Age comparison at 120 minutes.** This graph represents the changes in muscle power at the 120-minute mark of the experimental protocol, when comparing between the two aged models (representative graph only). A = Peak force; B = Muscle shortening. C = Passive re-lengthening; and D = Activation rate.

### 4.3.3 Western Blot

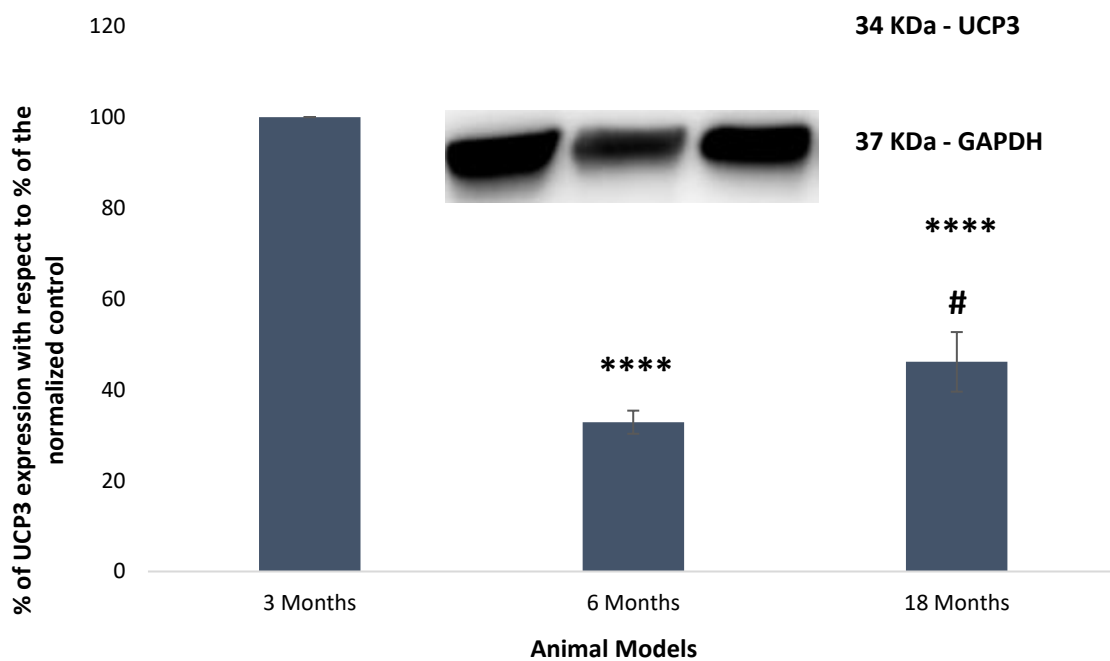
Pyruvate dehydrogenase (PDH) and Uncoupling protein 3 (UCP3) were assessed using western blotting in order to assess the impact of key mitochondrial regulators in cardiac function. All of the represented graphs were plotted after correcting for protein loading and the 3-month controls were normalised.

Figure 4.3.3.1 shows the percentage of phosphorylated PDH in untreated heart tissue as a % of the control and in differently aged rat models, respectively. The 3-month model was used as a control, while the 6 and 18-month models were used as the aged models. As seen by the figure, both the 6 and the 18-month models showed significant decreases in expression when compared to the control, with the 6-month model showing a  $-67\% \pm 4.4$  (SEM) decrease in phosphorylated protein loading ( $p < 0.0001$ ) and the 18-month model showing a decrease of  $-53\% \pm 4.0$  (SEM) in phosphorylated protein loading ( $p < 0.0001$ ).



**Figure 4.3.3.1 – Phosphorylated PDH expression in differently aged models (n = 4 for all).** This graph represents the effects of age on the levels of phosphorylated PDH, as a percentage of total PDH (6-month model: \*\*\*\* in relation to the 3-month model; 18-month model: \*\*\*\* =  $p < 0.0001$  in relation to the 3-month model and ## =  $p < 0.01$ , in relation to the 6-month model). The top blot is a representative image of phospho-PDH, while the bottom blot represents total-PDH. The presented results are all corrected for GAPDH.

Figure 4.3.3.2 shows the percentage of UCP3 in heart tissue as a % of the control and in differently aged rat models. The 3-month model was used as a control and normalised, while the 6 and 18-month models were used as the aged models. As seen by the figure, Both the 6 and the 18-month models were significant decreased when compared to the control, with the 6-month model showing a  $-68\% \pm 2.5$  (SEM) decrease in UCP3 protein loading ( $p < 0.0001$ ) and the 18-month model showing a decrease of  $-54\% \pm 6.5$  (SEM) in UCP3 protein loading ( $p < 0.0001$ ).



**Figure 4.3.3.2 – UCP3 expression in differently aged models (n = 4 for all).** This graph represents the effects of age on the levels of UCP3, as a percentage of GAPDH (6-month model: \*\*\*\* in relation to the 3-month model; 18-month model: \*\*\*\* =  $p < 0.0001$  in relation to the 3-month model and # =  $p < 0.05$ , in relation to the 6-month model). The top blot is a representative image of UCP3, while the bottom blot is a representative image of GAPDH. The presented results are all corrected for GAPDH.

#### 4.4 Discussion and Conclusion

The primary aim of this chapter was to investigate how cardiac function changes in 3, 6 and 18-months animal and how this can alter the mitochondrial energetic metabolism. In this study it was established that the aged models mimicked the old heart (via measures of CF, LVDP, HR, MPR and MPD) and its muscle function (via measures of total work produced by the papillary muscle), as well as key metabolic agents, analysed via western blotting and the hypotheses proposed were confirmed: on the isolated heart model, changes in performance were analysed, based on the absolute values, for the 6 and 18-month groups in comparison to the 3-month group, during the first 15-minutes of the protocol, with significant changes being recorded for both MPR and RPP. When running the papillary muscle performance assay, significant decreases in muscle performance and overall power output between the 3 and 6-month models were observed. Furthermore, the PDH and UCP3 analysis pointed towards a reduced effectiveness in ATP production and synthesis in older models, which has been seen before in previous literature.

Absolute values (figure 3.3.1.1) showed us that while no changes were seen on the MPR and MPD, the 18-month model starting values for RPP were observed to be higher than the 3 and 6-month models; however, it was also observed that a higher rate of decrease in performance when compared to the younger models, a pattern that was also seen when looking at the % of stabilisation, as the aged models (6 and 18-months) showed significant differences, displaying changes in both the cardiac function of the heart (via the RPP calculations) and its power production and regulation. Previous literature has shown that the performance of the heart is diminished with age, especially regarding power output and overall muscle performance.

The most common causes for this include arterial stiffness, changes in calcium modulation, increased wall thickness (Csiszar et al. 2008) and ventricular vascular interactions, such as prolonged myocardial contractions, as a consequence of left ventricular hypertrophy (Csiszar et al. 2008; Lakatta and Levy 2003). This LV hypertrophy is of particular performance and has been linked to an increase in the LV mass because of aging, derived from an increase in myocyte cell volumes, starting at an increase of 53% on the left ventricle of rats aged 3-10 months and increasing to up to 90% in rats between 18-20-month-old. Aging also shows an 18% cell number loss in 12- and 20-month-old rats, followed by subsequent myocardial fibrosis (Anversa et al. 1986; Yin et al. 1982). This decrease in myocyte count has been previously linked to a decrease in left ventricular function, but that was once again not documented in this project. Nonetheless, the RPP traces on both the 6-month and the 18-month models showed a clear decrease in cardiac function when compared to the 3-month model. The addition of more n numbers would have been helpful in confirming this, but with the current data it is possible to extrapolate that a decrease in contractility is definitely present in the aged models. Another important factor in decreased vascular loading of the heart is the decreased effect of  $\beta$ -adrenergic stimulation on the vasculature of the heart. This decrease is commonly associated with a decrease in heart rate but has been mainly tested when comparing between resting heart rate and heart rate during exercise (Lakatta 1993). While a significant decrease in the heart rate of the aged models was not observed throughout the protocol presented in this project, both the LVDP and the RPP (which is calculated using the HR and the LVDP) showed an exacerbated decrease in both the 6-month and 18-month models.

It is therefore proposed that the HR might be the less impactful of the two parameters, when assessing age dysfunction in the heart. Calcium changes have also been documented and aged hearts have shown to not only have limited  $\beta$ -adrenergic stimulation, but also an intrinsic decline in their abilities to increase transient  $\text{Ca}^{2+}$  (Feridooni, Dibb and Howlett 2015; Orchard and Lakatta 1985; Xiao et al. 1994a). This decline has been shown by both Leblanc et al and Nair and Nair in more than one occasion, in both male and female rats of different age groups, which highlighted a clear relation between age and a dysfunction in the L-type calcium channels (Leblanc et al. 1998; Nair and Nair 2001). Based on these results, it is proposed that there may be a potential explanation as to why a decline was recorded in this project, in addition to potential tissue fatigue. Two of the age groups used in most of the old and current studies were rats aged between 6 and 15-months (Capasso et al. 1983; Feridooni et al. 2017); between these two age groups, there was little to no change in mechanical and energetic muscle characteristics. However, in 27- and 32-month-old models, which presented themselves with age related decreases in muscle shortening and contractile protein activity, reductions in peak tension rise and fall, decreases in the resting length-tension relationship (between  $L_{\text{max}}$  and 98%  $L_{\text{max}}$ ) and reductions in ATPase levels (Kiriakis and Gibbs 2000; Wong et al. 2010).

To this effect, the work-loop assay was used as a 2-point verification, showing a clear difference in the performance of the cardiac muscles of the aged model, with a clear decrease in performance after the first 40 minutes of the experimental protocol. The 45-minute mark comparison of the two aged models showed an initial decrease in muscle activation rate, as well as the total work done by the 6-month muscle. This change was consistent throughout the experimental protocol and was applicable to both the 6-month and the 18-month models.

In the study on the papillary muscles, a significant decrease on the 6 and 18-month model was recorded and compared to the 3-month model, which has previously demonstrated in studies that showed significant differences between the work produced by a 6-month animal and the work produced by a 27-month animal (Capasso et al. 1983; Capasso et al. 1986; Kiriakis and Gibbs 2000), a change that has its proposed origin on a significant decrease in muscle shortening as a function of load between each age group, which was not confirmed in the presented work-loops but recorded in the isolated hearts, via changes to  $dP/dt_{max}$ .

To follow up on this, Capitanio et al investigated the proteomics and protein expression in young and aged rat models (Capitanio et al. 2016) and found that certain contractile and structural proteins are altered older rats when compared to younger ones, such as an isoform of myosin binding protein C (Mybpc3), which when lowered have been shown to have a negative effect on the contractility of the heart (Cheng et al. 2013). In addition to this, Capitanio et al also found that the Acyl-CoA synthetase family was significantly reduced in aged rats; this metabolic protein is linked to fatty acid oxidation and its reduced expression has been previously proposed to be linked to a reduction in ATP production, with a consequent reduction in available energy for cardiac contraction (Chakravarti et al. 2008). This study was incredibly useful, as it established that there is a decrease in ATP productions mechanism in the hearts of aged models, which was originally proposed in the aims section and will now be further discussed.

There is a lot of work published on the mechanical and energetic effect of cardiac overload in aged models; however, there is very limited work on the energetic consequences of aging on the myocardium. It is commonly known that old age is directly associated with not only a prolongation of the contractile duration of the heart, but also a reduction in force generation by the heart muscles (Capasso et al. 1983; Froehlich et al. 1978).

It is suggested that pyruvate and fatty acid uptake declines in aged models, which causes a shortage of the fuel necessary for ATP production (Lesnefsky, Chen and Hoppel 2016; McMillin et al. 1993); however, the ATP levels in the heart have not always been reported to decrease as expected of the aged models, with an increase in glucose oxidation being the most suggested explanation behind this (Barton et al. 2016; McMillin et al. 1993). As the pyruvate dehydrogenase complex (PDC) is known to be involved in this process, it is theorised that it plays a role in the compensatory mechanism of the aged heart (Moreau et al. 2004). Researchers found that the PDC was heavily related to a compensatory mechanism involving an increase in NADH levels and the enzymes responsible for producing it and that this accounted for the marked increase in glucose-derived pyruvate measured in both young and aged hearts (Moreau et al. 2003; Moreau et al. 2004; Nakai et al. 1997). These studies found that adaptive changes in the PDC kinetics had an effect on PDH and this is the core of the adaptive mechanism often observed in aged heart models. A study conducted by Chuffa et al found that PDH expression was significantly reduced in older rats when compared to younger ones, alongside other biomarkers of the glycolytic pathway, which led to a measurable reduction in energy generation and myocardial contractility in aged rats (Chuffa, Luiz Gustavo de Almeida and Seiva 2013). In addition to this, Hyyti et al have shown that age reduces fatty acid oxidation and favours glucose oxidation. Due to effects of PDH on glucose regulation, it is likely that this is the reason for an increase in its expression in aged rat hearts (Hyyti et al. 2010).

Research shows, to this day, conflicting evidence in regard to PDH expression and its effects in the aged heart, as seen in the discussion above. In this study, PDH did change with age, but a decrease in active PDH on the 6-month models was recorded, followed by its increase in the 18-month models, albeit still lower than the 3-month controls.

UCPs are known to mediate proton leaks and can change the mitochondrial membrane potential (Bellanti et al. 2013). Studies have shown that depressed heart function in aged hearts is associated with increased oxygen costs and decreased membrane potential, as well as increased proton leaks; it is also known that UCP3 mRNA levels tend to increase in aged models (Goshovska et al. 2010). All of this combined leads to a reduction in mitochondrial efficiency in aged tissue, and a shift to glycolysis as a source of ATP production, which directly correlates with what was shown in this thesis (Bellanti et al. 2013; Edwards et al. 2003). Studies have also shown that UCP3 decreases in abundance in the mitochondria of aged hearts, due to the mentioned shift from fatty acid oxidation to a more carbohydrate-based metabolism (Hilse et al. 2016; Hilse et al. 2018). This study has shown that UCP3 is decreased in an age-dependant fashion, which carries significant impact in fatty acid oxidation rates due to its role as a fatty acid anion transporter.

It is therefore proposed that there is a dependence of glucose oxidation in younger and older rats, while in middle aged rats that is not the case and there is a preference for fatty acid oxidation, which also explains the observed increase in phosphorylated PDH levels, as was mentioned before. The UCP3 levels are also align with this hypothesis, but based on the results collected, it is likely that they are less impactful in the overall fatty acid oxidation process in age and other metabolic agents might take precedence in facilitating this process.

There are, however, some concerns amongst the scientific community regarding the mRNA expression of UCP3 vs its protein expression (Pecqueur et al. 2001; Rupprecht et al. 2012; Rupprecht et al. 2019), due to the fact that UCP3 has an upstream open reading frame, or UORF (Hurtaud et al. 2006). UORFs are mRNA elements that can, in certain conditions, cause a reduction in protein expression by up to 80% (Calvo, Pagliarini and Mootha 2009), which makes UCP3 a very difficult protein to reliably investigate.

It is therefore important to continue the investigation on this mitochondrial agent as much as possible, in order to widen the understanding of its pathways and regulators and how age can impact its expression.

#### **4.5 Summary, limitations and final comments**

This project established the aged data for cardiac function and added important contributions to the current literature on the subject. It has been established that the cardiac function of the heart is diminished with age, showing severe decreases in the 6 and 18-month aged models; in addition to this, it was also shown that the muscles of the heart suffer severe drops in performance as an effect of ageing and that this translates to reductions in power output and total net-work done by the muscles of the 6 and 18-month models. Finally, alongside previous literature and the original hypothesis for this study, it was shown that ATP production is impaired with age and that both PDH and UCP3 are key agents in this effect and that their changes in expression are, to an extent, behind the overall decreases in overall contractile performance.

Limitations for this project include the limited n numbers due to animal housing issues and due to the fact that many of the 18-month animals did not survive until they were ready to be sacrificed. In addition to this, female rats were not tested and previous research has shown that male and female rats express different genes and female rats have actually shown significant decreases in overall cardiac function and structure in an age-dependant fashion, which is a phenomenon that has not always been observed in male rats (Fannin et al. 2014). No investigation was done on the main cardiac contractility related proteins, like the  $\alpha$  and  $\beta$ -myosin heavy chains, cardiac troponin T, C and myosin binding protein C, as it was decided from the beginning to focus on the energy metabolism of the heart.

In addition, for the study on the contractile function of the heart to be more comprehensive, the mentioned proteins should be considered for future studies. In addition to this, investigating the mRNA levels of PDH, PPAR $\alpha$  and UCP3 would have been useful to complement the western blot results, as it would show whether there are gene expression changes directly or indirectly tied to the protein levels; for UCP3 this would be of particular importance due to previously published discrepancies between protein and mRNA levels.

The next chapter will focus on investigating how obesity induces changes in the contractile function of the heart, in differently aged models, and how it can cause changes in the expression of both PDH and UCP3.

# **Chapter Five: The effects of high fat -diet- induced obesity on the contractile function of the heart**

Some of the data in this chapter was presented as following:

- **Coventry University Symposium 2016 – Poster presentation**
- **“Working Across Boundaries” HLS Conference 2016 – Poster presentation**

Manuscripts in preparation which will include part of the data presented in this chapter:

- The impact of a high-fat diet on rat heart contractility, in different aged models  
– *RA Ribeiro, Maddock, H, Tallis, J, Dodd, M, Gharanei, AM – The Journal of Experimental Biology.*

## 5.1 Introduction

The cardiovascular dysfunction often associated with obesity results from a remodelling that occurs via different cardiac and metabolic mechanistic alterations (Alpert et al. 1995; Eckel, Grundy and Zimmet 2005; Lavie et al. 2013; Trayhurn and Wood 2004), as mentioned in section 1.2.2; however, it can be linked to three main factors: the first one is cardiac lipotoxicity (Drosatos and Schulze 2013; Ren et al. 2010), nitric oxide (NO) changes, which play an active role in cardiac contractility and have been shown to cause reduced contractile responses to  $\beta$ -receptor stimulation (Dawson et al. 2005) and inflammation, which can influence left ventricular function through adipokines and inflammatory markers, to name a few (Csiszar et al. 2008; Trayhurn and Wood 2005). This dysfunction can manifest as various morphological and, consequently, haemodynamic alterations, with the most impactful one being translated as an increase in ventricular mass and wall thickness (Avelar et al. 2007). This is of particular importance due to its impact on the cardiac contractile function of obese hearts via changes to the LV preload and afterload, increases in LV stroke work and abnormal changes to the LV end-diastolic pressure (Berkalp et al. 1995; Haggerty et al. 2015; Liu, X. et al. 2016; Messerli et al. 1982). It is therefore clear that obesity can cause severe functional and mechanistic changes to the heart; thus, it is paramount to understand how this happens, in order to potentially develop therapies to counter it.

The combined effects of obesity and age have been studied in the past (Alpert et al. 2018; Hyyti et al. 2010; Qiang et al. 2007); in addition, obesity in the elderly is a very serious concern due to its increasing prevalence in the general population (Gregg and Shaw 2017; Tremmel et al. 2017; WHO 2020). Previous studies have shown that obesity shares similarities with ageing due to its effects on metabolic dysfunction as a direct result of measurable increases in oxidative stress and consequent apoptosis and telomere shortening (Niemann et al. 2011).

It is known that ATP dysfunction in obesity comes as a result of increased fat mass and studies have identified common functional genes and biomarkers in both obesity and ageing, such as the p53 protein (Edwards et al. 2007; Yokoyama et al. 2014); in addition to this, studies have also shown that white adipose tissue in obese patients shows hypoxic traits which can exacerbate the already decreased O<sub>2</sub> supply in aged tissues (Dodd et al. 2018; Valli, Harris and Kessler 2015; Ye et al. 2007). As seen in previous literature, cardiac function changes at both a cellular and molecular level; these changes have been observed in cardiac myocytes of both obese and lean animals in different age models, by first stimulating the cells with a frequency of 0.5 Hz and measuring the changes in cell length, peak shortening, velocity of shortening and relengthening, time to peak shortening and time to 90% relengthening and then measuring intracellular Ca<sup>2+</sup> and the levels of active AKT; it was concluded that there was a significant reduction in the velocity of the lengthening and shortening of the cardiomyocytes, as well as a reduction in their peak shortening and an increase in time to 90% relengthening, which together caused an overall reduction in contractile function via changes in the levels of phosphorylated AKT and changes to the handling of intracellular Ca<sup>2+</sup> (Ren et al. 2010).

Studies have also shown that there are several associations between cardiac dysfunction and mitochondrial functional changes, mostly in ATP production, respiration and biogenesis and signalling pathway alterations (Boudina et al. 2005; Boudina and Abel 2006; Boudina et al. 2007). Finally, in the previous chapter it was established that there was an age-dependant decrease in contractility linked to changes in the expression of key elements (pyruvate dehydrogenase and uncoupling protein 3) involved in mitochondrial regulation, which aligns with all of the previously mentioned literature (Boudina et al. 2012; Crewe, Kinter and Szweda 2013; Finck 2007; Moreau et al. 2004; Pohl et al. 2019).

Previous studies have proposed that there is a relation between cardiac contractile dysfunction, FA uptake and FA oxidation in obesity, with a common link in myocardial lipid accumulation (Christoffersen et al. 2003; Drosatos et al. 2011; Drosatos 2016; Szczepaniak et al. 2003). This FA oxidation change is, to an extent, known to be regulated by mitochondrial uncoupling, as well as the pyruvate complex (please see sections 1.6.2 and 1.6.3, respectively, for an in-depth review of these two mitochondrial agents). A study showed the effects of pyruvate on the heart and it was concluded that there was an impairment in the PDHc, as well as reduced oxidative mitochondrial capacity, which led the researchers to conclude that FAs induce uncoupling in obese hearts, usually accompanied by a severe reduction in ATP production (Boudina et al. 2005). Studies have also recently risen to support these findings. In one case, a team of researchers found that deleting specific PDH genes and restricting glucose oxidation led to cardiac complications mimicking those of a cardiomyopathy, in the form of diastolic dysfunction and cardiac hypertrophy (Gopal et al. 2018). These conclusions agree with other studies that have shown how PDH activity is directly linked to glucose oxidation rates and how changes to any of these pathways leads to cardiac defects (Lydell et al. 2002; Sheeran et al. 2019; Sun et al. 2015).

UCP3 is known to be regulated by PPAR $\alpha$  in aged hearts and to be expressed in the presence of increased free FA conditions (Stavinoha et al. 2004; Young, M., Patil et al. 2001). Studies have proposed that increases in FA mitochondrial fluxes can lead to the activation of UCP3 (Boudina et al. 2005), a hypothesis that has been linked to increased generations of superoxides, compounds directly linked to UCP activation (Echtay et al. 2002). Studies have also shown a reduction in the cardiac function of obesity-related diabetic hearts, usually accompanied by a mitochondrial ROS increase (Boudina and Abel 2006; Boudina et al. 2007).

In these studies, researchers established that UCP3 seemed to play a protective role, suggesting that UCPs can, under certain conditions, work as protective mediators against ROS production and against triglyceride accumulation within the mitochondria, further showing an antioxidant protection against FAs (Goglia and Skulachev 2003; Schrauwen et al. 2002). Other researchers, however, have disproved this hypothesis, by claiming that no correlation exists between the UCP3 levels and ROS production (Goglia and Skulachev 2003; Hilse et al. 2018; Shabalina and Nedergaard 2011). Regardless of this, it has been clearly established that UCP3s function as markers of FA oxidation and it can, therefore, be used as a criterion for heart dysfunction and cardiomyocyte changes (Hilse et al. 2016). It is also clear that the mechanism behind UCP3 is not fully understood and it is therefore imperative that more work is done to better understand how it affects FA metabolism.

The aim here was to investigate the independent effects of HFD and the synergistic effects of age (6- and 18-months) and HFD on whole heart cardiac functions, isolated muscle contractions and intracellular proteins associated with mitochondrial energetic metabolism. The main hypotheses for this chapter were **(a)** that HFD will cause a decrease in overall cardiac and muscular functions, and this effect will be aggravated at 18-months and **(b)** that the combined effect of age and obesity will also cause significant impairment in muscular power output and a decrease in the phosphorylation levels of PDH, due to its vital function in glucose metabolism, and an increase in UCP3, due to its function as an obesity marker.

The main objectives for this study were: **(a)** to assess whether the isolated heart and the work-loop models can be used to evaluate cardiac contractile function in the presence of high-fat diet-induced obesity **(b)** to determine the synergistic effect of ageing and HFD in order to investigate how it can affect the energy metabolism of the heart and **(c)** to investigate whether these changes occur as a result of metabolic changes to the pathways involving pyruvate dehydrogenase E1- $\alpha$  subunit (PDH) and uncoupling protein 3 (UCP3).

## 5.2 Materials and Methods

### 5.2.1 Animal Models

Following ethics approval from the host institute, 3-month animals were purchased from Charles River UK Limited (Margate, UK) and received human care in accordance with the guidelines of the British Home Office Animals (Scientific Procedures) Act 1986 (Hollands 1986). Animals were aged in cages of 3 to 5 individuals, in 12h light and dark cycles at around 50% relative humidity. The diets used in this project were the same as the ones seen in a recent study published by Messa et al (Messa et al. 2020) and their caloric composition were as follows: (**STANDARD CHOW**): protein 17.5%, fat 7.4%, carbohydrate, 75.1%; gross energy 3.52 kcal.g<sup>-1</sup>; metabolizable energy 2.57 kcal.g<sup>-1</sup> (CRM(P) SDS/Dietex International Ltd, Whitham, UK) and (**HIGH FAT DIET**): protein 18.0%, fat 63.7%, carbohydrate, 18.4%; gross energy 5.2 kcal.g<sup>-1</sup>; metabolizable energy 3.8 kcal.g<sup>-1</sup> (Advance protocol PicoLab, Fort Worth, USA). All of the animal groups were given *ad libitum* access to their respective diet and water and feeding began 16 weeks prior to starting the experiments. For the 6 and 18-month lean and high-fat diet groups, animals were divided into randomized sample sizes of 60 and 80 Sprague-Dawley male rats, respectively. For the 6-month group, 30 were given standard chow *ad libitum* (average body mass of 539g ± 15.5 (SEM)) and the other 30 were given the high fat diet *ad libitum* (average body mass of 638g ± 7.2 (SEM)). For the 18-month group, 40 were given standard chow *ad libitum* (average body mass of 793g ± 8.4 (SEM)) and the other 40 were given the high fat diet *ad libitum* (average body mass of 930g ± 10.5 (SEM)). The body mass measurements of the animals were measured bi-weekly (see figure 5.2.1.1 and table 5.2.1.1) and both the mesenteric and epididymal pads were weighed (see table 5.2.1.1) after the sacrifice of the animals to provide a two-step verification in their body mass difference (Woods et al. 2003).

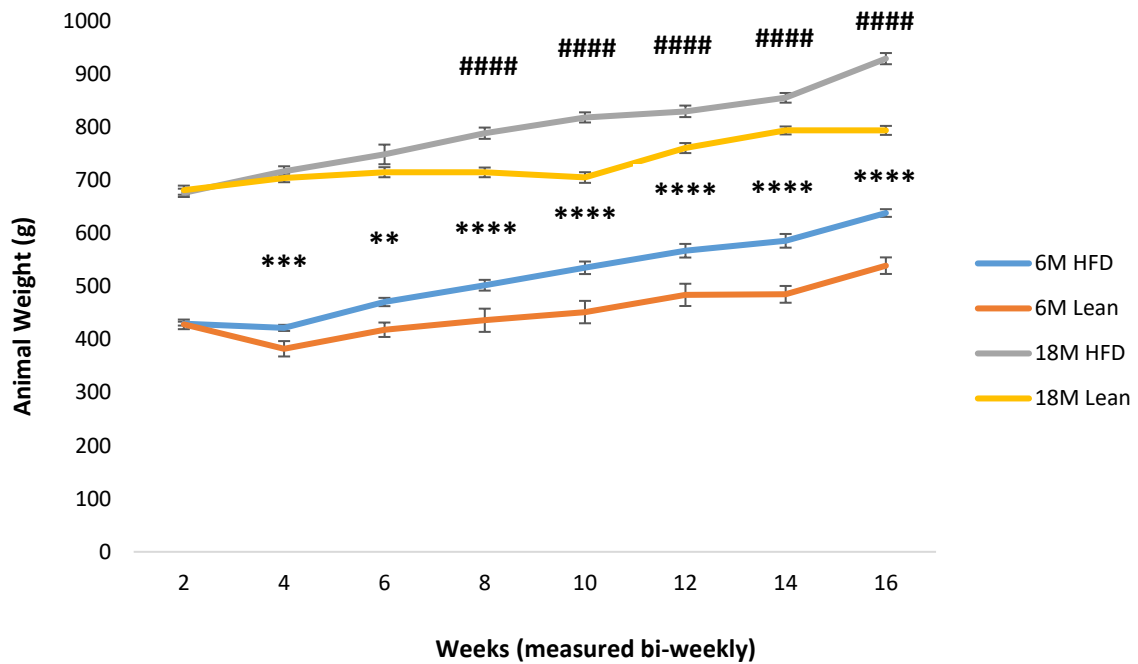


**Figure 5.2.1.1 – Comparison of animal body mass in both the 6 and the 18-month aged models, measured bi-weekly, for a total of 16 weeks.** Significance was shown after the first month of feeding between the lean and the HFD models within each aged model (\*\*\*\* and #### =  $p < 0.0001$ ; \* = 6-month model; # = 18-month model).

**Table 5.2.1.1 – Table with the comparison of parameters between lean models and HFD models, in 6-month and 18-month aged animals.** The mean values are a representation of the parameters at the start of the experimental protocols (\*\* =  $p < 0.01$ ; \*\*\* =  $p < 0.001$  and \*\*\*\* =  $p < 0.0001$ , compared to the 6-month lean group and ### =  $p < 0.001$  and #### =  $p < 0.0001$ , compared to the 18-month lean group).

Age group	6M Lean Mean $\pm$ SEM	6M HFD Mean $\pm$ SEM	18M Lean Mean $\pm$ SEM	18M HFD Mean $\pm$ SEM
<b>Body mass (g)</b>	539 $\pm$ 15.5	638 $\pm$ 7.2 ****	794 $\pm$ 8.4	929 $\pm$ 10.5 ####
<b>Body length (cm)</b>	43 $\pm$ 0.5	44 $\pm$ 0.4	49.5 $\pm$ 0.4	48.5 $\pm$ 0.4
<b>Left epididymal fat pad mass (g)</b>	7.01 $\pm$ 0.6	8.65 $\pm$ 0.5 ***	6.93 $\pm$ 0.4	12.05 $\pm$ 0.6 ####
<b>Right epididymal fat pad mass (g)</b>	6.64 $\pm$ 0.6	8.72 $\pm$ 0.5 **	6.97 $\pm$ 0.3	12.50 $\pm$ 0.6 ####
<b>Mesenteric fat pad mass (g)</b>	6.50 $\pm$ 0.6	10.63 $\pm$ 0.8 ****	8.70 $\pm$ 0.3	11.42 $\pm$ 0.4 ###
<b>Body circumference (cm)</b>	21.75 $\pm$ 0.2	25.75 $\pm$ 0.2 ****	26.25 $\pm$ 0.2	33.75 $\pm$ 0.3 ####

Regarding the animals in the obesity projects, previous rodent models have been used for similar studies (with slight modifications in feeding time and diet supplements) in order to induce obesity, as their neuroanatomy and energy homeostasis control resembles that of a human being (Barrett, Mercer and Morgan 2016; Marques et al. 2016; Wilson, C. et al. 2007; Woods et al. 2003). A more detailed explanation of the animal model and how it compares to previous research can be found in section 3.1. As it was also mentioned before in section 3.1, for the purposes of this study 3-month rats have been equated, in age, to a human child between 10-18 years, 6-month rats have been equated to a young adult between 20-30 years and 18-month rats have been equated to an older adult between 54-69 years (Andreollo et al. 2012; Capitanio et al. 2016; Jackson et al. 2017; Sengupta 2013). It was decided that the entirety of the previous published literature would be utilised to define the age groups for this thesis.

### **5.2.2 Langendorff Isolated Heart Model (full review in section 3.2)**

The technique starts with the perfusion of the heart with Krebs-Henseleit buffer (maintained at a constant temperature of  $37^{\circ}\text{C} \pm 0.5$  at a pH of 7.4) and gassed with 95%  $\text{O}_2$  and 5%  $\text{CO}_2$ , by means of cannulating the aorta, in a retrograde fashion, forcing the closing of the aortic valve as a result of a change in pressure. The buffer then passes through a vascular bed before being drawn to the coronary sinus in the right atria. This allows the preparation to be maintained without any fluid filling the ventricular chambers (Skrzypiec-Spring et al. 2007). The Langendorff preparations were run as described in section 3.2.2 and as seen in figure 5.2.2.1, under normal physiological conditions.

Measurements for the coronary flow (CF), left ventricular developed pressure (LVDP), heart rate (HR) and the Maximum ventricular pressure increase (+dP/dtmax) and decrease (-dP/dTmax) were recorded using a physiological pressure transducer connected to the latex balloon and to a PowerLab (ADInstruments, UK) linked to a PC with LabChart® software v7 and the rate pressure product (RPP) was calculated using the function mentioned in section 3.2.2. At the end of the protocol, the left ventricle was excised from each heart and divided into two; tissues were then rapidly frozen in liquid nitrogen before being stored at -80°C for future use. For a full background review, please refer to section 3.2.

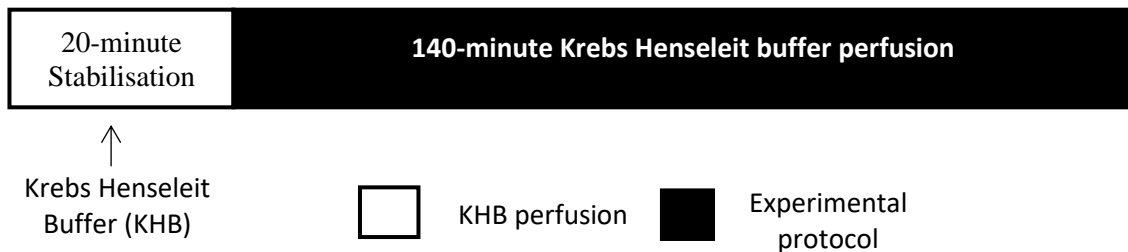


**Figure 5.2.2.1 - Langendorff Protocol.** This was the protocol used for this chapter. The hearts were perfused with KHB for a total run time of 160 minutes.

### 5.2.3 Work-loop Assay (full review in section 3.3)

This technique was only carried out for the 6-month animals. Following the sacrifice of the animal, the diaphragm was cut to expose the thoracic cavity and the thorax was subsequently opened to expose the heart. The excised hearts were immediately placed in ice cold modified Ringers buffer (NaCl, 144mM; sodium pyruvate, 10mM; KCl, 6mM; MgCl<sub>2</sub>, 1mM; CaCl<sub>2</sub>, 2mM; NaH<sub>2</sub>PO<sub>4</sub>, 1mM; MgSO<sub>4</sub>, 1mM; Hepes, 10mM; with a pH of 7.4 at room temperature and oxygenated with 100% O<sub>2</sub>) and held in place on a silicone petri dish. This preparation was then placed under a microscope, to dissect the muscle as quickly as possible.

Muscles containing branches or smaller muscles attached to them were excluded due to the potential to disturb forces production and recording. The chosen muscles were carefully trimmed and dissected and were then clamped at both the tendon and the ventricular chamber wall by small aluminium foil T-shaped clips. The muscle was left untouched to avoid potential damage. The dissected muscle was then placed on a horizontal chamber in an organ bath with circulating modified Ringers buffer and maintained at 37°C.

The muscles were also connected to a 50nM force transducer and a high-speed length controller that were later used to stimulate the muscles at a 60-mA amplitude. (Layland, Young and Altringham 1995). The resulting developed force was calculated by subtracting the maximum produced force from the minimum produced force.

The optimal muscle length was obtained by gradually increasing the muscle length using a micromanipulator (all products were purchased from Aurora Scientific, Canada) until the maximum developed force was reached ( $L_{max}$ ). Once reached the muscle length was measured with an eyepiece. For the actual work-loop protocol, the muscles were set to 95% of their original maximum length ( $L_{95\%}$ ) and allowed a 30-minute stabilisation period.

Once the  $L_{95\%}$  was calculated, the work-loop protocol (see figure 5.2.3.1) was carried out at a frequency of 6Hz and a strain amplitude of  $\pm 6\%$  which, again, has been shown to produce the maximum power output in the cardiac muscle (Layland, Young and Altringham 1995). This protocol was repeated every 5 minutes for a total of 120 minutes (for a total of 24 loops produced per protocol).

At the end of the 120 minutes, the muscle was weighed to the nearest 0.00001g using an electronic balance. Instantaneous power output was calculated for every data point by multiplying instantaneous force generated by instantaneous velocity. This was done for each loop (1863 total data points per loop) and then averaged to generate a net-work value for each instance of a completed loop (Gharanei et al. 2014).

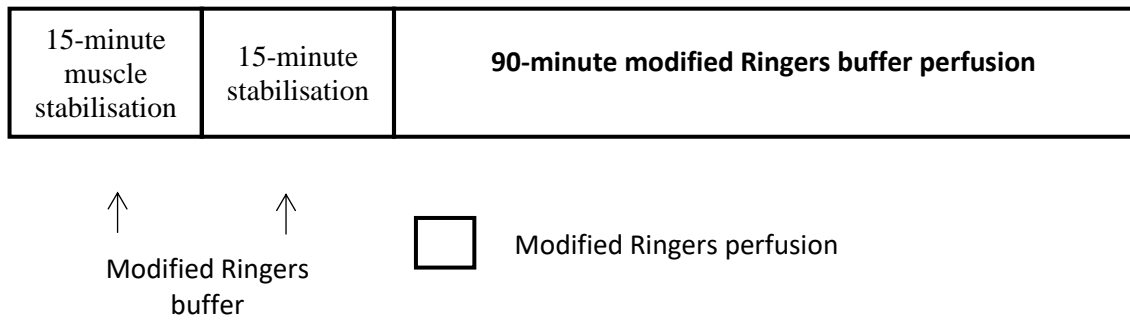


**Figure 5.2.3.1 – Work-loop protocol.** This was the protocol used for this chapter. The hearts were perfused with modified Ringers buffer for a total run time of 120-minutes.

#### 5.2.4 Western Blotting (full review in section 3.4)

Cardiac tissue was collected from each treatment group, as mentioned in table 3.1.2.2. Approximately half of the left ventricle (50 mg) was then homogenized with lysis buffer (100 mM NaCl, 10 mM Tris base - pH 8.0, 1 mM EDTA - pH 8.0, 2 mM sodium pyrophosphate, 2 mM NaF, 2 mM  $\beta$ -glycerophosphate, SigmaFAST™ protease inhibitor cocktail tablets – 1 tablet/100ml and PhosStop™ - 1 tablet/10ml) on a IKA Ultra-Turrax® T 25 basic disperser, set to a speed of 21,500 RPM.

This tissue was then centrifuged for 10 minutes at 11,000 RPM at 4°C to obtain the desired supernatant, which was then transferred into clean 1.5ml microcentrifuge tubes. Samples were diluted using Laemmli buffer (250 mM Tris-HCl – pH 6.8, 10% glycerol, 0.006% bromophenol blue, 4% SDS,  $\beta$ -mercaptoethanol – pH 6.8) and incubated at 100°C for 5 minutes before being stored at –20°C. Prior to using the samples, they were defrosted on ice and diluted further using Laemmli buffer to obtain a protein concentration of 50 $\mu$ g. To calculate the protein content of homogenised samples, a colorimetric Pierce™ BCA Protein assay kit (Thermo Fisher Scientific, UK) was used. Concentrated albumin standards were serially diluted using lysis buffer to obtain a concentration range of 0 - 2000 $\mu$ g/ml.

BCA working reagent was prepared following a 50:1 ratio of reagent A and reagent B, respectively. Standards and samples were pipetted at a volume of 10 $\mu$ l, in triplicate, onto a 96-well plate. Following this, 200 $\mu$ l of working reagent was added to each well. Plates were then covered to protect from light and incubated for 30 minutes at 37°C, before being left to cool to room temperature. The plate reader was set to 562 nm and the measured absorbance values were then used to calculate the total protein content per unknown sample.

The previously collected samples were further diluted using laemmli buffer to obtain a concentration of 50 $\mu$ g/ $\mu$ l. These samples were then centrifuged at 1200 RPM for 2 minutes, at 4°C, before being loaded onto Precast TGX™ (Tris/glycine) gradient gels (Bio-Rad, UK). The gels were then placed inside of a Mini-PROTEAN™ vertical electrophoresis assembly unit before filling the chamber and outer tank with running buffer (14.42g/L Glycine, 1.0g/L SDS, 3.03g/L Tris base). The samples were then loaded into the wells, with at least one well loaded with a molecular protein marker acquired from Cell Signalling UK. Gels were run at 110V for 60 minutes using a Power-PAC 3000 (Bio-Rad, UK).

Following electrophoretic separation, the gels were removed from their compartments and placed onto Trans-Blot® Turbo™ transfer packs, consisting of filter paper, buffer and a polyvinylidene fluoride (PVDF) membrane. The assembled cassettes were loaded into the Trans-Blot system (Bio-Rad, UK) and ran for the mixed molecular weight transfer protocol for a total of 7 minutes. Following transfer, the membranes were cut into two using a scalpel blade. Blots were then incubated at room temperature in blocking buffer (5% w/v milk powder in Tris-buffered saline with Tween 20 (TBST) for 60 minutes on an orbital shaker (Cassambai et al. 2019). Blots were then incubated overnight in 5% w/v bovine serum albumin (BSA) in TBST - 1/1000, at 4°C, with anti-UCP3 antibody and phosphorylated Pyruvate Dehydrogenase E1-alpha subunit purchased from Abcam (UK).

The following day, blots were then incubated with secondary antibody (anti-rabbit HRP IgG – 1/1000, Cell Signalling, UK) in blocking solution (5% w/v milk powder in TBST) and incubated for 1 hour at room temperature on an orbital shaker. To visualise the membranes, they were first placed onto an acetate sheet and coated with approximately 1 mL of SuperSignal West Femto kit (Thermo-Scientific), in a 1:1 dilution, to amplify the signals from the membranes. Images were then captured and visualised using a ChemiDoc with the ImageLab™ Touch software (Bio-Rad, UK). Membranes were exposed for 3 to 5 seconds (see representative blot in figure 2.4.6.1) in order to detect the bands corresponding to the proteins of interest. Images were subsequently analysed using the java-based software ImageJ (National Institutes of Health, USA). After visualising the membranes, they were stripped using Restore™ Western Blot Stripping Buffer (Thermo Fisher Scientific, UK) and re-probed for the total form of Pyruvate Dehydrogenase E1-alpha subunit and GAPDH, to be used as controls for the data.

### **5.2.5 Statistical Analysis (full review in section 3.6)**

Animal body mass and fat pad weight was plotted as average mass/weight  $\pm$  standard error of the mean (SEM) and statistically analysed using One-Way analysis of variance (ANOVA) with Tukey's post hoc test, on IBM SPSS® Statistics 25 (IBM Corporation USA). A p value of  $p < 0.05$  was considered statistically significant. The haemodynamics and work-loop data were plotted as a percentage of the average stabilisation (mean  $\pm$  standard error of the mean (SEM)). Two-Way analysis of variance (ANOVA) was used with Tukey's LSD (least significant difference) for each time point as a function of each age group, for both the Langendorff and the work-loop data. Fisher's LSD was used for the western blot data, as the main interest was in finding the minimum difference between protein expression. A p-value of  $p < 0.05$  was considered statistically significant.

## 5.3 Results

### 5.3.1 Langendorff Isolated Heart Model

As explained in section 3.6, a two-way ANOVA was done to examine the effect of age and time on the maximum pressure rise, maximum pressure drop and rate pressure product. No statistically significant interaction was recorded (p values of 1.0, 0.94 and 1.0, respectively), but the post hoc tests showed significances in the independent variables (p values of 0.000 for both MPR and RPP). Performance variation was also analysed, based on the average absolute values, for the 6 and 18-month groups, and their respective HFD model, during the first 20-minutes of the protocol, which shows that there are significant changes in performance between HFD and lean hearts (table 5.3.1.1). For the 6-month group, the HFD starting numbers were significant when compared to the 6-month lean model for MPR ( $+1389 \pm 212.5$  (SEM),  $p < 0.0001$ ), MPD ( $+1513 \pm 344.3$  (SEM),  $p < 0.0001$ ) and RPP ( $+20676 \pm 3652$  (SEM),  $p < 0.0001$ ). For the 18-month group, no significant differences were recorded. Finally, the results were plotted and analysed after normalising them to stabilisation values, as seen in the graphs below.

**Table 5.3.1.1 – Performance assessment of the four HFD models in the first 20-minutes of the experimental protocol.** The table shows the absolute values of each of the haemodynamic parameters for each HFD group. The 6-month lean group showed lower values when compared to its respective HFD group. The 18-month group shows higher initial numbers for all parameters, when compared to the 6-month models, but no significance was found between the HFD and lean models. (6-month model: \*\*\*\* =  $p < 0.0001$  in relation to the 6-month lean control).

Diet models	6-month Lean	6-month HFD	6-month significance	18-month Lean	18-month HFD
<b>MPR</b>					
Mean $\pm$ SEM	$4757.5 \pm 55.2$	$6146 \pm 212.5$	****	$6022.7 \pm 636.4$	$5278.2 \pm 521.4$
<b>MPD</b>					
Mean $\pm$ SEM	$-4686.5 \pm 310.1$	$-6199 \pm 344.3$	****	$-5169.5 \pm 425.7$	$-4951 \pm 443.3$
<b>RPP</b>					
Mean $\pm$ SEM	$35524.6 \pm 2619$	$56200.5 \pm 3652$	****	$51477.9 \pm 5847.6$	$37703.6 \pm 9281.6$

Figure 5.3.1.1 represents the rate at which the pressure on the left ventricle of the heart develops. The HFD models showed no difference between the two age groups, when compared to their respective lean control (A: 6-month:  $p = 0.96$  and B: 18-month:  $p = 0.99$ ).

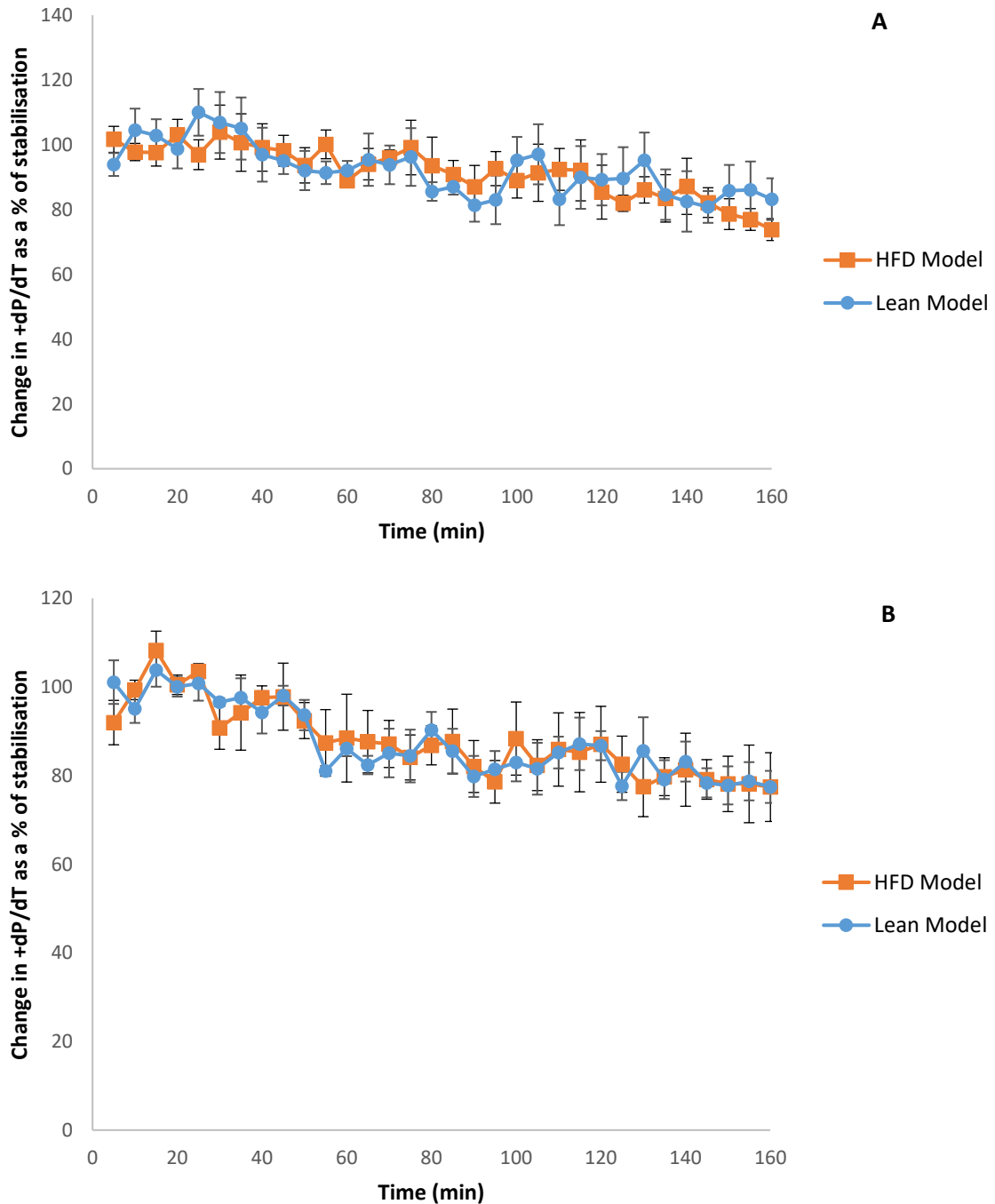
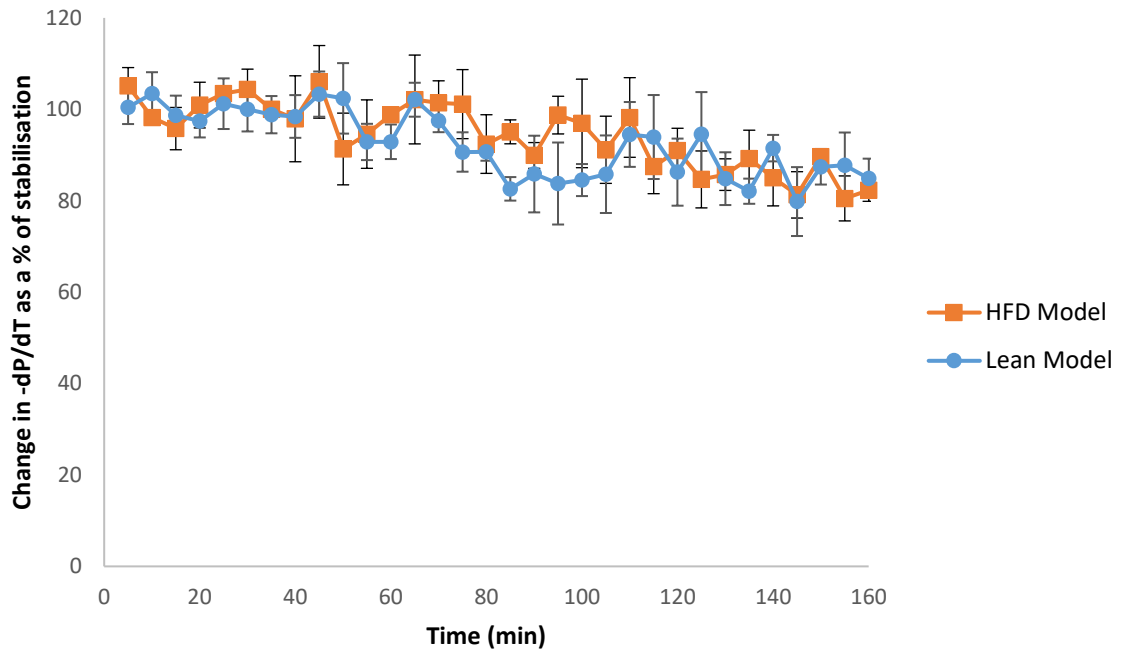
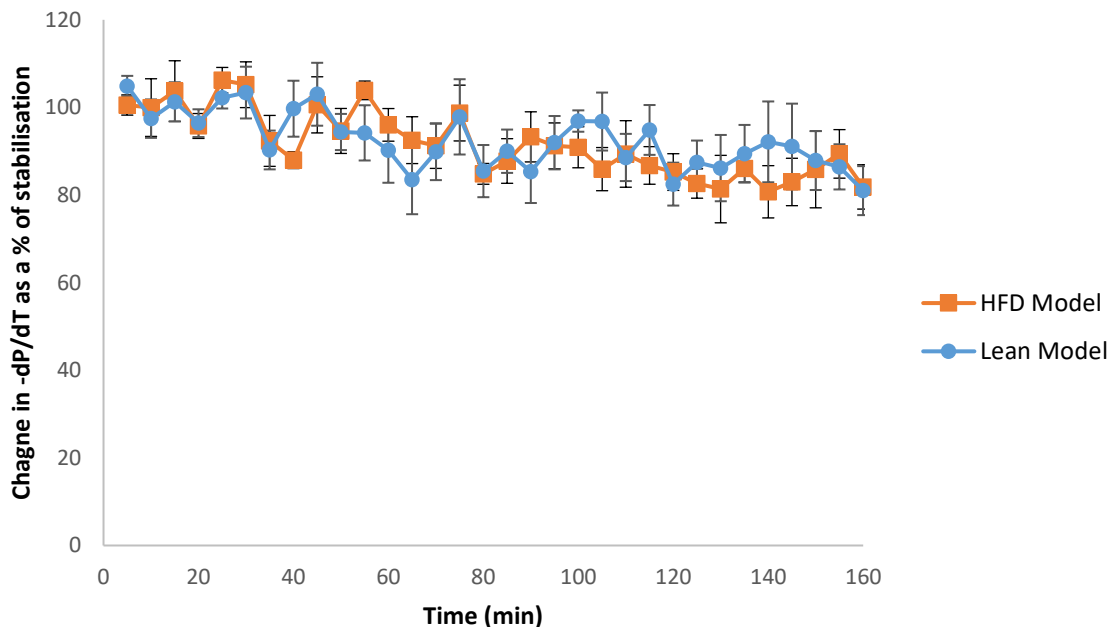


Figure 5.3.1.1 - +dP/dTmax for the 6-month models as seen in graph A and for the 18-month models as seen in graph B (n = 4 for both models). Hearts were allowed a 20-minute stabilisation period and were then subsequently perfused with KH buffer for another 140 minutes.

Both figures (5.3.1.2 and 5.3.1.3) represent the rate at which the pressure on the left ventricle of the heart decays. The HFD models showed no differences as a function of age or time, when compared to their respective lean control (6-month:  $p = 0.43$  and 18-month:  $p = 0.90$ ).

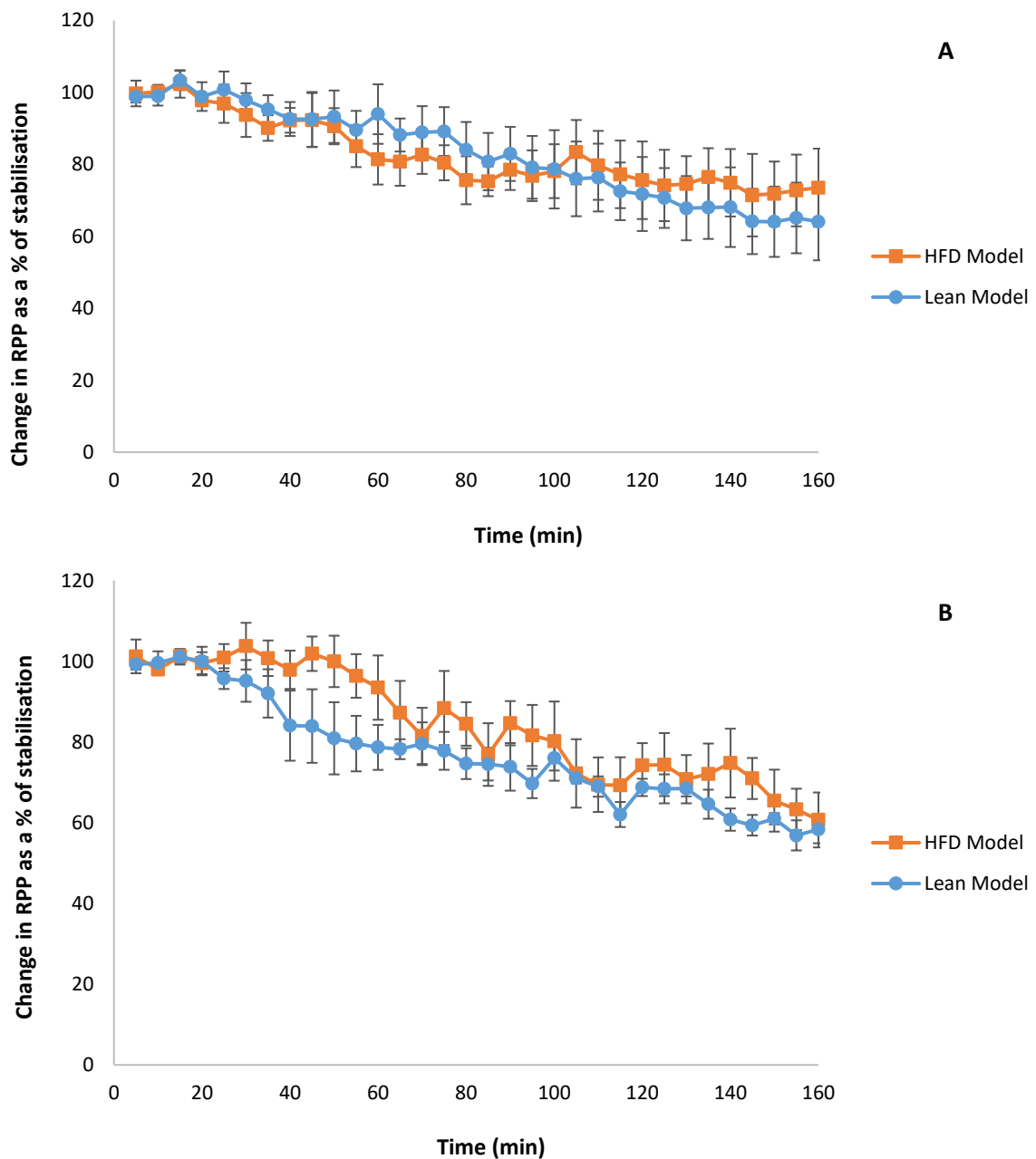


**Figure 5.3.1.2 -  $-dP/dT_{max}$  for the lean and HFD 6-month models ( $n = 4$  for both models).** Hearts were allowed a 20-minute stabilisation period and were then subsequently perfused with KH buffer for another 140 minutes. Measurements for maximum ventricular pressure drop are displayed above.



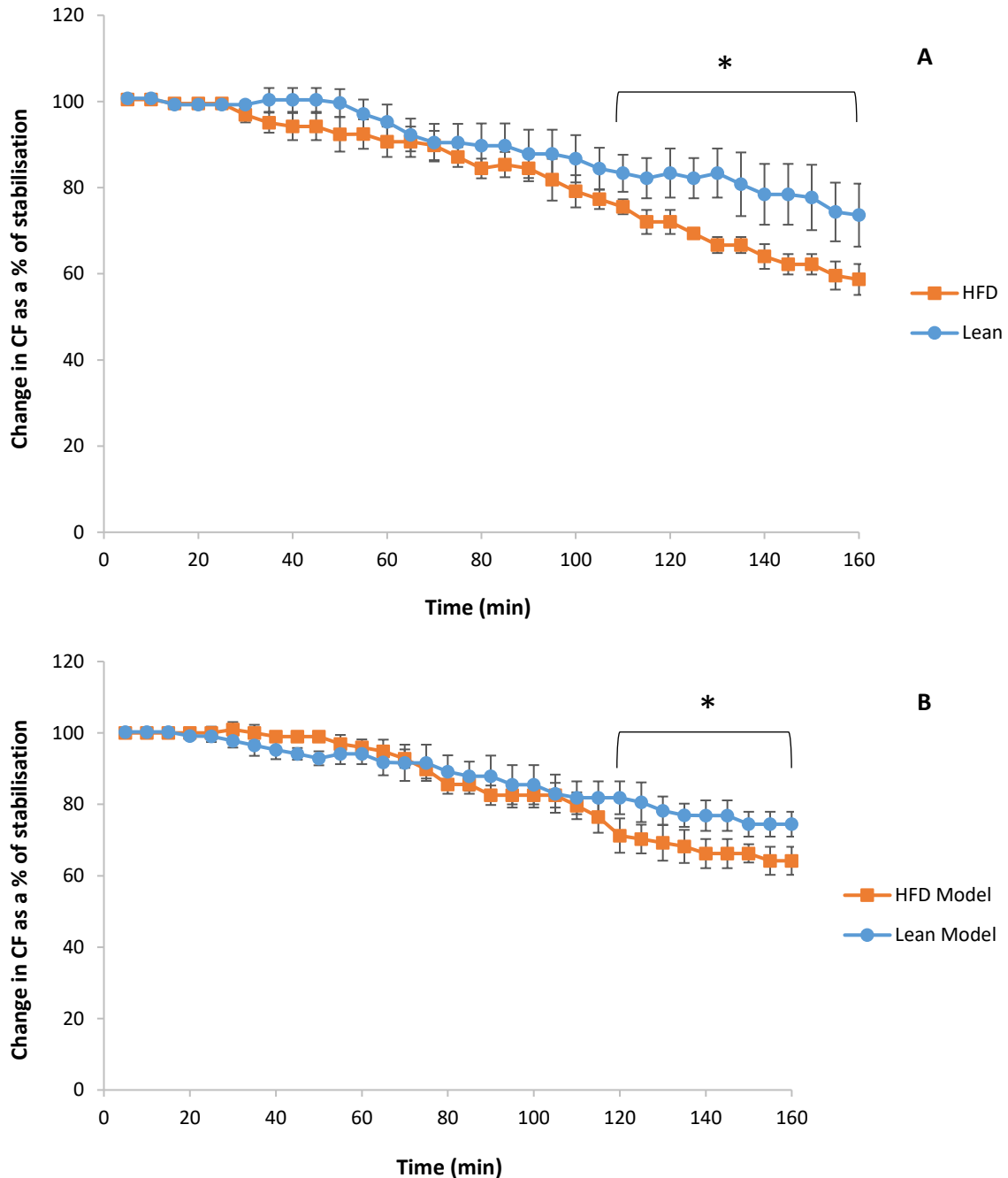
**Figure 5.3.1.3 -  $-dP/dT_{max}$  for the lean and HFD 18-month models ( $n = 4$  for both models).** Hearts were allowed a 20-minute stabilisation period and were then subsequently perfused with KH buffer for another 140 minutes. Measurements for maximum ventricular pressure drop are displayed above.

Figure 5.3.1.4 represents a calculation for the total myocardial workload of the heart, by multiplying the LVDP by the HR. No significance was recorded for the 6-month group nor the 18-month group, apart from an anomaly between the 45 and the 60-minute mark. However, while this may have occurred as a result of a compensatory effect of the heart, it is also likely that it occurred due to spontaneous contractions and was deemed to be of no statistical significance.



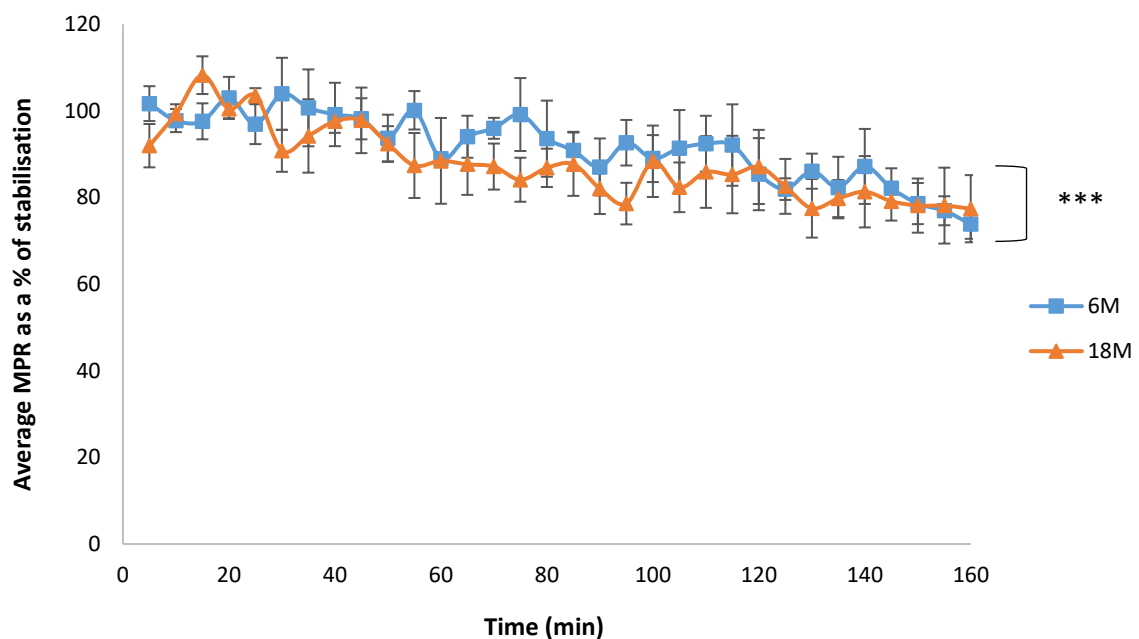
**Figure 5.3.1.4 - RPP for the 6 (A) and 18-month (B) lean and HFD models (n = 4 for both models).** Hearts were allowed a 20-minute stabilisation period and were then subsequently perfused with KH buffer for another 140 minutes. Measurements for maximum ventricular pressure drop are displayed above.

Figure 5.3.1.5 represents the rate of cardiac tissue perfusion in 6-month (A) and 18-month (B) animals (B). Both the 6 (A) and the 18-month (B) model showed a similar pattern, with both post hoc tests showing a significant decrease of -15%,  $p < 0.05$  in relation to the lean control, starting at the 110-minute mark and lasting until the end of the protocol.



**Figure 5.3.1.5 - CF for the 6 (A) and 18-month (B) lean and HFD models (n = 4 for both models).** Hearts were allowed a 20-minute stabilisation period and were then subsequently perfused with KH buffer for another 140 minutes. Measurements for coronary flow are displayed above (\* =  $p < 0.05$  in relation to the lean control model).

The next three graphs represent the comparison between the haemodynamic parameters of the 6-month HFD model when compared to the 18-month HFD model. Figure 5.3.1.6 represents the MPR comparison between the two models. When looking at the % of stabilisation, the Two-Way ANOVA and the post hoc tests showed a significant effect of HFD on the 18-month tissue viability and performance on the Langendorff isolated heart ( $-4.9\% \pm 1.3$  (SEM),  $p < 0.001$  when compared to the 6-month HFD data. However, no time-dependant significant effect was recorded between the three age models.



**Figure 5.3.1.6 - MPR for the 6- and 18-month HFD models (n = 4 for both models).** Hearts were allowed a 20-minute stabilisation period and were then subsequently perfused with KH buffer for another 140 minutes. Measurements for MPR are displayed above (\*\*\*) =  $p < 0.001$  in relation to the 6-month HFD model).

As seen by figure 5.3.1.7, no significance was found when looking at the MPD of the hearts in the 6- and 18-month HFD models.

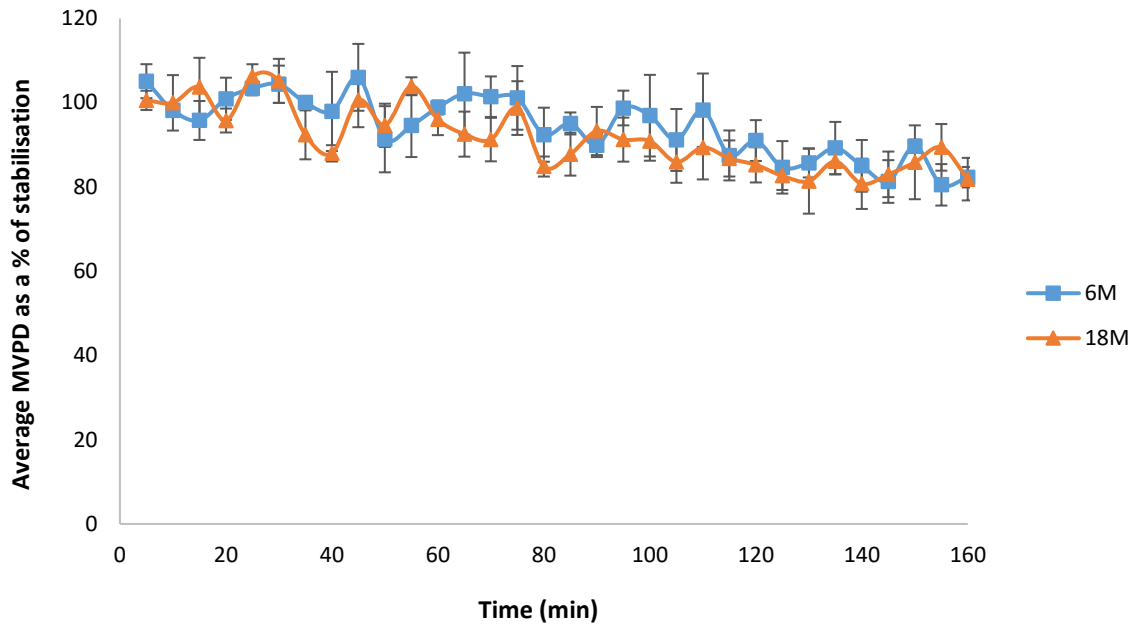


**Figure 5.3.1.7 - MPD for the 6- and 18-month HFD models (n = 4 for both models).** Hearts were allowed a 20-minute stabilisation period and were then subsequently perfused with KH buffer for another 140 minutes. Measurements for MPD are displayed above.

Figure 5.3.1.8 represents the RPP comparison between the two models. When looking at the % of stabilisation, the Two-Way ANOVA and the post hoc tests showed a significant effect of ageing on the 18-month tissue viability and performance on the Langendorff isolated heart ( $-6.03\% \pm 1.4$  (SEM),  $p < 0.0001$  when compared to the 6-month HFD data. However, no time-dependant significant effect was recorded between the three age models.

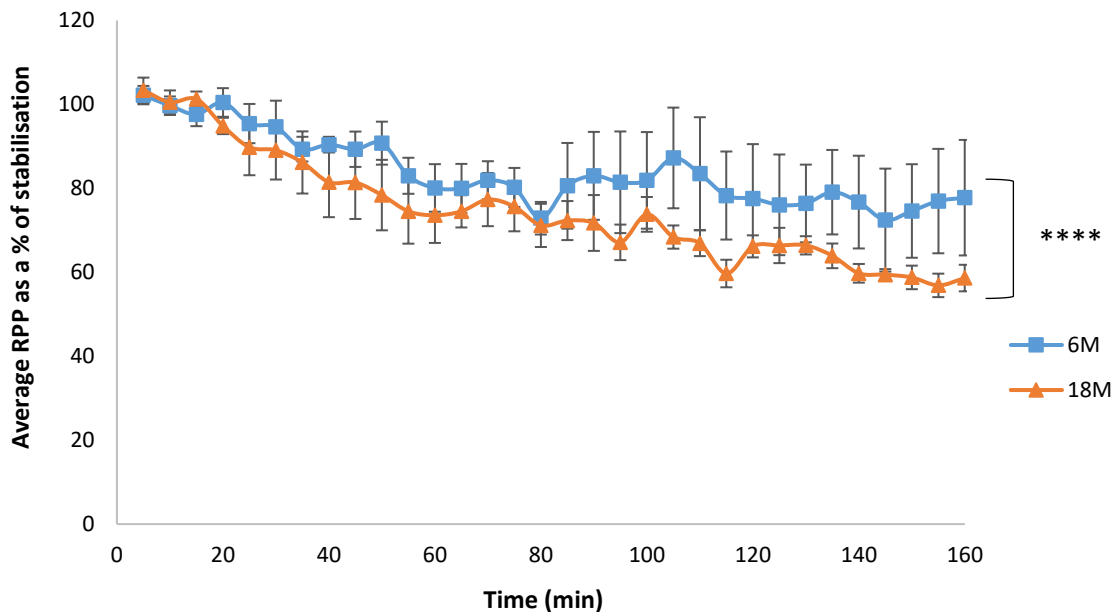


**Figure 5.3.1.8 - RPP for the 6- and 18-month HFD models (n = 4 for both models).** Hearts were allowed a 20-minute stabilisation period and were then subsequently perfused with KH buffer for another 140 minutes. Measurements for RPP are displayed above (\*\*\*) =  $p < 0.0001$  in relation to the 6-month HFD model).

### 5.3.2 Work-Loop Assay

The data presented in this section represents the 6-month set of lean and HFD data for the cardiac muscle assay. The two-way anova showed a significant interaction between HFD\*TIME, with a p value of 0.01. The independent variables were also investigated, as seen in figure 5.3.2.1. Figure 5.3.2.1 shows the power output over time and there was a clear significant difference when comparing the power outputs between the two models, with the HFD model showing an initial significant decrease at the 45-minute mark ( $-8\% \pm 3.3$  (SEM),  $p < 0.01$ ). At the 100-minute mark, a further significant decrease was recorded ( $-24\% \pm 6.6$  (SEM),  $p < 0.01$ ) that lasted until finally showing maximal significant decrease of  $-28\% \pm 11.4$  (SEM),  $p < 0.01$  in power output, at the 120-minute mark.

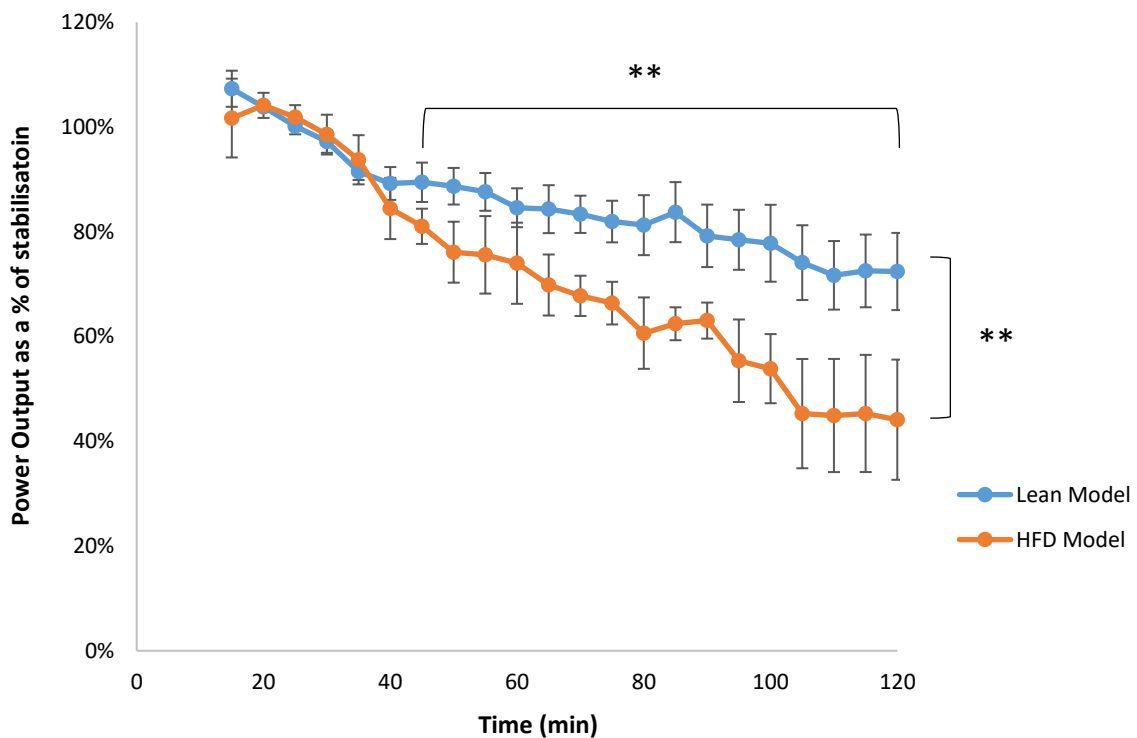
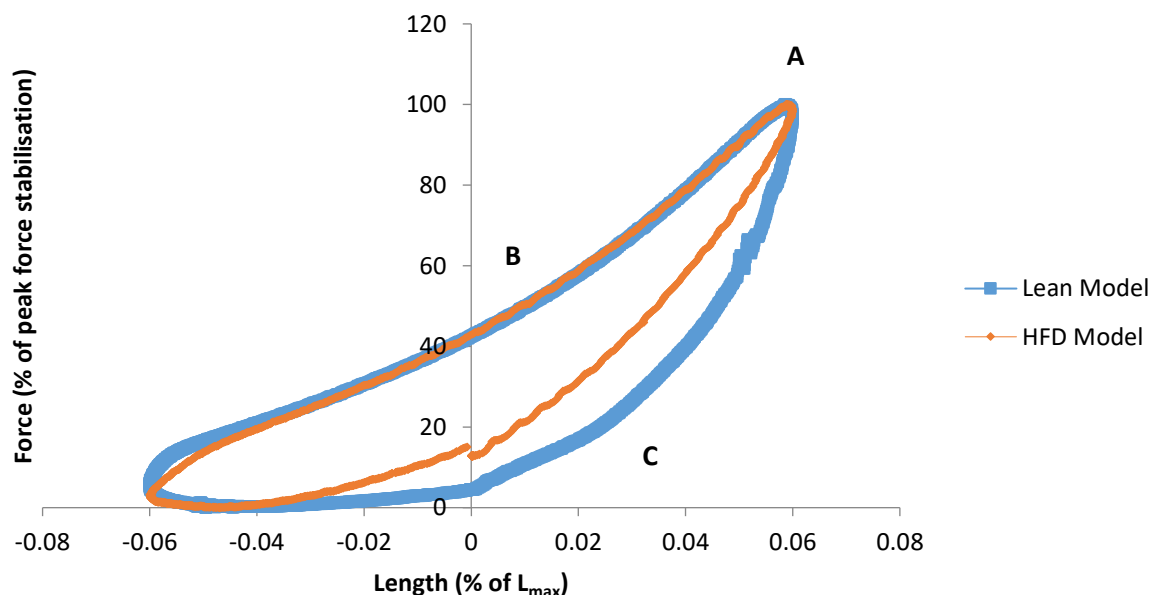
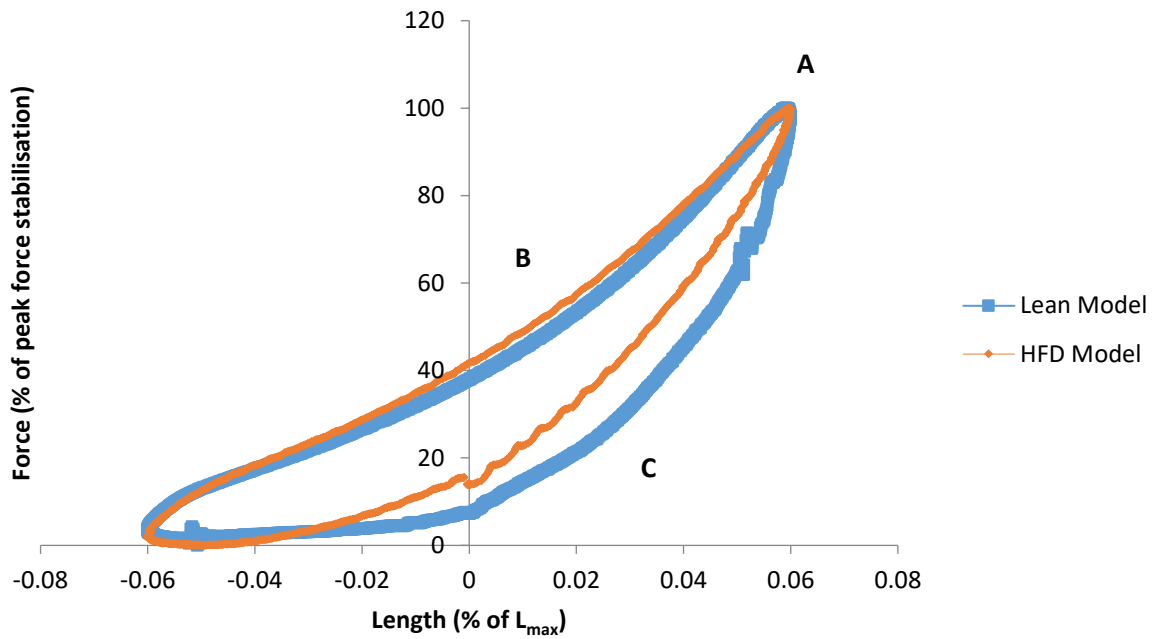


Figure 5.3.2.1 – Power output for the lean and HFD 6-month models (n = 6 and 5, respectively). Work produced by the muscle under similar conditions but in two different diet models. A significant change was observed after the 35-minute mark (\*\* =  $p < 0.01$ ).

The next three graphs (figures 5.3.2.2 to 5.3.2.4) represent the force of the muscles plotted against the % in length change, at three different time points (45, 100 and 120 minutes). They are presented as a plot of force against % length change (or strain). The loops presented are all averages of the work produced by the muscles. No change was documented in peak force measurements, based on visual inspection (**A**), but the work required by the muscle during shortening was reduced (**B**), at the 120-minute mark, for both models. The lean model showed no changes in activation rate throughout the experimental protocol. The HFD muscle, on the other hand, showed a higher demand in the muscle activation rate across all time points (**C**), including the non-presented ones. Finally, the total net-work done by the muscle was significantly reduced on the HFD model, which can be seen by a reduction in the total area of the loop, with its lowest value seen at the 120-minute mark. An important note here that the HFD muscles performed significantly worse on the work-loop assay and did not withstand the full 120-minute protocol before being unable to be stimulated into further contractions. It is therefore clear that HFD causes significant impairment in overall muscle contractions.



**Figure 5.3.2.2 - Comparison between a lean and an HFD model at the 45-minute mark.** This graph represents the changes in muscle power at the 45-minute mark of the experimental protocol, when comparing between the diet models (representative graph only). A = Peak force; B = Muscle Shortening; C = Activation rate.



**Figure 5.3.2.3 - Comparison between a lean and an HFD model at the 100-minute mark.** This graph represents the changes in muscle power at the 100-minute mark of the experimental protocol, when comparing between the diet models (representative graph only). A = Peak force; B = Muscle Shortening; C = Activation rate.

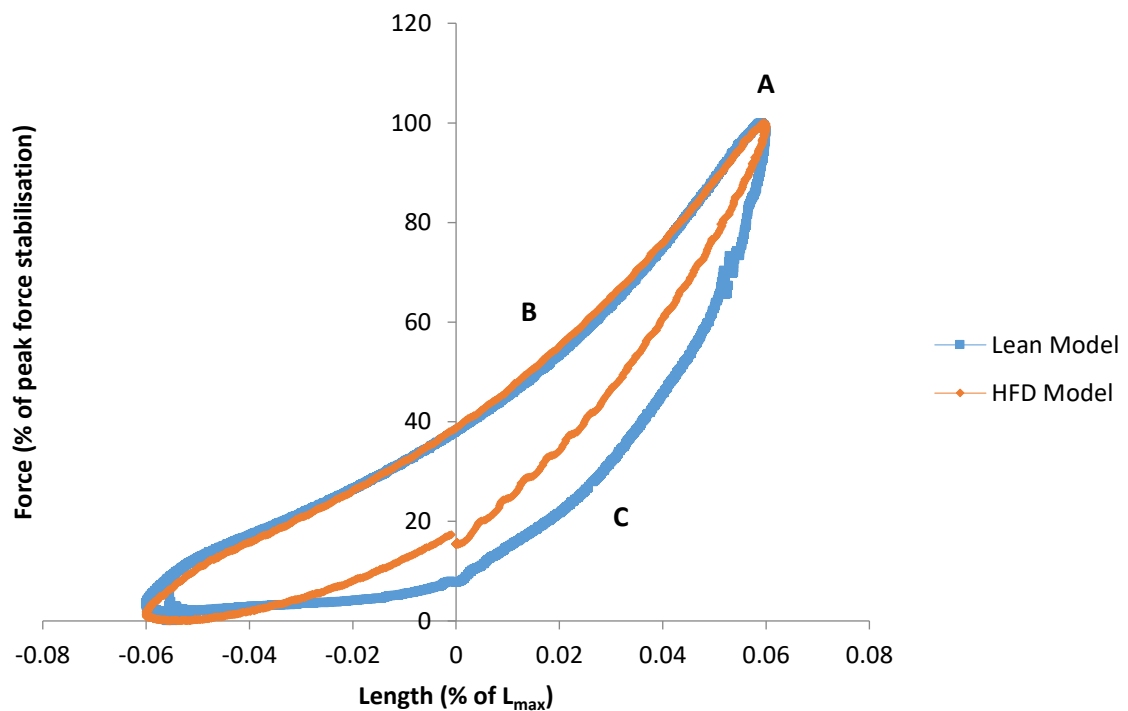
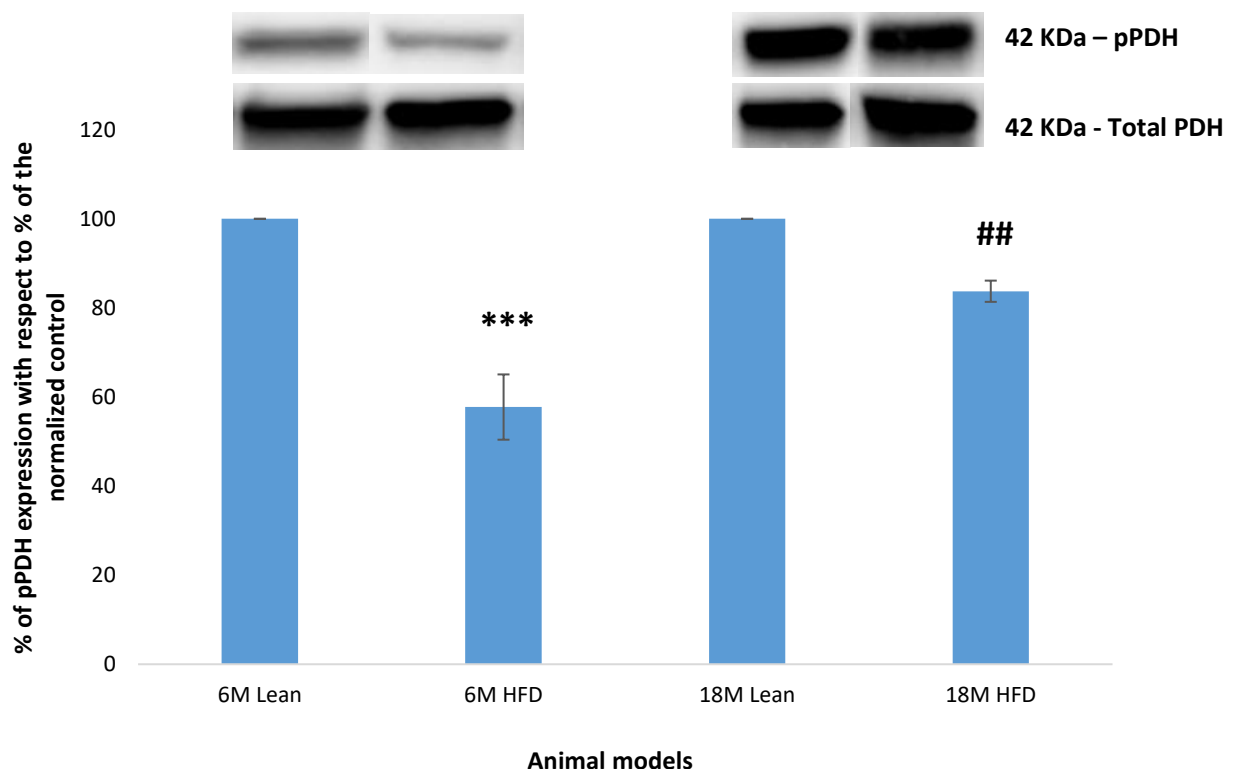


**Figure 5.3.2.4 - Comparison between a lean and an HFD model at the 120-minute mark.** This graph represents the changes in muscle power at the 120-minute mark of the experimental protocol, when comparing between the diet models (representative graph only). A = Peak force; B = Muscle Shortening; C = Activation rate.

### 5.3.3 Western Blot

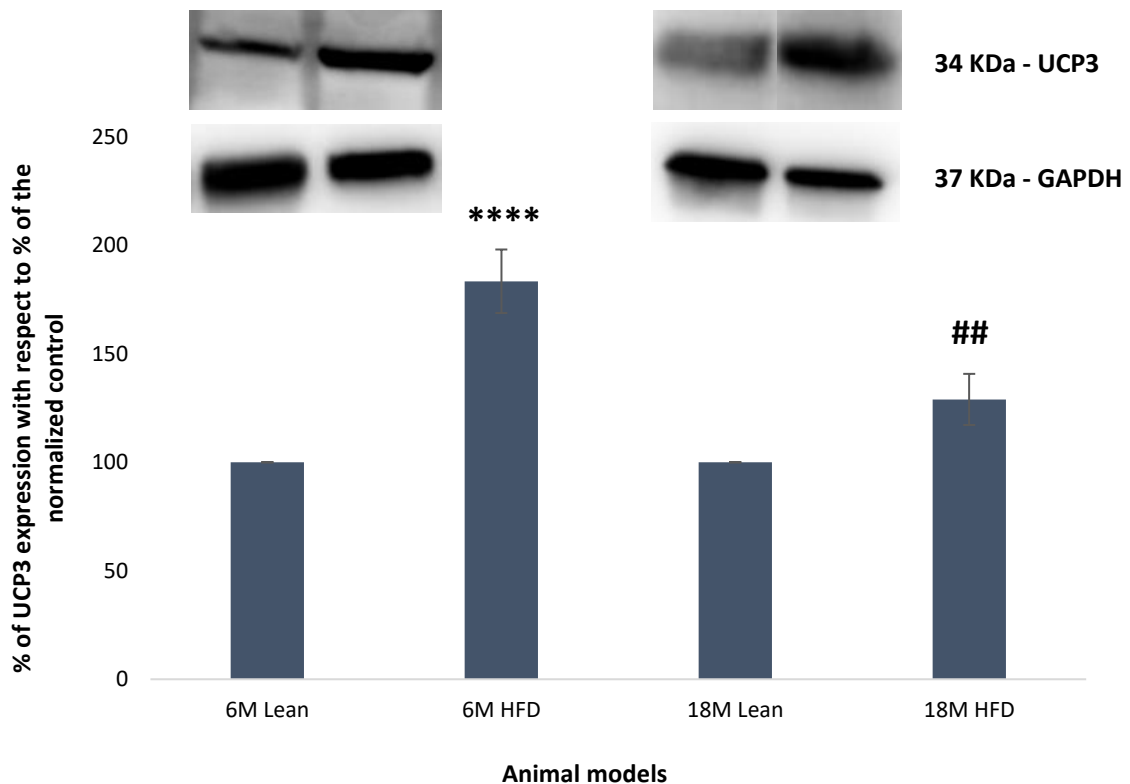
Pyruvate dehydrogenase (PDH) and Uncoupling protein 3 (UCP3) were assessed using western blotting in order to assess the impact of key mitochondrial regulators in cardiac function. All of the represented graphs were plotted after correcting for protein loading and the lean controls were normalised.

Figure 5.3.3.1 shows the percentage of phosphorylated PDH in 6 and 18-month HFD heart tissue as a % of the 6 and 18-month lean controls. As seen by figure 5.3.3.1, the effect of the HFD on the 6-month animals caused a decrease in the active portion of PDH, with a decrease of  $-43\% \pm 7.3$  (SEM) observed when compared to the total ( $p < 0.001$ ). As for the 18-month models, the effect of the HFD on the animals caused a decrease in the active portion of PDH, with a decrease of  $-17\% \pm 2.3$  (SEM) observed when compared to the total ( $p < 0.01$ ).



**Figure 5.3.3.1 – Phosphorylated PDH expression in 6- and 18-month-old HFD and lean animal models (n = 4 for all).** This graph represents the effects of HFD on the levels of phosphorylated PDH, as a percentage of total PDH (\*\*\*) =  $p < 0.001$  compared to the 6-month lean group and ## =  $p < 0.01$  compared to the 18-month lean group). The top blot is a representative image of phospho-PDH, while the bottom blot represents total-PDH. The presented results are all corrected for GAPDH.

Figure 5.3.3.2 shows the percentage of active UCP3 in 6 and 18-month HFD heart tissue as a % of the 6 and 18-month lean control. As seen by figure 5.3.3.2, the presence of HFD on the animals caused a significant increase of  $+83\% \pm 14.6$  (SEM) in UCP3 expression when compared to the total form of the protein ( $p < 0.0001$ ). As for the 18-month model, the presence of HFD on the animals caused a significant increase of  $+29\% \pm 11.7$  (SEM) in UCP3 expression when compared to the total form of the protein ( $p < 0.01$ ).



**Figure 5.3.3.2 – Active UCP3 expression in 6- and 18-month-old HFD and lean animal models (n = 4 for all).** This graph represents the effects of HFD on the levels of UCP3, as a percentage of GAPDH (\*\*\*\* =  $p < 0.0001$  compared to the 6-month lean group and ## =  $p < 0.01$  compared to the 18-month lean group). The top blot is a representative image of UCP3, while the bottom blot represents GAPDH. The presented results are all corrected for GAPDH.

## 5.4 Discussion and Conclusion

The primary aim of this chapter was to investigate how cardiac function changes in lean and HFD animal models (aged 6 and 18-months) and how this can alter the mitochondrial energetic metabolism. In this study, aged models were established as reproducible models of heart (via measures of CF, LVDP, HR, MPR and MPD) and muscle function (via measures of total work produced by the papillary muscle), as well as key metabolic agents, analysed via western blotting. The proposed hypotheses were confirmed on the isolated heart model, as changes in variation in performance were analysed, based on the absolute values, for the 6-month lean group, when compared to the 6-month HFD group, during the first 15-minutes of the protocol, with significant changes being recorded for MPR, MPD and RPP. The papillary muscle assay also showed a significant change in power output and muscle performance on the 6-month HFD data and based on the data reported in chapter 4, it is possible to extrapolate that a steeper decline in performance would have been recorded for the 18-month model as well. In addition to this, the CF results suggest the presence of vascular remodelling in both the 6-month and the 18-month HFD models, with a significant decrease being documented throughout the protocol for both age models, which is in accordance with both the age and the stress levels of the HFD models, as previously documented (Abel, Litwin and Sweeney 2008; Stapleton et al. 2008). In addition to this, PDH and UCP3 were shown to be good biomarkers of obesity, as the formers levels decreased in the presence of the high-fat diet, while the latter increased significantly. PDH, specifically, seemed to show an age-dependant change, as it was shown to be less decreased in the 18-month HFD model, which indicates a reduction in fatty acid usage, even though HFD was present.

Vasoconstriction in obesity has been attributed to a variety of factors, from an increase in proinflammatory adipokines and cytokines to a dysfunction in the levels of endothelin-1 (ET-1), as obesity has been shown to change the endothelial vasoconstrictor responses (Ferri et al. 1997). A link to the Prostaglandin H<sub>2</sub>/Thromboxane A<sub>2</sub> (PGH<sub>2</sub>/TxA<sub>2</sub>) receptor, an important mediator of the chronic basal vasoconstriction system, has also been suggested as a result of both an increase in TP-mediated vasoconstriction and a decrease in PGI<sub>2</sub>-induced vasodilation (Abel, Litwin and Sweeney 2008; Xiang et al. 2006). The work done in this chapter does not confirm these changes, but it does seem to indicate that the vasoconstriction previously reported in obesity (commonly linked to hypertrophy, which will be further explained) was, to an extent, a factor in the changes seen in the HFD hearts shown here.

As mentioned in the previous paragraph, hypertrophy is very important when looking at obese models, as increased cardiac myocyte volume and diameter has also been vastly documented as the one of the main causes of hypertrophy and heart failure in both animals and patients (Wong et al. 2010). Consequently, a decrease in contractility on obese models is linked to a decrease in cardiomyocyte number of the left ventricle, but with an increase in their total volume, when compared to normal diet models (Schipke et al. 2014). Published work has also linked a reduced effectiveness of isolated papillary muscles to myocardial and cytoskeletal stiffness in obese rats, with significant differences observed in most cases (Leopoldo et al. 2010). Previous researchers have also hypothesised that the lower efficiency of the muscles in hypertrophy can be due to changes to the myosin heavy chain (MHC). The proposed idea is that the shift from the  $\alpha$ -MHC isoform to the  $\beta$ -MHC is somehow causing the observed decreased efficiency. This shift has been replicated in hypoxia and it has been proposed that a similar event occurs during myocardial hypertrophy and this is the cause of a reduction in contractile efficiency of hypertrophic muscles (Razeghi et al. 2003).

Whilst hypertrophy levels for this project were not directly measured, a significant increase in the measured absolute values for the 6-month HFD models was recorded; the same difference was not seen on the 18-month animals potentially due to the fact that hypertrophy is an established characteristic of the ageing heart (Feridooni et al. 2017). These results seem to indicate that a degree of hypertrophy was present (as previously mentioned); it was therefore important to mention it in order to explain the results shown in table 4.3.1.1.

The Langendorff heart technique is one of the most reliable contractility assessment tools available to researchers; however, it is lacking in assessing biomechanical function and cardiac output. To this effect, the work-loop assay is a reliable contractile assessment tool because it allows researchers to directly investigate the mechanical work done by the heart. since it is a technique designed to measure changes in force, velocity, activation rate, frequency and total cardiac work. When analysing the results from the papillary muscle assay, the HFD model performed substantially worse than the lean models, showing deterioration in the power output over time, as well as a decreased total net-work and muscle activation rate, a change that has been previously associated with another consequence of obesity, the hypertrophy of the heart (Correia et al. 2013). This is of particular relevance, as it shows that there is an exacerbation in muscle performance decline in an HFD-dependant fashion, which can have very serious implications for the contractile function of the heart. In addition to this, papillary muscles have also been shown to have a significant impairment in O<sub>2</sub> consumption during contraction, which has been linked to decreases in both total work output and mechanical efficiency (Wong et al. 2010). Wong et al therefore concluded that hypertrophy played a major role in the reduction in contraction on isolated papillary muscles, which is the proposed cause for both the absolute values shown in table 5.3.1.1 and the results from the work-loop assay (section 5.3.2).

Mitochondrial metabolism is a crucial component of cardiac function due to its role in ATP production, which is done either by fatty acid oxidation or from carbon substrate metabolism (Korvald, Elvenes and Myrmed 2000; Kühlbrandt 2015). It is of particular importance in both obesity and ageing due to the previously discussed mitochondrial dysfunction normally associated with both conditions (for a full review on this, please refer to section 1.6). To this effect, for this project the investigation was done to two primary agents involved in mitochondrial function: pyruvate dehydrogenase and uncoupling protein 3.

PDH activity in obesity has been previously reported in three key papers (Crewe, Kinter and Szweda 2013; Gopal et al. 2018; Lydell et al. 2002). Lydell et al confirmed that there are significant limitations in glucose oxidation in hypertrophied rat hearts which, have we mentioned before, is a well-documented heart dysfunction that occurs in both obesity and ageing (Avelar et al. 2007; Feridooni et al. 2017; Jalili, Manning and Kim 2003). Crewe et al followed this up with a more detailed study on mice models of high-fat diet and observed that, after just 1 day of feeding, there was already a significant decrease in pyruvate utilisation (Crewe, Kinter and Szweda 2013). Finally, Gopal et al, recorded a significant reduction in glucose oxidation as an effect of PDH deletion, in addition to an associated diastolic dysfunction (Gopal et al. 2018). In this study, the 6-month showed a significant decrease in PDH activity on the HFD models, with a decrease when compared to the lean controls, as seen in the previous research mentioned above. However, the 18-month models did not show a significant change between the models. As we saw in the previous chapter, age seems to have an effect on the expression of PDH, with a slight increase being observed when comparing between the 6 and the 18-month, albeit non-significant; in addition to this, it is known that there is a shift to glycolysis as a source of ATP in aged tissue (Bellanti et al. 2013; Edwards et al. 2003).

Therefore, it is likely that the increase in PDH levels in the HFD models comes from a shift to a glucose-reliant ATP production; while it was mentioned that there is a decrease in glucose oxidation with HFD, ageing seems to be a more significant factor in affecting the activity of PDH.

UCP3 plays a major role in FA oxidation and has been shown to be linked to fatty acid metabolism mechanisms via direct mediation in obese and diabetic hearts, independent of expression levels (Boudina et al. 2007; Hilse et al. 2018; Holloway et al. 2009) and, while not clear, it is safe to say that UCP3 has a direct effect in cardiac efficiency, as deletion of the UCP3 expression gene has been shown to induce a reduction in FA oxidation and a consequent reduction in ATP production as a result (Wilson, C. et al. 2007; Wright et al. 2009). In addition to this, studies have also shown that UCP3 decreases in abundance in the mitochondria of aged hearts, due to the mentioned shift from fatty acid oxidation to a more carbohydrate-based metabolism (Hilse et al. 2016; Hilse et al. 2018). In this study, the 6-month showed a significant increase in UCP3 expression, in an HFD-dependant manner, as seen in previous literature, likely due to an increase in FAs present on the tissue. The 18-month model, however, showed a non-significant HFD-dependant increase in UCP3, but the statistical analysis showed a p value of 0.058; these results correlate with the previously mentioned studies that have shown a reduction in UCP3 with age, something that the chapter 3 observations confirmed. However, these results have shown that there is a blunting in UCP3 expression in an age-dependant fashion. It was proposed that this effect is a consequence of PPAR $\alpha$  modulation, as it has been shown to be affected in aged models; furthermore, PPARs regulate gene expression in cardiomyocytes and changes in these genes cause a reduction in fatty-acid availability and oxidation with an accompanying glucose oxidation increase, which can cause cardiac dysfunctions (Haemmerle et al. 2011; Leone, Weinheimer and Kelly 1999).

Due to their vital role in UCP regulation, it is likely that there may be changes in PPAR expression that are causing the observed changes in UCP3 expression; however, further studies assessing PPAR $\alpha$  modulation are required to confirm this hypothesis.

## **5.5 Summary, limitations and final comments**

Similar to what was done in chapter 3, HFD models have been established for future research and, in addition to this, important contributions to the current literature on the subject have been made. It has been established that the presence of HFD causes non-significant changes on cardiac function in the isolated heart model, despite showing indications of hypertrophy, but does so in both the work-loop and protein expression studies. For the latter, specifically, it was found that the combination of HFD and age was causing increases in both phosphorylated PDH and available UCP3 expression (figures 4.3.3.1 and 4.3.3.2), but it is possible that this is most likely due to the presence of HFD as opposed to being an age-dependant change, as seen in previous literature.

The main limitations for this project, similarly to what was found in chapter 3, was the limited number of animals used due to animal housing issues and due to the fact that many of the 18-month animals did not survive until they were ready to be sacrificed. In addition to this, the use of female rats was also a potential direction to take the study, as previous research has shown that male and female rats express different genes and female rats have actually shown significant decreases in overall cardiac function and, which has not always been observed in male rats (Fannin et al. 2014). Another limitation was that only performance level changes of the papillary muscle in the presence of HFD was assessed, as none of the data supports the existence of contractile functional changes.

Finally, a lot of potential mitochondrial targets were not investigated due to the immense scope of the field. For this particular investigation, it would have been important to look at PPAR $\alpha$  activity to better understand the UCP3 and PDH results. Further research should, therefore, take this into account when investigating these particular mitochondrial agents. There is still a lot of work that can be done on this, but it has now been established that energy generation changes should be considered when investigating heart contractility and that there are significant variations on the energy production of both diet-induced obese animals and aged animals. In addition to this, investigating the mRNA levels of PDH, PPAR $\alpha$  and UCP3 would have been useful to complement the western blot results, as it would show whether there are gene expression changes directly or indirectly tied to the protein levels; for UCP3 this would be of particular importance due to previously published discrepancies between protein and mRNA levels.

The next chapter will focus on investigating how ageing induces changes in the contractile function of the heart change in when in the presence of different inotropic drugs, and how these drugs cause changes the expression of the active forms of both PDH and UCP3.

# **Chapter Six: Inotropic drug effects on the contractile function of the heart in an age-dependant study**

Some of the data in this chapter was presented as following:

- **Coventry University Symposium 2017 – Poster presentation**

Manuscripts in preparation which will include part of the data presented in this chapter:

- Inotropic functional changes of the heart in the presence of a high-fat diet, in differently aged models – *RA Ribeiro, Maddock, H, Tallis, J, Dodd, M, Gharanei, AM – Toxicology and Applied Pharmacology.*

## 6.1 Introduction

As it was mentioned in chapters 3 and 4, various functional, structural, cellular and molecular effects are involved in the aged heart, leading to age associated cardiac pathologies such as vascular thickening and arterial stiffness, impaired endothelial function, hypertrophy and fibrosis (Cheng et al. 2009; North and Sinclair 2012; Paneni et al. 2017). These changes can lead to various effects upon cardiac function, such as elevated systolic pressure and decreased diastolic pressure dysfunctions as a result of the aforementioned vascular stiffness ; in addition, the thickening of the vascular walls can also lead to a decline in endothelial cell function, as well as a loss of proliferation and movement, partially due to a reduction in endothelial nitric oxide synthetase activity (Izzo Jr and Shykoff 2001).

Studies have also looked at different molecular systems directly impacted by age, with three main regulation mechanisms being at the centre of it: the Renin Angiotensin Aldosterone System (RAAS), and cardiomyocyte relaxation impairment via the excitation-contraction coupling in the myocardium (Domenighetti et al. 2005), the adrenergic signalling level, most notably adenylyl cyclase type 5 (AC-5) on the extracellular signal-regulated kinase pathway, which has been previously shown to provide a degree of protection against oxidative stress (Yan et al. 2007) and the triggering of apoptotic events via mitochondrial ROS changes (Di Lisa and Bernardi 2006). Previous papers have also proven the existence of an impairment in certain mitochondrial proteins, as well as the existence of damaged mitochondria, in senescent rat hearts, that contribute to this link between mitochondrial dysfunctions and aged heart vulnerabilities. (Nitta et al. 1994; Tani et al. 2001). For an in-depth review on the effects of aging on cardiac function, please refer back to sections 1.4 and 1.6, as well as chapter 3 for a full physiological investigation. b

Due to this, studying the importance of the inotropic function of the heart is of particular importance. The inotropy of the heart is described as any force that increases myocardial contractile strength (Hasenfuss, Gerd and Teerlink 2011). The heart possesses three main endogenous inotropic mechanisms: a length-dependant cross-bridge activation, a heart rate dependant activation of contractile force and a catecholamine-mediated inotropy (Bers 2008). The most important of the three is the length-dependant activation (refer to section 1.3.4 for a detailed review), which occurs when the stroke volume of the left ventricle increases due to an increase in the total left ventricular volume (Ochsner et al. 2017); the heart rate dependant activation is calcium dependant, as an increase in heart rate implicates an increase in calcium levels and overall availability within the cardiomyocytes, which leads to an increase in contractility and the catecholamine-mediated inotropy is based on the usage of the  $\beta$ -adrenoceptor-adenylyl cyclase system to phosphorylate L-type calcium channels, via protein kinase A, in order to increase calcium influx and RyRs; phospholamban is also activated in order to accelerate calcium accumulation within the sarcoplasmic reticulum (Farrell and Howlett 2008; Grossman and Messerli 1998; Vallet, Dupuis and Chopin 1991). Isoprenaline, dobutamine, atenolol and itraconazole were the chosen drugs for this study due to their widespread usage worldwide (a full review on the mechanisms of each one can be found in chapters 1.7.1 to 1.7.4).

Guarnieri et al have previously shown that isoprenaline ( $5\mu\text{M}$ ) has an age-dependant effect in 7- and 22-month-old rats rat hearts (Guarnieri et al. 1980); in their study, the researchers used Wistar rats and mounted their hearts on a Langendorff apparatus before administrating increasingly high concentrations of isoprenaline ( $500\text{ nM}$ ) in 15-minute intervals. In addition to this, Guarnieri et al also ran protein assays to test for cAMP levels and myocardial membrane assays to test for cardiac  $\beta$ -adrenergic receptor activity.

The group found that the aged hearts respond with up to 40% less efficiency to  $\beta$ -receptor stimulation, with an associated increase in cyclic adenosine monophosphate (cAMP) levels; Guarnieri et al attributed this to a decrease in calcium handling within the myocytes but also suggest that there may be other factors in place. Lakatta et al did a study where they mounted the trabecular muscle of the heart on a stimulator and measured their power output; in addition, the group used increasing concentrations of both norepinephrine and isoprenaline to see how their effects changed in 6, 12 and 25-month rat models (Lakatta et al. 1975). The group found that both drugs caused a significant decrease in the maximal rate of tension development (dT/dt) of the aged hearts, which the researchers proposed to be linked to a decrease in available intracellular calcium and due to an intrinsic decrease in inotropic response in aged hearts.

Cardiac ageing is characterized by  $\beta$ -adrenoreceptor desensitization, with previous studies linking the phenomenon to changes in phosphorylation of the receptor structures (Abrass, Davis and Scarpace 1982; Hashimoto, Nakashima and Sugino 1983; Jiang, M., Moffat and Narayanan 1993); in addition, previous studies have also shown that, in terms of hemodynamic profiling, younger  $\beta$ -blocked patients and healthy elderly patients, without heart failure, have shown significant similarities in their impaired function, which provided researchers with further proof of this desensitization (Abrass, Davis and Scarpace 1982; Fleg, Aronow and Frishman 2011; Xiao et al. 1994b). Another study by Leineweber et al proposed that catecholamine levels play an important role in this desensitization of the aging heart, as the level of circulating catecholamines rises with the age associated plasma spill over from the tissues, which consequently causes a reduction of the catecholamines re-uptake transporter localized in the sympathetic nerve terminals (Leineweber et al. 2002).

The researchers further suggested that the  $\beta$ -adrenoceptor desensitization and down-regulation was one of the most important mechanisms to explain age-related decrease in  $\beta$ -adrenoceptor response to agonists. In addition to this, a more recent study found that the positive inotropic effect of  $\beta$ -receptor agonist is altered and reduced due to dysfunctions in the  $\beta_1$  and  $\beta_3$ -adrenoreceptors and in ATP production within the cells (Carillion et al. 2015).

Atenolol is a second-generation cardio-selective  $\beta_1$  receptor antagonist with both negative inotropic and chronotropic properties (see 1.7.3 for a full review on Atenolol). Atenolol has been previously used on cardiac research and has been shown to not only severely decrease the myocardial contractile force, but also the transmural flow and vascular resistance of the heart, in normal conditions (Berdeaux and Giudicelli 1982; Guth et al. 2015). On the isolated heart model, Atenolol has been shown to cause impaired coronary resistance during ischaemia, as well as a reduction in LVDP, HR, +dP/dt and -dP/dt when compared to control hearts (Allibardi et al. 1999; Lavanchy, Martin and Rossi 1988). It has also been shown to increase the risk of mortality in the elder population, especially in patients suffering from high pulse arterial pressure (Testa et al. 2014). In another study using 18-month mice models, it was found that Atenolol not only reduced the membrane fatty acid unsaturation of the heart, but also decreased the various markers of oxidative stress within the animals (Gómez et al. 2014; Sanchez-Roman et al. 2010; Sanchez-Roman et al. 2014). The Gómez study also recorded changes in the heart rate, systolic pressure and diastolic pressure in the hearts treated with atenolol, when compared to the control groups.

Itraconazole is a triazole antifungal agent (refer to section 1.7.4 for a full review on Itraconazole) that carries severe adverse effects, the most common ones being heart failure and a severe drop in left ventricular pressure (Fung, Chau and Yew 2008; Qu et al. 2013).

Studies have shown that patients are more likely to develop congestive heart failure when under treatments with Itraconazole, even when different protocols were used to measure the negative inotropic effect of the drug (Guth et al. 2015; Okuyan and Altin 2013). It has also been investigated in the isolated heart model and showed severe decreases in the heart rate, coronary flow, LVDP and the ventricular pressure rise and drop, starting at concentrations as low as 0.3  $\mu$ M (Qu et al. 2013). There is a very limited amount of information on Itraconazole but it is known that it is involved in CYP expression and a recent study used CYP2J2 cardiac expression models to show that, while younger mice retained their contractile function, the effect of CYP caused severe impairment in contractile function with age, due partially to a loss of cardioprotective mechanism against oxidative stress and decreased protein phosphatase 2A (Chaudhary et al. 2013). A study by Jamieson et al used echocardiography on 3- and 16-month-old soluble epoxide hydrolase (or sHE, a metabolite commonly linked to CYP function) mice to assess cardiac function and showed that there was a significant decline in cardiac function observed with age when compared to younger models (Jamieson et al. 2017).

The primary aims of this chapter were to investigate how different ages (3, 6 and 18-months) can affect whole heart cardiac functions, isolated muscle contractions and intracellular proteins associated with mitochondrial energetic metabolism, when under the effect of isoprenaline, dobutamine, atenolol and itraconazole. The main hypotheses for this chapter were **(a)** that due to  $\beta$ -receptor desensitization in ageing, Dobutamine and Atenolol measurements will show significant impaired effects on the haemodynamic function of the heart, **(b)** that Itraconazole will cause a significant decrease in the haemodynamic function of the heart, in an age-dependant fashion, due to changes in CYP expression and **(c)** that PDH and UCP3 Phosphorylation levels will be reduced in the presence of Dobutamine but will not change significantly in the presence of Atenolol and Itraconazole.

The main objectives of this study were: **(a)** to elucidate how Dobutamine, Itraconazole, Atenolol and Isoprenaline change the contractile function of a 3, 6 and 18-month heart using the Langendorff isolated heart model and the work-loop assay and **(b)** to investigate whether these changes occur partially as a result of mitochondrial energy metabolism changes, notably on the pathways involving pyruvate dehydrogenase E1- $\alpha$  subunit (PDH) and uncoupling protein 3 (UCP3).

## **6.2 Materials and Methods**

### **6.2.1 Animal Models**

Following ethics approval from the host institute, 3-month animals were purchased from Charles River UK Limited (Margate, UK) and received human care in accordance with the guidelines of the British Home Office Animals (Scientific Procedures) Act 1986 (Hollands 1986). 3, 6 and 18-month models were used due to these ages being representative of a young middle-aged and adult rat (as mentioned before in section 3.1, 3-month rats have been equated to a human child between 10-18 years, 6-month rats have been equated to a young adult between 20-30 years and 18-month rats have been equated to an older adult between 54-69 years (Andreollo et al. 2012; Capitanio et al. 2016; Jackson et al. 2017; Sengupta 2013)). The 3-month animals were used as controls for the studies. The body mass measurements for the animals were as follows: 3-month group (n=11) with an average body mass of  $350\text{g} \pm 3.2$  (SEM), 6-month group (n=10) with an average body mass of  $539\text{g} \pm 15.5$  (SEM) and 18-month group (n=4) with an average body mass of  $794\text{g} \pm 8.4$ (SEM). All animals were sacrificed by means of cervical dislocation, in accordance with the British Home Office Animals (Scientific Procedures) Act 1986, Schedule 1 (Hollands 1986).

### **6.2.2 Langendorff Isolated Heart Model (full review in section 3.2)**

The technique starts with the perfusion of the heart with Krebs-Henseleit buffer (maintained at a constant temperature of  $37^{\circ}\text{C} \pm 0.5$  at a pH of 7.4) and gassed with 95%  $\text{O}_2$  and 5%  $\text{CO}_2$ , by means of cannulating the aorta, in a retrograde fashion, forcing the closing of the aortic valve as a result of a change in pressure. The buffer then passes through a vascular bed before being drawn to the coronary sinus in the right atria. This allows the preparation to be maintained without any fluid filling the ventricular chambers (Skrzypiec-Spring et al. 2007). Measurements for the coronary flow (CF), left ventricular developed pressure (LVDP), heart rate (HR) and the Maximum ventricular pressure increase (+dP/dtmax) and decrease (-dP/dTmax) were recorded using a physiological pressure transducer connected to the latex balloon and to a PowerLab (ADInstruments, UK) linked to a PC with LabChart<sup>®</sup> software v7 and the rate pressure product (RPP) was calculated using the function mentioned in section 3.2.2. At the end of the protocol, the left ventricle was excised from each heart and divided into two; tissues were then rapidly frozen in liquid nitrogen before being stored at  $-80^{\circ}\text{C}$  for future use. For a full background review, please refer to section 3.2. The experimental protocol for each of the inotropes used (Dobutamine, Itraconazole and Atenolol) was split into a 20-minute stabilisation period and 140 minutes of increasingly high drug concentrations for all hearts (ranging from 1nM to  $30\mu\text{M}$ , for a total of seven different concentrations); a 20-minute cumulative protocol was chosen based on preliminary data that indicated that it was the adequate time to achieve a steady contractile response with the used inotropic drugs (see figure 6.2.2.1).

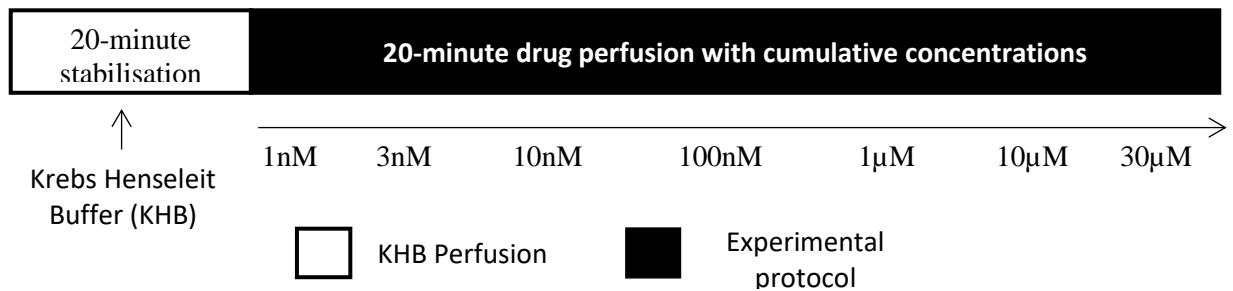


**Figure 6.2.2.1 - Langendorff protocol.** Diagram for the cumulative dose-controlled protocol for the Langendorff isolated heart model used in this project, per drug.

### 6.2.3 Work-loop assay (full review in section 3.3)

Following the sacrifice of the animal, the diaphragm was cut to expose the thoracic cavity and the thorax was subsequently opened to expose the heart. The excised hearts were immediately placed in ice cold modified Ringers buffer (NaCl, 144mM; sodium pyruvate, 10mM; KCl, 6mM; MgCl<sub>2</sub>, 1mM; CaCl<sub>2</sub>, 2mM; NaH<sub>2</sub>PO<sub>4</sub>, 1mM; MgSO<sub>4</sub>, 1mM; Hepes, 10mM; with a pH of 7.4 at room temperature and oxygenated with 100% O<sub>2</sub>) and held in place on a silicone petri dish.

This preparation was then placed under a microscope, to dissect the muscle as quickly as possible. Muscles containing branches or smaller muscles attached to them were excluded due to the potential to disturb forces production and recording. The chosen muscles were carefully trimmed and dissected and were then clamped at both the tendon and the ventricular chamber wall by small aluminium foil T-shaped clips. The muscle was left untouched to avoid potential damage. The dissected muscle was then placed on a horizontal chamber in an organ bath with circulating modified Ringers buffer and maintained at 37°C. The muscles were also connected to a 50nM force transducer and a high-speed length controller that were later used to stimulate the muscles at a 60-mA amplitude. (Layland, Young and Altringham 1995). The resulting developed force was calculated by subtracting the maximum produced force from the minimum produced force.

The optimal muscle length was obtained by gradually increasing the muscle length using a micromanipulator (all products were purchased from Aurora Scientific, Canada) until the maximum developed force was reached ( $L_{max}$ ). Once reached the muscle length was measured with an eyepiece. For the actual work-loop protocol, the muscles were set to 95% of their original maximum length ( $L_{95\%}$ ) and allowed a 30-minute stabilisation period.

Once the  $L_{95\%}$  was calculated, the work-loop protocol (see figure 4.2.3.1) was carried out at a frequency of 6Hz and a strain amplitude of  $\pm 6\%$  which, again, has been shown to produce the maximum power output in the cardiac muscle (Layland, Young and Altringham 1995). The heart muscles were allowed to stabilise for the first 30 minutes of the protocol before being perfused with one of the selected inotropes for 90 minutes (concentrations used for each drug were based on the current clinically relevant concentrations: Dobutamine –  $5\mu\text{M}$ ; Isoprenaline –  $100\text{nM}$ ; Atenolol –  $20\mu\text{M}$  and Itraconazole –  $10\mu\text{M}$ ). The loops were repeated every 5 minutes, for a total of 120 minutes (24 loops per muscle run). At the end of the protocol (see figure 6.2.3.1 for a simplified diagram), the muscles were then weighed using an electronic balance. Instantaneous power was calculated for every data point in each loop (1864 total data points per loop) and was then averaged to generate a net-work value for each loop. At the end of the 120 minutes, the muscle was weighed to the nearest  $0.00001\text{g}$  using an electronic balance. Instantaneous power output was calculated for every data point by multiplying instantaneous force generated by instantaneous velocity. This was done for each loop (1863 total data points per loop) and then averaged to generate a net-work value for each instance of a completed loop (Gharanei et al. 2014).



**Figure 5.2.3.1 – Work-loop protocol.** Diagram of the work-loop protocol used for this project.

#### 6.2.4 Western Blotting (full review in section 3.4)

Cardiac tissue was collected from each treatment group, as mentioned in table 3.1.2.2. Approximately half of the left ventricle (50 mg) was then homogenized with lysis buffer (100 mM NaCl, 10 mM Tris base - pH 8.0, 1 mM EDTA - pH 8.0, 2 mM sodium pyrophosphate, 2 mM NaF, 2 mM  $\beta$ -glycerophosphate, SigmaFAST™ protease inhibitor cocktail tablets – 1 tablet/100ml and PhosStop™ - 1 tablet/10ml) on a IKA Ultra-Turrax® T 25 basic disperser, set to a speed of 21,500 RPM.

This tissue was then centrifuged for 10 minutes at 11,000 RPM at 4°C to obtain the desired supernatant, which was then transferred into clean 1.5ml microcentrifuge tubes. Samples were diluted using Laemmli buffer (250 mM Tris-HCl – pH 6.8, 10% glycerol, 0.006% bromophenol blue, 4% SDS,  $\beta$ -mercaptoethanol – pH 6.8) and incubated at 100°C for 5 minutes before being stored at –20°C. Prior to using the samples, they were defrosted on ice and diluted further using Laemmli buffer to obtain a protein concentration of 50 $\mu$ g. To calculate the protein content of homogenised samples, a colorimetric Pierce™ BCA Protein assay kit (Thermo Fisher Scientific, UK) was used. Concentrated albumin standards were serially diluted using lysis buffer to obtain a concentration range of 0 - 2000 $\mu$ g/ml.

BCA working reagent was prepared following a 50:1 ratio of reagent A and reagent B, respectively. Standards and samples were pipetted at a volume of 10 $\mu$ l, in triplicate, onto a 96-well plate. Following this, 200 $\mu$ l of working reagent was added to each well.

Plates were then covered to protect from light and incubated for 30 minutes at 37°C, before being left to cool to room temperature. The plate reader was set to 562 nm and the measured absorbance values were then used to calculate the total protein content per unknown sample. The previously collected samples were further diluted using laemmli buffer to obtain a concentration of 50µg/µl. These samples were then centrifuged at 1200 RPM for 2 minutes, at 4°C, before being loaded onto Precast TGX™ (Tris/glycine) gradient gels (Bio-Rad, UK). The gels were then placed inside of a Mini-PROTEAN™ vertical electrophoresis assembly unit before filling the chamber and outer tank with running buffer (14.42g/L Glycine, 1.0g/L SDS, 3.03g/L Tris base). The samples were then loaded into the wells, with at least one well loaded with a molecular protein marker acquired from Cell Signalling UK. Gels were run at 110V for 60 minutes using a Power-PAC 3000 (Bio-Rad, UK).

Following electrophoretic separation, the gels were removed from their compartments and placed onto Trans-Blot® Turbo™ transfer packs, consisting of filter paper, buffer and a polyvinylidene fluoride (PVDF) membrane. The assembled cassettes were loaded into the Trans-Blot system (Bio-Rad, UK) and ran for the mixed molecular weight transfer protocol for a total of 7 minutes. Following transfer, the membranes were cut into two using a scalpel blade. Blots were then incubated at room temperature in blocking buffer (5% w/v milk powder in Tris-buffered saline with Tween 20 (TBST) for 60 minutes on an orbital shaker (Cassambai et al. 2019). Blots were then incubated overnight in 5% w/v bovine serum albumin (BSA) in TBST - 1/1000, at 4°C, with anti-UCP3 antibody and phosphorylated Pyruvate Dehydrogenase E1-alpha subunit purchased from Abcam (UK).

The following day, blots were then incubated with secondary antibody (anti-rabbit HRP IgG – 1/1000, Cell Signalling, UK) in blocking solution (5% w/v milk powder in TBST) and incubated for 1 hour at room temperature on an orbital shaker.

To visualise the membranes, they were first placed onto an acetate sheet and coated with approximately 1 mL of SuperSignal West Femto kit (Thermo-Scientific), in a 1:1 dilution, to amplify the signals from the membranes. Images were then captured and visualised using a ChemiDoc with the ImageLab™ Touch software (Bio-Rad, UK). Membranes were exposed for 3 to 5 seconds (see representative blot in figure 2.4.6.1) in order to detect the bands corresponding to the proteins of interest. Images were subsequently analysed using the java-based software ImageJ (National Institutes of Health, USA). After visualising the membranes, they were stripped using Restore™ Western Blot Stripping Buffer (Thermo Fisher Scientific, UK) and re-probed for the total form of Pyruvate Dehydrogenase E1-alpha subunit and GAPDH, to be used as controls for the data.

#### **6.2.5 Statistical Analysis (full review in section 3.6)**

The haemodynamics and work-loop data were plotted as a percentage of the average stabilisation (mean  $\pm$  standard error of the mean (SEM)). Two-Way analysis of variance (ANOVA) was used with Tukey's LSD (least significant difference) for each time point as a function of each age group and each treatment, for both the Langendorff and the work-loop data. Fisher's LSD was used for the western blot data, as the main interest was in finding the minimum difference between protein expression. A p-value of  $p < 0.05$  was considered statistically significant. Origin Pro 2015 (Origin Lab Corporation, USA) was used to plot all of the dose response graphs for each of the inotropes.

## 6.3 Results

### 6.3.1 Langendorff Isolated Heart Model

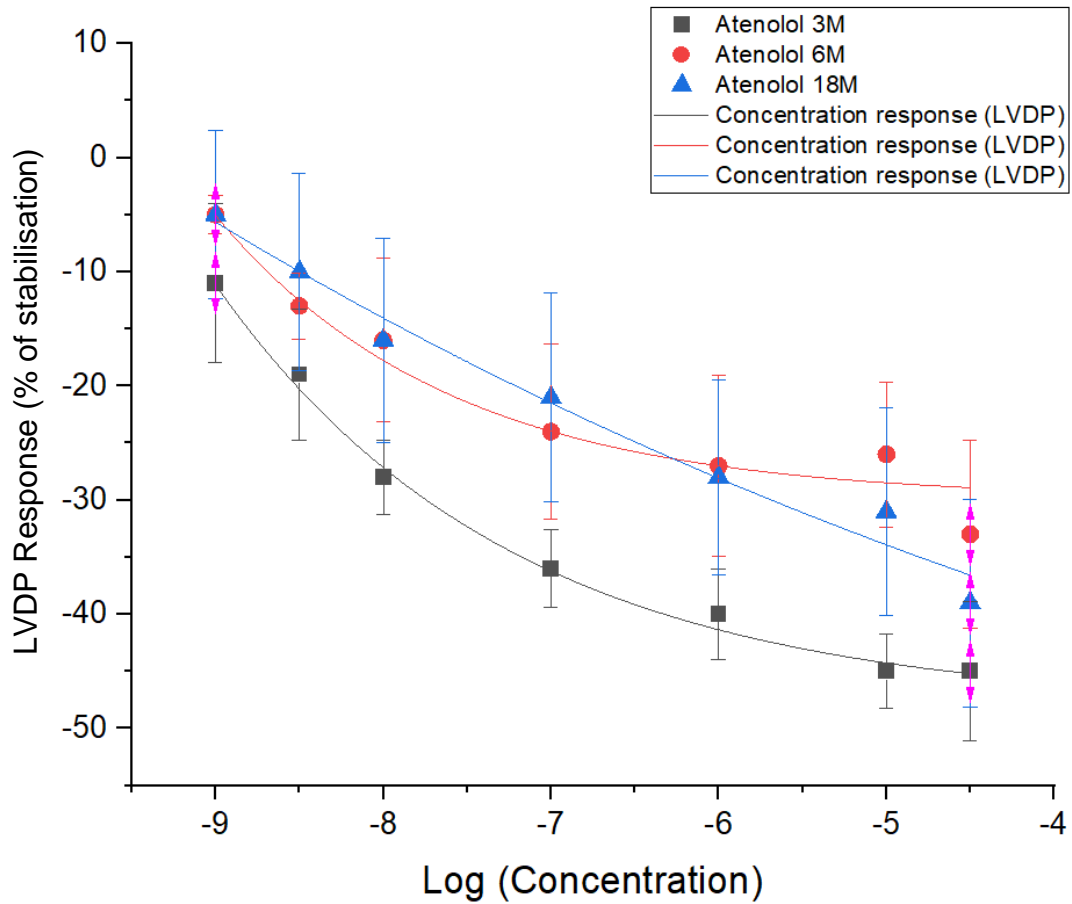
In order to present the Langendorff data, a table was necessary in addition to the concentration response curves, in order to highlight the changes in response occurring on the isolated heart. Table 6.3.1.1 contains the maximum and minimum responses for the relevant haemodynamic parameters, per inotropic drugs, in addition to their EC50 values.

Significances for these parameters have been depicted in figures 6.3.1.1 to 6.3.1.13.

**Table 6.3.1.1 – Table with the minimum and maximum drug response on the isolated heart, and respective EC50 value.** The values shown on the table represent the minimum and maximum response of the heart after being exposed to increasingly higher drug concentrations. The EC50 is also presented, showing the half maximal concentration required to induce a response.

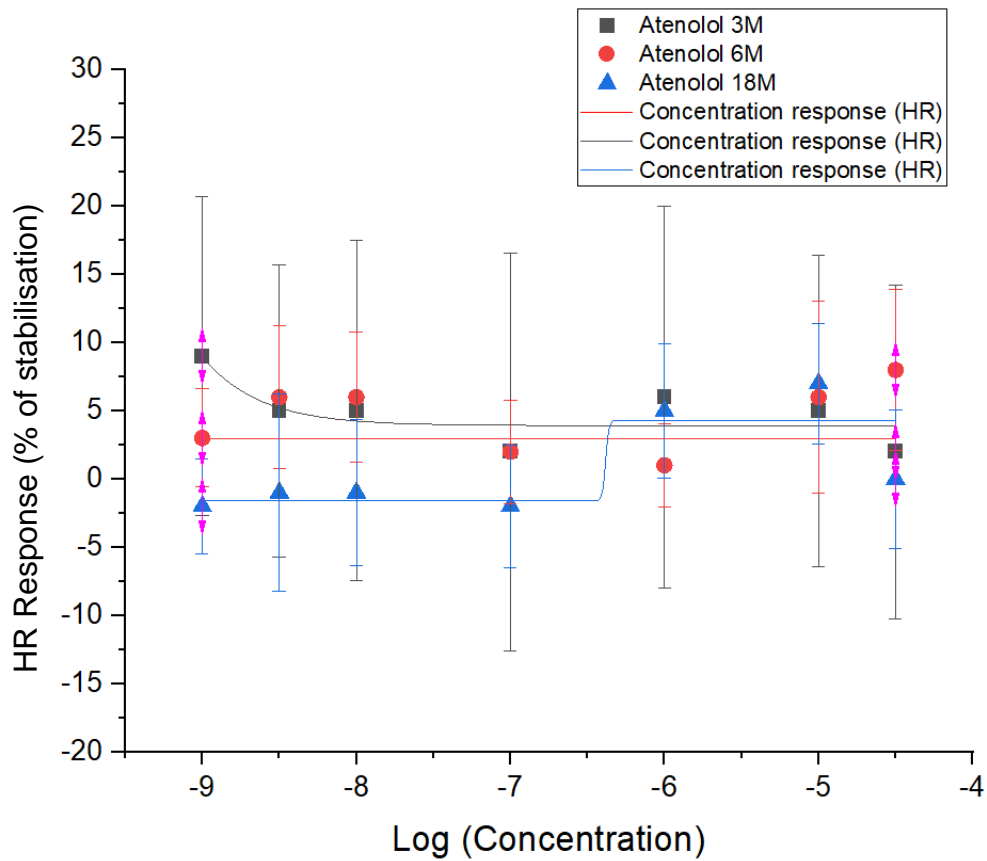
		Minimum response (% of stabilisation)			Maximum response (% of stabilisation)			EC50 (M)		
		3	6	18	3	6	18	3	6	18
<b>Age (months)</b>										
<b>LVDP (mmHg)</b>	Atenolol	-11	-5	-5	-45	-33	-39	1x10 <sup>-8</sup>	2.4x10 <sup>-8</sup>	1.4x10 <sup>-7</sup>
	Itraconazole	-3	1	-8	-50	-55	-60	5x10 <sup>-8</sup>	5.3x10 <sup>-7</sup>	2.7x10 <sup>-7</sup>
	Dobutamine	0	18	25	13	45	51	2.4x10 <sup>-5</sup>	3.9x10 <sup>-8</sup>	1.5x10 <sup>-6</sup>
<b>HR (bpm)</b>	Atenolol	2	1	0	9	8	7	3.2x10 <sup>-6</sup>	1.8x10 <sup>-9</sup>	5.6x10 <sup>-6</sup>
	Itraconazole	2	-5	0	14	-16	20	1.5x10 <sup>-5</sup>	2.2x10 <sup>-6</sup>	1x10 <sup>-7</sup>
	Dobutamine	1	3	-10	17	49	21	1.5x10 <sup>-7</sup>	5.8x10 <sup>-8</sup>	1.1x10 <sup>-6</sup>
<b>MPR (mmHg/s)</b>	Atenolol	9	1	-2	-10	-14	-17	2.7x10 <sup>-8</sup>	1.2x10 <sup>-6</sup>	1.8x10 <sup>-8</sup>
	Itraconazole	5	1	8	-26	-34	-17	1.3x10 <sup>-8</sup>	2.5x10 <sup>-6</sup>	6.8x10 <sup>-8</sup>
	Dobutamine	8	10	0	45	51	16	5x10 <sup>-8</sup>	1.3x10 <sup>-7</sup>	2.3x10 <sup>-7</sup>
<b>MPD (mmHg/s)</b>	Atenolol	6	-2	-1	-7	-15	-14	4.5x10 <sup>-6</sup>	3.2x10 <sup>-7</sup>	5.6x10 <sup>-8</sup>
	Itraconazole	6	1	2	-12	-22	-14	3.2x10 <sup>-9</sup>	6.2x10 <sup>-7</sup>	3.2x10 <sup>-8</sup>
	Dobutamine	-1	-3	-6	31	50	22	1.5x10 <sup>-6</sup>	5.3x10 <sup>-7</sup>	1x10 <sup>-9</sup>
<b>RPP (mmHg/min)</b>	Atenolol	-3	-3	-7	-45	-26	-39	1x10 <sup>-8</sup>	4.8x10 <sup>-8</sup>	2.2x10 <sup>-7</sup>
	Itraconazole	2	-3	-6	-44	-62	-52	1x10 <sup>-8</sup>	7.5x10 <sup>-7</sup>	3.5x10 <sup>-7</sup>
	Dobutamine	8	21	13	29	104	63	2.4x10 <sup>-7</sup>	4.1x10 <sup>-8</sup>	1.7x10 <sup>-9</sup>

Figure 6.3.1.1 represents the LVDP, or the difference between the systolic and diastolic pressure, plotted as both a % of the stabilisation time. When looking at the % of stabilisation, the post-hoc tests carried out showed no significance among the different for the atenolol-treated aged hearts.



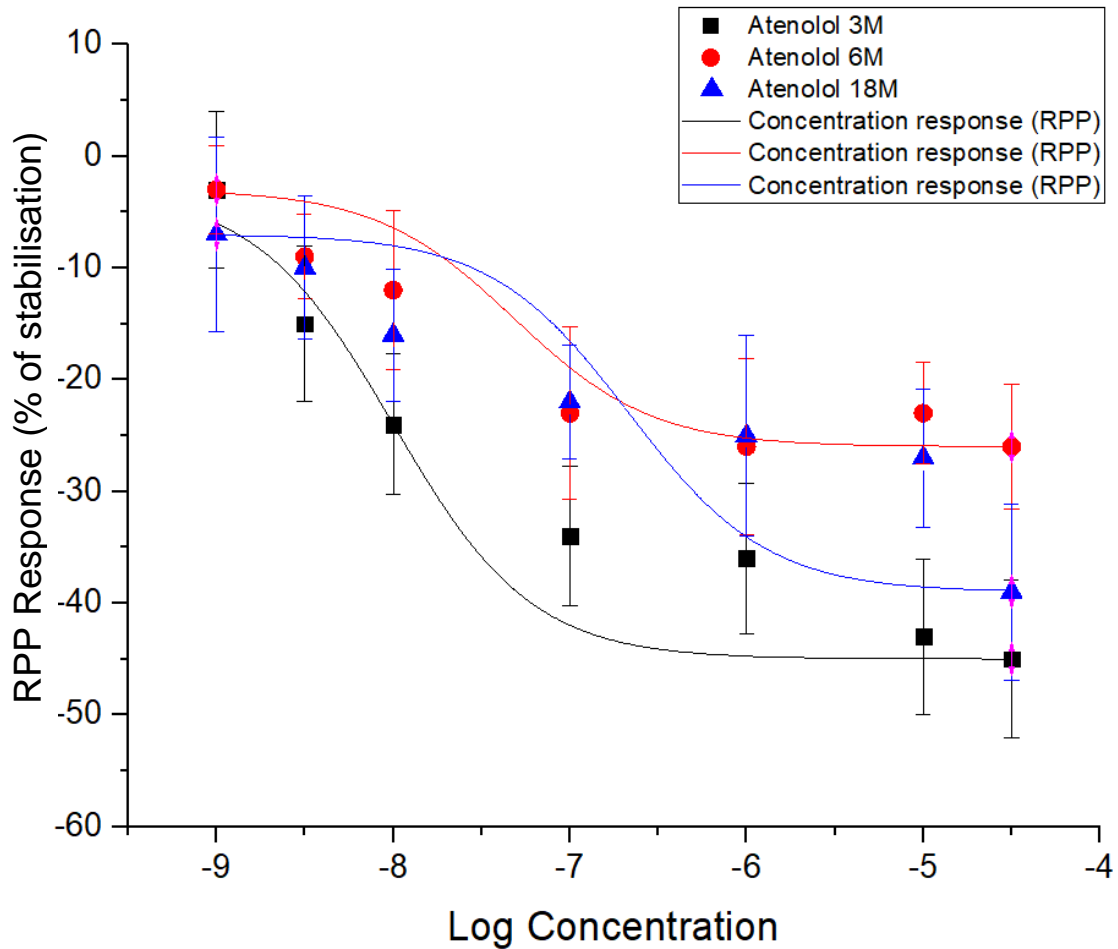
**Figure 6.3.1.1 – LVDP for Atenolol across the different aged models (n = 4 for all).** Hearts were allowed a 20-minute stabilisation period followed by increasing concentrations of each compound: 1 nM = 20-40 mins; 3 nM = 40-60 mins; 10 nM = 60-80 mins; 100 nM = 80-100 mins; 1  $\mu$ M = 100-120 mins; 10  $\mu$ M = 120-140 mins and 30  $\mu$ M = 140-160 mins.

Figure 6.3.1.2 represents the HR, or the number of heart beats per minute, plotted as both a % of the stabilisation time. When looking at the % of stabilisation, the post-hoc test showed no significance for the atenolol-treated hearts.



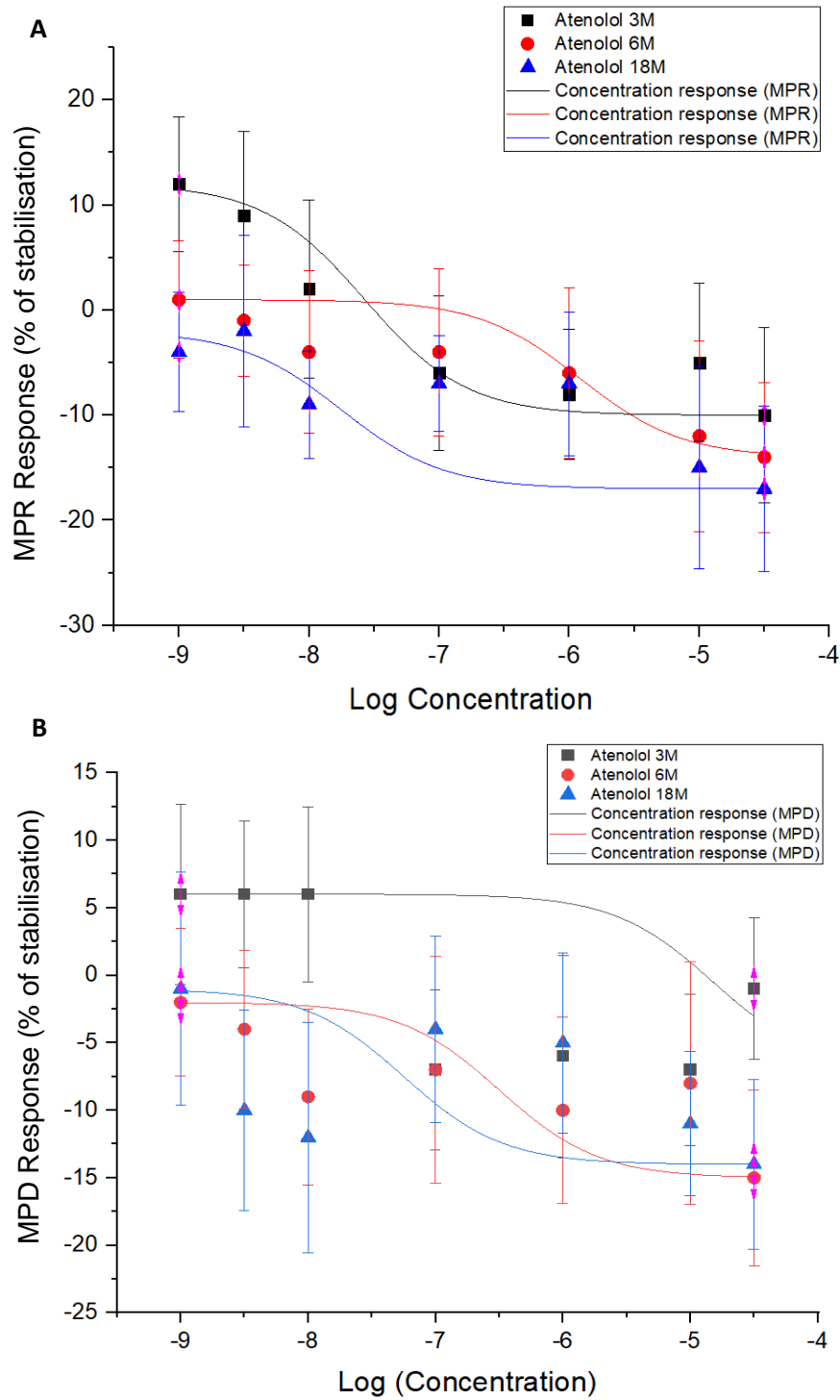
**Figure 6.3.1.2 – HR for Atenolol across the different aged models (n = 4 for all).** Hearts were allowed a 20-minute stabilisation period followed by increasing concentrations of each compound: 1 nM = 20-40 mins; 3 nM = 40-60 mins; 10 nM = 60-80 mins; 100 nM = 80-100 mins; 1 μM = 100-120 mins; 10 μM = 120-140 mins and 30 μM = 140-160 mins.

The RPP (figure 6.3.1.3) represents a calculation for the total myocardial workload of the heart, by multiplying the LVDP by the HR, plotted as a % of the stabilisation time. The RPP showed no significant changes when comparing between any of the three aged models.



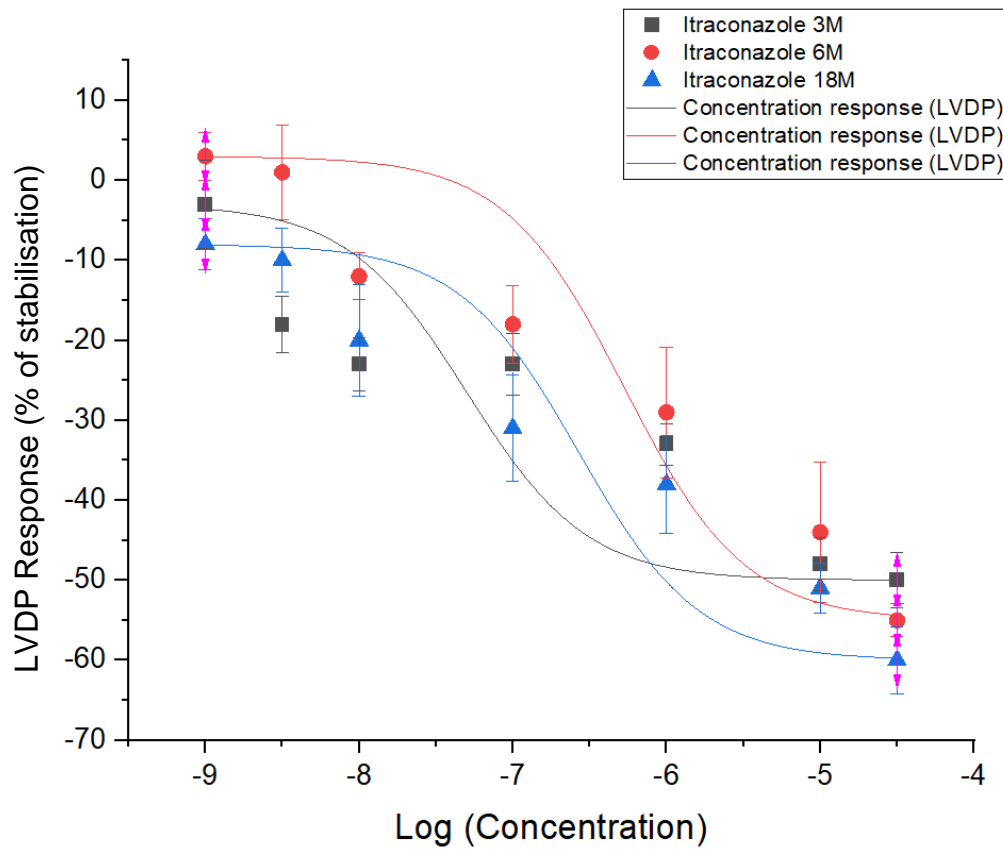
**Figure 6.3.1.3 – RPP for Atenolol across the different aged models (n = 4).** Hearts were allowed a 20-minute stabilisation period followed by increasing concentrations of each compound: 1 nM = 20-40 mins; 3 nM = 40-60 mins; 10 nM = 60-80 mins; 100 nM = 80-100 mins; 1 μM = 100-120 mins; 10 μM = 120-140 mins and 30 μM = 140-160 mins.

The MPR (graph A) and MPD (graph B) showed (6.3.1.4), yet again, no significant changes throughout the protocol.



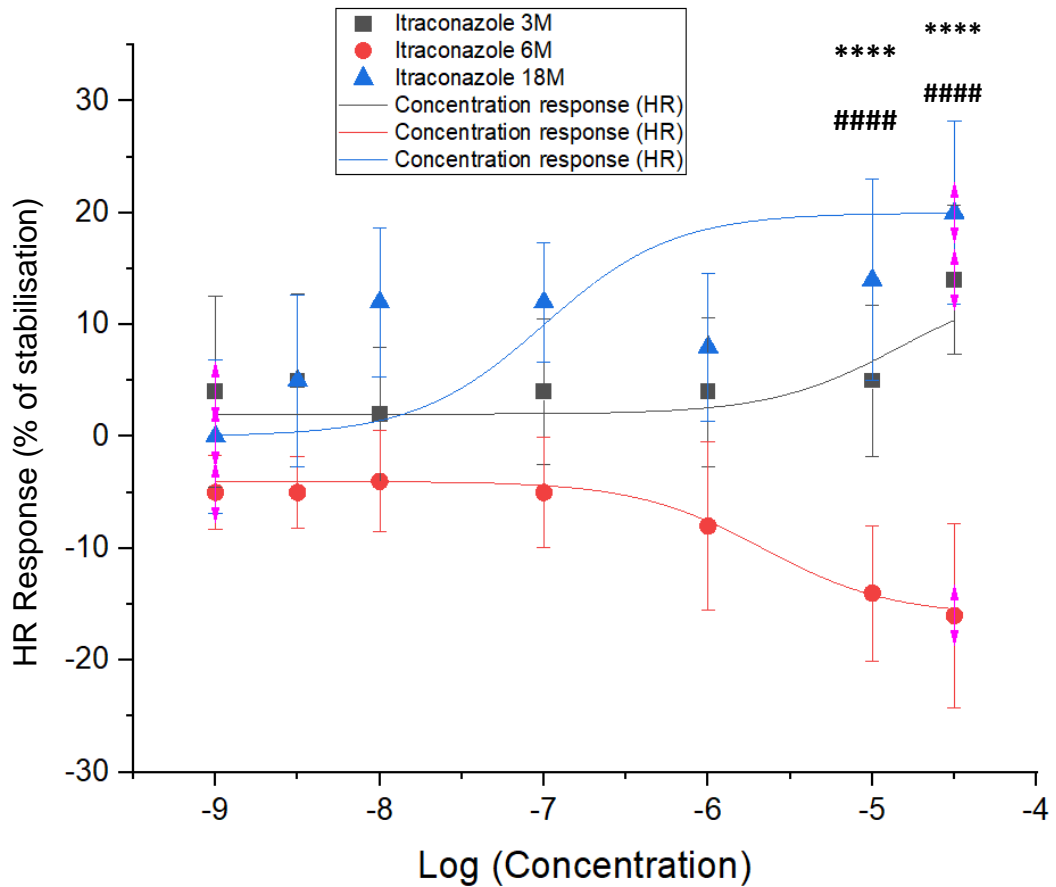
**Figure 6.3.1.4 – +dP/dTmax (A) and – dP/dTmax (B) for Atenolol across the different aged models (n = 4 for all).** Hearts were allowed a 20-minute stabilisation period followed by increasing concentrations of each compound: 1 nM = 20-40 mins; 3 nM = 40-60 mins; 10 nM = 60-80 mins; 100 nM = 80-100 mins; 1  $\mu$ M = 100-120 mins; 10  $\mu$ M = 120-140 mins and 30  $\mu$ M = 140-160 mins.

The LVDP (figure 6.3.1.5) for the itraconazole-treated hearts showed no significance between the three different models, but a negative inotropic was recorded.



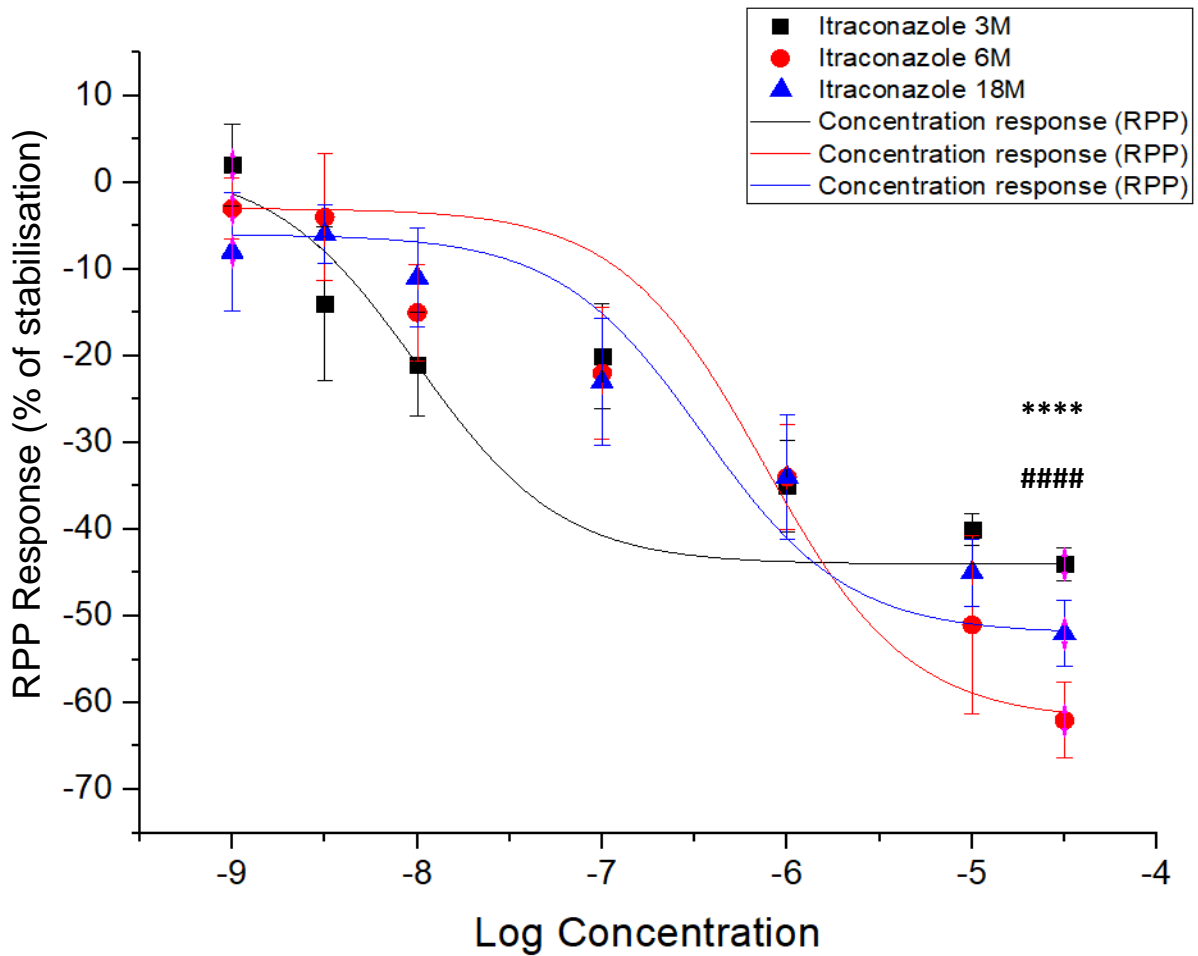
**Figure 6.3.1.5 – LVDP for Itraconazole across the different aged models (n = 4 for all).** Hearts were allowed a 20-minute stabilisation period followed by increasing concentrations of each compound: 1 nM = 20-40 mins; 3 nM = 40-60 mins; 10 nM = 60-80 mins; 100 nM = 80-100 mins; 1 μM = 100-120 mins; 10 μM = 120-140 mins and 30 μM = 140-160 mins.

As for the HR (figure 6.3.1.6), significance was observed for both the 10 and 30 μM concentrations (-29% and -30% ± 6.0 and 8.2 (SEM),  $p < 0.0001$ , respectively), for the 6-month hearts, when compared to the 3-month control. No significance was observed for the 18-month models.



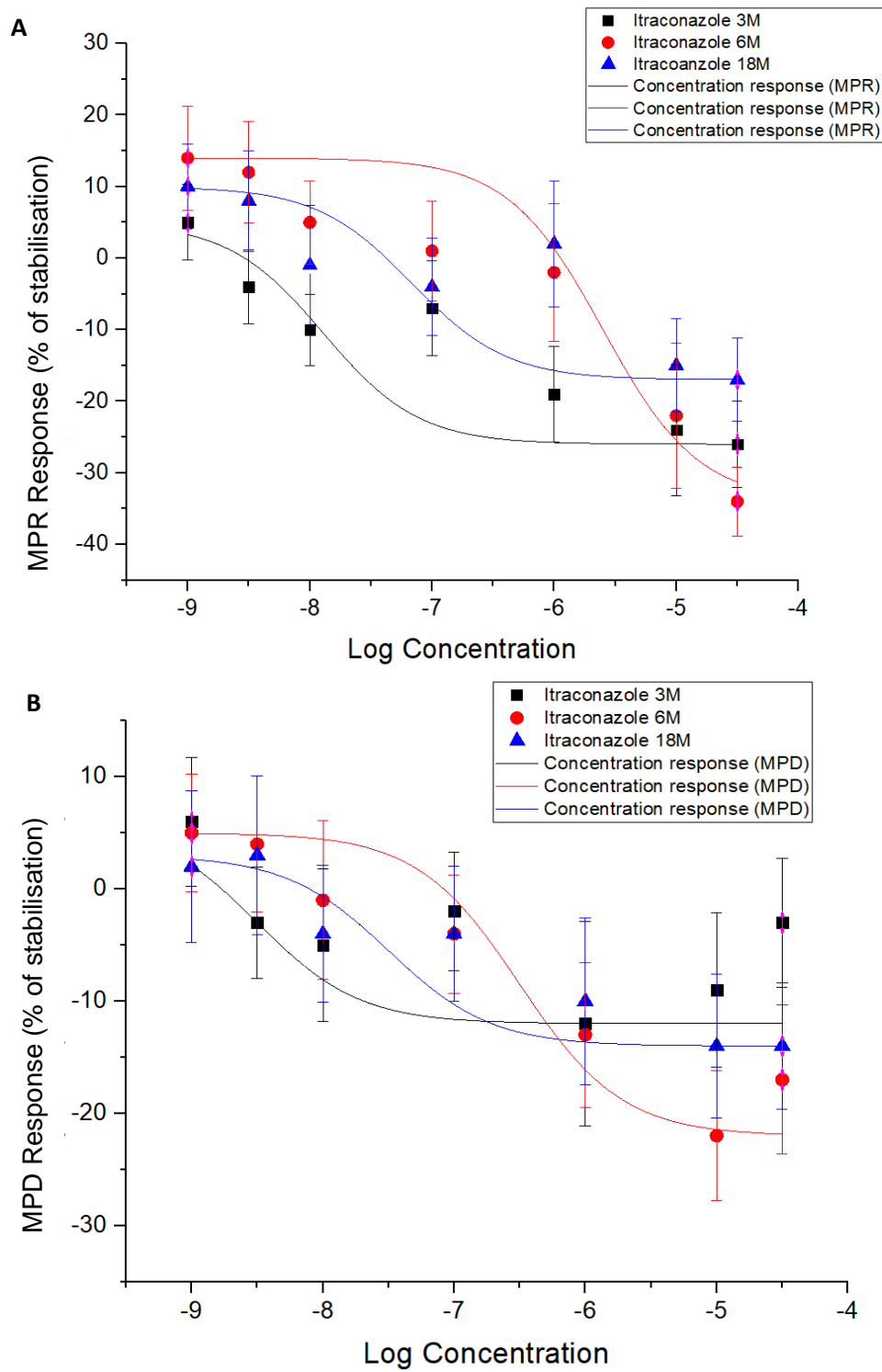
**Figure 6.3.1.6 – HR for Itraconazole across the different aged models (n = 4 for all).** Hearts were allowed a 20-minute stabilisation period followed by increasing concentrations of each compound: 1 nM = 20-40 mins; 3 nM = 40-60 mins; 10 nM = 60-80 mins; 100 nM = 80-100 mins; 1  $\mu$ M = 100-120 mins; 10  $\mu$ M = 120-140 mins and 30  $\mu$ M = 140-160 mins. Measurements for HR when treated with Itraconazole are displayed above (6-month model: \*\*\*\* =  $p < 0.0001$  in relation to the 3-month model and #### =  $p < 0.0001$ , in relation to the 18-month model).

For the RPP (see figure 6.3.1.7), the three models followed a similar pattern, as seen by the concentration response curves, but without any significant changes when comparing them to each other up until the highest concentration (30 $\mu$ M), with a decrease of -20% ( $p < 0.0001$ ) on the 6-month model and -15% ( $p < 0.01$ ) on the 18-month model, when compared to the 3-month control.



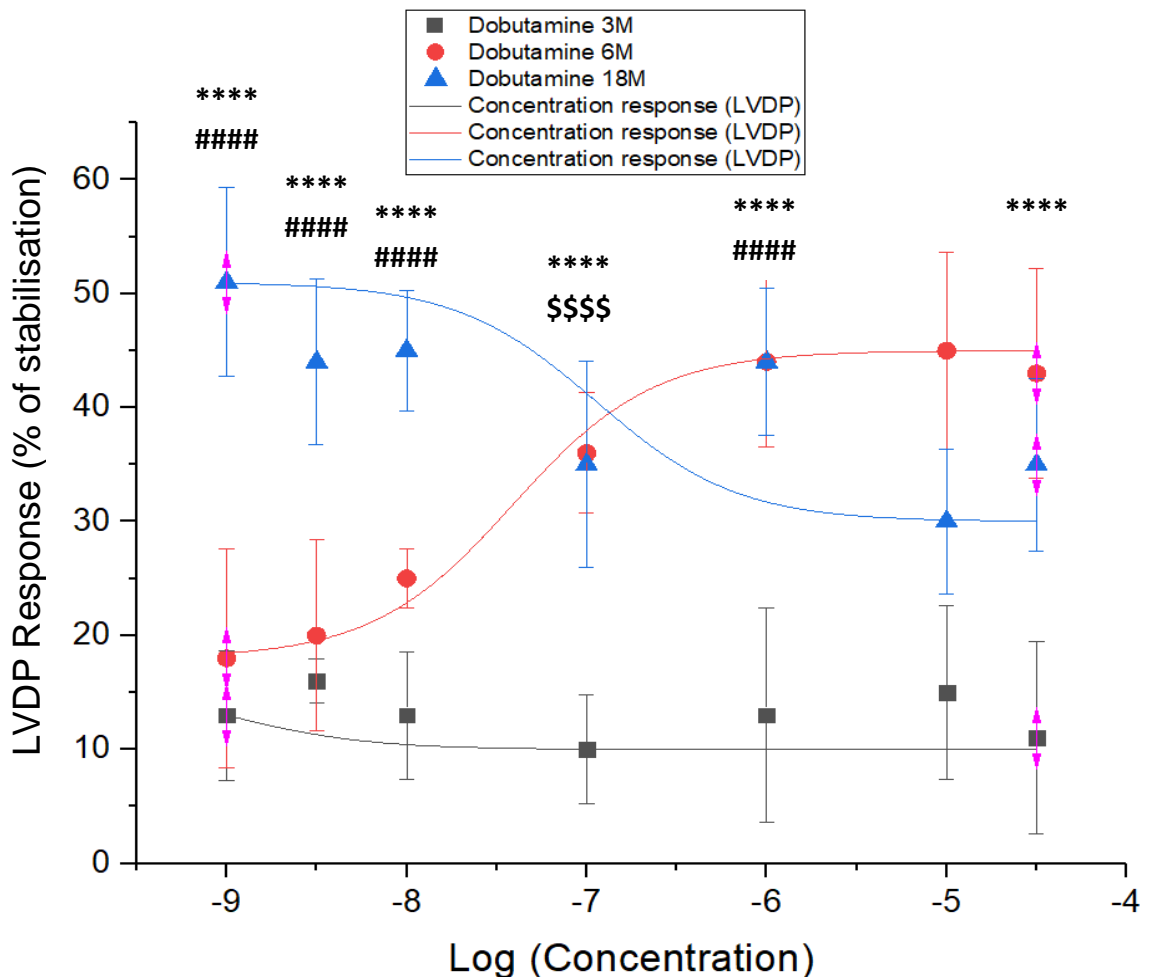
**Figure 6.3.1.7 – RPP for Itraconazole across the different aged models (n = 4 for all).** Hearts were allowed a 20-minute stabilisation period followed by increasing concentrations of each compound: 1 nM = 20-40 mins; 3 nM = 40-60 mins; 10 nM = 60-80 mins; 100 nM = 80-100 mins; 1  $\mu$ M = 100-120 mins; 10  $\mu$ M = 120-140 mins and 30  $\mu$ M = 140-160 mins (6-month model: \*\*\*\* =  $p < 0.0001$  in relation to the 3-month model and ##### =  $p < 0.0001$ , in relation to the 18-month model).

Both the MPR and MPD (Figure 6.3.1.8, graphs A and B, showed no significance across the three aged models, although the expected decline in response seen in chapter 4 was still recorded.



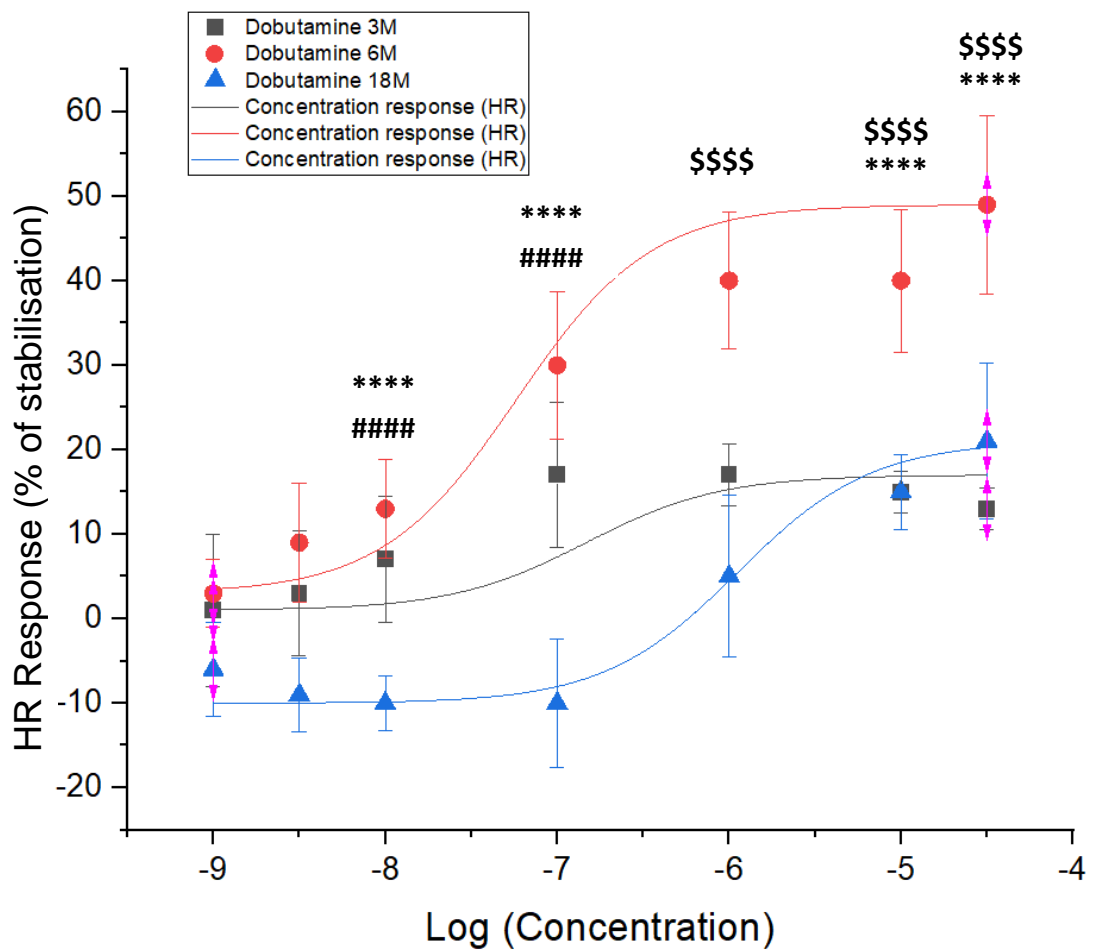
**Figure 6.3.1.8 – +dP/dTmax (A) and -dP/dTmax (B) for Itraconazole across the different aged models (n = 4 for all).** Hearts were allowed a 20-minute stabilisation period followed by increasing concentrations of each compound: 1 nM = 20-40 mins; 3 nM = 40-60 mins; 10 nM = 60-80 mins; 100 nM = 80-100 mins; 1 μM = 100-120 mins; 10 μM = 120-140 mins and 30 μM = 140-160 mins.

Figure 6.3.1.9 represents the LVDP, or the difference between the systolic and diastolic pressure, plotted as both a % of the stabilisation time. When looking at the % of stabilisation, the 18-month model showed a very strong significant response to Dobutamine, with an increase of  $+41\% \pm 7.5$  (SEM) at the 1nM concentration, when compared to the 3-month control ( $p < 0.0001$ ). The 6-month model showed no initial significance, but that changed at the 100nM concentration ( $+25\% \pm 2.5$  (SEM),  $p < 0.0001$ ), reaching its peak significant increase at the  $10\mu\text{M}$  concentration ( $+43\% \pm 8.6$  (SEM),  $p < 0.0001$ ), in relation to the 3-month control. In addition, the 3-month model seems to show little to no significant increase when comparing between doses.



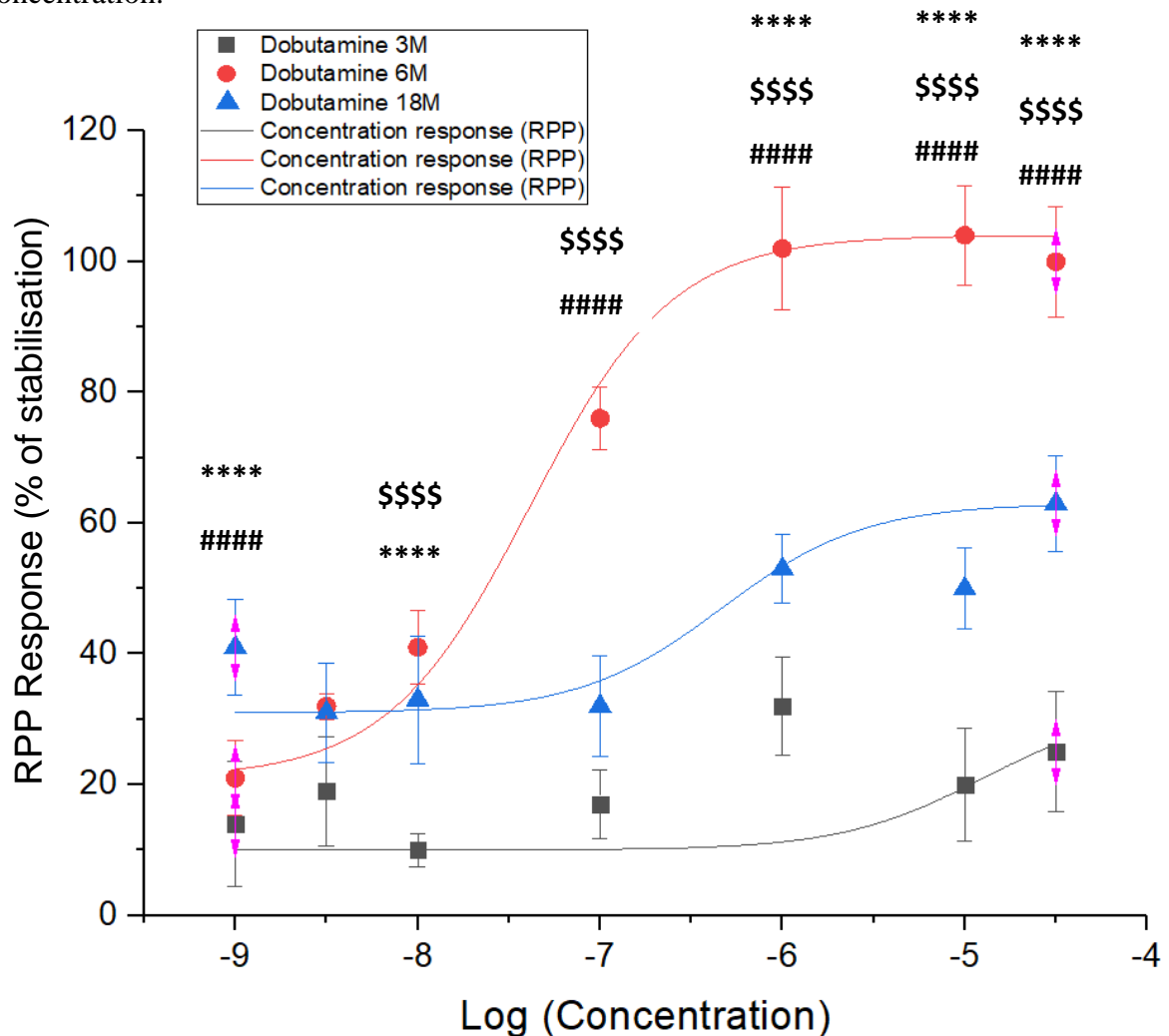
**Figure 6.3.1.9 – LVDP for Dobutamine across the different aged models (n = 4 for all).** Hearts were allowed a 20-minute stabilisation period followed by increasing concentrations of each compound: 1 nM = 20-40 mins; 3 nM = 40-60 mins; 10 nM = 60-80 mins; 100 nM = 80-100 mins; 1 µM = 100-120 mins; 10 µM = 120-140 mins and 30 µM = 140-160 mins. Measurements for LVDP when treated with Dobutamine are displayed above (6-month model: \$\$\$ =  $p < 0.0001$  in relation to the 3-month model; 18-month model: \*\*\*\* =  $p < 0.0001$  in relation to the 3-month model and ##### =  $p < 0.0001$ , in relation to the 6-month model).

Figure 6.3.1.10 represents the HR, or the number of heart beats per minute, plotted as both a % of the stabilisation time. When looking at the % of stabilisation, the 6-month model mimics the 3-month control group for the first 4 concentrations, before showing a significant increase at the 1 $\mu$ M (+23%  $\pm$  8.0 (SEM),  $p < 0.0001$ ), an increase that is maintained until the end of the protocol. The 18-month model, on the other hand, showed a significant decrease at the 10 and 100nM concentrations (-17%  $\pm$  3.2 (SEM) and -27%  $\pm$  7.6 (SEM), respectively,  $p < 0.0001$ ), before equalising with the 3-month control.



**Figure 6.3.1.10 – HR for Dobutamine across the different aged models (n = 4 for all).** Hearts were allowed a 20-minute stabilisation period followed by increasing concentrations of each compound: 1 nM = 20-40 mins; 3 nM = 40-60 mins; 10 nM = 60-80 mins; 100 nM = 80-100 mins; 1  $\mu$ M = 100-120 mins; 10  $\mu$ M = 120-140 mins and 30  $\mu$ M = 140-160 mins. Measurements for HR when treated with Dobutamine are displayed above (6-month model: \$\$\$\$ =  $p < 0.0001$  in relation to the 3-month model; 18-month model: ##### =  $p < 0.0001$  in relation to the 3-month model and ##### =  $p < 0.0001$ , in relation to the 6-month model).

For RPP (figure 6.3.1.11), Dobutamine showed a significant change for both 6 and 18-month models, when compared to the 3-month model. The 6-month model showed a significant increase of  $+30\% \pm 10.3$  (SEM),  $p < 0.0001$ , at the 10nM concentration before peaking at  $+73\% \pm 8.1$  (SEM),  $p < 0.0001$ , at the  $1\mu\text{M}$  concentration. The 18-month model showed an initial significant increase of  $+29\% \pm 8.3$  (SEM),  $p < 0.0001$ , at the 1nM concentration, before equalising the values on the 3-month model throughout the 3nM, 10nM and 100nM concentration; it then increased significantly by  $+24\% \pm 8.1$  (SEM),  $p < 0.0001$ , before finally reaching its peak increase of  $+41\% \pm 15.6$  (SEM),  $p < 0.0001$ , at the  $30\mu\text{M}$  concentration.



**Figure 6.3.1.11 – RPP for Dobutamine across the different aged models (n = 4 for all).** Hearts were allowed a 20-minute stabilisation period followed by increasing concentrations of each compound: 1 nM = 20-40 mins; 3 nM = 40-60 mins; 10 nM = 60-80 mins; 100 nM = 80-100 mins; 1  $\mu\text{M}$  = 100-120 mins; 10  $\mu\text{M}$  = 120-140 mins and 30  $\mu\text{M}$  = 140-160 mins. Measurements for RPP when treated with Dobutamine are displayed above (6-month model:  $\text{\$}\text{\$}\text{\$}\text{\$}$  =  $p < 0.0001$  in relation to the 3-month model; 18-month model:  $\text{\*\*\*\*}$  =  $p < 0.0001$  in relation to the 3-month model and  $\text{\#\#\#\#}$  =  $p < 0.0001$ , in relation to the 6-month model).

The MPR (figure 6.3.1.12) showed a clear change when comparing between the age groups. Both the 3 and 6-month models mimic each other throughout the protocol. However, the 18-month model showed an impairment in drug effect when compared to both the 3 and 6-month models, with a reduction in response starting at  $-13\% \pm 2.8$  (SEM),  $p < 0.0001$ , at the 1nM concentration, going up to  $-29\% \pm 4.8$  (SEM),  $p < 0.0001$ , at the 30 $\mu$ M concentration.

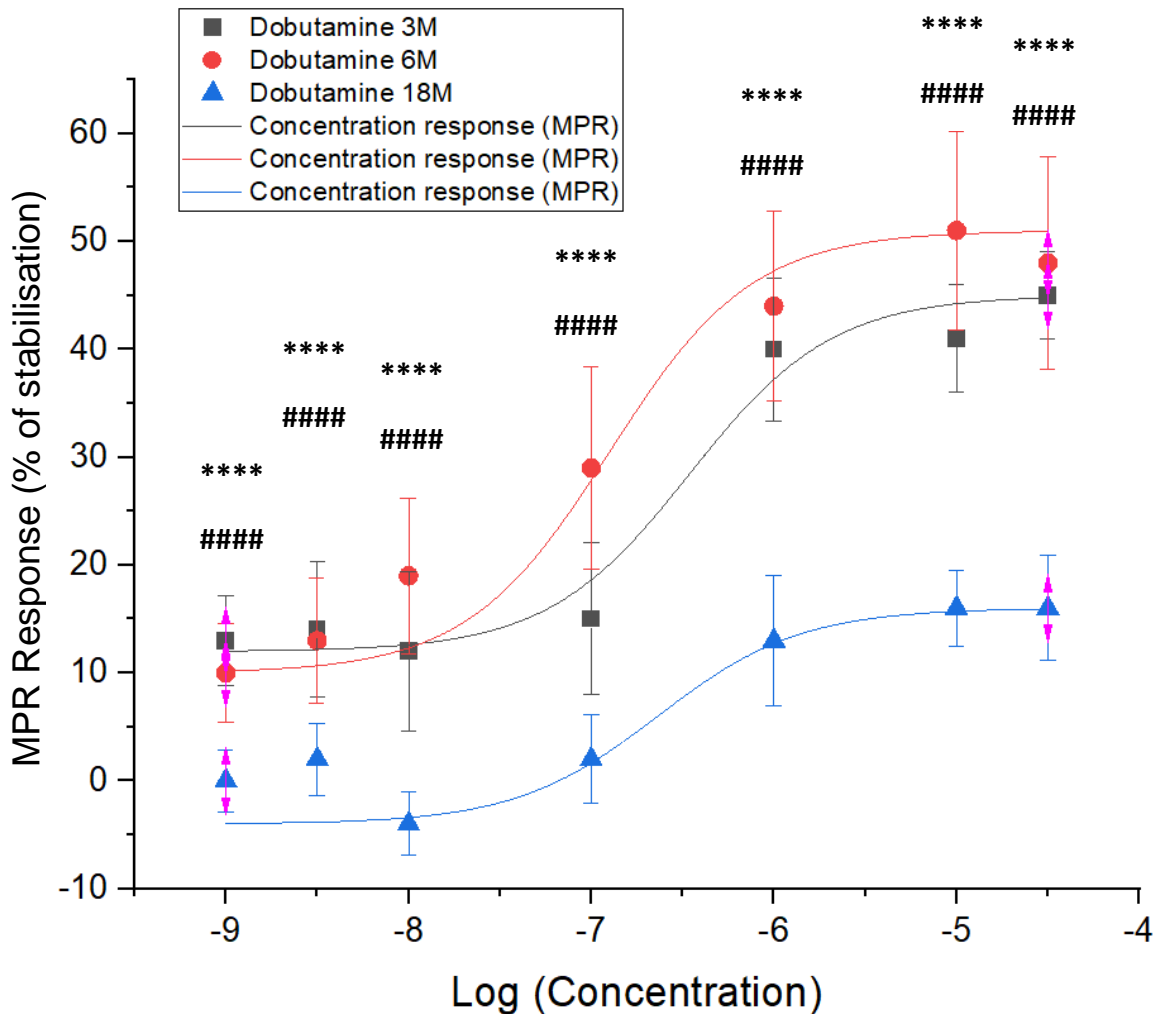


**Figure 6.3.1.12 – +dP/dTmax for Dobutamine across the different aged models (n = 4 for all).** Hearts were allowed a 20-minute stabilisation period followed by increasing concentrations of each compound: 1 nM = 20-40 mins; 3 nM = 40-60 mins; 10 nM = 60-80 mins; 100 nM = 80-100 mins; 1  $\mu$ M = 100-120 mins; 10  $\mu$ M = 120-140 mins and 30  $\mu$ M = 140-160 mins. Measurements for MPR when treated with Dobutamine are displayed above (18-month model: \*\*\*\* =  $p < 0.0001$  in relation to the 3-month model and ##### =  $p < 0.0001$ , in relation to the 6-month model).

The MPD (figure 6.3.1.13) showed no significance between the 3 and 6-month models, but it did show an impairment in drug effect on the 18-month model, starting at the 10 $\mu$ M concentration, with a decrease in response of -20%  $\pm$  (p<0.05) that stayed consistent until the end of the protocol.

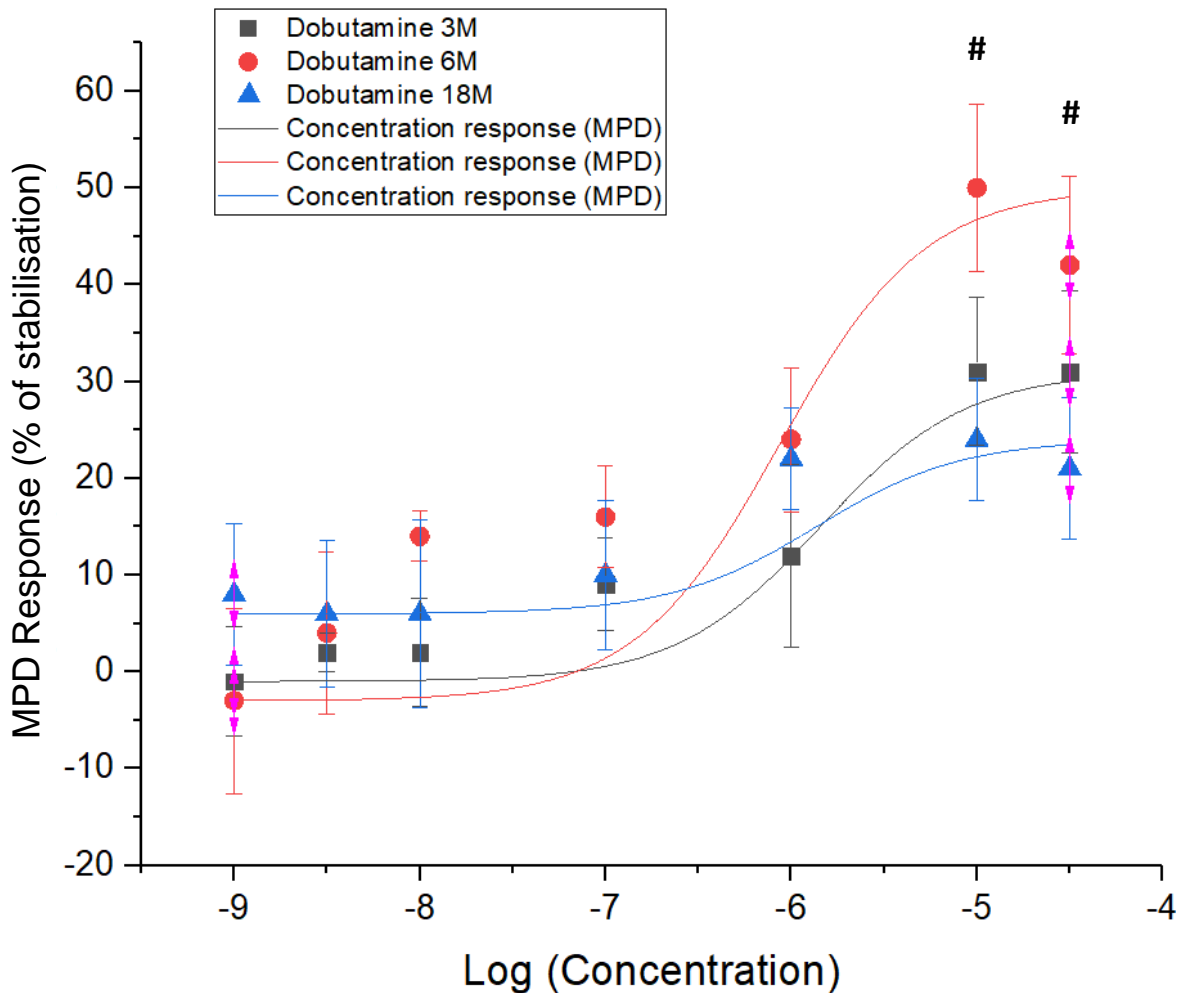
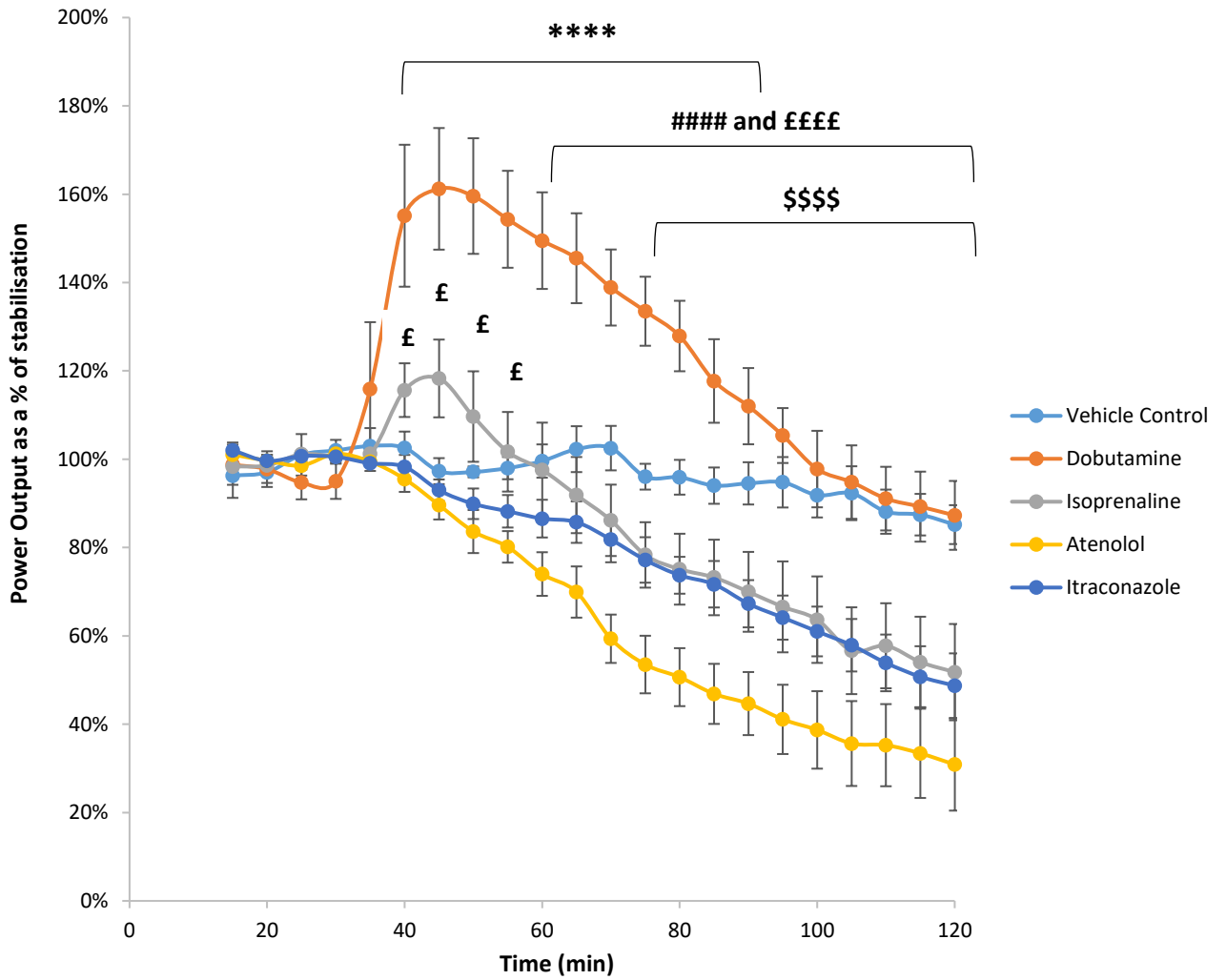


**Figure 6.3.1.13 – -dP/dTmax for Dobutamine across the different aged models (n = 4 for all).** Hearts were allowed a 20-minute stabilisation period followed by increasing concentrations of each compound: 1 nM = 20-40 mins; 3 nM = 40-60 mins; 10 nM = 60-80 mins; 100 nM = 80-100 mins; 1  $\mu$ M = 100-120 mins; 10  $\mu$ M = 120-140 mins and 30  $\mu$ M = 140-160 mins. Measurements for MPD when treated with Dobutamine are displayed above (18-month model: # = p < 0.05, in relation to the 6-month model).

### 6.3.2 Work-loop Assay

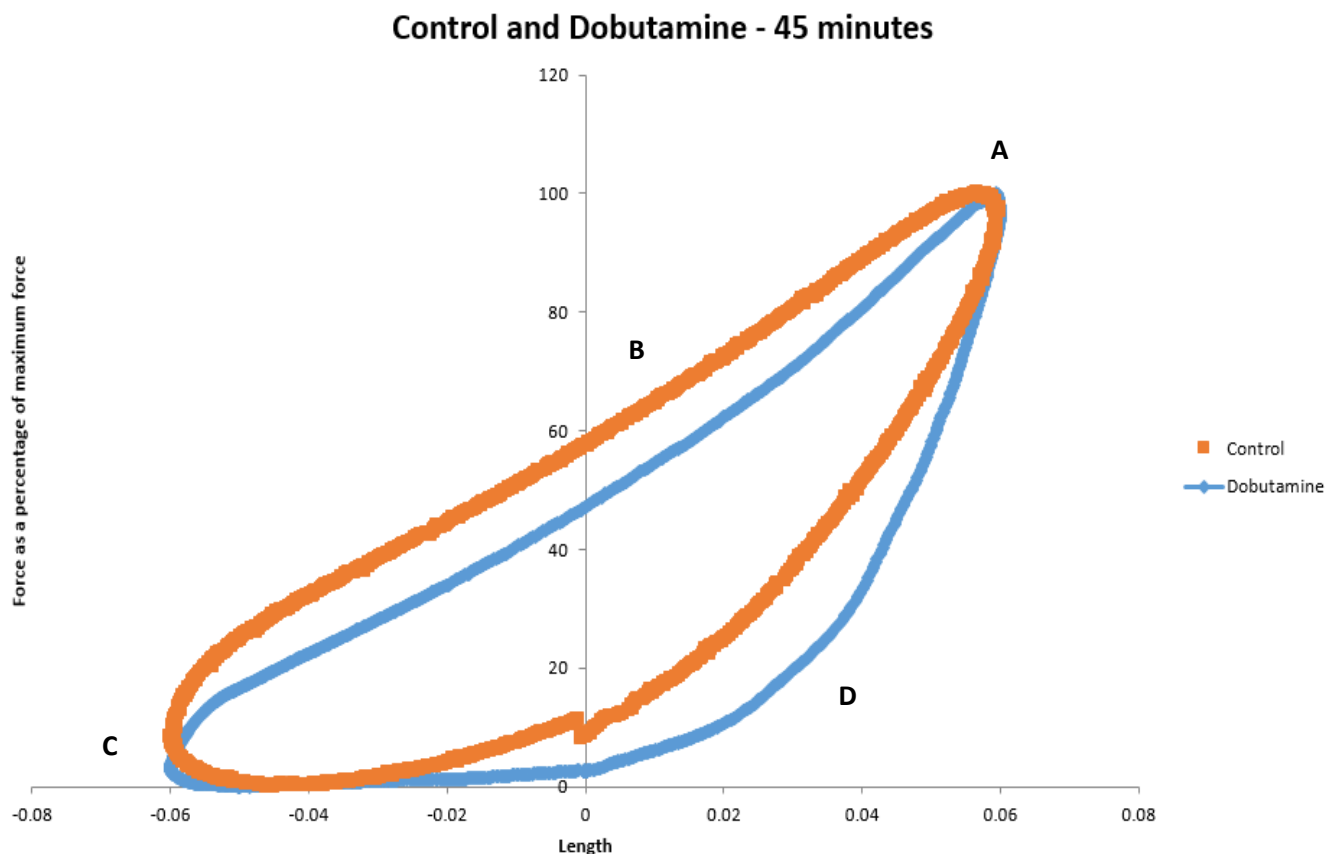
The next section will cover the results obtained from the work-loop muscle assay; unlike the isolated heart, this data pertains only to the 3-month animals. This data will be crucial in understanding how the papillary muscle of the heart undergoes mechanistic changes when under the effects of Dobutamine, Atenolol, Itraconazole and Isoprenaline. The first results shown are for the power outputs per drug treatment (figure 6.3.2.1), followed by representative loops obtained from each treatment.

Dobutamine showed a significant increase when compared to the control, especially at the 45-minute mark ( $+64\% \pm 13.7$  (SEM) increase in power output,  $p < 0.0001$ ). After 90-minutes, the muscle resumed a function similar to the control muscle. Atenolol showed a pronounced and significant decrease in muscle performance, starting at the 55-minute mark ( $-18\% \pm 3.5$  (SEM) decrease in performance,  $p < 0.05$ , before plateauing at the 100-minute mark ( $-53\% \pm 8.7$  (SEM) decrease in performance,  $p < 0.0001$ ). Itraconazole showed a pronounced and significant decrease in muscle performance, starting at the 55-minute mark ( $-10\% \pm 3.6$  (SEM) decrease in performance,  $p < 0.05$ ) and continuing to decrease until the end of the experimental protocol ( $-34\% \pm 5.6$  (SEM) decrease in performance,  $p < 0.001$  at the 100-minute mark and  $-36\% \pm 7.3$  (SEM) at the 120-minute mark). Isoprenaline showed a very interesting result, as it showed a significant increase when compared to the control, starting at the 40-minute mark ( $+13\% \pm 6.1$  (SEM) increase in muscle performance,  $p < 0.01$ ), with a peak at the 45-minute mark ( $+21\% \pm 8.8$  (SEM) increase in muscle performance,  $p < 0.01$ ). However, after the 75-minute mark ( $-18\% \pm 7.4$  (SEM),  $p < 0.01$ ), the muscles showed a pronounced and significant decrease in performance that reached a maximal decrease of  $-33\% \pm 10.9$  (SEM,  $p < 0.01$ ), at the 120-minute mark.



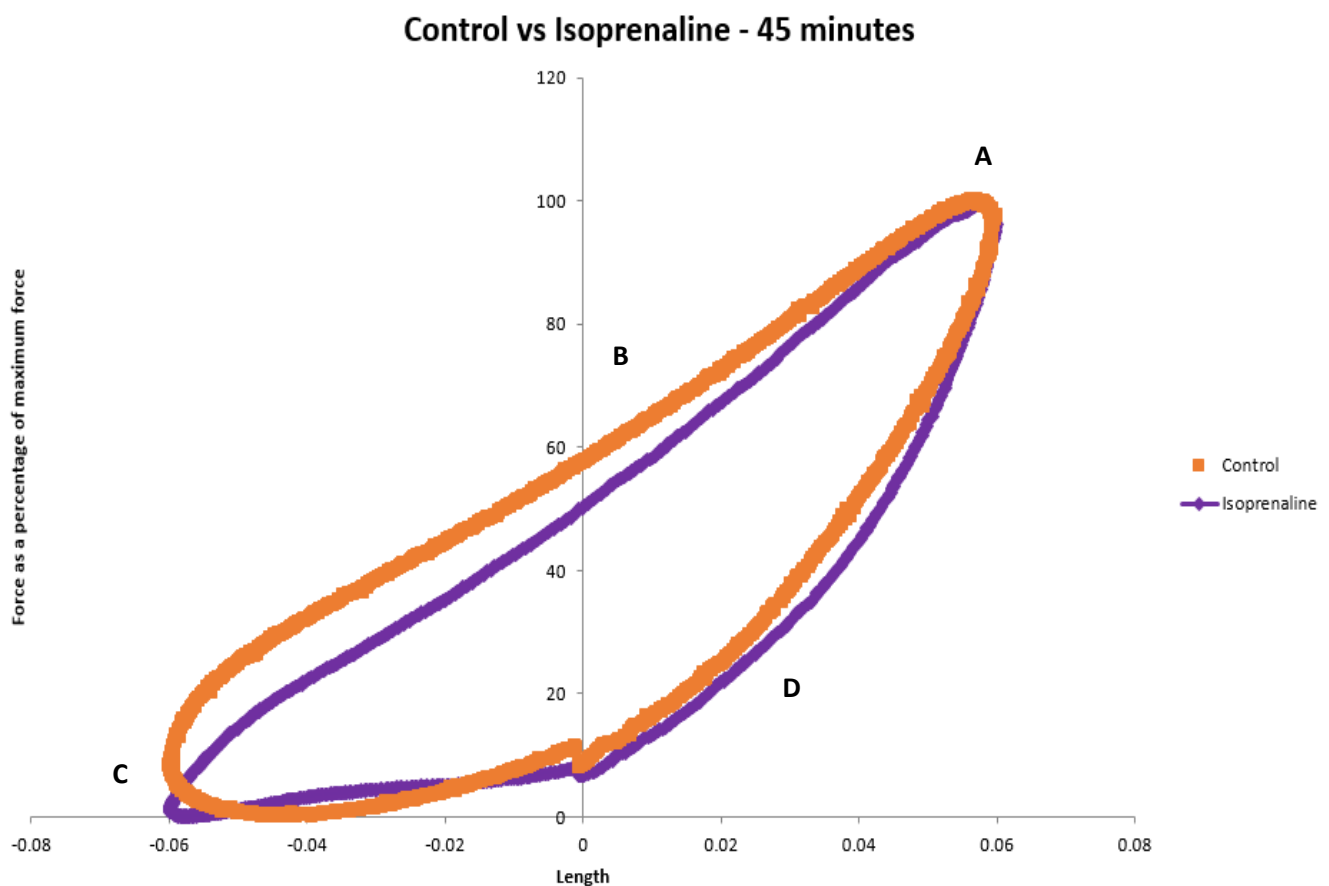
**Figure 6.3.2.1 – Power output for Dobutamine, Isoprenaline, Atenolol and Itraconazole (n = 7, 5, 5 and 5, respectively).** Work produced by the muscle in control conditions and under the effects of a 5µM Dobutamine concentration (\*\*\*\* = p<0.0001); a 20µM Atenolol concentration (##### = p<0.0001); a 10µM Itraconazole concentration (\$\$\$\$ = p<0.0001) and a 100nM Isoprenaline concentration (£ = p<0.05). All of the treatments were grouped together in the same graph to provide context on how each one affects the papillary muscle, when compared to the control.

Figure 6.3.2.2 contains a representation of the change in the loop shape of a muscle under normal conditions and a muscle under the effect of Dobutamine, at the 45-minute mark. The loops are plotted as force against % length change and are averages of the work produced by the muscles. As also seen in the figure, the loop shape is very different between the two presented groups. While peak force measurements remained the same between the two models (**A**), Dobutamine decreased the force produced during shortening (**B**), slightly increased the passive re-lengthening of the muscle (**C**) and increased the activation rate of the muscle (**D**), while also increasing the total net-work done by the muscle (total area inside the loop), when compared to the control data.



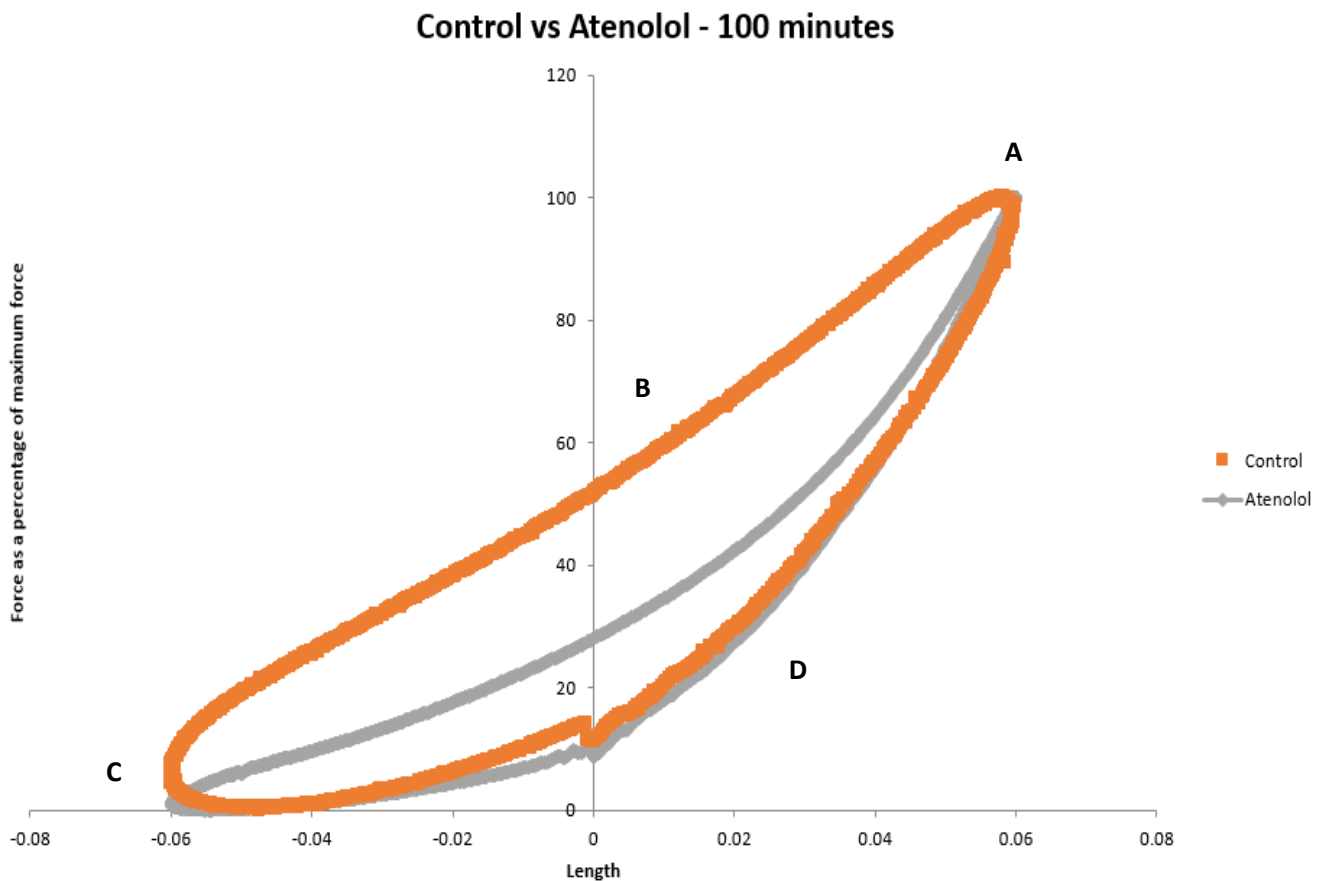
**Figure 6.3.2.2 – Comparison between control and Dobutamine treated muscles.** Effects of Dobutamine on the loop shape of a representative 3-month muscle at the 45-minute mark. A = Peak force; B = Muscle shortening. C = Passive re-lengthening; and D = Activation rate.

Figure 6.3.2.3 contains a representation of the change in the loop shape of a muscle under normal conditions and a muscle under the effect of Isoprenaline, at the 45-minute mark. The loops are plotted as force against % length change and are averages of the work produced by the muscles. As with Dobutamine, no changes were recorded regarding peak force measurements (**A**). a decrease in the passive re-lightning (**B**) and shortening force (**C**) of the muscle was recorded, as well as a slight increase in activation rate (**D**). The total net-work produced by the muscle (total area inside the loop) was increased as well.



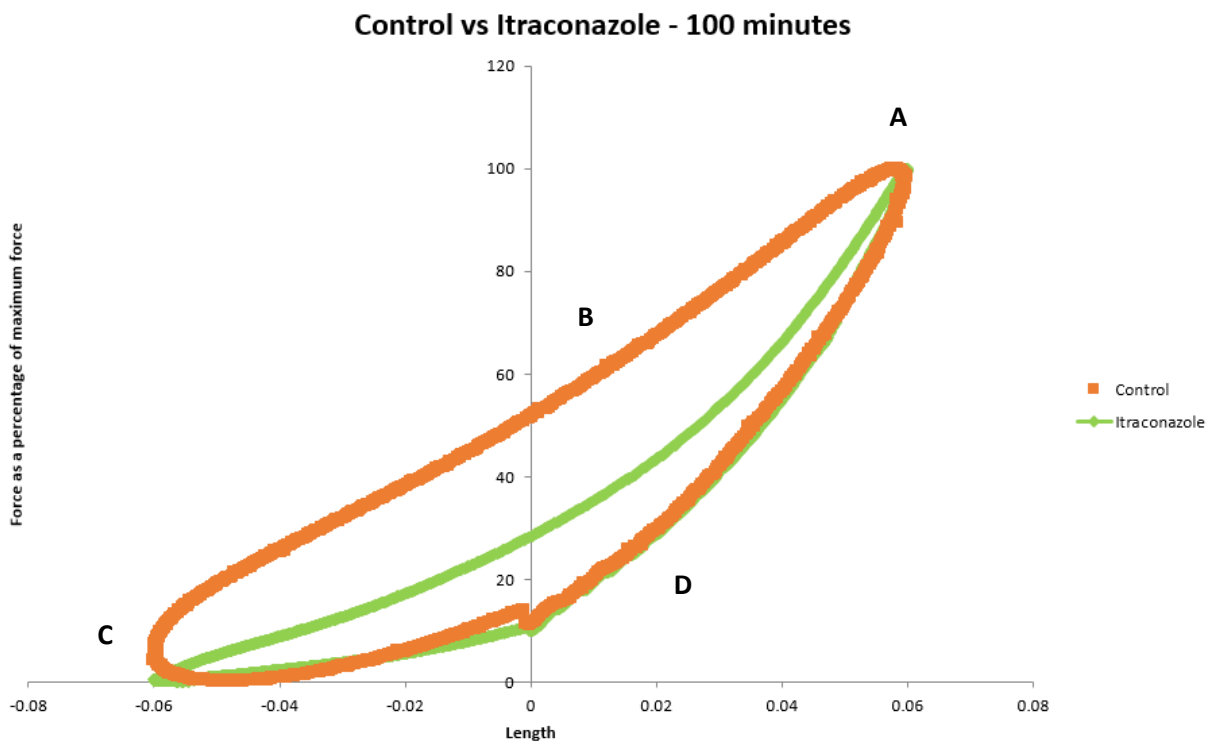
**Figure 6.3.2.3 - Comparison between control and Isoprenaline treated muscles.** Effects of Isoprenaline on the loop shape of a representative 3-month muscle at the 100-minute mark. A = Peak force; B = Muscle shortening. C = Passive re-lengthening; and D = Activation rate.

Figure 6.3.2.4 (representative graph) contains a representation of the change in the loop shape of a muscle under normal conditions and a muscle under the effect of Atenolol, at the 100-minute mark. The loops are plotted as force against % length change and are averages of the work produced by the muscles. No changes were recorded regarding peak force measurements (**A**) or activation rate (**D**). However, atenolol caused a severe impairment in the force produced by the muscle during shortening (**B**) and decreased its passive re-lengthening (**C**). In addition, it also decreased the total net-work produced by the muscle (total area inside the loop).



**Figure 6.3.2.4 - Comparison between control and Atenolol treated muscles.** Effects of Atenolol on the loop shape of a representative 3-month muscle at the 100-minute mark. A = Peak force; B = Muscle shortening. C = Passive re-lengthening; and D = Activation rate.

Figure 6.3.2.5 contains a representation of the change in the loop shape of a muscle under normal conditions and a muscle under the effect of Itraconazole, at the 100-minute mark. The loops are plotted as force against % length change and are averages of the work produced by the muscles. No changes were recorded regarding peak force measurements (A) or activation rate of the muscle (D). Not unlike Atenolol, Itraconazole caused a severe impairment in the force shortening of the muscle (B) and its passive re-lengthening (C), as well as a reduction in the total net-work produced by the muscle (total area inside the loop).



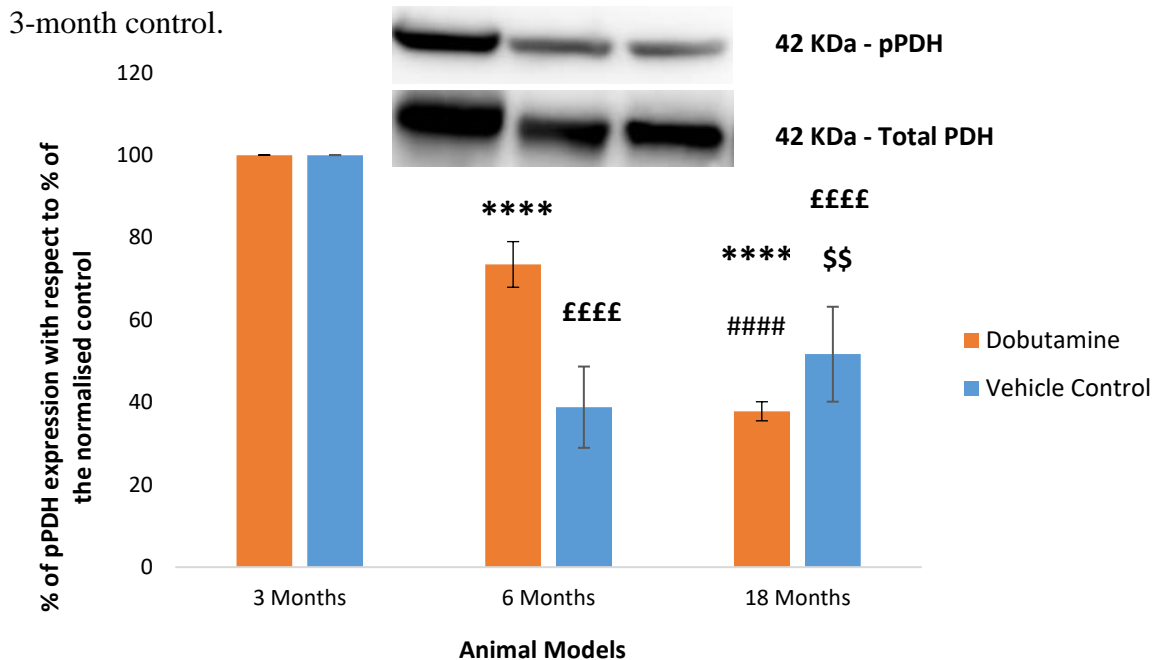
**Figure 6.3.2.5 - Comparison between control and Itraconazole treated muscles.** Effects of Itraconazole on the loop shape of a representative 3-month muscle at the 100-minute mark. A = Peak force; B = Muscle shortening. C = Passive re-lengthening; and D = Activation rate.

### 6.3.3 Western Blots

Pyruvate dehydrogenase (PDH) and Uncoupling protein 3 (UCP3) were assessed using western blotting in order to assess the impact of key mitochondrial regulators in cardiac function. All of the represented graphs were plotted after correcting for protein loading and the 3-month controls were normalised.

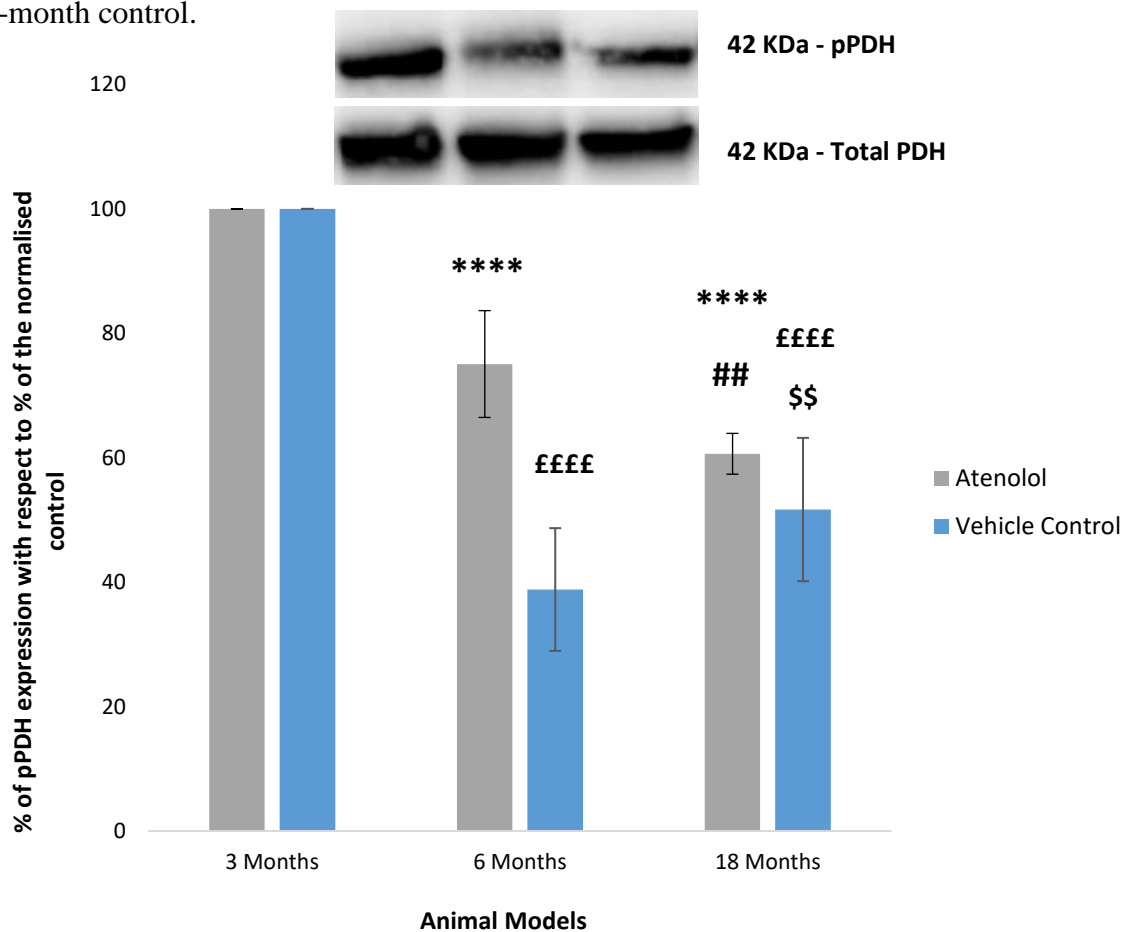
#### 6.3.3.1 Pyruvate Dehydrogenase

Figure 6.3.3.1.1 shows the percentage of phosphorylated PDH in dobutamine-treated heart tissue as a % of the 3-month control, in differently aged rat models. The 6-month treated hearts showed a significant decrease in phospho-PDH ( $-27\% \pm 5.5$  (SEM),  $p < 0.0001$ ) when compared to the 3-month treated control and the 18-month treated hearts showed a significant reduction ( $-62\% \pm 2.3$  (SEM),  $p < 0.0001$ ) in phospho-PDH when compared to the 3-month control.



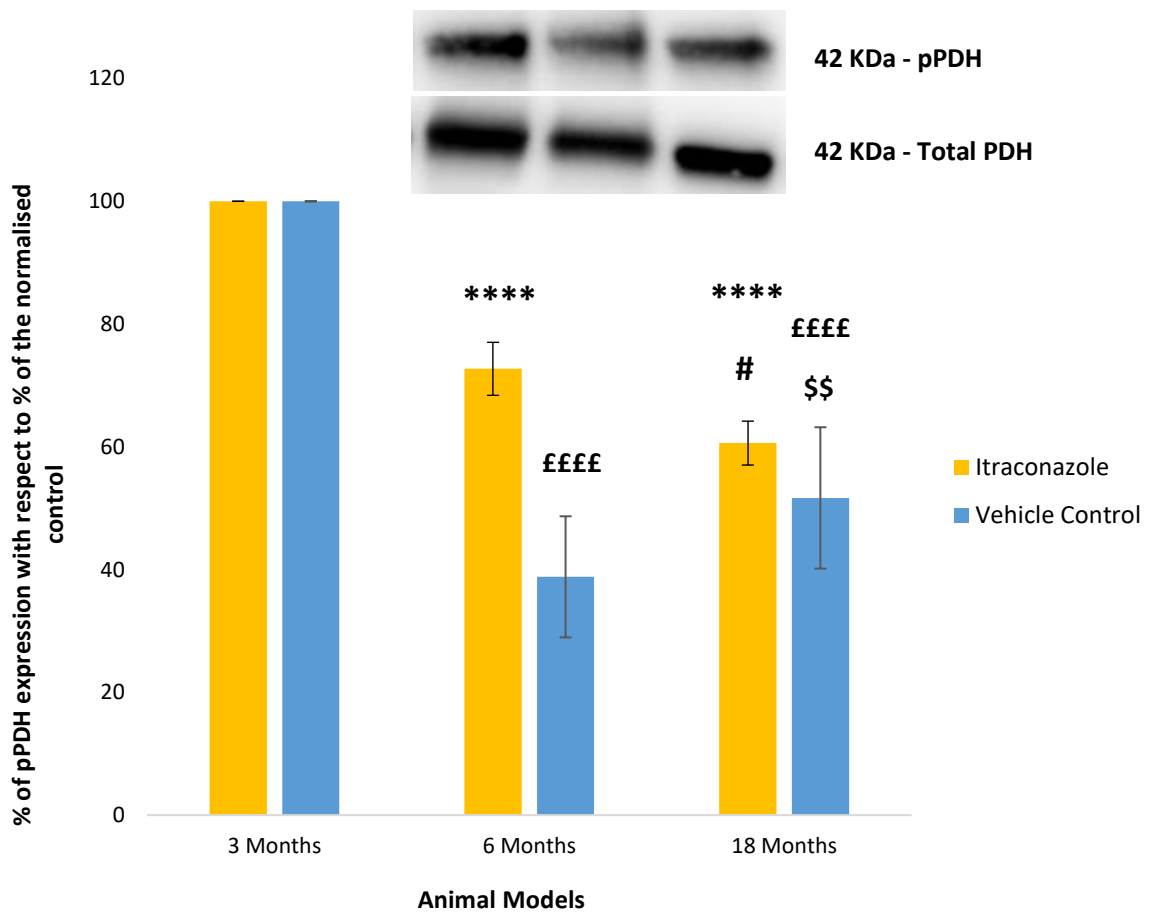
**Figure 6.3.3.1.1 – Phosphorylated PDH expression in different dobutamine-treated aged models (n = 4 for all).** This graph represents the effects of age on the levels of phosphorylated PDH in dobutamine-treated heart tissue, as a percentage of total PDH (6-month model: \*\*\*\* in relation to the 3-month model; 18-month model: \*\*\*\* =  $p < 0.0001$  in relation to the 3-month model and ##### =  $p < 0.01$ , in relation to the 6-month model). The top blot is a representative image of phospho-PDH, while the bottom blot represents total-PDH. The presented results are all corrected for GAPDH. The vehicle control values from chapter 4 are also present, with their significance indicated by the “£” and “\$” symbols (££££ =  $p < 0.0001$  and \$\$ =  $p < 0.01$ , in relation to the 3 and 6-month model, respectively).

Figure 6.3.3.1.2 shows the percentage of phosphorylated PDH in atenolol-treated heart tissue as a % of the control and in differently aged rat models. The 3-month model was used as a control, while the 6 and 18-month models were used as the aged models. The 6-month treated hearts showed a significant decrease in phospho-PDH ( $-25\% \pm 8.5$  (SEM),  $p < 0.0001$ ) when compared to the 3-month treated control and the 18-month treated hearts showed a significant reduction ( $-40\% \pm 3.0$  (SEM),  $p < 0.0001$ ) in phospho-PDH when compared to the 3-month control.



**Figure 6.3.3.1.2 – Phosphorylated PDH expression in different atenolol-treated aged models (n = 4 for all).** This graph represents the effects of age on the levels of phosphorylated PDH in atenolol-treated heart tissue, as a percentage of total PDH (6-month model: \*\*\*\* in relation to the 3-month model; 18-month model: \*\*\*\* =  $p < 0.0001$  in relation to the 3-month model and ## =  $p < 0.01$ , in relation to the 6-month model). The top blot is a representative image of phospho-PDH, while the bottom blot represents total-PDH. The presented results are all corrected for GAPDH. The vehicle control values from chapter 4 are also present, with their significance indicated by the “£” and “\$” symbols (££££ =  $p < 0.0001$  and \$\$ =  $p < 0.01$ , in relation to the 3 and 6-month model, respectively).

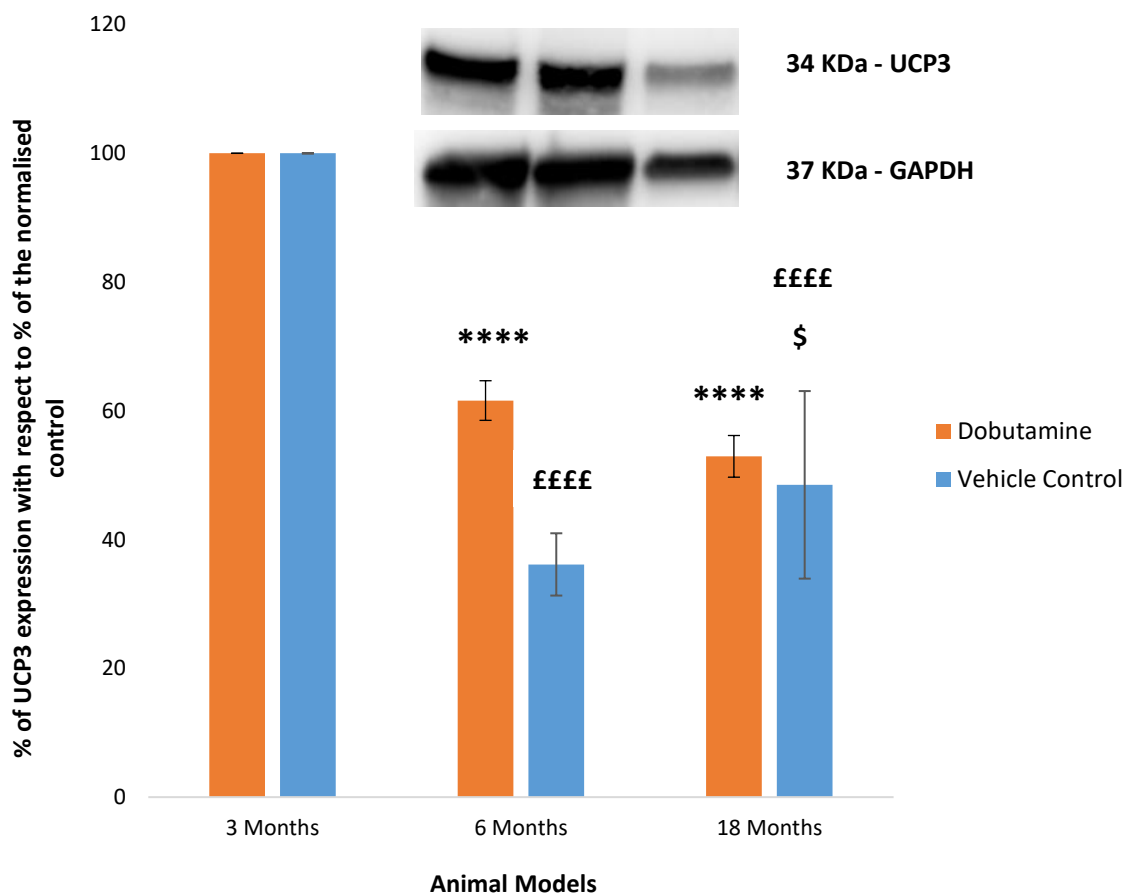
Figure 6.3.3.1.3 shows the percentage of phosphorylated PDH in itraconazole-treated heart tissue as a % of the control and in differently aged rat models. The 3-month model was used as a control, while the 6 and 18-month models were used as the aged models. The 6-month treated hearts showed a significant decrease in phospho-PDH ( $-28\% \pm 4.3$  (SEM),  $p < 0.001$ ) when compared to the 3-month treated control and the 18-month treated hearts showed a significant reduction ( $-40\% \pm 3.5$  (SEM),  $p < 0.0001$ ) in phospho-PDH when compared to the 3-month control.



**Figure 6.3.3.1.3 – Phosphorylated PDH expression in different itraconazole-treated aged models (n = 4 for all).** This graph represents the effects of age on the levels of phosphorylated PDH in itraconazole-treated heart tissue, as a percentage of total PDH (6-month model: \*\*\*\* in relation to the 3-month model; 18-month model: \*\*\*\* =  $p < 0.0001$  in relation to the 3-month model and # =  $p < 0.05$ , in relation to the 6-month model). The top blot is a representative image of phospho-PDH, while the bottom blot represents total-PDH. The presented results are all corrected for GAPDH. The vehicle control values from chapter 4 are also present, with their significance indicated by the “£” and “\$” symbols (##### =  $p < 0.0001$  and \$\$ =  $p < 0.01$ , in relation to the 3 and 6-month model, respectively).

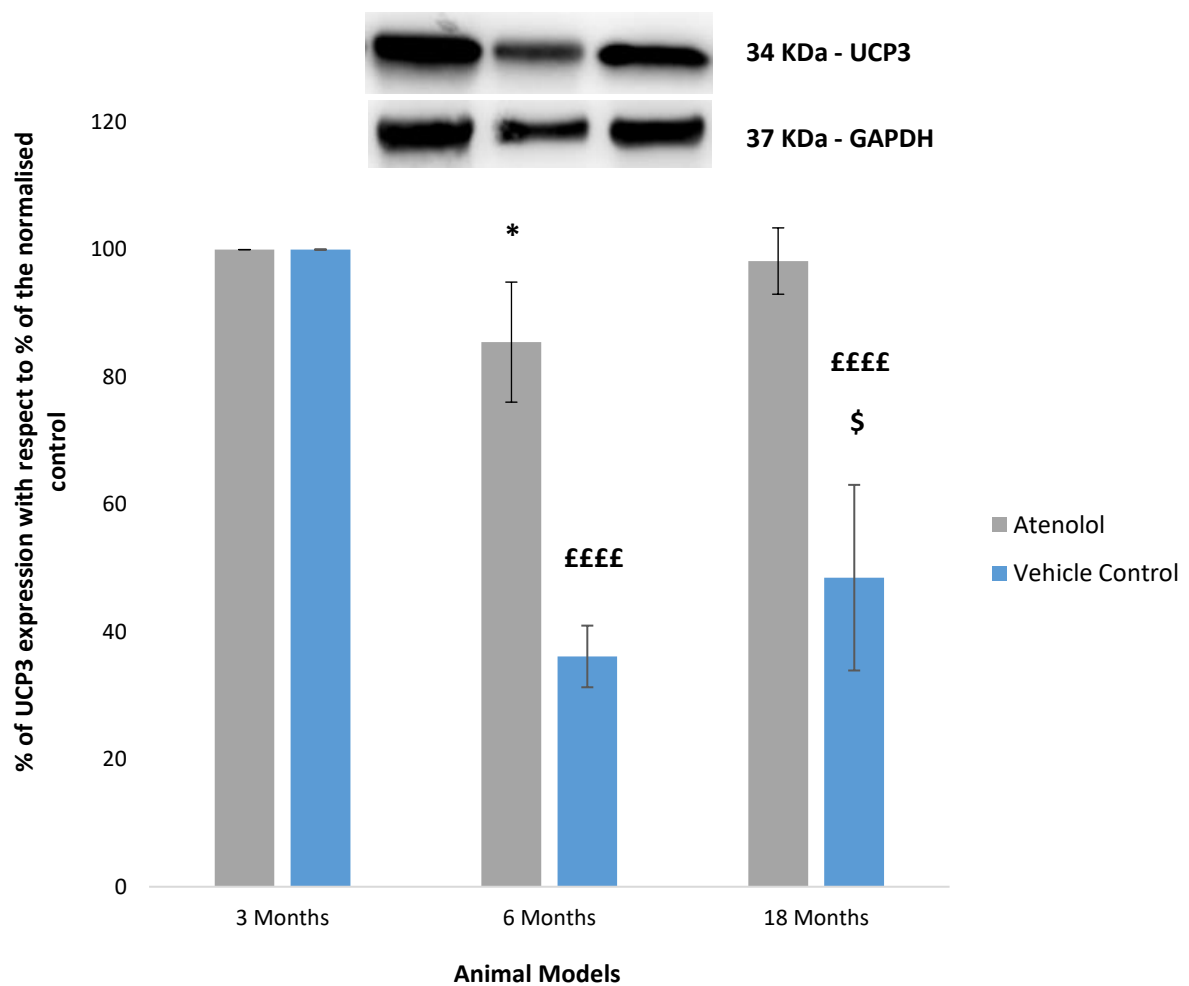
### 6.3.3.2 UCP3

Figure 6.3.3.2.1 shows the percentage of UCP3 in dobutamine-treated heart tissue as a % of the control and in differently aged rat models. The 3-month model was used as a control, while the 6 and 18-month models were used as the aged models. The 6-month treated hearts showed a significant decrease in UCP3 ( $-39\% \pm 3.0$  (SEM),  $p < 0.0001$ ) when compared to the 3-month treated control and the 18-month treated hearts showed a significant reduction ( $-48\% \pm 3.2$  (SEM),  $p < 0.0001$ ) in UCP3 when compared to the 3-month control.



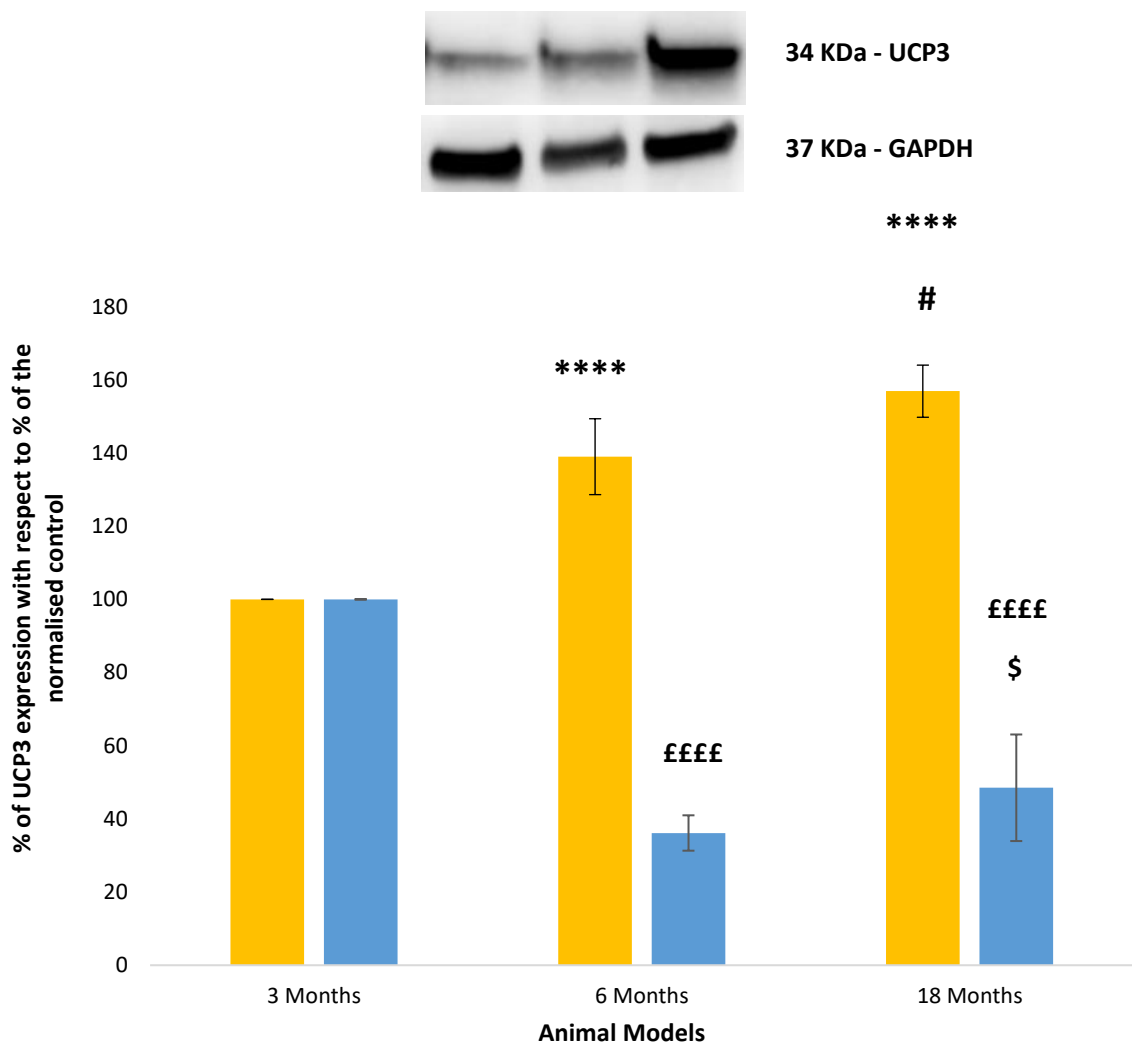
**Figure 6.3.3.2.1 – UCP3 expression in different dobutamine-treated aged models (n = 4 for all).** This graph represents the effects of age on the levels of UCP3 in dobutamine-treated heart tissue, as a percentage of the 3-month controls (\* =  $p < 0.05$ ; \*\* =  $p < 0.01$ , \*\*\* =  $p < 0.001$ , \*\*\*\* =  $p < 0.0001$ ). The top blot is a representative image of UCP3, while the bottom blot represents GAPDH. The presented results are all corrected for GAPDH. The vehicle control values from chapter 4 are also present, with their significance indicated by the “£” and “\$” symbols (££££ =  $p < 0.0001$  and \$ =  $p < 0.05$ , in relation to the 3 and 6-month model, respectively).

Figure 6.3.3.2.2 shows the percentage of UCP3 in atenolol-treated heart tissue as a % of the control and in differently aged rat models. The 3-month model was used as a control, while the 6 and 18-month models were used as the aged models. The 6-month treated hearts showed a significant decrease in UCP3 ( $-15\% \pm 9.4$  (SEM),  $p < 0.01$ ) when compared to the 3-month treated control and the 18-month treated hearts showed no significance in UCP3 when compared to the 3-month control.



**Figure 6.3.3.2.2 – UCP3 expression in different atenolol-treated aged models (n = 4 for all).** This graph represents the effects of age on the levels of UCP3 in atenolol-treated heart tissue, as a percentage of the 3-month controls (6-month model: \* in relation to the 3-month model). The top blot is a representative image of UCP3, while the bottom blot represents GAPDH. The presented results are all corrected for GAPDH. The vehicle control values from chapter 4 are also present, with their significance indicated by the “£” and “\$” symbols (££££ =  $p < 0.0001$  and \$\$ =  $p < 0.01$ , in relation to the 3 and 6-month model, respectively).

Figure 6.3.3.2.3 shows the percentage of UCP3 in itraconazole-treated heart tissue as a % of the control and in differently aged rat models. The 3-month model was used as a control, while the 6 and 18-month models were used as the aged models. The 6-month treated hearts showed a significant increase in UCP3 ( $+39\% \pm 10.3$  (SEM),  $p < 0.0001$ ) when compared to the 3-month treated control and the 18-month treated hearts showed a significant increase ( $+56\% \pm 7.1$  (SEM),  $p < 0.0001$ ) in UCP3 when compared to the 3-month control.



**Figure 6.3.3.2.3 – UCP3 expression in different itraconazole-treated aged models (n = 4 for all).** This graph represents the effects of age on the levels of UCP3 in itraconazole-treated heart tissue, as a percentage of the 3-month controls (6-month model: \*\*\*\* in relation to the 3-month model; 18-month model: \*\*\*\* =  $p < 0.0001$  in relation to the 3-month model and # =  $p < 0.05$ , in relation to the 6-month model). The top blot is a representative image of UCP3, while the bottom blot represents GAPDH. The presented results are all corrected for GAPDH. The vehicle control values from chapter 4 are also present, with their significance indicated by the “€” and “\$” symbols (€€€€ =  $p < 0.0001$  and \$\$ =  $p < 0.01$ , in relation to the 3 and 6-month model, respectively).

## 6.4 Discussion and Conclusion

In chapters 3 it was shown how age can change the function of the heart and found that, whilst no changes were recorded in the isolated heart, the molecular assays revealed protein expression changes directly linked to an aging effect. For this chapter, a similar investigation was conducted but it was hypothesised that age would cause changes in the effects of dobutamine, atenolol and itraconazole. Dobutamine was shown to have an effect directly tied to age, as the haemodynamic parameters measured were lower when compared to the younger models, which were proposed to be an effect known as  $\beta$ -receptor desensitization (this can be further seen in Table 6.3.1.1, where the EC50 for the HR, MPD and RPP seems to indicate a significant increase in the dobutamine effect on the 6-month models when compared to the 18-month models); atenolol, on the other hand, did not seem to have an effect directly linked to age, as no significant changes were recorded for any of the parameters. As for itraconazole, the expected negative inotropic effect was recorded but little to no change was seen between the different aged models. In regard to the results from the work-loop assay when using catecholamine, dobutamine showed the expected increases in net-work and power output associated with  $\beta$ -stimulation (Gharanei, Wallis and Maddock 2015; Layland, J. and Kentish 2000). However, significant change in muscle performance over-time were recorded, when under the effect of Isoprenaline, which might have occurred due to the drugs extreme chronotropic properties (Fletcher et al. 2020). The work produced by the muscles under the effect of Atenolol and Itraconazole was significantly impaired and the total net-work of the muscles was also significantly impaired, as expected from negative inotropes; however, atenolol was shown to cause more significant changes, as the decrease in power output was more exacerbated when comparing between atenolol and itraconazole (Fletcher et al. 2020).

As for the protein results, the following was observed: PDH protein expression showed a decrease across all models, potentially due to the effect of age on the hearts treated with each inotrope; interestingly, dobutamine seemed to have the sharpest decrease in PDH phosphorylation, which may indicate an exacerbated increase in glucose metabolism to keep up with the energy demands triggered by  $\beta$ -receptor stimulation. It is clear from the data that the expression of pPDH varies amongst the different aged groups due to drug administration; this effect is independent of the aged models used as the drug administered show differences compared to the vehicle controls. As for the UCP3 protein expression, it did not change in atenolol or itraconazole across the different aged models, but increased in relation to the controls; dobutamine, on the other hand, showed a decrease in UCP3 levels on the 18-month model, and an overall increase when compared to the controls. Based on the present results it appears that there may be a minimal impact of UCP3 on the contractility of the heart, when treated with these drugs. However, the increases measured may indicate that other negative mechanisms and pathways are being activated within the heart when treated with these inotropes, across all ages. It is therefore clear that more work is still necessary to understand the exact effect of UCP3 in cardiac functions. Similar to what was observed with pPDH, it is clear from the data that the expression of UCP3 varies amongst the different aged groups due to drug administration; this effect is independent of the aged models used as the drug administered show differences compared to the vehicle controls.

The left ventricular wall thickens with age due to collagen deposition and fibrous tissues (Rossi et al. 2008). This change causes an increased vulnerability of the elder population to cardiovascular diseases (Cheng et al. 2009) and is, at least partially, the reason why there is an observable decrease in contractile forces of the heart in elder patients.

The use of catecholamines in aged models, as mentioned in sections 1.7.1 and 1.7.2, has been extensively researched in the past and Lakatta et al recorded a reduction in the maximal rate of tension development (dt/dt) of the trabecular muscle, in aged models, as a direct effect of not only a thickening of the ventricular wall, but also what the research group said was an age-related intrinsic loss of inotropic responses (Lakatta et al. 1975). A further study by Guarnieri et al used the isolated septa of the heart to test for the maximum rate of force development (dF/dt) and cAMP levels under the effect of isoprenaline and confirmed the findings of Lakatta et al that there is an age-dependant catecholamine response change, with the aged heart tissue showing up to 40% less dF/dt response to  $\beta$ -receptor stimulation, with an associated increase in cyclic adenosine monophosphate (cAMP) levels; the researchers proposed that, based on their observation, the diminished response to receptor stimulation stemmed not from a reduced contractile response to  $\text{Ca}^{2+}$ , but as a result of protein kinase-mediated  $\text{Ca}^{2+}$  (Guarnieri et al. 1980). A study by Dobson et al on both rat and guinea pig isolated hearts was carried out to measure the levels of myocardial adenosine and to confirm whether it did or did not mediate the responsiveness of  $\beta$ -receptor stimulation in aged tissue (Dobson, Fenton and Romano 1990); the researchers found that not only was there a decrease in catecholamine contractile stimulation from 113% in young hearts to 69% in aged ones, but isoprenaline was also causing an increase in adenosine release in both groups.

Dobson et al then ran the same experimental protocol but with an adenosine antagonist (Theophylline) being co-administrated with Isoprenaline on the isolated hearts and found that the previously observed difference between the young and aged hearts was prevented and stimulation of the  $\beta$ -receptors was restored in the aged hearts; the researchers concluded that, based on these results, the reduced contractile response of older hearts to  $\beta$ -receptor stimulation may occur partially due to enhanced adenosine levels in the aged myocardium.

In addition to this, previous studies have also shown a catecholamine-related preference for the  $\alpha$ -receptors in senescent rat hearts, as well as a  $\beta$ -adrenoreceptor desensitization (Ferrara et al. 2014; Jiang, M., Moffat and Narayanan 1993). This was tested using phenylephrine and the results obtained showed a shift in mediation from both receptors to the  $\alpha$ -receptor, in 7-month-old rats.

A similar study used Isoprenaline and documented a clear decrease in myocardial  $\beta$ -receptor affinity, which was linked to a decrease in catecholamine responsiveness (Abrass, Davis and Scarpace 1982; Dobson, Fenton and Romano 1990; Ferrara et al. 2014; Hashimoto, Nakashima and Sugino 1983). Another study has also conducted experiments on Dobutamine in young (4-month-old) and aged (20-month-old) mice and it was found that the drug had a much lower response rate on the haemodynamic parameters of the older rats, with reduced heart rate, ventricular end-diastolic volume and overall systolic function (Hirleman, Yu and Larson 2008). Based on the previous literature, the most important observation to be made in this chapter, in regard to the results, is how different drugs seemed to interact on different aged models. Regarding the positive inotropes used, it was previously mentioned that Isoprenaline can have limited effects on the aged myocardium (Hacker et al. 2006; Lakatta et al. 1975) derived from the previously mentioned  $\beta$ -adrenoreceptor desensitization. The effect of Dobutamine on the HR, MPR and RPP of the 18-month hearts was shown to be significantly reduced, when comparing to the two younger models (figures 5.3.2.6, 7 and 8). This has been similarly shown before, in models of myocardial infarction and, because the aged hearts mimic the signs of an MI, which would trigger a differential effect of  $\beta$ -receptor stimulation on the systolic activities of the heart and would explain the changes in  $+dP/dt_{max}$  expression in the different models (Abrass, Davis and Scarpace 1982; Cove et al. 1995; Dobson, Fenton and Romano 1990; Hacker et al. 2006).

This  $\beta$ -adrenoreceptor desensitization has also been previously linked to a deficit in  $\text{Ca}^{2+}$  modulation and to a diminished response in contraction, especially in rats aged 20-months or more (Xiao et al. 1994a). This calcium dysfunction was then further investigated in two papers published by Farrell and Howlett.

The first study was an investigation on whether the age-related decrease in catecholamine sensitivity was being induced by changes in  $\text{Ca}^{2+}$  homeostasis (Farrell and Howlett 2007); for this paper, the researchers used isoprenaline treated male rats aged 3 and 24-months and isolated cardiac myocytes from the animals, before doing voltage clamp and calcium measurements. The group found that there was an age-dependant reduction in cell contraction, with an associated reduction in diastolic  $\text{Ca}^{2+}$  and a lower occurrence of electrical and contractile cardiac activity; the diastolic  $\text{Ca}^{2+}$  changes are of particular importance and Farrell and Howlett then propose that the decreased inotropic response to  $\beta$ -adrenoreceptor stimulation occurs, partially, due to this  $\text{Ca}^{2+}$  decrease. The second study then followed, using the same animal models but treated with dobutamine, where the researchers investigated the effects of age on the  $\beta$ -adrenergic receptor signalling pathway by measuring intracellular  $\text{Ca}^{2+}$  and cAMP (Farrell and Howlett 2008). In this study, the researchers found that, first and foremost, aged cells required a higher concentration of dobutamine in order to increase the contraction amplitude of the cells. In addition to this, Farrell and Howlett also recorded an age-dependant decrease in cAMP production as a response to  $\beta$ -receptor stimulation. However, the researchers also found that this was only the case for  $\beta_1$ -receptor stimulation and proposed that the age-related decrease in catecholamine sensitivity, or  $\beta$ -desensitization, may be linked to upstream elements of both the cAMP and the  $\beta$ -adrenoreceptor signalling pathways. Results seem to suggest that the data collected by Farrell and Howlett may indeed be the cause for the  $\beta$ -desensitization, but for the present project this is not conclusive without measuring  $\text{Ca}^{2+}$  levels.

Despite this potential presence of  $\beta$ -desensitization, a reduction on the RPP of the heart was measured when using Atenolol, but that effect was only seen at the higher concentrations of the compound (figures 5.3.1.1 and 5.3.1.3), which seems to support the idea that the aforementioned desensitization only occurs in the presence of stimulation and not inhibition. Although this effect shows a decrease in % response at higher concentrations for the dose response curve, it is clear from the individual concentrations on the graph that there is a deviation from the data point and the fitted curve, which overshadows the actual relationship of the response to the concentration point. The results on the isolated heart seem to suggest that, while the lower concentrations of Atenolol do not trigger a change in response in an age-dependant fashion, the cumulative administration of Atenolol still causes severe negative inotropic effects. It is also important to note that aging seemed to have an effect similar to the negative inotropic effect caused by Atenolol. The relaxation time for contractions has been shown to be prolonged in myocytes from aged mice. This is attributable to, not unlike what was reviewed for  $\beta$ -receptor agonists, changes in the underlying  $\text{Ca}^{2+}$  transients. In a study by Lim et al, the researchers used left ventricular myocytes to measure  $\text{Ca}^{2+}$  levels; the researchers obtained results that suggested that  $\text{Ca}^{2+}$  transients are much smaller and the rates of decay are slower in aged myocytes when compared to myocytes from younger mice (Lim et al. 2000). This study, alongside the studies conducted by Farrell and Howlett (see above), seem to point towards a calcium related  $\beta$ -receptor aging-dependant desensitization and seem to indicate that, in order to accurately measure contractile parameters in aged models, future research should focus on the calcium pathway alongside the  $\beta$ -receptor signalling pathway.

Itraconazole has been tested in both animal and human models and it has been mostly associated with congestive heart failure and QRS and PR interval prolongation, especially in middle-aged and elder patients (Ahmad, Singer and Leissa 2001; Fung, Chau and Yew 2008; Okuyan and Altin 2013). The isolated heart models using itraconazole have shown a decrease in the baseline values of all measured parameters, in a concentration dependent manner (Markert et al. 2012; Qu et al. 2013). This effect has been linked to an inhibition in the Na<sup>+</sup> channel function, which has been previously linked to depressed cardiac contractility (Gottlieb 1989; Guth et al. 2015).

This occurs due to a dysfunction in the voltage-gated Na<sup>+</sup> channel but it has only been observed at high concentrations of itraconazole (3μM or higher). Itraconazole has also been reported to have little to no effect on the adenosine receptors of the heart but has been linked to an inhibition of the MEK5 kinase (Cleary and Stover 2015; Qu et al. 2013). Although this exact interaction is not heavily documented, the published work indicates that there the mechanism being the inotropy of Itraconazole might be directly related to this. For this study Itraconazole showed similar effects to the ones seen in previous literature that looked at its effect on the heart, with significant reductions in the RPP and ventricular pressure of the hearts tested. While the negative effect on Itraconazole was observed in the study, it was also found that age does not seem to play a major part in either a blunting or exacerbation of the drug effect. The concentration response curves produced showed that there are little to no changes in the negative inotropy of Itraconazole in the presence or absence of age.

In regard to the results from the work-loop assay when using catecholamine, dobutamine showed the expected increases in net-work and power output associated with β-stimulation (Fletcher et al. 2020; Gharanei, Wallis and Maddock 2015; Layland, J. and Kentish 2000).

However, with Isoprenaline it was found that even though it has a similar mechanism to Dobutamine, there is a reduced inotropic effect on this particular muscle setup; in addition to this, the muscles suffered a significant drop in performance after the 50-minute mark and after perfusion with Isoprenaline for 30-minutes. Previous to this drop the muscles exhibited abnormally high twitches, visible on the work-loop setup, which was proposed to be due to the chronotropic effect associated with the drug, as well as the high frequencies used, as Layland et al have found that 4Hz seems to be a more adequate frequency when compared to the 6Hz used for the studies, as it provides a more reliable power and net-work assessment (Layland, J. and Kentish 2000). The drop in performance may therefore be independent of a reduced drug effect and linked to the reported fasciculation.

In regard to the Atenolol work-loop, previous studies have used this drug in papillary muscles to study its effects on different rat models (Ban et al. 1985; Manley et al. 1986; Nagamine et al. 1989). The results documented have shown on more than one occasion that Atenolol reduces the overall contraction force of the muscles and causes a shift in the concentration-response curve of plotted muscles even in the presence of certain positive inotropic compounds (Hasenfuss, G. et al. 1992; Mügge et al. 1985). In the results presented here, a similar pattern was documented. The work produced by the muscles under the effect of Atenolol were significantly impaired and the total net-work of the muscles was also significantly impaired. Due to its effect as a  $\beta$ -receptor antagonist, it is expected for the drug to cause a significant reduction in total muscle performance, especially when exposing the muscle to a constant perfusion with the compound. The results obtained, in the younger animals, match the previously proposed hypothesis as well as the documented work done and set the ground for the next portion of this study: the use of this drug in aged isolated papillary muscles.

It has been previously mentioned how itraconazole causes heart failure and interval prolongations in heart contractility. The investigation on this drug is incredibly limited, in the context of cardiac contractile function, but not only was a negative inotropic effect on the whole heart model recorded, but also on the work-loop, as the isolated muscles showed a significant drop in power output when compared to the control muscles. It is hypothesized that itraconazole plays a role in the Na<sup>+</sup> channels of the heart and can cause depolarizing shifts (Guth et al. 2015; Qu et al. 2013); it is therefore possible that the negative inotropic effect recorded for the work-loop has, to an extent, a link to this. However, more work is still needed to improve the understanding of how itraconazole decreases the inotropy of the heart.

In chapter 3 it was established that levels of phospho-PDH under physiological conditions are reduced in an age-dependant fashion. Previous papers have suggested that PDH increases in response to an increase in Ca<sup>2+</sup> cytosolic transient (Spriet and Heigenhauser 2002), which has been justified to be potentially linked to the β-receptor desensitization in cardiac aging. A supporting study was then published by Sharma et al that measured cardiac tissue ATP with an assay kit and PDH levels with gas chromatography mass spectrometer (Sharma et al. 2005b). In their study, Sharma et al found that PDH was significantly increased in Dobutamine treated myocardial biopsies, with an associated increase in glucose oxidation; the researchers proposed that this PDH activity increase was associated with an increase in mitochondrial Ca<sup>2+</sup>, as it has been shown to occur in the presence of β-receptor stimulation.

As seen in figure 5.3.3.1.1, the dobutamine treated tissue showed no changes between the 3 and 6-month aged models but showed a significant decrease on the 18-month model. Interestingly, when compared to the control data, it was found that the dobutamine-treated 3-month phospho-PDH levels was actually lower when compared to the control, an effect that was not seen on the 6-month treated tissue, where an increase in active PDH was observed instead.

These levels then significantly dropped on the 18-month treated hearts. As it was mentioned above, Sharma et al showed that PDH significantly increased in the presence of  $\beta$ -receptor stimulation, an effect that was also detected (data not shown) in this study (Sharma et al. 2005b). The significant drop in levels with age confirms that there is a  $\beta$ -receptor desensitization that is age-dependant and that it can affect cardiac energy production and the contractility of the heart (as seen in figure 5.3.2.3), even in the presence of  $\beta$ -agonists; in addition to this, reduced intracellular calcium levels and mitochondrial dysfunction are also common effects of ageing (Domeier et al. 2014; Guo et al. 2014; Zhu et al. 2005) . For this study it was proposed that the mentioned age-dependant cardiac changes in contractility in the presence of dobutamine are, to an extent, linked to the PDH levels of the heart.

It is also important here to talk about Atenolol, as it mimicked the controls when comparing between the PDH levels across the three different age models, similar to what was seen in the isolated heart data, with the work-loop model being the only data set that showed changes in atenolol effects across ages; however, due to the fact that the 6 and 18-month muscles were not tested, this is just a potential extrapolation and more work would be required to confirm it.

The PDH levels on itraconazole-treated hearts were surprisingly similar to dobutamine, with the exception of the 18-month models, where the levels were shown to be on par with the untreated controls. In the review on itraconazole (section 1.7.4), it was mentioned that there is a limited amount of information on the drug, so this data is mostly speculative. It is known from a previous paper the drug has been shown to reduce the ATP levels in hepatocytes (Somchit et al. 2009); however, the difference between the PDH levels in different aged models seemed to play a lesser role in the overall contractility of the heart, as there was no significance between the three ages, as seen by figure 6.3.2.6.

It is therefore concluded, based on these observations, that the negative inotropy associated with itraconazole is not PDH dependant and other mitochondrial mechanisms may be active instead.

Cardiac energy deficits have been shown to occur in heart failure as a result of reductions in ATP production, as well as increases in cardiac work (Neubauer et al. 1997; Neubauer 2007; Stanley and Chandler 2002). This production depends on the energy of the proton gradient across the membrane, which is regulated by the uncoupling protein family, as it allows for the movement of protons from the outside of the mitochondrial matrix to its inside (Goglia and Skulachev 2003). Papers have shown that the presence of free circulating fatty acids can cause an increase in mitochondrial UCP expression and a subsequent lowering of the proton gradient, without ATP generation, which leads to reduced myocardial energy availability and contractility (Scheuermann-Freestone et al. 2003; Van Bilsen et al. 2002).

In other words, an increase in mitochondrial UCPs leads to a less efficient ATP synthesis. This is not an independent mechanism, as an increase in free fatty acids also causes a reduction in the GLUT4 protein, responsible for glucose uptake in the heart; this reduction reduces cardiac glycolytic ATP and the combination of the two mechanisms has been proposed as a potential explanation for the energy deficit observed in the heart; in addition to this,  $\beta$ -receptor stimulation has also been linked to an increase in free fatty acids into the plasma (Hoeks et al. 2003; Murray et al. 2004). Due to this, it is possible that the increase recorded for UCP3 levels on the itraconazole tissue may be behind the decrease seen in the ventricular relaxation rate of the isolated heart model, as there is an inefficient energy production due to the effects of age; in addition, Itraconazole may also be triggering additional molecular pathways that were not investigated in this chapter.

It is clear that work is still needed to understand the exact impact of these drugs on mitochondrial efficiency, but these results are vital in order to understand how cardiac remodelling as a consequence of age can cause shifts in protein expression when in the presence of specific compounds.

## **6.5 Summary, limitations and final comments**

To the best of our knowledge, this study was the first of its kind to investigate the effects of a range of both positive and negative inotropes (Dobutamine, Atenolol, Itraconazole and Isoprenaline) (Amin and Maleki 2012; Berry and McKenzie 2010; Opasich et al. 2000; Stangl et al. 2002) in a whole heart Langendorff model and on the work-loop assay, in order to compare their mechanistic differences in age-dependant animal models. Significant differences in the contractile properties of differently aged hearts were found and a potentially link was established between these changes and the previously reported  $\beta$ -desensitization in aged cardiac models, but more work is still necessary in order to confirm this.

In addition to this, significant changes in the active and total protein expressions of PDH when treated with Dobutamine and Itraconazole were measured, with no major changes in the hearts treated with atenolol. UCP3 showed increases when compared to the controls, but the results suggest that it does not impact cardiac contractility but may still impact other areas of cardiac function. There is therefore still a lot of work that can be done, but the work presented here proposes that energy generation molecular pathways changes should be considered when investigating these particular inotropic compounds.

The main limitations for this project, similarly to what was found in chapter 3, was the limited number of animals used due to animal housing issues and due to the fact that many of the 18-month animals did not survive until they were ready to be sacrificed.

Other limitations for this project rest on the fact that no investigation was done on various potential molecular targets due to the immense scope of the field and limited time; however, a link was confirmed, based on previously published literature, that connects calcium signalling and energy metabolism dysfunctions to the  $\beta$ -receptor desensitization recorded in aged hearts. In addition to this, and as it was mentioned previously, investigating the mRNA levels of PDH, PPAR $\alpha$  and UCP3 would have been useful to complement the western blot results, as it would show if there were gene expression changes directly or indirectly tied to the protein levels; for UCP3 this would be of particular importance due to previously published discrepancies between protein and mRNA levels.

The next chapter will focus on investigating obesity-induced changes in the contractile function of the heart under, the effect of the aforementioned inotropes, in an age-dependant fashion. It is now known that there are changes in ATP production due to age and will now focus on how they vary in HFD models.

## **Chapter Seven: Inotropic drug effects on the contractile function of the heart in High-fat diet-induced obesity, in differently aged animals**

Some of the data in this chapter was presented as following:

- **Coventry University Symposium 2017 – Poster presentation**
- **Sports, Exercise and Life Sciences Seminar Series 2018 – Oral presentation**

Manuscripts in preparation which will include part of the data presented in this chapter:

- Inotropic functional changes of the heart in the presence of a high-fat diet, in differently aged models – *RA Ribeiro, Maddock, H, Tallis, J, Dodd, M, Gharanei, AM – Toxicology and Applied Pharmacology.*

## 7.1 Introduction

As it has been recorded in the last three experimental chapters, both age and high-fat diet induced obesity play a major focus in cardiac dysfunction, with left ventricular hypertrophy being one of the major concerns (Lakatta and Levy 2003; Selthofer-Relatić, Bošnjak and Kibel 2016; Stapleton et al. 2008). This has been heavily supported by papers that have shown an age-dependant increase in cardiac stiffness, which causes the contractility of the heart to be significantly impaired (Biernacka and Frangogiannis 2011; Csiszar et al. 2008; Lakatta and Levy 2003). Studies have also looked at different molecular systems directly impacted by age, with three main mechanisms being at the centre of it: cardiomyocyte relaxation impairment via the excitation-contraction coupling in the myocardium (Domenighetti et al. 2005), the adrenergic signalling pathway (Yan et al. 2007) and the mitochondrial ROS involvement, as it is known that the aged myocardium has a lower threshold for ROS associated changes and dysfunctions associated with it can trigger apoptotic responses in cells (Crow et al. 2004; Sparagna et al. 2000). Previous papers have proven the existence of an impairment in certain mitochondrial proteins, as well as the existence of damaged mitochondria, in senescent rat hearts, that contribute to this link between mitochondrial dysfunctions and aged heart vulnerabilities. (Nitta et al. 1994; Tani et al. 2001). As it was also reviewed, the cardiovascular dysfunction often associated with obesity results from a remodelling that occurs via three main mechanistic alterations (Alpert et al. 1995; Eckel, Grundy and Zimmet 2005; Lavie et al. 2013; Trayhurn and Wood 2004): cardiac lipotoxicity (Drosatos and Schulze 2013; Ren et al. 2010), nitric oxide changes (Rastaldo et al. 2007) and inflammation (Csiszar et al. 2008; Trayhurn and Wood 2005). For an in-depth review on the effects of aging and obesity on cardiac function, please refer back to sections 1.4, 1.5 and 1.6, as well as chapters 3 and 4 for a full physiological investigation.

For this chapter, the effects of obesity on inotropic drug changes were studied with the aid of three inotropic drugs: dobutamine, atenolol and itraconazole (their mechanisms can be found between sections 1.7.1 and 1.7.4). Dobutamine is a catecholamine and one of the most commonly used positive inotropic agents worldwide (Machen and Sleeper 2015). There is a well documented phenomenon known as a “ $\beta$ -adrenoreceptor desensitization” and it is commonly observed during physical stress (Abrass, Davis and Scarpace 1982; Ferrara et al. 2014; Hashimoto, Nakashima and Sugino 1983). A different study by Bussey et al found that there is also a decrease in  $\beta$ 1-adrenoreceptor responsiveness in obese and high-fat diet induced obesity rat models, when they tested the AMPK signalling changes in the presence of obesity (Bussey et al. 2018). In this study, the researchers found that the  $\beta$ -adrenergic signalling was impaired in obese hearts and found that there was an equally reduced AMPK phosphorylation; Bussey et al proposed that AMPK downstream signalling may be a potential target in the restoration of the reduced responsiveness in the adrenoreceptors. AMPK has also been previously linked to PDH regulation and Klein et al showed that this was not so much a direct effect, but an indirect one likely due to the role of AMPK on energy homeostasis (Klein et al. 2007). Chambers et al conducted a follow-up study and found that in cardiac pyruvate dehydrogenase overexpressed mice, AMPK was overexpressed as an adaptive mechanism in order to maintain adequate levels of mitochondrial oxidation, but also to promote re-entry of FAs into the mitochondrion via an increase in PGC-1 $\alpha$  levels (Chambers et al. 2011).

Atenolol is a second-generation cardio-selective  $\beta$ 1 receptor antagonist with both negative inotropic and chronotropic properties (see 1.4.4 for a full review on Atenolol). On the isolated heart model, Atenolol has been shown to cause impaired coronary resistance during ischaemia, as well as a reduction in LVDP, HR, +dP/dt and -dP/dt when compared to control hearts (Allibardi et al. 1999; Lavanchy, Martin and Rossi 1988).

It has also been shown to increase the risk of mortality in the elder population, especially in patients suffering from high pulse arterial pressure (Testa et al. 2014). In another study using 18-month mice models, it was found that Atenolol not only reduced the membrane fatty acid unsaturation of the heart, but also decreased the various markers of oxidative stress within the animals (Gómez et al. 2014; Sanchez-Roman et al. 2010; Sanchez-Roman et al. 2014); in addition, Gómez et al also recorded changes in the heart rate, systolic pressure and diastolic pressure in the hearts treated with atenolol, when compared to the control groups.

In obesity, atenolol was shown by Wójcicki et al to have minimal and non-significant changes in both systolic and diastolic pressure and heart rate, when comparing them between lean and obese models (Wojcicki et al. 2003); however, this study was conducted on a very limited number of subjects and researchers only measured the plasma concentrations of the volunteers. A different study was carried out by Williams et al, which aimed to investigate the effects of a diet-induced obesity on cardiac regulation in mice, while under the effect of an atenolol treatment regime, under standard laboratory temperatures (22°C) and thermoneutral temperatures (30°C) conditions (Williams et al. 2003); in their study, the researchers found that there was a non-significant effect of atenolol on the mean arterial pressure (also known as average blood pressure) of obesity, but a significant decrease in heart rate which seemed to be attenuated or exacerbated under certain dark and light periods. Williams et al concluded that the  $\beta_1$ -adrenoceptor-blockade effects are, for the most part, unchanged in the presence or absence of obesity. These results, alongside the ones published by Klein et al, seem to indicate that there is a reduced effectiveness of beta-signalling stimulation (Klein et al. 2007), but not beta-signalling blocking, in obese models.

Parikh et al conducted a more recent study to investigate this, as researchers measured various haemodynamic parameters like systolic (SBP) and diastolic blood pressures (DBP) on a group of human participants split into three categories: normal weight, overweight and obese, under both normal conditions and under high blood pressure medication treatments (Parikh et al. 2018). Parikh et al found that between the three categories, there were no significant changes in any of the parameters measured for the three patient categories being treated with beta-blockers and calcium channel blockers. A pattern seems to emerge from these studies, as beta-blockers seem to be unaffected by obesity and retain the same effectiveness regardless of its presence.

Finally, Itraconazole is a synthetic triazole antifungal agent commonly used in the treatment of most systemic fungal infections (please refer to section 1.7.4 for a full review on Itraconazole). Amongst the most severe adverse effects of the drug, the most commonly observed is heart failure and a severe drop in left ventricular pressure (Fung, Chau and Yew 2008; Qu et al. 2013). Studies have shown that patients are more likely to develop congestive heart failure when under treatments with Itraconazole, even when different protocols were used to measure the negative inotropic effect of the drug (Guth et al. 2015; Okuyan and Altin 2013). It has also been investigated in the isolated heart model and showed severe decreases in the heart rate, coronary flow, LVDP and the ventricular pressure rise and drop, starting at concentrations as low as 0.3  $\mu\text{M}$  (Qu et al. 2013). Chaudhary et al showed, on the isolated heart model, that age also plays an effect in CYP expression and a recent study has shown that younger mice overexpress CYPs and that this effect is lost with age, due partially to oxidative stress (Chaudhary et al. 2013). These studies, while limited, suggest that age has a significant effect in heart function and that this is linked to changes to the CYP superfamily expression, which itraconazole inhibits.

In obesity, Fluconazole is the only one of the triazole antifungals that has been investigated and a very limited amount of data exists on the pharmacokinetics (PK) of most of them in both lean and obese patients, with no data available in murine models (Neofytos, Avdic and Magiorakos 2010). It is known that both fluconazole and itraconazole share very similar mechanism of action and, therefore, a brief review will be made on these drugs in the context of obesity. Fluconazole has been shown to have different PKs, depending on who it is used on; in healthy patients, it has shown a favourable safety profile (Lewis 2011), while in critically ill patients it has shown to have a change in its PKs to a less effective safety profile (Sinnollareddy et al. 2015). The exact reasons behind this are not fully understood. Alobaid et al conducted a study on participants divided into three groups: normal weight, obese and morbidly obese (Alobaid et al. 2016); plasma samples were taken and the research team found that the dosage required to achieve the same effect was significant different between the three groups, which Alobaid et al then concluded to be directly linked to the effects of obesity on the organism.

In addition to this, studies have been done on the changes in CYP450 enzymes as a result of obesity and a recent study by Drolet et al found that there was a significant reduction in CYP family enzyme protein expression in cardiac tissue of type 2 diabetes mice models (Drolet et al. 2017); the researchers concluded that this change was a potential exacerbator of risk factors of cardiovascular disease via a disruption in the equilibrium between cardioprotective and cardiotoxic metabolites of arachidonic acid. In this study it was proposed that these changes are also occurring on the carbon metabolic pathway, and it is suggested that these potential changes are happening via changes in ATP production and synthesis, potentially through pathways involving pyruvate dehydrogenase and UCP3.

Due to the lack of data on obese patients or models with itraconazole, this study crucial as a pioneering pre-clinical investigation to predict how itraconazole pharmacokinetics change in the presence of high-fat diet induced obesity, and whether it is heavily impacted by mitochondrial energy metabolic protein changes. In addition, the effect of different  $\beta$ -receptor agonists and antagonists are of particular importance due to the limited information on the combined effects of age and HFD, as it is likely that the  $\beta$ -receptor desensitization mentioned in previous chapters may occur in the presence of HFD.

The primary aims of this chapter were **a)** to investigate the effects of obesity on whole heart cardiac function when under the effect of isoprenaline, dobutamine, atenolol and itraconazole on an isolated heart model, **b)** to investigate the synergistic effects of age and high-fat diet-induced obesity on an isolated heart model and **c)** investigate how mitochondrial metabolism changes in the combined presence of obesity and the aforementioned inotropic drugs. The main hypotheses for this chapter were **(a)** HFD will cause a blunted effect of Dobutamine and will exacerbate the negative inotropic effects of Atenolol and Itraconazole, across all age groups and **(b)** PDH phosphorylation levels will be significantly decreased in the combined presence of HFD and age for Dobutamine, Atenolol and Itraconazole. Due to the presence of HFD, UCP3 levels will not show significant differences between the three drugs.

The main objectives of this study were: **(a)** to elucidate how Dobutamine, Itraconazole, Atenolol and Isoprenaline change the contractile function of the heart under naïve, HFD and HFD and ageing conditions, using the Langendorff isolated heart model and **(b)** to investigate whether these changes occur partially as a result of mitochondrial energy metabolism changes, notably on the pathways involving pyruvate dehydrogenase E1- $\alpha$  subunit (PDH) and uncoupling protein 3 (UCP3).

## 7.2 Materials and Methods

### 7.2.1 Animal Models

Following ethics approval from the host institute, 3-month animals were purchased from Charles River UK Limited (Margate, UK) and received human care in accordance with the guidelines of the British Home Office Animals (Scientific Procedures) Act 1986 (Hollands 1986). Animals were aged in cages of 3 to 5 individuals, in 12h light and dark cycles at around 50% relative humidity. The diets used for this project were the same as the ones seen in a recent study published by Messa et al (Messa et al. 2020) and their caloric composition were as follows: (**STANDARD CHOW**): protein 17.5%, fat 7.4%, carbohydrate, 75.1%; gross energy 3.52 kcal.g<sup>-1</sup>; metabolizable energy 2.57 kcal.g<sup>-1</sup> (CRM(P) SDS/Dietex International Ltd, Whitham, UK) and (**HIGH FAT DIET**): protein 18.0%, fat 63.7%, carbohydrate, 18.4%; gross energy 5.2 kcal.g<sup>-1</sup>; metabolizable energy 3.8 kcal.g<sup>-1</sup> (Advance protocol PicoLab, Fort Worth, USA). All of the animal groups were given *ad libitum* access to their respective diet and water and feeding began 16 weeks prior to starting the experiments. For the 6 and 18-month lean and high-fat diet groups, animals were divided into randomized sample sizes of 60 and 80 Sprague-Dawley male rats, respectively. For the 6-month group, 30 were given standard chow *ad libitum* (average body mass of 539g ± 15.5 (SEM)) and the other 30 were given the high fat diet *ad libitum* (average body mass of 638g ± 7.2 (SEM)). For the 18-month group, 40 were given standard chow *ad libitum* (average body mass of 793g ± 8.4 (SEM)) and the other 40 were given the high fat diet *ad libitum* (average body mass of 930g ± 10.5 (SEM)). The body mass measurements of the animals were measured bi-weekly (see figures 7.2.1.1 and table 7.2.1.1) and both the mesenteric and epididymal pads were weighed (see figure 7.2.1.1) after the sacrifice of the animals to provide a two-step verification in their body mass difference (Woods et al. 2003).

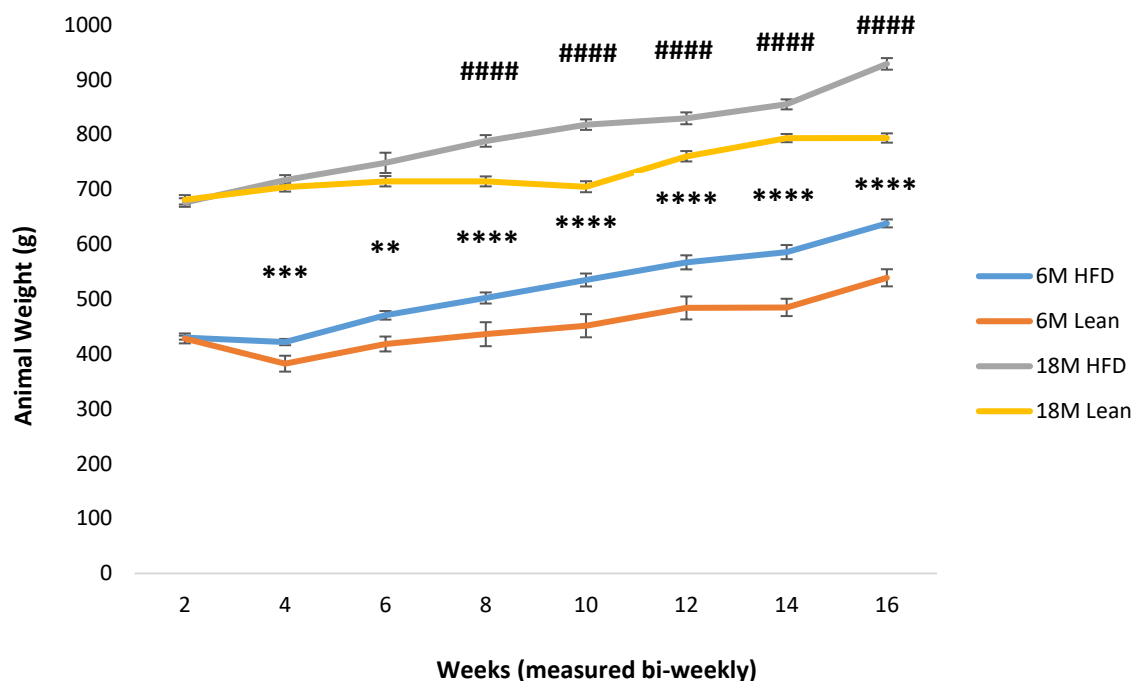


Figure 7.2.1.1 – Comparison of animal body mass in both the 6 and the 18-month aged models, measured bi-weekly, for a total of 16 weeks. Significance was shown after the first month of feeding between the lean and the HFD models within each aged model (\*\*\*\* and #### =  $p < 0.0001$ ; \* = 6-month model; # = 18-month model).

Table 7.2.1.1 – Table with the comparison of parameters between lean models and HFD models, in 6-month and 18-month aged animals. The mean values are a representation of the parameters at the start of the experimental protocols (\*\* =  $p < 0.01$ ; \*\*\* =  $p < 0.001$  and \*\*\*\* =  $p < 0.0001$ , compared to the 6-month lean group and ### =  $p < 0.001$  and #### =  $p < 0.0001$ , compared to the 18-month lean group).

Age group	6M Lean Mean $\pm$ SEM	6M HFD Mean $\pm$ SEM	18M Lean Mean $\pm$ SEM	18M HFD Mean $\pm$ SEM
Body mass (g)	539 $\pm$ 15.5	638 $\pm$ 7.2 ****	794 $\pm$ 8.4	929 $\pm$ 10.5 ####
Body length (cm)	43 $\pm$ 0.5	44 $\pm$ 0.4	49.5 $\pm$ 0.4	48.5 $\pm$ 0.4
Left epididymal fat pad mass (g)	7.01 $\pm$ 0.6	8.65 $\pm$ 0.5 ***	6.93 $\pm$ 0.4	12.05 $\pm$ 0.6 ####
Right epididymal fat pad mass (g)	6.64 $\pm$ 0.6	8.72 $\pm$ 0.5 **	6.97 $\pm$ 0.3	12.50 $\pm$ 0.6 ####
Mesenteric fat pad mass (g)	6.50 $\pm$ 0.6	10.63 $\pm$ 0.8 ****	8.70 $\pm$ 0.3	11.42 $\pm$ 0.4 ###
Body circumference (cm)	21.75 $\pm$ 0.2	25.75 $\pm$ 0.2 ****	26.25 $\pm$ 0.2	33.75 $\pm$ 0.3 ####

Regarding the animals in the obesity projects, previous rodent models have been used for similar studies (with slight modifications in feeding time and diet supplements) in order to induce obesity, as their neuroanatomy and energy homeostasis control resembles that of a human being (Barrett, Mercer and Morgan 2016; Marques et al. 2016; Wilson, C. et al. 2007; Woods et al. 2003). A more detailed explanation of the animal model and how it compares to previous research can be found in section 3.1.

### **7.2.2 Langendorff Isolated Heart Model (full review in section 3.2)**

The technique starts with the perfusion of the heart with Krebs-Henseleit buffer (maintained at a constant temperature of  $37^{\circ}\text{C} \pm 0.5$  at a pH of 7.4) and gassed with 95% O<sub>2</sub> and 5% CO<sub>2</sub>, by means of cannulating the aorta, in a retrograde fashion, forcing the closing of the aortic valve as a result of a change in pressure. The buffer then passes through a vascular bed before being drawn to the coronary sinus in the right atria. This allows the preparation to be maintained without any fluid filling the ventricular chambers (Skrzypiec-Spring et al. 2007). Measurements for the coronary flow (CF), left ventricular developed pressure (LVDP), heart rate (HR) and the Maximum ventricular pressure increase (+dP/dtmax) and decrease (-dP/dTmax) were recorded using a physiological pressure transducer connected to the latex balloon and to a PowerLab (ADInstruments, UK) linked to a PC with LabChart<sup>®</sup> software v7 and the rate pressure product (RPP) was calculated using the function mentioned in section 3.2.2. At the end of the protocol, the left ventricle was excised from each heart and divided into two; tissues were then rapidly frozen in liquid nitrogen before being stored at -80°C for future use. For a full background review, please refer to section 3.2.

The experimental protocol for each of the inotropes used (Dobutamine, Itraconazole and Atenolol) was split into a 20-minute stabilisation period and 140 minutes of increasingly high drug concentrations for all hearts (ranging from 1nM to 30µM, for a total of seven different concentrations); a 20-minute cumulative protocol was chosen based on preliminary data that indicated that it was the adequate time to achieve a steady contractile response with the used inotropic drugs (see figure 7.2.2.1).

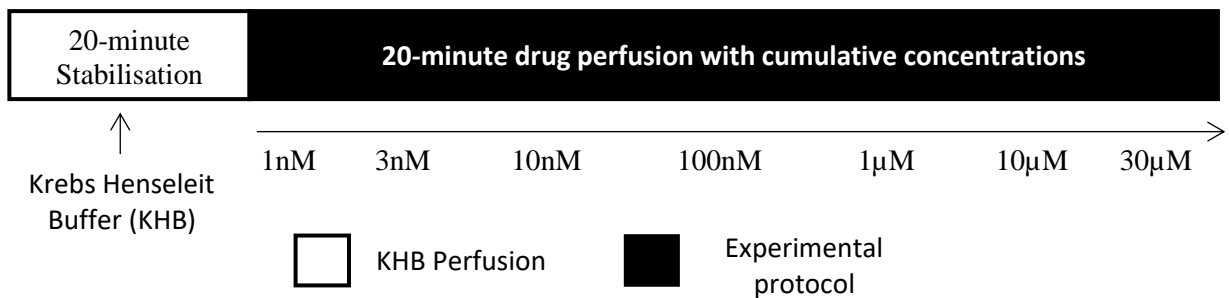


**Figure 7.2.2.1 – Langendorff protocol** - Diagram for the cumulative dose-controlled protocol for the Langendorff isolated heart model used in this project, per drug.

### 7.2.3 Western Blotting (full review in section 3.4)

Cardiac tissue was collected from each treatment group, as mentioned in table 3.1.2.2. Approximately half of the left ventricle (50 mg) was then homogenized with lysis buffer (100 mM NaCl, 10 mM Tris base - pH 8.0, 1 mM EDTA - pH 8.0, 2 mM sodium pyrophosphate, 2 mM NaF, 2 mM β-glycerophosphate, SigmaFAST™ protease inhibitor cocktail tablets – 1 tablet/100ml and PhosStop™ - 1 tablet/10ml) on a IKA Ultra-Turrax® T 25 basic disperser, set to a speed of 21,500 RPM.

This tissue was then centrifuged for 10 minutes at 11,000 RPM at 4°C to obtain the desired supernatant, which was then transferred into clean 1.5ml microcentrifuge tubes. Samples were diluted using Laemmli buffer (250 mM Tris-HCl – pH 6.8, 10% glycerol, 0.006% bromophenol blue, 4% SDS, β-mercaptoethanol – pH 6.8) and incubated at 100°C for 5 minutes before being stored at –20°C. Prior to using the samples, they were defrosted on ice and diluted further using Laemmli buffer to obtain a protein concentration of 50µg.

To calculate the protein content of homogenised samples, a colorimetric Pierce™ BCA Protein assay kit (Thermo Fisher Scientific, UK) was used. Concentrated albumin standards were serially diluted using lysis buffer to obtain a concentration range of 0 - 2000µg/ml.

BCA working reagent was prepared following a 50:1 ratio of reagent A and reagent B, respectively. Standards and samples were pipetted at a volume of 10µl, in triplicate, onto a 96-well plate. Following this, 200µl of working reagent was added to each well. Plates were then covered to protect from light and incubated for 30 minutes at 37°C, before being left to cool to room temperature. The plate reader was set to 562 nm and the measured absorbance values were then used to calculate the total protein content per unknown sample.

The previously collected samples were further diluted using laemmli buffer to obtain a concentration of 50µg/µl. These samples were then centrifuged at 1200 RPM for 2 minutes, at 4°C, before being loaded onto Precast TGX™ (Tris/glycine) gradient gels (Bio-Rad, UK). The gels were then placed inside of a Mini-PROTEAN™ vertical electrophoresis assembly unit before filling the chamber and outer tank with running buffer (14.42g/L Glycine, 1.0g/L SDS, 3.03g/L Tris base). The samples were then loaded into the wells, with at least one well loaded with a molecular protein marker acquired from Cell Signalling UK. Gels were run at 110V for 60 minutes using a Power-PAC 3000 (Bio-Rad, UK).

Following electrophoretic separation, the gels were removed from their compartments and placed onto Trans-Blot® Turbo™ transfer packs, consisting of filter paper, buffer and a polyvinylidene fluoride (PVDF) membrane. The assembled cassettes were loaded into the Trans-Blot system (Bio-Rad, UK) and ran for the mixed molecular weight transfer protocol for a total of 7 minutes. Following transfer, the membranes were cut into two using a scalpel blade. Blots were then incubated at room temperature in blocking buffer (5% w/v milk powder in Tris-buffered saline with Tween 20 (TBST) for 60 minutes on an orbital shaker (Cassambai et al. 2019).

Blots were then incubated overnight in 5% w/v bovine serum albumin (BSA) in TBST - 1/1000, at 4°C, with anti-UCP3 antibody and phosphorylated Pyruvate Dehydrogenase E1-alpha subunit purchased from Abcam (UK). The following day, blots were then incubated with secondary antibody (anti-rabbit HRP IgG – 1/1000, Cell Signalling, UK) in blocking solution (5% w/v milk powder in TBST) and incubated for 1 hour at room temperature on an orbital shaker.

To visualise the membranes, they were first placed onto an acetate sheet and coated with approximately 1 mL of SuperSignal West Femto kit (Thermo-Scientific), in a 1:1 dilution, to amplify the signals from the membranes. Images were then captured and visualised using a ChemiDoc with the ImageLab™ Touch software (Bio-Rad, UK). Membranes were exposed for 3 to 5 seconds (see representative blot in figure 2.4.6.1) in order to detect the bands corresponding to the proteins of interest. Images were subsequently analysed using the java-based software ImageJ (National Institutes of Health, USA). After visualising the membranes, they were stripped using Restore™ Western Blot Stripping Buffer (Thermo Fisher Scientific, UK) and re-probed for the total form of Pyruvate Dehydrogenase E1-alpha subunit and GAPDH, to be used as controls for the data.

#### **7.2.4 Statistical Analysis (full review in section 3.6)**

Animal body mass and fat pad weight was plotted as average mass/weight  $\pm$  standard error of the mean (SEM) and statistically analysed using One-Way analysis of variance (ANOVA) with Tukey's post hoc test, on IBM SPSS® Statistics 25 (IBM Corporation USA). A p value of  $p < 0.05$  was considered statistically significant. The haemodynamics and work-loop data were plotted as a percentage of the average stabilisation (mean  $\pm$  standard error of the mean (SEM)).

Two-Way analysis of variance (ANOVA) was used with Tukey's LSD (least significant difference) for each time point as a function of each age group and each treatment, for both the Langendorff and the work-loop data. Fisher's LSD was used for the western blot data, as the main interest was in finding the minimum difference between protein expression. A p-value of  $p < 0.05$  was considered statistically significant. Origin Pro 2015 (Origin Lab Corporation, USA) was used to plot all of the dose response graphs for each of the inotropes.

### **7.3 Results**

The data will be presented for the Langendorff isolated heart model, similarly to the previous chapter. Measurements for the different haemodynamic parameters will be presented, as well as the comparison between muscle mechanics when comparing a high-fat diet model to a lean model. Two different age group models were used for the isolated heart project: a 6-month model and an 18-month model. Data collection was divided into these two age groups. Parameters documented remained unchanged.

#### **7.3.1 Langendorff Isolated Heart Model**

The following section contains the recorded data for the Langendorff isolated heart model, showing a comparison between the drugs tested on lean models and the same drug administered to the HFD models. Stabilisation parameters were very similar, with no significance between the models. In order to present the Langendorff data, a table was necessary in addition to the concentration response curves, in order to highlight the changes in response occurring on the isolated heart. Table 7.3.1.1 contains the maximum and minimum responses for the relevant haemodynamic parameters on the 6-month lean and HFD models, per inotropic drugs, in addition to their EC50 values. Significances for these parameters have been depicted in figures 7.3.1.1 to 7.3.1.21.

**Table 7.3.1.1 – Table with the minimum and maximum drug response on the 6-month lean and HFD isolated hearts, and respective EC50 value.** The values shown on the table represent the minimum and maximum response of the heart after being exposed to increasingly higher drug concentrations. The EC50 is also presented, showing the half maximal concentration required to induce a response.

Age (months)		Minimum response (% of stabilisation)		Maximum response (% of stabilisation)		EC50 (M)	
		6 Lean	6 HFD	6 Lean	6 HFD	6 Lean	6 HFD
LVDP (mmHg)	Atenolol	-5	2	-33	-26	$2.4 \times 10^{-8}$	$2.7 \times 10^{-7}$
	Itraconazole	1	-9	-55	-60	$5.3 \times 10^{-7}$	$2 \times 10^{-7}$
	Dobutamine	18	18	45	32	$3.9 \times 10^{-8}$	$1.8 \times 10^{-6}$
HR (bpm)	Atenolol	1	2	8	9	$1.8 \times 10^{-9}$	$1.8 \times 10^{-8}$
	Itraconazole	-5	1	-16	13	$2.2 \times 10^{-6}$	$1.4 \times 10^{-8}$
	Dobutamine	3	-2	49	17	$5.8 \times 10^{-8}$	$5.2 \times 10^{-8}$
MPR (mmHg/s)	Atenolol	1	1	-14	-14	$1.2 \times 10^{-6}$	$2.4 \times 10^{-7}$
	Itraconazole	1	-6	-34	-35	$2.5 \times 10^{-6}$	$1.5 \times 10^{-7}$
	Dobutamine	10	19	51	55	$1.3 \times 10^{-7}$	$7.9 \times 10^{-8}$
MPD (mmHg/s)	Atenolol	-2	11	-15	-15	$3.2 \times 10^{-7}$	$1.6 \times 10^{-7}$
	Itraconazole	1	-6	-22	-23	$6.2 \times 10^{-7}$	$2 \times 10^{-8}$
	Dobutamine	-3	4	50	37	$5.3 \times 10^{-7}$	$7.9 \times 10^{-6}$
RPP (mmHg/min)	Atenolol	-3	4	-26	-24	$4.8 \times 10^{-8}$	$2.5 \times 10^{-7}$
	Itraconazole	-3	-6	-62	-56	$7.5 \times 10^{-7}$	$1 \times 10^{-8}$
	Dobutamine	21	15	104	43	$4.1 \times 10^{-8}$	$5.6 \times 10^{-6}$

Table 7.3.1.2 contains the maximum and minimum responses for the relevant haemodynamic parameters on the 18-month lean and HFD models, per inotropic drugs, in addition to their EC50 values. Significances for these parameters have been depicted in figures 7.3.1.1 to 7.3.1.21.

**Table 7.3.1.2 – Table with the minimum and maximum drug response on the 18-month lean and HFD isolated hearts, and respective EC50 value.** The values shown on the table represent the minimum and maximum response of the heart after being exposed to increasingly higher drug concentrations. The EC50 is also presented, showing the half maximal concentration required to induce a response.

Age (months)		Minimum response (% of stabilisation)		Maximum response (% of stabilisation)		EC50 (M)	
		18 Lean	18 HFD	18 Lean	18 HFD	18 Lean	18 HFD
LVDP (mmHg)	Atenolol	-5	-9	-39	-41	$1.4 \times 10^{-7}$	$4 \times 10^{-7}$
	Itraconazole	-8	-13	-60	-68	$2.7 \times 10^{-7}$	$1.5 \times 10^{-7}$
	Dobutamine	25	4	51	23	$1.5 \times 10^{-6}$	$1.5 \times 10^{-6}$
HR (bpm)	Atenolol	0	4	7	-6	$5.6 \times 10^{-6}$	$4.6 \times 10^{-7}$
	Itraconazole	0	-6	20	-27	$1 \times 10^{-7}$	$7.2 \times 10^{-9}$
	Dobutamine	-10	5	21	24	$1.1 \times 10^{-6}$	$3.5 \times 10^{-7}$
MPR (mmHg/s)	Atenolol	-2	-7	-17	-21	$1.8 \times 10^{-8}$	$1.2 \times 10^{-8}$
	Itraconazole	8	-5	-17	-39	$6.8 \times 10^{-8}$	$4.6 \times 10^{-7}$
	Dobutamine	0	1	16	21	$2.3 \times 10^{-7}$	$5.6 \times 10^{-8}$
MPD (mmHg/s)	Atenolol	-1	-1	-14	-22	$5.6 \times 10^{-8}$	$1 \times 10^{-8}$
	Itraconazole	2	-2	-14	-37	$3.2 \times 10^{-8}$	$2.4 \times 10^{-8}$
	Dobutamine	-6	-1	22	18	$1 \times 10^{-9}$	$1 \times 10^{-7}$
RPP (mmHg/min)	Atenolol	-7	-6	-39	-45	$2.2 \times 10^{-7}$	$2.7 \times 10^{-7}$
	Itraconazole	-6	-26	-52	-77	$3.5 \times 10^{-7}$	$3.2 \times 10^{-7}$
	Dobutamine	13	10	63	51	$1.7 \times 10^{-9}$	$2.9 \times 10^{-8}$

### *Atenolol (6-month data)*

No significant changes were recorded for either model (HFD and lean) for both LVDP and HR (data not presented here). In addition, no significant changes were seen on either the MPR (A) nor the MPD (B) of the hearts (figure 7.3.1.1) treated with Atenolol.

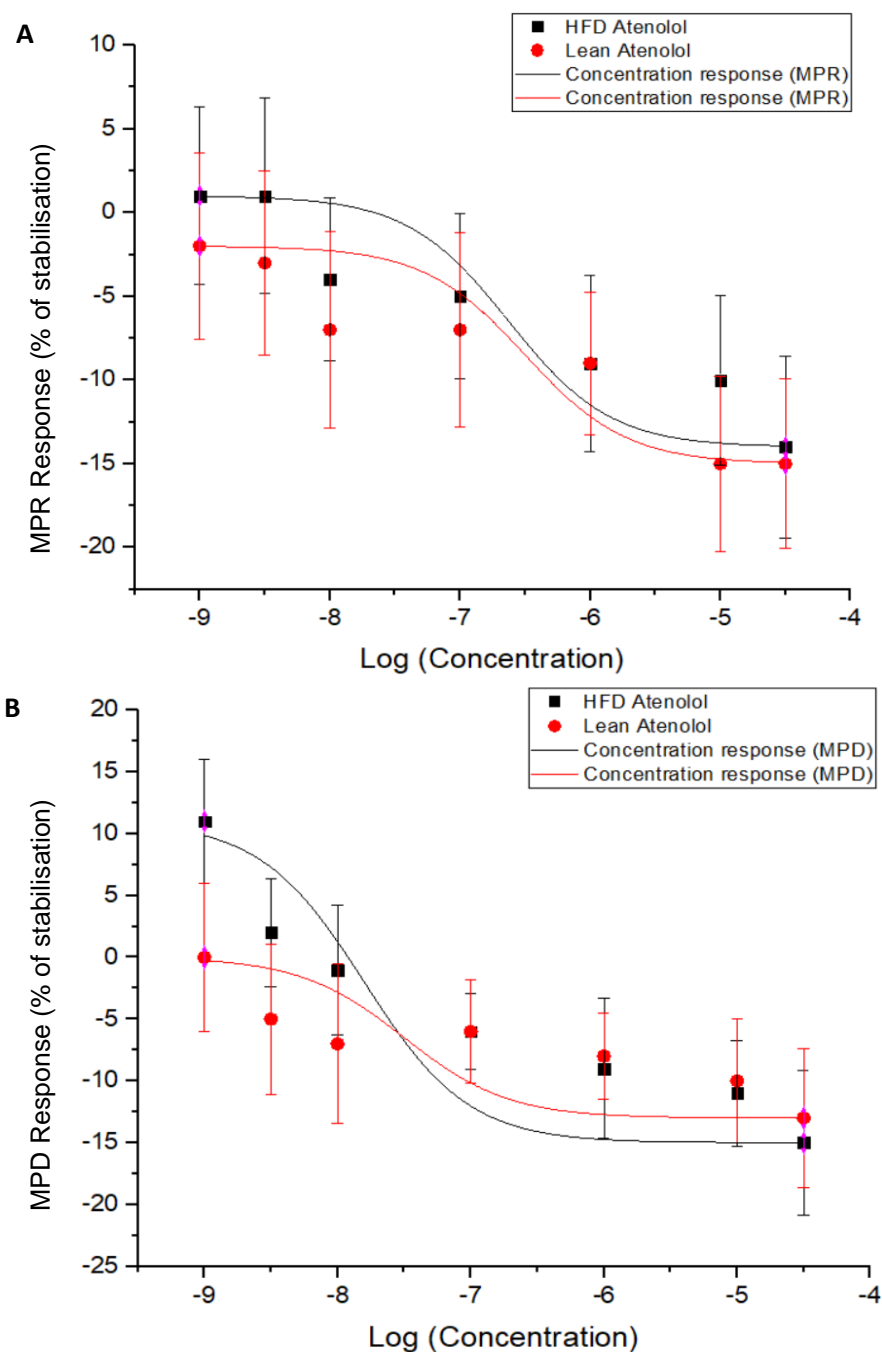


**Figure 7.3.1.1 - + dP/dTmax (A) and -dP/dTmax (B) for the 6-month atenolol-treated lean and HFD models (n = 4 for both).** Hearts were allowed a 20-minute stabilisation period followed by increasing concentrations of each compound: 1 nM = 20-40 mins; 3 nM = 40-60 mins; 10 nM = 60-80 mins; 100 nM = 80-100 mins; 1  $\mu$ M = 100-120 mins; 10  $\mu$ M = 120-140 mins and 30  $\mu$ M = 140-160 mins.

The RPP (figure 7.3.1.2) showed significance at the 100nM and 1µM concentrations, where the HDF hearts showed a significant increase of  $+20\% \pm 10.2$  (SEM), in relation to the lean hearts ( $p < 0.05$ ).

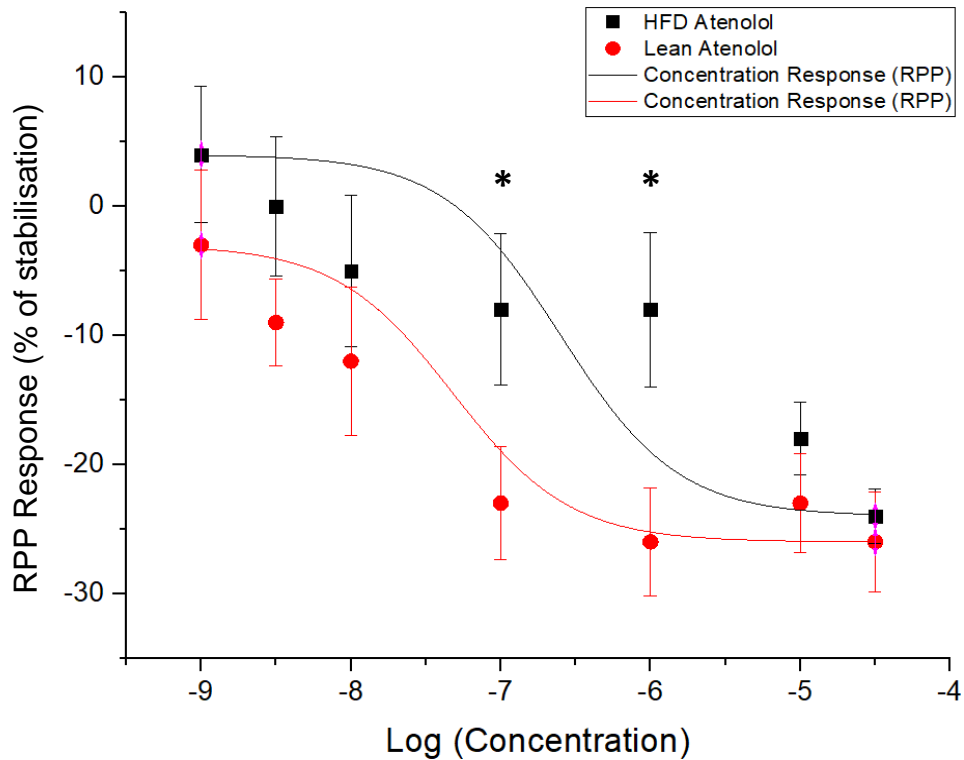


**Figure 7.3.1.2 – RPP for the 6-month atenolol-treated lean and HFD models (n = 4 for both).** Hearts were allowed a 20-minute stabilisation period followed by increasing concentrations of each compound: 1 nM = 20-40 mins; 3 nM = 40-60 mins; 10 nM = 60-80 mins; 100 nM = 80-100 mins; 1 µM = 100-120 mins; 10 µM = 120-140 mins and 30 µM = 140-160 mins. Measurements for RPP when treated with Atenolol are displayed above (\* =  $p < 0.05$ , in relation to the lean control).

### *Atenolol (18-month data)*

Similar to what was seen before, the LVDP and HR showed no significance between the two models (data not shown). In addition, the MPR (A) and MPD (B) also did not significantly change between the two models, when treated with Atenolol (figure 7.3.1.3). In addition, no significant changes were observed for the RPP of the hearts (figure 7.3.1.4).

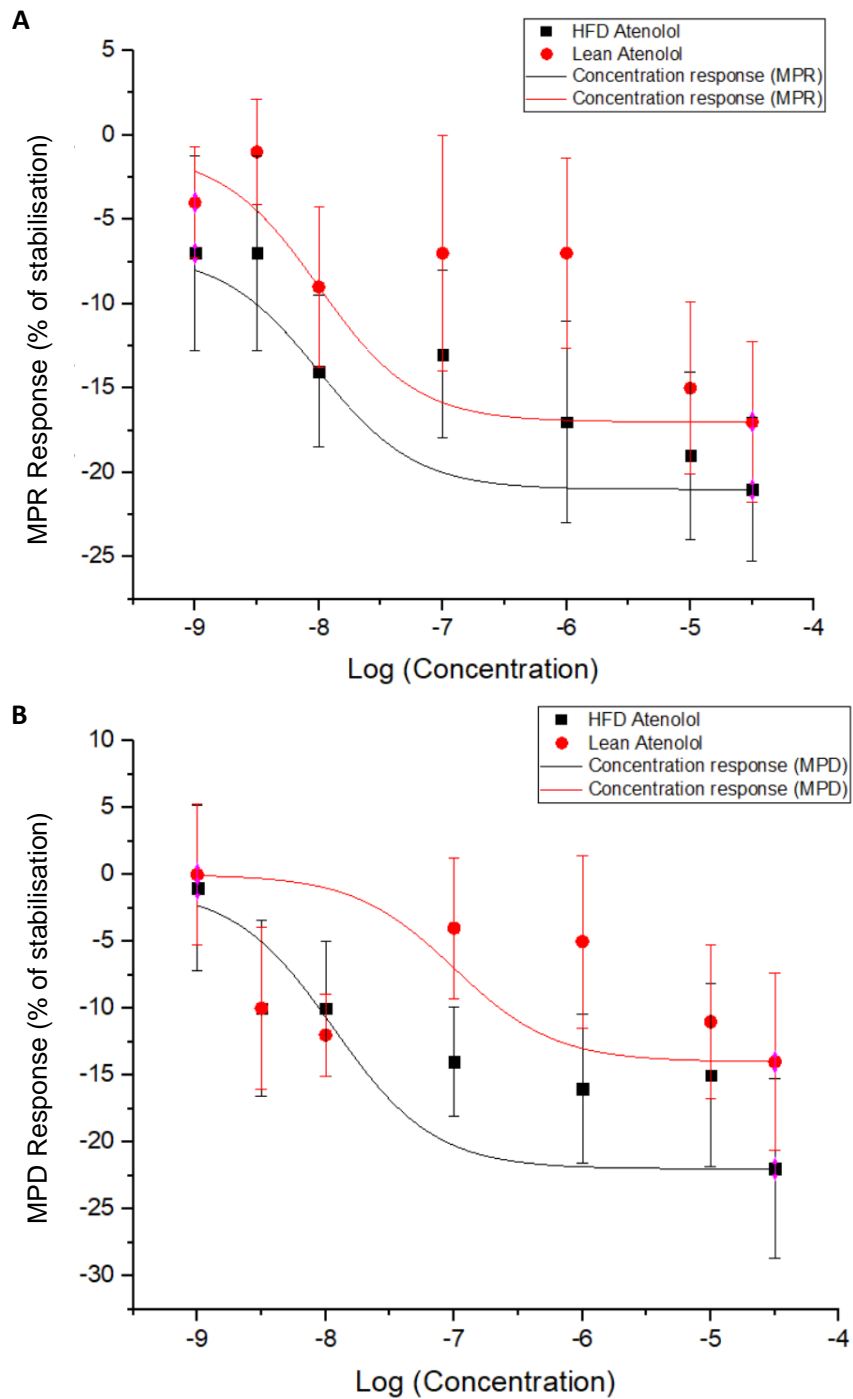


**Figure 7.3.1.3 - +dP/dTmax (A) and -dP/dTmax (B) for the 18-month atenolol-treated lean and HFD models (n = 4 for both).** Hearts were allowed a 20-minute stabilisation period followed by increasing concentrations of each compound: 1 nM = 20-40 mins; 3 nM = 40-60 mins; 10 nM = 60-80 mins; 100 nM = 80-100 mins; 1  $\mu$ M = 100-120 mins; 10  $\mu$ M = 120-140 mins and 30  $\mu$ M = 140-160 mins.

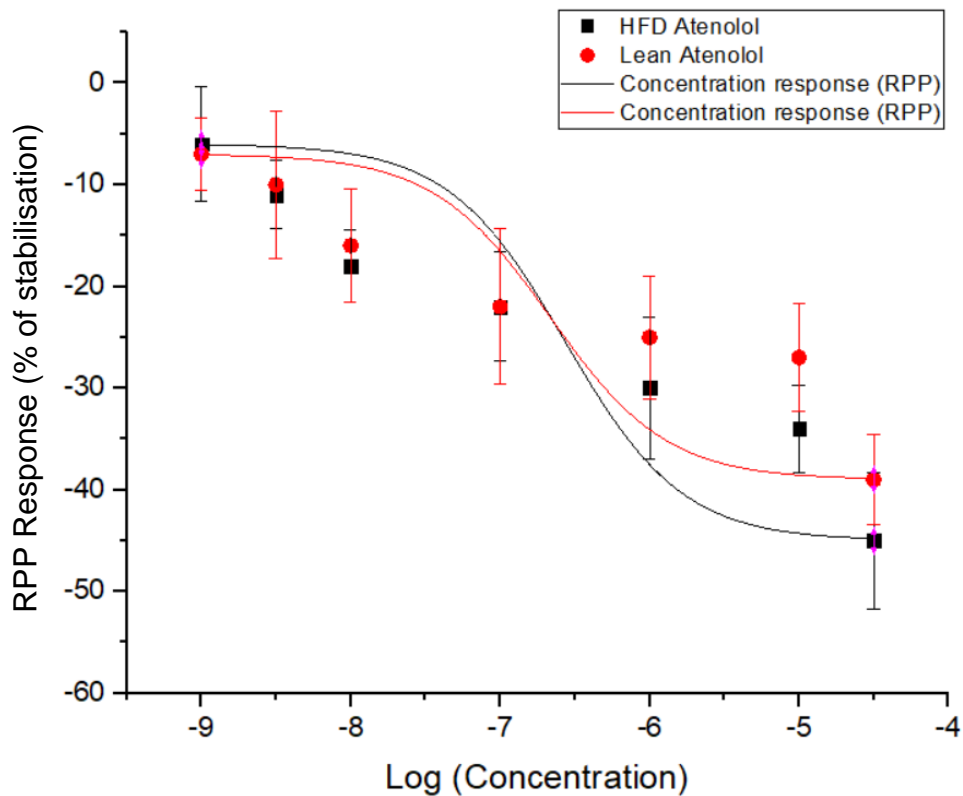


**Figure 7.3.1.4 – RPP for the 18-month atenolol-treated lean and HFD models (n = 4 for both).** Hearts were allowed a 20-minute stabilisation period followed by increasing concentrations of each compound: 1 nM = 20-40 mins; 3 nM = 40-60 mins; 10 nM = 60-80 mins; 100 nM = 80-100 mins; 1  $\mu$ M = 100-120 mins; 10  $\mu$ M = 120-140 mins and 30  $\mu$ M = 140-160 mins.

### ***Itraconazole (6-month data)***

The LVDP (figure 7.3.1.5) for the itraconazole-treated hearts showed an exacerbated negative inotropic effect of the drug upon the HFD model, with a significant decrease between the 1nM concentration ( $+12\% \pm 5.2$  (SEM),  $p < 0.05$ ) and the 100nM concentration ( $-15\% \pm 4.1$  (SEM),  $p < 0.05$ ), before equalising with the lean model.

As for the HR (figure 7.3.1.6), the two models were even up until the last two concentrations ( $-14\%$  and  $-29\% \pm 6.0$  and  $8.2$  (SEM), respectively,  $p < 0.01$ ), where the HFD model displayed a significant increase, when compared to the lean model.

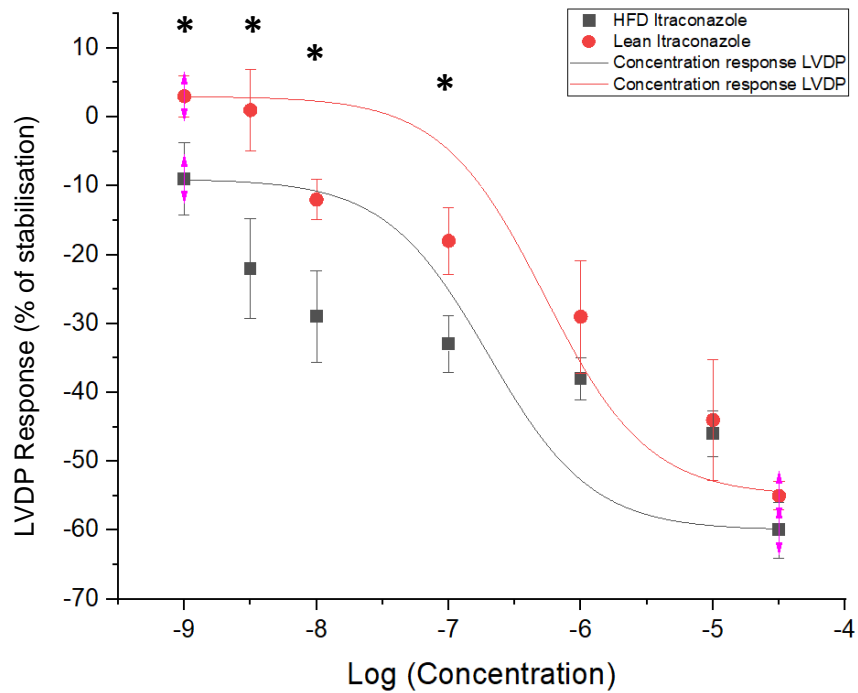


**Figure 7.3.1.5 – LVDP for the 6-month itraconazole-treated lean and HFD models (n = 4 for both).** Hearts were allowed a 20-minute stabilisation period followed by increasing concentrations of each compound: 1 nM = 20-40 mins; 3 nM = 40-60 mins; 10 nM = 60-80 mins; 100 nM = 80-100 mins; 1 µM = 100-120 mins; 10 µM = 120-140 mins and 30 µM = 140-160 mins. Measurements for LVDP when treated with Itraconazole are displayed above (\* =  $p < 0.05$ , in relation to the lean control).

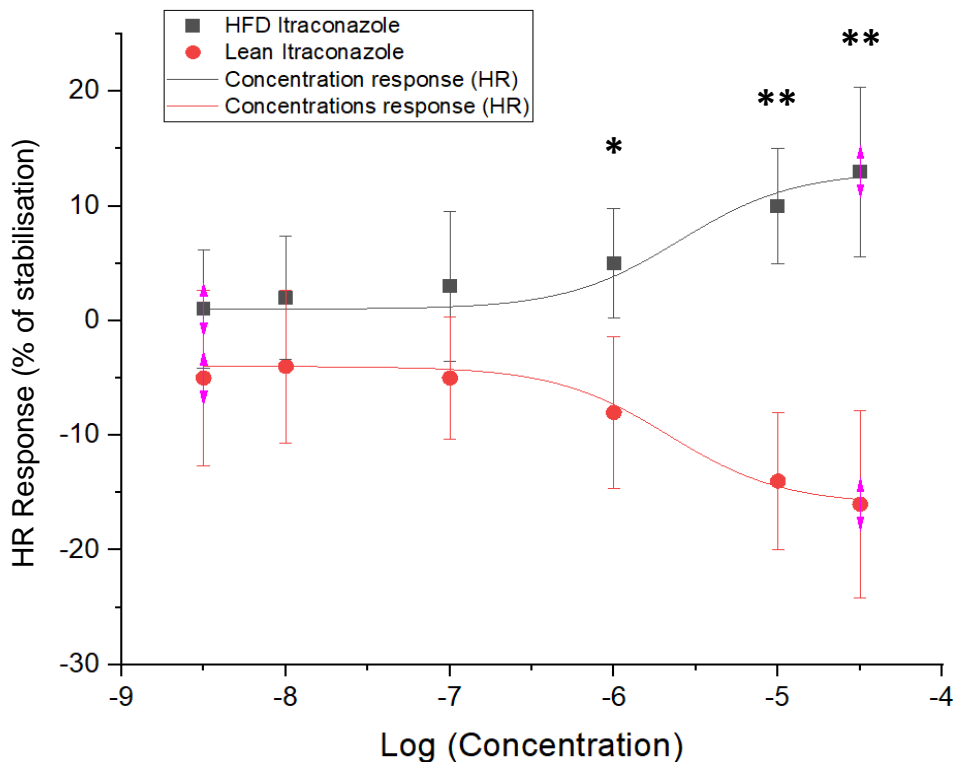


**Figure 7.3.1.6 – HR for the 6-month itraconazole-treated lean and HFD models (n = 4 for both).** Hearts were allowed a 20-minute stabilisation period followed by increasing concentrations of each compound: 1 nM = 20-40 mins; 3 nM = 40-60 mins; 10 nM = 60-80 mins; 100 nM = 80-100 mins; 1 µM = 100-120 mins; 10 µM = 120-140 mins and 30 µM = 140-160 mins. Measurements for HR when treated with Itraconazole are displayed above (\* =  $p < 0.05$ ; \*\* =  $p < 0.01$ ; in relation to the lean control).

The ventricular pressure rise (figure 7.3.1.7) differences were immediate for the hearts treated with Itraconazole. The compound seemed to have an exacerbated negative effect on the HFD models when compared to the lean models, starting at the 1nM concentration ( $-8\% \pm 7.2$  (SEM),  $p < 0.05$ ) until the  $1\mu\text{M}$  concentration ( $-21\% \pm 9.6$  (SEM),  $p < 0.05$ ). The last two concentrations showed a similar effect in both models.

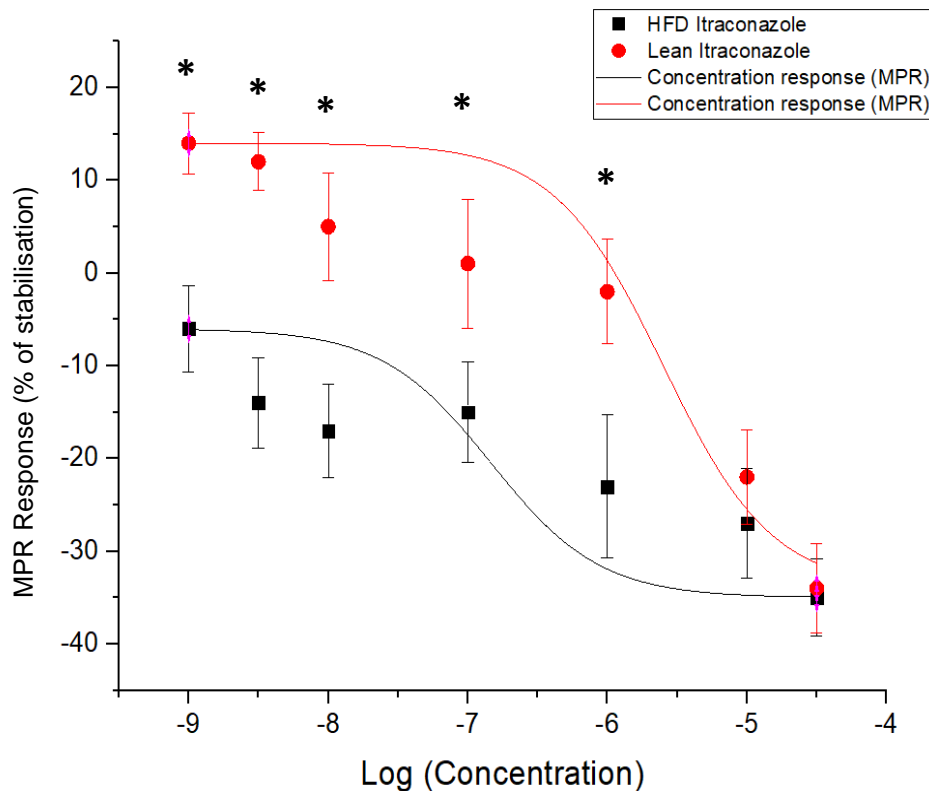


**Figure 7.3.1.7 – +dP/dTmax for the 6-month itraconazole-treated lean and HFD models (n = 4 for both).** Hearts were allowed a 20-minute stabilisation period followed by increasing concentrations of each compound: 1 nM = 20-40 mins; 3 nM = 40-60 mins; 10 nM = 60-80 mins; 100 nM = 80-100 mins; 1  $\mu\text{M}$  = 100-120 mins; 10  $\mu\text{M}$  = 120-140 mins and 30  $\mu\text{M}$  = 140-160 mins. Measurements for +dP/dTmax when treated with Itraconazole are displayed above (\* =  $p < 0.05$ , in relation to the lean control).

As for the MPD (figure 7.3.1.8), we observed a significant decrease at the 3nM ( $-8\% \pm 6.3$  (SEM),  $p < 0.05$ ) and 10nM ( $-13\% \pm 7.0$  (SEM),  $p < 0.05$ ) concentrations, when compared to the lean model.

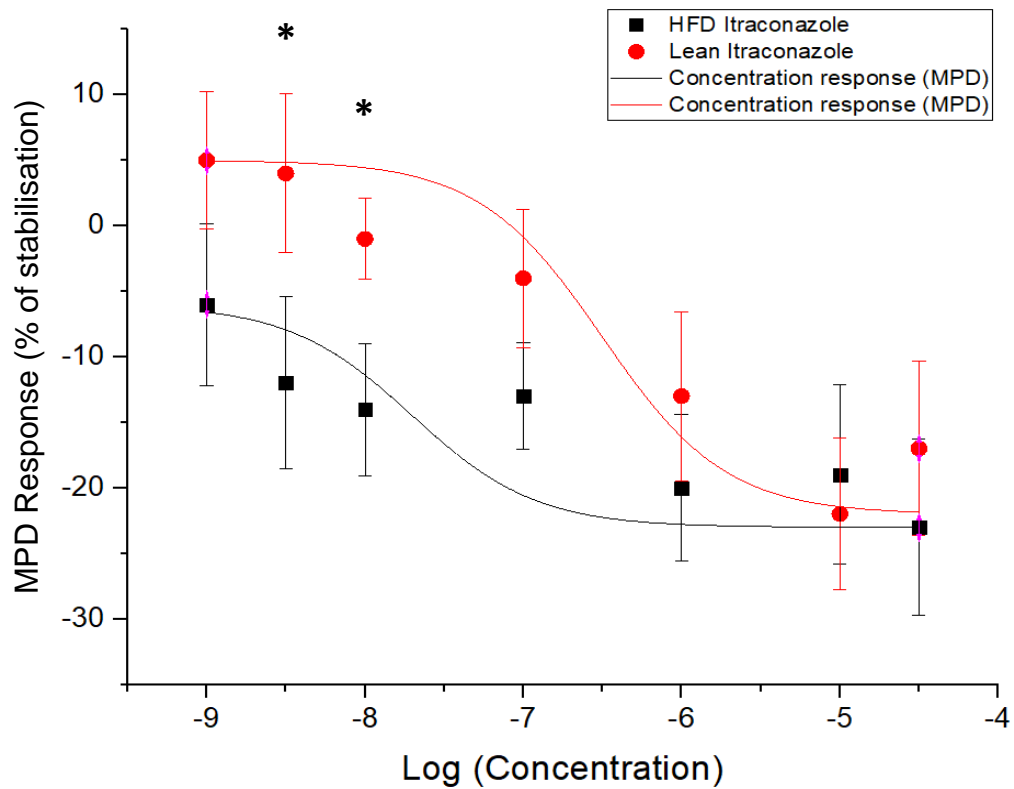


**Figure 7.3.1.8 –  $-dP/dT_{max}$  for the 6-month itraconazole-treated lean and HFD models (n = 4 for both).** Hearts were allowed a 20-minute stabilisation period followed by increasing concentrations of each compound: 1 nM = 20-40 mins; 3 nM = 40-60 mins; 10 nM = 60-80 mins; 100 nM = 80-100 mins; 1  $\mu$ M = 100-120 mins; 10  $\mu$ M = 120-140 mins and 30  $\mu$ M = 140-160 mins. Measurements for  $-dP/dT_{max}$  when treated with Itraconazole are displayed above (\* = p < 0.05, in relation to the lean control).

The RPP (figure 7.3.1.9) showed a significant exacerbation of the effect of the drug for the 3, 10 and 100 nM (-18, -15 and -13%  $\pm$  7.2, 5.5 and 7.6 (SEM), respectively, p<0.05).

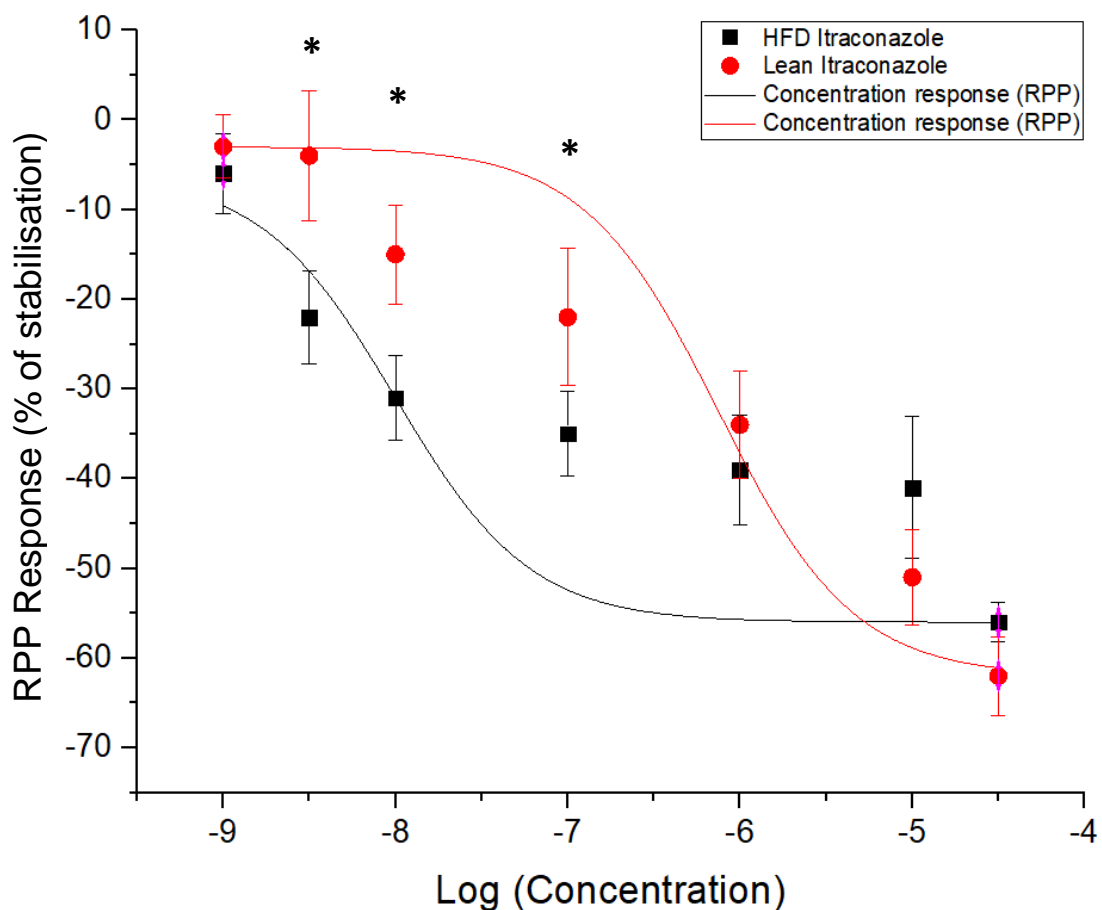


**Figure 7.3.1.9 – Rate Pressure Product for the 6-month itraconazole-treated lean and HFD models (n = 4 for both).** Hearts were allowed a 20-minute stabilisation period followed by increasing concentrations of each compound: 1 nM = 20-40 mins; 3 nM = 40-60 mins; 10 nM = 60-80 mins; 100 nM = 80-100 mins; 1 μM = 100-120 mins; 10 μM = 120-140 mins and 30 μM = 140-160 mins. Measurements for RPP when treated with Itraconazole are displayed above (\* = p < 0.05, in relation to the lean control).

### ***Itraconazole (18-month data)***

The LVDP (figure 7.3.1.10) showed no significance between the two models but did show the expected negative inotropic effect of the drug.

The HR (figure 7.3.1.11), on the other hand, showed a significant decrease for the HFD model, when compared to the lean model, across all concentrations, starting with a significant decrease at the 1nM concentration ( $-15\% \pm 6.2$  (SEM),  $p < 0.05$ ). This decrease was then increased at the 100nM concentration ( $-23\% \pm 6.5$  (SEM),  $p < 0.05$ ), before reaching its maximum difference at the 30μM concentration ( $-47\% \pm 7.4$  (SEM),  $p < 0.001$ ).

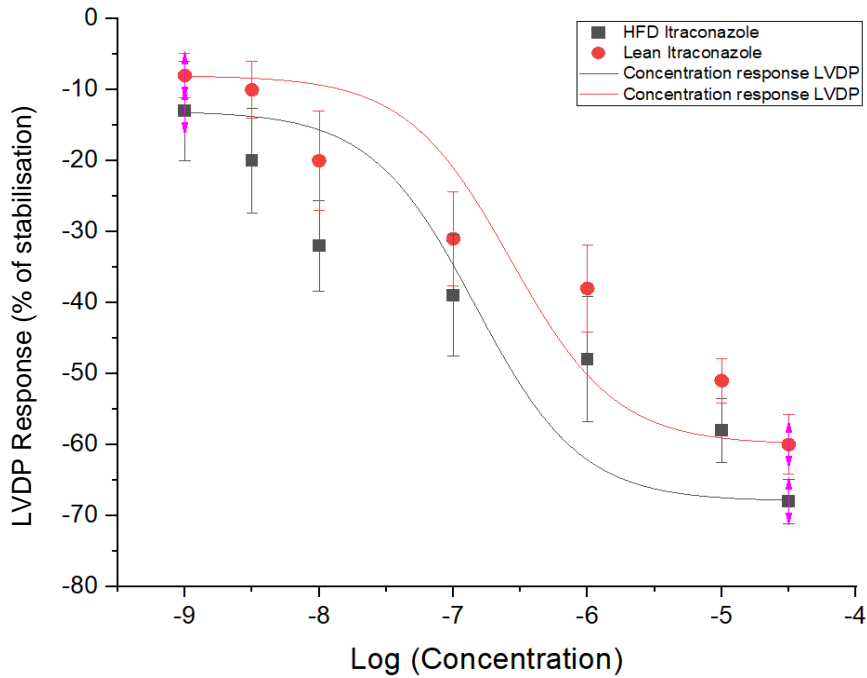


**Figure 7.3.1.10 –LVDP for the 18-month itraconazole-treated lean and HFD models (n = 4 for both).** Hearts were allowed a 20-minute stabilisation period followed by increasing concentrations of each compound: 1 nM = 20-40 mins; 3 nM = 40-60 mins; 10 nM = 60-80 mins; 100 nM = 80-100 mins; 1 µM = 100-120 mins; 10 µM = 120-140 mins and 30 µM = 140-160 mins.

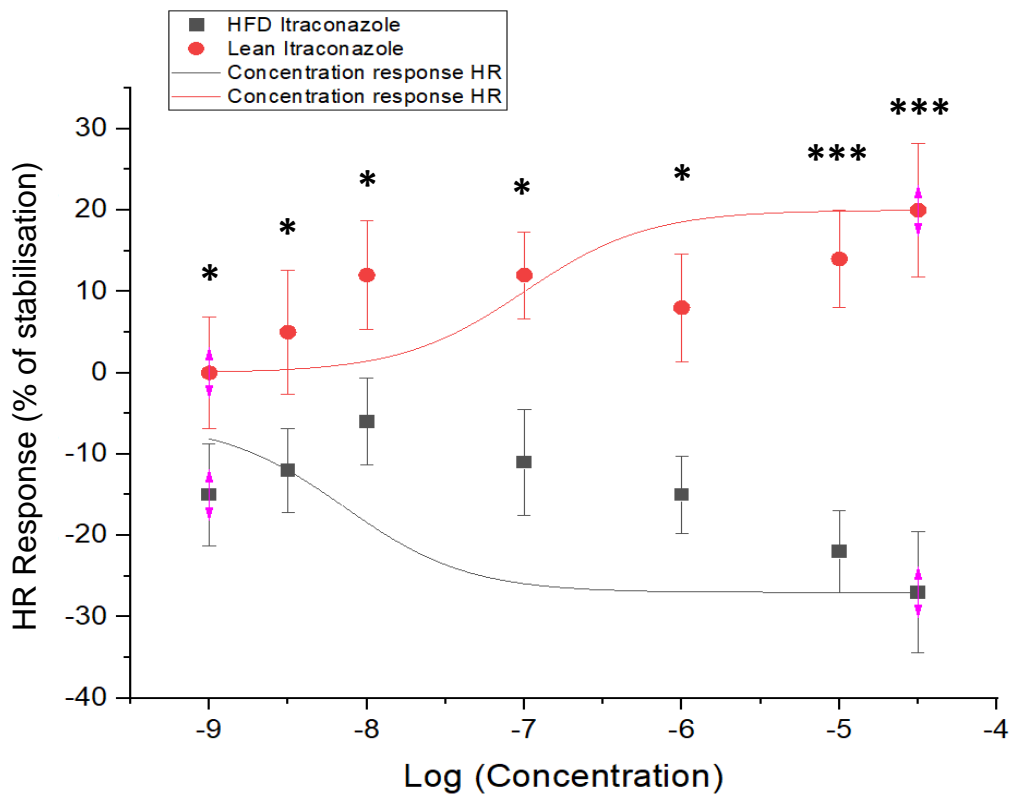


**Figure 7.3.1.11 – HR for the 18-month itraconazole-treated lean and HFD models (n = 4 for both).** Hearts were allowed a 20-minute stabilisation period followed by increasing concentrations of each compound: 1 nM = 20-40 mins; 3 nM = 40-60 mins; 10 nM = 60-80 mins; 100 nM = 80-100 mins; 1 µM = 100-120 mins; 10 µM = 120-140 mins and 30 µM = 140-160 mins. Measurements for HR when treated with Itraconazole are displayed above (\* = p < 0.05 and \*\*\* = p < 0.001, in relation to the lean control).

The ventricular pressure rise (A) and drop (B) showed very similar patterns throughout the protocol (figure 7.3.1.12). Itraconazole was shown to have a clear exacerbation of the negative inotropic effect on the HFD models, as shown by its effect on the MPR starting at the 10nM concentration ( $-10\% \pm 8.3$  (SEM),  $p < 0.05$ ), followed by a reduction at the 100nM concentration ( $-14\% \pm 6.7$  (SEM),  $p < 0.05$ ). A peak significant decrease was then recorded at the 1 $\mu$ M concentration ( $-26\% \pm 8.8$  (SEM),  $p < 0.01$ ), which stayed consistent until the end of the protocol. A similar pattern was recorded for the MPD, starting at the 3nM concentration ( $-13\% \pm 7.0$  (SEM),  $p < 0.05$ ) and reaching peak significant decrease at the 30 $\mu$ M concentration ( $-23\% \pm 5.5$  (SEM),  $p < 0.01$ ).

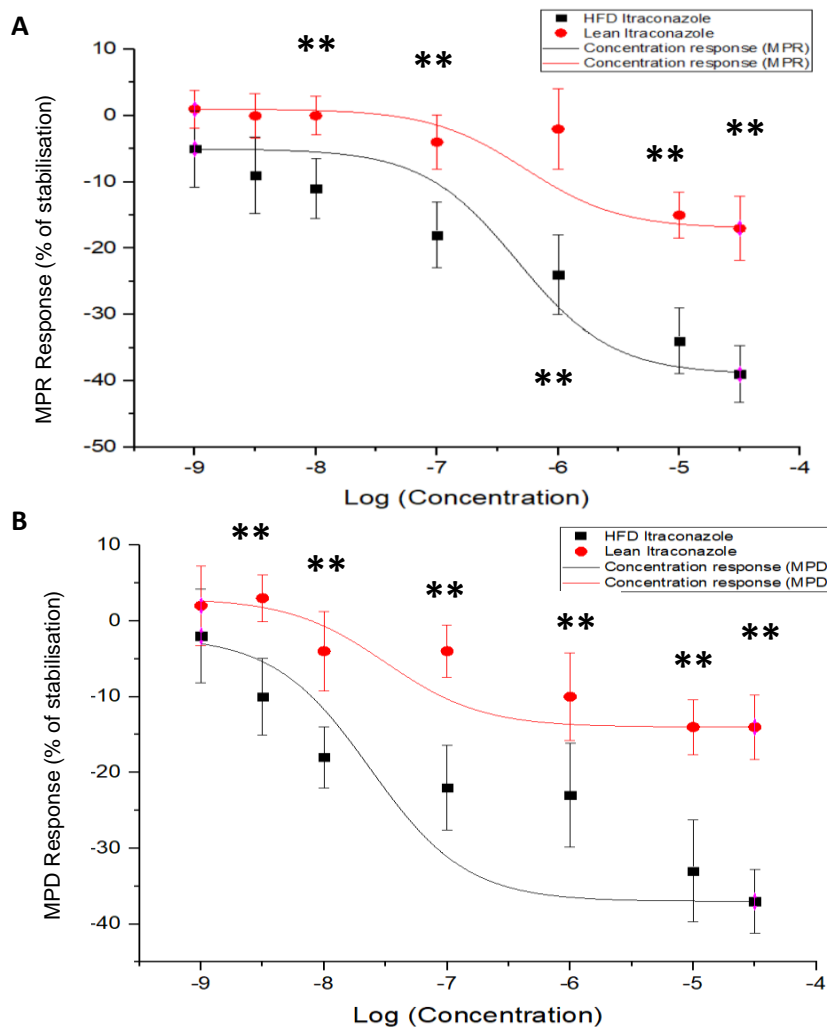


**Figure 7.3.1.12** – + dP/dTmax (A) and – dP/dTmax (B) for the 18-month itraconazole-treated lean and HFD models (n = 4 for both). Hearts were allowed a 20-minute stabilisation period followed by increasing concentrations of each compound: 1 nM = 20-40 mins; 3 nM = 40-60 mins; 10 nM = 60-80 mins; 100 nM = 80-100 mins; 1  $\mu$ M = 100-120 mins; 10  $\mu$ M = 120-140 mins and 30  $\mu$ M = 140-160 mins. Measurements for + and – dP/dTmax when treated with Itraconazole are displayed above (\*\* =  $p < 0.01$ ; in relation to the lean control).

The RPP for Itraconazole showed (figure 7.3.1.13), yet again, a clear exacerbation of the negative inotropic effect of the drug on the heart. From the 1nM concentration to the 30 $\mu$ M, the significant difference is within the range of -18 to -25%  $\pm$  6.7 to 3.8 (SEM), respectively, (p<0.01) in RPP measurements between the models.

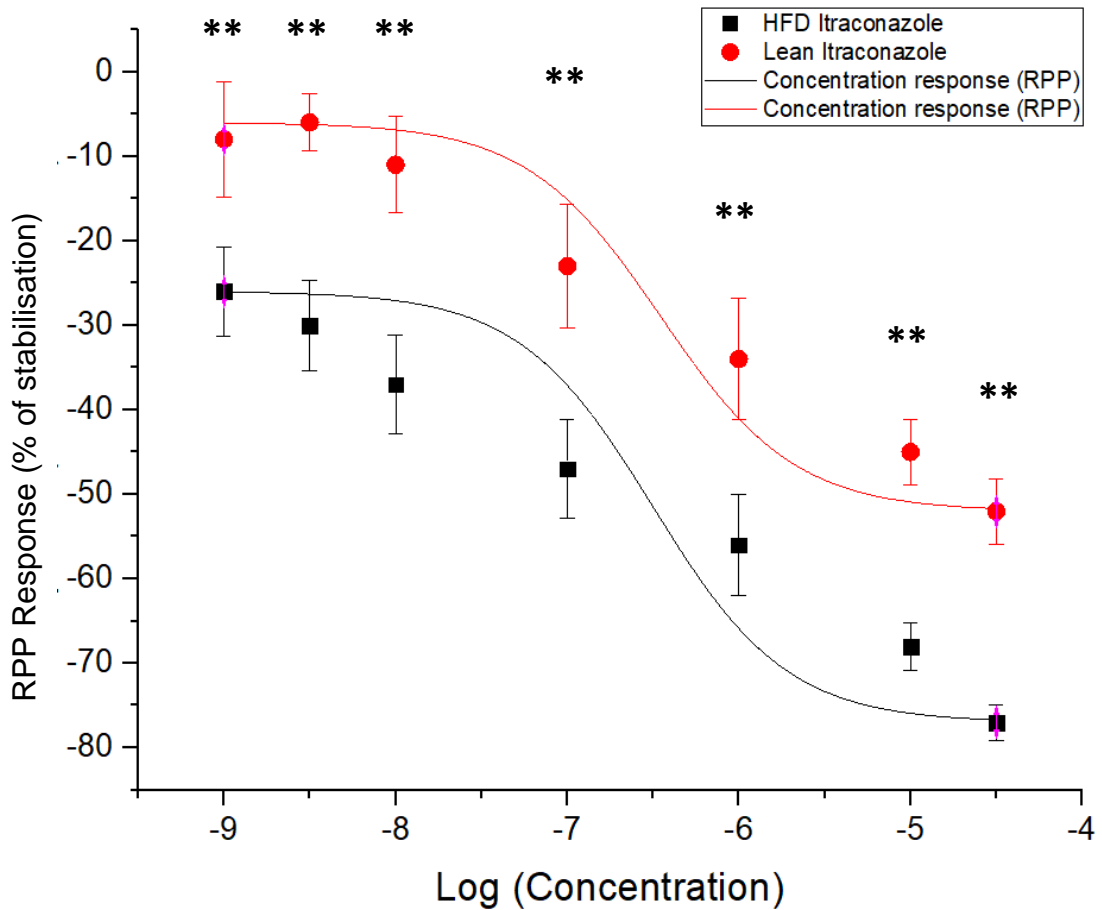


**Figure 7.3.1.13 – Rate Pressure Product for the 18-month itraconazole-treated lean and HFD models (n = 4 for both).** Hearts were allowed a 20-minute stabilisation period followed by increasing concentrations of each compound: 1 nM = 20-40 mins; 3 nM = 40-60 mins; 10 nM = 60-80 mins; 100 nM = 80-100 mins; 1  $\mu$ M = 100-120 mins; 10  $\mu$ M = 120-140 mins and 30  $\mu$ M = 140-160 mins. Measurements for RPP when treated with Itraconazole are displayed above (\*\* = p < 0.01; in relation to the lean control).

### ***Dobutamine (6-month data)***

An initial significant difference was documented on the LVDP when treating the HFD hearts with Dobutamine (figure 7.3.1.14), as we saw a significant decrease in the inotropic effect of the drug, starting at the 1 $\mu$ M concentration (-26%  $\pm$  7.4 (SEM),  $p < 0.001$ ) and persisting up until the 30 $\mu$ M concentration (-10%  $\pm$  9.1 (SEM),  $p < 0.01$ ).

As for the HR (figure 7.3.1.15), we observed a significantly decreased chronotropic effect of Dobutamine on the HFD model, starting at the 10 $\mu$ M concentration (-12%  $\pm$  8.7 (SEM),  $p < 0.01$ ) and lasting until the 30 $\mu$ M concentration (-14%  $\pm$  10.5 (SEM),  $p < 0.05$ ). Both parameters were shown to be significantly decreased in the HFD model, when compared to the lean one.

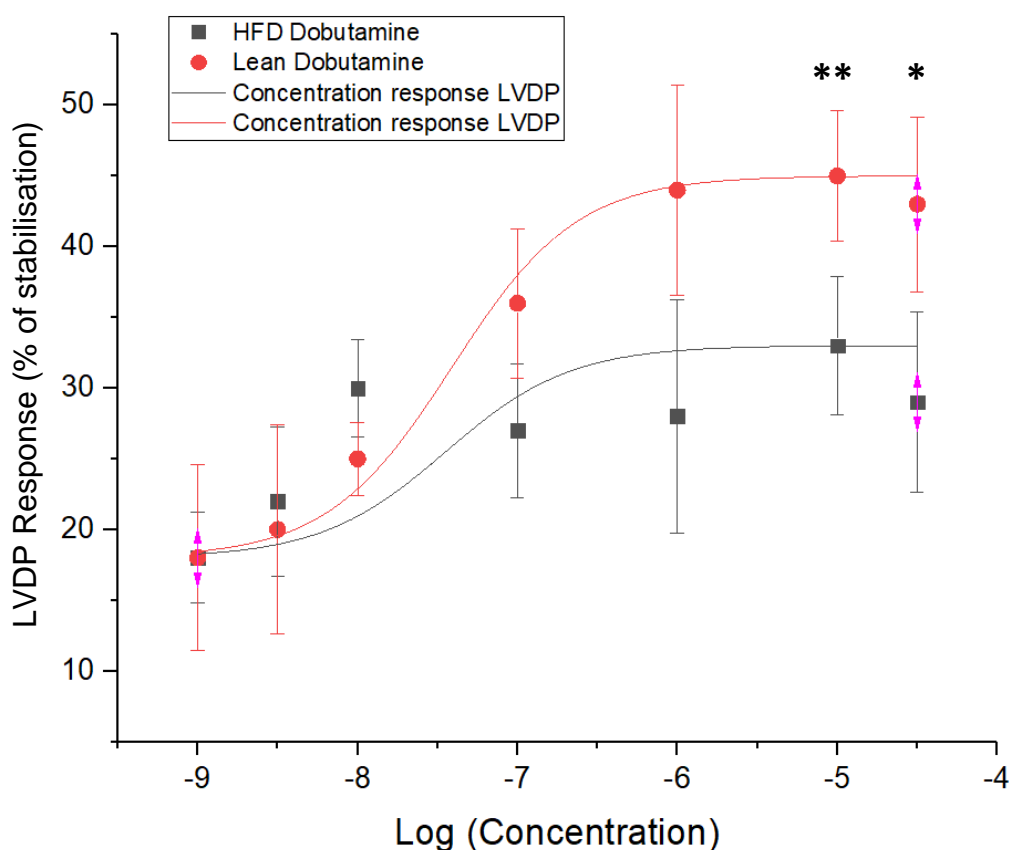


**Figure 7.3.1.14 - LVDP for the 6-month dobutamine-treated lean and HFD models (n = 4 for both).** Hearts were allowed a 20-minute stabilisation period followed by increasing concentrations of each compound: 1 nM = 20-40 mins; 3 nM = 40-60 mins; 10 nM = 60-80 mins; 100 nM = 80-100 mins; 1  $\mu$ M = 100-120 mins; 10  $\mu$ M = 120-140 mins and 30  $\mu$ M = 140-160 mins. Measurements for LVDP when treated with Dobutamine are displayed above (\* =  $p < 0.05$  and \*\* =  $p < 0.01$ ; in relation to the lean control).

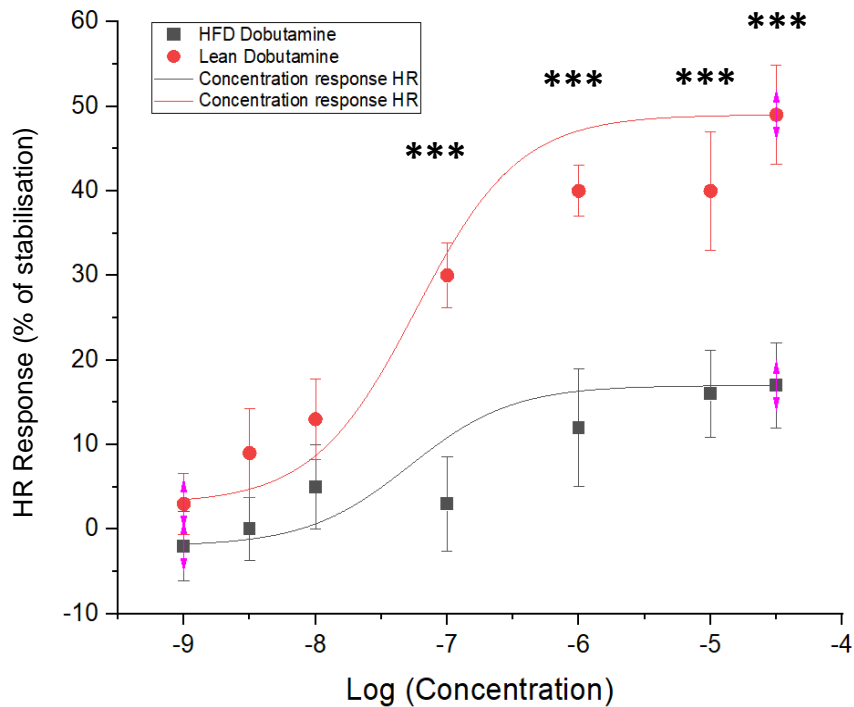


**Figure 7.3.1.15 – HR for the 6-month dobutamine-treated lean and HFD models (n = 4 for both).** Hearts were allowed a 20-minute stabilisation period followed by increasing concentrations of each compound: 1 nM = 20-40 mins; 3 nM = 40-60 mins; 10 nM = 60-80 mins; 100 nM = 80-100 mins; 1  $\mu$ M = 100-120 mins; 10  $\mu$ M = 120-140 mins and 30  $\mu$ M = 140-160 mins. Measurements for HR when treated with Dobutamine are displayed above (\*\*\*) =  $p < 0.001$ ; in relation to the lean control).

An initial significant difference was documented on the MPR (A) when treating the HFD hearts with Dobutamine (figure 7.3.1.16), as they displayed a stronger response to the drug (up to  $+20\% \pm 7.2$  (SEM), in relation to the lean heart, between the 3nM and the 100nM concentrations, ( $p < 0.05$ ), before equalizing at the 30 $\mu$ M concentration. The MPD (B) for the HFD hearts only showed a significant decrease at the 10 $\mu$ M concentration ( $-19\% \pm 8.5$  (SEM),  $p < 0.05$ ).

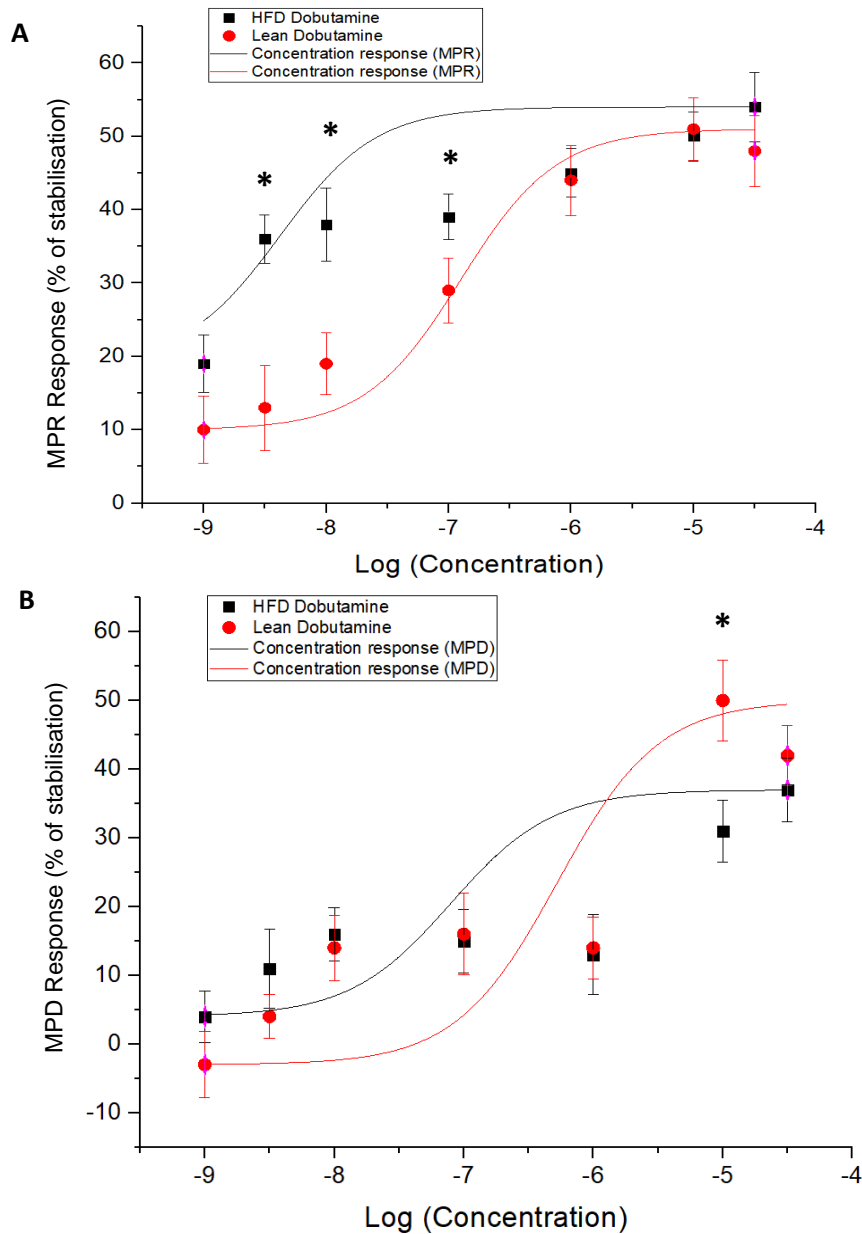


**Figure 7.3.1.16** - + dP/dTmax (A) and -dP/dTmax (B) for the 6-month dobutamine-treated lean and HFD models (n = 4 for both). Hearts were allowed a 20-minute stabilisation period followed by increasing concentrations of each compound: 1 nM = 20-40 mins; 3 nM = 40-60 mins; 10 nM = 60-80 mins; 100 nM = 80-100 mins; 1  $\mu$ M = 100-120 mins; 10  $\mu$ M = 120-140 mins and 30  $\mu$ M = 140-160 mins. Measurements for MPR and MPD when treated with Dobutamine are displayed above (\* = p < 0.05; in relation to the lean control).

The major results for this set of data came from the RPP of the hearts treated with Dobutamine (figure 7.3.1.17). The initial response showed a significant decrease at the 100nM concentration ( $-45\% \pm 15.8$  (SEM) for the HFD hearts ( $p < 0.01$ ) that was exacerbated to  $-62\% \pm 8.5$  after the 1 $\mu$ M concentration ( $p < 0.01$ ), when compared to the lean hearts.

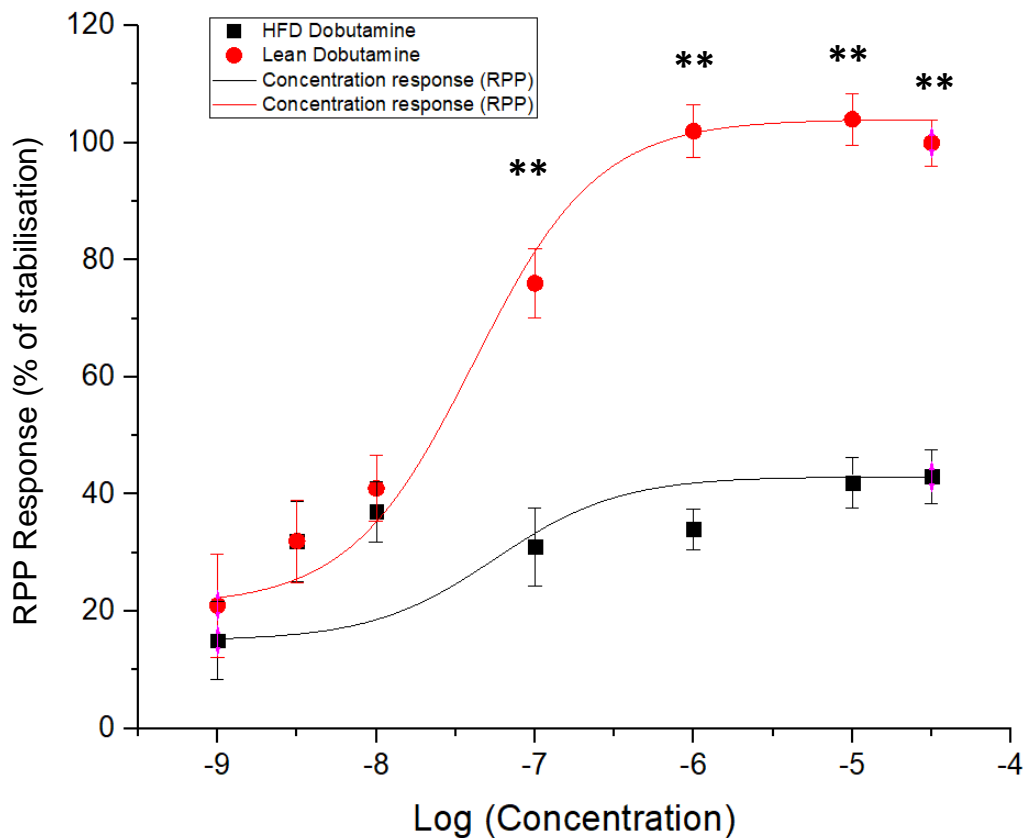


**Figure 7.3.1.17 – RPP for the 6-month dobutamine-treated lean and HFD models (n = 4 for both).** Hearts were allowed a 20-minute stabilisation period followed by increasing concentrations of each compound: 1 nM = 20-40 mins; 3 nM = 40-60 mins; 10 nM = 60-80 mins; 100 nM = 80-100 mins; 1  $\mu$ M = 100-120 mins; 10  $\mu$ M = 120-140 mins and 30  $\mu$ M = 140-160 mins. Measurements for RPP when treated with Dobutamine are displayed above (\*\* = p < 0.01; in relation to the lean control).

### ***Dobutamine (18-month data)***

The LVDP for the 18-month dobutamine treated hearts is shown in figure 7.3.1.18. Unlike the LVDP for the 6-month groups (figure 7.3.1.14), the 18-month lean group showed an initial response to the drug that decreased in effectiveness as we administered higher concentrations of the drug. On the other hand, the HFD animal group showed a significantly impaired drug effect, starting at the 1nM concentration ( $-34\% \pm 7.6$  (SEM),  $p < 0.01$ ) and lasting until the 1 $\mu$ M concentration ( $-19\% \pm 8.6$  (SEM),  $p < 0.05$ ), before equalizing its effect to the lean group. The patterns displayed seem to mirror each other for the duration of the drug administration.

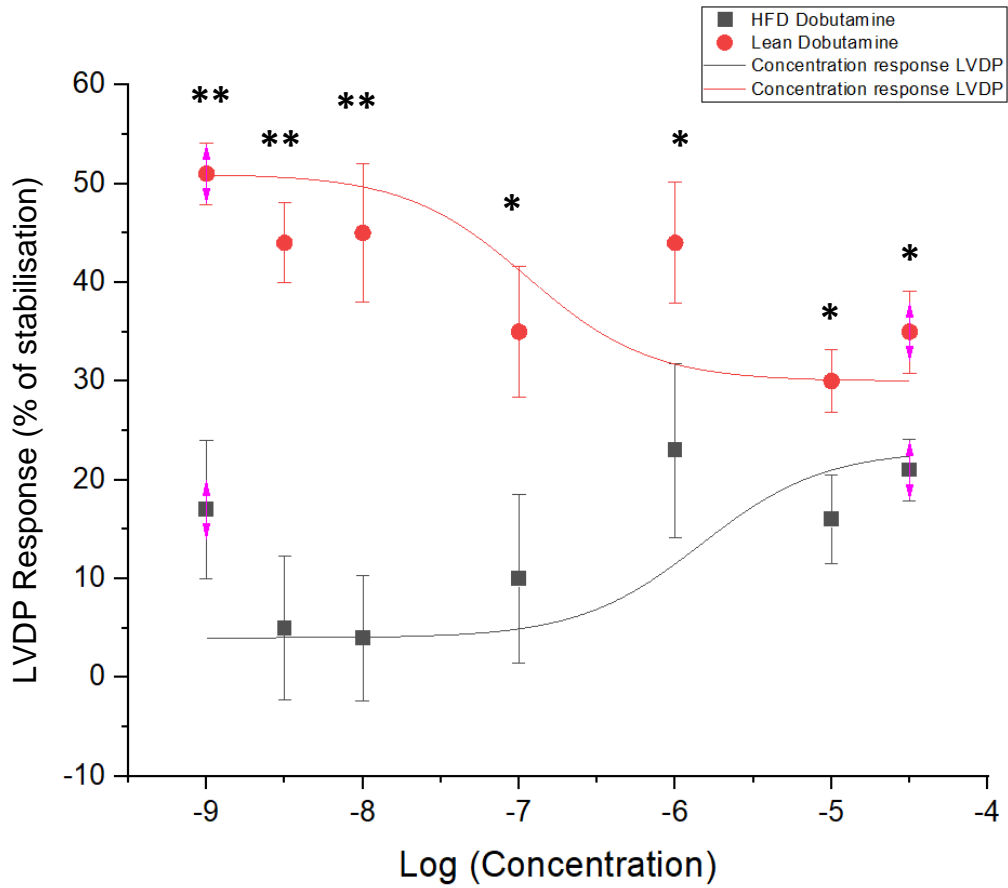


**Figure 7.3.1.18 – LVDP for the 18-month dobutamine-treated lean and HFD models (n = 4 for both).** Hearts were allowed a 20-minute stabilisation period followed by increasing concentrations of each compound: 1 nM = 20-40 mins; 3 nM = 40-60 mins; 10 nM = 60-80 mins; 100 nM = 80-100 mins; 1 μM = 100-120 mins; 10 μM = 120-140 mins and 30 μM = 140-160 mins. Measurements for LVDP when treated with Dobutamine are displayed above (\* = p < 0.05 and \*\* = p < 0.01; in relation to the lean control).

No significance was found for the HR (figure 7.3.1.19) when comparing between the 18-month HFD and lean dobutamine treated hearts.

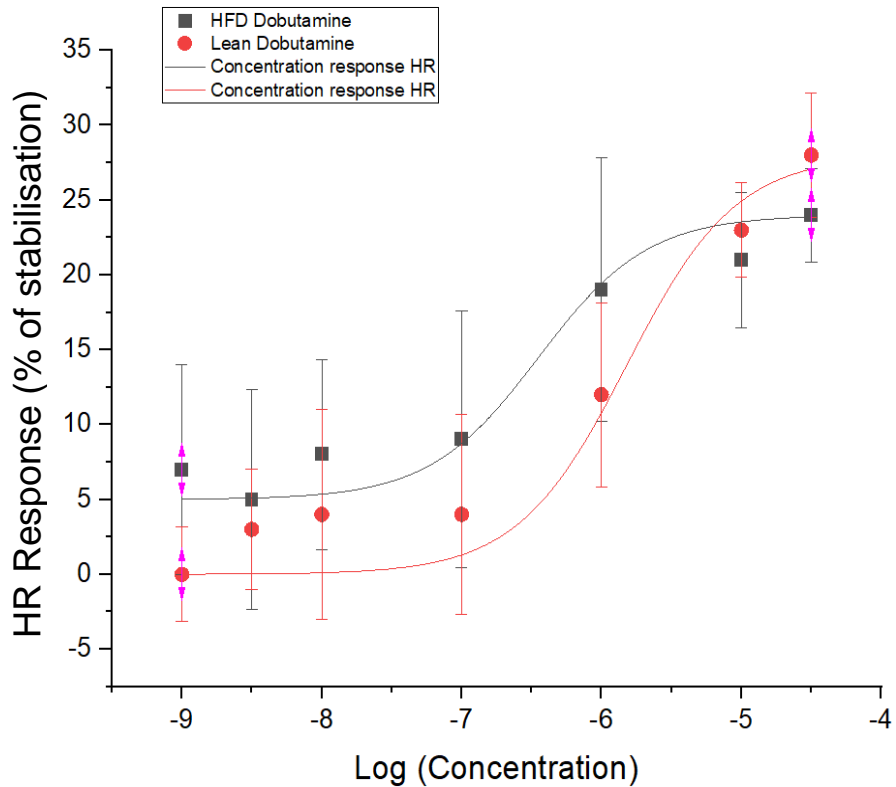


**Figure 7.3.1.19 – HR for the 18-month dobutamine-treated lean and HFD models (n = 4 for both).** Hearts were allowed a 20-minute stabilisation period followed by increasing concentrations of each compound: 1 nM = 20-40 mins; 3 nM = 40-60 mins; 10 nM = 60-80 mins; 100 nM = 80-100 mins; 1  $\mu$ M = 100-120 mins; 10  $\mu$ M = 120-140 mins and 30  $\mu$ M = 140-160 mins.

The ventricular pressure rise (A) and drop (B) for the 18-month data (figure 7.3.1.20) showed no significance at any point of the experimental protocol, with both models mimicking each other.

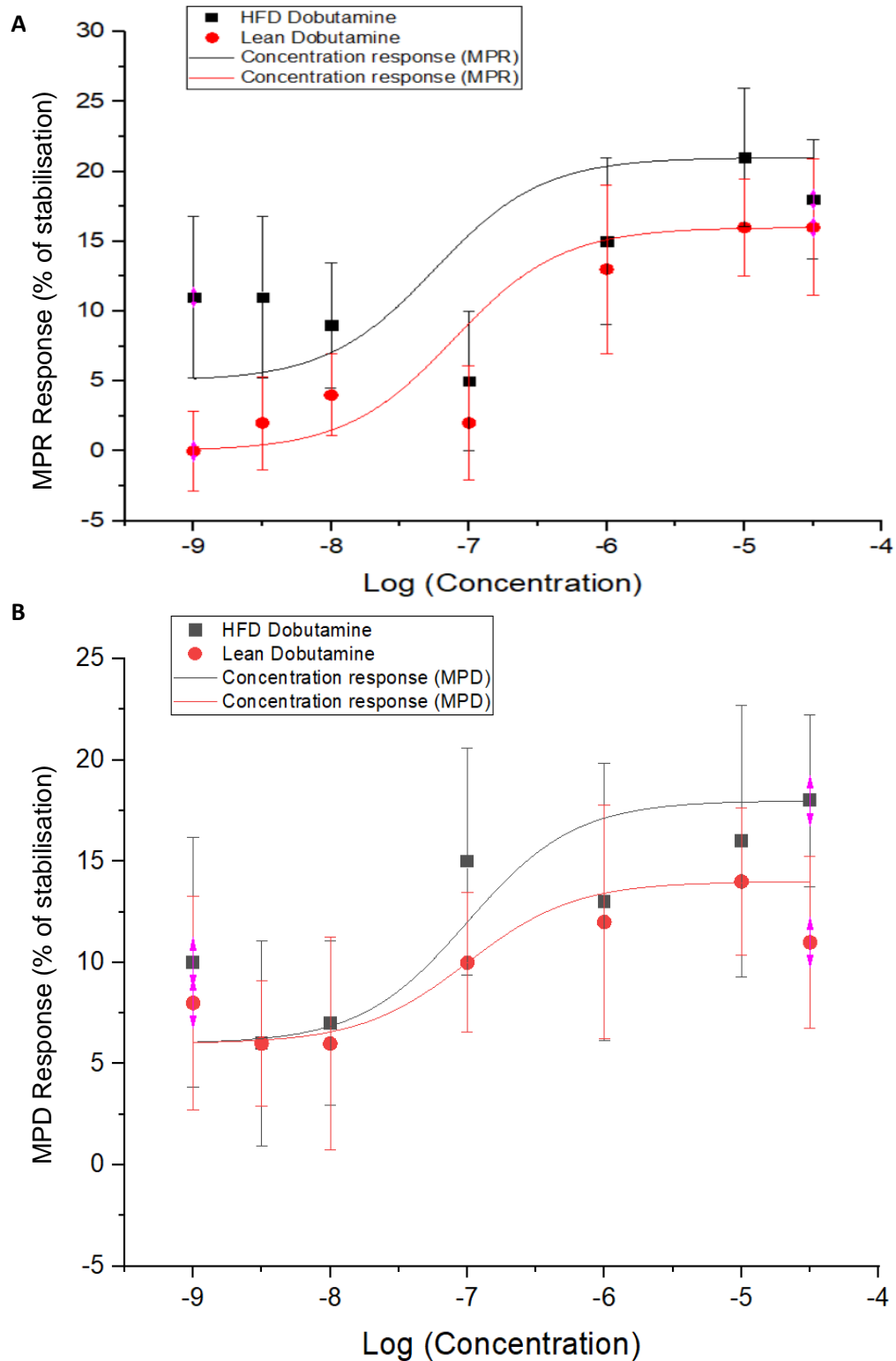


**Figure 7.3.1.20** – + dP/dTmax (A) and – dP/dTmax (B) for the 18-month dobutamine-treated lean and HFD models (n = 4 for both). Hearts were allowed a 20-minute stabilisation period followed by increasing concentrations of each compound: 1 nM = 20-40 mins; 3 nM = 40-60 mins; 10 nM = 60-80 mins; 100 nM = 80-100 mins; 1  $\mu$ M = 100-120 mins; 10  $\mu$ M = 120-140 mins and 30  $\mu$ M = 140-160 mins.

The RPP for Dobutamine (figure 7.3.1.21) showed an initial impairment in drug effect on the HFD heart, when compared to the lean heart, at the 1nM concentration ( $-26\% \pm 12.6$  (SEM),  $p < 0.05$ ). A further decrease in drug effect is then seen again at the  $1\mu\text{M}$  ( $-16\% \pm 13.9$  (SEM),  $p < 0.05$ ), with an exacerbation of this effect seen at the  $30\mu\text{M}$  concentration ( $-21\% \pm 6.4$  (SEM),  $p < 0.05$ ). The pattern for the RPP showed a decreased drug effectiveness throughout the protocol, for the HFD model.

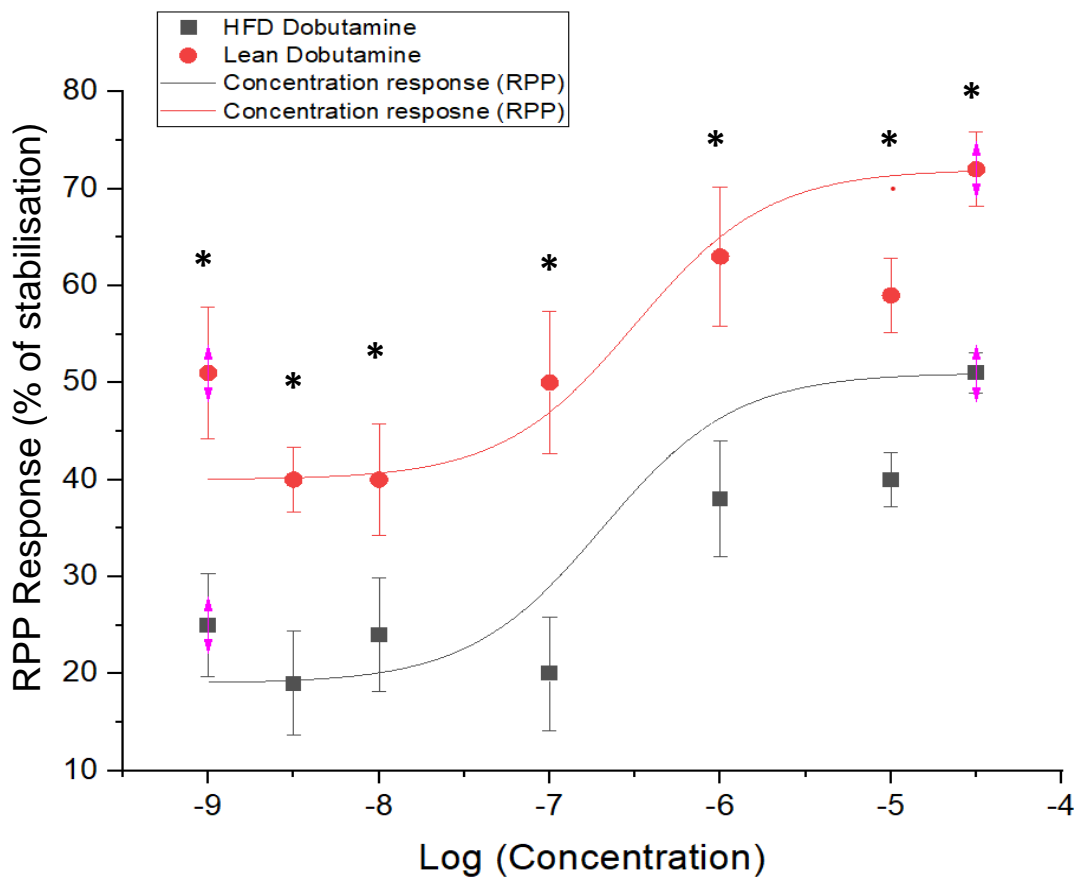


**Figure 7.3.1.21 – RPP for the 18-month dobutamine-treated lean and HFD models (n = 4 for both).** Hearts were allowed a 20-minute stabilisation period followed by increasing concentrations of each compound: 1 nM = 20-40 mins; 3 nM = 40-60 mins; 10 nM = 60-80 mins; 100 nM = 80-100 mins; 1  $\mu\text{M}$  = 100-120 mins; 10  $\mu\text{M}$  = 120-140 mins and 30  $\mu\text{M}$  = 140-160 mins. Measurements for RPP when treated with Dobutamine are displayed above (\* =  $p < 0.05$ ; in relation to the lean control).

### *Atenolol (6 vs 18-month HFD data)*

Figures 7.3.1.22 to 7.3.1.24 show the comparison for MPR, MPD and RPP on the 6- and 18-month HFD models treated with Atenolol. As seen by the graphs, no significance was recorded when comparing between the two models.

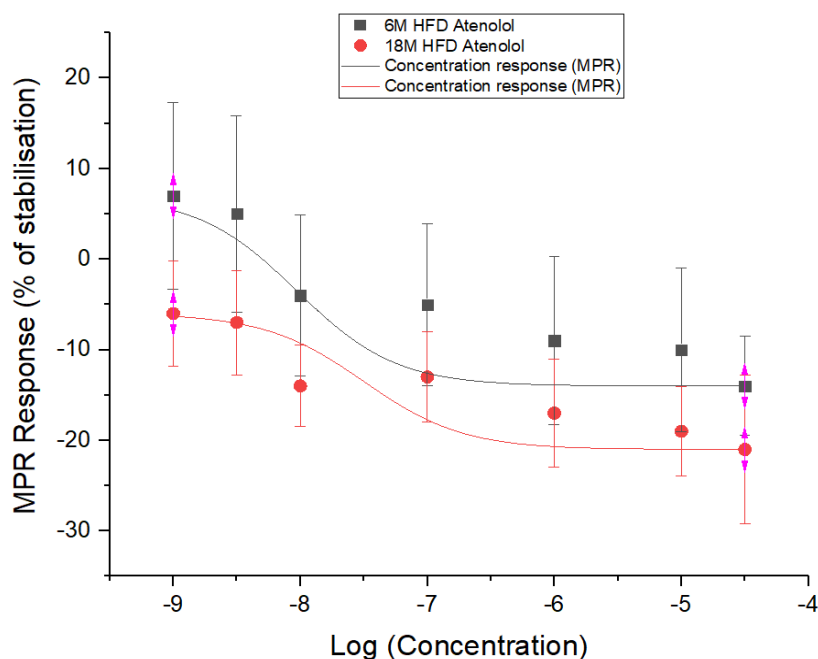


**Figure 7.3.1.22 – MPR for the 6- and 18-month HFD hearts treated with Atenolol (n = 4 for both).** Hearts were allowed a 20-minute stabilisation period followed by increasing concentrations of each compound: 1 nM = 20-40 mins; 3 nM = 40-60 mins; 10 nM = 60-80 mins; 100 nM = 80-100 mins; 1  $\mu$ M = 100-120 mins; 10  $\mu$ M = 120-140 mins and 30  $\mu$ M = 140-160 mins.

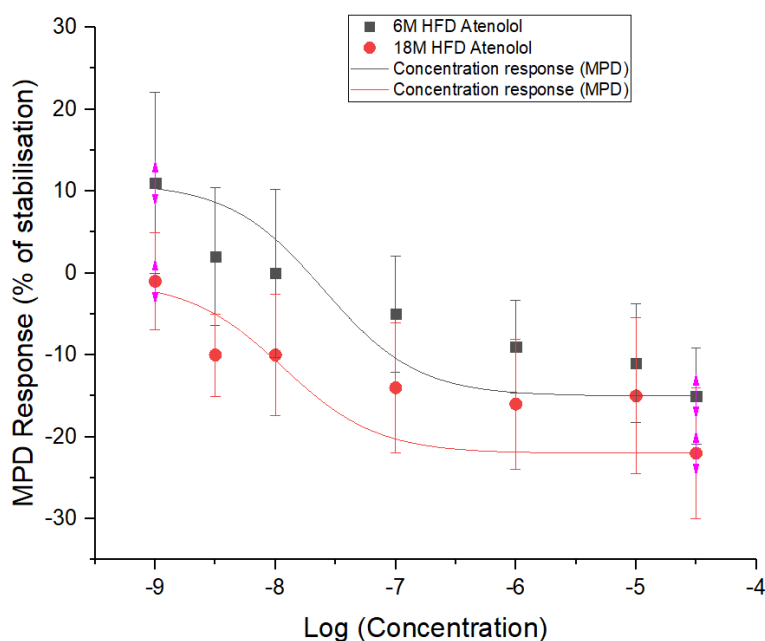


**Figure 7.3.1.23 – MPD for the 6- and 18-month HFD hearts treated with Atenolol (n = 4 for both).** Hearts were allowed a 20-minute stabilisation period followed by increasing concentrations of each compound: 1 nM = 20-40 mins; 3 nM = 40-60 mins; 10 nM = 60-80 mins; 100 nM = 80-100 mins; 1  $\mu$ M = 100-120 mins; 10  $\mu$ M = 120-140 mins and 30  $\mu$ M = 140-160 mins.

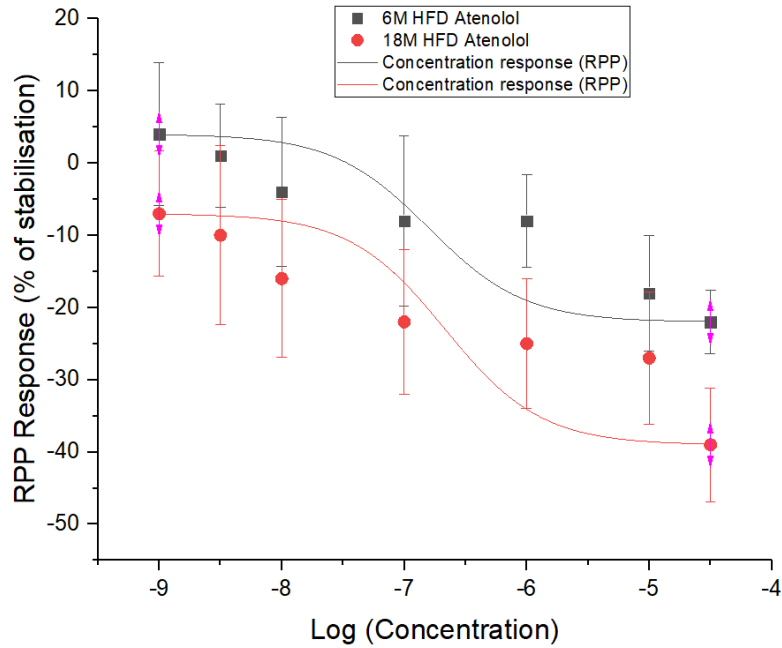


**Figure 7.3.1.24 – RPP for the 6- and 18-month HFD hearts treated with Atenolol (n = 4 for both).** Hearts were allowed a 20-minute stabilisation period followed by increasing concentrations of each compound: 1 nM = 20-40 mins; 3 nM = 40-60 mins; 10 nM = 60-80 mins; 100 nM = 80-100 mins; 1  $\mu$ M = 100-120 mins; 10  $\mu$ M = 120-140 mins and 30  $\mu$ M = 140-160 mins.

### ***Itraconazole (6 vs 18-month HFD data)***

Figures 7.3.1.25 to 7.3.1.27 show the comparison for MPR, MPD and RPP on the 6- and 18-month HFD models treated with Itraconazole. No significance was recorded on the MPR, as seen in figure 7.3.1.25.

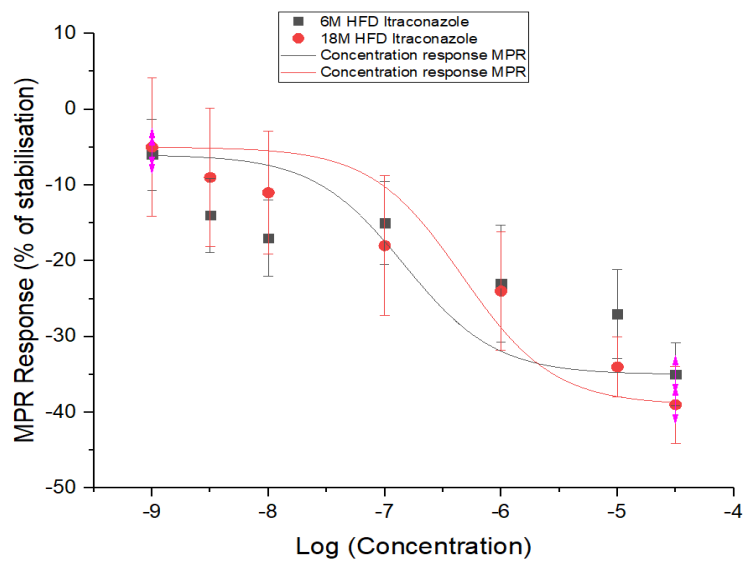


**Figure 7.3.1.25 – MPR for the 6- and 18-month HFD hearts treated with Itraconazole (n = 4 for both).** Hearts were allowed a 20-minute stabilisation period followed by increasing concentrations of each compound: 1 nM = 20-40 mins; 3 nM = 40-60 mins; 10 nM = 60-80 mins; 100 nM = 80-100 mins; 1  $\mu$ M = 100-120 mins; 10  $\mu$ M = 120-140 mins and 30  $\mu$ M = 140-160 mins.

As seen by figure 7.3.1.26, significance was recorded for the last two concentrations of itraconazole on the 18-month models, with peak difference being seen for the 30 $\mu$ M concentration (-14%  $\pm$  3.7 (SEM), p<0.05).

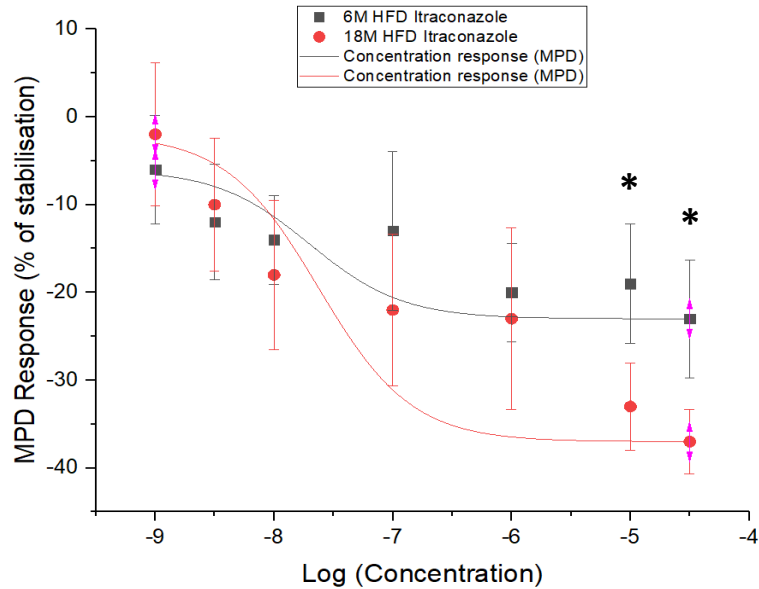


**Figure 7.3.1.26 – MPD for the 6- and 18-month HFD hearts treated with Itraconazole (n = 4 for both).** Hearts were allowed a 20-minute stabilisation period followed by increasing concentrations of each compound: 1 nM = 20-40 mins; 3 nM = 40-60 mins; 10 nM = 60-80 mins; 100 nM = 80-100 mins; 1  $\mu$ M = 100-120 mins; 10  $\mu$ M = 120-140 mins and 30  $\mu$ M = 140-160 mins. Measurements for MPD when treated with Itraconazole are displayed above (\* = p < 0.05; in relation to the 6-month HFD heart).

As seen by figure 7.3.1.27, the RPP showed significant changes for the last 3 concentrations, starting at the 1 $\mu$ M concentration (-17%  $\pm$  7.1 (SEM), p<0.05) and with peak significance being seen for the 30 $\mu$ M concentration (-21%  $\pm$  3.8 (SEM), p<0.05).

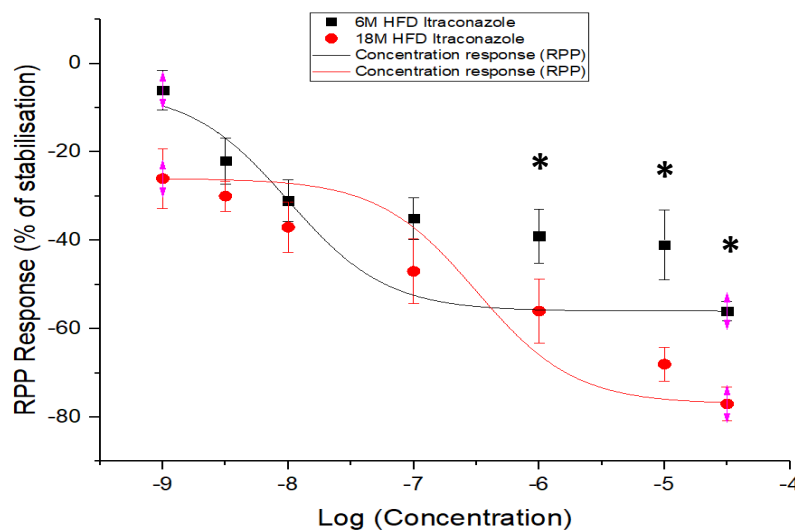


**Figure 7.3.1.27 – RPP for the 6- and 18-month HFD hearts treated with Itraconazole (n = 4 for both).** Hearts were allowed a 20-minute stabilisation period followed by increasing concentrations of each compound: 1 nM = 20-40 mins; 3 nM = 40-60 mins; 10 nM = 60-80 mins; 100 nM = 80-100 mins; 1  $\mu$ M = 100-120 mins; 10  $\mu$ M = 120-140 mins and 30  $\mu$ M = 140-160 mins. Measurements for RPP when treated with Itraconazole are displayed above (\* = p < 0.05; in relation to the 6-month HFD heart).

### ***Dobutamine (6 vs 18-month HFD data)***

Figures 7.3.1.28 to 7.3.1.30 show the comparison for MPR, MPD and RPP on the 6- and 18-month HFD models treated with Dobutamine. As seen by figure 7.3.1.28, the MPR showed significant changes between the two aged models, starting at the 3nM concentration ( $-16\% \pm 5.8$  (SEM),  $p < 0.05$ ) and achieving peak response difference at the 30 $\mu$ M concentration ( $-37\% \pm 9.8$  (SEM),  $p < 0.01$ ).

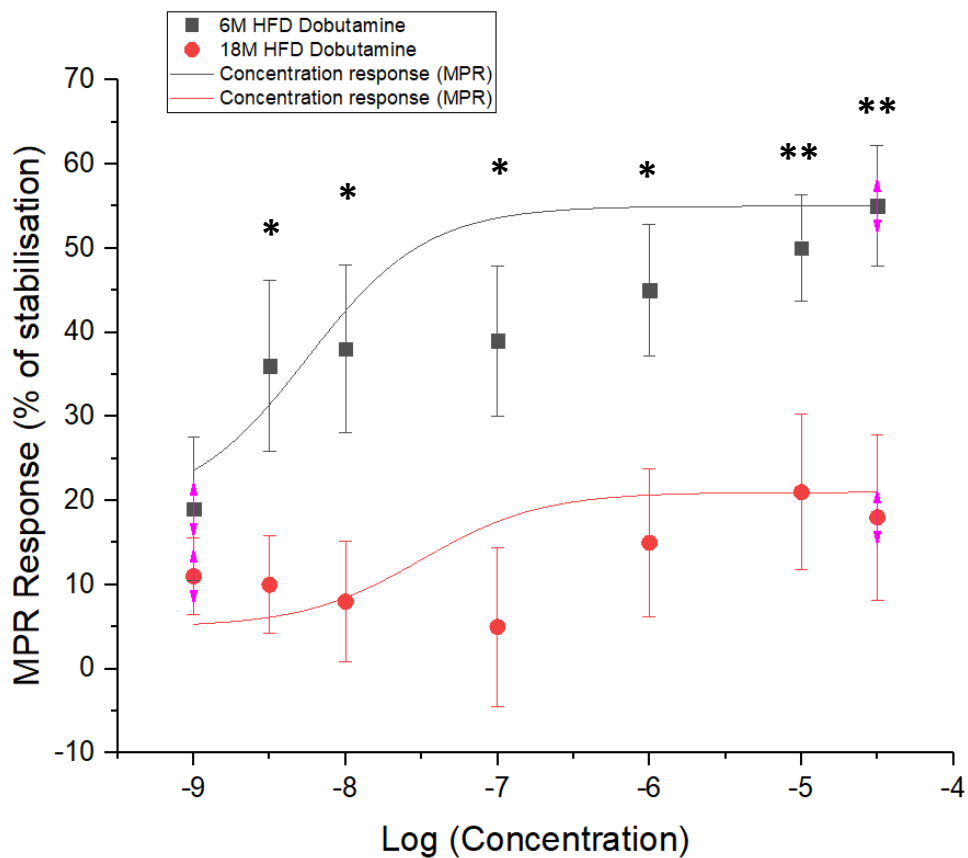


**Figure 7.3.1.28 – MPR for the 6- and 18-month HFD hearts treated with Dobutamine (n = 4 for both).** Hearts were allowed a 20-minute stabilisation period followed by increasing concentrations of each compound: 1 nM = 20-40 mins; 3 nM = 40-60 mins; 10 nM = 60-80 mins; 100 nM = 80-100 mins; 1  $\mu$ M = 100-120 mins; 10  $\mu$ M = 120-140 mins and 30  $\mu$ M = 140-160 mins. Measurements for MPR when treated with Dobutamine are displayed above (\* =  $p < 0.05$  and \*\* =  $p < 0.01$ ; in relation to the 6-month HFD heart).

No significance was recorded when comparing between the 6- and 18-month HFD models for the MPD and RPP, as seen in figures 7.3.1.29 and 7.3.1.30.

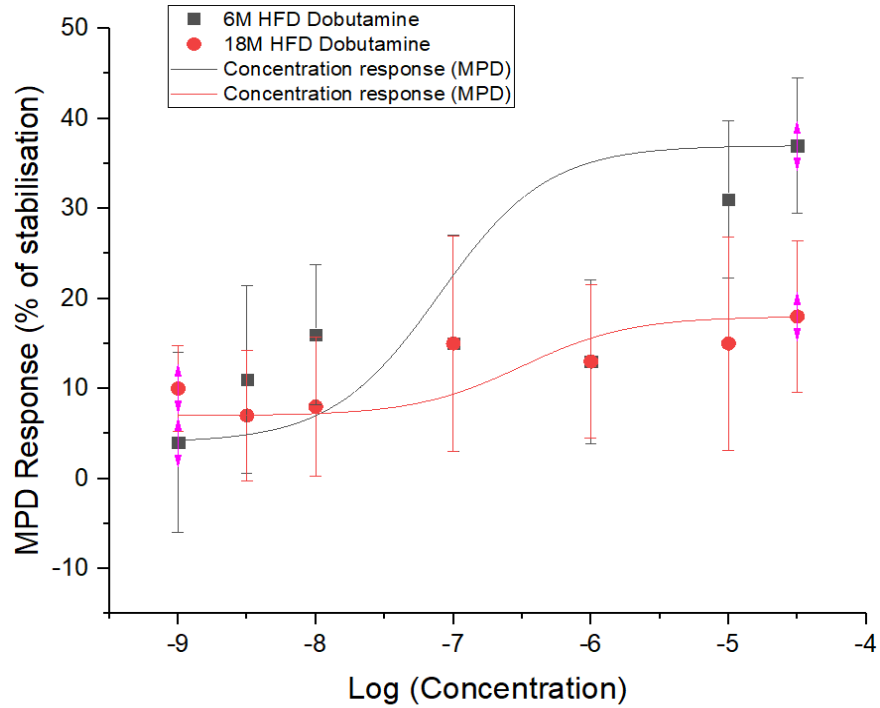


**Figure 7.3.1.29 – MPD for the 6- and 18-month HFD hearts treated with Dobutamine (n = 4 for both).** Hearts were allowed a 20-minute stabilisation period followed by increasing concentrations of each compound: 1 nM = 20-40 mins; 3 nM = 40-60 mins; 10 nM = 60-80 mins; 100 nM = 80-100 mins; 1 µM = 100-120 mins; 10 µM = 120-140 mins and 30 µM = 140-160 mins.

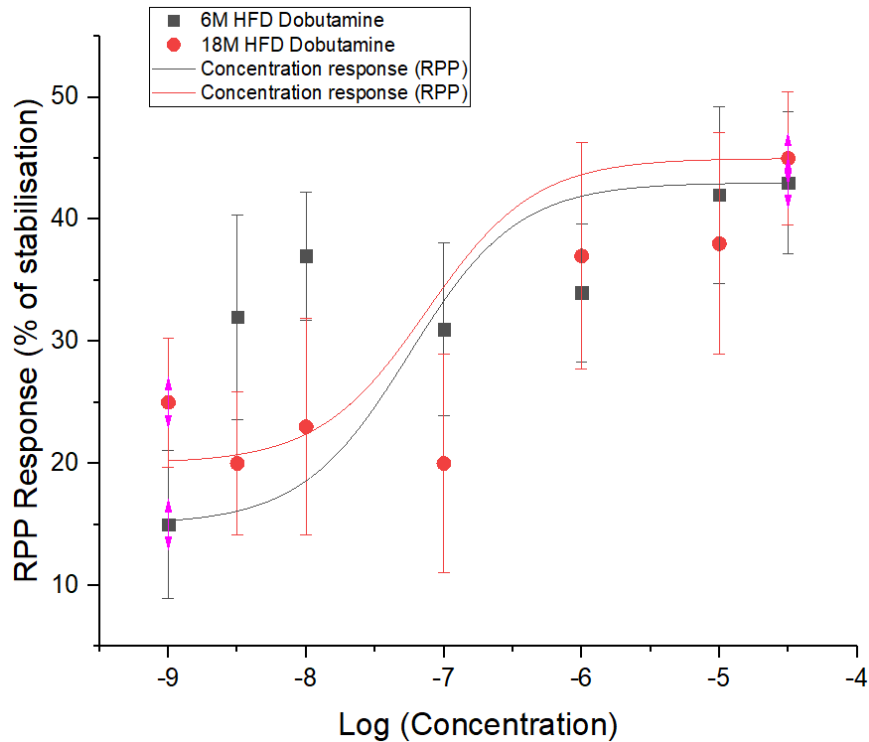


**Figure 7.3.1.30 – RPP for the 6- and 18-month HFD hearts treated with Dobutamine (n = 4 for both).** Hearts were allowed a 20-minute stabilisation period followed by increasing concentrations of each compound: 1 nM = 20-40 mins; 3 nM = 40-60 mins; 10 nM = 60-80 mins; 100 nM = 80-100 mins; 1 µM = 100-120 mins; 10 µM = 120-140 mins and 30 µM = 140-160 mins.

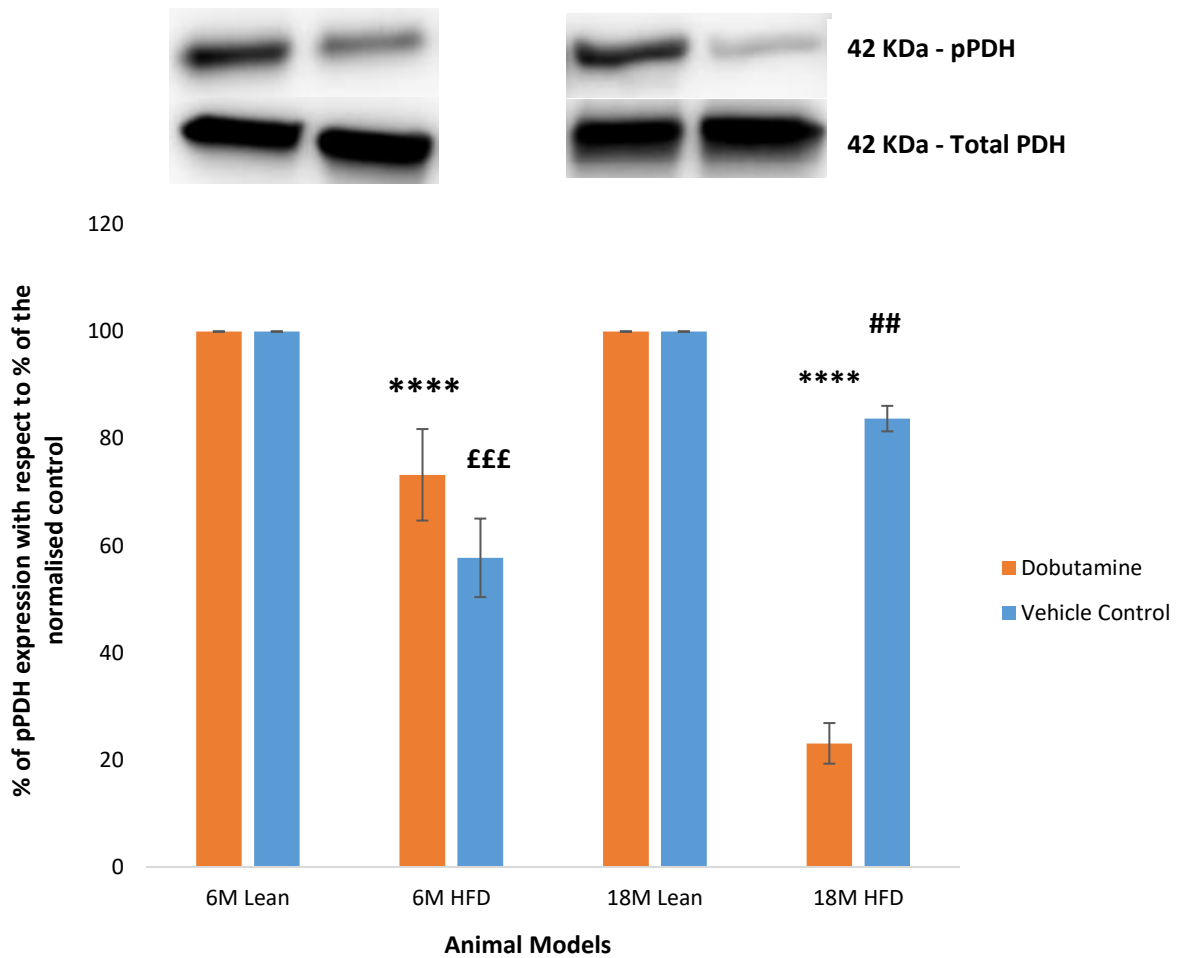
### **7.3.2 Western Blots**

Pyruvate dehydrogenase (PDH) and Uncoupling protein 3 (UCP3) were assessed using western blotting in order to assess the impact of key mitochondrial regulators in cardiac function. All of the represented graphs were plotted after correcting for protein loading and the lean controls were normalised.

#### **7.3.2.1 Pyruvate Dehydrogenase**

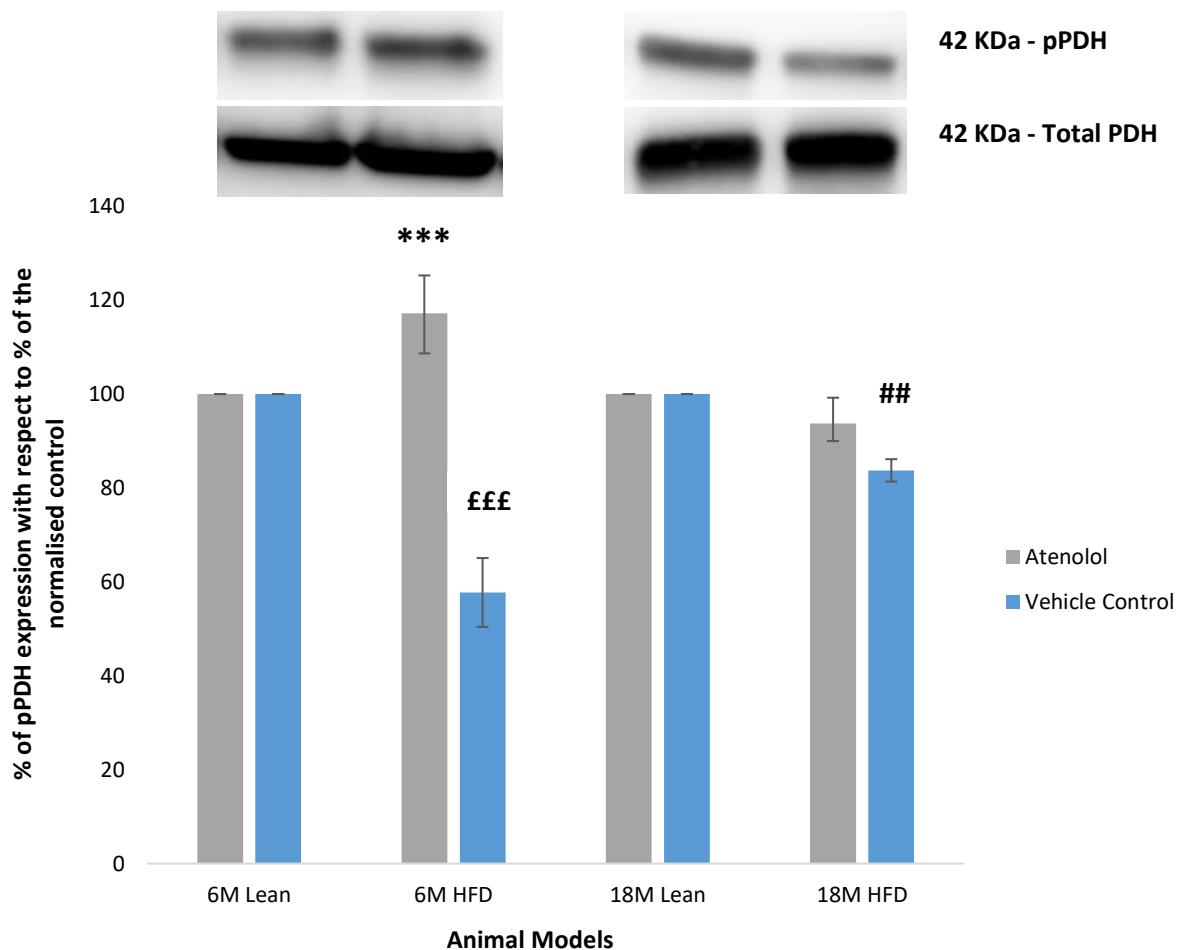
Figure 7.3.2.1.1 shows the percentage of phosphorylated PDH in dobutamine-treated heart tissue as a % of the control in 6 and 18-month lean and HFD rat models. The drug-treated lean models were used as controls for their respective age drug-treated HFD counterpart.

The 6-month treated HFD hearts showed a significant decrease in phosphorylated-PDH ( $-27\% \pm 8.5$  (SEM),  $p < 0.0001$ ) when compared to the 6-month treated lean control. The 18-month HFD treated hearts showed a significant decrease in phospho-PDH ( $-77\% \pm 3.7$  (SEM),  $p < 0.0001$ ) when compared to the 18-month treated lean control.



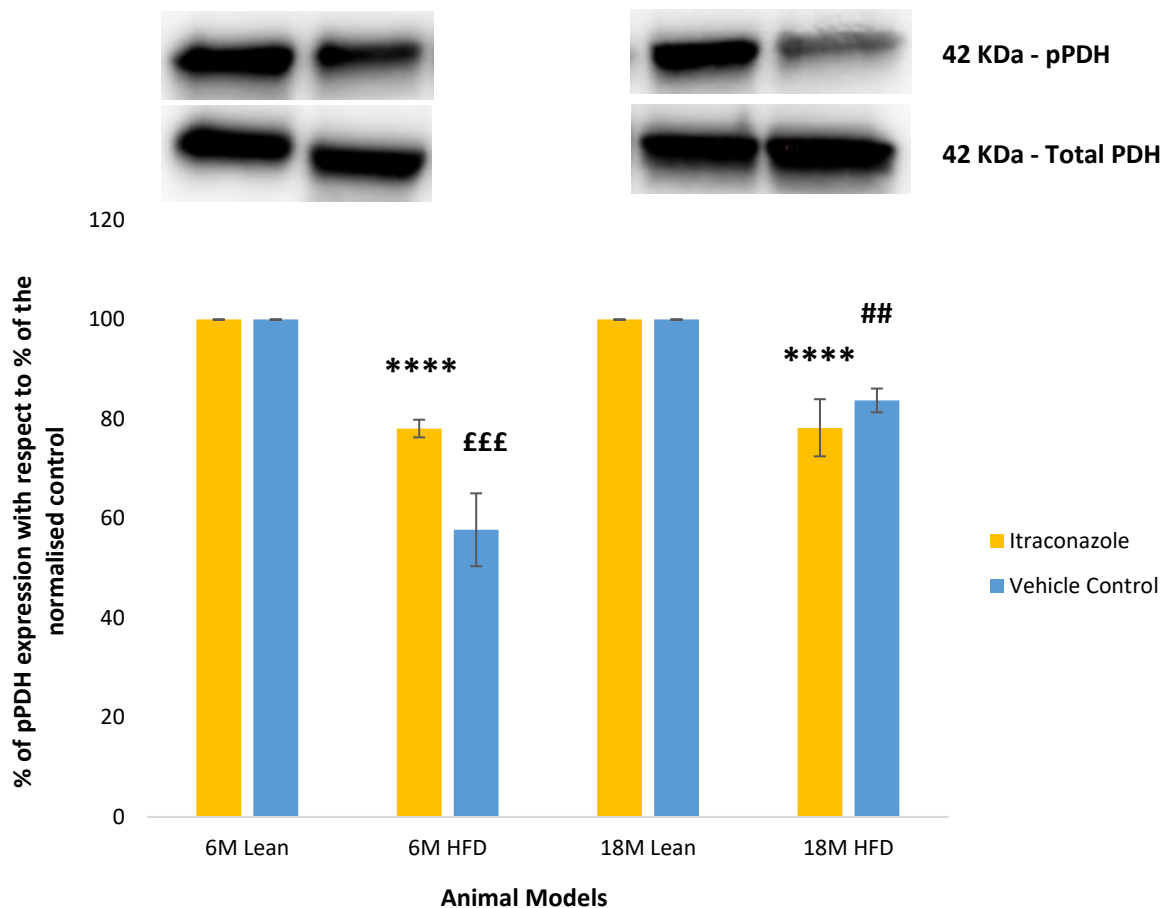
**Figure 7.3.2.1.1 – Phosphorylated PDH expression in 6- and 18-month-old HFD and lean Dobutamine treated animal models (n = 4 for all).** This graph represents the effects of HFD on the levels of phosphorylated PDH in dobutamine-treated heart tissue, as a percentage of total PDH (\*\*\*\* =  $p < 0.0001$ ). The top blot is a representative image of phospho-PDH, while the bottom blot represents total-PDH. The presented results are all corrected for GAPDH. The vehicle control values from chapter 5 are also present, with their significance indicated by the “£” and “\$” symbols (££££ =  $p < 0.0001$  and \$\$ =  $p < 0.01$ , in relation to the 6 and 18-month lean controls respectively).

Figure 7.3.2.1.2 shows the percentage of phosphorylated PDH in atenolol-treated heart tissue as a % of the control in 6 and 18-month lean and HFD rat models. The lean models were used as controls for their respective age HFD counterpart. The 6-month treated hearts showed a significant increase in phospho-PDH (+17%  $\pm$  8.0 (SEM),  $p < 0.001$ ) when compared to the 6-month treated lean control. The 18-month HFD treated hearts showed no significance in phospho-PDH when compared to the 18-month treated lean control. The vehicle control results from chapter 4 are also represented, to show the changes between the untreated hearts and the treated ones.



**Figure 7.3.2.1.2 – Phosphorylated PDH expression in 6- and 18-month-old HFD and lean Atenolol treated animal models (n = 4 for all).** This graph represents the effects of HFD on the levels of phosphorylated PDH in atenolol-treated heart tissue, as a percentage of total PDH (\*\*\*) =  $p < 0.001$ ). The top blot is a representative image of phospho-PDH, while the bottom blot represents total-PDH. The presented results are all corrected for GAPDH. The presented results are all corrected for GAPDH. The vehicle control values from chapter 5 are also present, with their significance indicated by the “£” and “\$” symbols (££££ =  $p < 0.0001$  and \$\$ =  $p < 0.01$ , in relation to the 6 and 18-month lean controls respectively).

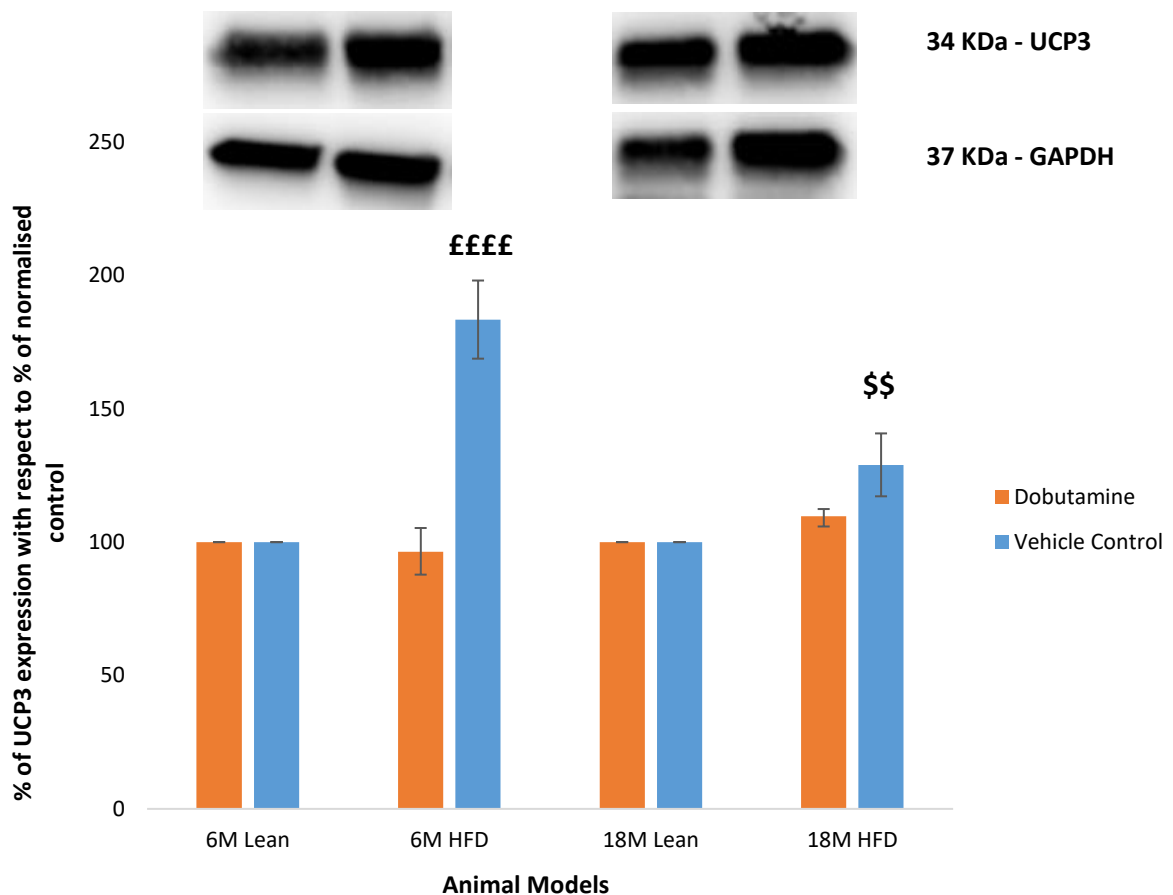
Figure 7.3.2.1.3 shows the percentage of phosphorylated PDH in itraconazole-treated heart tissue as a % of the control in 6 and 18-month lean and HFD rat models. The lean models were used as controls for their respective age HFD counterpart. The lean models were used as a control. The 6-month HFD treated hearts showed a significant decrease in phospho-PDH ( $-22\% \pm 1.7$  (SEM),  $p < 0.0001$ ) when compared to the 6-month treated lean control. The 18-month HFD treated hearts showed a significant decrease in phospho-PDH ( $-22\% \pm 5.7$  (SEM),  $p < 0.0001$ ) when compared to the 18-month treated lean control. The vehicle control results from chapter 4 are also represented, to show the changes between the untreated hearts and the treated ones.



**Figure 7.3.2.1.3 – Phosphorylated PDH expression 6- and 18-month-old HFD old HFD and lean Itraconazole treated animal models (n = 4 for all).** This graph represents the effects of HFD on the levels of phosphorylated PDH in itraconazole-treated heart tissue, as a percentage of total PDH (\*\*\*\* =  $p < 0.0001$ ). The top blot is a representative image of phospho-PDH, while the bottom blot represents total-PDH. The presented results are all corrected for GAPDH. The vehicle control values from chapter 5 are also present, with their significance indicated by the “£” and “\$” symbols (££££ =  $p < 0.0001$  and \$\$ =  $p < 0.01$ , in relation to the 6 and 18-month lean controls respectively).

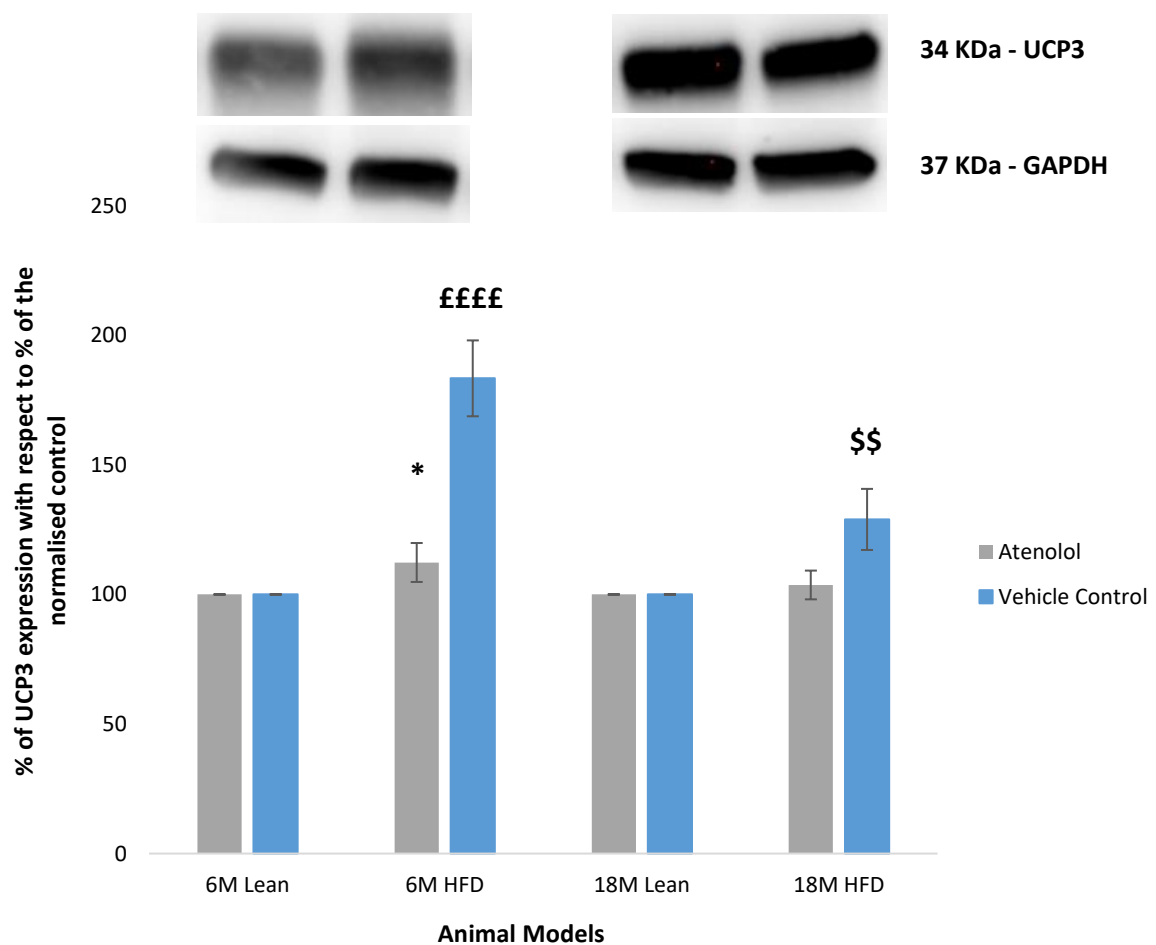
### 7.3.2.2 UCP3

Figure 7.3.2.2.1 shows the percentage of UCP3 in dobutamine-treated heart tissue as a % of the control in lean and HFD 6-month rat models. The lean models were used as a control. The 6-month HFD treated hearts showed no significant changes in UCP3 when compared to the 6-month treated lean control. The 18-month HFD treated hearts showed no significance in phospho-PDH when compared to the 18-month treated lean control. The vehicle control results from chapter 4 are also represented, to show the changes between the untreated hearts and the treated ones.



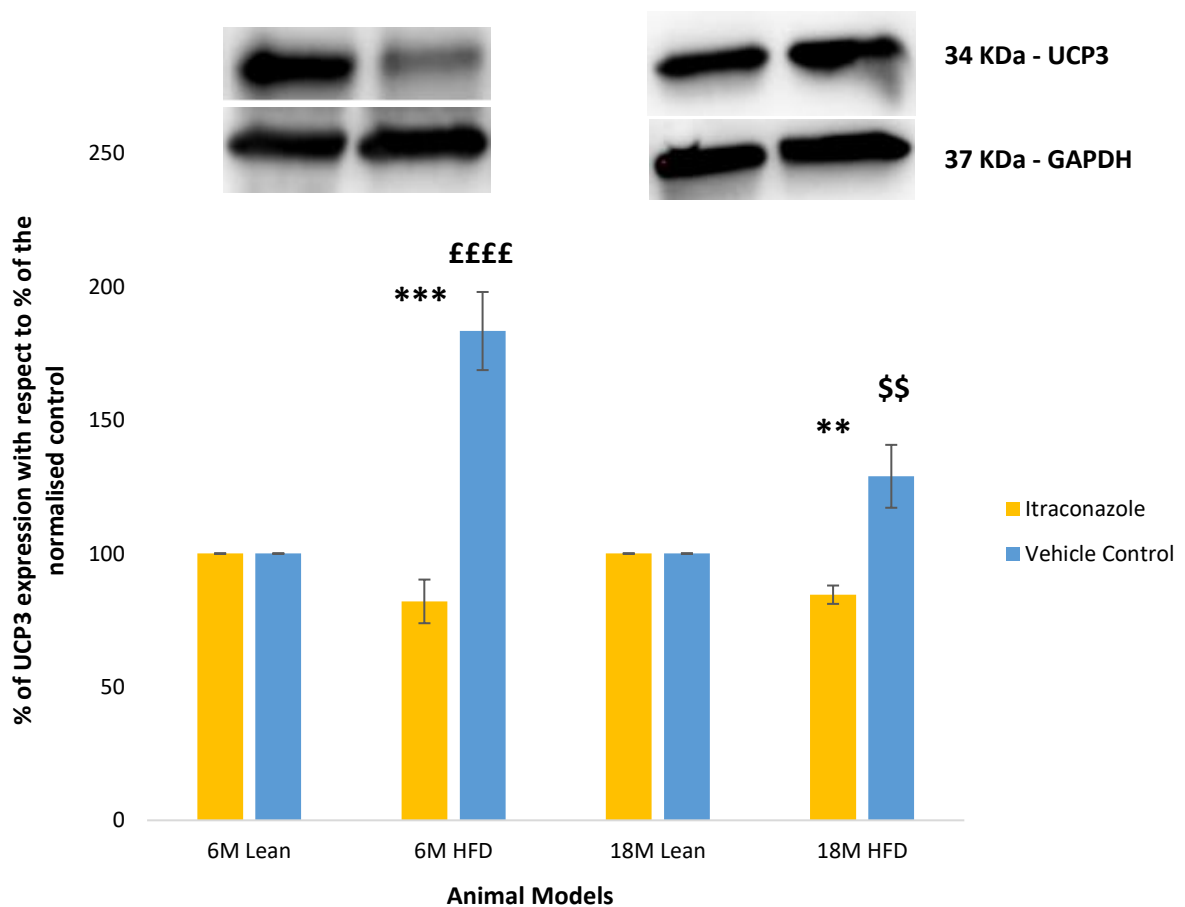
**Figure 7.3.2.2.1 – UCP3 expression in 6- and 18-month-old HFD and lean Dobutamine treated animal models (n = 4 for all).** This graph represents the effects of HFD on the levels of UCP3 in dobutamine-treated heart tissue, as a percentage of GAPDH. The top blot is a representative image of UCP3, while the bottom blot represents GAPDH. The presented results are all corrected for GAPDH. The presented results are all corrected for GAPDH. The vehicle control values from chapter 5 are also present, with their significance indicated by the “£” and “\$” symbols (££££ = p<0.0001 and \$\$ = p<0.01, in relation to the 6 and 18-month lean controls respectively).

Figure 7.3.2.2.2 shows the percentage of UCP3 in atenolol-treated heart tissue as a % of the control in lean and HFD 6-month rat models. The lean models were used as a control. The 6-month HFD treated hearts showed a significant increase in UCP3 ( $+12\% \pm 7.5$  (SEM),  $p < 0.05$ ), when compared to the 6-month treated lean control. The 18-month HFD treated hearts showed no significance when compared to the 18-month treated lean control. The vehicle control results from chapter 4 are also represented, to show the changes between the untreated hearts and the treated ones.



**Figure 7.3.2.2.2 – UCP3 expression in 6- and 18-month-old HFD and lean Atenolol treated animal models (n = 4 for all).** This graph represents the effects of HFD on the levels of UCP3 in atenolol-treated heart tissue, as a percentage of GAPDH ( $* = p < 0.05$ ). The top blot is a representative image of UCP3, while the bottom blot represents GAPDH. The presented results are all corrected for GAPDH. The vehicle control values from chapter 5 are also present, with their significance indicated by the “£” and “\$” symbols (££££ =  $p < 0.0001$  and \$\$ =  $p < 0.01$ , in relation to the 6 and 18-month lean controls respectively).

Figure 7.3.2.2.3 shows the percentage of UCP3 in itraconazole-treated heart tissue as a % of the control in lean and HFD 6-month rat models. The lean models were used as a control. The 6-month HFD treated hearts showed a significant decrease in UCP3 ( $-18\% \pm 8.1$  (SEM),  $p < 0.001$ ), when compared to the 6-month treated lean control. The 18-month HFD treated hearts showed a significant decrease in UCP3 ( $-16\% \pm 3.4$  (SEM),  $p < 0.01$ ), when compared to the 18-month treated lean control. The vehicle control results from chapter 4 are also represented, to show the changes between the untreated hearts and the treated ones.



**Figure 7.3.2.2.3 – UCP3 expression in 6- and 18-month-old HFD and lean Itraconazole treated animal models (n = 4 for all).** This graph represents the effects of HFD on the levels of UCP3 in itraconazole-treated heart tissue, as a percentage of GAPDH (\*\* =  $p < 0.01$ , \*\*\* =  $p < 0.001$ ). The top blot is a representative image of UCP3, while the bottom blot represents GAPDH. The presented results are all corrected for GAPDH. The presented results are all corrected for GAPDH. The vehicle control values from chapter 5 are also present, with their significance indicated by the “£” and “\$” symbols (££££ =  $p < 0.0001$  and \$\$ =  $p < 0.01$ , in relation to the 6 and 18-month lean controls respectively).

## 7.4 Discussion and Conclusion

In chapters 3 and 4 significant functional changes between lean and the HFD heart models were shown. This chapter aimed to investigate whether these changes could have an effect on the haemodynamic parameters of HFD rat models when treated with inotropic drugs. It was found that, on the Langendorff model, Atenolol showed no significant changes between the two models; however, Dobutamine was shown to have reduced effectiveness on the HFD models (as seen by the significantly reduced positive inotropic effect of the drug) and Itraconazole was shown to have an exacerbated effect on the HFD models (seen by a significant reduction in ventricular parameters of the heart). In addition, it was found that PDH seemed to affect the inotropic effect of dobutamine (via changes in its expression), whilst having limited or no effect on both atenolol and itraconazole. UCP3 was shown to be unchanged in dobutamine-treated hearts but showed an increase in atenolol-treated hearts and a decrease in itraconazole treated hearts. Overall, UCP3 does not seem to have a measurable effect on the contractile function of the heart while under the effect of these drugs. Contrary to the original hypotheses, Atenolol showed no significant changes in the presence and absence of HFD; this will be explored and discussed further below.

Previous research has shown that cardiac remodelling in obesity occurs via recorded changes to ventricular walls, depressed systolic function, hypertrophy and impaired vascular function (Selthofer-Relatić, Bošnjak and Kibel 2016; Stapleton et al. 2008). Lipotoxicity is also a common problem in obesity models, with some studies showing a development of a lipotoxic cardiomyopathy associated with increased FAO, decreased glucose oxidation, and increased peroxisomal production of ROS via an overexpression of Peroxisome proliferator-activated receptor- $\alpha$ , or PPAR- $\alpha$ , which controls the expression of fatty acid utilization genes and the cardiac energy metabolism (Finck et al. 2002).

In both diabetic and high-fat fed models, cardiomyopathic remodelling occurs as a partial result of reactive oxygen species being accumulated in the myocardium (Finck 2007).

Research has shown that PPAR expression and activation is induced by the presence of fatty acids as a result of obesity, insulin-deficiency or diabetes type 2 (Buchanan et al. 2005; Finck et al. 2002; Finck et al. 2003). Studies have also shown that, in both high fat fed and diabetic isolated hearts, PPAR expression is reduced even though there is an increase in fatty acid availability (Young, Guthrie, Razeghi, Leighton, Abbasi, Patil, Youker and Taegtmeier 2002; Zhou et al. 2000). This has been linked to both a decrease in contractility and a general reduction in haemodynamic function (Luptak, Balschi et al. 2005). Due to the role of PPAR- $\alpha$  and other fatty acid metabolites in the expression of PDH and UCP3, it was hypothesised that changes to their expression were causing the recorded shift in haemodynamic parameters, mainly in the rate of contraction and the RPP. Previous studies have shown that obesity and aging can impair cardiac contractility via changes to the phosphorylation of Akt and eNOS, as well as ERK and AMPK (Ren et al. 2010). However, in this paper the researchers claimed that their data was insufficient to fully understand the role of either of these pathways on the recorded contractile impairment. It is also important to note that they associated leptin to these changes, as opposed to any changes in mitochondrial regulation, even though both ERK and MAPK can have an effect on the modulation of PPARs (Burns and Heuvel 2007; Liao, P. et al. 2002). Papers have found a connection between aging and a reduction in PPAR expression, although these changes were not apparent on the echocardiograms of the test subjects (Barton et al. 2016; Kar and Bandyopadhyay 2018; Lesnefsky, Chen and Hoppel 2016; Sung et al. 2004); however, when tested on a molecular level this changed, with PPAR- $\alpha$  showing a significant reduced expression on the aged group.

Other studies related to this have also highlighted that not only is age a major factor in blunted PPAR- $\alpha$  expression (Francis, Annicotte and Auwerx 2003; Toth and Tchernof 2000), but also of other cardiac factors such as reductions in cardiac electrical activity and a desensitisation of the cardiac  $\beta$ 1-adrenergic receptors (Loichot et al. 2006; Sung, B. et al. 2004).

Atenolol is an adrenergic antagonist used in the treatment of high blood pressure (Carlberg, Samuelsson and Lindholm 2004; Wilkinson, McEniery and Cockcroft 2006). Atenolol has been previously shown to have a very limited effect on the heart at lower concentrations, and it has been reported to have, to an extent, a repairing effect on the RyR, SERCA2a and PLN protein contents of ischaemic hearts via its effect on the proteolysis of said proteins (Temsah et al. 2000). Even though this effect is not heavily researched, it is important for this study to understand that there is a limitation to the negative inotropic effect of Atenolol, alongside a potential cardioprotective effect, which might explain why there was a lack of significance amongst the recorded results. In addition to this, it is important to refer to a secondary effect of Atenolol that has been recently reported, which is its ability to decrease membrane fatty acid unsaturation (Sanchez-Roman et al. 2010; Sanchez-Roman et al. 2014) and lowering the oxidative damage to cardiac tissue in animal models of most age groups, apart from 35-month animal models (Gómez et al. 2014); however, the lack of significance amongst the recorded parameters can be explained by the findings made by Gómez et al, as atenolol-induced changes are not a factor in younger aged models. Wójcicki et al conducted a study using lean, high BMI and obese patients to investigate the pharmacokinetics and pharmacodynamics of atenolol in obesity (Wojcicki et al. 2003) and found that there were minimal and non-significant changes in the systolic and diastolic pressures and heart rate of obese patients, when compared to the lean control group; the researchers therefore concluded that the effect of atenolol is independent of the presence of absence of obesity.

In addition to this, a study by Williams et al which aimed to investigate the effects of a diet-induced obesity on cardiac regulation in mice, while under the effect of an atenolol treatment regime (Williams et al. 2003), also found that there was a non-significant effect of atenolol on the mean arterial pressure in obesity, but a significant decrease in heart rate. Observations made in this chapter provide no evidence to counteract the previously recorded data.

Dobutamine is heavily prescribed worldwide for treatment of heart failure and cardiogenic shock (DeWitt et al. 2016; Tariq and Aronow 2015). It can, in some reported cases, increase the myocardial oxygen demand when used in high doses, which can lead to tachycardic episodes (DeWitt et al. 2016; Wang, XC, Zhu and Shan 2015). Previous studies have shown that there is a correlation between  $\beta$ -adrenergic receptors and age, with the former being a direct function of the latter, which opposes the earlier papers that found no significance between the two factors (Abrass, Davis and Scarpace 1982; Ferrara et al. 2014; Xiao et al. 1994b). This phenomenon, aptly named  $\beta$ -adrenergic desensitization, stems from an understanding that ageing is associated with decreases in systolic cardiac function and an overall reduction in left ventricle inotropic reserves (Heller and Whitehorn 1972; Jiang, M., Moffat and Narayanan 1993; Xiao et al. 1994b). A more recent study used Dobutamine as a stress factor on a high fat diet-induced model and recorded significant blunting of contractile reserve functions, which the researchers hypothesized and was then further confirmed (Haggerty et al. 2015). The presented study showed a change in the effect of Dobutamine on the rate of contraction and on the RPP of the heart, with a clear blunting in the drug effect when comparing between the two models; in addition to this, age seemed to exacerbate this blunted effect, as the lean model on the 18-month data set seemed to match the HFD model on the 6-month data. This clearly shows that there are severe changes occurring within the heart to cause this effect.

The  $\beta$ -adrenergic desensitization seems to be a likely reasoning behind it, but other options have also been raised, mainly involving changes in mitochondrial components (e.g.: PPAR-alpha and PDH). To note that some research has also involved mitochondrial processes as the cause of the aforementioned  $\beta$ -adrenergic desensitization (Corbi et al. 2013; De Lucia, Eguchi and Koch 2018; Kontogiannis et al. 2018).

To add to this, lipid accumulation in obesity has also been directly linked to various factors heavily involved in contractile changes, mostly via the aforementioned ones, as they are sub-components of cardiac lipotoxicity (Drosatos et al. 2011; Drosatos 2016). However, in this study there were no means to directly confirm this event, but evidence was found to support the existence of factors involved with it, in the form of a blunted response of Dobutamine and a reduced PPAR- $\alpha$  expression in the heart tissues of high fat diet-induced rats.

Itraconazole is a commonly prescribed antifungal that has, on more than one occasion, been linked to a negative inotropic effect on the heart and severe cases of heart failure (Ahmad, Singer and Leissa 2001). Researchers have found that Itraconazole decreases the left ventricular contractility of the heart and, while the exact mechanism is not known, the results indicated that it was not related to any inhibition of the  $\text{Na}^+$  and  $\text{Ca}^{2+}$  channels, kinase inhibition or mitochondrial dysfunctions (Qu et al. 2013). However, a different study focused on the cardiac toxicity of Itraconazole found that the drug decreased, in a dose dependant manner, the mitochondrial oxidative phosphorylation and consequent oxygen consumption of myocardial tissue, by 20% (Cleary et al. 2013). The scientific community is split with the mechanisms behind the negative inotropy of Itraconazole, but the focus keeps turning towards mitochondrial dysfunction as the most likely cause, due to its involvement in mechanism of inotropy in the heart (Paul and Rawal 2017).

In this study, the MPD was significantly reduced in both 6 and 18-month HFD models, while the MPR was only significant towards the end of the protocol and only for the 18-month HFD model, indicating that a dose-response effect is present and exacerbated in the presence of both age and high-fat. The RPP on the 18-month model showed a clear exacerbation of the drug effect, starting at the lowest concentration and continuing all the way to the highest concentration used.

Previous studies have shown how itraconazole can be cytotoxic to cells, with studies showing a direct correlation between ATP level reductions and cytochrome P450 inhibition, which itraconazole inhibits (Somchit et al. 2009). However, as mentioned in the introduction, there is very limited research on azole antifungals and their effect on the cardiac function of obese patients and most of this data comes from patient data, as highlighted above; therefore, most of these conclusions will be extrapolations and hypothesis of this data. Studies have been conducted using Fluconazole and it was found that the drug was less effective in obese and morbidly obese patients, when compared to nonobese patients (Alobaid et al. 2016; Lopez and Phillips 2014; Sinnollareddy et al. 2015). While the negative effect on Itraconazole was observed in the present study, it was also found that age seems to play a lesser part on the drug effect, when compared to the effect of high-fat diet induced obesity. Therefore, it is proposed that Itraconazole must, to an extent, have a secondary interaction with an HFD-related agent, thus causing the recorded exacerbated negative inotropy on the hearts.

In chapter 5, significant differences were measured in the contractile properties of differently aged hearts, as well as in the active and total protein expressions of PDH when treated with Dobutamine and Itraconazole, with no major changes in the hearts treated with atenolol.

UCP3 showed increases when compared to the controls, but these results suggest that it does not impact cardiac contractility when treated with the drugs used for this project but may still impact other areas of cardiac function. PDH is a common target for metabolic studies due to its role as a key enzyme in the regulation of the balance between carbohydrate and fat metabolism in the heart (Hall et al. 1996; Le Page et al. 2015). In the previous studies it was confirmed that a decrease in PDH phosphorylation correlated with an increase in FA usage, as previously reported (Lloyd, Brocks and Chatham 2003; Moreau et al. 2004; Rinnankoski-Tuikka et al. 2012).

This is particularly true for aged models, as there is a previously recorded shift to a more glucose oxidation dependant mechanism for ATP production (Moreau et al. 2004). In the present study a decrease in the expression of phosphorylated PDH in our Dobutamine-treated hearts was observed, with a severe significant reduction in our 18-month treated hearts, specifically.  $\beta$ -receptor desensitization was mentioned in the introduction to this chapter and it is likely that this is the case with the data collected here, based on the changes in PDH expression, as it is likely that the extreme change in PDH expression for the 18-month model is age-dependant, with HFD having less of an effect upon it; this also goes in agreement with the observations in chapter 5, where an age-dependant reduction in PDH levels in Dobutamine-treated whole hearts was observed.

Interestingly, Atenolol showed a significant increase in the expression on the 6-month HFD model but no significance between the two diet models for the 18-month group. In chapter 5, a progressive decline in PDH activity in an age-dependant fashion for the Atenolol treated hearts was recorded. the data indicates that, although some changes in PDH expression were observed, Atenolol does not seem to cause significant changes to ATP production in HFD hearts.

Finally, Itraconazole showed a significant decrease for both models, which aligns with the observations in chapter 5 that there may not be a direct effect of PDH on the negative inotropic effect of Itraconazole on the heart. In addition to this, studies have been done on the changes in CYP450 enzymes as a result of obesity and a recent study by Drolet et al found that there was a significant reduction in CYP family enzyme protein expression in cardiac tissue of type 2 diabetes mice models (Drolet et al. 2017); the researchers concluded that this change was a potential exacerbator of risk factors of cardiovascular disease via a disruption in the equilibrium between cardioprotective and cardiotoxic metabolites of arachidonic acid.

Based on these observations, it is likely that these changes are also occurring on the carbon metabolic pathway, via pyruvate dehydrogenase and UCP3 expression changes, which were previously confirmed in chapters 3, 4 and 5. It is therefore likely that, while not directly, the potential changes in ATP production and synthesis via pyruvate dehydrogenase are compromised in hearts under the effect of Itraconazole; however more work is still needed to confirm this observation. In the present studies, UCP3 protein expression did not change in Dobutamine between the two models but was shown to be reduced when compared to the controls. Atenolol showed an increase in UCP3 levels on the 6-month HFD model when compared to the lean model but showed no changes in the 18-month models. Similar to what was seen for Dobutamine, Atenolol showed a reduction in UCP3 expression when compared to the controls. Finally, Itraconazole showed a significant decrease in both HFD models, when compared to their respective lean models, and an overall significant decrease when compared to the controls, as seen with the previous two drug treatments. Based on this data, it is likely that the conclusion from chapter 5 applies here as well and UCP3 does not have a particular effect upon the contractile function of the hearts treated with the aforementioned inotropic agents.

## 7.5 Summary, limitations and final comments

To the best of our knowledge, this study was the first of its kind to investigate the effects of a range of both positive and negative inotropes - Dobutamine, Atenolol, Itraconazole in a whole heart Langendorff model, in order to compare their mechanistic differences when applied to hearts from HFD animal models. Many studies have conducted work based on obese and type 2 diabetes models, but this is the first study to investigate the effects of inotropic drugs on obese models, with the added variable of age.

Significant differences were found in the contractile properties of differently aged hearts, as well as in the active and total protein expressions of PDH when treated with Dobutamine and Itraconazole, with no major changes in the hearts treated with atenolol. To confirm this effect, it is proposed that future studies run activity assays on the heart tissues to confirm the exact level of activity of PDH on the heart. UCP3 showed increases when compared to the controls, but the results suggest that it does not impact cardiac contractility but may still impact other areas of cardiac function.

The main limitations for this project, similarly to what was found in chapter 3, was the limited number of animals used due to animal housing issues and due to the fact that many of the 18-month animals did not survive until they were ready to be sacrificed. The other limitation of this project rests on the fact, that gender was not considered, as previous research has shown that male and female rats express different genes. While a potential link was investigated between mitochondrial energy regulation, a lot of other potential mitochondrial targets were not looked at due to the immense scope of the field.

In addition to this, and as it was mentioned previously, investigating the mRNA levels of PDH, PPAR $\alpha$  and UCP3 would have been useful to complement the western blot results, as it would show if there were gene expression changes directly or indirectly tied to the protein levels; for UCP3 this would be of particular importance due to previously published discrepancies between protein and mRNA levels.

There is still a lot of work to do, but it has been established that energy generation changes should be considered when investigating these particular inotropes, but not necessarily at the mitochondrial transporter level (UCP3).

# **Chapter Eight: General conclusions**

This study investigated the effect of age and HFD on cardiac contractile function in the presence and absence of inotropic drugs. Both can have negative effects on the contractility of the heart but the investigation into their combined effects is limited in published literature. Dobutamine and Atenolol have been shown to have different effects on haemodynamic function in the presence and absence of age and obesity, separately, but the synergistic effect is not clear. In contrast, Itraconazole has been shown to have a severe negative inotropic effect leading to heart failure but there is limited research exploring the mechanisms behind this effect. The main motivations behind this project were to assess how age, obesity and a synergistic effect of both affect the heart and whether the function of widely used inotropes, part of the WHO list of essential medications, is affected as a result (WHO 2019).

## **8.1 Summary of key findings**

The first aim of this thesis was to investigate the effect of age and HFD on cardiac contractility. The physiological effects of ageing and HFD, independently and synergistically, were found to negatively impact the cardiac papillary muscle power output via significant decrease in muscle work during shortening and muscle activation rates, both of which resulted from muscle fatigue; the total power output of the muscle was also reduced as a result. In addition, significant decreases in metabolic pathways involving both PDH and UCP3 were also recorded. Curiously, no significant changes were observed on the Langendorff isolated heart model (chapters 4 and 5). While the aforementioned effects were observed in both models independently, they were significantly exacerbated when both age and HFD were combined.

The second and third aims of this thesis were to investigate how Dobutamine, Itraconazole and Atenolol affect the contractile function of the heart under the effect of ageing, HFD and a combined effect of both and whether this relates to changes in metabolic pathways involving PDH and UCP3, which will be explored in detail in the next few paragraphs.

In the inotropic age study (chapter 6), significant age-dependant decreases in the haemodynamic parameters of 3, 6 and 18-month hearts were recorded to suggest a potential link between them and the previously reported  $\beta$ -receptor desensitization in aged cardiac models (Farrell and Howlett 2007; Farrell and Howlett 2008; Ferrara et al. 2014; Lim et al. 2000). In addition, significant age-dependant reductions were also measured for the active and total protein expressions of PDH when treated with dobutamine, atenolol and itraconazole. UCP3 showed an age-dependant decrease for dobutamine, no change across atenolol and a significant age-dependant increases in itraconazole-treated hearts; this was observed for the 6 and 18-month models when compared to the 3-month ones.

The effect of Dobutamine on phosphorylated PDH and UCP3 suggests that there may be an impairment in mitochondrial cardiac energy production, as the reduction in their levels was accompanied by decreased ventricular relaxation and the rate pressure product of the isolated heart. This effect was profound in aged models (as seen by the results for the 6 and 18-month models). An age-dependant decrease in phosphorylation of PDH and increased UCP3 in the itraconazole-treated hearts seem to suggest a link between the negative inotropic effect of the drug and an increase in cardiac fatty acid oxidation, as ATP production derived from fatty acids has been previously linked, in untreated hearts, to decreases in cardiac efficiency.

In the inotropic HFD study (chapter 7), the contractile properties of the 6 and 18-month HFD hearts were measured, when treated with dobutamine, atenolol and itraconazole. Atenolol was shown to have no significant effect on cardiac contractility in the presence or absence of HFD. The effect of Dobutamine on cardiac contractility were shown to be significantly impaired in the presence of HFD for both aged models, with an exacerbation being recorded on the 18-month model, as the effectiveness of the drug across all ranges was reduced in comparison with the lean model and the 6-months data.

This data combined with the data from the age study (chapter 5) confirms the hypothesis that not only is there a confirmed presence of the aforementioned  $\beta$ -receptor desensitization on the heart, but also that the combined effect of age and HFD might be causing an exacerbation of this phenomenon. The effects of the Dobutamine on the mitochondrial metabolism were then investigated and it was found that there was a significant decrease in the expression of PDH on the 18-month hearts. It is therefore proposed that the reduction in haemodynamic parameters measured on the isolated heart model is due to changes in energy production as a result of the synergistic effect of HFD and age on the heart.

As for the itraconazole data, an exacerbation of its negative inotropic effect was measured, in a concentration-dependant fashion, for both the 6 and 18-month hearts. For this project, the data suggests that the mitochondrial metabolism was being changed as an effect of the drug. Investigation into PDH activity showed that, while there was an increase in its phosphorylated levels in the 6-month hearts, the 18-month hearts actually showed a significantly increased level of PDH expression when compared to its younger counterpart. UCP3 levels are also reduced in the 18-month HFD models, when compared to the 6-month HFD, but increased when compared to the lean models. These results suggest that itraconazole causes the heart to shift to a more ineffective ATP production, which in turn leads to cardiac deficiency and exacerbates the negative inotropic mechanism of the drug.

The outcome of this thesis has highlighted the importance of preclinical studies to acutely assess drug safety and capabilities across different aged and HFD phenotypes, as well as in the presence of both. The current study also highlighted the importance of assessing these parameters in hearts without cardiovascular complications such as myocardial ischaemia, but the findings showed that even in the absence of these complications, there can still be adverse effects of certain drugs in the presence of age and HFD. It is therefore of vital importance that safety assessments are carried out in different cardiac models, both in the presence and absence of disease. There is a limited scope of the use of Dobutamine, Atenolol and Itraconazole in HFD and ageing clinical settings, which emphasizes the importance of these preclinical safety assessments, in order to develop cardioprotective strategies and interventions to ensure the safety of all patients, regardless of their pre-existing conditions, when being treated with these drugs. This project has furthered the understanding of these drugs under specific models of disease and age and supports future studies which may observe adverse cardiac events as a result of their use.

## **8.2 Study limitations**

The main limitation for this project was the limited sample size for the studies, although low sample sizes have been used in the past to great effect (Cassambai et al. 2019; Gudmundsdottir, Benediktsdottir and Gudbjarnason 1991), due to the fact that many of the 18-month animals did not survive until they were ready to be sacrificed due to their advanced age (see section 3.1.1 for a Kaplan-Meier curve to showcase this). An unavoidable selection bias was also present via a “survival of the fittest” situation and it is therefore possible that the aged models do not accurately mimic the exact phenotype of their age range as a result.

Another limitation was the use of male-only models, as previous research has shown that male and female rats express different genes and female rats have actually shown significant decreases in overall cardiac function and structure in an age-dependant fashion, which is a phenomenon that has not always been observed in males (Fannin et al. 2014). Female models have also been investigated to a lesser extent when compared to male models due to hormonal factors; because of their lower testosterone levels, female models tend to express higher levels of leptin and adiponectin, which influence their abilities to consume food and energy, as well as their ability to gain weight (Aronne and Segal 2002). This would therefore be an interesting study to carry out and compare those results with the ones presented here.

Three age groups were used for this project, which do not account for senescent animals. It is therefore necessary for future studies to potentially include 20- to 24-month-old animals to better understand some of these results, especially when applied to drug studies (Capitanio et al. 2016; Moreau et al 2004; Iemitsu et al 2002). Finally, the Langendorff isolated model allows for the recording of direct effects of inotropic agents on the heart but the results are less clinically relevant due to being an isolated organ model and lacking neuronal regulation, limited oxygen carrying capabilities of the buffer used and a vulnerability of the heart to injury while being mounted on the apparatus (Bell, Mocanu and Yellon 2011; Skrzypiec-Spring et al. 2007).

## **Chapter Nine: Future work**

The data presented throughout this thesis have produced some valuable results in the context of cardiac physiology, pharmacology and energy metabolism. Due to time, animal upkeep capacity, decrease survival of aged models (as highlighted in section 3.1.1) and a conscious reduction of animal usage, other investigations which could have supplemented the findings for this study could not be implemented. However, proposed further studies including the techniques mentioned but not utilised (section 3.7) for this project are outlined.

Whilst several haemodynamic parameters were measured in this study with the Langendorff model to account for cardiac contractility, there was no investigation into how the composition of Krebs-Henseleit buffer (KHB) can account for cardiac metabolism. The sole use of glucose as energy source in KHB has been mentioned multiple times as being a vital component in mitochondrial metabolism (Gopal et al. 2018; Le Page et al. 2015; Qiang et al. 2007). Due to this, injections of glucose inhibitors or antagonists onto the whole heart model at timed intervals would be the first step into quantifying how glucose uptake differs between lean and obese models, across different ages (Tessier et al. 2003).

As an integral part of this work, ATP and mitochondrial studies are proposed to play a large role in the changes observed between the HFD and aged models. ATP synthase assays and mitochondrial isolations and tracing (which would show dynamic metabolism, as opposed to western blotting which is static) would confirm changes to ATP metabolism dependent on HFD or age and the additional effect of inotropes. Measurement of mitochondrial channel activity could also be used to investigate whether the observed changes in HFD and aged models could be due to mitochondrial oxidative stress (Balderas-Villalobos et al. 2013; Bers 2000; Reho and Rahmouni 2017).

The PPAR $\alpha$  pathway is an important cardiac metabolic regulator, therefore observing the effect of HFD and ageing on specific genes such as PPAR $\alpha$ , UCP3 and PDK4, would elucidate the role of the mitochondria on the observed metabolic and contractile changes in this study (Finck et al. 2003; Francis, Annicotte and Auwerx 2003; Kar and Bandyopadhyay 2018; Pol, Lieu and Drosatos 2015). Although PCR was used to investigate this pathway, the results were not conclusive and a more thorough investigation is therefore required.

Leptin has been previously shown to be directly linked to contractile function via different pathways such as the NADPH oxidase pathway and the Leptin receptor pathway (Dong et al. 2006; Dong, Zhang and Ren 2006; Nickola et al. 2000; Unger and Zhou 2001). It would therefore be interesting to measure how leptin receptor activity changes in the presence and absence of a high-fat diet, under the differently aged models used here, especially due to some of the results indicating changes linked to high-fat diet changes (Chapters 5 and 7).

Previous literature has shown that intracellular Ca<sup>2+</sup> levels are lowered in obese rats, with leptin playing a key role via increases in NO production and via the NADPH oxidase-mediated pathway (Dong, Zhang and Ren 2006; Nickola et al. 2000). Measuring calcium levels would therefore be a crucial next step for further studies, by looking at both intracellular Ca<sup>2+</sup> movement and the calcium signalling pathway, as both would prove vital to investigate the link between calcium impairment and the changes observed in this project with the inotropic drugs, and whether the effects of age and HFD significantly changed this; furthermore, calcium metabolism levels in the mitochondria have been previously linked to a decrease in the active length-tension relationship of hypertrophied myocardial samples (Cooper et al. 1973). While this could explain the reduction in the net-work produced by the papillary muscles isolated from the HFD models analysed in this project, the current data is not enough to support this and more work is therefore still needed.

Finally, and as it was mentioned extensively throughout this project, investigating the mRNA levels of PDH, PPAR $\alpha$  and UCP3 would have been useful to complement the western blot results, as it would highlight changes in gene expression, directly or indirectly tied to the protein level. For UCP3 this would be of particular importance due to previously published discrepancies between protein and mRNA levels. This was started but due to insufficient tissue it was not completed, but it would be helpful to add to future research as a two-step verification for the results presented here.

In the context of the drugs used, Dobutamine and Itraconazole showed significant changes in the presence of obesity; based on this, there are a few potential mechanisms worth exploring. While Dobutamine has been investigated in the past, this project conducted these investigations in both a cumulative fashion and across differently aged obese hearts; the results obtained indicated significant changes to its inotropic effect in both lean and obese hearts. The reason behind this was, unfortunately, not clarified with this project but future work on beta-receptor desensitisation is crucial to better understand how the effect occurs and its exact link to obesity and ageing. Looking at ECG models as well as sympathetic and parasympathetic nerve responses would be a very valuable project to undertake in order to clarify some of the results obtained for this project (Allen et al. 2018; Chauhan et al. 2018).

In respect to Itraconazole, close to no research is currently available on its effect on the cardiac function on the heart, but most researchers agree that it has a severe negative inotropic effect (Qu et al. 2013; Tokarev and Benditt 2015). The results obtained in this project have shown a potential exacerbation of this negative effect in the presence of obesity. Due to its link to Itraconazole, cytochrome P450 measurements using modern proteomic methods (electrophoresis, mass spectrometry or liquid chromatography) applied to the models used for this project would be beneficial in understanding whether there is a link between its expression and the changes in itraconazole function recorded.

## References

- Abel, Litwin, and Sweeney (2008) 'Cardiac Remodeling in Obesity'. *Physiological Reviews* 88 (2), 389-419
- Abrass, I. B., Davis, J. L., and Scarpace, P. J. (1982) 'Isoproterenol Responsiveness and Myocardial B-Adrenergic Receptors in Young and Old Rats'. *Journal of Gerontology* 37 (2), 156-160
- Afilalo, J., Karunanathan, S., Eisenberg, M. J., Alexander, K. P., and Bergman, H. (2009) 'Role of Frailty in Patients with Cardiovascular Disease'. *The American Journal of Cardiology* 103 (11), 1616-1621
- Ahmad, S. R., Singer, S. J., and Leissa, B. G. (2001) 'Congestive Heart Failure Associated with Itraconazole'. *The Lancet* 357 (9270), 1766-1767
- Al Ali, A. M., Straatman, L. P., Allard, M. F., and Ignaszewski, A. P. (2006) 'Eosinophilic Myocarditis: Case Series and Review of Literature'. *Canadian Journal of Cardiology* 22 (14), 1233-1237
- Albarwani, S. A., Mansour, F., Khan, A. A., Al-Lawati, I., Al-Kaabi, A., Al-Busaidi, A., Al-Hadhrami, S., Al-Husseini, I., Al-Siyabi, S., and Tanira, M. O. (2016) 'Aging Reduces L-Type Calcium Channel Current and the Vasodilatory Response of Small Mesenteric Arteries to Calcium Channel Blockers'. *Frontiers in Physiology* 7, 171
- Allen, Coote, J. H., Grubb, B. D., Batten, T. F. C., Pauza, D. H., Ng, G. A., and Brack, K. E. (2018) 'Electrophysiological Effects of Nicotinic and Electrical Stimulation of Intrinsic Cardiac Ganglia in the Absence of Extrinsic Autonomic Nerves in the Rabbit Heart'. *Heart Rhythm* 15 (11), 1698-1707
- Allibardi, S., Merati, G., Chierchia, S., and Samaja, M. (1999) 'Atenolol Depresses Post-Ischaemic Recovery in the Isolated Rat Heart'. *Pharmacological Research* 39 (6), 431-435
- Alobaid, A. S., Wallis, S. C., Jarrett, P., Starr, T., Stuart, J., Lassig-Smith, M., Mejia, J. L., Roberts, M. S., Sinnollareddy, M. G., Roger, C., Lipman, J., and Roberts, J. A. (2016) 'Effect of Obesity on the Population Pharmacokinetics of Fluconazole in Critically Ill Patients'. *Antimicrobial Agents and Chemotherapy* 60 (11), 6550-6557
- Alpert, M. A., Karthikeyan, K., Abdullah, O., and Ghadban, R. (2018) 'Obesity and Cardiac Remodeling in Adults: Mechanisms and Clinical Implications'. *Progress in Cardiovascular Diseases* 61 (2), 114-123
- Alpert, M. A., Lambert, C. R., Panayiotou, H., Terry, B. E., Cohen, M. V., Massey, C. V., Hashimi, M. W., and Mukerji, V. (1995) 'Relation of Duration of Morbid Obesity to Left Ventricular Mass, Systolic Function, and Diastolic Filling, and Effect of Weight Loss'. *The American Journal of Cardiology* 76 (16), 1194-1197

- Amin, A. and Maleki, M. (2012) 'Positive Inotropes in Heart Failure: A Review Article'. *Heart Asia* 4 (1), 16-22
- Andreollo, N. A., Santos, E. F. d., Araújo, M. R., and Lopes, L. R. (2012) 'Rat's Age Versus Human's Age: What is the Relationship?'. *ABCD.Arquivos Brasileiros De Cirurgia Digestiva (São Paulo)* 25 (1), 49-51
- Antzelevitch, C. (2005) 'Cardiac Repolarization. the Long and Short of It'. *EP Europace* 7 (s2), S3-S9
- Anversa, P., Hiler, B., Ricci, R., Guideri, G., and Olivetti, G. (1986) 'Myocyte Cell Loss and Myocyte Hypertrophy in the Aging Rat Heart'. *Journal of the American College of Cardiology* 8 (6), 1441-1448
- Arany, Z., He, H., Lin, J., Hoyer, K., Handschin, C., Toka, O., Ahmad, F., Matsui, T., Chin, S., and Wu, P. (2005) 'Transcriptional Coactivator PGC-1 $\alpha$  Controls the Energy State and Contractile Function of Cardiac Muscle'. *Cell Metabolism* 1 (4), 259-271
- Aronne and Segal (2002) 'Adiposity and Fat Distribution Outcome Measures: Assessment and Clinical Implications'. *Obesity* 10 (s11), 14S
- Aurigemma, G. P., de Simone, G., and Fitzgibbons, T. P. (2013) 'Cardiac Remodeling in Obesity'. *Circulation: Cardiovascular Imaging* 6 (1), 142-152
- Avelar, E., Cloward, T. V., Walker, J. M., Farney, R. J., Strong, M., Pendleton, R. C., Segerson, N., Adams, T. D., Gress, R. E., and Hunt, S. C. (2007) 'Left Ventricular Hypertrophy in Severe Obesity: Interactions among Blood Pressure, Nocturnal Hypoxemia, and Body Mass'. *Hypertension* 49 (1), 34-39
- Averin, A. S., Zakharova, N. M., Ignat'ev, D. A., Tarlachkov, S. V., and Nakipova, O. V. (2010) 'Effect of Isoproterenol on Contractility of the Heart Papillary Muscles of a Ground Squirrel'. *Biofizika* 55 (5), 910-917
- Avierinos, J., Tribouilloy, C., Grigioni, F., Suri, R., Barbieri, A., Michelena, H. I., Ionico, T., Rusinaru, D., Ansal di, S., and Habib, G. (2013) 'Impact of Ageing on Presentation and Outcome of Mitral Regurgitation due to Flail Leaflet: A Multicentre International Study'. *European Heart Journal* 34 (33), 2600-2609
- Baker, C. (2018) *Obesity Statistics*. United Kingdom: House of Commons Library
- Balderas-Villalobos, J., Molina-Muñoz, T., Mailloux-Salinas, P., Bravo, G., Carvajal, K., and Gómez-Viquez, N. L. (2013) 'Oxidative Stress in Cardiomyocytes Contributes to Decreased SERCA2a Activity in Rats with Metabolic Syndrome'. *American Journal of Physiology-Heart and Circulatory Physiology* 305 (9), H1344-H1353
- Ban, T., Sada, S., Takahashi, Y., Sada, H., and Fujita, T. (1985) 'Effects of Para-Substituted Beta-Adrenoceptor Blocking Agents and Methyl-Substituted Phenoxypropanolamine Derivatives on Maximum Upstroke Velocity of Action Potential in Guinea-Pig Papillary Muscles'. *Naunyn-Schmiedeberg's Archives of Pharmacology* 329 (1), 77-85

- Barazzoni, R. and Nair, K. S. (2001) 'Changes in Uncoupling Protein-2 and-3 Expression in Aging Rat Skeletal Muscle, Liver, and Heart'. *American Journal of Physiology-Endocrinology and Metabolism* 280 (3), E413-E419
- Barnes, L. A., Opitz, J. M., and Gilbert-Barnes, E. (2007) 'Obesity: Genetic, Molecular, and Environmental Aspects'. *American Journal of Medical Genetics Part A* 143 (24), 3016-3034
- Barrett, P., Mercer, J. G., and Morgan, P. J. (2016) 'Preclinical Models for Obesity Research'. *Disease Models & Mechanisms* 9 (11), 1245-1255
- Barton, G. P., Sepe, J. J., McKiernan, S. H., Aiken, J. M., and Diffie, G. M. (2016) 'Mitochondrial and Metabolic Gene Expression in the Aged Rat Heart'. *Frontiers in Physiology* 7, 352
- Basford, J. R. (2002) 'The Law of Laplace and its Relevance to Contemporary Medicine and Rehabilitation'. *Archives of Physical Medicine and Rehabilitation* 83 (8), 1165-1170
- Bass, J. J., Wilkinson, D. J., Rankin, D., Phillips, B. E., Szewczyk, N. J., Smith, K., and Atherton, P. J. (2017) 'An Overview of Technical Considerations for Western Blotting Applications to Physiological Research'. *Scandinavian Journal of Medicine & Science in Sports* 27 (1), 4-25
- Belin, R. J., Sumandea, M. P., Allen, E. J., Schoenfelt, K., Wang, H., Solaro, R. J., and de Tombe, P. P. (2007) 'Augmented Protein Kinase C-Alpha-Induced Myofilament Protein Phosphorylation Contributes to Myofilament Dysfunction in Experimental Congestive Heart Failure'. *Circulation Research* 101 (2), 195-204
- Bell, R. M., Mocanu, M. M., and Yellon, D. M. (2011) 'Retrograde Heart Perfusion: The Langendorff Technique of Isolated Heart Perfusion'. *Journal of Molecular and Cellular Cardiology* 50 (6), 940-950
- Bellanti, F., Romano, A. D., Giudetti, A. M., Rollo, T., Blonda, M., Tamborra, R., Vendemiale, G., and Serviddio, G. (2013a) 'Many Faces of Mitochondrial Uncoupling during Age: Damage Or Defense?'. *Journals of Gerontology Series A: Biomedical Sciences and Medical Sciences* 68 (8), 892-902
- Ben-Haim, M. S., Kanfi, Y., Mitchell, S. J., Maoz, N., Vaughan, K. L., Amariglio, N., Lerrer, B., De Cabo, R., Rechavi, G., and Cohen, H. Y. (2017) 'Breaking the Ceiling of Human Maximal Life Span'. *The Journals of Gerontology: Series A* 73 (11), 1465-1471
- Berdeaux, A. and Giudicelli, J. (1982) 'Intrinsic Sympathomimetic Activity and Coronary Blood Flow.'. *British Journal of Clinical Pharmacology* 13 (S2)
- Bergman, H., Ferrucci, L., Guralnik, J., Hogan, D. B., Hummel, S., Karunanathan, S., and Wolfson, C. (2007) 'Frailty: An Emerging Research and Clinical Paradigm--Issues and Controversies'. *The Journals of Gerontology. Series A, Biological Sciences and Medical Sciences* 62 (7), 731-737

- Berkalp, Cesur, V., Corapcioglu, D., Erol, C., and Baskal, N. (1995) 'Obesity and Left Ventricular Diastolic Dysfunction'. *International Journal of Cardiology* 52 (1), 23-26
- Berry, W. and McKenzie, C. (2010) 'Use of Inotropes in Critical Care'. *Clinical Pharmacist* 2, 395
- Bers, D. M. (2008) 'Calcium Cycling and Signaling in Cardiac Myocytes'. *Annu.Rev.Physiol.* 70, 23-49
- Bers, D. M. (2000) 'Calcium Fluxes Involved in Control of Cardiac Myocyte Contraction'. *Circulation Research* 87 (4), 275-281
- Betts, DeSaix, P., Johnson, E., Johnson, J. E., Korol, O., Kruse, D. H., Poe, B., Wise, J. A., and Young, K. A. (2014) 'Anatomy and Physiology'
- BHF (2020) *CVD Statistics - BHF UK Factsheet* [online] available from <https://www.bhf.org.uk/what-we-do/our-research/heart-statistics> [2020]
- Bieche, I., Narjoz, C., Asselah, T., Vacher, S., Marcellin, P., Lidereau, R., Beaune, P., and de Waziers, I. (2007) 'Reverse Transcriptase-PCR Quantification of mRNA Levels from Cytochrome (CYP) 1, CYP2 and CYP3 Families in 22 Different Human Tissues'. *Pharmacogenetics and Genomics* 17 (9), 731-742
- Biernacka, A. and Frangogiannis, N. G. (2011) 'Aging and Cardiac Fibrosis'. *Aging and Disease* 2 (2), 158-173
- Birbrair, A., Zhang, T., Wang, Z., Messi, M. L., Enikolopov, G. N., Mintz, A., and Delbono, O. (2013) 'Role of Pericytes in Skeletal Muscle Regeneration and Fat Accumulation'. *Stem Cells and Development* 22 (16), 2298-2314
- Bitto, A., Wang, A. M., Bennett, C. F., and Kaerberlein, M. (2015) 'Biochemical Genetic Pathways that Modulate Aging in Multiple Species'. *Cold Spring Harbor Perspectives in Medicine* 5 (11), 10.1101/cshperspect.a025114
- Bodi, I., Mikala, G., Koch, S. E., Akhter, S. A., and Schwartz, A. (2005) 'The L-Type Calcium Channel in the Heart: The Beat Goes On'. *The Journal of Clinical Investigation* 115 (12), 3306-3317
- Borgers, M. and Ven, M. (1989) 'Mode of Action of Itraconazole: Morphological Aspects'. *Mycoses* 32 (s1), 53-59
- Boudina, Han, Y. H., Pei, S., Tidwell, T. J., Henrie, B., Tuinei, J., Olsen, C., Sena, S., and Abel, E. D. (2012) 'UCP3 Regulates Cardiac Efficiency and Mitochondrial Coupling in High Fat-Fed Mice but Not in Leptin-Deficient Mice'. *Diabetes* 61 (12), 3260-3269
- Boudina, Sena, S., Theobald, H., Sheng, X., Wright, J. J., Hu, X. X., Aziz, S., Johnson, J. I., Bugger, H., Zaha, V. G., and Abel, E. D. (2007) 'Mitochondrial Energetics in the Heart in Obesity-Related Diabetes: Direct Evidence for Increased Uncoupled Respiration and Activation of Uncoupling Proteins'. *Diabetes* 56 (10), 2457-2466

- Boudina and Abel (2006) 'Mitochondrial Uncoupling: A Key Contributor to Reduced Cardiac Efficiency in Diabetes'. *Physiology* 21 (4), 250-258
- Boudina, Sena, S., O'Neill, B., Tathireddy, P., Young, M., and Abel, E. (2005) 'Reduced Mitochondrial Oxidative Capacity and Increased Mitochondrial Uncoupling Impair Myocardial Energetics in Obesity' 112 (17), 2686
- Brand, M. D. and Esteves, T. C. (2005) 'Physiological Functions of the Mitochondrial Uncoupling Proteins UCP2 and UCP3'. *Cell Metabolism* 2 (2), 85-93
- Bristow, M. R., Ginsburg, R., Umans, V., Fowler, M., Minobe, W., Rasmussen, R., Zera, P., Menlove, R., Shah, P., and Jamieson, S. (1986) 'Beta 1- and Beta 2-Adrenergic-Receptor Subpopulations in Nonfailing and Failing Human Ventricular Myocardium: Coupling of both Receptor Subtypes to Muscle Contraction and Selective Beta 1-Receptor Down-Regulation in Heart Failure'. *Circulation Research* 59 (3), 297-309
- Brooks, W. W. and Conrad, C. H. (2009) 'Isoproterenol-Induced Myocardial Injury and Diastolic Dysfunction in Mice: Structural and Functional Correlates'. *Comparative Medicine* 59 (4), 339-343
- Buchanan, J., Mazumder, P. K., Hu, P., Chakrabarti, G., Roberts, M. W., Yun, U. J., Cooksey, R. C., Litwin, S. E., and Abel, E. D. (2005) 'Reduced Cardiac Efficiency and Altered Substrate Metabolism Precedes the Onset of Hyperglycemia and Contractile Dysfunction in Two Mouse Models of Insulin Resistance and Obesity'. *Endocrinology* 146 (12), 5341-5349
- Burnette, W. N. (1981) "'Western Blotting": Electrophoretic Transfer of Proteins from Sodium Dodecyl Sulfate--Polyacrylamide Gels to Unmodified Nitrocellulose and Radiographic Detection with Antibody and Radioiodinated Protein A'. *Analytical Biochemistry* 112 (2), 195-203
- Burns, K. A. and Heuvel, J. P. V. (2007) 'Modulation of PPAR Activity Via Phosphorylation'. *Biochimica Et Biophysica Acta (BBA)-Molecular and Cell Biology of Lipids* 1771 (8), 952-960
- Bussey, C. T., Thaug, H. A., Hughes, G., Bahn, A., and Lamberts, R. R. (2018) 'Cardiac B-adrenergic Responsiveness of Obese Zucker Rats: The Role of AMPK'. *Experimental Physiology* 103 (8), 1067-1075
- Calvo, S. E., Pagliarini, D. J., and Mootha, V. K. (2009) 'Upstream Open Reading Frames Cause Widespread Reduction of Protein Expression and are Polymorphic among Humans'. *Proceedings of the National Academy of Sciences of the United States of America* 106 (18), 7507-7512
- Camici, G. G., Savarese, G., Akhmedov, A., and Lüscher, T. F. (2015) 'Molecular Mechanism of Endothelial and Vascular Aging: Implications for Cardiovascular Disease'. *European Heart Journal* 36 (48), 3392-3403

- Campbell, F. M., Kozak, R., Wagner, A., Altarejos, J. Y., Dyck, J. R., Belke, D. D., Severson, D. L., Kelly, D. P., and Lopaschuk, G. D. (2002) 'A Role for Peroxisome Proliferator-Activated Receptor Alpha (PPARalpha ) in the Control of Cardiac Malonyl-CoA Levels: Reduced Fatty Acid Oxidation Rates and Increased Glucose Oxidation Rates in the Hearts of Mice Lacking PPARalpha are Associated with Higher Concentrations of Malonyl-CoA and Reduced Expression of Malonyl-CoA Decarboxylase'. *The Journal of Biological Chemistry* 277 (6), 4098-4103
- Capasso, J. M., Malhotra, A., Scheuer, J., and Sonnenblick, E. H. (1986) 'Myocardial Biochemical, Contractile, and Electrical Performance After Imposition of Hypertension in Young and Old Rats'. *Circulation Research* 58 (4), 445-460
- Capasso, J. M., Malhotra, A., Remily, R. M., Scheuer, J., and Sonnenblick, E. H. (1983) 'Effects of Age on Mechanical and Electrical Performance of Rat Myocardium'. *The American Journal of Physiology* 245 (1), H72-81
- Capitanio, D., Leone, R., Fania, C., Torretta, E., and Gelfi, C. (2016) 'Sprague Dawley Rats: A Model of Successful Heart Aging'. *EuPA Open Proteomics* 12, 22-30
- Carbone, S., Lavie, C. J., Elagizi, A., Arena, R., and Ventura, H. O. (2020) *The Impact of Obesity in Heart Failure* [online] . available from <<http://www.sciencedirect.com/science/article/pii/S1551713619300923>>
- Carillion, Feldman, S., Jiang, C., Atassi, F., Na, N., Mougenot, N., Besse, S., Hulot, J., Riou, B., and Amour, J. (2015) 'Overexpression of Cyclic Adenosine Monophosphate Effluent Protein MRP4 Induces an Altered Response to B-Adrenergic Stimulation in the Senescent Rat Heart'. *Anesthesiology: The Journal of the American Society of Anesthesiologists* 122 (2), 334-342
- Carlberg, B., Samuelsson, O., and Lindholm, L. H. (2004) 'Atenolol in Hypertension: Is it a Wise Choice?'. *The Lancet* 364 (9446), 1684-1689
- Carroll, J. F., Jones, A. E., Hester, R. L., Reinhart, G. A., Cockrell, K., and Mizelle, H. L. (1997) 'Reduced Cardiac Contractile Responsiveness to Isoproterenol in Obese Rabbits'. *Hypertension* 30 (6), 1376-1381
- Cassambai, S., Mee, C. J., Renshaw, D., and Hussain, A. (2019) 'Tiotropium Bromide, a Long Acting Muscarinic Receptor Antagonist Triggers Intracellular Calcium Signalling in the Heart'. *Toxicology and Applied Pharmacology*, 114778
- Ceesay, M. M., Couchman, L., Smith, M., Wade, J., Flanagan, R. J., and Pagliuca, A. (2016) 'Triazole Antifungals used for Prophylaxis and Treatment of Invasive Fungal Disease in Adult Haematology Patients: Trough Serum Concentrations in Relation to Outcome'. *Medical Mycology* 54 (7), 691-698
- Chakravarti, B., Oseguera, M., Dalal, N., Fathy, P., Mallik, B., Raval, A., and Chakravarti, D. N. (2008) 'Proteomic Profiling of Aging in the Mouse Heart: Altered Expression of Mitochondrial Proteins'. *Archives of Biochemistry and Biophysics* 474 (1), 22-31

- Chambers, K. T., Leone, T. C., Sambandam, N., Kovacs, A., Wagg, C. S., Lopaschuk, G. D., Finck, B. N., and Kelly, D. P. (2011) 'Chronic Inhibition of Pyruvate Dehydrogenase in Heart Triggers an Adaptive Metabolic Response'. *The Journal of Biological Chemistry* 286 (13), 11155-11162
- Chaudhary, K. R., Zordoky, B. N., Edin, M. L., Alsaleh, N., El-Kadi, A. O., Zeldin, D. C., and Seubert, J. M. (2013) 'Differential Effects of Soluble Epoxide Hydrolase Inhibition and CYP2J2 Overexpression on Postischemic Cardiac Function in Aged Mice'. *Prostaglandins & Other Lipid Mediators* 104, 8-17
- Chaudhary, K. R., Batchu, S. N., and Seubert, J. M. (2009) 'Cytochrome P450 Enzymes and the Heart'. *IUBMB Life* 61 (10), 954-960
- Chauhan, R., Coote, J., Allen, E., Pongpaopattanakul, P., Brack, K. E., and Ng, G. A. (2018) 'Functional Selectivity of Cardiac Preganglionic Sympathetic Neurons in the Rabbit Heart'. *International Journal of Cardiology* 264, 70-78
- Chehal, M. K. and Granville, D. J. (2006) 'Cytochrome p450 2C (CYP2C) in Ischemic Heart Injury and Vascular Dysfunction'. *Canadian Journal of Physiology and Pharmacology* 84 (1), 15-20
- Chen, N., Zhou, M., Yang, M., Guo, J., Zhu, C., Yang, J., Wang, Y., Yang, X., and He, L. (2010) 'Calcium Channel Blockers Versus Other Classes of Drugs for Hypertension'. *The Cochrane Library*
- Chen, M. A. (2015) 'Frailty and Cardiovascular Disease: Potential Role of Gait Speed in Surgical Risk Stratification in Older Adults'. *Journal of Geriatric Cardiology : JGC* 12 (1), 44-56
- Cheng, Y., Wan, X., McElfresh, T. A., Chen, X., Gresham, K. S., Rosenbaum, D. S., Chandler, M. P., and Stelzer, J. E. (2013) 'Impaired Contractile Function due to Decreased Cardiac Myosin Binding Protein C Content in the Sarcomere'. *American Journal of Physiology-Heart and Circulatory Physiology* 305 (1), H52-H65
- Cheng, S., Fernandes, V. R., Bluemke, D. A., McClelland, R. L., Kronmal, R. A., and Lima, J. A. (2009) 'Age-Related Left Ventricular Remodeling and Associated Risk for Cardiovascular Outcomes: The Multi-Ethnic Study of Atherosclerosis'. *Circulation. Cardiovascular Imaging* 2 (3), 191-198
- Choksi, K. B. and Papaconstantinou, J. (2008) 'Age-Related Alterations in Oxidatively Damaged Proteins of Mouse Heart Mitochondrial Electron Transport Chain Complexes'. *Free Radical Biology and Medicine* 44 (10), 1795-1805
- Christoffersen, C., Bollano, E., Lindegaard, M. L., Bartels, E. D., Goetze, J. P., Andersen, C. B., and Nielsen, L. B. (2003) 'Cardiac Lipid Accumulation Associated with Diastolic Dysfunction in Obese Mice'. *Endocrinology* 144 (8), 3483-3490
- Chuffa, Luiz Gustavo de Almeida and Seiva, F. R. F. (2013) 'Combined Effects of Age and Diet-Induced Obesity on Biochemical Parameters and Cardiac Energy Metabolism in Rats'

- Chung, S., Arrell, D. K., Faustino, R. S., Terzic, A., and Dzeja, P. P. (2010) 'Glycolytic Network Restructuring Integral to the Energetics of Embryonic Stem Cell Cardiac Differentiation'. *Journal of Molecular and Cellular Cardiology* 48 (4), 725-734
- Cleary, J. D. and Stover, K. R. (2015) 'Antifungal-Associated Drug-Induced Cardiac Disease'. *Clinical Infectious Diseases* 61 (suppl\_6), S662-S668
- Cleary, J. D., Stover, K. R., Farley, J., Daley, W., Kyle, P. B., and Hosler, J. (2013) 'Cardiac Toxicity of Azole Antifungals'
- Cnop, M., Foufelle, F., and Velloso, L. A. (2012) 'Endoplasmic Reticulum Stress, Obesity and Diabetes'. *Trends in Molecular Medicine* 18 (1), 59-68
- Coelho, M., Oliveira, T., and Fernandes, R. (2013) 'Biochemistry of Adipose Tissue: An Endocrine Organ'. *Archives of Medical Science : AMS* 9 (2), 191-200
- Cohen, M. L., Bloomquist, W., Kriauciunas, A., Shuker, A., and Calligaro, D. (1999) 'Aryl Propanolamines: Comparison of Activity at Human B3 Receptors, Rat B3 Receptors and Rat Atrial Receptors Mediating Tachycardia'. *British Journal of Pharmacology* 126 (4), 1018-1024
- Cooley, D. A. (2010) 'Review of Carpentier's Reconstructive Valve Surgery: From Valve Analysis to Valve Reconstruction'. *Texas Heart Institute Journal* 37 (3), 382
- Cooper, G., 4th, Satava, R. M., Jr, Harrison, C. E., and Coleman, H. N., 3rd (1973) 'Mechanisms for the Abnormal Energetics of Pressure-Induced Hypertrophy of Cat Myocardium'. *Circulation Research* 33 (2), 213-223
- Corbi, G., Conti, V., Russomanno, G., Longobardi, G., Furgi, G., Filippelli, A., and Ferrara, N. (2013) 'Adrenergic Signaling and Oxidative Stress: A Role for Sirtuins?'. *Frontiers in Physiology* 4, 324
- Correia, A. S., Pinho, T., Madureira, A. J., Araujo, V., and Maciel, M. J. (2013) 'Isolated Papillary Muscle Hypertrophy: A Variant of Hypertrophic Cardiomyopathy, but further Evidences are Still Needed: Reply'. *European Heart Journal—Cardiovascular Imaging* 14 (8), 827-828
- Cove, C. J., Widman, S. C., Liang, C., Schenk, E. A., and Hood, W. B. (1995) 'Dobutamine Effects on Systole and Diastole in Rats with Myocardial Infarction'. *The American Journal of the Medical Sciences* 309 (1), 5-12
- Crane, J. D., Devries, M. C., Safdar, A., Hamadeh, M. J., and Tarnopolsky, M. A. (2010) 'The Effect of Aging on Human Skeletal Muscle Mitochondrial and Intramyocellular Lipid Ultrastructure'. *Journals of Gerontology Series A: Biomedical Sciences and Medical Sciences* 65 (2), 119-128
- Crewe, C., Kinter, M., and Szweda, L. I. (2013) 'Rapid Inhibition of Pyruvate Dehydrogenase: An Initiating Event in High Dietary Fat-Induced Loss of Metabolic Flexibility in the Heart'. *PloS One* 8 (10), e77280

- Crimmins, E. M. (2015) 'Lifespan and Healthspan: Past, Present, and Promise'. *The Gerontologist* 55 (6), 901-911
- Crow, Mani, K., Nam, Y., and Kitsis, R. N. (2004) 'The Mitochondrial Death Pathway and Cardiac Myocyte Apoptosis'. *Circulation Research* 95 (10), 957-970
- Csiszar, A., Wang, M., Lakatta, E. G., and Ungvari, Z. (2008) 'Inflammation and Endothelial Dysfunction during Aging: Role of NF-kappaB'. *Journal of Applied Physiology (Bethesda, Md.: 1985)* 105 (4), 1333-1341
- Davis, J. P. and Tikunova, S. B. (2008) 'Ca(2+) Exchange with Troponin C and Cardiac Muscle Dynamics'. *Cardiovascular Research* 77 (4), 619-626
- Dawson, D., Lygate, C., Zhang, M., Hulbert, K., Neubauer, S., and Casadei, B. (2005) 'nNOS Gene Deletion Exacerbates Pathological Left Ventricular Remodelling and Functional Deterioration After Myocardial Infarction'
- De Lucia, C., Eguchi, A., and Koch, W. J. (2018) 'New Insights in Cardiac B-Adrenergic Signaling during Heart Failure and Aging'. *Frontiers in Pharmacology* 9, 904
- Dewey, S., Lai, X., Witzmann, F. A., Sohal, M., and Gomes, A. V. (2013) 'Proteomic Analysis of Hearts from Akita Mice Suggests that Increases in Soluble Epoxide Hydrolase and Antioxidative Programming are Key Changes in Early Stages of Diabetic Cardiomyopathy'. *Journal of Proteome Research* 12 (9), 3920-3933
- DeWitt, E. S., Black, K. J., Thiagarajan, R. R., DiNardo, J. A., Colan, S. D., McGowan, F. X., and Kheir, J. N. (2016) 'Effects of Commonly used Inotropes on Myocardial Function and Oxygen Consumption Under Constant Ventricular Loading Conditions'. *Journal of Applied Physiology* 121 (1), 7-14
- Dhingra, R. and Vasan, R. S. (2012) 'Age as a Risk Factor'. *Medical Clinics of North America* 96 (1), 87-91
- Di Lisa, F. and Bernardi, P. (2006) 'Mitochondria and Ischemia-reperfusion Injury of the Heart: Fixing a Hole'. *Cardiovascular Research* 70 (2), 191-199
- DiNicolantonio, J. J., Fares, H., Niazi, A. K., Chatterjee, S., D'Ascenzo, F., Cerrato, E., Biondi-Zoccai, G., Lavie, C. J., Bell, D. S., and O'Keefe, J. H. (2015) 'B-Blockers in Hypertension, Diabetes, Heart Failure and Acute Myocardial Infarction: A Review of the Literature'. *Open Heart* 2 (1), e000230
- Dobson, J. G., Jr, Fenton, R. A., and Romano, F. D. (1990) 'Increased Myocardial Adenosine Production and Reduction of Beta-Adrenergic Contractile Response in Aged Hearts'. *Circulation Research* 66 (5), 1381-1390
- Dodd, M. S., Fialho, Maria da Luz Sousa, Aparicio, C. N. M., Kerr, M., Timm, K. N., Griffin, J. L., Luiken, J. J., Glatz, J. F., Tyler, D. J., and Heather, L. C. (2018) 'Fatty Acids Prevent Hypoxia-Inducible Factor-1 $\alpha$  Signaling through Decreased Succinate in Diabetes'. *JACC: Basic to Translational Science* 3 (4), 485-498

- Domeier, T. L., Roberts, C. J., Gibson, A. K., Hanft, L. M., McDonald, K. S., and Segal, S. S. (2014) 'Dantrolene Suppresses Spontaneous Ca<sup>2+</sup> Release without Altering Excitation-Contraction Coupling in Cardiomyocytes of Aged Mice'. *American Journal of Physiology-Heart and Circulatory Physiology* 307 (6), H818-H829
- Domenighetti, A. A., Wang, Q., Egger, M., Richards, S. M., Pedrazzini, T., and Delbridge, L. M. (2005) 'Angiotensin II-mediated Phenotypic Cardiomyocyte Remodeling Leads to Age-Dependent Cardiac Dysfunction and Failure'. *Hypertension* 46 (2), 426-432
- Dong, Zhang, X., and Ren, J. (2006) 'Leptin Regulates Cardiomyocyte Contractile Function through Endothelin-1 receptor-NADPH Oxidase Pathway'. *Hypertension* 47 (2), 222-229
- Dong, Zhang, X., Yang, X., Esberg, L. B., Yang, H., Zhang, Z., Culver, B., and Ren, J. (2006) 'Impaired Cardiac Contractile Function in Ventricular Myocytes from Leptin-Deficient Ob/Ob Obese Mice'. *The Journal of Endocrinology* 188 (1), 25-36
- Driscoll, D. J., Gillette, P. C., Lewis, R. M., Hartley, C. J., Schwartz, A., and Dunn, F. (1979) 'Comparative Hemodynamic Effects of Isoproterenol, Dopamine, and Dobutamine in the Newborn Dog'. *Pediatric Research* 13 (9), 1006-1009
- Drolet, B., Pilote, S., Galinas, C., Kamaliza, A., Blais-Boilard, A., Virgili, J., Patoine, D., and Simard, C. (2017) 'Altered Protein Expression of Cardiac CYP2J and Hepatic CYP2C, CYP4A, and CYP4F in a Mouse Model of Type II Diabetes—A Link in the Onset and Development of Cardiovascular Disease?'. *Pharmaceutics* 9 (4), 44
- Drosatos (2016) 'Fatty Old Hearts: Role of Cardiac Lipotoxicity in Age-Related Cardiomyopathy'. *Pathobiology of Aging & Age-Related Diseases* 6 (1), 32221
- Drosatos and Schulze (2013) 'Cardiac Lipotoxicity: Molecular Pathways and Therapeutic Implications'. *Current Heart Failure Reports* 10 (2), 109-121
- Drosatos, Bharadwaj, K. G., Lymperopoulos, A., Ikeda, S., Khan, R., Hu, Y., Agarwal, R., Yu, S., Jiang, H., Steinberg, S. F., Blaner, W. S., Koch, W. J., and Goldberg, I. J. (2011) 'Cardiomyocyte Lipids Impair Beta-Adrenergic Receptor Function Via PKC Activation'. *American Journal of Physiology. Endocrinology and Metabolism* 300 (3), E489-99
- Durand, M. J., Ait-Aissa, K., and Gutterman, D. D. (2017) 'Regenerative Angiogenesis: Quality Over Quantity'. *Circulation Research* 120 (9), 1379-1380
- Echtay, K. S., Roussel, D., St-Pierre, J., Jekabsons, M. B., Cadenas, S., Stuart, J. A., Harper, J. A., Roebuck, S. J., Morrison, A., and Pickering, S. (2002) 'Superoxide Activates Mitochondrial Uncoupling Proteins'. *Nature* 415 (6867), 96
- Eckel, R. H., Grundy, S. M., and Zimmet, P. Z. (2005) 'The Metabolic Syndrome'. *The Lancet* 365 (9468), 1415-1428

- Edwards, M. G., Anderson, R. M., Yuan, M., Kendzierski, C. M., Weindruch, R., and Prolla, T. A. (2007) 'Gene Expression Profiling of Aging Reveals Activation of a p53-Mediated Transcriptional Program'. *BMC Genomics* 8 (1), 80
- Edwards, M. G., Sarkar, D., Klopp, R., Morrow, J. D., Weindruch, R., and Prolla, T. A. (2003) 'Age-Related Impairment of the Transcriptional Responses to Oxidative Stress in the Mouse Heart'. *Physiological Genomics* 13 (2), 119-127
- Eisner, D. A., Caldwell, J. L., Kistamás, K., and Trafford, A. W. (2017) 'Calcium and Excitation-Contraction Coupling in the Heart'. *Circulation Research* 121 (2), 181-195
- Eizirik, D. L., Cardozo, A. K., and Cnop, M. (2008) 'The Role for Endoplasmic Reticulum Stress in Diabetes Mellitus'. *Endocrine Reviews* 29 (1), 42-61
- Elmore, S. P., Qian, T., Grissom, S. F., and Lemasters, J. J. (2001) 'The Mitochondrial Permeability Transition Initiates Autophagy in Rat Hepatocytes'. *The FASEB Journal* 15 (12), 2286-2287
- Elsen, M., Raschke, S., and Eckel, J. (2014) 'Browning of White Fat: Does Irisin Play a Role in Humans?'. *The Journal of Endocrinology* 222 (1), R25-38
- Engelhardt, S., Hein, L., Wiesmann, F., and Lohse, M. J. (1999) 'Progressive Hypertrophy and Heart Failure in Beta1-Adrenergic Receptor Transgenic Mice'. *Proceedings of the National Academy of Sciences of the United States of America* 96 (12), 7059-7064
- Engvall, E., Jonsson, K., and Perlmann, P. (1971) 'Enzyme-Linked Immunosorbent Assay. II. Quantitative Assay of Protein Antigen, Immunoglobulin G, by Means of Enzyme-Labelled Antigen and Antibody-Coated Tubes'. *Biochimica Et Biophysica Acta (BBA)-Protein Structure* 251 (3), 427-434
- Fannin, J., Rice, K. M., Thulluri, S., Dornon, L., Arvapalli, R. K., Wehner, P., and Blough, E. R. (2014) 'Age-Associated Alterations of Cardiac Structure and Function in the Female F344xBN Rat Heart'. *Age* 36 (4), 9684
- Farrell, S. R. and Howlett, S. E. (2008a) 'The Age-Related Decrease in Catecholamine Sensitivity is Mediated by  $\beta$ 1-Adrenergic Receptors Linked to a Decrease in Adenylate Cyclase Activity in Ventricular Myocytes from Male Fischer 344 Rats'. *Mechanisms of Ageing and Development* 129 (12), 735-744
- Farrell, S. R. and Howlett, S. E. (2007) 'The Effects of Isoproterenol on Abnormal Electrical and Contractile Activity and Diastolic Calcium are Attenuated in Myocytes from Aged Fischer 344 Rats'. *Mechanisms of Ageing and Development* 128 (10), 566-573
- Feridooni, Kane, A. E., Ayaz, O., Boroumandi, A., Polidovitch, N., Tsushima, R. G., Rose, R. A., and Howlett, S. E. (2017) 'The Impact of Age and Frailty on Ventricular Structure and Function in C57BL/6J Mice'. *The Journal of Physiology* 595 (12), 3721-3742
- Feridooni, Dibb, K. M., and Howlett, S. E. (2015) 'How Cardiomyocyte Excitation, Calcium Release and Contraction Become Altered with Age'. *Journal of Molecular and Cellular Cardiology* 83, 62-72

- Feridooni, H. A., Sun, M. H., Rockwood, K., and Howlett, S. E. (2014) 'Reliability of a Frailty Index Based on the Clinical Assessment of Health Deficits in Male C57BL/6J Mice'. *Journals of Gerontology Series A: Biomedical Sciences and Medical Sciences* 70 (6), 686-693
- Ferrara, N., Komici, K., Corbi, G., Pagano, G., Furgi, G., Rengo, C., Femminella, G. D., Leosco, D., and Bonaduce, D. (2014) 'B-Adrenergic Receptor Responsiveness in Aging Heart and Clinical Implications'. *Frontiers in Physiology* 4, 396
- Ferri, C., Bellini, C., Desideri, G., Baldoncini, R., Properzi, G., Santucci, A., and De Mattia, G. (1997) 'Circulating Endothelin-1 Levels in Obese Patients with the Metabolic Syndrome'. *Experimental and Clinical Endocrinology & Diabetes* 105 (S 02), 38-40
- Ferron, Jacobsen, B. B., Sant'Ana, P. G., de Campos, D. H., de Tomasi, L. C., Luvizotto Rde, A., Cicogna, A. C., Leopoldo, A. S., and Lima-Leopoldo, A. P. (2015) 'Cardiac Dysfunction Induced by Obesity is Not Related to Beta-Adrenergic System Impairment at the Receptor-Signalling Pathway'. *PloS One* 10 (9), e0138605
- Finck (2007) 'The PPAR Regulatory System in Cardiac Physiology and Disease'. *Cardiovascular Research* 73 (2), 269-277
- Finck, Han, X., Courtois, M., Aimond, F., Nerbonne, J. M., Kovacs, A., Gross, R. W., and Kelly, D. P. (2003) 'A Critical Role for PPARalpha-Mediated Lipotoxicity in the Pathogenesis of Diabetic Cardiomyopathy: Modulation by Dietary Fat Content'. *Proceedings of the National Academy of Sciences of the United States of America* 100 (3), 1226-1231
- Finck, Lehman, J. J., Leone, T. C., Welch, M. J., Bennett, M. J., Kovacs, A., Han, X., Gross, R. W., Kozak, R., and Lopaschuk, G. D. (2002) 'The Cardiac Phenotype Induced by PPAR $\alpha$  Overexpression Mimics that Caused by Diabetes Mellitus'. *The Journal of Clinical Investigation* 109 (1), 121-130
- Fleg, J. L., Aronow, W. S., and Frishman, W. H. (2011) 'Cardiovascular Drug Therapy in the Elderly: Benefits and Challenges'. *Nature Reviews Cardiology* 8 (1), 13-28
- Fleming, I., Michaelis, U. R., Bredenkötter, D., Fisslthaler, B., Dehghani, F., Brandes, R. P., and Busse, R. (2001) 'Endothelium-Derived Hyperpolarizing Factor Synthase (Cytochrome P450 2C9) is a Functionally Significant Source of Reactive Oxygen Species in Coronary Arteries'. *Circulation Research* 88 (1), 44-51
- Fletcher, S., Maddock, H., James, R. S., Wallis, R., and Gharanei, M. (2020) 'The Cardiac Work-Loop Technique: An in Vitro Model for Identifying and Profiling Drug-Induced Changes in Inotropy using Rat Papillary Muscles'. *Scientific Reports* 10 (1), 1-13
- Fleury Curado, T., Pho, H., Berger, S., Caballero-Eraso, C., Shin, M., Sennes, L. U., Pham, L., Schwartz, A. R., and Polotsky, V. Y. (2018) 'Sleep-Disordered Breathing in C57BL/6J Mice with Diet-Induced Obesity'. *Sleep* 41 (8), zsy089

- Follath, F., Cleland, J., Just, H., Papp, J., Scholz, H., Peuhkurinen, K., Harjola, V., Mitrovic, V., Abdalla, M., and Sandell, E. (2002) 'Efficacy and Safety of Intravenous Levosimendan Compared with Dobutamine in Severe Low-Output Heart Failure (the LIDO Study): A Randomised Double-Blind Trial'. *The Lancet* 360 (9328), 196-202
- Francis, G. A., Annicotte, J., and Auwerx, J. (2003) 'PPAR-A Effects on the Heart and Other Vascular Tissues'. *American Journal of Physiology-Heart and Circulatory Physiology* 285 (1), H1-H9
- Freemantle, N., Cleland, J., Young, P., Mason, J., and Harrison, J. (1999) 'Beta Blockade After Myocardial Infarction: Systematic Review and Meta Regression Analysis'. *BMJ (Clinical Research Ed.)* 318 (7200), 1730-1737
- Fried, L. P., Tangen, C. M., Walston, J., Newman, A. B., Hirsch, C., Gottdiener, J., Seeman, T., Tracy, R., Kop, W. J., Burke, G., McBurnie, M. A., and Cardiovascular Health Study Collaborative Research Group (2001) 'Frailty in Older Adults: Evidence for a Phenotype'. *The Journals of Gerontology.Series A, Biological Sciences and Medical Sciences* 56 (3), M146-56
- Froehlich, Lakatta, E., Beard, E., Spurgeon, H., Weisfeldt, M., and Gerstenblith, G. (1978) 'Studies of Sarcoplasmic Reticulum Function and Contraction Duration in Young Adult and Aged Rat Myocardium'. *Journal of Molecular and Cellular Cardiology* 10 (5), 427-438
- Fung, S. L., Chau, C. H., and Yew, W. W. (2008) 'Cardiovascular Adverse Effects during Itraconazole Therapy'. *The European Respiratory Journal* 32 (1), 240
- García, E. H., Perna, E. R., Farías, E. F., Obregón, R. O., Macin, S. M., Parras, J. I., Agüero, M. A., Moratorio, D. A., Pitzus, A. E., and Tassano, E. A. (2006) 'Reduced Systolic Performance by Tissue Doppler in Patients with Preserved and Abnormal Ejection Fraction: New Insights in Chronic Heart Failure'. *International Journal of Cardiology* 108 (2), 181-188
- Ghannoum, M. A. and Rice, L. B. (1999) 'Antifungal Agents: Mode of Action, Mechanisms of Resistance, and Correlation of these Mechanisms with Bacterial Resistance'. *Clinical Microbiology Reviews* 12 (4), 501-517
- Gharanei, M., Wallis, R., and Maddock, H. (2015) 'Validation of the Rat Papillary Work-Loop Assay to Assess Inotropic Drug Effects'. *Journal of Pharmacological and Toxicological Methods* (75), 177
- Gharanei, M., Hussain, A., James, R. S., Janneh, O., and Maddock, H. (2014a) 'Investigation into the Cardiotoxic Effects of Doxorubicin on Contractile Function and the Protection Afforded by Cyclosporin A using the Work-Loop Assay'. *Toxicology in Vitro* 28 (5), 722-731
- Gheorghiadu, M., Filippatos, G., and Felker, G. (2012) 'Diagnosis and Management of Acute Heart Failure Syndromes'. *Braunwald's Heart Disease: A Textbook of Cardiovascular Medicine.9th Ed.Philadelphia: Elsevier*, 517-542

- Gogiraju, R., Bochenek, M. L., and Schäfer, K. (2019) 'Angiogenic Endothelial Cell Signaling in Cardiac Hypertrophy and Heart Failure'. *Frontiers in Cardiovascular Medicine* 6, 20
- Goglia, F. and Skulachev, V. (2003) 'A Function for Novel Uncoupling Proteins: Antioxidant Defense of Mitochondrial Matrix by Translocating Fatty Acid Peroxides from the Inner to the Outer Membrane Leaflet.'. *FASEB Journal: Official Publication of the Federation of American Societies for Experimental Biology* 17 (12), 1585-1591
- Gómez, A., Sánchez-Roman, I., Gomez, J., Cruces, J., Mate, I., Lopez-Torres, M., Naudi, A., Portero-Otin, M., Pamplona, R., and De la Fuente, M. (2014) 'Lifelong Treatment with Atenolol Decreases Membrane Fatty Acid Unsaturation and Oxidative Stress in Heart and Skeletal Muscle Mitochondria and Improves Immunity and Behavior, without Changing Mice Longevity'. *Aging Cell* 13 (3), 551-560
- Gopal, K., Almutairi, M., Al Batran, R., Eaton, F., Gandhi, M., and Ussher, J. R. (2018) 'Cardiac-Specific Deletion of Pyruvate Dehydrogenase Impairs Glucose Oxidation Rates and Induces Diastolic Dysfunction'. *Frontiers in Cardiovascular Medicine* 5, 17
- Gorré, F. and Vandekerckhove, H. (2010) 'Beta-Blockers: Focus on Mechanism of Action'. *Acta Cardiologica* 65 (5), 565
- Goshovska, Y. V., Lisovyi, O. O., Shimanskaya, T. V., and Sagach, V. F. (2010) 'Changes in UCP2 and UCP3 Genes Expression, in Heart Function and Oxygen Cost of Myocardial Work Under Aging and Ischemia-Reperfusion'. *International Journal of Physiology and Pathophysiology* 1 (3)
- Gottlieb, S. S. (1989) 'The use of Antiarrhythmic Agents in Heart Failure: Implications of CAST'. *American Heart Journal* 118 (5 Pt 1), 1074-1077
- Green, P., Kodali, S., Leon, M. B., and Maurer, M. S. (2011) 'Echocardiographic Assessment of Pressure Volume Relations in Heart Failure and Valvular Heart Disease: Using Imaging to Understand Physiology'. *Minerva Cardioangiologica* 59 (4), 375-389
- Gregg, E. W. and Shaw, J. E. (2017) 'Global Health Effects of Overweight and Obesity'. *The New England Journal of Medicine* 377 (1), 80-81
- Grossman, E. and Messerli, F. H. (1998) 'Effect of Calcium Antagonists on Sympathetic Activity'. *European Heart Journal* 19 Suppl F, F27-31
- Guarente, L. and Kenyon, C. (2000) 'Genetic Pathways that Regulate Ageing in Model Organisms'. *Nature* 408 (6809), 255
- Guarnieri, T., Filburn, C., Zitnik, G., Roth, G., and Lakatta, E. (1980) 'Contractile and Biochemical Correlates of B-Adrenergic Stimulation of the Aged Heart'. *Am J Physiol* 239, H501-H508
- Gudmundsdottir, E., Benediksdottir, V. E., and Gudbjarnason, S. (1991) 'Combined Effects of Age and Dietary Fat on Beta 1-Receptors and Ca<sup>2+</sup> Channels in Rat Hearts'. *The American Journal of Physiology* 260 (1 Pt 2), H66-72

- Guellich, A., Damy, T., Conti, M., Claes, V., Samuel, J., Pineau, T., Lecarpentier, Y., and Coirault, C. (2013) 'Tempol Prevents Cardiac Oxidative Damage and Left Ventricular Dysfunction in the PPAR-A KO Mouse'. *American Journal of Physiology-Heart and Circulatory Physiology* 304 (11), H1505-H1512
- Guo, X., Yuan, S., Liu, Z., and Fang, Q. (2014) 'Oxidation-and CaMKII-Mediated Sarcoplasmic Reticulum Ca<sup>2</sup> Leak Triggers Atrial Fibrillation in Aging'. *Journal of Cardiovascular Electrophysiology* 25 (6), 645-652
- Guth, B. D., Chiang, A. Y., Doyle, J., Engwall, M. J., Guillon, J., Hoffmann, P., Koerner, J., Mittelstadt, S., Ottinger, S., and Pierson, J. B. (2015) 'The Evaluation of Drug-Induced Changes in Cardiac Inotropy in Dogs: Results from a HESI-Sponsored Consortium'. *Journal of Pharmacological and Toxicological Methods* 75, 70-90
- Hacker, T. A., McKiernan, S. H., Douglas, P. S., Wanagat, J., and Aiken, J. M. (2006) 'Age-Related Changes in Cardiac Structure and Function in Fischer 344 X Brown Norway Hybrid Rats'. *American Journal of Physiology.Heart and Circulatory Physiology* 290 (1), H304-11
- Haemmerle, G., Moustafa, T., Woelkart, G., Büttner, S., Schmidt, A., Van De Weijer, T., Hesselink, M., Jaeger, D., Kienesberger, P. C., and Zierler, K. (2011) 'ATGL-Mediated Fat Catabolism Regulates Cardiac Mitochondrial Function Via PPAR-A and PGC-1'. *Nature Medicine* 17 (9), 1076
- Haggerty, C. M., Mattingly, A. C., Kramer, S. P., Binkley, C. M., Jing, L., Suever, J. D., Powell, D. K., Charnigo, R. J., Epstein, F. H., and Fornwalt, B. K. (2015) 'Left Ventricular Mechanical Dysfunction in Diet-Induced Obese Mice is Exacerbated during Inotropic Stress: A Cine DENSE Cardiovascular Magnetic Resonance Study'. *Journal of Cardiovascular Magnetic Resonance* 17 (1), 75
- Hall, J. L., Stanley, W. C., Lopaschuk, G. D., Wisneski, J. A., Pizzurro, R. D., Hamilton, C. D., and McCormack, J. G. (1996) 'Impaired Pyruvate Oxidation but Normal Glucose Uptake in Diabetic Pig Heart during Dobutamine-Induced Work'. *The American Journal of Physiology* 271 (6 Pt 2), H2320-9
- Hamilton, W. (1953) 'The Physiology of the Cardiac Output'. *Circulation* 8 (527), 6STARR
- Hamlin, S. K., Villars, P. S., Kanusky, J. T., and Shaw, A. D. (2004) 'Role of Diastole in Left Ventricular Function, II: Diagnosis and Treatment'. *American Journal of Critical Care* 13 (6), 453-466
- Hasenfuss, G. and Teerlink, J. R. (2011) 'Cardiac Inotropes: Current Agents and Future Directions'. *European Heart Journal* 32 (15), 1838-1845
- Hasenfuss, G., Mulieri, L. A., Leavitt, B. J., Allen, P. D., Haeberle, J. R., and Alpert, N. R. (1992) 'Alteration of Contractile Function and Excitation-Contraction Coupling in Dilated Cardiomyopathy'. *Circulation Research* 70 (6), 1225-1232

- Hashimoto, H., Nakashima, M., and Sugino, N. (1983) 'Age-dependent Differences in the Positive Inotropic Effect of Phenylephrine on Rat Isolated Atria'. *British Journal of Pharmacology* 79 (2), 499-507
- Haslam, D. (2007) 'Obesity: A Medical History'. *Obesity Reviews* 8 (s1), 31-36
- Haycraft, J. B. and Paterson, D. R. (1896) 'The Time of Contraction of the Papillary Muscles'. *The Journal of Physiology* 19 (3), 262-265
- Heidenreich, P. A., Trogdon, J. G., Khavjou, O. A., Butler, J., Dracup, K., Ezekowitz, M. D., Finkelstein, E. A., Hong, Y., Johnston, S. C., and Khera, A. (2011) 'Forecasting the Future of Cardiovascular Disease in the United States: A Policy Statement from the American Heart Association'. *Circulation* 123 (8), 933-944
- Heller, L. J. and Whitehorn, W. V. (1972) 'Age-Associated Alterations in Myocardial Contractile Properties'. *The American Journal of Physiology* 222 (6), 1613-1619
- Henderson, K. A., Borders, R. B., Ross, J. B., Huwar, T. B., Travis, C. O., Wood, B. J., Ma, Z. J., Hong, S. P., Vinci, T. M., and Roche, B. M. (2013) 'Effects of Tyrosine Kinase Inhibitors on Rat Isolated Heart Function and Protein Biomarkers Indicative of Toxicity'. *Journal of Pharmacological and Toxicological Methods* 68 (1), 150-159
- Henry, T. D., Annex, B. H., McKendall, G. R., Azrin, M. A., Lopez, J. J., Giordano, F. J., Shah, P. K., Willerson, J. T., Benza, R. L., Berman, D. S., Gibson, C. M., Bajamonde, A., Rundle, A. C., Fine, J., McCluskey, E. R., and VIVA Investigators (2003) 'The VIVA Trial: Vascular Endothelial Growth Factor in Ischemia for Vascular Angiogenesis'. *Circulation* 107 (10), 1359-1365
- Hildebrand, S., Stümer, J., and Pfeifer, A. (2018) 'PVAT and its Relation to Brown, Beige, and White Adipose Tissue in Development and Function'. *Frontiers in Physiology* 9, 70
- Hilse, K. E., Rupprecht, A., Zimmermann, L., Egerbacher, M., Seiler Wulczyn, A. E., and Pohl, E. E. (2018) 'The Expression of Uncoupling Protein 3 Coincides with the Fatty Acid Oxidation Type of Metabolism in Adult Murine Heart.'. *Frontiers in Physiology* 9, 747
- Hilse, K. E., Kalinovich, A. V., Rupprecht, A., Smorodchenko, A., Zeitz, U., Staniek, K., Erben, R. G., and Pohl, E. E. (2016) 'The Expression of UCP3 Directly Correlates to UCP1 Abundance in Brown Adipose Tissue'. *Biochimica Et Biophysica Acta (BBA)-Bioenergetics* 1857 (1), 72-78
- Hirleman, Yu, and Larson (2008) 'Lusitropic Effects of Dobutamine in Young and Aged Mice in Vivo'. *The Journal of Extra-Corporeal Technology* 40 (1), 10-15
- Hoeks, J., van Baak, M. A., Hesselink, M. K., Hul, G. B., Vidal, H., Saris, W. H., and Schrauwen, P. (2003) 'Effect of B1-and B2-Adrenergic Stimulation on Energy Expenditure, Substrate Oxidation, and UCP3 Expression in Humans'. *American Journal of Physiology-Endocrinology and Metabolism* 285 (4), E775-E782

- Hoffman, B. B. (2001) 'Catecholamines, Sympathomimetic Drugs, & Adrenergic Receptor Antagonists'. *Goodman and Gilman's the Pharmacological Basis of Therapeutics*
- Hoffmann, C., Leitz, M., Oberdorf-Maass, S., Lohse, M., and Klotz, K. (2004) 'Comparative Pharmacology of Human B-Adrenergic Receptor Subtypes—characterization of Stably Transfected Receptors in CHO Cells'. *Naunyn-Schmiedeberg's Archives of Pharmacology* 369 (2), 151-159
- Hollands, C. (1986) 'The Animals (Scientific Procedures) Act 1986'. *The Lancet* 328 (8497), 32-33
- Holloway, G. P., Jain, S. S., Bezaire, V., Han, X. X., Glatz, J. F., Luiken, J. J., Harper, M., and Bonen, A. (2009) 'FAT/CD36-Null Mice Reveal that Mitochondrial FAT/CD36 is Required to Upregulate Mitochondrial Fatty Acid Oxidation in Contracting Muscle'. *American Journal of Physiology-Regulatory, Integrative and Comparative Physiology* 297 (4), R960-R967
- Holness, M. J., Kraus, A., Harris, R. A., and Sugden, M. C. (2000) 'Targeted Upregulation of Pyruvate Dehydrogenase Kinase (PDK)-4 in Slow-Twitch Skeletal Muscle Underlies the Stable Modification of the Regulatory Characteristics of PDK Induced by High-Fat Feeding'. *Diabetes* 49 (5), 775-781
- Holubarsch, C., Ruf, T., Goldstein, D. J., Ashton, R. C., Nickl, W., Pieske, B., Pioch, K., Lu" demann, J., Wiesner, S., and Hasenfuss, G. (1996) 'Existence of the Frank-Starling Mechanism in the Failing Human Heart: Investigations on the Organ, Tissue, and Sarcomere Levels'. *Circulation* 94 (4), 683-689
- Hom, J. R., Quintanilla, R. A., Hoffman, D. L., de Mesy Bentley, Karen L, Molkentin, J. D., Sheu, S., and Porter Jr, G. A. (2011) 'The Permeability Transition Pore Controls Cardiac Mitochondrial Maturation and Myocyte Differentiation'. *Developmental Cell* 21 (3), 469-478
- Ho-Pham, L. T., Lai, T. Q., Nguyen, M. T., and Nguyen, T. V. (2015) 'Relationship between Body Mass Index and Percent Body Fat in Vietnamese: Implications for the Diagnosis of Obesity'. *PloS One* 10 (5), e0127198
- HSE (2019) *Adult Obesity in England* [online] available from <<https://digital.nhs.uk/data-and-information/publications/statistical/health-survey-for-england/2017>> []
- Hua, Y., Zhang, Y., Ceylan-Isik, A. F., Wold, L. E., Nunn, J. M., and Ren, J. (2011) 'Chronic Akt Activation Accentuates Aging-Induced Cardiac Hypertrophy and Myocardial Contractile Dysfunction: Role of Autophagy'. *Basic Research in Cardiology* 106 (6), 1173-1191
- Huang, B., Gudi, R., Wu, P., Harris, R. A., Hamilton, J., and Popov, K. M. (1998) 'Isoenzymes of Pyruvate Dehydrogenase Phosphatase. DNA-Derived Amino Acid Sequences, Expression, and Regulation'. *The Journal of Biological Chemistry* 273 (28), 17680-17688

- Hurtaud, C., Gelly, C., Bouillaud, F., and Levi-Meyrueis, C. (2006) 'Translation Control of UCP2 Synthesis by the Upstream Open Reading Frame'. *Cellular and Molecular Life Sciences* 63 (15), 1780
- Huss, J. M. and Kelly, D. P. (2005) 'Mitochondrial Energy Metabolism in Heart Failure: A Question of Balance'. *The Journal of Clinical Investigation* 115 (3), 547-555
- Hyyti, O. M., Ledee, D., Ning, X., Ge, M., and Portman, M. A. (2010) 'Aging Impairs Myocardial Fatty Acid and Ketone Oxidation and Modifies Cardiac Functional and Metabolic Responses to Insulin in Mice'. *American Journal of Physiology-Heart and Circulatory Physiology* 299 (3), H868-H875
- Iemitsu, M., Miyauchi, T., Maeda, S., Tanabe, T., Takanashi, M., Irukayama-Tomobe, Y., Sakai, S., Ohmori, H., Matsuda, M., and Yamaguchi, I. (2002) 'Aging-Induced Decrease in the PPAR-A Level in Hearts is Improved by Exercise Training'. *American Journal of Physiology-Heart and Circulatory Physiology* 283 (5), H1750-H1760
- Ingwall, J. S. (2008) 'Energy Metabolism in Heart Failure and Remodelling'. *Cardiovascular Research* 81 (3), 412-419
- Izzo Jr, J. L. and Shykoff, B. E. (2001) 'Arterial Stiffness: Clinical Relevance, Measurement, and Treatment'. *Rev Cardiovasc Med* 2 (1), 29-40
- Jackson, S. J., Andrews, N., Ball, D., Bellantuono, I., Gray, J., Hachoumi, L., Holmes, A., Latcham, J., Petrie, A., and Potter, P. (2017) 'Does Age Matter? the Impact of Rodent Age on Study Outcomes'. *Laboratory Animals* 51 (2), 160-169
- Jacob, Dierberger, and Kissling (1992) 'Functional Significance of the Frank-Starling Mechanism Under Physiological and Pathophysiological Conditions'. *European Heart Journal* 13 (suppl\_E), 7-14
- Jalili, T., Manning, J., and Kim, S. (2003) 'Increased Translocation of Cardiac Protein Kinase C Beta2 Accompanies Mild Cardiac Hypertrophy in Rats Fed Saturated Fat'. *The Journal of Nutrition* 133 (2), 358-361
- Jamieson, K. L., Samokhvalov, V., Akhnokh, M. K., Lee, K., Cho, W. J., Takawale, A., Wang, X., Kassiri, Z., and Seubert, J. M. (2017) 'Genetic Deletion of Soluble Epoxide Hydrolase Provides Cardioprotective Responses Following Myocardial Infarction in Aged Mice'. *Prostaglandins & Other Lipid Mediators* 132, 47-58
- Jia, W., Li, Y. C., Zhu, Y. Q., Li, G. H., Zhou, Y. L., Zhang, D. R., Zhao, X. Y., and Gao, S. L. (2010) 'The Clinical Efficacy and Cardiac Safety of Itraconazole Injection in Treatment of Acute Pulmonary Invasive Fungal Infection in Chronic Pulmonary Diseases in the Elderly'. *Zhonghua Nei Ke Za Zhi* 49 (3), 230-233
- Jiang, C., Carillion, A., Na, N., De Jong, A., Feldman, S., Lacorte, J., Bonnefont-Rousselot, D., Riou, B., and Amour, J. (2015) 'Modification of the B-Adrenoceptor Stimulation Pathway in Zucker Obese and Obese Diabetic Rat Myocardium'. *Critical Care Medicine* 43 (7), e241-e249

- Jiang, M., Moffat, M., and Narayanan, N. (1993) 'Age-Related Alterations in the Phosphorylation of Sarcoplasmic Reticulum and Myofibrillar Proteins and Diminished Contractile Response to Isoproterenol in Intact Rat Ventricle'. *Circulation Research* 72 (1), 102-111
- Kahn, S. E., Hull, R. L., and Utzschneider, K. M. (2006) 'Mechanisms Linking Obesity to Insulin Resistance and Type 2 Diabetes'. *Nature* 444 (7121), 840-846
- Kahn, B. B. and Flier, J. S. (2000) 'Obesity and Insulin Resistance'. *The Journal of Clinical Investigation* 106 (4), 473-481
- Kane, A. E., Hilmer, S. N., Mach, J., Mitchell, S. J., de Cabo, R., and Howlett, S. E. (2016) 'Animal Models of Frailty: Current Applications in Clinical Research'. *Clinical Interventions in Aging* 11, 1519-1529
- Kar, D. and Bandyopadhyay, A. (2018) 'Targeting Peroxisome Proliferator Activated Receptor Alpha (PPAR Alpha) for the Prevention of Mitochondrial Impairment and Hypertrophy in Cardiomyocytes'. *Cellular Physiology and Biochemistry : International Journal of Experimental Cellular Physiology, Biochemistry, and Pharmacology* 49 (1), 245-259
- Karbowska, J., Kochan, Z., and Smolenski, R. T. (2003) 'Peroxisome Proliferator-Activated Receptor Alpha is Downregulated in the Failing Human Heart'. *Cellular and Molecular Biology Letters* 8 (1), 49-54
- Kass, R. S. and Tsien, R. W. (1976) 'Control of Action Potential Duration by Calcium Ions in Cardiac Purkinje Fibers'. *The Journal of General Physiology* 67 (5), 599-617
- Katholi, R. E. and Couri, D. M. (2011) 'Left Ventricular Hypertrophy: Major Risk Factor in Patients with Hypertension: Update and Practical Clinical Applications'. *International Journal of Hypertension* 2011, 495349
- Katragadda, D., Batchu, S., Cho, W., Chaudhary, K., Falck, J., and Seubert, J. (2009) 'Epoxyeicosatrienoic Acids Limit Damage to Mitochondrial Function Following Stress in Cardiac Cells'. *Journal of Molecular and Cellular Cardiology* 46 (6), 867-875
- Katz (1988) 'Cellular Mechanisms in Congestive Heart Failure'. *The American Journal of Cardiology* 62 (2), 3A-8A
- Keller, K. M. and Howlett, S. E. (2016) 'Sex Differences in the Biology and Pathology of the Aging Heart'. *Canadian Journal of Cardiology* 32 (9), 1065-1073
- Kersten, S. (2014) 'Integrated Physiology and Systems Biology of PPAR $\alpha$ '. *Molecular Metabolism* 3 (4), 354-371
- Khurana, R., Simons, M., Martin, J. F., and Zachary, I. C. (2005) 'Role of Angiogenesis in Cardiovascular Disease: A Critical Appraisal'. *Circulation* 112 (12), 1813-1824

- Kienesberger, Pulinilkunnil, T., Sung, M. M., Nagendran, J., Haemmerle, G., Kershaw, E. E., Young, M. E., Light, P. E., Oudit, G. Y., and Zechner, R. (2012) 'Myocardial ATGL Overexpression Decreases the Reliance on Fatty Acid Oxidation and Protects Against Pressure Overload-Induced Cardiac Dysfunction'. *Molecular and Cellular Biology* 32 (4), 740-750
- Kim, Park, and O'Rourke (2015) 'Vasculopathy of Aging and the Revised Cardiovascular Continuum'. *Pulse (Basel, Switzerland)* 3 (2), 141-147
- Kim, Uotani, S., Pierroz, D. D., Flier, J. S., and Kahn, B. B. (2000) 'In Vivo Administration of Leptin Activates Signal Transduction Directly in Insulin-Sensitive Tissues: Overlapping but Distinct Pathways from Insulin 1'. *Endocrinology* 141 (7), 2328-2339
- Kiriazis, H. and Gibbs, C. L. (2000) 'Effects of Aging on the Work Output and Efficiency of Rat Papillary Muscle'. *Cardiovascular Research* 48 (1), 111-119
- Klein, Pilegaard, H., Trebak, J. T., Jensen, T. E., Viollet, B., Schjerling, P., and Wojtaszewski, J. F. (2007) 'Lack of AMPK $\alpha$ 2 Enhances Pyruvate Dehydrogenase Activity during Exercise'. *American Journal of Physiology-Endocrinology and Metabolism* 293 (5), E1242-E1249
- Klein, Burstow, D. J., Tajik, A. J., Zachariah, P. K., Taliercio, C. P., Taylor, C. L., Bailey, K. R., and Seward, J. B. (1990) 'Age-Related Prevalence of Valvular Regurgitation in Normal Subjects: A Comprehensive Color Flow Examination of 118 Volunteers'. *Journal of the American Society of Echocardiography : Official Publication of the American Society of Echocardiography* 3 (1), 54-63
- Kleipool, E. E., Hoogendijk, E. O., Trappenburg, M. C., Handoko, M. L., Huisman, M., Peters, M. J., and Muller, M. (2018) 'Frailty in Older Adults with Cardiovascular Disease: Cause, Effect Or both?'. *Aging and Disease* 9 (3), 489-497
- Kless, C., Rink, N., Rozman, J., and Klingenspor, M. (2017) 'Proximate Causes for Diet-Induced Obesity in Laboratory Mice: A Case Study'. *European Journal of Clinical Nutrition* 71 (3), 306-317
- Kobayashi, T. and Solaro, R. J. (2005) 'Calcium, Thin Filaments, and the Integrative Biology of Cardiac Contractility'. *Annu.Rev.Physiol.* 67, 39-67
- Kolwicz Jr, S. C., Purohit, S., and Tian, R. (2013) 'Cardiac Metabolism and its Interactions with Contraction, Growth, and Survival of Cardiomyocytes'. *Circulation Research* 113 (5), 603-616
- Konrady, A., Kasherininov, Y., Shavarov, A., Shavarova, E., Vachrameeva, N., Krutikov, A., Smirnova, E., and Shlyakhto, E. (2006) 'How can we Block Sympathetic Overactivity? Effects of Rilmenidine and Atenolol in Overweight Hypertensive Patients'. *Journal of Human Hypertension* 20 (6), 398-406

- Kontogiannis, C., Kosmopoulos, M., Georgiopoulos, G., Spartalis, M., Paraskevaidis, I., and Chatzidou, S. (2018) 'Mitochondria in B-Adrenergic Signaling: Emerging Therapeutic Perspectives in Heart Failure and Ventricular Arrhythmias'. *Journal of Thoracic Disease* 10 (Suppl 33), S4183
- Korvald, C., Elvenes, O. P., and Myrnes, T. (2000) 'Myocardial Substrate Metabolism Influences Left Ventricular Energetics in Vivo'. *American Journal of Physiology-Heart and Circulatory Physiology* 278 (4), H1345-H1351
- Koshman, Y. E., Herzberg, B. R., Seifert, T. R., Polakowski, J. S., and Mittelstadt, S. W. (2018) 'The Evaluation of Drug-Induced Changes in Left Ventricular Function in Pentobarbital-Anesthetized Dogs'. *Journal of Pharmacological and Toxicological Methods* 91, 27-35
- Kovacic, J. C., Moreno, P., Nabel, E. G., Hachinski, V., and Fuster, V. (2011) 'Cellular Senescence, Vascular Disease, and Aging: Part 2 of a 2-Part Review: Clinical Vascular Disease in the Elderly'. *Circulation* 123 (17), 1900-1910
- Kranias, E. G. and Hajjar, R. J. (2012) 'Modulation of Cardiac Contractility by the Phospholamban/SERCA2a Regulatome'. *Circulation Research* 110 (12), 1646-1660
- Krell, M. J., Kline, E. M., Bates, E. R., Hodgson, J. M., Dilworth, L. R., Laufer, N., Vogel, R. A., and Pitt, B. (1986) 'Intermittent, Ambulatory Dobutamine Infusions in Patients with Severe Congestive Heart Failure'. *American Heart Journal* 112 (4), 787-791
- Krug, J. W., Rose, G., Clifford, G. D., and Oster, J. (2013) 'ECG-Based Gating in Ultra High Field Cardiovascular Magnetic Resonance using an Independent Component Analysis Approach'. *Journal of Cardiovascular Magnetic Resonance* 15 (1), 104
- Kühlbrandt, W. (2015) 'Structure and Function of Mitochondrial Membrane Protein Complexes'. *BMC Biology* 13 (1), 89
- Kuller, L. H., Lopez, O. L., Mackey, R. H., Rosano, C., Edmundowicz, D., Becker, J. T., and Newman, A. B. (2016) 'Subclinical Cardiovascular Disease and Death, Dementia, and Coronary Heart Disease in Patients 80 Years'. *Journal of the American College of Cardiology* 67 (9), 1013-1022
- la Cour Poulsen, L., Siersbæk, M., and Mandrup, S. (eds.) (2012) *Seminars in Cell & Developmental Biology*. 'PPARs: Fatty Acid Sensors Controlling Metabolism': Elsevier
- Lakatta and Levy (2003) 'Arterial and Cardiac Aging: Major Shareholders in Cardiovascular Enterprises. Part II: The Aging Heart in Health: Links to Heart Disease'. *Circulation* 107, 346-354
- Lakatta (1993) 'Cardiovascular Regulatory Mechanisms in Advanced Age'. *Physiological Reviews* 73 (2), 413-467
- Lakatta, Gerstenblith, Angell, Shock, and Weisfeldt (1975) 'Diminished Inotropic Response of Aged Myocardium to Catecholamines'. *Circulation Research* 36 (2), 262-269

- Lavanchy, N., Martin, J., and Rossi, A. (1988) 'Comparative Study of the Effects of Acebutolol, Atenolol, D-Propranolol and DL-Propranolol on the Alterations in Energy Metabolism Caused by Ischemia and Reperfusion: A <sup>31</sup>P NMR Study on the Isolated Rat Heart'. *Cardiovascular Drugs and Therapy* 2 (4), 501-512
- Lavie, C. J., Alpert, M. A., Arena, R., Mehra, M. R., Milani, R. V., and Ventura, H. O. (2013) 'Impact of Obesity and the Obesity Paradox on Prevalence and Prognosis in Heart Failure'. *JACC: Heart Failure* 1 (2), 93-102
- Layland, Young, and Altringham (1995) 'The Effect of Cycle Frequency on the Power Output of Rat Papillary Muscles in Vitro'. *The Journal of Experimental Biology* 198 (Pt 4), 1035-1043
- Layland, J. and Kentish, J. (2000) 'Effects of A1-or B-adrenoceptor Stimulation on Work-loop and Isometric Contractions of Isolated Rat Cardiac Trabeculae'. *The Journal of Physiology* 524 (1), 205-219
- Layland, J., Young, I., and Altringham, J. (1995) 'The Length Dependence of Work Production in Rat Papillary Muscles in Vitro'. *The Journal of Experimental Biology* 198 (Pt 12), 2491-2499
- Le Page, L. M., Rider, O. J., Lewis, A. J., Ball, V., Clarke, K., Johansson, E., Carr, C. A., Heather, L. C., and Tyler, D. J. (2015) 'Increasing Pyruvate Dehydrogenase Flux as a Treatment for Diabetic Cardiomyopathy: A Combined <sup>13</sup>C Hyperpolarized Magnetic Resonance and Echocardiography Study'. *Diabetes* 64 (8), 2735-2743
- Lean, M. (2000) 'Pathophysiology of Obesity'. *Proceedings of the Nutrition Society* 59 (03), 331-336
- Leblanc, N., Chartier, D., Gosselin, H., and Rouleau, J. (1998) 'Age and Gender Differences in Excitation-contraction Coupling of the Rat Ventricle'. *The Journal of Physiology* 511 (2), 533-548
- Lee, J. and Smith, N. P. (2012) 'The Multi-Scale Modelling of Coronary Blood Flow'. *Annals of Biomedical Engineering* 40 (11), 2399-2413
- Leineweber, K., Wangemann, T., Giessler, C., Bruck, H., Dhein, S., Kostelka, M., Mohr, F., Silber, R., and Brodde, O. (2002) 'Age-Dependent Changes of Cardiac Neuronal Noradrenaline Reuptake Transporter (Uptake1) in the Human Heart'. *Journal of the American College of Cardiology* 40 (8), 1459-1465
- Leone, T. C., Weinheimer, C. J., and Kelly, D. P. (1999) 'A Critical Role for the Peroxisome Proliferator-Activated Receptor Alpha (PPARalpha) in the Cellular Fasting Response: The PPARalpha-Null Mouse as a Model of Fatty Acid Oxidation Disorders'. *Proceedings of the National Academy of Sciences of the United States of America* 96 (13), 7473-7478

- Leopoldo, A. S., Sugizaki, M. M., Lima-Leopoldo, A. P., do Nascimento, A. F., Luvizotto, Renata de Azevedo Melo, de Campos, Dijon Henrique Salomé, Okoshi, K., Dal Pai-Silva, M., Padovani, C. R., and Cicogna, A. C. (2010) 'Cardiac Remodeling in a Rat Model of Diet-Induced Obesity'. *Canadian Journal of Cardiology* 26 (8), 423-429
- Lesnefsky, E. J., Chen, Q., and Hoppel, C. L. (2016) 'Mitochondrial Metabolism in Aging Heart'. *Circulation Research* 118 (10), 1593-1611
- Lewis, R. E. (ed.) (2011) *Mayo Clinic Proceedings*. 'Current Concepts in Antifungal Pharmacology': Elsevier
- Liao, P., Wang, S., Wang, S., Zheng, M., Zheng, M., Zhang, S., Cheng, H., Wang, Y., and Xiao, R. (2002) 'p38 Mitogen-Activated Protein Kinase Mediates a Negative Inotropic Effect in Cardiac Myocytes'. *Circulation Research* 90 (2), 190-196
- Liao, Y., Chen, Z. Y., Wang, Y. X., Lin, Y., Yang, F., and Zhou, Q. L. (2014) 'New Progress in Angiogenesis Therapy of Cardiovascular Disease by Ultrasound Targeted Microbubble Destruction'. *BioMed Research International* 2014, 872984
- Lim, C., Apstein, C. S., Colucci, W. S., and Liao, R. (2000) 'Impaired Cell Shortening and Relengthening with Increased Pacing Frequency are Intrinsic to the Senescent Mouse Cardiomyocyte'. *Journal of Molecular and Cellular Cardiology* 32 (11), 2075-2082
- Linn, T. C., Pettit, F. H., and Reed, L. J. (1969) 'Alpha-Keto Acid Dehydrogenase Complexes. X. Regulation of the Activity of the Pyruvate Dehydrogenase Complex from Beef Kidney Mitochondria by Phosphorylation and Dephosphorylation'. *Proceedings of the National Academy of Sciences of the United States of America* 62 (1), 234-241
- Lipskaia, L., Chemaly, E. R., Hadri, L., Lompre, A., and Hajjar, R. J. (2010) 'Sarcoplasmic Reticulum Ca<sup>2+</sup> ATPase as a Therapeutic Target for Heart Failure'. *Expert Opinion on Biological Therapy* 10 (1), 29-41
- Liu, Jia, H., Chang, X., Ding, G., Zhang, H., and Zou, Z. (2013) 'The Metabolic Disturbances of Isoproterenol Induced Myocardial Infarction in Rats Based on a Tissue Targeted Metabonomics'. *Molecular BioSystems* 9 (11), 2823-2834
- Liu, X., Liu, F., Deng, C., Zhang, M., Yang, M., Xiao, D., Lin, Q., Cai, S., Kuang, S., and Chen, J. (2016) 'Left Ventricular Deformation Associated with Cardiomyocyte Ca<sup>2+</sup> Transients Delay in Early Stage of Low-Dose of STZ and High-Fat Diet Induced Type 2 Diabetic Rats'. *BMC Cardiovascular Disorders* 16 (1), 41
- Lloyd, S., Brocks, C., and Chatham, J. C. (2003) 'Differential Modulation of Glucose, Lactate, and Pyruvate Oxidation by Insulin and Dichloroacetate in the Rat Heart'. *American Journal of Physiology-Heart and Circulatory Physiology* 285 (1), H163-H172

- Loichot, C., Jesel, L., Tesse, A., Taberero, A., Schoonjans, K., Roul, G., Carpusca, I., Auwerx, J., and Andriantsitohaina, R. (2006) 'Deletion of Peroxisome Proliferator-Activated Receptor- $\alpha$  Induces an Alteration of Cardiac Functions'. *American Journal of Physiology-Heart and Circulatory Physiology* 291 (1), H161-H166
- Lopaschuk, G. D., Ussher, J. R., Folmes, C. D., Jaswal, J. S., and Stanley, W. C. (2010) 'Myocardial Fatty Acid Metabolism in Health and Disease'. *Physiological Reviews* 90 (1), 207-258
- Lopez, N. D. and Phillips, K. M. (2014) 'Fluconazole Pharmacokinetics in a Morbidly Obese, Critically Ill Patient Receiving Continuous Venovenous Hemofiltration'. *Pharmacotherapy: The Journal of Human Pharmacology and Drug Therapy* 34 (9), e162-e168
- Lu, T., Hoshi, T., Weintraub, N. L., Spector, A. A., and Lee, H. (2001) 'Activation of ATP-sensitive K Channels by Epoxyeicosatrienoic Acids in Rat Cardiac Ventricular Myocytes'. *The Journal of Physiology* 537 (3), 811-827
- Lu, Y., Liu, X., Liang, X., Xiang, L., and Zhang, W. (2011) 'Metabolomic Strategy to Study Therapeutic and Synergistic Effects of Tanshinone IIA, Salvianolic Acid B and Ginsenoside Rb1 in Myocardial Ischemia Rats'. *Journal of Ethnopharmacology* 134 (1), 45-49
- Luo, C. H. and Rudy, Y. (1991) 'A Model of the Ventricular Cardiac Action Potential. Depolarization, Repolarization, and their Interaction'. *Circulation Research* 68 (6), 1501-1526
- Luptak, Balschi, J. A., Xing, Y., Leone, T. C., Kelly, D. P., and Tian, R. (2005) 'Decreased Contractile and Metabolic Reserve in Peroxisome Proliferator-Activated Receptor- $\alpha$ -Null Hearts can be Rescued by Increasing Glucose Transport and Utilization'. *Circulation* 112 (15), 2339-2346
- Lydell, C. P., Chan, A., Wambolt, R. B., Sambandam, N., Parsons, H., Bondy, G. P., Rodrigues, B., Popov, K. M., Harris, R. A., and Brownsey, R. W. (2002) 'Pyruvate Dehydrogenase and the Regulation of Glucose Oxidation in Hypertrophied Rat Hearts'. *Cardiovascular Research* 53 (4), 841-851
- Ma, B., Xiong, X., Chen, C., Li, H., Xu, X., Li, X., Li, R., Chen, G., Dackor, R. T., and Zeldin, D. C. (2013) 'Cardiac-Specific Overexpression of CYP2J2 Attenuates Diabetic Cardiomyopathy in Male Streptozotocin-Induced Diabetic Mice'. *Endocrinology* 154 (8), 2843-2856
- Machen, M. C. and Sleeper, M. (2015) 'Ventricular Failure and Myocardial Infarction'. in *Small Animal Critical Care Medicine (Second Edition)*. ed. by Anon: Elsevier, 214-218
- MacLennan, D. H. and Kranias, E. G. (2003) 'Phospholamban: A Crucial Regulator of Cardiac Contractility'. *Nature Reviews Molecular Cell Biology* 4 (7), 566-577

- Maertens, J., Marchetti, O., Herbrecht, R., Cornely, O., Flückiger, U., Frere, P., Gachot, B., Heinz, W., Lass-Flörl, C., and Ribaud, P. (2011) 'European Guidelines for Antifungal Management in Leukemia and Hematopoietic Stem Cell Transplant Recipients: Summary of the ECIL 3—2009 Update'. *Bone Marrow Transplantation* 46 (5), 709-718
- Mahmood, T. and Yang, P. C. (2012) 'Western Blot: Technique, Theory, and Trouble Shooting'. *North American Journal of Medical Sciences* 4 (9), 429-434
- Manley, B. S., Alexopoulos, D., Robinson, G. J., and Cobbe, S. M. (1986) 'Subsidiary Class III Effects of Beta Blockers? A Comparison of Atenolol, Metoprolol, Nadolol, Oxprenolol and Sotalol'. *Cardiovascular Research* 20 (10), 705-709
- Marín-Royo, G., Ortega-Hernández, A., Martínez-Martínez, E., Jurado-López, R., Luaces, M., Islas, F., Gómez-Garre, D., Delgado-Valero, B., Lagunas, E., and Ramchandani, B. (2019) 'The Impact of Cardiac Lipotoxicity on Cardiac Function and Mirnas Signature in Obese and Non-Obese Rats with Myocardial Infarction'. *Scientific Reports* 9 (1), 444
- Markert, M., Trautmann, T., Groß, M., Ege, A., Mayer, K., and Guth, B. (2012) 'Evaluation of a Method to Correct the Contractility Index LVdP/Dtmax for Changes in Heart Rate'. *Journal of Pharmacological and Toxicological Methods* 66 (2), 98-105
- Marks, A. R. (2013) 'Calcium Cycling Proteins and Heart Failure: Mechanisms and Therapeutics'. *The Journal of Clinical Investigation* 123 (1), 46-52
- Marques, C., Meireles, M., Norberto, S., Leite, J., Freitas, J., Pestana, D., Faria, A., and Calhau, C. (2016) 'High-Fat Diet-Induced Obesity Rat Model: A Comparison between Wistar and Sprague Dawley Rat-Implications of Gut Microbiota'
- Marzilli, M., Sabbah, H. N., and Stein, P. D. (1980) 'Mitral Regurgitation in Ventricular Premature Contractions: The Role of the Papillary Muscle'. *Chest* 77 (6), 736-740
- Marzilli, M., Sabbah, H., Lee, T., and Stein, P. D. (1980) 'Role of the Papillary Muscle in Opening and Closure of the Mitral Valve'. *American Journal of Physiology-Heart and Circulatory Physiology* 238 (3), H348-H354
- Masamura, K., Tanaka, N., Yoshida, M., Kato, M., Kawai, Y., Oida, K., and Miyamori, I. (2003) 'Myocardial Metabolic Regulation through Peroxisome Proliferator-Activated Receptor Alpha After Myocardial Infarction'. *Experimental and Clinical Cardiology* 8 (2), 61-66
- Mazumder, P. K., O'Neill, B. T., Roberts, M. W., Buchanan, J., Yun, U. J., Cooksey, R. C., Boudina, S., and Abel, E. D. (2004) 'Impaired Cardiac Efficiency and Increased Fatty Acid Oxidation in Insulin-Resistant Ob/Ob Mouse Hearts'. *Diabetes* 53 (9), 2366-2374
- McMillin, J. B., Taffet, G. E., Taegtmeier, H., Hudson, E. K., and Tate, C. A. (1993) 'Mitochondrial Metabolism and Substrate Competition in the Aging Fischer Rat Heart'. *Cardiovascular Research* 27 (12), 2222-2228

- Meletiadiis, J., Al-Saigh, R., Velegraki, A., Walsh, T. J., Roilides, E., and Zerva, L. (2012) 'Pharmacodynamic Effects of Simulated Standard Doses of Antifungal Drugs Against Aspergillus Species in a New in Vitro Pharmacokinetic/Pharmacodynamic Model'. *Antimicrobial Agents and Chemotherapy* 56 (1), 403-410
- Messa, G., Piasecki, M., Hurst, J., Hill, C., Tallis, J., and Degens, H. (2020) 'The Impact of a High-Fat Diet in Mice is Dependent on Duration and Age, and Differs between Muscles'. *The Journal of Experimental Biology* 223 (Pt 6), 10.1242/jeb.217117
- Messerli, Ventura, H. O., Reisin, E., Dreslinski, G. R., Dunn, F. G., MacPhee, A. A., and Frohlich, E. (1982) 'Borderline Hypertension and Obesity: Two Prehypertensive States with Elevated Cardiac Output.'. *Circulation* 66 (1), 55-60
- Meyer, C., Rana, O. R., Saygili, E., Gemein, C., Becker, M., Nolte, K. W., Weis, J., Schimpf, T., Knackstedt, C., Mischke, K., Hoffmann, R., Kelm, M., Pauza, D., and Schauerte, P. (2010) 'Augmentation of Left Ventricular Contractility by Cardiac Sympathetic Neural Stimulation'. *Circulation* 121 (11), 1286-1294
- Minhas, K. M., Khan, S. A., Raju, S. V., Phan, A. C., Gonzalez, D. R., Skaf, M. W., Lee, K., Tejani, A. D., Saliaris, A. P., and Barouch, L. A. (2005) 'Leptin Repletion Restores Depressed B-adrenergic Contractility in Ob/Ob Mice Independently of Cardiac Hypertrophy'. *The Journal of Physiology* 565 (2), 463-474
- Mitchell, J. R. and Wang, J. (2014) 'Expanding Application of the Wiggers Diagram to Teach Cardiovascular Physiology'. *Advances in Physiology Education* 38 (2), 170-175
- Moisan, Lee, Y., Zhang, J. D., Hudak, C. S., Meyer, C. A., Prummer, M., Zoffmann, S., Truong, H. H., Ebeling, M., and Kiiialainen, A. (2015) 'White-to-Brown Metabolic Conversion of Human Adipocytes by JAK Inhibition'. *Nature Cell Biology* 17 (1), 57-67
- Moraga, A., Lao, K. H., and Zeng, L. (2017) 'Angiogenesis and Cardiovascular Diseases: The Emerging Role of HDACs'. *Physiologic and Pathologic Angiogenesis: Signaling Mechanisms and Targeted Therapy*, 149
- Moreau, R., Heath, S. D., Doneanu, C. E., Harris, R. A., and Hagen, T. M. (2004) 'Age-Related Compensatory Activation of Pyruvate Dehydrogenase Complex in Rat Heart'. *Biochemical and Biophysical Research Communications* 325 (1), 48-58
- Moreau, R., Heath, S. D., Doneanu, C. E., Lindsay, J. G., and Hagen, T. M. (2003) 'Age-Related Increase in 4-Hydroxynonenal Adduction to Rat Heart A-Ketoglutarate Dehydrogenase does Not Cause Loss of its Catalytic Activity'. *Antioxidants and Redox Signaling* 5 (5), 517-527
- Morita, H., Wu, J., and Zipes, D. P. (2008) 'The QT Syndromes: Long and Short'. *The Lancet* 372 (9640), 750-763
- Mügge, A., Posselt, D., Reimer, U., Schmitz, W., and Scholz, H. (1985) 'Effects of the Beta 2-Adrenoceptor Agonists Fenoterol and Salbutamol on Force of Contraction in Isolated Human Ventricular Myocardium'. *Klinische Wochenschrift* 63 (1), 26-31

- Murray, A. J., Anderson, R. E., Watson, G. C., Radda, G. K., and Clarke, K. (2004) 'Uncoupling Proteins in Human Heart'. *The Lancet* 364 (9447), 1786-1788
- Myslivičėk, J., Řiční, J., Kolář, F., and Tuček, S. (2003) 'The Effects of Hydrocortisone on Rat Heart Muscarinic and Adrenergic A1, B1 and B2 Receptors, Propranolol-Resistant Binding Sites and on some Subsequent Steps in Intracellular Signalling'. *Naunyn-Schmiedeberg's Archives of Pharmacology* 368 (5), 366-376
- Nagamine, F., Murakami, K., Mimura, G., and Sakanashi, M. (1989) 'Effects of Beta-Adrenoceptor Blocking Agents on Isolated Atrial and Papillary Muscles from Experimentally Diabetic Rats'. *Japanese Journal of Pharmacology* 49 (1), 67-76
- Nagatsu, T. (2006) 'The Catecholamine System in Health and Disease'. *Proceedings of the Japan Academy, Series B* 82 (10), 388-415
- Nair, R. R. and Nair, P. (2001) 'Age-Dependent Variation in Contractility of Adult Cardiac Myocytes'. *The International Journal of Biochemistry & Cell Biology* 33 (2), 119-125
- Naito, J., Masuyama, T., Mano, T., Yamamoto, K., Doi, Y., Kondo, H., Nagano, R., Inoue, M., and Hori, M. (1996) 'Influence of Preload, Afterload, and Contractility on Myocardial Ultrasonic Tissue Characterization with Integrated Backscatter'. *Ultrasound in Medicine & Biology* 22 (3), 305-312
- Nakai, N., Sato, Y., Oshida, Y., Yoshimura, A., Fujitsuka, N., and Shimomura, Y. (1997) 'Effects of Aging on the Activities of Pyruvate Dehydrogenase Complex and its Kinase in Rat Heart'. *Life Sciences* 60 (25), 2309-2314
- Narayan, P., Valdivia, H. H., Mentzer Jr, R. M., and Lasley, R. D. (1998) 'Adenosine A 1 Receptor Stimulation Antagonizes the Negative Inotropic Effects of the PKC Activator Dioctanoylglycerol'. *Journal of Molecular and Cellular Cardiology* 30 (5), 913-921
- NC3Rs (2019) *The 3Rs* [online] available from <<https://www.nc3rs.org.uk/the-3rs>> []
- Nedergaard, J., Ricquier, D., and Kozak, L. P. (2005) 'Uncoupling Proteins: Current Status and Therapeutic Prospects'. *EMBO Reports* 6 (10), 917-921
- Nedergaard, J. and Cannon, B. (2003) 'The "Novel" Uncoupling Proteins UCP2 and UCP3: What do they really do? Pros and Cons for Suggested Functions'. *Experimental Physiology* 88 (1), 65-84
- Neofytos, D., Avdic, E., and Magiorakos, A. P. (2010) 'Clinical Safety and Tolerability Issues in use of Triazole Derivatives in Management of Fungal Infections'. *Drug, Healthcare and Patient Safety* 2, 27-38
- Nerbonne, J. M. and Kass, R. S. (2005) 'Molecular Physiology of Cardiac Repolarization'. *Physiological Reviews* 85 (4), 1205-1253
- Neubauer, S. (2007) 'The Failing Heart—an Engine Out of Fuel'. *New England Journal of Medicine* 356 (11), 1140-1151

- Neubauer, S., Horn, M., Cramer, M., Harre, K., Newell, J. B., Peters, W., Pabst, T., Ertl, G., Hahn, D., and Ingwall, J. S. (1997) 'Myocardial Phosphocreatine-to-ATP Ratio is a Predictor of Mortality in Patients with Dilated Cardiomyopathy'. *Circulation* 96 (7), 2190-2196
- Newman, A. B., Naydeck, B. L., Ives, D. G., Boudreau, R. M., Sutton-Tyrrell, K., O'Leary, D. H., and Kuller, L. H. (2008) 'Coronary Artery Calcium, Carotid Artery Wall Thickness, and Cardiovascular Disease Outcomes in Adults 70 to 99 Years Old'. *The American Journal of Cardiology* 101 (2), 186-192
- Nickola, M. W., Wold, L. E., Colligan, P. B., Wang, G., Samson, W. K., and Ren, J. (2000) 'Leptin Attenuates Cardiac Contraction in Rat Ventricular Myocytes: Role of NO'. *Hypertension* 36 (4), 501-505
- Niemann, B., Chen, Y., Teschner, M., Li, L., Silber, R., and Rohrbach, S. (2011) 'Obesity Induces Signs of Premature Cardiac Aging in Younger Patients: The Role of Mitochondria'. *Journal of the American College of Cardiology* 57 (5), 577-585
- Nitta, Y., Abe, K., Aoki, M., Ohno, I., and Isoyama, S. (1994) 'Diminished Heat Shock Protein 70 mRNA Induction in Aged Rat Hearts After Ischemia'. *The American Journal of Physiology* 267 (5 Pt 2), H1795-803
- Noble, D., Noble, S., Bett, G., Earm, Y., Ho, W., and So, I. (1991) 'The Role of Sodium-Calcium Exchange during the Cardiac Action Potential A'. *Annals of the New York Academy of Sciences* 639 (1), 334-353
- North, B. and Sinclair, D. (2012) 'The Intersection between Aging and Cardiovascular Disease'. *Circulation Research* 110 (8), 1097-1108
- Norton, J. M. (2001) 'Toward Consistent Definitions for Preload and Afterload'. *Advances in Physiology Education* 25 (1-4), 53-61
- Ochsner, G., Wilhelm, M. J., Amacher, R., Petrou, A., Cesarovic, N., Stauffert, S., Röhrnbauer, B., Maisano, F., Hierold, C., and Meboldt, M. (2017) 'In Vivo Evaluation of Physiologic Control Algorithms for Left Ventricular Assist Devices Based on Left Ventricular Volume Or Pressure'. *ASAIO Journal* 63 (5), 568-577
- Oka, S., Zhai, P., Yamamoto, T., Ikeda, Y., Byun, J., Hsu, C. P., and Sadoshima, J. (2015) 'Peroxisome Proliferator Activated Receptor-Alpha Association with Silent Information Regulator 1 Suppresses Cardiac Fatty Acid Metabolism in the Failing Heart'. *Circulation.Heart Failure* 8 (6), 1123-1132
- Okuyan, H. and Altin, C. (2013) 'Heart Failure Induced by Itraconazole'. *Indian Journal of Pharmacology* 45 (5), 524-525
- Oni-Orisan, A., Alsaleh, N., Lee, C. R., and Seubert, J. M. (2014) 'Epoxyeicosatrienoic Acids and Cardioprotection: The Road to Translation'. *Journal of Molecular and Cellular Cardiology* 74, 199-208

- Opasich, C., Russo, A., Mingrone, R., Zambelli, M., and Tavazzi, L. (2000) 'Intravenous Inotropic Agents in the Intensive Therapy Unit: Do they really make a Difference?'. *European Journal of Heart Failure* 2 (1), 7-11
- Orchard and Lakatta (1985) 'Intracellular Calcium Transients and Developed Tension in Rat Heart Muscle. A Mechanism for the Negative Interval-Strength Relationship'. *The Journal of General Physiology* 86 (5), 637-651
- Paneni, F., Cañestro, C. D., Libby, P., Lüscher, T. F., and Camici, G. G. (2017) 'The Aging Cardiovascular System: Understanding it at the Cellular and Clinical Levels'. *Journal of the American College of Cardiology* 69 (15), 1952-1967
- Parikh, J. S., Randhawa, A. K., Wharton, S., Edgell, H., and Kuk, J. L. (2018) 'The Association between Antihypertensive Medication use and Blood Pressure is Influenced by Obesity'. *Journal of Obesity* 2018
- Park, Kim, S. H., Cho, G., Baik, I., Kim, N. H., Lim, H. E., Kim, E. J., Park, C. G., Lim, S. Y., and Kim, Y. H. (2011) 'Obesity Phenotype and Cardiovascular Changes'. *Journal of Hypertension* 29 (9), 1765-1772
- Park, Cho, Y. R., Kim, H. J., Higashimori, T., Danton, C., Lee, M. K., Dey, A., Rothermel, B., Kim, Y. B., Kalinowski, A., Russell, K. S., and Kim, J. K. (2005) 'Unraveling the Temporal Pattern of Diet-Induced Insulin Resistance in Individual Organs and Cardiac Dysfunction in C57BL/6 Mice'. *Diabetes* 54 (12), 3530-3540
- Paul, V. and Rawal, H. (2017) 'Cardiotoxicity with Itraconazole'. *BMJ Case Reports* 2017, 10.1136/bcr-2017-219376
- Pavek, P. and Dvorak, Z. (2008) 'Xenobiotic-Induced Transcriptional Regulation of Xenobiotic Metabolizing Enzymes of the Cytochrome P450 Superfamily in Human Extrahepatic Tissues'. *Current Drug Metabolism* 9 (2), 129-143
- Pecqueur, C., Alves-Guerra, M. C., Gelly, C., Levi-Meyrueis, C., Couplan, E., Collins, S., Ricquier, D., Bouillaud, F., and Miroux, B. (2001) 'Uncoupling Protein 2, in Vivo Distribution, Induction upon Oxidative Stress, and Evidence for Translational Regulation'. *The Journal of Biological Chemistry* 276 (12), 8705-8712
- Poehlman, E. T., McAuliffe, T. L., Van Houten, D. R., and Danforth, E., Jr (1990) 'Influence of Age and Endurance Training on Metabolic Rate and Hormones in Healthy Men'. *The American Journal of Physiology* 259 (1 Pt 1), E66-72
- Pohl, E. E., Rupperecht, A., Macher, G., and Hilse, K. (2019) 'Important Trends in UCP3 Investigation'. *Frontiers in Physiology* 10, 470
- Pol, Lieu, M., and Drosatos (2015) 'PPARs: Protectors Or Opponents of Myocardial Function?'. *PPAR Research* 2015
- Prosdocimo, D., John, J. E., Zhang, L., Efrain, E. S., Zhang, R., Liao, X., and Jain, M. K. (2015) 'KLF15 and PPAR $\alpha$  Cooperate to Regulate Cardiomyocyte Lipid Gene Expression and Oxidation'. *PPAR Research* 2015

- Qiang, W., Weiqiang, K., Qing, Z., Pengju, Z., and Yi, L. (2007) 'Aging Impairs Insulin-Stimulated Glucose Uptake in Rat Skeletal Muscle Via Suppressing AMPK $\alpha$ '. *Experimental & Molecular Medicine* 39 (4), 535-543
- Qu, Y., Fang, M., Gao, B., Amouzadeh, H. R., Li, N., Narayanan, P., Acton, P., Lawrence, J., and Vargas, H. M. (2013) 'Itraconazole Decreases Left Ventricular Contractility in Isolated Rabbit Heart: Mechanism of Action'. *Toxicology and Applied Pharmacology* 268 (2), 113-122
- Rastaldo, R., Pagliaro, P., Cappello, S., Penna, C., Mancardi, D., Westerhof, N., and Losano, G. (2007) 'Nitric Oxide and Cardiac Function'. *Life Sciences* 81 (10), 779-793
- Ratshin, R. A., Rackley, C. E., and Russell Jr, R. O. (1974) 'Determination of Left Ventricular Preload and Afterload by Quantitative Echocardiography in Man: Calibration of the Method'. *Circulation Research* 34 (5), 711-718
- Razeghi, P., Essop, M. F., Huss, J. M., Abbasi, S., Manga, N., and Taegtmeier, H. (2003) 'Hypoxia-Induced Switches of Myosin Heavy Chain Iso-Gene Expression in Rat Heart'. *Biochemical and Biophysical Research Communications* 303 (4), 1024-1027
- Redinger, R. N. (2007) 'The Pathophysiology of Obesity and its Clinical Manifestations'. *Gastroenterology & Hepatology* 3 (11), 856-863
- Reho, J. J. and Rahmouni, K. (2017) 'Oxidative and Inflammatory Signals in Obesity-Associated Vascular Abnormalities'. *Clinical Science (London, England : 1979)* 131 (14), 1689-1700
- Ren, J., Dong, F., Cai, G., Zhao, P., Nunn, J. M., Wold, L. E., and Pei, J. (2010) 'Interaction between Age and Obesity on Cardiomyocyte Contractile Function: Role of Leptin and Stress Signaling'. *PLoS One* 5 (4), e10085
- Reznick, R. M., Zong, H., Li, J., Morino, K., Moore, I. K., Hannah, J. Y., Liu, Z., Dong, J., Mustard, K. J., and Hawley, S. A. (2007) 'Aging-Associated Reductions in AMP-Activated Protein Kinase Activity and Mitochondrial Biogenesis'. *Cell Metabolism* 5 (2), 151-156
- Rinnankoski-Tuikka, R., Silvennoinen, M., Torvinen, S., Hulmi, J. J., Lehti, M., Kivelä, R., Reunanen, H., and Kainulainen, H. (2012) 'Effects of High-Fat Diet and Physical Activity on Pyruvate Dehydrogenase Kinase-4 in Mouse Skeletal Muscle'. *Nutrition & Metabolism* 9 (1), 53
- Roberts, F. and Freshwater-Turner, D. (2007) 'Pharmacokinetics and Anaesthesia'. *Continuing Education in Anaesthesia, Critical Care & Pain* 7 (1), 25-29
- Roberts, W. and Cohen, L. (1972) 'Left Ventricular Papillary Muscles. Description of the Normal and a Survey of Conditions Causing them to be Abnormal'. *Circulation* 46 (1), 138-154

- Roche, C., Besnier, M., Cassel, R., Harouki, N., Coquerel, D., Guerrot, D., Nicol, L., Loizon, E., Remy-Jouet, I., and Morisseau, C. (2015) 'Soluble Epoxide Hydrolase Inhibition Improves Coronary Endothelial Function and Prevents the Development of Cardiac Alterations in Obese Insulin-Resistant Mice'. *American Journal of Physiology-Heart and Circulatory Physiology* 308 (9), H1020-H1029
- Rockwood, K., Blodgett, J. M., Theou, O., Sun, M. H., Feridooni, H. A., Mitnitski, A., Rose, R. A., Godin, J., Gregson, E., and Howlett, S. E. (2017) 'A Frailty Index Based on Deficit Accumulation Quantifies Mortality Risk in Humans and in Mice'. *Scientific Reports* 7, 43068
- Rodriguez, P. and Kranias, E. G. (2005) 'Phospholamban: A Key Determinant of Cardiac Function and Dysfunction'. *Archives Des Maladies Du Coeur Et Des Vaisseaux* 98 (12), 1239-1243
- Rojas, J. M., Bolze, F., Thorup, I., Nowak, J., Dalsgaard, C. M., Skydsgaard, M., Berthelsen, L. O., Keane, K. A., Soeborg, H., Sjogren, I., Jensen, J. T., Fels, J. J., Offenber, H. K., Andersen, L. W., and Dalgaard, M. (2018) 'The Effect of Diet-Induced Obesity on Toxicological Parameters in the Polygenic Sprague-Dawley Rat Model'. *Toxicologic Pathology* 46 (7), 777-798
- Rosell, M., Kafrou, M., Frontini, A., Okolo, A., Chan, Y., Nikolopoulou, E., Millership, S., Fenech, M. E., MacIntyre, D., and Turner, J. O. (2014) 'Brown and White Adipose Tissues: Intrinsic Differences in Gene Expression and Response to Cold Exposure in Mice'. *American Journal of Physiology-Endocrinology and Metabolism* 306 (8), E945-E964
- Ross Jr, J. and Sobel, B. (1972) 'Regulation of Cardiac Contraction'. *Annual Review of Physiology* 34 (1), 47-90
- Rossi, S., Baruffi, S., Bertuzzi, A., Miragoli, M., Corradi, D., Maestri, R., Alinovi, R., Mutti, A., Musso, E., Sgoifo, A., Brisinda, D., Fenici, R., and Macchi, E. (2008) 'Ventricular Activation is Impaired in Aged Rat Hearts'. *American Journal of Physiology.Heart and Circulatory Physiology* 295 (6), H2336-47
- Ruffolo, R. R., Jr (1987) 'The Pharmacology of Dobutamine'. *The American Journal of the Medical Sciences* 294 (4), 244-248
- Rupprecht, A., Moldzio, R., Mödl, B., and Pohl, E. E. (2019) 'Glutamine Regulates Mitochondrial Uncoupling Protein 2 to Promote Glutaminolysis in Neuroblastoma Cells'. *Biochimica Et Biophysica Acta (BBA)-Bioenergetics* 1860 (5), 391-401
- Rupprecht, A., Bräuer, A. U., Smorodchenko, A., Goyn, J., Hilse, K. E., Shabalina, I. G., Infante-Duarte, C., and Pohl, E. E. (2012) 'Quantification of Uncoupling Protein 2 Reveals its Main Expression in Immune Cells and Selective Up-Regulation during T-Cell Proliferation'. *PLoS One* 7 (8), e41406

- Russell, L. K., Mansfield, C. M., Lehman, J. J., Kovacs, A., Courtois, M., Saffitz, J. E., Medeiros, D. M., Valencik, M. L., McDonald, J. A., and Kelly, D. P. (2004) 'Cardiac-Specific Induction of the Transcriptional Coactivator Peroxisome Proliferator-Activated Receptor  $\gamma$  Coactivator-1 $\alpha$  Promotes Mitochondrial Biogenesis and Reversible Cardiomyopathy in a Developmental Stage-Dependent Manner'. *Circulation Research* 94 (4), 525-533
- Sanchez-Roman, I., Gomez, A., Naudí, A., Jove, M., Gómez, J., Lopez-Torres, M., Pamplona, R., and Barja, G. (2014) 'Independent and Additive Effects of Atenolol and Methionine Restriction on Lowering Rat Heart Mitochondria Oxidative Stress'. *Journal of Bioenergetics and Biomembranes* 46 (3), 159-172
- Sanchez-Roman, I., Gomez, J., Naudi, A., Ayala, V., Portero-Otín, M., Lopez-Torres, M., Pamplona, R., and Barja, G. (2010) 'The B-Blocker Atenolol Lowers the Longevity-Related Degree of Fatty Acid Unsaturation, Decreases Protein Oxidative Damage, and Increases Extracellular Signal-Regulated Kinase Signaling in the Heart of C57BL/6 Mice'. *Rejuvenation Research* 13 (6), 683-693
- Sandri, M., Lin, J., Handschin, C., Yang, W., Arany, Z. P., Lecker, S. H., Goldberg, A. L., and Spiegelman, B. M. (2006) 'PGC-1 $\alpha$  Protects Skeletal Muscle from Atrophy by Suppressing FoxO3 Action and Atrophy-Specific Gene Transcription'. *Proceedings of the National Academy of Sciences of the United States of America* 103 (44), 16260-16265
- Santana, L. F., Cheng, E. P., and Lederer, W. J. (2010) 'How does the Shape of the Cardiac Action Potential Control Calcium Signaling and Contraction in the Heart?'. *Journal of Molecular and Cellular Cardiology* 49 (6), 901-903
- Scheuermann-Freestone, M., Madsen, P. L., Manners, D., Blamire, A. M., Buckingham, R. E., Styles, P., Radda, G. K., Neubauer, S., and Clarke, K. (2003) 'Abnormal Cardiac and Skeletal Muscle Energy Metabolism in Patients with Type 2 Diabetes'. *Circulation* 107 (24), 3040-3046
- Schipke, J., Banmann, E., Nikam, S., Voswinckel, R., Kohlstedt, K., Loot, A. E., Fleming, I., and Mühlfeld, C. (2014) 'The Number of Cardiac Myocytes in the Hypertrophic and Hypotrophic Left Ventricle of the Obese and Calorie-restricted Mouse Heart'. *Journal of Anatomy* 225 (5), 539-547
- Scholz, H. (1984) 'Inotropic Drugs and their Mechanisms of Action'. *Journal of the American College of Cardiology* 4 (2), 389-397
- Schrauwen, P., Hinderling, V., Hesselink, M. K., Schaart, G., Kornips, E., Saris, W. H., Westerterp-Plantenga, M., and Langhans, W. (2002) 'Etomoxir-Induced Increase in UCP3 Supports a Role of Uncoupling Protein 3 as a Mitochondrial Fatty Acid Anion Exporter'. *The FASEB Journal* 16 (12), 1688-1690
- Scorrano, L., Oakes, S. A., Opferman, J. T., Cheng, E. H., Sorcinelli, M. D., Pozzan, T., and Korsmeyer, S. J. (2003) 'BAX and BAK Regulation of Endoplasmic Reticulum Ca<sup>2+</sup>: A Control Point for Apoptosis'. *Science (New York, N.Y.)* 300 (5616), 135-139

- Selthofer-Relatić, K., Bošnjak, I., and Kibel, A. (2016) 'Obesity Related Coronary Microvascular Dysfunction: From Basic to Clinical Practice'. *Cardiology Research and Practice* 2016
- Sengupta, P. (2013) 'The Laboratory Rat: Relating its Age with Human'S'. *International Journal of Preventive Medicine* 4 (6), 624-630
- Seo, A., Joseph, A. M., Dutta, D., Hwang, J. C., Aris, J. P., and Leeuwenburgh, C. (2010) 'New Insights into the Role of Mitochondria in Aging: Mitochondrial Dynamics and More'. *Journal of Cell Science* 123 (Pt 15), 2533-2542
- Seo, A., Xu, J., Servais, S., Hofer, T., Marzetti, E., Wohlgemuth, S. E., Knutson, M. D., Chung, H. Y., and Leeuwenburgh, C. (2008) 'Mitochondrial Iron Accumulation with Age and Functional Consequences'. *Aging Cell* 7 (5), 706-716
- Seo, A., Hofer, T., Sung, B., Judge, S., Chung, H. Y., and Leeuwenburgh, C. (2006) 'Hepatic Oxidative Stress during Aging: Effects of 8% Long-Term Calorie Restriction and Lifelong Exercise'. *Antioxidants & Redox Signaling* 8 (3-4), 529-538
- Shabalina, I. G. and Nedergaard, J. (2011) 'Mitochondrial ('mild') Uncoupling and ROS Production: Physiologically Relevant Or Not?'. *Biochemical Society Transactions* 39 (part 5)
- Shamliyan, T., Talley, K. M., Ramakrishnan, R., and Kane, R. L. (2013) 'Association of Frailty with Survival: A Systematic Literature Review'. *Ageing Research Reviews* 12 (2), 719-736
- Sharma, N., Okere, I. C., Brunengraber, D. Z., McElfresh, T. A., King, K. L., Sterk, J. P., Huang, H., Chandler, M. P., and Stanley, W. C. (2005) 'Regulation of Pyruvate Dehydrogenase Activity and Citric Acid Cycle Intermediates during High Cardiac Power Generation'. *The Journal of Physiology* 562 (2), 593-603
- Sheeran, F. L., Angerosa, J., Liaw, N. Y., Cheung, M. M., and Pepe, S. (2019) 'Adaptations in Protein Expression and Regulated Activity of Pyruvate Dehydrogenase Multienzyme Complex in Human Systolic Heart Failure'. *Oxidative Medicine and Cellular Longevity* 2019
- Shiou, Y., Huang, I., Lin, H., and Lee, H. (2018) 'High Fat Diet Aggravates Atrial and Ventricular Remodeling of Hypertensive Heart Disease in Aging Rats'. *Journal of the Formosan Medical Association* 117 (7), 621-631
- Sindone, A. P., Keogh, A. M., Macdonald, P. S., McCosker, C. J., and Kaan, A. F. (1997) 'Continuous Home Ambulatory Intravenous Inotropic Drug Therapy in Severe Heart Failure: Safety and Cost Efficacy'. *American Heart Journal* 134 (5), 889-900
- Sinnollareddy, M. G., Roberts, J. A., Lipman, J., Akova, M., Bassetti, M., De Waele, J. J., Kaukonen, K., Koulenti, D., Martin, C., and Montravers, P. (2015) 'Pharmacokinetic Variability and Exposures of Fluconazole, Anidulafungin, and Caspofungin in Intensive Care Unit Patients: Data from Multinational Defining Antibiotic Levels in Intensive Care Unit (DALI) Patients Study'. *Critical Care* 19 (1), 33

- Skrzypiec-Spring, M., Grotthus, B., Szeląg, A., and Schulz, R. (2007) 'Isolated Heart Perfusion According to Langendorff—still Viable in the New Millennium'. *Journal of Pharmacological and Toxicological Methods* 55 (2), 113-126
- Sohn, Song, W., Kim, B., Kang, M., Lee, S., Suh, J., Yoon, Y. E., Kim, S., Youn, T., and Cho, S. (2015) 'Eosinophilic Myocarditis: Case Series and Literature Review'. *Asia Pacific Allergy* 5 (2), 123-127
- Somchit, N., Ngee, C. S., Yaakob, A., Ahmad, Z., and Zakaria, Z. A. (2009) 'Effects of Cytochrome p450 Inhibitors on Itraconazole and Fluconazole Induced Cytotoxicity in Hepatocytes'. *Journal of Toxicology* 2009, 912320
- Son, N. H., Yu, S., Tuinei, J., Arai, K., Hamai, H., Homma, S., Shulman, G. I., Abel, E. D., and Goldberg, I. J. (2010) 'PPARgamma-Induced Cardiolipotoxicity in Mice is Ameliorated by PPARalpha Deficiency Despite Increases in Fatty Acid Oxidation'. *The Journal of Clinical Investigation* 120 (10), 3443-3454
- Sparagna, G. C., Hickson-Bick, D. L., Buja, L. M., and McMillin, J. B. (2000) 'A Metabolic Role for Mitochondria in Palmitate-Induced Cardiac Myocyte Apoptosis'. *American Journal of Physiology. Heart and Circulatory Physiology* 279 (5), H2124-32
- Spriet, L. L. and Heigenhauser, G. J. (2002) 'Regulation of Pyruvate Dehydrogenase (PDH) Activity in Human Skeletal Muscle during Exercise'. *Exercise and Sport Sciences Reviews* 30 (2), 91-95
- Stangl, V., Baumann, G., Stangl, K., and Felix, S. B. (2002) 'Negative Inotropic Mediators Released from the Heart After Myocardial Ischaemia–reperfusion'. *Cardiovascular Research* 53 (1), 12-30
- Stanley, W. C. and Chandler, M. P. (2002) 'Energy Metabolism in the Normal and Failing Heart: Potential for Therapeutic Interventions'. *Heart Failure Reviews* 7 (2), 115-130
- Stapleton, P. A., James, M. E., Goodwill, A. G., and Frisbee, J. C. (2008) 'Obesity and Vascular Dysfunction'. *Pathophysiology : The Official Journal of the International Society for Pathophysiology* 15 (2), 79-89
- Stavinoha, RaySpellicy, J. W., Essop, M. F., Graveleau, C., Abel, E. D., Hart-Sailors, M. L., Mersmann, H. J., Bray, M. S., and Young, M. E. (2004) 'Evidence for Mitochondrial Thioesterase 1 as a Peroxisome Proliferator-Activated Receptor-A-Regulated Gene in Cardiac and Skeletal Muscle'. *American Journal of Physiology-Endocrinology and Metabolism* 287 (5), E888-E895
- Stegeman, J. J., Woodin, B. R., Klotz, A. V., Wolke, R. E., and Orme-Johnson, N. R. (1982) 'Cytochrome P-450 and Monooxygenase Activity in Cardiac Microsomes from the Fish *Stenotomus Chrysops*'. *Molecular Pharmacology* 21 (2), 517-526
- Steinberg, S. F. (2013) 'Oxidative Stress and Sarcomeric Proteins'. *Circulation Research* 112 (2), 393-405

- Sugden, M. C. and Holness, M. J. (2003) 'Recent Advances in Mechanisms Regulating Glucose Oxidation at the Level of the Pyruvate Dehydrogenase Complex by PDKs'. *American Journal of Physiology-Endocrinology and Metabolism* 284 (5), E855-E862
- Sun, W., Liu, Q., Leng, J., Zheng, Y., and Li, J. (2015a) 'The Role of Pyruvate Dehydrogenase Complex in Cardiovascular Diseases'. *Life Sciences* 121, 97-103
- Sung, Park, S., Yu, B. P., and Chung, H. Y. (2004) 'Modulation of PPAR in Aging, Inflammation, and Calorie Restriction'. *The Journals of Gerontology Series A: Biological Sciences and Medical Sciences* 59 (10), B997-B1006
- Sutherland, F. J. and Hearse, D. J. (2000) 'The Isolated Blood and Perfusion Fluid Perfused Heart'. *Pharmacological Research* 41 (6), 613-627
- Szczepaniak, L. S., Dobbins, R. L., Metzger, G. J., Sartoni-D'Ambrosia, G., Arbique, D., Vongpatanasin, W., Unger, R., and Victor, R. G. (2003) 'Myocardial Triglycerides and Systolic Function in Humans: In Vivo Evaluation by Localized Proton Spectroscopy and Cardiac Imaging'. *Magnetic Resonance in Medicine: An Official Journal of the International Society for Magnetic Resonance in Medicine* 49 (3), 417-423
- Taegtmeyer, H., Wilson, C. R., Razeghi, P., and Sharma, S. (2005) 'Metabolic Energetics and Genetics in the Heart'. *Annals of the New York Academy of Sciences* 1047, 208-218
- Tani, M., Honma, Y., Hasegawa, H., and Tamaki, K. (2001) 'Direct Activation of Mitochondrial KATP Channels Mimics Preconditioning but Protein Kinase C Activation is Less Effective in Middle-Aged Rat Hearts'. *Cardiovascular Research* 49 (1), 56-68
- Tariq, S. and Aronow, W. S. (2015) 'Use of Inotropic Agents in Treatment of Systolic Heart Failure'. *International Journal of Molecular Sciences* 16 (12), 29060-29068
- Taylor, J. (2014) 'The Effects of Obesity and Ageing on the Heart: Are they so Different?'. *European Heart Journal* 35 (23), 1502
- Teerlink, J. R. (2009) 'A Novel Approach to Improve Cardiac Performance: Cardiac Myosin Activators'. *Heart Failure Reviews* 14 (4), 289
- Temsah, R. M., Dyck, C., Neticadan, T., Chapman, D., Elimban, V., and Dhalla, N. S. (2000) 'Effect of Beta-Adrenoceptor Blockers on Sarcoplasmic Reticular Function and Gene Expression in the Ischemic-Reperfused Heart'. *The Journal of Pharmacology and Experimental Therapeutics* 293 (1), 15-23
- Tessier, Thurner, Jungling, Luckhoff, and Fischer (2003) 'Impairment of Glucose Metabolism in Hearts from Rats Treated with Endotoxin'. *Cardiovascular Research* 60 (1), 119-130
- Testa, G., Cacciatore, F., Della-Morte, D., Mazzella, F., Mastrobuoni, C., Galizia, G., Gargiulo, G., Rengo, F., Bonaduce, D., and Abete, P. (2014) 'Atenolol use is Associated with Long-term Mortality in Community-dwelling Older Adults with Hypertension'. *Geriatrics & Gerontology International* 14 (1), 153-158

- Tokarev, J. and Benditt, D. G. (2015) 'Sinus Bradycardia and Chronotropic Incompetence Associated with Single-Agent Itraconazole Antifungal Therapy: A Case Report'. *HeartRhythm Case Reports* 1 (1), 6-9
- Toth, M. and Tchernof, A. (2000) 'Lipid Metabolism in the Elderly'. *European Journal of Clinical Nutrition* 54 (S3), S121
- Towbin, H., Staehelin, T., and Gordon, J. (1979) 'Electrophoretic Transfer of Proteins from Polyacrylamide Gels to Nitrocellulose Sheets: Procedure and some Applications'. *Proceedings of the National Academy of Sciences of the United States of America* 76 (9), 4350-4354
- Trayhurn, P. and Wood, I. (2005) 'Signalling Role of Adipose Tissue: Adipokines and Inflammation in Obesity'. *Biochemical Society Transactions* 33 (Pt 5), 1078-1081
- Trayhurn, P. and Wood, I. (2004) 'Adipokines: Inflammation and the Pleiotropic Role of White Adipose Tissue'. *British Journal of Nutrition* 92 (3), 347-355
- Tremmel, M., Gerdtham, U., Nilsson, P. M., and Saha, S. (2017) 'Economic Burden of Obesity: A Systematic Literature Review'. *International Journal of Environmental Research and Public Health* 14 (4), 435
- Triposkiadis, F., Karayannis, G., Giamouzis, G., Skoularigis, J., Louridas, G., and Butler, J. (2009) 'The Sympathetic Nervous System in Heart Failure: Physiology, Pathophysiology, and Clinical Implications'. *Journal of the American College of Cardiology* 54 (19), 1747-1762
- Tucker, R., Haq, Y., Denning, D., and Stevens, D. (1990) 'Adverse Events Associated with Itraconazole in 189 Patients on Chronic Therapy'. *Journal of Antimicrobial Chemotherapy* 26 (4), 561-566
- Turpin, S. M., Lancaster, G. I., Darby, I., Febbraio, M. A., and Watt, M. J. (2006) 'Apoptosis in Skeletal Muscle Myotubes is Induced by Ceramides and is Positively Related to Insulin Resistance'. *American Journal of Physiology. Endocrinology and Metabolism* 291 (6), E1341-50
- Tuttle, R. (1958) 'Development of New Catecholamine to Selectively in Crease Cardiac Contractility.'. *Circ Res* 36, 25-27
- Unger, R. H. and Zhou, Y. T. (2001) 'Lipotoxicity of Beta-Cells in Obesity and in Other Causes of Fatty Acid Spillover'. *Diabetes* 50 Suppl 1, S118-21
- Vallet, B., Dupuis, B., and Chopin, C. (1991) 'Dobutamine: Mechanisms of Action and use in Acute Cardiovascular Pathology'. *Annales De Cardiologie Et D'Angeiologie* 40 (6), 397-402
- Valli, A., Harris, A. L., and Kessler, B. M. (2015) 'Hypoxia Metabolism in Ageing'. *Aging* 7 (7), 465-466

- Van Bilsen, M., van der Vusse, Ger J, Gilde, A. J., Lindhout, M., and van der Lee, Karin AJM (2002) 'Peroxisome Proliferator-Activated Receptors: Lipid Binding Proteins Controlling Gene Expression'. in *Cellular Lipid Binding Proteins*. ed. by Anon: Springer, 131-138
- van Eerd, J. and Takahashi, K. (1975) 'The Amino Acid Sequence of Bovine Cardiac Troponin-C. Comparison with Rabbit Skeletal Troponin-C'. *Biochemical and Biophysical Research Communications* 64 (1), 122-127
- Van Weemen, B. and Schuurs, A. (1971) 'Immunoassay using Antigen—enzyme Conjugates'. *FEBS Letters* 15 (3), 232-236
- Vileigas, D. F., de Deus, A. F., da Silva, D. C., de Tomasi, L. C., de Campos, D. H., Adorni, C. S., de Oliveira, S. M., Sant'Ana, P. G., Okoshi, K., and Padovani, C. R. (2016) 'Saturated High-fat Diet-induced Obesity Increases Adenylate Cyclase of Myocardial B-adrenergic System and does Not Compromise Cardiac Function'. *Physiological Reports* 4 (17)
- Vincent, J. (2008) 'Understanding Cardiac Output'. *Critical Care* 12 (4), 1
- Voci, P., Bilotta, F., Caretta, Q., Mercanti, C., and Marino, B. (1995) 'Papillary Muscle Perfusion Pattern. A Hypothesis for Ischemic Papillary Muscle Dysfunction'. *Circulation* 91 (6), 1714-1718
- Vornanen, M. (1996) 'Excitation-Contraction Coupling of the Developing Rat Heart'. *Molecular and Cellular Biochemistry* 163 (1), 5-11
- Wakasaki, H., Koya, D., Schoen, F. J., Jirousek, M. R., Ways, D. K., Hoit, B. D., Walsh, R. A., and King, G. L. (1997) 'Targeted Overexpression of Protein Kinase C Beta2 Isoform in Myocardium Causes Cardiomyopathy'. *Proceedings of the National Academy of Sciences of the United States of America* 94 (17), 9320-9325
- Wang, Zhu, D., and Shan, Y. (2015) 'Dobutamine Therapy is Associated with Worse Clinical Outcomes Compared with Nesiritide Therapy for Acute Decompensated Heart Failure: A Systematic Review and Meta-Analysis'. *American Journal of Cardiovascular Drugs* 15 (6), 429-437
- Wang, K., Xu, Y., Sun, Q., Long, J., Liu, J., and Ding, J. (2018) 'Mitochondria Regulate Cardiac Contraction through ATP-Dependent and Independent Mechanisms'. *Free Radical Research* 52 (11-12), 1256-1265
- Wang, X., West, J. A., Murray, A. J., and Griffin, J. L. (2015) 'Comprehensive Metabolic Profiling of Age-Related Mitochondrial Dysfunction in the High-Fat-Fed Ob/Ob Mouse Heart'. *Journal of Proteome Research* 14 (7), 2849-2862
- Watanabe, T., Delbridge, L. M., Bustamante, J. O., and McDonald, T. F. (1983) 'Heterogeneity of the Action Potential in Isolated Rat Ventricular Myocytes and Tissue'. *Circulation Research* 52 (3), 280-290

- Waumsley, J., Atter, N., Boyle, S., and Buckroyd, J. (2011) 'Obesity in the UK: A Psychological Perspective'. *Obesity Working Group*, 1-84
- Wende, A. R. and Abel, E. D. (2010) 'Lipotoxicity in the Heart'. *Biochimica Et Biophysica Acta (BBA)-Molecular and Cell Biology of Lipids* 1801 (3), 311-319
- WHO (2020) *Obesity and Overweight* [online] available from <<https://www.who.int/news-room/fact-sheets/detail/obesity-and-overweight>> [05 2020]
- WHO (2019) *World Health Organization Model List of Essential Medicines: 21st List 2019* [online] available from [2020]
- Wiener, C., Fauci, A., Braunwald, E., Kasper, D., Hauser, S., Longo, D., Jameson, J., Loscalzo, J., and Brown, C. (2012) *Harrisons Principles of Internal Medicine Self-Assessment and Board Review 18th Edition.*: McGraw Hill Professional
- Wikoff, W. R., Frye, R. F., Zhu, H., Gong, Y., Boyle, S., Churchill, E., Cooper-Dehoff, R. M., Beitelshes, A. L., Chapman, A. B., Fiehn, O., Johnson, J. A., Kaddurah-Daouk, R., and Pharmacometabolomics Research Network (2013) 'Pharmacometabolomics Reveals Racial Differences in Response to Atenolol Treatment'. *PloS One* 8 (3), e57639
- Wilkinson, I. B., McEniery, C. M., and Cockcroft, J. R. (2006) 'Atenolol and Cardiovascular Risk: An Issue Close to the Heart'. *Lancet (London, England)* 367 (9511), 627-629
- Williams, T., Chambers, J., Roberts, L., Henderson, R., and Overton, J. (2003) 'Diet-induced Obesity and Cardiovascular Regulation in C57BL/6J Mice'. *Clinical and Experimental Pharmacology and Physiology* 30 (10), 769-778
- Wilson, C., Tran, M. K., Salazar, K. L., Young, M. E., and Taegtmeier, H. (2007) 'Western Diet, but Not High Fat Diet, Causes Derangements of Fatty Acid Metabolism and Contractile Dysfunction in the Heart of Wistar Rats'. *The Biochemical Journal* 406 (3), 457-467
- Wilson, D., Jackson, T., Sapey, E., and Lord, J. M. (2017) 'Frailty and Sarcopenia: The Potential Role of an Aged Immune System'. *Ageing Research Reviews*
- Wofford, M. R., Anderson, D. C., Brown, C. A., Jones, D. W., Miller, M. E., and Hall, J. E. (2001) 'Antihypertensive Effect of A-and B-Adrenergic Blockade in Obese and Lean Hypertensive Subjects'. *American Journal of Hypertension* 14 (7), 694-698
- Wohlgemuth, Seo, A. Y., Marzetti, E., Lees, H. A., and Leeuwenburgh, C. (2010) 'Skeletal Muscle Autophagy and Apoptosis during Aging: Effects of Calorie Restriction and Life-Long Exercise'. *Experimental Gerontology* 45 (2), 138-148
- Wojcicki, J., Jaroszynska, M., Drozdik, M., Pawlik, A., Gawronska-Szklarz, B., and Sterna, R. (2003) 'Comparative Pharmacokinetics and Pharmacodynamics of Propranolol and Atenolol in Normolipaeamic and Hyperlipidaemic Obese Subjects'. *Biopharmaceutics & Drug Disposition* 24 (5), 211-218

- Wong, Y. Y., Handoko, M. L., Mouchaers, K. T., de Man, F. S., Vonk-Noordegraaf, A., and van der Laarse, W. J. (2010) 'Reduced Mechanical Efficiency of Rat Papillary Muscle Related to Degree of Hypertrophy of Cardiomyocytes'. *American Journal of Physiology. Heart and Circulatory Physiology* 298 (4), H1190-7
- Woodcock, E. A. and Matkovich, S. J. (2005) 'Cardiomyocytes Structure, Function and Associated Pathologies'. *The International Journal of Biochemistry & Cell Biology* 37 (9), 1746-1751
- Woods, S. C., Seeley, R. J., Rushing, P. A., D'Alessio, D., and Tso, P. (2003) 'A Controlled High-Fat Diet Induces an Obese Syndrome in Rats'. *The Journal of Nutrition* 133 (4), 1081-1087
- Wright, J. J., Kim, J., Buchanan, J., Boudina, S., Sena, S., Bakirtzi, K., Ilkun, O., Theobald, H. A., Cooksey, R. C., and Kandror, K. V. (2009) 'Mechanisms for Increased Myocardial Fatty Acid Utilization Following Short-Term High-Fat Feeding'. *Cardiovascular Research* 82 (2), 351-360
- Wu, S., Chen, W., Murphy, E., Gabel, S., Tomer, K. B., Foley, J., Steenbergen, C., Falck, J. R., Moomaw, C. R., and Zeldin, D. C. (1997) 'Molecular Cloning, Expression, and Functional Significance of a Cytochrome P450 Highly Expressed in Rat Heart Myocytes'. *The Journal of Biological Chemistry* 272 (19), 12551-12559
- Xiang, L., Naik, J. S., Hodnett, B. L., and Hester, R. L. (2006) 'Altered Arachidonic Acid Metabolism Impairs Functional Vasodilation in Metabolic Syndrome'. *American Journal of Physiology-Regulatory, Integrative and Comparative Physiology* 290 (1), R134-R138
- Xiao, R. P., Spurgeon, H. A., O'Connor, F., and Lakatta, E. G. (1994a) 'Age-Associated Changes in Beta-Adrenergic Modulation on Rat Cardiac Excitation-Contraction Coupling'. *The Journal of Clinical Investigation* 94 (5), 2051-2059
- Xiao, R. P., Spurgeon, H. A., O'Connor, F., and Lakatta, E. G. (1994b) 'Age-Associated Changes in Beta-Adrenergic Modulation on Rat Cardiac Excitation-Contraction Coupling'. *The Journal of Clinical Investigation* 94 (5), 2051-2059
- Xu, H., Garver, H., Fernandes, R., Phelps, J. T., Harkema, J. J., Galligan, J. J., and Fink, G. D. (2015) 'BK Channel Beta1-Subunit Deficiency Exacerbates Vascular Fibrosis and Remodelling but does Not Promote Hypertension in High-Fat Fed Obesity in Mice'. *Journal of Hypertension* 33 (8), 1611-1623
- Xue, H., Lu, Z., Tang, W. L., Pang, L. W., Wang, G. M., Wong, G. W., and Wright, J. M. (2015) 'First-line Drugs Inhibiting the Renin Angiotensin System Versus Other First-line Antihypertensive Drug Classes for Hypertension'. *The Cochrane Library*
- Yamakage, M. and Namiki, A. (2002) 'Calcium Channels—basic Aspects of their Structure, Function and Gene Encoding; Anesthetic Action on the Channels—a Review'. *Canadian Journal of Anesthesia* 49 (2), 151-164

- Yan, L., Vatner, D. E., O'Connor, J. P., Ivessa, A., Ge, H., Chen, W., Hirotani, S., Ishikawa, Y., Sadoshima, J., and Vatner, S. F. (2007) 'Type 5 Adenylyl Cyclase Disruption Increases Longevity and Protects Against Stress'. *Cell* 130 (2), 247-258
- Ye, J., Gao, Z., Yin, J., and He, Q. (2007) 'Hypoxia is a Potential Risk Factor for Chronic Inflammation and Adiponectin Reduction in Adipose Tissue of Ob/Ob and Dietary Obese Mice'. *American Journal of Physiology-Endocrinology and Metabolism* 293 (4), E1118-E1128
- Yin, F. C., Spurgeon, H. A., Rakusan, K., Weisfeldt, M. L., and Lakatta, E. G. (1982) 'Use of Tibial Length to Quantify Cardiac Hypertrophy: Application in the Aging Rat'. *The American Journal of Physiology* 243 (6), H941-7
- Yokoyama, M., Okada, S., Nakagomi, A., Moriya, J., Shimizu, I., Nojima, A., Yoshida, Y., Ichimiya, H., Kamimura, N., and Kobayashi, Y. (2014) 'Inhibition of Endothelial p53 Improves Metabolic Abnormalities Related to Dietary Obesity'. *Cell Reports* 7 (5), 1691-1703
- Young, Guthrie, P. H., Razeghi, P., Leighton, B., Abbasi, S., Patil, S., Youker, K. A., and Taegtmeier, H. (2002) 'Impaired Long-Chain Fatty Acid Oxidation and Contractile Dysfunction in the Obese Zucker Rat Heart'. *Diabetes* 51 (8), 2587-2595
- Young, M., Laws, F. A., Goodwin, G. W., and Taegtmeier, H. (2001) 'Reactivation of Peroxisome Proliferator-Activated Receptor Alpha is Associated with Contractile Dysfunction in Hypertrophied Rat Heart'. *The Journal of Biological Chemistry* 276 (48), 44390-44395
- Young, M., Patil, S., Ying, J., Depre, C., Ahuja, H. S., Shipley, G. L., Stepkowski, S. M., Davies, P. J., and Taegtmeier, H. (2001) 'Uncoupling Protein 3 Transcription is Regulated by Peroxisome Proliferator-Activated Receptor (Alpha) in the Adult Rodent Heart'. *FASEB Journal : Official Publication of the Federation of American Societies for Experimental Biology* 15 (3), 833-845
- Zachary, I. and Morgan, R. D. (2011) 'Therapeutic Angiogenesis for Cardiovascular Disease: Biological Context, Challenges, Prospects'. *Heart (British Cardiac Society)* 97 (3), 181-189
- Zhang, Y., Wang, W. E., Zhang, X., Li, Y., Chen, B., Liu, C., Ai, X., Zhang, X., Tian, Y., and Zhang, C. (2019) 'Cardiomyocyte PKA Ablation Enhances Basal Contractility while Eliminates Cardiac B-Adrenergic Response without Adverse Effects on the Heart'. *Circulation Research* 124 (12), 1760-1777
- Zhou, Y. T., Grayburn, P., Karim, A., Shimabukuro, M., Higa, M., Baetens, D., Orci, L., and Unger, R. H. (2000) 'Lipotoxic Heart Disease in Obese Rats: Implications for Human Obesity'. *Proceedings of the National Academy of Sciences of the United States of America* 97 (4), 1784-1789
- Zhu, X., Altschaf, B. A., Hajjar, R. J., Valdivia, H. H., and Schmidt, U. (2005) 'Altered Ca<sup>2+</sup> Sparks and Gating Properties of Ryanodine Receptors in Aging Cardiomyocytes'. *Cell Calcium* 37 (6), 583-591

- Zimmer, H. G. (1999) 'The Contributions of Carl Ludwig to Cardiology'. *The Canadian Journal of Cardiology* 15 (3), 323-329
- Zimmer, H. G. (1998) 'The Isolated Perfused Heart and its Pioneers'. *News in Physiological Sciences : An International Journal of Physiology Produced Jointly by the International Union of Physiological Sciences and the American Physiological Society* 13, 203-210
- Zurbier, C. and Van Beek, J. (1997) 'Mitochondrial Response to Heart Rate Steps in Isolated Rabbit Heart is Slowed After Myocardial Stunning'. *Circulation Research* 81 (1), 69-75

# Appendix

**Appendix 1** – The data shown below represents the coronary flow measurements for the 3, 6 and 18-month control models, as presented in chapter 4. Both the raw values and the normalised to stabilisation values are presented.

CHAPTER 4 - CONTROL DATA																		
Time	3M Avg.	SD	SEM	3M Avg. %	SD	SEM	6M Avg.	SD	SEM	6M Avg. %	SD	SEM	18M Avg.	SD	SEM	18M Avg. %	SD	SEM
5	19	1.915	1.106	100.397	0.794	0.458	26	6.455	3.727	100.735	1.471	0.849	21	1.000	0.577	100.287	0.575	0.332
10	19	1.915	1.106	100.397	0.794	0.458	26	6.455	3.727	100.735	1.471	0.849	21	1.000	0.577	100.287	0.575	0.332
15	19	1.915	1.106	100.397	0.794	0.458	25	5.477	3.162	99.265	1.471	0.849	21	1.000	0.577	100.287	0.575	0.332
20	18	2.363	1.364	98.810	2.381	1.375	25	5.477	3.162	99.265	1.471	0.849	20	0.500	0.289	99.138	1.724	0.995
25	18	1.708	0.986	99.147	2.864	1.654	25	5.477	3.162	99.265	1.471	0.849	20	1.258	0.726	99.037	2.746	1.585
30	18	1.633	0.943	97.897	5.317	3.070	25	5.477	3.162	99.265	1.471	0.849	20	1.414	0.816	97.787	3.253	1.878
35	18	1.633	0.943	97.897	5.317	3.070	25	5.439	3.140	100.360	4.790	2.765	20	1.708	0.986	96.537	5.111	2.951
40	18	1.633	0.943	97.897	5.317	3.070	25	5.439	3.140	100.360	4.790	2.765	20	1.732	1.000	95.287	4.564	2.635
45	18	1.291	0.745	95.258	4.776	2.758	25	5.439	3.140	100.360	4.790	2.765	19	1.258	0.726	94.138	2.854	1.648
50	17	0.957	0.553	94.008	5.470	3.158	25	4.967	2.867	99.625	5.620	3.244	19	1.414	0.816	92.888	3.394	1.960
55	17	1.414	0.816	92.421	2.814	1.625	24	4.031	2.327	97.059	5.882	3.396	19	1.500	0.866	94.138	4.981	2.876
60	17	1.414	0.816	92.421	2.814	1.625	24	3.594	2.075	95.282	6.942	4.008	19	1.500	0.866	94.138	4.981	2.876
65	17	1.414	0.816	92.421	2.814	1.625	23	3.559	2.055	92.220	6.582	3.800	19	1.500	0.866	91.739	6.238	3.601
70	17	0.957	0.553	94.008	5.470	3.158	23	3.109	1.795	90.443	7.556	4.363	19	2.217	1.280	91.638	8.798	5.079
75	17	1.500	0.866	93.869	5.791	3.344	22	3.202	1.848	89.401	7.618	4.398	19	2.217	1.280	91.638	8.798	5.079
80	17	0.957	0.553	94.008	5.470	3.158	22	2.708	1.563	88.666	8.932	5.157	18	2.217	1.280	89.138	7.957	4.594
85	18	1.291	0.745	95.258	4.776	2.758	22	2.708	1.563	88.666	8.932	5.157	18	2.160	1.247	87.888	7.073	4.084
90	18	1.291	0.745	95.258	4.776	2.758	22	2.380	1.374	86.794	9.393	5.423	18	2.582	1.491	87.888	10.001	5.774
95	17	1.826	1.054	92.282	3.309	1.910	21	2.500	1.443	85.752	9.519	5.496	18	2.380	1.374	85.489	9.529	5.502
100	17	1.414	0.816	92.421	2.814	1.625	21	2.708	1.563	84.616	8.952	5.169	18	2.380	1.374	85.489	9.529	5.502
105	17	1.708	0.986	93.671	2.470	1.426	21	3.109	1.795	82.289	6.954	4.015	17	2.449	1.414	82.989	9.259	5.346
110	18	1.291	0.745	95.258	4.776	2.758	21	3.109	1.795	82.289	6.954	4.015	17	2.062	1.190	81.839	7.970	4.602
115	17	1.500	0.866	93.869	5.791	3.344	20	3.403	1.965	81.153	7.413	4.280	17	2.062	1.190	81.839	7.970	4.602
120	17	1.155	0.667	92.619	6.002	3.465	21	3.317	1.915	82.343	9.498	5.484	17	2.062	1.190	81.839	7.970	4.602
125	17	1.155	0.667	92.619	6.002	3.465	20	3.403	1.965	81.153	7.413	4.280	17	2.380	1.374	80.589	9.622	5.555
130	17	1.155	0.667	92.619	6.002	3.465	21	3.317	1.915	82.343	9.498	5.484	16	1.826	1.054	78.190	6.940	4.007
135	17	1.500	0.866	93.869	5.791	3.344	20	2.872	1.658	79.736	12.227	7.059	16	1.708	0.986	76.940	5.632	3.251
140	17	1.500	0.866	93.869	5.791	3.344	19	3.266	1.886	76.368	10.800	6.236	16	2.217	1.280	76.839	7.397	4.271
145	17	1.500	0.866	91.032	2.853	1.647	19	3.266	1.886	76.368	10.800	6.236	16	2.217	1.280	76.839	7.397	4.271
150	17	1.732	1.000	89.643	4.878	2.816	19	2.872	1.658	75.633	11.658	6.731	15	1.893	1.093	74.440	6.026	3.479
155	17	1.732	1.000	89.643	4.878	2.816	18	3.266	1.886	72.264	10.327	5.962	15	1.893	1.093	74.440	6.026	3.479
160	17	1.732	1.000	89.643	4.878	2.816	18	2.887	1.667	70.487	10.878	6.280	15	1.893	1.093	74.440	6.026	3.479

**Appendix 2** – The data shown below represents the left ventricular developed pressure measurements for the 3, 6 and 18-month control models, as presented in chapter 4. Both the raw values and the normalised to stabilisation values are presented.

CHAPTER 4 - CONTROL DATA																		
Time	3M Avg.	SD	SEM	3M Avg. %	SD	SEM	6M Avg.	SD	SEM	6M Avg. %	SD	SEM	18M Avg.	SD	SEM	18M Avg. %	SD	SEM
5	120.11	16.334	9.431	135.108	18.018	10.403	148.37	21.886	12.636	101.546	3.245	1.874	98.41	0.642	0.371	102.279	1.084	0.626
10	117.14	18.358	10.599	137.583	16.608	9.589	147.22	23.496	13.565	98.766	1.653	0.954	100.39	3.881	2.241	101.348	1.292	0.746
15	117.43	20.535	11.856	140.833	19.366	11.181	145.14	22.844	13.189	98.792	1.989	1.148	102.54	1.469	0.848	99.924	0.470	0.271
20	119.85	20.310	11.726	135.590	19.699	11.373	140.23	23.075	13.322	100.896	2.028	1.171	98.66	3.312	1.912	96.449	1.150	0.664
25	120.27	15.744	9.090	136.838	19.954	11.520	133.68	30.424	17.566	101.721	2.907	1.679	99.57	3.786	2.186	91.194	7.487	4.322
30	119.96	16.669	9.624	135.498	19.240	11.108	131.31	30.334	17.514	101.368	2.743	1.584	98.61	2.075	1.198	89.561	7.384	4.263
35	119.27	18.465	10.661	133.720	24.657	14.236	127.83	29.079	16.789	100.586	1.183	0.683	96.98	7.196	4.155	87.301	7.016	4.050
40	115.47	16.669	9.624	131.010	25.533	14.741	122.61	30.892	17.836	97.619	5.925	3.421	95.02	9.647	5.570	83.484	8.900	5.138
45	114.87	12.992	7.501	126.708	21.052	12.155	121.52	30.387	17.544	97.608	9.251	5.341	92.20	8.446	4.876	82.701	8.777	5.067
50	112.19	12.841	7.413	121.548	18.284	10.556	116.92	29.233	16.878	95.165	6.490	3.747	88.52	6.525	3.767	79.676	8.750	5.052
55	108.89	13.422	7.749	119.060	20.133	11.624	111.14	24.624	14.217	92.251	5.078	2.932	86.53	6.756	3.901	75.984	5.896	3.404
60	107.99	14.156	8.173	118.505	18.627	10.754	106.74	19.252	11.115	91.418	5.872	3.390	86.25	6.487	3.745	73.382	3.698	2.135
65	107.64	12.806	7.393	117.455	19.387	11.193	106.47	17.940	10.358	91.201	4.864	2.808	85.40	6.242	3.604	73.339	4.085	2.359
70	107.29	14.577	8.416	114.948	21.044	12.149	109.05	21.171	12.223	90.693	2.696	1.557	83.44	7.397	4.271	75.003	6.795	3.923
75	105.24	14.070	8.123	114.178	23.397	13.508	105.11	19.830	11.449	88.992	2.778	1.604	82.83	10.172	5.873	72.372	6.644	3.836
80	104.64	13.524	7.808	110.830	22.020	12.713	99.68	18.371	10.606	88.587	4.576	2.642	80.51	10.023	5.787	68.718	6.511	3.759
85	101.52	15.929	9.197	111.085	21.249	12.268	101.08	16.221	9.365	85.647	3.062	1.768	80.85	10.699	6.177	69.814	5.686	3.283
90	101.40	16.363	9.447	109.888	20.498	11.835	99.51	16.732	9.660	85.494	2.713	1.566	80.14	11.449	6.610	68.749	6.518	3.763
95	100.51	16.663	9.620	105.385	18.124	10.464	97.61	18.137	10.471	84.689	2.994	1.729	77.31	13.602	7.853	67.240	6.130	3.539
100	98.22	18.544	10.707	105.088	20.089	11.598	102.51	14.647	8.456	82.532	3.566	2.059	77.01	14.283	8.246	70.783	3.087	1.782
105	98.51	15.537	8.970	100.778	19.362	11.179	98.46	12.542	7.241	83.146	4.213	2.432	73.82	13.844	7.993	68.080	2.821	1.629
110	97.86	17.323	10.001	101.558	19.874	11.474	95.23	8.887	5.131	82.404	4.573	2.640	74.37	13.390	7.731	66.167	5.527	3.191
115	97.34	17.905	10.338	99.770	17.491	10.099	93.39	10.685	6.169	81.807	2.941	1.698	73.19	12.546	7.244	64.778	5.188	2.995
120	96.05	19.689	11.368	98.430	20.024	11.561	97.28	11.907	6.874	80.539	4.448	2.568	72.43	15.651	9.036	67.297	3.035	1.752
125	95.23	19.716	11.383	98.390	20.581	11.883	94.78	12.382	7.149	79.830	4.367	2.521	72.45	15.910	9.185	65.579	4.739	2.736
130	95.50	17.638	10.183	96.540	18.115	10.459	88.95	9.530	5.502	80.265	2.753	1.590	71.25	15.285	8.825	61.652	3.488	2.014
135	93.44	19.745	11.400	96.400	19.494	11.255	91.91	11.468	6.621	77.700	5.440	3.141	71.01	15.343	8.859	63.648	4.869	2.811
140	94.14	19.117	11.037	93.513	19.056	11.002	90.30	11.095	6.405	78.931	3.910	2.258	69.14	16.554	9.557	62.456	2.410	1.392
145	94.10	17.287	9.980	90.493	19.757	11.407	88.25	11.794	6.809	79.113	3.776	2.180	66.95	17.192	9.926	61.009	3.956	2.284
150	94.45	20.360	11.755	91.768	19.269	11.125	87.64	12.980	7.494	79.116	6.264	3.616	67.86	16.796	9.697	60.449	2.666	1.539
155	94.00	19.742	11.398	91.555	17.526	10.119	83.52	11.142	6.433	78.769	5.615	3.242	67.60	14.940	8.625	57.696	2.439	1.408
160	93.58	19.091	11.022	89.268	20.856	12.041	86.79	10.288	5.940	78.461	5.087	2.937	65.91	16.840	9.722	60.169	5.088	2.938

**Appendix 3** – The data shown below represents the heart rate measurements for the 3, 6 and 18-month control models, as presented in chapter 4. Both the raw values and the normalised to stabilisation values are presented.

CHAPTER 4 - CONTROL DATA																		
Time	3M Avg.	SD	SEM	3M Avg. %	SD	SEM	6M Avg.	SD	SEM	6M Avg. %	SD	SEM	18M Avg.	SD	SEM	18M Avg. %	SD	SEM
5	308	9.574	5.528	99.633	1.417	0.818	275	3.245	1.874	98.408	0.642	0.371	345	9.574	5.528	101.077	4.537	2.619
10	313	12.583	7.265	101.249	2.787	1.609	270	1.653	0.954	100.394	3.881	2.241	340	12.583	7.265	99.176	3.841	2.217
15	308	18.930	10.929	99.564	3.623	2.091	275	1.989	1.148	102.536	1.469	0.848	348	18.930	10.929	101.377	2.740	1.582
20	308	17.078	9.860	99.554	1.387	0.801	275	2.028	1.171	98.662	3.312	1.912	338	17.078	9.860	98.370	2.370	1.368
25	308	20.616	11.902	99.533	3.373	1.948	278	2.907	1.679	99.574	3.786	2.186	338	20.616	11.902	98.195	4.741	2.737
30	295	10.000	5.774	95.589	2.256	1.303	273	2.743	1.584	98.611	2.075	1.198	340	10.000	5.774	99.213	6.535	3.773
35	303	9.574	5.528	98.073	4.242	2.449	270	1.183	0.683	96.975	7.196	4.155	338	9.574	5.528	98.453	9.209	5.317
40	295	18.380	10.612	95.511	2.348	1.356	268	5.925	3.421	95.019	9.647	5.570	333	17.321	10.000	97.209	9.263	5.348
45	295	10.000	5.774	95.589	2.256	1.303	275	9.251	5.341	92.200	8.446	4.876	335	10.000	5.774	97.918	8.698	5.022
50	300	14.142	8.165	97.206	3.783	2.184	288	6.490	3.747	88.519	6.525	3.767	335	14.142	8.165	97.918	8.698	5.022
55	303	18.930	10.929	97.975	4.388	2.533	283	5.078	2.932	86.534	6.756	3.901	335	18.930	10.929	97.693	12.008	6.933
60	308	24.612	14.210	99.357	9.744	5.626	298	5.872	3.390	86.249	6.487	3.745	345	7.291	4.210	100.150	12.840	7.413
65	305	12.679	7.321	98.666	6.425	3.710	283	4.864	2.808	85.398	6.242	3.604	350	12.679	7.321	101.807	9.537	5.506
70	293	12.583	7.265	94.742	1.352	0.780	290	2.696	1.557	83.443	7.397	4.271	355	12.583	7.265	103.144	10.642	6.144
75	293	22.174	12.802	94.673	4.664	2.693	295	2.778	1.604	82.835	10.172	5.873	360	4.853	2.802	104.562	9.798	5.657
80	308	15.419	8.902	99.533	3.373	1.948	285	4.576	2.642	80.506	10.023	5.787	358	15.419	8.902	103.807	10.562	6.098
85	295	13.412	7.744	95.531	6.502	3.754	273	3.062	1.768	80.854	10.699	6.177	358	13.412	7.744	103.733	8.962	5.174
90	293	11.781	6.802	94.673	4.664	2.693	283	2.713	1.566	80.138	11.449	6.610	360	11.781	6.802	104.254	11.134	6.428
95	298	11.402	6.583	96.212	5.843	3.373	280	2.994	1.729	77.313	13.602	7.853	345	11.402	6.583	100.158	9.954	5.747
100	288	12.540	7.240	92.959	6.009	3.469	278	3.566	2.059	77.005	14.283	8.246	360	12.540	7.240	104.378	9.943	5.741
105	293	15.227	8.791	94.497	8.987	5.189	280	4.213	2.432	73.824	13.844	7.993	348	15.227	8.791	100.803	10.510	6.068
110	303	15.227	8.791	97.741	8.875	5.124	280	4.573	2.640	74.374	13.390	7.731	350	15.227	8.791	101.485	9.107	5.258
115	300	17.563	10.140	96.971	7.376	4.259	270	2.941	1.698	73.190	12.546	7.244	318	17.321	10.000	92.249	6.046	3.491
120	290	17.607	10.165	93.806	5.299	3.059	270	4.448	2.568	72.428	15.651	9.036	340	9.760	5.635	98.676	10.245	5.915
125	293	7.679	4.434	94.654	5.079	2.932	268	4.367	2.521	72.446	15.910	9.185	348	7.679	4.434	101.216	6.925	3.998
130	305	6.484	3.744	98.745	5.379	3.105	260	2.753	1.590	71.246	15.285	8.825	373	6.484	3.744	108.228	11.247	6.494
135	303	18.930	10.929	98.335	4.140	2.390	263	5.440	3.141	71.005	15.343	8.859	345	18.930	10.929	100.751	9.325	5.384
140	303	7.679	4.434	97.897	5.013	2.894	268	3.910	2.258	69.144	16.554	9.557	330	7.679	4.434	95.967	9.475	5.470
145	305	7.846	4.530	98.676	4.352	2.513	263	3.776	2.180	66.954	17.192	9.926	335	7.846	4.530	97.670	5.998	3.463
150	298	11.402	6.583	96.271	6.634	3.830	258	6.264	3.616	67.862	16.796	9.697	335	11.402	6.583	97.385	8.843	5.106
155	303	14.695	8.484	97.819	6.706	3.872	263	5.615	3.242	67.603	14.940	8.625	338	14.695	8.484	98.632	7.610	4.394
160	305	7.846	4.530	98.676	4.352	2.513	265	5.087	2.937	65.910	16.840	9.722	338	7.846	4.530	97.773	9.863	5.694

**Appendix 4** – The data shown below represents the coronary flow measurements for the 6 and 18-month lean and HFD control models, as presented in chapter 5. Both the raw values and the normalised to stabilisation values are presented.

CHAPTER 5 - CONTROL DATA																								
Time	6M Lean Avg.	SD	SEM	6M Lean Avg. %	SD	SEM	6M HFD Avg.	SD	SEM	6M HFD Avg. %	SD	SEM	18M Lean Avg.	SD	SEM	18M Lean Avg. %	SD	SEM	18M HFD Avg.	SD	SEM	18M HFD Avg. %	SD	SEM
5	26	6.455	3.727	100.735	1.471	0.849	28	0.500	0.289	100.455	0.909	0.525	21	1.000	0.577	100.287	0.575	0.332	25	1.000	0.577	100.005	0.851	0.491
10	26	6.455	3.727	100.735	1.471	0.849	28	0.500	0.289	100.455	0.909	0.525	21	1.000	0.577	100.287	0.575	0.332	25	1.000	0.577	100.005	0.851	0.491
15	25	5.477	3.162	99.265	1.471	0.849	28	0.816	0.471	99.545	0.909	0.525	21	1.000	0.577	100.287	0.575	0.332	25	1.000	0.577	100.005	0.851	0.491
20	25	5.477	3.162	99.265	1.471	0.849	28	0.816	0.471	99.545	0.909	0.525	20	0.500	0.289	99.138	1.724	0.995	25	1.291	0.745	99.984	2.552	1.473
25	25	5.477	3.162	99.265	1.471	0.849	28	0.816	0.471	99.545	0.909	0.525	20	1.258	0.726	99.037	2.746	1.585	25	1.291	0.745	99.995	3.057	1.765
30	25	5.477	3.162	99.265	1.471	0.849	27	0.957	0.553	96.898	3.040	1.755	20	1.414	0.816	97.787	3.253	1.878	25	1.708	0.986	100.956	3.613	2.086
35	25	5.439	3.140	100.360	4.790	2.765	27	1.500	0.866	95.079	4.029	2.326	20	1.708	0.986	96.537	5.111	2.951	25	1.291	0.745	100.016	3.921	2.264
40	25	5.439	3.140	100.360	4.790	2.765	27	1.915	1.106	94.170	5.445	3.144	20	1.732	1.000	95.287	4.564	2.635	24	1.258	0.726	98.964	2.254	1.301
45	25	5.439	3.140	100.360	4.790	2.765	27	1.915	1.106	94.170	5.445	3.144	19	1.258	0.726	94.138	2.854	1.648	24	1.258	0.726	98.964	2.254	1.301
50	25	4.967	2.867	99.625	5.620	3.244	26	2.309	1.333	92.385	6.976	4.027	19	1.414	0.816	92.888	3.394	1.960	24	1.258	0.726	98.964	2.254	1.301
55	24	4.031	2.327	97.059	5.882	3.396	26	1.826	1.054	92.432	5.921	3.418	19	1.500	0.866	94.138	4.981	2.876	24	1.708	0.986	96.891	4.414	2.549
60	24	3.594	2.075	95.282	6.942	4.008	26	1.915	1.106	90.646	6.106	3.525	19	1.500	0.866	94.138	4.981	2.876	24	1.291	0.745	95.930	3.901	2.252
65	23	3.559	2.055	92.220	6.582	3.800	26	1.915	1.106	90.646	6.106	3.525	19	1.500	0.866	91.739	6.238	3.601	23	1.708	0.986	94.888	5.603	3.235
70	23	3.109	1.795	90.443	7.556	4.363	25	1.708	0.986	89.784	5.883	3.396	19	2.217	1.280	91.638	8.798	5.079	23	1.708	0.986	92.804	4.472	2.582
75	23	3.109	1.795	90.443	7.556	4.363	25	1.291	0.745	87.105	3.980	2.298	19	2.217	1.280	91.638	8.798	5.079	22	1.633	0.943	89.749	4.357	2.516
80	22	2.630	1.518	89.707	8.994	5.193	24	1.258	0.726	84.441	3.967	2.290	18	2.217	1.280	89.138	7.957	4.594	21	2.000	1.155	85.581	4.540	2.621
85	22	2.630	1.518	89.707	8.994	5.193	24	1.414	0.816	85.350	5.090	2.939	18	2.160	1.247	87.888	7.073	4.084	21	2.000	1.155	85.581	4.540	2.621
90	22	2.363	1.364	87.836	9.723	5.613	24	1.258	0.726	84.488	5.188	2.995	18	2.582	1.491	87.888	10.001	5.774	20	1.893	1.093	82.547	4.718	2.724
95	22	2.363	1.364	87.836	9.723	5.613	23	2.160	1.247	81.841	8.407	4.854	18	2.380	1.374	85.489	9.529	5.502	20	2.062	1.190	82.558	5.989	3.458
100	22	2.646	1.528	86.699	9.507	5.489	22	1.708	0.986	79.146	6.480	3.741	18	2.380	1.374	85.489	9.529	5.502	20	2.062	1.190	82.558	5.989	3.458
105	21	3.162	1.826	84.373	8.457	4.883	22	1.258	0.726	77.328	3.976	2.295	17	2.449	1.414	82.989	9.259	5.346	20	2.062	1.190	82.558	5.989	3.458
110	21	3.096	1.787	83.331	7.456	4.305	21	0.957	0.553	75.556	2.993	1.728	17	2.062	1.190	81.839	7.970	4.602	20	1.732	1.000	79.604	6.500	3.753
115	21	3.416	1.972	82.195	8.084	4.667	20	1.258	0.726	72.030	4.833	2.790	17	2.062	1.190	81.839	7.970	4.602	19	2.217	1.280	76.468	7.662	4.423
120	21	3.304	1.908	83.385	9.864	5.695	20	1.258	0.726	72.030	4.833	2.790	17	2.062	1.190	81.839	7.970	4.602	18	2.646	1.528	71.248	8.327	4.807
125	21	3.416	1.972	82.195	8.084	4.667	20	0.577	0.333	69.336	1.501	0.867	17	2.380	1.374	80.589	9.622	5.555	17	2.217	1.280	70.287	6.973	4.026
130	21	3.304	1.908	83.385	9.864	5.695	19	0.957	0.553	66.672	3.222	1.860	16	1.826	1.054	78.190	6.940	4.007	17	2.582	1.491	69.256	8.721	5.035
135	20	2.944	1.700	80.778	12.800	7.390	19	0.957	0.553	66.672	3.222	1.860	16	1.708	0.986	76.940	5.632	3.251	17	2.500	1.443	68.214	8.027	4.634
140	20	3.416	1.972	78.451	12.229	7.061	18	1.414	0.816	64.008	4.982	2.877	16	2.217	1.280	76.839	7.397	4.271	16	2.217	1.280	66.200	7.065	4.079
145	20	3.416	1.972	78.451	12.229	7.061	18	1.291	0.745	62.206	4.098	2.366	16	2.217	1.280	76.839	7.397	4.271	16	2.217	1.280	66.200	7.065	4.079
150	19	3.096	1.787	77.716	13.149	7.592	18	1.291	0.745	62.206	4.098	2.366	15	1.893	1.093	74.440	6.026	3.479	16	1.500	0.866	66.269	4.426	2.555
155	19	3.416	1.972	74.347	11.799	6.812	17	1.500	0.866	59.589	5.652	3.263	15	1.893	1.093	74.440	6.026	3.479	16	2.062	1.190	64.186	6.800	3.926
160	18	3.096	1.787	73.612	12.660	7.309	17	1.732	1.000	58.679	6.218	3.590	15	1.893	1.093	74.440	6.026	3.479	16	2.062	1.190	64.186	6.800	3.926

**Appendix 5** – The data shown below represents the left ventricular developed pressure measurements for the 6 and 18-month lean and HFD control models, as presented in chapter 5. Both the raw values and the normalised to stabilisation values are presented.

CHAPTER 5 - CONTROL DATA																								
Time	6M Lean Avg.	SD	SEM	6M Lean Avg. %	SD	SEM	6M HFD Avg.	SD	SEM	6M HFD Avg. %	SD	SEM	18M Lean Avg.	SD	SEM	18M Lean Avg. %	SD	SEM	18M HFD Avg.	SD	SEM	18M HFD Avg. %	SD	SEM
5	148.37	21.886	12.636	101.546	3.245	1.874	174.310	14.425	8.328	100.187	1.497	0.864	98.41	0.642	0.371	102.279	1.084	0.626	174.310	14.425	8.328	100.187	1.497	0.864
10	147.22	23.496	13.565	98.766	1.653	0.954	175.960	17.810	10.283	101.000	2.184	1.261	100.39	3.881	2.241	101.348	1.292	0.746	175.960	17.810	10.283	101.000	2.184	1.261
15	145.14	22.844	13.189	98.792	1.989	1.148	171.890	17.150	9.902	98.673	1.538	0.888	102.54	1.469	0.848	99.924	0.470	0.271	171.890	17.150	9.902	98.673	1.538	0.888
20	140.23	23.075	13.322	100.896	2.028	1.171	174.013	11.309	6.529	100.140	2.643	1.526	98.66	3.312	1.912	96.449	1.150	0.664	174.013	11.309	6.529	100.140	2.643	1.526
25	133.68	30.424	17.566	101.721	2.907	1.679	174.058	20.829	12.026	99.820	4.293	2.478	99.57	3.786	2.186	91.194	7.487	4.322	174.058	20.829	12.026	99.820	4.293	2.478
30	131.31	30.334	17.514	101.368	2.743	1.584	172.735	21.630	12.488	98.996	4.320	2.494	98.61	2.075	1.198	89.561	7.384	4.263	172.735	21.630	12.488	98.996	4.320	2.494
35	127.83	29.079	16.789	100.586	1.183	0.683	171.595	18.666	10.777	98.468	3.448	1.991	96.98	7.196	4.155	87.301	7.016	4.050	171.595	18.666	10.777	98.468	3.448	1.991
40	122.61	30.892	17.836	97.619	5.925	3.421	169.078	12.426	7.174	97.284	3.592	2.074	95.02	9.647	5.570	83.484	8.900	5.138	169.078	12.426	7.174	97.284	3.592	2.074
45	121.52	30.387	17.544	97.608	9.251	5.341	168.030	20.616	11.902	96.451	6.635	3.831	92.20	8.446	4.876	82.701	8.777	5.067	168.030	20.616	11.902	96.451	6.635	3.831
50	116.92	29.233	16.878	95.165	6.490	3.747	166.415	24.102	13.915	95.458	9.055	5.228	88.52	6.525	3.767	79.676	8.750	5.052	166.415	24.102	13.915	95.458	9.055	5.228
55	111.14	24.624	14.217	92.251	5.078	2.932	164.488	24.451	14.117	94.294	8.742	5.047	86.53	6.756	3.901	75.984	5.896	3.404	164.488	24.451	14.117	94.294	8.742	5.047
60	106.74	19.252	11.115	91.418	5.872	3.390	159.548	22.252	12.847	91.460	7.357	4.247	86.25	6.487	3.745	73.382	3.698	2.135	159.548	22.252	12.847	91.460	7.357	4.247
65	106.47	17.940	10.358	91.201	4.864	2.808	157.788	19.542	11.283	90.707	8.557	4.940	85.40	6.242	3.604	73.339	4.085	2.359	157.788	19.542	11.283	90.707	8.557	4.940
70	109.05	21.171	12.223	90.693	2.696	1.557	155.968	19.984	11.538	89.717	9.585	5.534	83.44	7.397	4.271	75.003	6.795	3.923	155.968	19.984	11.538	89.717	9.585	5.534
75	105.11	19.830	11.449	88.992	2.778	1.604	151.608	22.996	13.277	87.138	10.999	6.350	82.83	10.172	5.873	72.372	6.644	3.836	151.608	22.996	13.277	87.138	10.999	6.350
80	99.68	18.371	10.606	88.587	4.576	2.642	146.373	25.374	14.650	83.979	11.465	6.619	80.51	10.023	5.787	68.718	6.511	3.759	146.373	25.374	14.650	83.979	11.465	6.619
85	101.08	16.221	9.365	85.647	3.062	1.768	156.943	19.123	11.040	90.800	14.413	8.321	80.85	10.699	6.177	69.814	5.686	3.283	156.943	19.123	11.040	90.800	14.413	8.321
90	99.51	16.732	9.660	85.494	2.713	1.566	158.425	16.519	9.537	91.685	13.741	7.934	80.14	11.449	6.610	68.749	6.518	3.763	158.425	16.519	9.537	91.685	13.741	7.934
95	97.61	18.137	10.471	84.689	2.994	1.729	157.568	14.860	8.579	91.328	14.541	8.395	77.31	13.602	7.853	67.240	6.130	3.539	157.568	14.860	8.579	91.328	14.541	8.395
100	102.51	14.647	8.456	82.532	3.566	2.059	158.370	17.805	10.280	91.827	15.936	9.201	77.01	14.283	8.246	70.783	3.087	1.782	158.370	17.805	10.280	91.827	15.936	9.201
105	98.46	12.542	7.241	83.146	4.213	2.432	158.483	21.102	12.183	91.965	17.762	10.255	73.82	13.844	7.993	68.080	2.821	1.629	158.483	21.102	12.183	91.965	17.762	10.255
110	95.23	8.887	5.131	82.404	4.573	2.640	154.068	22.874	13.207	89.530	19.223	11.098	74.37	13.390	7.731	66.167	5.527	3.191	154.068	22.874	13.207	89.530	19.223	11.098
115	93.39	10.685	6.169	81.807	2.941	1.698	152.815	20.937	12.088	88.790	18.273	10.550	73.19	12.546	7.244	64.778	5.188	2.995	152.815	20.937	12.088	88.790	18.273	10.550
120	97.28	11.907	6.874	80.539	4.448	2.568	150.653	22.827	13.179	87.688	20.155	11.636	72.43	15.651	9.036	67.297	3.035	1.752	150.653	22.827	13.179	87.688	20.155	11.636
125	94.78	12.382	7.149	79.830	4.367	2.521	145.633	22.267	12.856	84.769	19.527	11.274	72.45	15.910	9.185	65.579	4.739	2.736	145.633	22.267	12.856	84.769	19.527	11.274
130	88.95	9.530	5.502	80.265	2.753	1.590	144.260	18.738	10.819	83.700	15.883	9.170	71.25	15.285	8.825	61.652	3.488	2.014	144.260	18.738	10.819	83.700	15.883	9.170
135	91.91	11.468	6.621	77.700	5.440	3.141	142.448	16.801	9.700	82.634	14.916	8.612	71.01	15.343	8.859	63.648	4.869	2.811	142.448	16.801	9.700	82.634	14.916	8.612
140	90.30	11.095	6.405	78.931	3.910	2.258	140.888	19.466	11.239	81.974	17.801	10.277	69.14	16.554	9.557	62.456	2.410	1.392	140.888	19.466	11.239	81.974	17.801	10.277
145	88.25	11.794	6.809	79.113	3.776	2.180	138.388	21.456	12.388	80.498	18.236	10.529	66.95	17.192	9.926	61.009	3.956	2.284	138.388	21.456	12.388	80.498	18.236	10.529
150	87.64	12.980	7.494	79.116	6.264	3.616	136.615	21.243	12.265	79.555	18.726	10.812	67.86	16.796	9.697	60.449	2.666	1.539	136.615	21.243	12.265	79.555	18.726	10.812
155	83.52	11.142	6.433	78.769	5.615	3.242	134.368	19.934	11.509	78.099	16.900	9.757	67.60	14.940	8.625	57.696	2.439	1.408	134.368	19.934	11.509	78.099	16.900	9.757
160	86.79	10.288	5.940	78.461	5.087	2.937	132.970	22.173	12.802	77.399	18.540	10.704	65.91	16.840	9.722	60.169	5.088	2.938	132.970	22.173	12.802	77.399	18.540	10.704

**Appendix 6** – The data shown below represents the heart rate measurements for the 6 and 18-month lean and HFD control models, as presented in chapter 5. Both the raw values and the normalised to stabilisation values are presented.

CHAPTER 5 - CONTROL DATA																								
Time	6M Lean Avg.	SD	SEM	6M Lean Avg. %	SD	SEM	6M HFD Avg.	SD	SEM	6M HFD Avg. %	SD	SEM	18M Lean Avg.	SD	SEM	18M Lean Avg. %	SD	SEM	18M HFD Avg.	SD	SEM	18M HFD Avg. %	SD	SEM
5	275	3.245	1.874	98.408	0.642	0.371	323	11.180	6.455	102.036	2.644	1.526	345	9.574	5.528	101.077	4.537	2.619	305	83.467	1.874	102.971	83.467	4.108
10	270	1.653	0.954	100.394	3.881	2.241	313	11.180	6.455	98.710	2.088	1.205	340	12.583	7.265	99.176	3.841	2.217	295	79.373	0.954	99.683	79.373	0.934
15	275	1.989	1.148	102.536	1.469	0.848	313	9.487	5.477	98.956	3.441	1.987	348	18.930	10.929	101.377	2.740	1.582	295	88.882	1.148	99.070	88.882	2.375
20	275	2.028	1.171	98.662	3.312	1.912	318	9.487	5.477	100.298	3.630	2.096	338	17.078	9.860	98.370	2.370	1.368	293	88.081	1.171	98.276	88.081	2.169
25	278	2.907	1.679	99.574	3.786	2.186	305	9.487	5.477	95.933	11.054	6.382	338	20.616	11.902	98.195	4.741	2.737	305	99.833	1.679	101.920	99.833	2.622
30	273	2.743	1.584	98.611	2.075	1.198	305	9.487	5.477	95.980	13.742	7.934	340	10.000	5.774	99.213	6.535	3.773	318	89.954	1.584	106.997	89.954	2.711
35	270	1.183	0.683	96.975	7.196	4.155	288	9.421	5.439	90.954	7.886	4.553	338	9.574	5.528	98.453	9.209	5.317	318	71.356	0.683	108.264	71.356	5.540
40	268	5.925	3.421	95.019	9.647	5.570	295	9.421	5.439	93.098	5.734	3.311	333	17.321	10.000	97.209	9.263	5.348	308	82.614	3.421	103.908	82.614	5.333
45	275	9.251	5.341	92.200	8.446	4.876	295	9.421	5.439	93.141	11.794	6.809	335	10.000	5.774	97.918	8.698	5.022	320	69.761	5.341	109.197	69.761	4.600
50	288	6.490	3.747	88.519	6.525	3.767	303	8.602	4.967	95.428	9.295	5.366	335	14.142	8.165	97.918	8.698	5.022	313	58.523	3.747	107.315	58.523	5.678
55	283	5.078	2.932	86.534	6.756	3.901	280	6.982	4.031	88.716	12.003	6.930	335	18.930	10.929	97.693	12.008	6.933	310	80.416	2.932	104.955	80.416	5.527
60	298	5.872	3.390	86.249	6.487	3.745	280	6.225	3.594	88.565	16.943	9.782	345	7.291	4.210	100.150	12.840	7.413	308	65.511	3.390	105.269	65.511	6.607
65	283	4.864	2.808	85.398	6.242	3.604	280	6.164	3.559	88.664	12.459	7.193	350	12.679	7.321	101.807	9.537	5.506	303	70.887	2.808	103.285	70.887	6.246
70	290	2.696	1.557	83.443	7.397	4.271	290	5.385	3.109	92.041	11.913	6.878	355	12.583	7.265	103.144	10.642	6.144	288	60.208	1.557	98.415	60.208	4.669
75	295	2.778	1.604	82.835	10.172	5.873	295	5.545	3.202	93.581	17.059	9.849	360	4.853	2.802	104.562	9.798	5.657	310	58.878	1.604	106.991	58.878	9.110
80	285	4.576	2.642	80.506	10.023	5.787	278	4.690	2.708	88.017	13.917	8.035	358	15.419	8.902	103.807	10.562	6.098	318	80.571	2.642	107.786	80.571	3.274
85	273	3.062	1.768	80.854	10.699	6.177	283	4.690	2.708	89.216	14.862	8.581	358	13.412	7.744	103.733	8.962	5.174	293	63.443	1.768	100.038	63.443	4.991
90	283	2.713	1.566	80.138	11.449	6.610	285	4.123	2.380	90.256	9.907	5.720	360	11.781	6.802	104.254	11.134	6.428	313	58.523	1.566	107.393	58.523	6.721
95	280	2.994	1.729	77.313	13.602	7.853	280	4.330	2.500	88.763	12.545	7.243	345	11.402	6.583	100.158	9.954	5.747	308	68.007	1.729	105.012	68.007	4.532
100	278	3.566	2.059	77.005	14.283	8.246	280	4.690	2.708	88.569	6.681	3.858	360	12.540	7.240	104.378	9.943	5.741	313	57.951	2.059	107.785	57.951	8.561
105	280	4.213	2.432	73.824	13.844	7.993	298	5.385	3.109	94.233	5.251	3.032	348	15.227	8.791	100.803	10.510	6.068	303	71.356	2.432	103.069	71.356	4.641
110	280	4.573	2.640	74.374	13.390	7.731	293	5.385	3.109	92.494	6.063	3.501	350	15.227	8.791	101.485	9.107	5.258	295	62.450	2.640	101.048	62.450	5.865
115	270	2.941	1.698	73.190	12.546	7.244	278	5.895	3.403	88.021	5.685	3.282	318	17.321	10.000	92.249	6.046	3.491	295	58.023	1.698	101.229	58.023	5.838
120	270	4.448	2.568	72.428	15.651	9.036	278	5.745	3.317	88.069	9.259	5.346	340	9.760	5.635	98.676	10.245	5.915	308	74.106	2.568	104.440	74.106	2.643
125	268	4.367	2.521	72.446	15.910	9.185	283	5.895	3.403	89.268	4.307	2.487	348	7.679	4.434	101.216	6.925	3.998	315	81.035	2.521	106.677	81.035	2.565
130	260	2.753	1.590	71.246	15.285	8.825	288	5.745	3.317	91.006	2.977	1.719	373	6.484	3.744	108.228	11.247	6.494	303	66.521	1.590	103.290	66.521	5.783
135	263	5.440	3.141	71.005	15.343	8.859	300	4.975	2.872	95.272	7.348	4.243	345	18.930	10.929	100.751	9.325	5.384	315	89.629	3.141	106.064	89.629	0.740
140	268	3.910	2.258	69.144	16.554	9.557	295	5.657	3.266	93.146	4.507	2.602	330	7.679	4.434	95.967	9.475	5.470	323	88.835	2.258	108.837	88.835	0.658
145	263	3.776	2.180	66.954	17.192	9.926	283	5.657	3.266	89.074	9.714	5.608	335	7.846	4.530	97.670	5.998	3.463	315	80.208	2.180	106.718	80.208	4.460
150	258	6.264	3.616	67.862	16.796	9.697	295	4.975	2.872	93.392	7.590	4.382	335	11.402	6.583	97.385	8.843	5.106	298	59.090	3.616	102.063	59.090	6.811
155	263	5.615	3.242	67.603	14.940	8.625	308	5.657	3.266	97.511	11.870	6.853	338	14.695	8.484	98.632	7.610	4.394	298	74.106	3.242	100.873	74.106	2.230
160	265	5.087	2.937	65.910	16.840	9.722	313	5.000	2.887	99.197	12.690	7.327	338	7.846	4.530	97.773	9.863	5.694	293	68.981	2.937	99.466	68.981	2.863

**Appendix 7** – The data shown below represents the coronary flow measurements for the 3, 6 and 18-month Dobutamine treated hearts, as presented in chapter 6. Both the raw values and the normalised to stabilisation values are presented.

CHAPTER 6 - DOBUTAMINE DATA																			
Concentration	Time	3M Avg.	SD	SEM	3M Avg. %	SD	SEM	6M Avg.	SD	SEM	6M Avg. %	SD	SEM	18M Avg.	SD	SEM	18M Avg. %	SD	SEM
Stabilisation	5	21	3.873	2.236	101.392	1.348	0.778	25	2.121	1.225	99.050	1.117	0.645	19	1.414	0.816	97.834	3.371	1.946
	10	21	3.873	2.236	101.392	1.348	0.778	25	2.502	1.444	99.050	1.117	0.645	20	1.225	0.707	101.235	2.619	1.512
	15	20	4.272	2.466	99.779	2.082	1.202	26	2.668	1.540	101.637	1.904	1.099	20	0.707	0.408	99.588	0.873	0.504
	20	20	4.031	2.327	97.436	1.760	1.016	25	2.806	1.620	100.262	1.767	1.020	20	0.000	0.000	101.343	4.226	2.440
1 nM	25	20	4.243	2.449	98.572	4.004	2.312	28	2.935	1.695	112.395	13.865	8.005	23	1.871	1.080	115.006	13.847	7.995
	30	20	4.397	2.539	98.446	2.434	1.405	28	2.935	1.695	112.395	13.865	8.005	23	2.121	1.225	116.673	14.290	8.250
	35	20	4.082	2.357	98.852	6.379	3.683	28	2.935	1.695	112.395	13.865	8.005	23	2.550	1.472	118.428	17.151	9.902
	40	20	4.425	2.555	97.239	5.682	3.281	28	2.468	1.425	112.557	13.242	7.645	23	2.550	1.472	118.428	17.151	9.902
3 nM	45	20	4.573	2.640	99.582	3.974	2.295	28	2.213	1.278	111.345	14.856	8.577	24	1.225	0.707	121.720	11.172	6.450
	50	20	3.862	2.230	100.185	4.325	2.497	28	2.428	1.402	109.970	15.960	9.215	24	1.871	1.080	123.474	14.714	8.495
	55	19	4.243	2.449	93.480	4.498	2.597	28	2.428	1.402	109.970	15.960	9.215	24	0.000	0.000	121.611	5.072	2.928
10 nM	60	19	4.243	2.449	93.480	4.498	2.597	27	2.405	1.388	108.581	13.019	7.516	24	0.707	0.408	123.278	5.112	2.952
	65	20	3.697	2.134	96.426	2.904	1.677	28	2.428	1.402	109.970	15.960	9.215	24	1.225	0.707	121.524	4.000	2.310
	70	20	4.435	2.560	95.823	4.043	2.334	27	2.368	1.367	105.995	15.746	9.091	24	1.225	0.707	121.524	4.000	2.310
	75	20	3.651	2.108	99.049	3.264	1.885	26	2.138	1.234	104.783	17.239	9.953	24	1.225	0.707	121.503	2.170	1.253
100 nM	80	21	4.243	2.449	103.665	3.747	2.163	26	2.090	1.207	103.394	14.336	8.277	24	2.550	1.472	119.728	9.205	5.315
	85	21	4.646	2.682	102.052	5.132	2.963	26	2.307	1.332	102.019	15.537	8.970	24	2.449	1.414	121.395	7.860	4.538
	90	22	4.435	2.560	106.008	2.490	1.437	26	2.307	1.332	102.019	15.537	8.970	24	2.449	1.414	121.395	7.860	4.538
	95	21	4.272	2.466	104.872	1.422	0.821	26	2.551	1.473	103.231	14.396	8.312	25	2.550	1.472	124.795	9.079	5.242
1 µM	100	22	4.435	2.560	106.008	2.490	1.437	24	2.890	1.669	95.118	15.847	9.149	25	3.240	1.871	126.441	12.564	7.254
	105	22	4.787	2.764	107.062	8.554	4.939	24	2.412	1.393	93.891	11.214	6.474	25	2.828	1.633	128.196	11.365	6.562
	110	21	3.916	2.261	103.862	2.371	1.369	23	2.893	1.670	92.340	10.984	6.342	25	1.414	0.816	124.904	5.355	3.092
	115	21	3.916	2.261	103.862	2.371	1.369	24	2.706	1.562	93.714	8.254	4.766	25	1.414	0.816	124.904	5.355	3.092
10 µM	120	22	4.349	2.511	107.342	3.956	2.284	23	2.640	1.524	89.739	8.274	4.777	24	1.871	1.080	123.237	8.829	5.097
	125	22	4.272	2.466	107.495	2.359	1.362	22	2.756	1.591	86.961	5.197	3.000	24	3.082	1.780	123.216	14.662	8.465
	130	22	4.397	2.539	108.631	1.339	0.773	22	3.152	1.820	86.784	8.249	4.762	25	1.871	1.080	124.991	10.775	6.221
	135	22	4.113	2.375	110.091	3.732	2.155	21	2.690	1.553	82.986	5.476	3.162	25	3.082	1.780	128.284	14.673	8.472
30 µM	140	22	4.856	2.804	109.488	4.579	2.643	20	2.261	1.305	79.187	5.643	3.258	26	3.082	1.780	130.038	15.974	9.223
	145	22	4.349	2.511	107.342	3.956	2.284	21	1.933	1.116	81.936	2.120	1.224	26	2.449	1.414	131.705	12.445	7.185
	150	22	3.916	2.261	108.955	2.890	1.669	20	2.171	1.253	79.172	1.010	0.583	27	3.742	2.160	134.997	17.348	10.016
	155	22	4.397	2.539	108.631	1.339	0.773	20	1.727	0.997	79.335	3.746	2.163	27	3.240	1.871	136.663	14.177	8.185
	160	22	4.397	2.539	108.631	1.339	0.773	21	1.933	1.116	81.936	2.120	1.224	27	3.536	2.041	134.909	14.609	8.434

**Appendix 8** – The data shown below represents the left ventricular developed pressure measurements for the 3, 6 and 18-month Dobutamine treated hearts, as presented in chapter 6. Both the raw values and the normalised to stabilisation values are presented.

CHAPTER 6 - DOBUTAMINE DATA																			
Concentration	Time	3M Avg.	SD	SEM	3M Avg. %	SD	SEM	6M Avg.	SD	SEM	6M Avg. %	SD	SEM	18M Avg.	SD	SEM	18M Avg. %	SD	SEM
Stabilisation	5	111.293	23.154	13.368	97.527	4.895	2.826	144.843	13.416	7.746	101.156	3.513	2.028	109.130	8.426	4.865	99.858	1.518	0.876
	10	111.313	24.204	13.974	97.406	4.626	2.671	142.650	12.023	6.941	99.629	1.160	0.670	108.837	10.611	6.126	99.535	3.570	2.061
	15	115.118	21.506	12.416	101.234	2.384	1.376	142.820	16.726	9.657	99.608	2.523	1.457	108.453	8.578	4.952	99.243	2.806	1.620
	20	117.375	17.960	10.369	103.834	6.804	3.928	142.627	13.106	7.567	99.607	3.796	2.192	110.737	7.484	4.321	101.364	2.279	1.316
1 nM	25	125.113	19.103	11.029	111.331	14.424	8.327	161.270	29.809	17.210	112.415	14.484	8.362	162.177	6.637	3.832	148.807	13.636	7.873
	30	128.870	16.334	9.430	114.677	12.680	7.321	173.640	36.572	21.115	120.899	17.586	10.153	161.593	7.514	4.338	148.181	11.743	6.780
	35	127.633	21.294	12.294	112.824	9.171	5.295	175.417	36.152	20.872	122.105	16.578	9.571	164.473	9.022	5.209	150.904	14.756	8.519
3 nM	40	127.400	22.760	13.141	112.185	3.210	1.853	168.140	38.633	22.305	116.884	17.619	10.172	170.010	4.616	2.665	155.950	12.256	7.076
	45	135.973	21.914	12.652	119.998	3.762	2.172	169.950	36.299	20.957	118.161	15.411	8.897	164.093	6.168	3.561	150.571	13.697	7.908
	50	129.868	21.050	12.153	114.611	4.656	2.688	170.100	34.684	20.025	118.272	13.877	8.012	162.537	5.458	3.151	149.143	13.325	7.693
10 nM	55	128.983	21.433	12.374	113.767	4.256	2.457	171.827	33.105	19.113	119.559	13.232	7.639	155.040	11.489	6.633	142.147	13.527	7.810
	60	129.390	23.735	13.703	113.791	0.899	0.519	176.677	36.771	21.230	122.881	15.618	9.017	144.483	20.036	11.568	132.400	19.402	11.202
	65	120.430	24.959	14.410	105.949	10.317	5.956	174.403	23.633	13.645	121.566	5.869	3.388	138.630	16.882	9.747	127.064	16.925	9.772
100 nM	70	117.163	17.393	10.042	103.752	7.611	4.394	174.423	19.179	11.073	121.693	3.399	1.962	134.167	1.514	0.874	123.039	8.141	4.700
	75	114.135	9.959	5.750	102.070	13.186	7.613	181.433	18.751	10.826	126.624	3.491	2.016	134.417	10.261	5.924	123.457	16.038	9.259
	80	112.148	15.205	8.778	99.420	7.596	4.386	183.910	15.821	9.134	128.472	5.022	2.900	137.920	8.563	4.944	126.591	13.910	8.031
1 μM	85	113.103	11.456	6.614	100.729	9.683	5.591	187.800	11.978	6.915	131.324	6.754	3.899	142.790	7.500	4.330	131.164	15.572	8.990
	90	112.888	14.751	8.517	100.110	6.886	3.975	192.280	5.851	3.378	134.627	9.634	5.562	144.307	9.443	5.452	132.538	16.301	9.411
	95	112.378	17.219	9.942	99.373	6.089	3.516	197.483	5.297	3.058	138.313	10.949	6.321	148.053	10.206	5.893	136.007	17.451	10.075
10 μM	100	114.070	24.842	14.343	100.377	10.539	6.085	196.923	7.759	4.480	137.841	9.250	5.340	150.560	10.604	6.122	138.304	17.769	10.259
	105	129.380	29.848	17.233	113.554	17.610	10.167	200.880	13.623	7.865	140.633	12.611	7.281	154.853	6.128	3.538	142.114	13.537	7.815
	110	133.085	31.736	18.323	116.451	16.549	9.554	203.747	13.995	8.080	142.552	10.626	6.135	158.630	8.602	4.966	145.774	18.382	10.613
30 μM	115	127.638	29.901	17.264	111.785	15.892	9.175	206.520	18.663	10.775	144.441	12.441	7.183	159.097	7.455	4.304	146.149	17.090	9.867
	120	125.640	29.396	16.972	110.075	15.100	8.718	210.943	20.169	11.645	147.652	15.904	9.182	157.330	20.643	11.918	143.778	10.945	6.319
	125	118.680	20.000	11.547	105.049	13.153	7.594	209.650	13.746	7.936	146.858	14.848	8.572	148.403	13.981	8.072	135.713	2.464	1.423
30 μM	130	117.330	20.000	11.547	103.829	13.080	7.552	211.720	12.914	7.456	148.346	15.400	8.891	142.320	10.014	5.781	130.251	0.857	0.495
	135	117.148	15.005	8.663	104.217	12.379	7.147	206.197	7.706	4.449	144.480	13.555	7.826	141.027	8.127	4.692	129.132	3.510	2.027
	140	119.800	15.780	9.110	106.680	14.316	8.265	200.827	5.173	2.987	140.862	15.963	9.216	136.937	13.050	7.535	125.240	4.198	2.424
30 μM	145	122.970	16.683	9.632	109.417	14.147	8.168	196.640	6.773	3.910	138.012	17.766	10.257	145.580	19.113	11.035	133.032	9.850	5.687
	150	125.550	16.833	9.718	111.724	14.446	8.340	191.503	6.182	3.569	134.366	16.529	9.543	146.400	16.876	9.743	134.057	14.465	8.351
	155	125.190	19.122	11.040	111.202	15.278	8.821	187.337	5.545	3.201	131.408	15.160	8.753	147.523	14.440	8.337	135.106	12.363	7.138
	160	125.030	19.706	11.377	110.914	14.545	8.397	184.073	6.338	3.659	129.079	14.208	8.203	148.690	13.815	7.976	136.230	13.101	7.564

**Appendix 9** – The data shown below represents the heart rate measurements for the 3, 6 and 18-month Dobutamine treated hearts, as presented in chapter 6. Both the raw values and the normalised to stabilisation values are presented.

CHAPTER 6 - DOBUTAMINE DATA																			
Concentration	Time	3M Avg.	SD	SEM	3M Avg. %	SD	SEM	6M Avg.	SD	SEM	6M Avg. %	SD	SEM	18M Avg.	SD	SEM	18M Avg. %	SD	SEM
Stabilisation	5	310	3.873	2.236	104.918	7.439	4.295	253	10.964	6.330	96.223	4.263	2.461	347	7.071	4.082	106.079	7.621	4.400
	10	300	3.873	2.236	101.623	5.917	3.416	257	10.964	6.330	97.535	6.718	3.879	353	7.071	4.082	108.180	9.451	5.456
	15	303	4.272	2.466	102.583	3.771	2.177	270	3.833	2.213	102.388	3.639	2.101	307	16.349	9.439	93.391	10.105	5.834
	20	268	4.031	2.327	90.876	12.368	7.141	273	10.964	6.330	103.855	4.450	2.569	303	16.349	9.439	92.349	8.974	5.181
1 nM	25	290	4.243	2.449	98.554	16.028	9.254	263	18.708	10.801	100.161	3.496	2.018	327	4.508	2.602	99.611	4.352	2.513
	30	293	4.397	2.539	99.292	15.239	8.798	260	12.247	7.071	99.002	5.720	3.303	297	7.288	4.208	90.281	16.335	9.431
	35	300	4.082	2.357	101.967	16.605	9.587	270	12.247	7.071	102.911	9.083	5.244	303	16.349	9.439	92.448	10.867	6.274
	40	305	4.425	2.555	103.639	14.504	8.374	290	5.895	3.404	109.682	9.525	5.499	303	4.729	2.730	92.515	7.241	4.180
3 nM	45	300	4.573	2.640	101.818	10.432	6.023	287	15.492	8.944	108.277	14.403	8.316	303	10.964	6.330	92.581	3.658	2.112
	50	308	3.862	2.230	104.375	11.189	6.460	287	4.607	2.660	108.492	11.264	6.503	297	11.727	6.771	90.364	7.952	4.591
	55	313	4.243	2.449	106.001	14.374	8.299	290	6.620	3.822	109.867	11.291	6.519	303	8.175	4.720	92.598	3.147	1.817
	60	298	4.243	2.449	101.108	15.044	8.686	293	16.349	9.439	111.242	12.046	6.955	293	8.357	4.825	89.156	15.499	8.949
10 nM	65	308	3.697	2.134	104.551	19.398	11.199	300	6.620	3.822	113.683	11.119	6.419	280	3.893	2.247	85.502	2.614	1.509
	70	310	4.435	2.560	105.142	12.448	7.187	293	10.964	6.330	111.487	4.763	2.750	307	7.071	4.082	93.839	6.805	3.929
	75	318	3.651	2.108	107.812	9.256	5.344	293	13.502	7.795	111.579	9.644	5.568	293	7.071	4.082	89.703	4.448	2.568
	80	320	4.243	2.449	108.674	10.503	6.064	300	14.349	8.284	113.991	15.210	8.782	297	13.502	7.795	90.630	8.320	4.804
100 nM	85	338	4.646	2.682	114.506	10.249	5.917	317	10.964	6.330	120.801	16.330	9.428	267	7.071	4.082	81.549	4.113	2.375
	90	358	5.917	3.416	121.082	16.392	9.464	330	21.213	12.247	125.899	15.186	8.768	287	8.175	4.720	87.686	9.090	5.248
	95	330	3.771	2.177	111.902	13.601	7.853	353	14.142	8.165	134.813	14.862	8.580	310	5.895	3.404	94.732	17.016	9.824
	100	350	12.368	7.141	118.554	19.121	11.040	360	0.000	0.000	137.378	14.276	8.242	317	15.492	8.944	97.016	22.560	13.025
1 µM	105	353	16.028	9.254	119.497	8.956	5.171	363	7.071	4.082	138.752	16.757	9.675	313	4.729	2.730	95.973	14.868	8.584
	110	340	15.239	8.798	115.187	6.146	3.548	367	7.071	4.082	140.034	16.927	9.773	340	9.518	5.495	104.360	19.132	11.046
	115	333	16.605	9.587	112.788	5.691	3.286	363	7.071	4.082	138.537	12.099	6.986	347	4.729	2.730	106.395	18.282	10.555
	120	358	14.504	8.374	121.299	4.380	2.529	370	12.247	7.071	140.978	10.068	5.813	373	4.729	2.730	114.218	13.883	8.016
10 µM	125	350	10.432	6.023	118.768	4.429	2.557	360	12.247	7.071	137.162	9.673	5.585	377	18.708	10.801	115.161	6.601	3.811
	130	330	11.189	6.460	111.981	4.176	2.411	363	7.071	4.082	138.752	16.757	9.675	370	15.083	8.708	113.010	7.417	4.282
	135	340	14.374	8.299	115.374	4.303	2.484	377	7.071	4.082	143.850	17.323	10.001	370	7.174	4.142	113.126	8.286	4.784
	140	330	12.540	7.240	111.981	4.176	2.411	370	0.000	0.000	141.194	14.672	8.471	393	6.729	3.885	119.841	8.401	4.850
30 µM	145	320	20.616	11.902	108.588	4.050	2.338	383	14.142	8.165	146.507	20.021	11.559	383	8.357	4.825	116.697	13.945	8.051
	150	330	7.174	4.142	111.981	4.176	2.411	393	10.964	6.330	150.138	19.282	11.133	387	12.265	7.081	117.557	16.355	9.443
	155	340	11.402	6.583	115.374	4.303	2.484	400	12.247	7.071	152.734	18.563	10.718	403	12.265	7.081	122.702	16.423	9.482
	160	340	14.553	8.402	115.374	4.303	2.484	387	7.071	4.082	147.544	15.485	8.940	413	12.265	7.081	125.746	17.138	9.895

**Appendix 10** – The data shown below represents the coronary flow measurements for the 3, 6 and 18-month Atenolol treated hearts, as presented in chapter 6. Both the raw values and the normalised to stabilisation values are presented.

CHAPTER 6 - ATENOLOL DATA																			
Concentration	Time	3M Avg.	SD	SEM	3M Avg. %	SD	SEM	6M Avg.	SD	SEM	6M Avg. %	SD	SEM	18M Avg.	SD	SEM	18M Avg. %	SD	SEM
Stabilisation	5	20	2.828	1.633	100.806	1.613	0.931	23	6.550	3.782	97.797	3.908	2.256	27	1.893	1.093	99.324	1.351	0.780
	10	20	2.828	1.633	100.806	1.613	0.931	23	6.111	3.528	101.186	1.167	0.674	27	2.000	1.155	100.225	0.450	0.260
	15	20	2.828	1.633	100.806	1.613	0.931	23	5.918	3.417	100.508	1.562	0.902	27	2.000	1.155	100.225	0.450	0.260
	20	19	1.500	0.866	97.581	4.839	2.794	23	5.918	3.417	100.508	1.562	0.902	27	2.000	1.155	100.225	0.450	0.260
1 nM	25	19	2.449	1.414	95.878	2.749	1.587	23	5.981	3.453	98.580	3.525	2.035	26	2.217	1.280	97.390	1.841	1.063
	30	19	2.062	1.190	94.803	3.972	2.293	22	6.050	3.493	96.612	3.489	2.014	26	2.217	1.280	97.390	1.841	1.063
3 nM	35	18	2.872	1.658	91.850	3.423	1.976	22	6.050	3.493	96.612	3.489	2.014	26	2.217	1.280	97.390	1.841	1.063
	40	18	2.872	1.658	91.850	3.423	1.976	22	5.829	3.365	93.261	6.987	4.034	27	2.380	1.374	98.291	2.533	1.462
	45	19	2.363	1.364	94.628	0.262	0.151	21	5.712	3.298	90.615	6.243	3.604	26	2.708	1.563	96.348	3.472	2.004
	50	19	1.915	1.106	93.553	2.169	1.252	20	5.303	3.062	86.675	8.875	5.124	25	2.708	1.563	92.620	3.738	2.158
	55	18	2.449	1.414	90.775	2.897	1.672	20	5.174	2.987	85.867	8.101	4.677	25	3.202	1.848	91.578	5.704	3.293
10 nM	60	18	2.449	1.414	90.775	2.897	1.672	19	5.027	2.903	81.968	14.172	8.182	25	3.109	1.795	90.677	5.541	3.199
	65	18	1.893	1.093	92.303	2.476	1.430	19	5.196	3.000	82.776	14.829	8.562	24	3.096	1.787	89.776	5.946	3.433
	70	18	1.500	0.866	92.478	4.312	2.490	19	5.027	2.903	81.968	14.172	8.182	24	2.944	1.700	88.884	5.587	3.226
	75	18	1.915	1.106	88.450	1.702	0.982	19	5.246	3.029	81.226	11.152	6.438	23	3.096	1.787	86.048	6.170	3.562
	80	18	1.915	1.106	88.450	1.702	0.982	19	5.566	3.213	79.976	13.195	7.618	23	2.872	1.658	84.262	5.951	3.436
100 nM	85	18	2.062	1.190	89.700	3.783	2.184	19	5.566	3.213	79.976	13.195	7.618	23	3.403	1.965	84.122	7.506	4.334
	90	18	2.449	1.414	90.775	2.897	1.672	18	5.218	3.012	75.713	11.100	6.408	23	3.403	1.965	84.122	7.506	4.334
	95	18	2.363	1.364	89.525	0.746	0.431	17	5.282	3.050	73.808	12.913	7.456	22	4.349	2.511	82.038	11.152	6.439
	100	18	2.363	1.364	89.525	0.746	0.431	16	4.922	2.842	70.506	11.623	6.710	22	3.948	2.279	80.245	9.603	5.544
	105	18	2.062	1.190	89.700	3.783	2.184	15	5.282	3.050	64.422	13.549	7.823	22	3.873	2.236	79.344	9.441	5.451
1 µM	110	18	2.062	1.190	89.700	3.783	2.184	15	5.360	3.094	61.686	15.341	8.857	21	4.082	2.357	77.409	10.282	5.936
	115	17	2.062	1.190	84.597	3.682	2.126	15	5.360	3.094	61.686	15.341	8.857	21	3.862	2.230	76.516	9.441	5.451
	120	17	2.062	1.190	84.597	3.682	2.126	14	5.790	3.343	59.146	16.664	9.621	20	4.082	2.357	73.681	10.568	6.101
	125	17	1.732	1.000	83.522	5.141	2.968	14	5.457	3.150	57.801	16.252	9.383	20	4.573	2.640	72.639	12.596	7.272
	130	17	1.732	1.000	83.522	5.141	2.968	13	5.317	3.070	55.025	14.748	8.515	19	5.252	3.032	68.762	15.590	9.001
10 µM	135	17	2.062	1.190	84.772	7.367	4.253	13	5.764	3.328	51.546	16.038	9.260	19	5.252	3.032	68.762	15.590	9.001
	140	17	2.309	1.333	85.847	6.149	3.550	13	5.764	3.328	51.546	16.038	9.260	18	4.761	2.749	66.075	13.842	7.991
	145	17	2.309	1.333	85.847	6.149	3.550	12	5.599	3.233	50.868	15.714	9.072	18	4.573	2.640	65.183	13.173	7.605
	150	16	2.309	1.333	80.744	6.173	3.564	11	5.599	3.233	46.175	16.546	9.553	17	4.924	2.843	63.248	14.746	8.514
	155	16	2.309	1.333	80.744	6.173	3.564	11	5.457	3.150	43.529	15.810	9.128	17	4.830	2.789	62.347	14.428	8.330
30 µM	160	16	2.630	1.518	81.994	8.672	5.007	11	4.845	2.797	43.304	12.467	7.198	17	4.830	2.789	62.347	14.428	8.330

**Appendix 11** – The data shown below represents the left ventricular developed pressure measurements for the 3, 6 and 18-month Atenolol treated hearts, as presented in chapter 6. Both the raw values and the normalised to stabilisation values are presented.

CHAPTER 6 - ATENOLOL DATA																			
Concentration	Time	3M Avg.	SD	SEM	3M Avg. %	SD	SEM	6M Avg.	SD	SEM	6M Avg. %	SD	SEM	18M Avg.	SD	SEM	18M Avg. %	SD	SEM
Stabilisation	5	141.460	10.819	6.246	101.375	3.715	2.145	137.246	18.305	10.568	97.913	1.535	0.886	139.240	15.833	9.141	98.637	1.693	0.977
	10	141.665	3.908	2.256	100.398	3.928	2.268	141.024	18.626	10.754	100.649	1.607	0.928	141.415	16.194	9.350	100.186	1.892	1.093
	15	139.093	15.203	8.778	99.043	1.960	1.132	139.960	17.470	10.086	99.950	1.254	0.724	141.230	16.381	9.457	100.020	0.503	0.290
	20	138.815	11.848	6.840	99.184	3.277	1.892	142.194	18.755	10.828	101.487	1.753	1.012	142.898	17.211	9.937	101.157	0.666	0.385
1 nM	25	127.110	6.825	3.940	91.674	11.544	6.665	136.768	17.919	10.346	97.623	1.605	0.927	134.290	10.612	6.127	95.120	7.616	4.397
	30	125.375	7.224	4.171	90.476	12.580	7.263	132.930	16.213	9.361	95.040	2.891	1.669	133.128	7.633	4.407	94.326	13.370	7.719
	35	121.503	8.308	4.797	87.460	12.526	7.232	129.330	14.007	8.087	92.631	3.549	2.049	132.370	9.464	5.464	93.897	15.598	9.006
3 nM	40	120.570	12.159	7.020	85.939	11.445	6.608	128.736	16.832	9.718	91.943	3.551	2.050	134.445	8.357	4.825	95.347	14.477	8.358
	45	118.843	10.034	5.793	84.855	9.774	5.643	125.208	16.743	9.666	89.434	4.382	2.530	134.410	6.073	3.506	95.492	14.182	8.188
	50	112.045	10.675	6.163	79.746	9.521	5.497	121.582	16.933	9.776	86.757	3.364	1.942	125.028	8.019	4.630	88.703	14.971	8.643
10 nM	55	114.363	12.959	7.482	81.066	10.848	6.263	122.676	18.284	10.556	87.557	6.050	3.493	124.315	9.543	5.510	88.289	16.672	9.625
	60	110.973	8.733	5.042	79.214	9.695	5.598	116.894	19.258	11.119	83.288	6.268	3.619	123.588	6.775	3.912	87.689	13.929	8.042
	65	104.495	7.359	4.249	74.590	8.167	4.715	117.122	18.318	10.576	83.849	9.693	5.596	121.035	7.907	4.565	86.045	16.052	9.267
100 nM	70	101.700	9.164	5.291	72.042	6.121	3.534	119.088	19.134	11.047	85.440	12.122	6.999	118.050	7.285	4.206	83.838	15.151	8.747
	75	104.353	4.348	2.510	74.627	2.457	1.419	117.500	20.127	11.620	84.378	14.124	8.155	116.103	9.750	5.629	82.189	15.350	8.862
	80	95.705	5.263	3.039	68.272	5.444	3.143	114.036	20.823	12.022	81.754	13.618	7.863	116.728	9.960	5.751	82.625	15.396	8.889
1 µM	85	89.983	19.923	11.503	64.359	5.493	3.172	109.948	21.656	12.503	78.583	12.736	7.353	114.240	9.227	5.327	80.926	15.452	8.921
	90	89.303	22.492	12.986	63.578	7.341	4.238	105.648	21.565	12.450	75.462	12.607	7.279	111.750	10.478	6.049	79.217	16.854	9.731
	95	93.370	6.137	3.543	66.190	5.221	3.014	106.690	22.601	13.049	76.230	13.830	7.985	109.583	9.046	5.223	77.675	15.805	9.125
10 µM	100	88.423	3.781	2.183	62.911	5.367	3.099	103.944	25.255	14.581	73.848	13.775	7.953	108.965	8.959	5.172	77.194	15.470	8.932
	105	85.873	3.918	2.262	61.152	7.113	4.107	101.652	21.913	12.651	72.554	13.020	7.517	105.435	7.505	4.333	74.701	14.445	8.340
	110	84.715	18.987	10.962	60.538	5.952	3.436	102.988	22.797	13.162	73.714	14.882	8.592	101.348	7.047	4.069	71.779	14.129	8.157
30 µM	115	85.500	20.103	11.606	60.961	6.801	3.926	101.658	23.123	13.350	72.554	13.700	7.909	100.835	7.730	4.463	71.507	15.159	8.752
	120	81.113	3.645	2.104	57.591	7.657	4.421	103.760	21.476	12.399	74.309	13.609	7.857	98.385	8.359	4.826	69.761	15.612	9.013
	125	76.820	19.602	11.317	54.502	6.026	3.479	104.254	19.564	11.295	74.510	10.784	6.226	100.165	9.417	5.437	70.989	16.117	9.305
	130	78.313	19.028	10.986	55.828	7.117	4.109	103.568	16.275	9.397	74.337	10.146	5.858	96.015	7.777	4.490	68.225	15.986	9.230
	135	79.273	19.177	11.072	56.551	4.050	2.338	103.638	18.192	10.503	74.172	10.568	6.101	94.263	7.201	4.158	66.947	15.458	8.925
	140	77.640	21.286	12.289	54.828	5.370	3.100	103.086	19.498	11.257	73.924	12.710	7.338	96.138	4.473	2.583	68.557	15.296	8.831
	145	79.500	7.679	4.434	55.810	10.411	6.011	98.760	16.638	9.606	71.223	13.169	7.603	88.905	7.114	4.108	63.144	15.518	8.959
	150	78.530	7.924	4.575	55.088	10.529	6.079	97.346	16.931	9.775	70.362	14.625	8.444	87.845	7.558	4.363	62.385	15.869	9.162
	155	77.370	8.236	4.755	54.225	10.673	6.162	96.826	16.561	9.562	69.931	14.089	8.134	86.338	9.338	5.391	61.183	16.517	9.536
	160	78.430	8.232	4.753	55.014	10.542	6.086	96.956	17.543	10.128	70.111	15.346	8.860	82.600	7.333	4.233	58.484	15.015	8.669

**Appendix 12** – The data shown below represents the heart rate measurements for the 3, 6 and 18-month Atenolol treated hearts, as presented in chapter 6. Both the raw values and the normalised to stabilisation values are presented.

CHAPTER 6 - ATENOLOL DATA																			
Concentration	Time	3M Avg.	SD	SEM	3M Avg. %	SD	SEM	6M Avg.	SD	SEM	6M Avg. %	SD	SEM	18M Avg.	SD	SEM	18M Avg. %	SD	SEM
Stabilisation	5	315	13.317	7.689	92.262	7.413	4.280	268	9.652	5.572	101.941	2.826	1.632	345	9.412	5.434	102.179	3.043	1.757
	10	348	16.594	9.580	101.562	2.479	1.431	252	8.947	5.166	95.794	1.583	0.914	328	5.373	3.102	97.016	2.305	1.331
	15	348	12.005	6.931	101.072	4.578	2.643	262	11.662	6.733	99.557	3.787	2.186	343	5.272	3.044	100.802	3.876	2.238
	20	363	10.457	6.037	105.104	9.678	5.588	270	11.402	6.583	102.708	4.158	2.401	338	5.412	3.124	100.003	3.025	1.746
1 nM	25	373	18.930	10.929	110.942	19.450	11.230	270	11.592	6.693	101.993	8.155	4.708	338	5.412	3.124	100.110	4.065	2.347
	30	378	7.291	4.210	112.598	23.228	13.411	272	15.883	9.170	103.333	4.965	2.867	315	5.484	3.166	93.333	4.715	2.722
	35	360	6.184	3.570	107.078	20.104	11.607	266	1.897	1.095	100.851	5.328	3.076	338	13.549	7.823	99.757	3.603	2.080
3 nM	40	350	8.564	4.944	103.851	18.343	10.590	276	7.629	4.405	105.263	6.480	3.741	333	5.718	3.301	98.204	11.729	6.772
	45	363	8.798	5.079	107.359	21.369	12.337	276	15.996	9.235	105.216	9.386	5.419	328	15.718	9.075	96.347	13.851	7.997
	50	363	9.885	5.707	106.894	18.482	10.670	284	10.473	6.047	108.847	13.368	7.718	333	11.702	6.756	97.851	11.839	6.835
	55	355	6.061	3.500	104.723	17.544	10.129	272	18.596	10.736	103.310	6.467	3.734	338	10.038	5.795	99.653	14.078	8.128
10 nM	60	335	12.679	7.321	99.485	16.825	9.714	276	16.554	9.558	104.971	6.880	3.972	348	15.718	9.075	101.874	10.365	5.984
	65	360	14.872	8.586	106.448	21.391	12.350	282	5.917	3.416	107.686	7.179	4.145	345	10.186	5.881	101.042	9.036	5.217
	70	353	16.534	9.546	104.153	21.014	12.132	276	5.263	3.038	105.580	9.375	5.412	345	8.393	4.845	101.859	12.358	7.135
100 nM	75	353	13.549	7.823	104.524	22.936	13.242	272	9.652	5.572	103.583	4.941	2.853	330	9.683	5.590	97.579	6.184	3.570
	80	353	7.587	4.380	104.083	21.026	12.139	280	7.785	4.495	106.491	11.628	6.713	330	8.607	4.969	97.070	9.298	5.368
	85	335	13.613	7.859	99.247	21.911	12.650	268	9.652	5.572	102.168	6.547	3.780	308	15.939	9.202	91.405	7.097	4.098
30 µM	90	353	7.587	4.380	104.330	22.806	13.167	266	5.263	3.038	101.534	6.087	3.515	323	17.240	9.954	95.895	7.411	4.279
	95	335	15.616	9.016	99.879	26.510	15.306	276	13.663	7.889	105.044	6.199	3.579	343	5.412	3.124	101.671	7.633	4.407
	100	355	10.091	5.826	105.842	29.910	17.268	262	9.652	5.572	99.238	7.496	4.328	358	13.332	7.697	104.966	9.043	5.221
1 µM	105	353	9.617	5.552	105.244	31.028	17.914	270	9.652	5.572	102.969	6.307	3.641	350	12.368	7.140	102.731	9.926	5.731
	110	343	16.534	9.546	101.016	19.675	11.359	262	16.994	9.812	99.389	4.918	2.840	358	9.617	5.552	105.206	10.344	5.972
	115	378	5.272	3.044	111.546	22.818	13.174	264	13.052	7.536	100.371	4.541	2.622	360	15.963	9.216	105.583	9.012	5.203
10 µM	120	360	8.357	4.825	106.640	23.518	13.578	268	8.224	4.748	102.121	5.172	2.986	360	11.134	6.428	105.857	4.997	2.885
	125	363	10.038	5.795	106.501	19.668	11.355	262	14.144	8.166	99.840	8.729	5.040	360	17.128	9.889	105.501	8.358	4.825
	130	333	6.385	3.687	98.598	19.964	11.526	280	4.759	2.748	107.463	12.522	7.229	375	3.026	1.747	109.910	8.560	4.942
30 µM	135	348	8.658	4.999	110.980	19.138	11.049	282	7.479	4.318	108.306	13.681	7.899	373	8.767	5.062	109.751	7.959	4.595
	140	350	9.683	5.590	103.555	20.443	11.803	280	7.174	4.142	107.551	13.737	7.931	348	16.534	9.546	102.552	5.607	3.237
	145	343	5.990	3.458	101.456	20.516	11.845	280	10.742	6.202	107.187	11.842	6.837	328	7.690	4.440	97.230	10.858	6.269
	150	343	5.990	3.458	101.456	20.516	11.845	278	8.224	4.748	106.383	10.231	5.907	338	13.549	7.823	99.700	7.406	4.276
	155	345	8.121	4.689	101.982	21.697	12.527	280	20.310	11.726	107.298	10.159	5.865	338	62.915	36.324	100.165	10.982	6.341
	160	348	10.422	6.017	103.008	22.181	12.806	286	23.399	13.509	109.345	8.503	4.909	348	10.038	5.795	102.034	5.991	3.459

**Appendix 13** – The data shown below represents the coronary flow measurements for the 3, 6 and 18-month Itraconazole treated hearts, as presented in chapter 6. Both the raw values and the normalised to stabilisation values are presented.

CHAPTER 6 - ITRACONAZOLE DATA																			
Concentration	Time	3M Avg.	SD	SEM	3M Avg. %	SD	SEM	6M Avg.	SD	SEM	6M Avg. %	SD	SEM	18M Avg.	SD	SEM	18M Avg. %	SD	SEM
Stabilisation	5	19	3.367	1.944	99.234	7.070	4.082	24	6.285	3.629	101.353	0.377	0.217	25	1.155	0.667	101.297	1.584	0.914
	10	20	3.304	1.908	103.028	3.210	1.854	24	6.285	3.629	101.353	0.377	0.217	25	1.155	0.667	101.297	1.584	0.914
	15	19	3.594	2.075	100.142	4.632	2.674	23	5.523	3.189	97.406	3.996	2.307	25	1.500	0.866	100.221	1.266	0.731
	20	19	2.082	1.202	97.596	10.783	6.226	24	6.481	3.742	99.888	3.388	1.956	24	1.633	0.943	97.185	3.257	1.880
1 nM	25	17	2.986	1.724	87.672	9.784	5.649	20	1.871	1.080	86.453	16.638	9.606	22	1.414	0.816	89.148	4.590	2.650
	30	16	2.887	1.667	81.167	10.422	6.017	20	2.121	1.225	84.765	13.309	7.684	22	1.414	0.816	89.148	4.590	2.650
	35	15	2.217	1.280	77.416	7.515	4.339	20	1.871	1.080	83.413	13.118	7.573	22	1.915	1.106	86.970	3.673	2.121
3 nM	40	14	1.826	1.054	73.754	8.339	4.815	20	1.871	1.080	83.413	13.118	7.573	20	2.363	1.364	81.835	5.935	3.426
	45	14	1.258	0.726	75.732	12.717	7.342	19	3.742	2.160	81.167	8.168	4.716	21	2.646	1.528	82.816	7.118	4.110
	50	14	1.732	1.000	71.580	12.175	7.029	19	3.742	2.160	81.167	8.168	4.716	21	2.986	1.724	83.796	8.591	4.960
	55	13	1.708	0.986	67.918	14.297	8.254	18	3.742	2.160	76.884	7.615	4.397	19	2.000	1.155	76.876	6.029	3.481
10 nM	60	12	2.160	1.247	63.365	11.121	6.421	19	3.082	1.780	78.572	7.982	4.608	18	2.828	1.633	72.642	8.403	4.852
	65	11	1.258	0.726	59.747	10.381	5.994	19	3.240	1.871	80.037	10.294	5.944	17	2.582	1.491	68.636	7.552	4.360
	70	11	0.500	0.289	57.347	10.730	6.195	19	2.828	1.633	78.907	12.519	7.228	16	2.582	1.491	64.577	7.717	4.456
100 nM	75	10	0.500	0.289	52.019	9.853	5.689	18	4.243	2.449	75.532	13.267	7.660	16	3.109	1.795	62.460	9.805	5.661
	80	10	0.577	0.333	50.889	11.116	6.418	17	3.742	2.160	73.272	16.663	9.620	15	2.646	1.528	58.463	8.188	4.727
	85	10	1.258	0.726	52.512	14.705	8.490	18	4.243	2.449	75.532	13.267	7.660	15	2.646	1.528	58.463	8.188	4.727
1 µM	90	9	0.957	0.553	47.227	13.413	7.744	18	4.243	2.449	75.532	13.267	7.660	14	2.872	1.658	55.365	9.067	5.235
	95	9	1.732	1.000	46.408	18.137	10.472	18	4.950	2.858	73.844	14.971	8.643	13	2.944	1.700	52.329	9.666	5.581
	100	8	2.380	1.374	41.570	21.413	12.363	16	4.950	2.858	65.278	15.040	8.683	12	3.304	1.908	47.214	11.597	6.696
	105	7	2.380	1.374	36.242	20.511	11.842	16	4.950	2.858	65.278	15.040	8.683	12	3.109	1.795	46.234	10.874	6.278
10 µM	110	6	2.160	1.247	33.355	18.321	10.578	15	4.416	2.550	63.018	17.103	9.874	11	3.594	2.075	45.158	13.004	7.508
	115	5	0.816	0.471	27.090	8.943	5.163	13	3.742	2.160	56.140	15.175	8.762	10	3.559	2.055	40.077	12.952	7.478
	120	4	0.500	0.289	20.094	4.988	2.880	12	4.637	2.677	51.299	16.096	9.293	9	3.416	1.972	34.014	12.556	7.249
30 µM	125	5	0.957	0.553	25.065	4.838	2.793	10	1.414	0.816	43.736	7.048	4.069	8	3.500	2.021	32.973	12.802	7.391
	130	5	1.000	0.577	23.846	5.617	3.243	9	1.871	1.080	39.789	10.953	6.324	7	3.162	1.826	27.934	11.640	6.720
	135	5	0.577	0.333	24.246	6.722	3.881	8	1.871	1.080	36.064	13.253	7.651	7	2.887	1.667	26.010	10.771	6.219
	140	4	0.816	0.471	21.804	8.158	4.710	8	2.449	1.414	34.934	15.624	9.020	6	3.367	1.944	23.894	12.743	7.357
30 µM	145	4	0.500	0.289	20.137	5.140	2.968	5	2.550	1.472	22.099	9.721	5.613	5	2.160	1.247	19.991	8.074	4.662
	150	4	0.500	0.289	20.137	5.140	2.968	4	1.414	0.816	18.039	4.315	2.491	3	0.500	0.289	11.101	1.716	0.991
	155	4	0.000	0.000	21.314	3.616	2.088	4	1.414	0.816	15.109	2.306	1.331	3	0.000	0.000	12.177	0.635	0.367
	160	4	0.577	0.333	18.829	5.546	3.202	1	0.269	0.155	9.696	0.960	0.554	2	0.500	0.289	9.193	2.489	1.437

**Appendix 14** – The data shown below represents the left ventricular developed pressure measurements for the 3, 6 and 18-month Itraconazole treated hearts, as presented in chapter 6. Both the raw values and the normalised to stabilisation values are presented.

CHAPTER 6 - ITRACONAZOLE DATA																			
Concentration	Time	3M Avg.	SD	SEM	3M Avg. %	SD	SEM	6M Avg.	SD	SEM	6M Avg. %	SD	SEM	18M Avg.	SD	SEM	18M Avg. %	SD	SEM
Stabilisation	5	130.638	19.972	11.531	97.347	2.198	1.269	130.587	19.733	11.393	97.476	0.912	0.527	155.288	16.442	9.493	98.424	0.543	0.314
	10	133.315	20.944	12.092	99.266	1.437	0.830	133.100	18.662	10.774	99.427	0.569	0.328	158.190	15.505	8.952	100.433	1.365	0.788
	15	137.755	25.470	14.705	102.214	2.463	1.422	135.417	18.560	10.716	101.180	1.026	0.593	158.415	17.089	9.866	100.400	1.718	0.992
	20	136.423	25.201	14.550	101.173	2.880	1.663	136.460	19.499	11.258	101.918	0.489	0.282	159.435	20.924	12.080	100.743	3.210	1.853
1 nM	25	138.190	12.814	7.398	102.115	10.234	5.909	136.793	19.534	11.278	102.168	0.742	0.428	146.890	15.026	8.675	93.338	6.230	3.597
	30	137.503	12.978	7.493	101.693	12.156	7.018	136.210	22.334	12.894	101.613	3.956	2.284	147.745	20.819	12.020	93.414	5.622	3.246
	35	128.313	23.595	13.623	95.304	7.306	4.218	140.773	10.534	6.082	104.752	6.576	3.797	144.768	3.768	2.175	91.486	3.737	2.157
3 nM	40	122.565	11.643	6.722	90.238	8.689	5.017	137.917	12.728	7.348	102.542	9.607	5.547	144.458	18.390	10.618	91.301	6.259	3.614
	45	115.268	9.444	5.453	84.914	6.656	3.843	134.433	14.005	8.086	99.864	11.036	6.371	149.295	22.451	12.962	94.177	6.463	3.732
	50	110.355	24.331	14.047	81.498	5.596	3.231	137.853	17.234	9.950	102.334	13.659	7.886	144.563	20.357	11.753	91.128	7.213	4.164
10 nM	55	110.273	8.832	5.099	81.161	6.666	3.849	135.913	9.162	5.290	101.292	9.075	5.239	141.105	17.085	9.864	88.877	8.142	4.701
	60	108.680	20.432	11.796	80.630	5.120	2.956	135.893	7.697	4.444	101.310	7.519	4.341	136.468	14.558	8.405	86.425	6.080	3.510
	65	104.785	18.976	10.956	77.825	5.094	2.941	125.533	13.798	7.966	94.039	6.093	3.518	131.613	15.888	9.173	83.029	14.240	8.221
100 nM	70	103.200	20.663	11.930	76.484	6.965	4.021	123.310	17.245	9.956	92.214	5.858	3.382	127.385	18.221	10.520	80.457	12.543	7.242
	75	104.028	18.053	10.423	77.327	4.515	2.607	113.773	20.280	11.708	84.767	3.277	1.892	123.130	16.641	9.608	77.710	10.867	6.274
	80	104.650	20.443	11.803	77.573	6.037	3.486	110.293	20.785	12.000	82.140	4.819	2.782	122.718	15.647	9.034	77.558	10.788	6.229
1 µM	85	104.525	18.056	10.425	77.816	4.565	2.636	108.160	22.870	13.204	80.492	7.754	4.477	113.900	15.372	8.875	71.861	11.579	6.685
	90	107.835	14.586	8.421	80.746	6.879	3.972	110.037	20.900	12.067	82.028	6.984	4.032	112.903	17.550	10.132	70.827	10.632	6.139
	95	102.913	12.272	7.085	77.154	6.237	3.601	111.010	19.320	11.154	82.926	8.077	4.664	107.623	15.619	9.017	67.368	13.079	7.551
10 µM	100	97.248	14.472	8.355	72.902	8.584	4.956	109.470	22.508	12.995	81.710	10.699	6.177	105.995	15.678	9.052	66.561	10.892	6.288
	105	92.440	11.230	6.484	69.464	7.685	4.437	103.217	19.487	11.251	77.277	11.622	6.710	102.070	16.342	9.435	63.873	10.316	5.956
	110	86.995	8.527	4.923	65.341	5.456	3.150	94.170	19.007	10.974	70.740	14.247	8.225	100.960	16.988	9.808	63.200	11.750	6.784
30 µM	115	80.228	11.992	6.924	59.811	2.251	1.300	94.663	17.343	10.013	71.164	13.794	7.964	97.453	14.532	8.390	61.124	10.523	6.075
	120	74.365	12.012	6.935	55.357	2.571	1.484	88.533	20.260	11.697	66.702	16.812	9.707	92.298	13.074	7.548	57.927	10.032	5.792
	125	73.100	15.000	8.660	54.167	5.683	3.281	85.857	20.699	11.951	64.626	16.405	9.471	81.820	7.981	4.608	51.328	6.525	3.767
30 µM	130	71.730	15.000	8.660	53.124	5.750	3.320	75.647	7.116	4.108	56.389	14.644	8.455	78.195	16.884	9.748	49.719	4.404	2.543
	135	68.770	15.000	8.660	50.870	5.914	3.414	73.087	10.662	6.156	54.152	16.039	9.260	76.425	15.040	8.684	48.788	5.111	2.951
	140	68.830	15.000	8.660	50.916	5.910	3.412	67.370	6.098	3.521	50.098	13.680	7.898	72.408	16.145	9.321	46.109	5.863	3.385
30 µM	145	67.870	15.000	8.660	50.185	5.969	3.446	61.117	14.795	8.542	45.363	5.295	3.057	69.628	17.589	10.155	44.066	4.893	2.825
	150	69.830	15.000	8.660	51.677	5.852	3.379	62.680	11.112	6.416	46.757	3.449	1.991	63.823	18.613	10.746	40.659	8.181	4.723
	155	66.620	15.000	8.660	49.233	6.049	3.492	59.927	10.919	6.304	44.640	2.077	1.199	61.238	18.713	10.804	38.849	7.716	4.455
	160	64.690	15.000	8.660	47.764	6.180	3.568	56.250	4.020	2.321	42.217	3.238	1.869	58.180	20.122	11.618	36.629	8.016	4.628

**Appendix 15** – The data shown below represents the heart rate measurements for the 3, 6 and 18-month Itraconazole treated hearts, as presented in chapter 6. Both the raw values and the normalised to stabilisation values are presented.

CHAPTER 6 - ITRACONAZOLE DATA																			
Concentration	Time	3M Avg.	SD	SEM	3M Avg. %	SD	SEM	6M Avg.	SD	SEM	6M Avg. %	SD	SEM	18M Avg.	SD	SEM	18M Avg. %	SD	SEM
Stabilisation	5	300	9.329	5.386	101.464	7.147	4.126	283	14.142	8.165	96.349	3.882	2.241	258	20.616	11.902	92.653	5.350	3.089
	10	288	22.174	12.802	97.710	4.780	2.760	307	18.035	10.412	104.108	6.937	4.005	270	14.142	8.165	97.193	3.093	1.786
	15	295	11.547	6.667	100.085	3.816	2.203	293	7.071	4.082	99.772	2.579	1.489	283	7.679	4.434	101.503	3.620	2.090
	20	298	17.679	10.207	100.740	2.149	1.241	293	7.071	4.082	99.772	2.579	1.489	303	16.714	9.650	108.652	7.949	4.589
1 nM	25	315	12.070	6.968	106.283	12.971	7.489	273	15.121	8.730	92.729	8.656	4.997	270	14.302	8.257	97.376	12.314	7.109
	30	318	8.533	4.927	106.835	13.709	7.915	280	12.247	7.071	95.370	8.634	4.985	263	17.078	9.860	94.721	8.818	5.091
	35	293	15.058	8.694	98.404	13.327	7.694	280	12.247	7.071	95.199	1.458	0.842	295	11.030	6.368	105.790	14.680	8.475
3 nM	40	315	9.044	5.222	105.623	19.038	10.992	280	7.174	4.142	95.114	4.167	2.406	283	14.373	8.298	101.618	11.964	6.907
	45	308	7.040	4.064	103.125	15.750	9.093	280	15.083	8.708	95.068	6.842	3.950	275	17.075	9.858	98.848	11.028	6.367
	50	308	8.767	5.062	103.404	17.415	10.055	283	14.142	8.165	96.389	5.739	3.313	295	12.641	7.298	105.744	14.248	8.226
10 nM	55	315	9.706	5.604	106.674	8.751	5.053	277	7.071	4.082	94.115	3.429	1.980	310	16.667	9.623	111.077	14.703	8.489
	60	313	9.885	5.707	105.266	11.572	6.681	277	18.708	10.801	94.095	6.264	3.617	295	10.451	6.034	105.974	13.045	7.531
	65	303	15.554	8.980	101.972	16.107	9.300	297	7.071	4.082	101.007	7.191	4.151	318	8.852	5.111	113.847	9.891	5.711
100 nM	70	323	9.344	5.395	108.678	11.026	6.366	273	14.142	8.165	93.117	9.142	5.278	298	14.603	8.431	106.951	15.541	8.973
	75	295	15.359	8.868	99.562	7.844	4.529	287	18.708	10.801	97.559	8.205	4.737	323	11.094	6.405	115.548	9.712	5.607
	80	293	9.177	5.298	99.054	6.669	3.850	277	7.071	4.082	94.201	6.863	3.962	318	15.276	8.819	113.641	10.973	6.335
1 µM	85	298	15.939	9.202	100.506	9.585	5.534	280	12.247	7.071	95.370	8.634	4.985	310	17.945	10.361	111.215	5.579	3.221
	90	290	17.871	10.318	97.842	12.052	6.958	280	12.247	7.071	95.370	8.634	4.985	325	17.958	10.368	116.364	12.994	7.502
	95	330	7.746	4.472	110.848	15.722	9.077	277	7.071	4.082	94.201	6.863	3.962	315	13.317	7.689	112.893	12.007	6.932
10 µM	100	320	15.025	8.674	108.165	7.453	4.303	277	9.907	5.720	94.160	10.072	5.815	303	15.720	9.076	108.606	6.420	3.707
	105	305	10.451	6.034	103.302	9.935	5.736	273	14.142	8.165	93.117	9.142	5.278	295	15.846	9.149	105.859	5.865	3.386
	110	323	8.798	5.079	108.644	10.201	5.890	273	28.284	16.330	93.157	13.215	7.630	318	17.879	10.322	113.594	12.464	7.196
30 µM	115	308	15.276	8.819	104.055	11.562	6.675	267	18.035	10.412	90.823	13.956	8.058	293	8.852	5.111	104.790	10.237	5.910
	120	293	16.046	9.264	98.272	14.473	8.356	263	18.035	10.412	89.865	16.016	9.247	300	8.591	4.960	107.399	17.219	9.942
	125	350	15.276	8.819	119.578	12.147	7.013	253	8.175	4.720	86.376	12.335	7.122	300	8.591	4.960	107.399	17.219	9.942
	130	330	16.046	9.264	112.745	11.453	6.612	257	8.175	4.720	87.435	11.501	6.640	300	12.121	6.998	107.376	15.531	8.967
	135	340	9.211	5.318	116.161	11.800	6.813	253	18.708	10.801	86.291	9.343	5.394	340	16.349	9.439	121.858	12.660	7.309
	140	330	7.746	4.472	112.745	11.453	6.612	243	14.142	8.165	82.908	8.653	4.996	328	11.166	6.447	117.571	17.012	9.822
	145	320	15.025	8.674	109.328	11.106	6.412	237	13.502	7.795	80.760	14.204	8.201	343	18.510	10.687	123.180	17.149	9.901
	150	330	10.451	6.034	112.745	11.453	6.612	250	7.785	4.495	85.166	16.144	9.321	325	11.906	6.874	116.824	14.312	8.263
	155	340	8.798	5.079	116.161	11.800	6.813	250	15.083	8.708	85.186	13.362	7.715	343	15.939	9.202	122.881	13.573	7.837
	160	340	11.800	6.813	116.161	11.800	6.813	250	15.083	8.708	85.186	13.362	7.715	330	18.373	10.608	118.663	11.530	6.657

**Appendix 16** – The data shown below represents the coronary flow measurements for the 6 and 18-month lean and HFD Dobutamine treated hearts, as presented in chapter 7. Both the raw values and the normalised to stabilisation values are presented.

CHAPTER 7 - DOBUTAMINE DATA																									
Concentration	Time	6M Lean Avg.	SD	SEM	6M Lean Avg. %	SD	SEM	6M HFD Avg.	SD	SEM	6M HFD Avg. %	SD	SEM	18M Lean Avg.	SD	SEM	18M Lean Avg. %	SD	SEM	18M HFD Avg.	SD	SEM	18M HFD Avg. %	SD	SEM
Stabilisation	5	25	2.121	1.225	99.050	1.117	0.645	30	7.348	4.243	102.950	3.208	1.852	19	1.414	0.816	97.834	3.371	1.946	26	2.363	1.364	100.556	1.111	0.642
	10	25	2.502	1.444	99.050	1.117	0.645	29	5.099	2.944	99.029	5.268	3.042	20	1.225	0.707	101.235	2.619	1.512	26	2.828	1.633	99.444	1.111	0.642
	15	26	2.668	1.540	101.637	1.904	1.099	29	6.819	3.937	99.571	1.874	1.082	20	0.707	0.408	99.588	0.873	0.504	26	2.630	1.518	98.552	1.761	1.017
	20	25	2.806	1.620	100.262	1.767	1.020	29	6.745	3.894	98.450	1.661	0.959	20	0.000	0.000	101.343	4.226	2.440	27	2.646	1.528	101.448	1.761	1.017
1 nM	25	28	2.935	1.695	112.395	13.865	8.005	31	2.828	1.633	109.500	19.268	11.124	23	1.871	1.080	115.006	13.847	7.995	29	4.272	2.466	109.896	10.799	6.235
	30	28	2.935	1.695	112.395	13.865	8.005	31	1.871	1.080	109.640	19.607	11.320	23	2.121	1.225	116.673	14.290	8.250	29	4.546	2.625	110.789	11.413	6.589
	35	28	2.935	1.695	112.395	13.865	8.005	30	1.871	1.080	106.121	18.788	10.848	23	2.550	1.472	118.428	17.151	9.902	29	4.856	2.804	111.682	12.258	7.077
	40	28	2.468	1.425	112.557	13.242	7.645	31	3.674	2.121	107.784	12.326	7.117	23	2.550	1.472	118.428	17.151	9.902	29	4.856	2.804	111.682	12.258	7.077
3 nM	45	28	2.213	1.278	111.345	14.856	8.577	32	2.550	1.472	110.918	22.276	12.861	24	1.225	0.707	121.720	11.172	6.450	29	4.761	2.749	111.007	14.172	8.182
	50	28	2.428	1.402	109.970	15.960	9.215	31	2.828	1.633	109.500	19.268	11.124	24	1.871	1.080	123.474	14.714	8.495	29	4.992	2.882	111.969	15.346	8.860
	55	28	2.428	1.402	109.970	15.960	9.215	31	3.082	1.780	109.202	15.282	8.823	24	0.000	0.000	121.611	5.072	2.928	29	4.992	2.882	111.969	15.346	8.860
	60	27	2.405	1.388	108.581	13.019	7.516	32	2.550	1.472	110.620	18.255	10.540	24	0.707	0.408	123.278	5.112	2.952	29	4.992	2.882	111.969	15.346	8.860
10 nM	65	28	2.428	1.402	109.970	15.960	9.215	31	2.828	1.633	109.500	19.268	11.124	24	1.225	0.707	121.524	4.000	2.310	30	4.349	2.511	114.191	14.961	8.638
	70	27	2.368	1.367	105.995	15.746	9.091	32	2.550	1.472	110.620	18.255	10.540	24	1.225	0.707	121.524	4.000	2.310	30	4.349	2.511	114.191	14.961	8.638
	75	26	2.138	1.234	104.783	17.239	9.953	31	2.449	1.414	108.222	16.687	9.634	24	1.225	0.707	121.503	2.170	1.253	30	4.349	2.511	114.191	14.961	8.638
	80	26	2.090	1.207	103.394	14.336	8.277	31	2.121	1.225	108.520	20.433	11.797	24	2.550	1.472	119.728	9.205	5.315	30	4.349	2.511	114.191	14.961	8.638
100 nM	85	26	2.307	1.332	102.019	15.537	8.970	30	2.449	1.414	104.702	15.866	9.160	24	2.449	1.414	121.395	7.860	4.538	30	3.202	1.848	116.195	11.469	6.622
	90	26	2.307	1.332	102.019	15.537	8.970	30	2.449	1.414	104.702	15.866	9.160	24	2.449	1.414	121.395	7.860	4.538	30	3.202	1.848	116.195	11.469	6.622
	95	26	2.551	1.473	103.231	14.396	8.312	30	3.674	2.121	104.264	11.510	6.645	25	2.550	1.472	124.795	9.079	5.242	31	3.162	1.826	118.942	9.685	5.592
	100	24	2.890	1.669	95.118	15.847	9.149	30	3.937	2.273	102.986	10.199	5.888	25	3.240	1.871	126.441	12.564	7.254	31	3.109	1.795	117.157	11.346	6.551
1 µM	105	24	2.412	1.393	93.891	11.214	6.474	29	5.099	2.944	99.029	5.268	3.042	25	2.828	1.633	128.196	11.365	6.562	31	3.559	2.055	118.942	11.305	6.527
	110	23	2.893	1.670	92.340	10.984	6.342	28	6.164	3.559	97.470	0.498	0.288	25	1.414	0.816	124.904	5.355	3.092	32	3.000	1.732	120.946	9.992	5.769
	115	24	2.706	1.562	93.714	8.254	4.766	28	5.523	3.189	95.369	2.655	1.533	25	1.414	0.816	124.904	5.355	3.092	31	2.754	1.590	119.985	8.851	5.110
	120	23	2.640	1.524	89.739	8.274	4.777	27	4.416	2.550	93.689	12.160	7.020	24	1.871	1.080	123.237	8.829	5.097	32	2.309	1.333	123.168	11.845	6.839
10 µM	125	22	2.756	1.591	86.961	5.197	3.000	26	6.124	3.536	90.011	16.996	9.812	24	3.082	1.780	123.216	14.662	8.465	33	3.000	1.732	124.954	12.033	6.947
	130	22	3.152	1.820	86.784	8.249	4.762	25	6.164	3.559	85.512	18.531	10.699	25	1.871	1.080	124.991	10.775	6.221	33	3.202	1.848	125.916	12.783	7.380
	135	21	2.690	1.553	82.986	5.476	3.162	25	6.164	3.559	85.512	18.531	10.699	25	3.082	1.780	128.284	14.673	8.472	33	3.512	2.028	125.023	14.535	8.392
	140	20	2.261	1.305	79.187	5.643	3.258	24	6.285	3.629	84.531	20.336	11.741	26	3.082	1.780	130.038	15.974	9.223	34	1.915	1.106	128.813	9.103	5.256
30 µM	145	21	1.933	1.116	81.936	2.120	1.224	24	6.964	4.021	82.132	22.169	12.800	26	2.449	1.414	131.705	12.445	7.185	33	1.708	0.986	127.920	9.754	5.631
	150	20	2.171	1.253	79.172	1.010	0.583	24	6.964	4.021	82.132	22.169	12.800	27	3.742	2.160	134.997	17.348	10.016	33	1.708	0.986	127.920	9.754	5.631
	155	20	1.727	0.997	79.335	3.746	2.163	24	6.164	3.559	81.992	18.308	10.570	27	3.240	1.871	136.663	14.177	8.185	33	1.708	0.986	127.920	9.754	5.631
	160	21	1.933	1.116	81.936	2.120	1.224	24	7.382	4.262	81.694	21.034	12.144	27	3.536	2.041	134.909	14.609	8.434	33	1.708	0.986	127.920	9.754	5.631

**Appendix 17** – The data shown below represents the left ventricular developed pressure measurements for the 6 and 18-month lean and HFD Dobutamine treated hearts, as presented in chapter 7. Both the raw values and the normalised to stabilisation values are presented.

CHAPTER 7 - DOBUTAMINE DATA																									
Concentration	Time	6M Lean Avg.	SD	SEM	6M Lean Avg. %	SD	SEM	6M HFD Avg.	SD	SEM	6M HFD Avg. %	SD	SEM	18M Lean Avg.	SD	SEM	18M Lean Avg. %	SD	SEM	18M HFD Avg.	SD	SEM	18M HFD Avg. %	SD	SEM
Stabilisation	5	144.84	13.416	7.746	101.156	3.513	2.028	139.403	12.807	7.394	96.834	2.908	1.679	109.13	8.426	4.865	99.858	1.518	0.876	172.168	12.619	7.285	98.285	2.555	1.475
	10	142.65	12.023	6.941	99.629	1.160	0.670	145.053	20.703	11.953	100.998	2.151	1.242	108.84	10.611	6.126	99.535	3.570	2.061	174.363	9.584	5.533	99.609	1.197	0.691
	15	142.82	16.726	9.657	99.608	2.523	1.457	144.860	22.444	12.958	100.767	1.653	0.954	108.45	8.578	4.952	99.243	2.806	1.620	176.148	9.129	5.270	100.662	2.587	1.494
	20	142.63	13.106	7.567	99.607	3.796	2.192	146.050	9.015	5.205	101.401	2.366	1.366	110.74	7.484	4.321	101.364	2.279	1.316	177.568	9.625	5.557	101.445	1.467	0.847
1 nM	25	161.27	12.489	7.210	112.415	14.484	8.362	159.497	7.734	4.465	110.992	6.446	3.722	162.18	6.637	3.832	148.807	13.636	7.873	203.635	22.132	12.778	116.548	13.527	7.810
	30	173.64	20.983	12.115	120.899	17.586	10.153	166.363	15.166	8.756	115.400	6.722	3.881	161.59	7.514	4.338	148.181	11.743	6.780	207.798	9.964	5.753	118.815	15.019	8.671
	35	175.42	18.831	10.872	122.105	16.578	9.571	174.653	20.944	12.092	120.909	7.175	4.143	164.47	9.022	5.209	150.904	14.756	8.519	205.943	12.041	6.952	117.803	16.689	9.635
3 nM	40	168.14	14.384	8.305	116.884	17.619	10.172	179.110	13.269	7.661	124.444	1.992	1.150	170.01	4.616	2.665	155.950	12.256	7.076	197.445	8.038	4.641	112.932	14.358	8.290
	45	169.95	18.978	10.957	118.161	15.411	8.897	185.603	12.080	6.975	129.161	8.086	4.668	164.09	6.168	3.561	150.571	13.697	7.908	186.905	21.640	12.494	107.080	14.328	8.272
	50	170.10	17.364	10.025	118.272	13.877	8.012	187.183	19.865	11.469	130.813	11.554	6.671	162.54	5.458	3.151	149.143	13.325	7.693	185.868	23.809	13.746	106.468	15.166	8.756
10 nM	55	171.83	15.785	9.113	119.559	13.232	7.639	191.267	20.586	11.885	133.523	7.751	4.475	155.04	11.489	6.633	142.147	13.527	7.810	179.690	22.487	12.983	102.950	14.640	8.452
	60	176.68	15.986	9.230	122.881	15.618	9.017	190.380	19.910	11.495	132.970	9.102	5.255	144.48	20.036	11.568	132.400	19.402	11.202	180.590	25.789	14.889	103.277	14.389	8.307
	65	174.40	23.633	13.645	121.566	5.869	3.388	188.510	24.164	13.951	131.530	9.483	5.475	138.63	16.882	9.747	127.064	16.925	9.772	182.128	14.650	8.458	104.019	16.706	9.645
100 nM	70	174.42	19.179	11.073	121.693	3.399	1.962	188.690	15.077	8.705	131.168	5.026	2.902	134.17	1.514	0.874	123.039	8.141	4.700	181.180	15.435	8.912	103.461	17.072	9.857
	75	181.43	18.751	10.826	126.624	3.491	2.016	187.523	17.689	10.213	130.146	3.166	1.828	134.42	10.261	5.924	123.457	16.038	9.259	181.115	16.178	9.340	103.464	17.836	10.298
	80	183.91	15.821	9.134	128.472	5.022	2.900	185.893	16.291	9.405	129.088	6.300	3.638	137.92	8.563	4.944	126.591	13.910	8.031	182.638	16.399	9.468	104.236	21.337	12.319
1 μM	85	187.80	11.978	6.915	131.324	6.754	3.899	186.777	13.320	7.691	129.972	9.888	5.709	142.79	7.500	4.330	131.164	15.572	8.990	188.148	8.973	5.181	107.289	11.490	6.634
	90	192.28	5.851	3.378	134.627	9.634	5.562	188.010	12.141	7.010	130.770	0.902	0.521	144.31	9.443	5.452	132.538	16.301	9.411	192.385	12.578	7.262	109.506	12.196	7.042
	95	197.48	5.297	3.058	138.313	10.949	6.321	177.883	14.021	8.095	123.782	10.078	5.819	148.05	10.206	5.893	136.007	17.451	10.075	195.530	10.093	5.827	111.378	10.821	6.247
10 μM	100	196.92	7.759	4.480	137.841	9.250	5.340	175.333	11.590	6.691	122.187	11.891	6.865	150.56	10.604	6.122	138.304	17.769	10.259	193.855	14.632	8.448	110.249	12.936	7.468
	105	200.88	13.623	7.865	140.633	12.611	7.281	172.660	16.057	9.271	120.700	14.773	8.529	154.85	6.128	3.538	142.114	13.537	7.815	212.925	18.206	10.511	121.494	4.809	2.777
	110	203.75	13.995	8.080	142.552	10.626	6.135	169.787	12.795	7.387	118.121	21.533	12.432	158.63	8.602	4.966	145.774	18.382	10.613	213.045	22.402	12.934	121.459	7.102	4.100
30 μM	115	206.52	18.663	10.775	144.441	12.441	7.183	161.450	8.664	5.002	112.629	26.618	15.368	159.10	7.455	4.304	146.149	17.090	9.867	213.883	14.853	8.575	122.180	5.243	3.027
	120	210.94	20.169	11.645	147.652	15.904	9.182	171.193	16.756	9.674	118.852	14.915	8.611	157.33	20.643	11.918	143.778	10.945	6.319	220.233	7.095	4.096	126.163	9.448	5.455
	125	209.65	13.746	7.936	146.858	14.848	8.572	173.047	21.851	12.616	119.981	9.258	5.345	148.40	13.981	8.072	135.713	2.464	1.423	201.685	16.779	9.687	115.560	12.392	7.155
	130	211.72	12.914	7.456	148.346	15.400	8.891	179.593	9.391	5.422	124.082	10.927	6.308	142.32	10.014	5.781	130.251	0.857	0.495	205.395	11.176	6.453	117.752	11.473	6.624
	135	206.20	7.706	4.449	144.480	13.555	7.826	182.373	22.475	12.976	126.350	6.595	3.807	141.03	8.127	4.692	129.132	3.510	2.027	204.815	13.086	7.555	117.358	11.125	6.423
	140	200.83	5.173	2.987	140.862	15.963	9.216	176.253	20.301	11.721	122.066	6.947	4.011	136.94	13.050	7.535	125.240	4.198	2.424	197.050	12.305	7.104	112.861	9.912	5.723
	145	196.64	6.773	3.910	138.012	17.766	10.257	183.600	13.204	7.623	132.762	13.243	7.646	145.58	19.113	11.035	133.032	9.850	5.687	211.835	14.556	8.404	120.978	3.813	2.202
	150	191.50	6.182	3.569	134.366	16.529	9.543	181.057	8.001	4.619	132.897	21.478	12.400	146.40	16.876	9.743	134.057	14.465	8.351	211.940	20.566	11.874	120.870	5.851	3.378
	155	187.34	5.545	3.201	131.408	15.160	8.753	178.250	16.718	9.652	128.657	15.699	9.064	147.52	14.440	8.337	135.106	12.363	7.138	214.660	18.348	10.593	122.525	5.714	3.299
	160	184.07	6.338	3.659	129.079	14.208	8.203	171.053	13.890	8.019	123.028	14.559	8.405	148.69	13.815	7.976	136.230	13.101	7.564	212.628	16.880	9.746	121.452	6.579	3.798

**Appendix 18** – The data shown below represents the heart rate measurements for the 6 and 18-month lean and HFD Dobutamine treated hearts, as presented in chapter 7. Both the raw values and the normalised to stabilisation values are presented.

CHAPTER 7 - DOBUTAMINE DATA																									
Concentration	Time	6M Lean Avg.	SD	SEM	6M Lean Avg. %	SD	SEM	6M HFD Avg.	SD	SEM	6M HFD Avg. %	SD	SEM	18M Lean Avg.	SD	SEM	18M Lean Avg. %	SD	SEM	18M HFD Avg.	SD	SEM	18M HFD Avg. %	SD	SEM
Stabilisation	5	253	10.964	6.330	96.223	4.263	2.461	337	8.454	4.881	104.645	4.649	2.684	347	7.071	4.082	106.079	7.621	4.400	323	11.402	6.583	101.412	3.957	2.284
	10	257	10.964	6.330	97.535	6.718	3.879	330	12.846	7.417	102.389	2.653	1.532	353	7.071	4.082	108.180	9.451	5.456	318	21.302	12.298	99.600	3.980	2.298
	15	270	3.833	2.213	102.388	3.639	2.101	300	9.518	5.495	93.477	3.183	1.838	307	16.349	9.439	93.391	10.105	5.834	320	7.174	4.142	100.730	4.896	2.827
	20	273	10.964	6.330	103.855	4.450	2.569	320	21.484	12.404	99.489	2.718	1.569	303	16.349	9.439	92.349	8.974	5.181	313	8.979	5.184	98.257	2.070	1.195
1 nM	25	263	18.708	10.801	100.161	3.496	2.018	330	7.174	4.142	103.997	19.857	11.465	327	4.508	2.602	99.611	4.352	2.513	343	11.817	6.822	107.324	5.266	3.040
	30	260	12.247	7.071	99.002	5.720	3.303	327	8.454	4.881	101.491	4.737	2.735	297	7.288	4.208	90.281	16.335	9.431	328	15.276	8.819	102.530	7.374	4.257
	35	270	12.247	7.071	102.911	9.083	5.244	297	14.142	8.165	93.342	14.970	8.643	303	16.349	9.439	92.448	10.867	6.274	348	22.597	13.047	108.861	9.050	5.225
	40	290	5.895	3.404	109.682	9.525	5.499	293	14.856	8.577	91.262	3.218	1.858	303	4.729	2.730	92.515	7.241	4.180	353	22.148	12.787	110.410	10.946	6.320
3 nM	45	287	15.492	8.944	108.277	14.403	8.316	313	13.502	7.795	98.628	18.329	10.582	303	10.964	6.330	92.581	3.658	2.112	333	8.852	5.111	104.233	4.757	2.747
	50	287	4.607	2.660	108.492	11.264	6.503	317	21.828	12.602	99.058	9.952	5.746	297	11.727	6.771	90.364	7.952	4.591	345	14.119	8.152	107.986	14.771	8.528
	55	290	6.620	3.822	109.867	11.291	6.519	317	23.238	13.417	98.721	11.127	6.424	303	8.175	4.720	92.598	3.147	1.817	320	15.025	8.674	100.191	7.660	4.422
	60	293	16.349	9.439	111.242	12.046	6.955	333	22.050	12.730	104.386	12.676	7.318	293	8.357	4.825	89.156	15.499	8.949	340	14.872	8.586	106.151	11.957	6.903
10 nM	65	300	6.620	3.822	113.683	11.119	6.419	340	25.106	14.495	106.134	5.948	3.434	280	3.893	2.247	85.502	2.614	1.509	350	12.368	7.140	109.189	18.336	10.586
	70	293	10.964	6.330	111.487	4.763	2.750	333	18.708	10.801	105.101	19.779	11.419	307	7.071	4.082	93.839	6.805	3.929	358	9.617	5.552	111.619	17.492	10.099
	75	293	13.502	7.795	111.579	9.644	5.568	333	8.371	4.833	106.077	32.965	19.033	293	7.071	4.082	89.703	4.448	2.568	358	15.325	8.848	111.462	18.655	10.770
	80	300	14.349	8.284	113.991	15.210	8.782	327	14.142	8.165	102.804	16.699	9.641	297	13.502	7.795	90.630	8.320	4.804	315	15.767	9.103	98.388	19.959	11.524
100 nM	85	317	10.964	6.330	120.801	16.330	9.428	310	15.083	8.708	97.393	15.903	9.181	267	7.071	4.082	81.549	4.113	2.375	335	10.179	5.877	104.740	24.561	14.180
	90	330	21.213	12.247	125.899	15.186	8.768	310	21.484	12.404	97.310	19.892	11.485	287	8.175	4.720	87.686	9.090	5.248	348	12.521	7.229	108.703	19.511	11.265
	95	353	14.142	8.165	134.813	14.862	8.580	337	8.371	4.833	106.129	23.169	13.377	310	5.895	3.404	94.732	17.016	9.824	358	9.617	5.552	111.842	17.823	10.290
	100	360	0.000	0.000	137.378	14.276	8.242	353	14.142	8.165	111.072	15.991	9.232	317	15.492	8.944	97.016	22.560	13.025	358	9.760	5.635	111.976	22.810	13.169
1 μM	105	363	7.071	4.082	138.752	16.757	9.675	357	14.142	8.165	112.348	19.371	11.184	313	4.729	2.730	95.973	14.868	8.584	365	14.979	8.648	114.664	24.198	13.970
	110	367	7.071	4.082	140.034	16.927	9.773	357	7.071	4.082	112.307	18.577	10.725	340	9.518	5.495	104.360	19.132	11.046	373	20.962	12.102	117.133	13.856	8.000
	115	363	7.071	4.082	138.537	12.099	6.986	350	12.247	7.071	110.683	24.422	14.100	347	4.729	2.730	106.395	18.282	10.555	380	15.025	8.674	119.514	11.959	6.904
	120	370	12.247	7.071	140.978	10.068	5.813	357	24.050	13.885	113.785	38.179	22.042	373	4.729	2.730	114.218	13.883	8.016	400	7.174	4.142	126.504	14.538	8.393
10 μM	125	360	12.247	7.071	137.162	9.673	5.585	357	25.495	14.720	113.152	29.589	17.083	377	18.708	10.801	115.161	6.601	3.811	388	12.540	7.240	122.850	18.182	10.497
	130	363	7.071	4.082	138.752	16.757	9.675	350	21.154	12.213	111.274	32.222	18.603	370	15.083	8.708	113.010	7.417	4.282	383	11.402	6.583	121.022	15.577	8.994
	135	377	7.071	4.082	143.850	17.323	10.001	373	18.585	10.730	117.256	18.705	10.799	370	7.174	4.142	113.126	8.286	4.784	373	11.402	6.583	118.234	18.342	10.590
	140	370	0.000	0.000	141.194	14.672	8.471	383	7.071	4.082	120.788	21.195	12.237	393	6.729	3.885	119.841	8.401	4.850	380	9.760	5.635	119.952	11.741	6.779
30 μM	145	383	14.142	8.165	146.507	20.021	11.559	363	18.708	10.801	115.072	27.590	15.929	383	8.357	4.825	116.697	13.945	8.051	403	14.056	8.115	125.991	11.369	6.564
	150	393	10.964	6.330	150.138	19.282	11.133	377	22.050	12.730	117.769	8.740	5.046	387	12.265	7.081	117.557	16.355	9.443	400	20.131	11.623	125.443	8.736	5.044
	155	400	12.247	7.071	152.734	18.563	10.718	370	19.422	11.213	115.809	10.987	6.344	403	12.265	7.081	122.702	16.423	9.482	388	15.720	9.076	121.913	5.761	3.326
	160	387	7.071	4.082	147.544	15.485	8.940	377	22.050	12.730	117.769	8.740	5.046	413	12.265	7.081	125.746	17.138	9.895	393	17.879	10.322	123.293	10.555	6.094

**Appendix 19** – The data shown below represents the coronary flow measurements for the 6 and 18-month lean and HFD Atenolol treated hearts, as presented in chapter 7. Both the raw values and the normalised to stabilisation values are presented.

CHAPTER 7 - ATENOLOL DATA																									
Concentration	Time	6M Lean Avg.	SD	SEM	6M Lean Avg. %	SD	SEM	6M HFD Avg.	SD	SEM	6M HFD Avg. %	SD	SEM	18M Lean Avg.	SD	SEM	18M Lean Avg. %	SD	SEM	18M HFD Avg.	SD	SEM	18M HFD Avg. %	SD	SEM
Stabilisation	5	23	6.550	3.782	97.797	3.908	2.256	28	2.630	1.518	101.345	6.698	3.867	27	1.893	1.093	99.324	1.351	0.780	23	1.414	0.816	101.189	1.748	1.009
	10	23	6.111	3.528	101.186	1.167	0.674	27	1.893	1.093	99.564	3.231	1.865	27	2.000	1.155	100.225	0.450	0.260	23	1.893	1.093	99.955	0.935	0.540
	15	23	5.918	3.417	100.508	1.562	0.902	27	1.893	1.093	99.546	2.342	1.352	27	2.000	1.155	100.225	0.450	0.260	23	1.893	1.093	99.955	0.935	0.540
	20	23	5.918	3.417	100.508	1.562	0.902	27	1.893	1.093	99.546	2.342	1.352	27	2.000	1.155	100.225	0.450	0.260	23	1.732	1.000	98.902	1.491	0.861
1 nM	25	23	5.981	3.453	98.580	3.525	2.035	26	2.872	1.658	94.065	8.500	4.907	26	2.217	1.280	97.390	1.841	1.063	23	1.732	1.000	98.902	1.491	0.861
	30	22	6.050	3.493	96.612	3.489	2.014	26	3.317	1.915	98.139	10.332	5.965	26	2.217	1.280	97.390	1.841	1.063	21	1.708	0.986	93.455	4.159	2.401
	35	22	6.050	3.493	96.612	3.489	2.014	25	2.986	1.724	92.142	7.523	4.344	26	2.217	1.280	97.390	1.841	1.063	21	2.160	1.247	92.221	4.709	2.719
	40	22	5.829	3.365	93.261	6.987	4.034	24	2.500	1.443	88.624	7.746	4.472	27	2.380	1.374	98.291	2.533	1.462	20	2.500	1.443	88.812	5.576	3.219
3 nM	45	21	5.712	3.298	90.615	6.243	3.604	24	2.630	1.518	86.865	9.374	5.412	26	2.708	1.563	96.348	3.472	2.004	19	2.000	1.155	83.378	3.294	1.902
	50	20	5.303	3.062	86.675	8.875	5.124	24	2.517	1.453	85.904	8.231	4.752	25	2.708	1.563	92.620	3.738	2.158	19	2.500	1.443	82.144	5.597	3.231
	55	20	5.174	2.987	85.867	8.101	4.677	23	2.217	1.280	85.070	8.297	4.790	25	3.202	1.848	91.578	5.704	3.293	19	2.380	1.374	81.102	5.688	3.284
	60	19	5.027	2.903	81.968	14.172	8.182	24	2.380	1.374	86.032	9.544	5.510	25	3.109	1.795	90.677	5.541	3.199	19	3.109	1.795	80.920	8.844	5.106
10 nM	65	19	5.196	3.000	82.776	14.829	8.562	23	3.594	2.075	85.105	13.714	7.918	24	3.096	1.787	89.776	5.946	3.433	15	2.217	1.280	64.697	7.105	4.102
	70	19	5.027	2.903	81.968	14.172	8.182	23	3.109	1.795	82.367	12.008	6.933	24	2.944	1.700	88.884	5.587	3.226	15	1.915	1.106	63.610	5.338	3.082
	75	19	5.246	3.029	81.226	11.152	6.438	22	3.464	2.000	80.608	13.870	8.008	23	3.096	1.787	86.048	6.170	3.562	14	1.708	0.986	62.523	3.994	2.306
	80	19	5.566	3.213	79.976	13.195	7.618	22	3.317	1.915	78.813	13.614	7.860	23	2.872	1.658	84.262	5.951	3.436	14	1.915	1.106	59.194	5.502	3.177
100 nM	85	19	5.566	3.213	79.976	13.195	7.618	20	3.304	1.908	74.315	14.035	8.103	23	3.403	1.965	84.122	7.506	4.334	13	2.062	1.190	56.002	7.361	4.250
	90	18	5.218	3.012	75.713	11.100	6.408	21	2.517	1.453	75.206	11.324	6.538	23	3.403	1.965	84.122	7.506	4.334	12	2.630	1.518	53.714	9.694	5.597
	95	17	5.282	3.050	73.808	12.913	7.456	20	3.304	1.908	72.392	13.367	7.717	22	4.349	2.511	82.038	11.152	6.439	12	2.363	1.364	51.540	8.450	4.878
	100	16	4.922	2.842	70.506	11.623	6.710	19	3.464	2.000	69.764	14.591	8.424	22	3.948	2.279	80.245	9.603	5.544	11	2.217	1.280	49.264	7.421	4.284
1 μM	105	15	5.282	3.050	64.422	13.549	7.823	19	3.317	1.915	67.895	13.826	7.983	22	3.873	2.236	79.344	9.441	5.451	11	2.582	1.491	48.030	8.777	5.067
	110	15	5.360	3.094	61.686	15.341	8.857	18	3.686	2.128	66.969	15.002	8.661	21	4.082	2.357	77.409	10.282	5.936	11	1.915	1.106	45.946	6.095	3.519
	115	15	5.360	3.094	61.686	15.341	8.857	17	3.304	1.908	63.323	13.699	7.909	21	3.862	2.230	76.516	9.441	5.451	10	2.363	1.364	44.712	8.028	4.635
	120	14	5.790	3.343	59.146	16.664	9.621	17	3.416	1.972	60.620	14.253	8.229	20	4.082	2.357	73.681	10.568	6.101	10	2.217	1.280	42.572	7.499	4.330
10 μM	125	14	5.457	3.150	57.801	16.252	9.383	17	2.887	1.667	60.584	12.273	7.086	20	4.573	2.640	72.639	12.596	7.272	9	2.500	1.443	40.251	8.638	4.987
	130	13	5.317	3.070	55.025	14.748	8.515	16	3.304	1.908	59.659	13.593	7.848	19	5.252	3.032	68.762	15.590	9.001	8	2.363	1.364	35.880	8.587	4.958
	135	13	5.764	3.328	51.546	16.038	9.260	15	3.686	2.128	55.976	14.729	8.504	19	5.252	3.032	68.762	15.590	9.001	8	2.828	1.633	34.646	10.802	6.236
	140	13	5.764	3.328	51.546	16.038	9.260	15	3.317	1.915	53.238	13.423	7.750	18	4.761	2.749	66.075	13.842	7.991	8	2.828	1.633	34.646	10.802	6.236
30 μM	145	12	5.599	3.233	50.868	15.714	9.072	14	3.686	2.128	52.312	14.644	8.455	18	4.573	2.640	65.183	13.173	7.605	7	2.872	1.658	31.282	11.213	6.474
	150	11	5.599	3.233	46.175	16.546	9.553	14	3.304	1.908	50.407	12.907	7.452	17	4.924	2.843	63.248	14.746	8.514	7	2.708	1.563	30.195	10.378	5.992
	155	11	5.457	3.150	43.529	15.810	9.128	13	4.082	2.357	47.722	15.916	9.189	17	4.830	2.789	62.347	14.428	8.330	7	2.380	1.374	28.067	8.954	5.170
	160	11	4.845	2.797	43.304	12.467	7.198	13	4.500	2.598	46.796	17.361	10.023	17	4.830	2.789	62.347	14.428	8.330	7	2.517	1.453	28.056	9.525	5.499

**Appendix 20** – The data shown below represents the left ventricular developed pressure measurements for the 6 and 18-month lean and HFD Atenolol treated hearts, as presented in chapter 7. Both the raw values and the normalised to stabilisation values are presented.

CHAPTER 7 - ATENOLOL DATA																									
Concentration	Time	6M Lean Avg.	SD	SEM	6M Lean Avg. %	SD	SEM	6M HFD Avg.	SD	SEM	6M HFD Avg. %	SD	SEM	18M Lean Avg.	SD	SEM	18M Lean Avg. %	SD	SEM	18M HFD Avg.	SD	SEM	18M HFD Avg. %	SD	SEM
Stabilisation	5	137.25	18.305	10.568	97.913	1.535	0.886	158.695	18.636	10.759	98.863	1.493	0.862	139.24	15.833	9.141	98.637	1.693	0.977	144.898	21.423	12.369	100.821	2.482	1.433
	10	141.02	18.626	10.754	100.649	1.607	0.928	161.785	20.893	12.063	100.673	1.404	0.811	141.42	16.194	9.350	100.186	1.892	1.093	144.270	19.306	11.146	100.781	1.569	0.906
	15	139.96	17.470	10.086	99.950	1.254	0.724	160.445	17.103	9.874	100.032	1.262	0.729	141.23	16.381	9.457	100.020	0.503	0.290	143.518	19.300	11.143	100.297	0.801	0.462
	20	142.19	18.755	10.828	101.487	1.753	1.012	161.340	20.119	11.616	100.432	2.514	1.452	142.90	17.211	9.937	101.157	0.666	0.385	140.310	18.569	10.721	98.101	2.855	1.648
1 nM	25	136.77	17.919	10.346	97.623	1.605	0.927	161.088	19.491	11.253	100.322	3.187	1.840	134.29	10.612	6.127	95.120	7.616	4.397	129.845	13.119	7.574	92.274	13.016	7.515
	30	132.93	16.213	9.361	95.040	2.891	1.669	166.883	9.441	5.450	103.737	9.003	5.198	133.13	7.633	4.407	94.326	13.370	7.719	128.538	10.127	5.847	91.304	9.940	5.739
	35	129.33	14.007	8.087	92.631	3.549	2.049	166.180	14.569	8.412	103.224	13.429	7.753	132.37	9.464	5.464	93.897	15.598	9.006	126.263	15.001	8.661	88.546	8.332	4.810
3 nM	40	128.74	16.832	9.718	91.943	3.551	2.050	160.060	16.832	9.718	99.284	14.759	8.521	134.45	8.357	4.825	95.347	14.477	8.358	127.478	10.142	5.856	90.319	8.474	4.892
	45	125.21	16.743	9.666	89.434	4.382	2.530	160.315	12.624	7.288	99.920	15.049	8.689	134.41	6.073	3.506	95.492	14.182	8.188	127.978	12.062	6.964	90.090	5.745	3.317
	50	121.58	16.933	9.776	86.757	3.364	1.942	155.113	11.549	6.668	96.815	15.992	9.233	125.03	8.019	4.630	88.703	14.971	8.643	125.173	12.011	6.935	87.806	4.605	2.658
10 nM	55	122.68	18.284	10.556	87.557	6.050	3.493	150.543	13.710	7.915	93.695	15.774	9.107	124.32	9.543	5.510	88.289	16.672	9.625	124.193	14.094	8.137	86.738	6.411	3.701
	60	116.89	19.258	11.119	83.288	6.268	3.619	143.608	13.201	7.621	89.485	16.669	9.624	123.59	6.775	3.912	87.689	13.929	8.042	120.385	5.926	3.421	85.530	7.856	4.536
	65	117.12	18.318	10.576	83.849	9.693	5.596	146.638	11.635	6.718	91.395	15.577	8.993	121.04	7.907	4.565	86.045	16.052	9.267	118.178	5.741	3.314	83.974	8.431	4.868
100 nM	70	119.09	19.134	11.047	85.440	12.122	6.999	149.885	22.338	12.897	93.667	12.594	7.271	118.05	7.285	4.206	83.838	15.151	8.747	116.885	6.052	3.494	83.040	9.067	5.235
	75	117.50	20.127	11.620	84.378	14.124	8.155	147.943	23.586	13.617	92.633	15.304	8.836	116.10	9.750	5.629	82.189	15.350	8.862	115.745	4.923	2.842	82.528	10.854	6.267
	80	114.04	20.823	12.022	81.754	13.618	7.863	149.933	23.489	13.561	93.753	14.131	8.158	116.73	9.960	5.751	82.625	15.396	8.889	115.648	4.092	2.362	82.468	9.699	5.600
1 µM	85	109.95	21.656	12.503	78.583	12.736	7.353	149.368	22.891	13.216	93.351	13.036	7.527	114.24	9.227	5.327	80.926	15.452	8.921	111.615	18.710	10.802	79.667	9.129	5.270
	90	105.65	21.565	12.450	75.462	12.607	7.279	140.390	10.023	5.787	87.856	17.227	9.946	111.75	10.478	6.049	79.217	16.854	9.731	109.425	16.661	9.619	78.620	11.112	6.416
	95	106.69	22.601	13.049	76.230	13.830	7.985	136.343	10.003	5.775	85.367	17.242	9.955	109.58	9.046	5.223	77.675	15.805	9.125	107.610	11.943	6.895	77.887	11.315	6.533
10 µM	100	103.94	25.255	14.581	73.848	13.775	7.953	137.573	11.828	6.829	85.901	16.986	9.807	108.97	8.959	5.172	77.194	15.470	8.932	102.970	8.614	4.973	75.411	14.842	8.569
	105	101.65	21.913	12.651	72.554	13.020	7.517	136.575	11.249	6.495	85.305	16.782	9.689	105.44	7.505	4.333	74.701	14.445	8.340	100.203	9.462	5.463	73.041	13.360	7.713
	110	102.99	22.797	13.162	73.714	14.882	8.592	136.388	9.718	5.611	85.192	15.966	9.218	101.35	7.047	4.069	71.779	14.129	8.157	100.388	7.301	4.215	73.674	15.027	8.676
30 µM	115	101.66	23.123	13.350	72.554	13.700	7.909	138.853	9.675	5.586	86.691	15.709	9.070	100.84	7.730	4.463	71.507	15.159	8.752	99.068	8.174	4.720	72.359	13.495	7.791
	120	103.76	21.476	12.399	74.309	13.609	7.857	137.813	10.597	6.118	85.932	15.580	8.995	98.39	8.359	4.826	69.761	15.612	9.013	97.788	8.033	4.638	71.688	15.007	8.664
	125	104.25	19.564	11.295	74.510	10.784	6.226	135.070	11.079	6.397	84.189	15.765	9.102	100.17	9.417	5.437	70.989	16.117	9.305	95.830	9.362	5.405	69.743	12.884	7.439
18M HFD	130	103.57	16.275	9.397	74.337	10.146	5.858	132.193	6.096	3.519	82.548	13.368	7.718	96.02	7.777	4.490	68.225	15.986	9.230	93.815	10.315	5.955	67.623	9.539	5.507
	135	103.64	18.192	10.503	74.172	10.568	6.101	128.640	6.335	3.657	80.455	14.843	8.569	94.26	7.201	4.158	66.947	15.458	8.925	92.608	5.222	3.015	67.535	11.304	6.526
	140	103.09	19.498	11.257	73.924	12.710	7.338	122.178	18.541	10.705	76.388	11.060	6.385	96.14	4.473	2.583	68.557	15.296	8.831	87.135	18.023	10.406	64.082	12.133	7.005
18M Lean	145	98.76	16.638	9.606	71.223	13.169	7.603	120.753	21.762	12.565	75.347	11.820	6.824	88.91	7.114	4.108	63.144	15.518	8.959	81.393	12.909	7.453	60.583	13.724	7.923
	150	97.35	16.931	9.775	70.362	14.625	8.444	119.518	18.842	10.878	74.772	11.355	6.556	87.85	7.558	4.363	62.385	15.869	9.162	81.693	9.025	5.211	61.681	16.647	9.611
	155	96.83	16.561	9.562	69.931	14.089	8.134	117.185	18.493	10.677	73.244	10.672	6.162	86.34	9.338	5.391	61.183	16.517	9.536	78.335	8.232	4.753	59.175	15.876	9.166
	160	96.96	17.543	10.128	70.111	15.346	8.860	115.028	17.290	9.982	71.893	9.887	5.708	82.60	7.333	4.233	58.484	15.015	8.669	72.838	8.223	4.747	55.508	16.753	9.673

**Appendix 21** – The data shown below represents the heart rate measurements for the 6 and 18-month lean and HFD Atenolol treated hearts, as presented in chapter 7. Both the raw values and the normalised to stabilisation values are presented.

CHAPTER 7 - ATENOLOL DATA																									
Concentration	Time	6M Lean Avg.	SD	SEM	6M Lean Avg. %	SD	SEM	6M HFD Avg.	SD	SEM	6M HFD Avg. %	SD	SEM	18M Lean Avg.	SD	SEM	18M Lean Avg. %	SD	SEM	18M HFD Avg.	SD	SEM	18M HFD Avg. %	SD	SEM
Stabilisation	5	268	9.652	5.572	101.941	2.826	1.632	298	22.174	12.802	99.529	7.666	4.426	345	9.412	5.434	102.179	3.043	1.757	325	19.648	11.344	102.677	1.698	0.981
	10	252	8.947	5.166	95.794	1.583	0.914	295	15.846	9.149	98.316	5.011	2.893	328	5.373	3.102	97.016	2.305	1.331	305	9.137	5.275	96.554	1.548	0.893
	15	262	11.662	6.733	99.557	3.787	2.186	308	17.078	9.860	102.886	6.353	3.668	343	5.272	3.044	100.802	3.876	2.238	313	16.714	9.650	98.792	2.565	1.481
	20	270	11.402	6.583	102.708	4.158	2.401	298	10.217	5.899	99.268	4.331	2.501	338	5.412	3.124	100.003	3.025	1.746	323	15.720	9.076	101.977	1.820	1.051
1 nM	25	270	11.592	6.693	101.993	8.155	4.708	288	17.679	10.207	95.870	7.164	4.136	338	5.412	3.124	100.110	4.065	2.347	350	20.131	11.623	110.552	12.048	6.956
	30	272	15.883	9.170	103.333	4.965	2.867	300	21.602	12.472	100.305	6.231	3.598	315	5.484	3.166	93.333	4.715	2.722	328	23.809	13.746	103.376	2.524	1.457
	35	266	1.897	1.095	100.851	5.328	3.076	295	19.149	11.055	98.696	6.797	3.924	338	13.549	7.823	99.757	3.603	2.080	308	20.429	11.794	97.257	6.897	3.982
	40	276	7.629	4.405	105.263	6.480	3.741	333	22.174	12.802	111.255	8.122	4.689	333	5.718	3.301	98.204	11.729	6.772	330	12.119	6.997	104.786	10.066	5.812
3 nM	45	276	15.996	9.235	105.216	9.386	5.419	315	11.547	6.667	105.081	3.585	2.070	328	15.718	9.075	96.347	13.851	7.997	318	21.302	12.298	100.400	7.041	4.065
	50	284	10.473	6.047	108.847	13.368	7.718	330	14.302	8.257	110.091	5.266	3.040	333	11.702	6.756	97.851	11.839	6.835	323	12.529	7.234	102.401	14.889	8.596
	55	272	18.596	10.736	103.310	6.467	3.734	308	20.429	11.794	102.606	9.860	5.693	338	10.038	5.795	99.653	14.078	8.128	323	18.619	10.750	102.224	9.401	5.428
	60	276	16.554	9.558	104.971	6.880	3.972	320	12.119	6.997	106.864	7.135	4.120	348	15.718	9.075	101.874	10.365	5.984	323	9.885	5.707	101.970	16.458	9.502
10 nM	65	282	5.917	3.416	107.686	7.179	4.145	328	12.540	7.240	109.555	10.086	5.823	345	10.186	5.881	101.042	9.036	5.217	315	8.316	4.801	99.624	16.246	9.380
	70	276	5.263	3.038	105.580	9.375	5.412	298	15.000	8.660	99.520	5.167	2.983	345	8.393	4.845	101.859	12.358	7.135	315	16.021	9.250	99.910	14.923	8.616
	75	272	9.652	5.572	103.583	4.941	2.853	290	12.119	6.997	96.913	8.548	4.935	330	9.683	5.590	97.579	6.184	3.570	325	9.952	5.746	102.669	15.798	9.121
	80	280	7.785	4.495	106.491	11.628	6.713	308	12.540	7.240	102.896	10.507	6.066	330	8.607	4.969	97.070	9.298	5.368	310	8.499	4.907	98.732	12.369	7.141
100 nM	85	268	9.652	5.572	102.168	6.547	3.780	305	19.648	11.344	101.983	11.852	6.843	308	15.939	9.202	91.405	7.097	4.098	328	11.402	6.583	103.839	7.344	4.240
	90	266	5.263	3.038	101.534	6.087	3.515	318	13.636	7.873	105.970	6.032	3.483	323	17.240	9.954	95.895	7.411	4.279	323	11.402	6.583	102.407	10.100	5.831
	95	276	13.663	7.889	105.044	6.199	3.579	313	15.720	9.076	104.860	15.113	8.726	343	5.412	3.124	101.671	7.633	4.407	310	20.000	11.547	98.593	9.830	5.675
	100	262	9.652	5.572	99.238	7.496	4.328	315	20.817	12.019	105.321	5.892	3.402	358	13.332	7.697	104.966	9.043	5.221	308	12.583	7.265	98.139	12.105	6.989
1 µM	105	270	9.652	5.572	102.969	6.307	3.641	320	20.977	12.111	106.673	8.110	4.682	350	12.368	7.140	102.731	9.926	5.731	305	12.910	7.454	97.298	11.652	6.727
	110	262	16.994	9.812	99.389	4.918	2.840	325	23.094	13.333	108.645	12.776	7.376	358	9.617	5.552	105.206	10.344	5.972	308	22.174	12.802	98.071	13.293	7.675
	115	264	13.052	7.536	100.371	4.541	2.622	328	11.817	6.822	109.357	13.565	7.832	360	15.963	9.216	105.583	9.012	5.203	305	12.910	7.454	97.088	9.482	5.475
	120	268	8.224	4.748	102.121	5.172	2.986	333	20.962	12.102	110.661	13.355	7.711	360	11.134	6.428	105.857	4.997	2.885	300	18.257	10.541	95.725	12.782	7.380
10 µM	125	262	14.144	8.166	99.840	8.729	5.040	328	11.094	6.405	109.180	10.937	6.315	360	17.128	9.889	105.501	8.358	4.825	315	19.648	11.344	100.449	15.870	9.163
	130	280	4.759	2.748	107.463	12.522	7.229	315	9.706	5.604	104.893	8.634	4.985	375	3.026	1.747	109.910	8.560	4.942	315	19.149	11.055	100.629	14.521	8.384
	135	282	7.479	4.318	108.306	13.681	7.899	280	12.119	6.997	93.493	7.093	4.095	373	8.767	5.062	109.751	7.959	4.595	315	23.805	13.744	100.239	11.490	6.634
	140	280	7.174	4.142	107.551	13.737	7.931	300	20.000	11.547	100.476	8.704	5.025	348	16.534	9.546	102.552	5.607	3.237	310	12.119	6.997	99.159	16.815	9.708
30 µM	145	280	10.742	6.202	107.187	11.842	6.837	308	8.979	5.184	102.737	6.591	3.806	328	7.690	4.440	97.230	10.858	6.269	305	7.846	4.530	97.410	15.254	8.807
	150	278	8.224	4.748	106.383	10.231	5.907	305	15.846	9.149	101.720	5.983	3.455	338	13.549	7.823	99.700	7.406	4.276	310	12.119	6.997	98.910	14.798	8.544
	155	280	20.310	11.726	107.298	10.159	5.865	303	21.302	12.298	100.989	10.630	6.137	338	10.954	6.324	100.165	10.982	6.341	293	17.078	9.860	93.091	9.489	5.478
	160	286	23.399	13.509	109.345	8.503	4.909	323	18.510	10.687	107.258	11.909	6.876	348	10.038	5.795	102.034	5.991	3.459	275	18.565	10.718	87.456	8.375	4.836

**Appendix 22** – The data shown below represents the coronary flow measurements for the 6 and 18-month lean and HFD Itraconazole treated hearts, as presented in chapter 7. Both the raw values and the normalised to stabilisation values are presented.

CHAPTER 7 - ITRACONAZOLE DATA																									
Concentration	Time	6M Lean Avg.	SD	SEM	6M Lean Avg. %	SD	SEM	6M HFD Avg.	SD	SEM	6M HFD Avg. %	SD	SEM	18M Lean Avg.	SD	SEM	18M Lean Avg. %	SD	SEM	18M HFD Avg.	SD	SEM	18M HFD Avg. %	SD	SEM
Stabilisation	5	26	6.455	3.727	100.735	1.471	0.849	29	1.414	0.816	101.420	1.597	0.922	21	1.000	0.577	100.287	0.575	0.332	25	3.464	2.000	102.005	2.466	1.424
	10	26	6.455	3.727	100.735	1.471	0.849	29	1.414	0.816	101.420	1.597	0.922	21	1.000	0.577	100.287	0.575	0.332	25	3.317	1.915	100.005	0.817	0.471
	15	25	5.477	3.162	99.265	1.471	0.849	29	0.707	0.408	99.150	1.038	0.599	21	1.000	0.577	100.287	0.575	0.332	24	3.304	1.908	98.995	1.429	0.825
	20	25	5.477	3.162	99.265	1.471	0.849	28	0.707	0.408	98.011	2.636	1.522	20	0.500	0.289	99.138	1.724	0.995	24	3.304	1.908	98.995	1.429	0.825
1 nM	25	25	5.477	3.162	99.265	1.471	0.849	26	0.707	0.408	91.090	2.473	1.428	20	1.258	0.726	99.037	2.746	1.585	23	2.500	1.443	93.209	4.810	2.777
	30	25	5.477	3.162	99.265	1.471	0.849	25	0.707	0.408	87.630	2.397	1.384	20	1.414	0.816	97.787	3.253	1.878	22	2.872	1.658	91.189	7.920	4.573
	35	25	5.439	3.140	100.360	4.790	2.765	25	1.414	0.816	85.300	3.752	2.166	20	1.708	0.986	96.537	5.111	2.951	22	2.828	1.633	90.198	8.180	4.723
3 nM	40	25	5.439	3.140	100.360	4.790	2.765	23	1.225	0.707	79.571	4.647	2.683	20	1.732	1.000	95.287	4.564	2.635	22	3.317	1.915	87.938	8.155	4.708
	45	25	5.439	3.140	100.360	4.790	2.765	23	1.225	0.707	79.571	4.647	2.683	19	1.258	0.726	94.138	2.854	1.648	21	3.594	2.075	84.948	10.738	6.199
	50	25	4.967	2.867	99.625	5.620	3.244	21	1.414	0.816	73.841	6.292	3.633	19	1.414	0.816	92.888	3.394	1.960	21	3.594	2.075	84.948	10.738	6.199
10 nM	55	24	4.031	2.327	97.059	5.882	3.396	20	0.707	0.408	68.061	3.973	2.294	19	1.500	0.866	94.138	4.981	2.876	20	3.559	2.055	81.555	7.190	4.151
	60	24	3.594	2.075	95.282	6.942	4.008	20	0.707	0.408	68.061	3.973	2.294	19	1.500	0.866	94.138	4.981	2.876	19	4.193	2.421	78.065	7.566	4.368
	65	23	3.559	2.055	92.220	6.582	3.800	18	0.707	0.408	61.141	3.778	2.181	19	1.500	0.866	91.739	6.238	3.601	19	3.742	2.160	77.172	5.807	3.352
100 nM	70	23	3.109	1.795	90.443	7.556	4.363	16	0.707	0.408	56.500	2.473	1.428	19	2.217	1.280	91.638	8.798	5.079	18	4.193	2.421	73.922	7.933	4.580
	75	23	3.109	1.795	90.443	7.556	4.363	16	0.707	0.408	56.500	2.473	1.428	19	2.217	1.280	91.638	8.798	5.079	18	4.500	2.598	71.902	10.366	5.985
	80	22	2.630	1.518	89.707	8.994	5.193	15	1.414	0.816	50.719	4.501	2.598	18	2.217	1.280	89.138	7.957	4.594	18	4.041	2.333	71.009	8.818	5.091
30 μM	85	22	2.630	1.518	89.707	8.994	5.193	14	1.871	1.080	49.590	6.526	3.768	18	2.160	1.247	87.888	7.073	4.084	16	4.031	2.327	65.713	8.825	5.095
	90	22	2.363	1.364	87.836	9.723	5.613	13	2.121	1.225	44.939	6.859	3.960	18	2.582	1.491	87.888	10.001	5.774	16	4.500	2.598	63.693	11.978	6.916
	95	22	2.363	1.364	87.836	9.723	5.613	12	2.828	1.633	42.619	9.270	5.352	18	2.380	1.374	85.489	9.529	5.502	14	5.315	3.069	57.193	15.153	8.748
1 μM	100	22	2.646	1.528	86.699	9.507	5.489	12	2.550	1.472	40.289	8.092	4.672	18	2.380	1.374	85.489	9.529	5.502	13	4.082	2.357	52.611	12.276	7.088
	105	21	3.162	1.826	84.373	8.457	4.883	11	1.871	1.080	36.819	5.462	3.154	17	2.449	1.414	82.989	9.259	5.346	13	4.573	2.640	51.504	14.095	8.138
	110	21	3.096	1.787	83.331	7.456	4.305	11	2.121	1.225	38.019	6.905	3.987	17	2.062	1.190	81.839	7.970	4.602	12	4.500	2.598	47.121	13.213	7.629
10 μM	115	21	3.416	1.972	82.195	8.084	4.667	11	2.550	1.472	36.829	8.149	4.705	17	2.062	1.190	81.839	7.970	4.602	12	4.796	2.769	45.871	14.303	8.258
	120	21	3.304	1.908	83.385	9.864	5.695	9	1.871	1.080	32.229	5.826	3.364	17	2.062	1.190	81.839	7.970	4.602	11	5.500	3.175	42.523	16.914	9.765
	125	21	3.416	1.972	82.195	8.084	4.667	9	1.871	1.080	32.229	5.826	3.364	17	2.380	1.374	80.589	9.622	5.555	10	5.377	3.105	40.380	16.807	9.703
30 μM	130	21	3.304	1.908	83.385	9.864	5.695	8	0.707	0.408	28.820	2.251	1.300	16	1.826	1.054	78.190	6.940	4.007	9	4.113	2.375	34.712	12.404	7.162
	135	20	2.944	1.700	80.778	12.800	7.390	8	0.707	0.408	26.490	1.586	0.916	16	1.708	0.986	76.940	5.632	3.251	7	3.697	2.134	25.715	11.429	6.599
	140	20	3.416	1.972	78.451	12.229	7.061	8	0.707	0.408	26.541	2.907	1.678	16	2.217	1.280	76.839	7.397	4.271	6	2.872	1.658	22.939	8.750	5.052
30 μM	145	20	3.416	1.972	78.451	12.229	7.061	6	1.414	0.816	21.839	4.225	2.440	16	2.217	1.280	76.839	7.397	4.271	5	2.217	1.280	19.134	7.067	4.080
	150	19	3.096	1.787	77.716	13.149	7.592	5	1.225	0.707	17.249	3.827	2.209	15	1.893	1.093	74.440	6.026	3.479	4	1.708	0.986	14.848	5.008	2.891
	155	19	3.416	1.972	74.347	11.799	6.812	4	1.414	0.816	12.659	4.716	2.723	15	1.893	1.093	74.440	6.026	3.479	3	0.816	0.471	12.072	1.754	1.013
	160	18	3.096	1.787	73.612	12.660	7.309	3	1.225	0.707	10.329	4.004	2.312	15	1.893	1.093	74.440	6.026	3.479	3	1.000	0.577	9.929	3.343	1.930

**Appendix 23** – The data shown below represents the left ventricular developed pressure measurements for the 6 and 18-month lean and HFD Itraconazole treated hearts, as presented in chapter 7. Both the raw values and the normalised to stabilisation values are presented.

CHAPTER 7 - ITRACONAZOLE DATA																									
Concentration	Time	6M Lean Avg.	SD	SEM	6M Lean Avg. %	SD	SEM	6M HFD Avg.	SD	SEM	6M HFD Avg. %	SD	SEM	18M Lean Avg.	SD	SEM	18M Lean Avg. %	SD	SEM	18M HFD Avg.	SD	SEM	18M HFD Avg. %	SD	SEM
Stabilisation	5	148.37	21.886	12.636	101.546	3.245	1.874	143.173	11.008	6.355	97.294	2.091	1.207	98.41	0.642	0.371	102.279	1.084	0.626	186.320	20.180	11.651	99.352	1.757	1.014
	10	147.22	23.496	13.565	98.766	1.653	0.954	145.147	8.865	5.118	98.685	2.163	1.249	100.39	3.881	2.241	101.348	1.292	0.746	187.745	23.848	13.768	99.928	2.436	1.406
	15	145.14	22.844	13.189	98.792	1.989	1.148	150.600	12.525	7.232	102.335	3.140	1.813	102.54	1.469	0.848	99.924	0.470	0.271	189.778	20.142	11.629	101.198	1.995	1.152
	20	140.23	23.075	13.322	100.896	2.028	1.171	149.657	11.889	6.864	101.686	0.962	0.555	98.66	3.312	1.912	96.449	1.150	0.664	186.695	20.428	11.794	99.522	0.569	0.329
1 nM	25	133.68	13.104	7.566	101.721	2.907	1.679	139.287	4.127	2.383	94.971	9.695	5.598	99.57	3.786	2.186	91.194	7.487	4.322	165.940	9.585	5.534	89.248	10.715	6.186
	30	131.31	13.014	7.514	101.368	2.743	1.584	135.707	4.824	2.785	92.516	9.399	5.427	98.61	2.075	1.198	89.561	7.384	4.263	164.913	9.147	5.281	88.822	12.177	7.030
	35	127.83	11.759	6.789	100.586	1.183	0.683	129.847	7.182	4.146	88.580	10.690	6.172	96.98	7.196	4.155	87.301	7.016	4.050	161.683	8.505	4.911	87.121	12.270	7.084
	40	122.61	13.572	7.836	97.619	5.925	3.421	130.540	3.115	1.798	88.909	6.299	3.637	95.02	9.647	5.570	83.484	8.900	5.138	156.843	14.515	8.380	84.542	13.416	7.746
3 nM	45	121.52	13.067	7.544	97.608	9.251	5.341	120.523	11.123	6.422	82.227	12.081	6.975	92.20	8.446	4.876	82.701	8.777	5.067	154.218	12.013	6.936	83.057	12.067	6.967
	50	116.92	11.912	6.878	95.165	6.490	3.747	115.473	11.892	6.866	78.844	13.052	7.536	88.52	6.525	3.767	79.676	8.750	5.052	149.323	12.130	7.003	80.597	13.312	7.686
	55	111.14	7.304	4.217	92.251	5.078	2.932	113.907	14.261	8.234	77.829	14.766	8.525	86.53	6.756	3.901	75.984	5.896	3.404	147.405	15.961	9.215	79.589	14.676	8.473
	60	106.74	19.252	11.115	91.418	5.872	3.390	107.990	7.568	4.370	73.718	10.443	6.029	86.25	6.487	3.745	73.382	3.698	2.135	141.140	12.364	7.138	75.940	10.661	6.155
10 nM	65	106.47	17.940	10.358	91.201	4.864	2.808	107.237	10.106	5.834	73.270	12.220	7.055	85.40	6.242	3.604	73.339	4.085	2.359	129.578	7.885	4.553	69.765	9.526	5.500
	70	109.05	21.171	12.223	90.693	2.696	1.557	107.093	11.418	6.592	73.200	13.132	7.582	83.44	7.397	4.271	75.003	6.795	3.923	128.145	9.100	5.254	69.152	11.327	6.539
	75	105.11	19.830	11.449	88.992	2.778	1.604	102.553	4.271	2.466	69.950	7.910	4.567	82.83	10.172	5.873	72.372	6.644	3.836	126.258	6.270	3.620	68.093	10.061	5.809
	80	99.68	18.371	10.606	88.587	4.576	2.642	96.100	15.035	8.680	65.629	12.933	7.467	80.51	10.023	5.787	68.718	6.511	3.759	117.240	12.371	7.143	63.504	13.220	7.632
100 nM	85	101.08	16.221	9.365	85.647	3.062	1.768	97.523	3.297	1.903	66.504	7.076	4.085	80.85	10.699	6.177	69.814	5.686	3.283	113.115	12.483	7.207	61.320	13.522	7.807
	90	99.51	16.732	9.660	85.494	2.713	1.566	101.430	3.566	2.059	69.161	7.165	4.137	80.14	11.449	6.610	68.749	6.518	3.763	113.788	13.574	7.837	61.801	14.694	8.484
	95	97.61	18.137	10.471	84.689	2.994	1.729	98.233	1.058	0.611	66.923	5.109	2.950	77.31	13.602	7.853	67.240	6.130	3.539	112.010	12.931	7.466	60.752	13.806	7.971
	100	102.51	14.647	8.456	82.532	3.566	2.059	95.633	9.275	5.355	65.208	9.179	5.299	77.01	14.283	8.246	70.783	3.087	1.782	107.190	18.116	10.459	58.521	17.317	9.998
1 µM	105	98.46	12.542	7.241	83.146	4.213	2.432	93.780	2.707	1.563	63.922	6.084	3.513	73.82	13.844	7.993	68.080	2.821	1.629	98.085	15.887	9.173	53.540	15.477	8.936
	110	95.23	8.887	5.131	82.404	4.573	2.640	93.047	10.848	6.263	63.146	2.973	1.717	74.37	13.390	7.731	66.167	5.527	3.191	98.143	15.201	8.776	53.536	15.073	8.703
	115	93.39	10.685	6.169	81.807	2.941	1.698	91.853	12.307	7.106	62.307	4.342	2.507	73.19	12.546	7.244	64.778	5.188	2.995	93.850	14.586	8.421	51.198	14.301	8.256
	120	97.28	11.907	6.874	80.539	4.448	2.568	86.683	17.182	9.920	58.680	7.864	4.540	72.43	15.651	9.036	67.297	3.035	1.752	92.608	17.385	10.037	50.689	16.145	9.321
10 µM	125	94.78	12.382	7.149	79.830	4.367	2.521	84.890	19.134	11.047	57.408	8.842	5.105	72.45	15.910	9.185	65.579	4.739	2.736	83.125	13.451	7.766	45.395	13.209	7.626
	130	88.95	9.530	5.502	80.265	2.753	1.590	82.217	13.000	7.506	55.752	5.879	3.394	71.25	15.285	8.825	61.652	3.488	2.014	79.378	6.123	3.535	42.957	8.078	4.664
	135	91.91	11.468	6.621	77.700	5.440	3.141	78.983	8.805	5.084	53.670	4.500	2.598	71.01	15.343	8.859	63.648	4.869	2.811	77.823	4.469	2.580	41.982	6.535	3.773
	140	90.30	11.095	6.405	78.931	3.910	2.258	72.003	6.778	3.913	48.955	3.732	2.155	69.14	16.554	9.557	62.456	2.410	1.392	71.853	2.347	1.355	38.585	3.516	2.030
30 µM	145	88.25	11.794	6.809	79.113	3.776	2.180	63.457	7.850	4.532	43.318	7.324	4.228	66.95	17.192	9.926	61.009	3.956	2.284	62.995	5.407	3.122	34.099	6.736	3.889
	150	87.64	12.980	7.494	79.116	6.264	3.616	60.373	6.290	3.631	41.184	6.013	3.472	67.86	16.796	9.697	60.449	2.666	1.539	61.190	4.674	2.698	33.158	6.632	3.829
	155	83.52	11.142	6.433	78.769	5.615	3.242	58.013	4.874	2.814	39.621	6.089	3.516	67.60	14.940	8.625	57.696	2.439	1.408	59.085	1.615	0.933	31.829	4.129	2.384
	160	86.79	10.288	5.940	78.461	5.087	2.937	51.470	9.815	5.667	35.253	8.882	5.128	65.91	16.840	9.722	60.169	5.088	2.938	55.075	2.977	1.719	29.675	4.120	2.379

**Appendix 24** – The data shown below represents the left ventricular developed pressure measurements for the 6 and 18-month lean and HFD Itraconazole treated hearts, as presented in chapter 7. Both the raw values and the normalised to stabilisation values are presented.

CHAPTER 7 - ITRACONAZOLE DATA																									
Concentration	Time	6M Lean Avg.	SD	SEM	6M Lean Avg. %	SD	SEM	6M HFD Avg.	SD	SEM	6M HFD Avg. %	SD	SEM	18M Lean Avg.	SD	SEM	18M Lean Avg. %	SD	SEM	18M HFD Avg.	SD	SEM	18M HFD Avg. %	SD	SEM
Stabilisation	5	275	3.245	1.874	98.408	0.642	0.371	290	15.083	8.708	95.586	10.590	6.114	345	9.574	5.528	101.077	4.537	2.619	355	17.561	10.139	98.271	2.881	1.663
	10	270	1.653	0.954	100.394	3.881	2.241	300	15.083	8.708	98.606	0.671	0.387	340	12.583	7.265	99.176	3.841	2.217	358	13.549	7.823	99.170	2.950	1.703
	15	275	1.989	1.148	102.536	1.469	0.848	320	21.484	12.404	104.931	10.241	5.913	348	18.930	10.929	101.377	2.740	1.582	360	10.820	6.247	100.570	4.851	2.801
	20	275	2.028	1.171	98.662	3.312	1.912	307	10.964	6.330	100.877	1.758	1.015	338	17.078	9.860	98.370	2.370	1.368	368	13.038	7.528	101.990	4.588	2.649
1 nM	25	278	2.907	1.679	99.574	3.786	2.186	313	20.586	11.885	102.741	9.427	5.443	338	20.616	11.902	98.195	4.741	2.737	310	18.900	10.912	86.640	10.301	5.947
	30	273	2.743	1.584	98.611	2.075	1.198	327	17.609	10.166	106.715	20.194	11.659	340	10.000	5.774	99.213	6.535	3.773	310	15.025	8.674	86.767	10.525	6.076
	35	270	1.183	0.683	96.975	7.196	4.155	330	11.678	6.742	108.032	10.574	6.105	338	9.574	5.528	98.453	9.209	5.317	288	22.174	12.802	81.322	13.135	7.584
	40	268	5.925	3.421	95.019	9.647	5.570	293	14.856	8.577	96.231	9.140	5.277	333	17.321	10.000	97.209	9.263	5.348	310	25.106	14.495	86.866	9.403	5.429
3 nM	45	275	9.251	5.341	92.200	8.446	4.876	313	15.492	8.944	102.482	12.759	7.367	335	10.000	5.774	97.918	8.698	5.022	315	17.798	10.276	88.396	8.988	5.189
	50	288	6.490	3.747	88.519	6.525	3.767	300	9.518	5.495	98.477	6.736	3.889	335	14.142	8.165	97.918	8.698	5.022	315	13.771	7.951	88.410	7.990	4.613
	55	283	5.078	2.932	86.534	6.756	3.901	293	20.586	11.885	96.256	12.404	7.161	335	18.930	10.929	97.693	12.008	6.933	303	7.679	4.434	85.298	11.595	6.694
	60	298	5.872	3.390	86.249	6.487	3.745	313	8.371	4.833	103.018	9.265	5.349	345	7.291	4.210	100.150	12.840	7.413	323	16.594	9.580	89.935	7.079	4.087
10 nM	65	283	4.864	2.808	85.398	6.242	3.604	290	15.083	8.708	95.303	0.969	0.560	350	12.679	7.321	101.807	9.537	5.506	348	11.094	6.405	97.493	11.685	6.746
	70	290	2.696	1.557	83.443	7.397	4.271	300	9.276	5.355	98.348	13.599	7.852	355	12.583	7.265	103.144	10.642	6.144	318	15.276	8.819	88.307	1.602	0.925
	75	295	2.778	1.604	82.835	10.172	5.873	297	8.371	4.833	97.444	7.818	4.514	360	4.853	2.802	104.562	9.798	5.657	330	20.131	11.623	92.188	10.889	6.287
	80	285	4.576	2.642	80.506	10.023	5.787	310	18.744	10.822	101.603	8.236	4.755	358	15.419	8.902	103.807	10.562	6.098	345	11.906	6.874	96.891	12.994	7.502
100 nM	85	273	3.062	1.768	80.854	10.699	6.177	310	21.484	12.404	101.683	10.702	6.179	358	13.412	7.744	103.733	8.962	5.174	315	23.805	13.744	88.904	12.466	7.197
	90	283	2.713	1.566	80.138	11.449	6.610	313	20.096	11.602	102.944	2.637	1.522	360	11.781	6.802	104.254	11.134	6.428	318	11.094	6.405	88.674	6.713	3.876
	95	280	2.994	1.729	77.313	13.602	7.853	280	19.422	11.213	91.974	4.572	2.640	345	11.402	6.583	100.158	9.954	5.747	308	20.616	11.902	86.757	11.424	6.596
	100	278	3.566	2.059	77.005	14.283	8.246	273	20.096	11.602	89.778	5.798	3.348	360	12.540	7.240	104.378	9.943	5.741	328	12.540	7.240	92.517	14.734	8.507
1 µM	105	280	4.213	2.432	73.824	13.844	7.993	280	21.213	12.247	92.306	7.673	4.430	348	15.227	8.791	100.803	10.510	6.068	325	21.409	12.361	91.434	12.671	7.315
	110	280	4.573	2.640	74.374	13.390	7.731	333	17.680	10.208	109.041	12.230	7.061	350	15.227	8.791	101.485	9.107	5.258	303	8.852	5.111	84.472	5.848	3.376
	115	270	2.941	1.698	73.190	12.546	7.244	297	21.863	12.622	96.988	15.803	9.124	318	17.321	10.000	92.249	6.046	3.491	305	8.948	5.166	85.477	9.946	5.742
	120	270	4.448	2.568	72.428	15.651	9.036	290	19.422	11.213	95.278	4.454	2.571	340	9.760	5.635	98.676	10.245	5.915	283	15.720	9.076	79.030	4.718	2.724
10 µM	125	268	4.367	2.521	72.446	15.910	9.185	317	14.085	8.132	103.313	17.514	10.112	348	7.679	4.434	101.216	6.925	3.998	288	17.679	10.207	81.463	16.756	9.674
	130	260	2.753	1.590	71.246	15.285	8.825	310	16.229	9.370	101.473	14.512	8.379	373	6.484	3.744	108.228	11.247	6.494	278	15.939	9.202	78.396	17.760	10.253
	135	263	5.440	3.141	71.005	15.343	8.859	370	10.609	6.125	120.712	20.413	11.786	345	18.930	10.929	100.751	9.325	5.384	275	22.805	13.166	77.631	18.758	10.830
	140	268	3.910	2.258	69.144	16.554	9.557	347	23.454	13.541	113.120	20.483	11.826	330	7.679	4.434	95.967	9.475	5.470	260	24.237	13.993	73.048	16.170	9.336
30 µM	145	263	3.776	2.180	66.954	17.192	9.926	340	23.184	13.385	111.077	21.976	12.688	335	7.846	4.530	97.670	5.998	3.463	258	21.302	12.298	72.284	10.245	5.915
	150	258	6.264	3.616	67.862	16.796	9.697	343	17.609	10.166	112.492	22.107	12.764	335	11.402	6.583	97.385	8.843	5.106	275	17.504	10.106	78.267	16.381	9.458
	155	263	5.615	3.242	67.603	14.940	8.625	350	10.609	6.125	114.178	22.150	12.788	338	14.695	8.484	98.632	7.610	4.394	255	9.137	5.275	72.168	13.325	7.693
	160	265	5.087	2.937	65.910	16.840	9.722	350	10.609	6.125	114.178	22.150	12.788	338	7.846	4.530	97.773	9.863	5.694	240	21.602	12.472	67.861	11.421	6.594